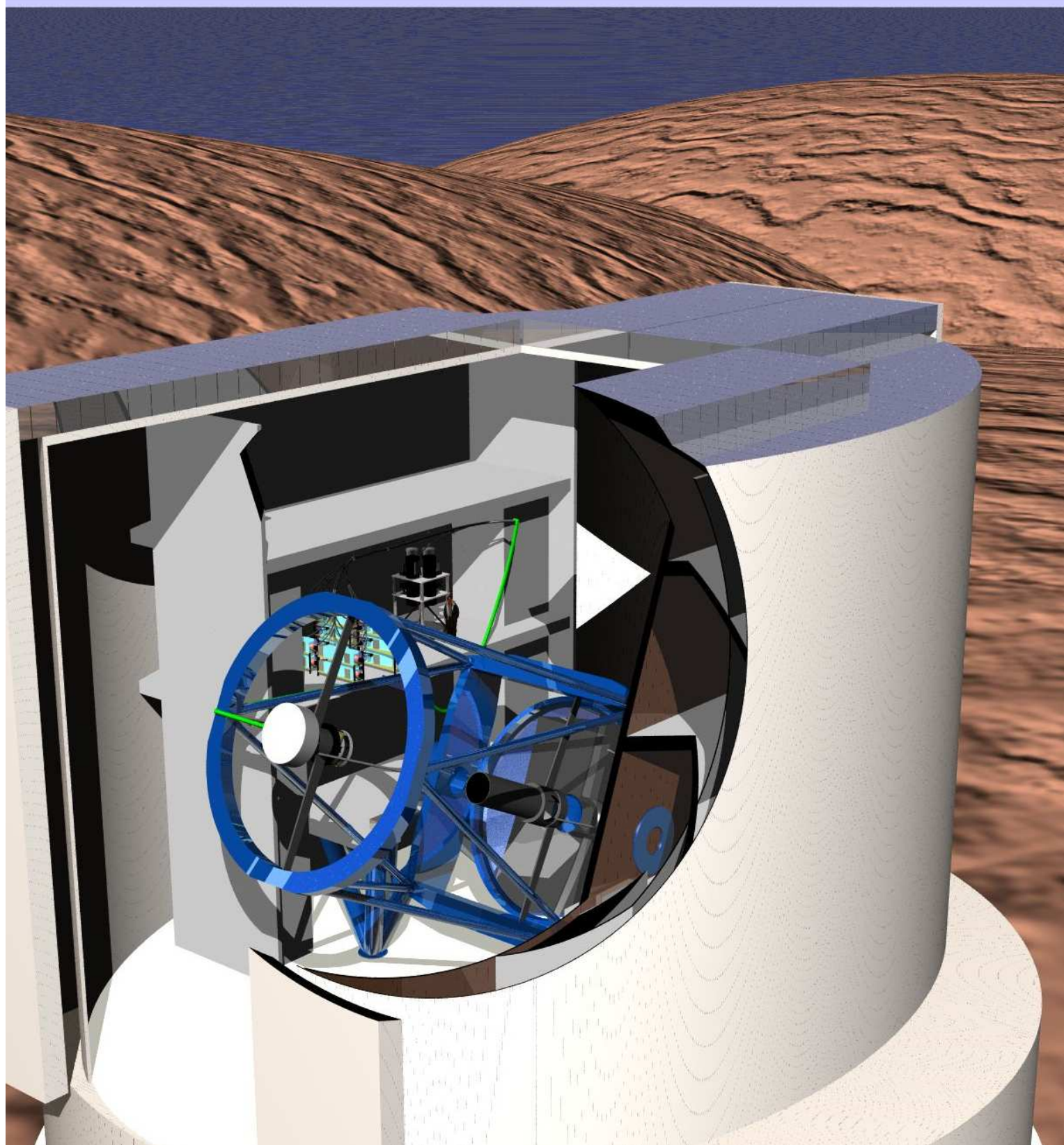


Gemini Wide-Field Fiber-Fed Optical Multi-Object Spectrograph (WFMOS)

Feasibility Study Report

(AURA Contract No. 0084699-GEM00385)





Gemini WFMOS

WFMOS FEASIBILITY STUDY REPORT

WFMOS Feasibility Study AURA Contract No. 0084699-GEM00385

CHANGE RECORD

ISSUE	DATE	SECTION/PAGE AFFECTED	REASON/REMARKS
0.4	07/09/04	All	Skeleton as submitted to Gemini
1	07/03/05	All	As submitted to Gemini for review

Prepared jointly by

Anglo-Australian Observatory
Canadian Astronomy Data Centre
Johns Hopkins University
National Optical Astronomy Observatory
University of Durham
University of Oxford
University of Portsmouth

A list of the contributors to this document can be found at the end.

Released By:

Samuel C. Barden 7 March 2005 _____

Name

Date

Signature

Executive Summary

What is dark energy? How does its equation of state vary as a function of time? How do galaxies form? What is the nature of dark matter on galactic scales? What formation mechanisms result in the observed structure of our Galaxy? Why is our Galaxy different in structure from other local group members? How does galaxy formation and evolution depend on the formation and evolution of large scale structure? How was the Universe reionized? What mechanisms govern the creation and dispersal of “metals” in the Universe? Such are some of the key questions facing today’s science of astronomy. The recent Gemini ASPEN workshop (Scientific Horizons at the Gemini Observatory: Exploring a Universe of Matter, Energy and Life) identified many of these questions as key areas in which the Gemini telescopes should be engaged over the coming decades.

A new facility capable of taking detailed spectroscopy of millions of objects in the Universe overcomes the statistical complexity of the Universe and allows us to answer these fundamental questions. In this document we present the scientific case, technical feasibility, and estimated cost of a wide-field, fiber-fed, multi-object spectrograph (WF MOS) for the Gemini/Subaru observatory.

This study is the result of a call by Gemini to examine such an instrument as an outcome of the ASPEN meeting. The Gemini observatory is exploring the possibility that this facility may actually be implemented on the Subaru telescope, but shared between the Gemini and Subaru communities in exchange for Subaru access to other key instruments on Gemini.

WF MOS provides Gemini/Subaru with the capability of simultaneously obtaining moderate to high-resolution ($R=1,000-40,000$) spectra of ~ 4500 targets in a field of view of 1.5 degrees in diameter. This capability would enable Gemini/Subaru to be uniquely capable, providing the Observatory with a 10-100 advantage over existing and planned multiobject spectrographs. WF MOS will deliver of order 20,000 astronomical spectra per night!

The two primary science drivers for WF MOS are (1) the determination of the equation of state of dark energy, and (2) the study of the origin of our Galaxy.

The dark energy science case can be summarized by the following:

- Acoustic oscillations provide an astrophysically robust cosmological standard ruler that can be used to study the nature of dark energy by the direct measurement of the variation in the angular diameter distance and the cosmological expansion rate as a function of redshift. The recent detection of the acoustic oscillations in the galaxy power spectrum at low- z , by the SDSS and 2DF teams, reinforces the viability of this method in providing a new, powerful probe of dark energy.
- WF MOS can provide unprecedented constraints on the nature of dark energy by undertaking uniquely large galaxy redshift surveys necessary to detect and robustly measure the scale length of the acoustic oscillations at high redshift (i.e., at $z\sim 1$ and $z\sim 3$). These surveys would require roughly 200 nights with GWF MOS but would take more

than 2000 nights with any existing spectrograph and are therefore currently infeasible.

- The acoustic peak method opens discovery space for the study of dark energy at $z > 1.5$ that the other current methods cannot provide. At the same time, it provides competitive and complementary constraints at lower redshifts.
- The data derived from the galaxy redshift surveys will also provide an unprecedented data set for the study of the evolution in the properties of galaxy populations over a large fraction of our Universe's history.

The Galactic archaeology and genesis case is summarized by:

- WFMOS enables an unprecedented study of the formation history of our Galaxy and its neighbours, and will provide the only robust means of distinguishing between competing formation scenarios for these systems.
- The high-resolution mode of WFMOS ($R \sim 40,000$) will be used to study a sample of roughly 1.5 million stars, the biggest spectroscopic survey ever conceived from the ground. This survey will provide exquisite abundance information on 100,000 thick disk stars and 30,000 halo stars. The chemical signatures will allow us to identify the rate of infall of distinct fragments of the protogalaxy into the different components of the Galaxy. Many of these structures will not be identifiable from their kinematic signatures alone. The high-resolution mode provides a unique scientific capability for Gemini's astronomical community.
- The low-resolution mode of WFMOS ($R \sim 1800$) will be used to conduct a kinematic survey of roughly half a million stars in our Galaxy and M31 to unravel their merger histories from phase space (kinematic and spatial) signatures.

Table 1. Summary of the Baseline Survey Parameters.

Survey	R_{lim} (AB mag)	Target Surface Density (deg⁻²)	Total Area (deg²)	Total Sample Size (# objects)	Total Survey Time¹ (hrs/nights)
<i>Dark Energy</i> $z = 0.5 - 1.3$	22.7	1000	2000	2×10^6	1530/153
<i>Dark Energy</i> $z = 2.3 - 3.3$	24.5	2000	300	6×10^5	1360/136
<i>Galactic High-Res</i>	17	500	3000	1.5×10^6	4900/490
<i>Galactic Low-Res</i>	21	1000	500	0.5×10^6	1400/140

¹ Includes factor of 1.7 to account for weather and assumes average of 10 hours per night.

WFMOS is mounted at the prime focus of either the Gemini or Subaru telescope. It contains a multi-element corrector, an atmospheric dispersion correcting prism assembly, and an Echidna-style fiber optic focal plane. If implemented on Gemini, the ADC would double as a wobble plate to provide a fast guiding capability and

the ability to beam switch. Faint object sky subtraction with WFMOS will be done using the nod-and-shuffle observing mode, which obviates many of the traditional limitations of fiber spectrographs. Configuring the fibers is done through a novel approach that images the focal plane and allows configuration of the ~4500 fibers in less than 10 minutes. The fibers feed to an array of spectrographs located in a spectrograph laboratory. WFMOS is a prime-focus instrument that will require a new top-end structure (for Gemini) which holds the corrector and the fiber assembly. Since the Subaru telescope already executes instrument changes at the top end, the WFMOS facility would only require some modification of the existing top end for optimal performance.

The study reveals technical challenges, but no technical show stoppers as the challenges all appear to be manageable. Among the challenges are: the large size of the front element of the corrector (1.2 meters if vignetting is allowed, 1.6 meters for an unvignetted system); the complexity of dealing with 4500 fibers; dealing with wind shake induced image motion on Gemini; and providing an efficient data pipeline for the spectra. The cost for the baseline concept appears to be \$45M without contingency and \$60M with the addition of 30% contingency (see Table 2). The development phase of the baseline instrument is 6 to 7 years.

The baseline concept assumed an implementation on the Subaru telescope with 4500 fibres over a 1.5 degree field. Alternative options explored included: implementation on Gemini, which would require a new top end; extension to 6000 fibres over a 2 degree field on Subaru; and the addition of IR spectrographs to the Subaru baseline.

The costs for the various components of the WFMOS baseline instrument are discussed in detail in *Chapter 27, Costs Structure and Costs Estimates*. A summary table of the costs is shown in Table 2 below.

Table 2. Table of cost estimates for WFMOS implementation.

WFMOS System Costs	
Subaru 1.5 deg – no IR (baseline concept)	\$45,400,000
	(\$59,000,000 with contingency)
Gemini 1.5 deg – no IR (KAOS concept)	\$44,800,000
(original baseline)	(\$58,240,000 with contingency)
Subaru 1.5 deg – with IR	\$51,800,000
	(\$67,340,000 with contingency)
Subaru 2.0 deg – no IR	\$54,500,000
	(\$70,850,000 with contingency)
WFMOS components	ROM Cost (USD)
Corrector	\$4,570,560
Top End Modifications	\$655,720
Positioner	\$8,258,768
Fibre Cable	\$1,877,040
Fibre Connector	\$1,019,955
Low-resolution spectrographs (10 off)	\$7,538,600
High-resolution spectrographs (double unit)	\$8,457,840

WF MOS System Costs

Acquisition and Guiding systems software	\$56,800
Wavefront Sensing (mirror control)	\$1,440,688
Calibration Systems	\$407,160
Systems software	\$1,464,400
Data reduction pipeline	\$2,599,652
Subaru infrastructure upgrades	\$1,258,400
Project Management & Logistics	\$4,489,320
Process costs	\$1,301,765
Estimated total of basic work scope	\$45,396,668
Gemini contingency (30%)	\$13,619,000
Estimated Project Total - incl. contingency	\$59,015,668

Optional components

NIR spectrograph	\$9,666,966
Gemini CFRP top end	\$800,000
Gemini Steel top end	\$597,000
Do-all spectrographs	\$13,179,860
Gemini infrastructure for WF MOS	\$500,000
Data Pipeline Package B	\$1,900,000

In Summary

This report clearly demonstrates in detail that it is feasible for Gemini to achieve fundamental new results in dark energy and galaxy archaeology through the construction of WF MOS on Subaru or Gemini with the baseline concept costing \$45M USD (\$60M with 30% contingency). Many in the Gemini community are ready, able, and anxious to build this facility!

Table of Contents

<u>SECTION I: INTRODUCTION TO THE WFMOS FEASIBILITY STUDY.....</u>	<u>24</u>
CHAPTER 1 GLOSSARY OF TERMS.....	25
CHAPTER 2 INTRODUCTION AND PURPOSE.....	29
2.1 GEMINI WFMOS FEASIBILITY STUDY.....	29
2.1.1 <i>Aspen Process</i>	30
2.1.2 <i>Strawman Concept</i>	30
2.1.3 <i>Purpose of the Feasibility Study</i>	32
2.2 APPLICABLE DOCUMENTATION.....	33
<u>SECTION II: WFMOS SCIENCE CASES.....</u>	<u>34</u>
CHAPTER 3 DARK ENERGY AND COSMIC SOUND: A NEW ROAD TO COSMIC ACCELERATION AND THE EQUATION OF STATE FROM GIANT GALAXY REDSHIFT SURVEYS.....	35
3.1 BACKGROUND.....	35
3.1.1 <i>Why dark energy is one of the most important problems in physics</i>	35
3.1.2 <i>Acoustic oscillations as a standard ruler and probe of dark energy</i>	36
3.1.3 <i>Theoretical Uncertainties in the Acoustic Oscillation Method</i>	38
3.1.4 <i>January 2005: Acoustic oscillations discovered</i>	38
3.2 GALAXY REDSHIFT SURVEYS FOR ACOUSTIC OSCILLATIONS.....	40
3.2.1 <i>Analytic assessments of performance</i>	41
3.2.2 <i>Numerical validation of analytic computations</i>	43
3.2.3 <i>Estimated performance as a function of survey size/redshift</i>	47
3.2.4 <i>Comparing and Constrasting the Acoustic Oscillation Method with Others</i>	47
3.3 POSSIBLE TARGETS FOR THE ACOUSTIC OSCILLATION SURVEYS.....	49
3.3.1 <i>Redshift range $0.5 < z < 1.3$</i>	50
3.3.1.1 <i>Red Sequence Galaxies at $z \sim 1$</i>	51
3.3.1.2 <i>Blue Sequence Galaxies at $z \sim 1$</i>	51
3.3.1.3 <i>Exposure Times for $z \sim 1$ Samples</i>	52
3.3.2 <i>Redshift range $2.3 < z < 3.5$</i>	52
3.3.3 <i>Redshift desert $1.3 < z < 2.3$</i>	53
3.3.3.1 <i>A red-optimized strategy</i>	54
3.3.3.2 <i>A near-IR strategy</i>	54
3.3.3.3 <i>A blue-optimized strategy</i>	55
3.3.3.4 <i>Number of redshift desert fibers</i>	55
3.3.4 <i>Nod & Shuffle and Exposure time</i>	55
3.4 OPTIMIZATION OF SURVEY SIZE AND REDSHIFT RANGE.....	56
3.4.1 <i>Where is the Best Place to Look for Interesting New Dark Energy Physics?</i>	56
3.4.2 <i>Two Baseline Surveys</i>	58
3.4.3 <i>A Program for Optimization of the Experimental Design</i>	61
3.4.3.1 <i>Overview</i>	61
3.4.3.2 <i>Testing analytical predictions of dark energy measurements for a fiducial ΛCDM model</i>	61
3.4.4 <i>Trade-off of exposure time versus science gain</i>	63
3.5 FLOW-DOWN TO INSTRUMENT REQUIREMENTS, GIVEN OPTIMISATION.....	63

3.5.1 Wavelength coverage and areal density.....	63
3.5.2 Fiber allocation (given a clustered target set and multiple spectrographs).....	64
3.5.3 Fiber rearrangement time, accuracy requirements.....	65
3.5.4 Acquisition and guiding requirements.....	65
3.5.5 Resolution and calibration requirements, including sky subtraction.....	65
3.5.6 Data reduction requirements.....	66
3.6 DISCUSSION OF THE AVAILABILITY OF THE REQUIRED IMAGING DATA.....	66
3.7 TELESCOPE IMPACT ON SCIENCE.....	67
3.7.1 Gemini North vs. Gemini South vs. Subaru.	67
3.7.2 Constraints on observatory operations.....	67
3.8 OPPORTUNITIES FOR ADDITIONAL SIMULTANEOUS, INDEPENDENT SCIENCE PROGRAMS.....	67
3.9 OTHER FACILITIES.....	68
3.9.1 Complementary Facilities.....	68
3.9.2 Competing Facilities, both spectroscopic surveys and photometric redshift surveys.	68
3.9.3 A Road-Map for Acoustic oscillation surveys over the next decade.....	69
3.10 KEY RISKS TO SCIENCE GOALS.....	71
3.10.1 Competition in 2012: How big a survey will be required?	71
3.10.2 Competition in 2012: Spectroscopic redshift surveys.	71
3.10.3 Competition in 2012: Photometric redshift surveys.	72
3.10.4 Exposure time estimates.....	72
3.10.5 The cosmological constant null result, i.e. would it be a failure if we just found $w=-1$?.....	72
3.10.6 Failure of the Planck mission.....	73
3.10.7 Telescope access.....	73
3.10.8 Imaging surveys for photometric pre-selection.....	73
3.11 REFERENCES.....	74
CHAPTER 4 STELLAR ARCHAEOLOGY AND GALAXY GENESIS.....	77
4.1 SCIENCE CASE – HOW DO GALAXIES FORM?.....	77
4.1.1 The High-Spectral-Resolution Survey.....	78
4.1.1.1 Identification of Distinct Stellar Populations.....	78
4.1.1.2 Chemical Tagging.....	80
4.1.1.3 Primary requirements of chemical tagging.....	81
4.1.1.4 Analysis of substructure in kinematic and elemental abundances.....	83
4.1.2 The Low-Spectral-Resolution Survey.....	83
4.1.2.1 The stellar halo - thick disk interface.....	84
4.1.2.2 The thick disk - thin disk interface.....	84
4.1.2.3 The central bulge–bar–inner disk.....	86
4.1.2.4 The extent of the dark halo.....	87
4.1.3 Investigations for requirements analysis.....	87
4.1.3.1 Detailed Simulations of the Merging of Substructure.....	87
4.1.3.1.1 Observing the Milky Way.....	88
4.1.3.1.2 Metallicity distributions.....	91
4.1.3.1.3 Observing another galaxy.....	92
4.1.3.2 Sky Coverage, Velocity Accuracy to Detect Streams.....	93
4.1.4 What will have been achieved for M31?.....	95
4.2 TELESCOPE IMPACT ON SCIENCE.....	98
4.2.1 Hemisphere Impact.....	98
4.2.2 Field of View.....	99
4.3 INSTRUMENT REQUIREMENTS.....	99
4.3.1 Basic Parameters.....	99
4.3.1.1 What Resolution and Wavelength Coverage are Required?.....	99

4.3.1.1.1 High-resolution survey.....	99
4.3.1.1.1.1 Spectral resolution.....	99
4.3.1.1.1.2 Wavelength Coverage.....	101
4.3.1.1.2 Low resolution survey.....	103
4.3.2 <i>Data Reduction Requirements</i>	103
4.3.3 <i>Acquisition Requirements</i>	104
4.3.4 <i>Calibration Requirements</i>	104
4.4 OBSERVING SCENARIOS.....	105
4.4.1 <i>Survey Parameters</i>	105
4.4.2 <i>The High-Resolution Survey</i>	105
4.4.3 <i>Low-Resolution Survey</i>	106
4.4.4 <i>Required support for observation preparation</i>	107
4.4.4.1 Precursor Surveys.....	107
4.4.5 <i>End-to-End observing cycle</i>	107
4.4.5.1 Operational model.....	107
4.4.5.2 Fiber assignment.....	111
4.5 OTHER FACILITIES.....	112
4.5.1 <i>Complementary</i>	112
4.5.2 <i>Competition</i>	113
4.6 RISKS TO THE SCIENCE.....	114
4.7 REFERENCES.....	114
CHAPTER 5 OTHER SCIENCE ENABLED BY WFMOS.....	117
5.1 BACKGROUND.....	117
5.2 VALUE ADDED SCIENCE.....	117
5.3 SCIENCE CASES ENABLED BY WFMOS AS DESIGNED.....	118
5.4 REFERENCES.....	119
<u>SECTION III: WFMOS TECHNICAL STUDY.....</u>	<u>121</u>
CHAPTER 6 WFMOS SUMMARY INSTRUMENT DESCRIPTION.....	122
6.1 PRIMARY DESCRIPTION.....	122
6.2 SYSTEM COMPONENTS.....	122
6.2.1 <i>Top End</i>	123
6.2.2 <i>Wide-Field Corrector</i>	124
6.2.3 <i>Atmospheric Dispersion Compensator</i>	124
6.2.4 <i>[Gemini Option: Image Stabilizer]</i>	124
6.2.5 <i>Acquisition and Guiding System</i>	125
6.2.6 <i>Wavefront Sensing System</i>	125
6.2.7 <i>Calibration System</i>	125
6.2.8 <i>Fiber Positioner</i>	125
6.2.9 <i>Instrument Rotator</i>	125
6.2.10 <i>Flexure Compensator</i>	126
6.2.11 <i>Fiber Cable</i>	126
6.2.12 <i>Fiber Connector</i>	126
6.2.13 <i>Low Dispersion and High Dispersion Spectrographs</i>	127
6.2.14 <i>Detector Systems</i>	127
6.2.15 <i>Instrument Control Computers/Software</i>	127
6.2.16 <i>Instrument Handling Facilities</i>	128
6.2.17 <i>Observing Preparation Software</i>	128
6.2.18 <i>Data Pipeline</i>	128
6.3 SYSTEM PERFORMANCE.....	129

CHAPTER 7 SYSTEMS ENGINEERING.....	131
7.1 SYSTEMS APPROACH.....	131
7.2 ARCHITECTURAL AND TELESCOPE CONSTRAINT ISSUES.....	132
7.3 SOFTWARE SYSTEMS OVERVIEW.....	134
7.3.1 <i>Strawman Design</i>	135
7.3.1.1 Top-level description of software functionality required to support science case.....	135
7.3.1.2 Block diagram level illustrations of major subsystems.....	136
7.3.1.3 Communications pathways.....	145
7.3.1.4 Data flows	145
7.3.1.5 Instrument Control Software Implementation notes.....	146
7.3.2 <i>Interfaces</i>	148
7.4 ELECTRICAL/ELECTRONIC SYSTEMS OVERVIEW.....	148
7.4.1 <i>Strawman Design</i>	148
7.4.1.1 Top End Sub Systems.....	148
7.4.1.2 Off Telescope Sub-systems.....	149
7.4.1.3 Top Level Control Computer.....	149
7.4.1.4 Block diagram level illustrations of major subsystems.....	150
7.4.2 <i>Conformance with Gemini Aspen Instrument Architecture</i>	150
7.4.3 <i>Interfaces</i>	151
7.4.4 <i>General Electronics System Engineering</i>	153
7.4.4.1 Equipment and Component Standardisation.....	153
7.4.4.2 Prototyping.....	153
7.4.4.3 Electronics Cooling.....	154
7.4.4.4 Power.....	154
7.4.4.5 Observatory Electronics Design Requirements.....	154
7.4.4.6 Safety.....	154
7.4.4.7 Environmental Requirements.....	154
7.4.4.8 Electro-Magnetic Compatibility (EMC).....	154
7.5 FAILURE MODE EFFECT ANALYSIS (FMEA).....	155
7.5.1 <i>Introduction</i>	155
7.5.2 <i>FMEA approach</i>	155
7.5.3 <i>Failure Mode Effect Analysis Rating Scales</i>	155
7.5.4 <i>Results of Feasibility Study FMEA</i>	156
CHAPTER 8 WIDE FIELD CORRECTOR.....	158
8.1 SUMMARY.....	158
8.1.1 <i>Baseline Corrector Design</i>	158
8.1.2 <i>Optical design exploration – Subaru and Hyper-SuprimeCam</i>	159
8.1.3 <i>Potential IR Performance</i>	161
8.2 OPTICAL TOLERANCING.....	161
8.3 WOBBLE PLATE FOR GEMINI IMPLEMENTATION.....	162
8.4 PRIME FOCUS MOUNTING STRUCTURE.....	162
8.5 COST TRADES.....	164
8.6 COST AND FEASIBILITY.....	165
8.6.1 <i>Optical elements</i>	165
8.6.2 <i>Mechanical Structure</i>	166
CHAPTER 9 WOBBLE PLATE.....	167
9.1 EFFECT OF WINDSHAKE ON GEMINI.....	167
9.2 WOBBLE PLATE SERVO CONCEPT.....	168
9.3 WOBBLE PLATE SOLUTION.....	169

9.3.1 Mechanical Design.....	169
9.3.2 Mass and Inertia Estimates.....	173
9.3.3 Actuator Selection.....	174
9.3.4 Finite Element Analysis.....	179
9.3.5 Variations on a Theme.....	186
9.4 WOBBLE PLATE SPECIFICATION.....	188
9.5 FEASIBILITY OF OPTICAL ELEMENTS.....	188
9.6 COST AND FEASIBILITY OF MOUNTING.....	189
9.7 COST AND FEASIBILITY OF CONTROL SYSTEM.....	189
9.8 COST AND FEASIBILITY OF ELECTRONICS AND SOFTWARE.....	190
9.9 FINAL COST AND RISK ANALYSIS.....	190
CHAPTER 10 TOP END STRUCTURE.....	192
10.1 TOP END STRUCTURE – SUBARU.....	192
10.1.1 Summary of Strawman specification.....	192
10.1.2 Design concepts.....	192
10.1.2.1 Existing top end.....	192
10.1.2.2 New top end.....	194
10.1.2.2.1 Allowing an Optimal Optical Design	194
10.1.2.2.2 Mechanical Design.....	194
10.1.2.2.3 Electronics Design.....	195
10.1.2.2.4 Software Effort.....	196
10.1.3 Cost Trades.....	196
10.1.4 Cost Forecast.....	198
10.2 TOP END STRUCTURE – GEMINI.....	198
10.2.1 Summary.....	198
10.2.2 Design Concepts.....	199
10.2.2.1 Steel Top End.....	199
10.2.2.1.1 Telescope Performance	200
10.2.2.1.2 Infrastructure Adequacy.....	200
10.2.2.2 Composite Top End.....	201
10.2.2.2.1 Telescope Performance	202
10.2.2.2.2 Infrastructure Adequacy.....	202
10.2.3 Operational Practices.....	202
10.2.4 Cost Trades.....	203
10.2.5 Cost Forecast.....	203
CHAPTER 11 POSITIONER.....	204
11.1 INTRODUCTION.....	204
11.2 SUMMARY OF STRAWMAN SPECIFICATION.....	205
11.3 POSITIONER STRAWMAN DESIGN.....	206
11.3.1 Positioner configuration.....	208
11.3.2 Position feedback – FPI and the STRIP concept.....	209
11.3.2.1 STRIP specifications.....	210
11.3.2.2 STRIP prototyping.....	211
11.3.2.3 Back-illumination requirements.....	213
11.3.3 Mechanical Design.....	213
11.3.3.1 Spherical Focal Plane implications.....	213
11.3.3.2 Adjustable length spines.....	213
11.3.3.3 Reduced actuator size.....	214
11.3.3.4 Streamlined design of spine drive actuators.....	214
11.3.3.5 Module base.....	215
11.3.3.6 Module Mounting Frame.....	216

11.3.3.7 Fiber routing within the positioner.....	217
11.3.3.8 Instrument rotator.....	217
11.3.3.9 Pointing and focus adjustment mechanism.....	217
11.3.3.10 Fiber and Cable Wrap.....	218
11.3.3.11 Electronics enclosures and support structure.....	219
11.3.3.12 Electronics cooling system.....	219
11.3.3.13 Positioner enclosure.....	219
11.3.3.14 Assembly and alignment process.....	220
<i>11.3.4 Positioner Electronics Design.....</i>	<i>220</i>
11.3.4.1 Introduction.....	220
11.3.4.2 Approach.....	220
11.3.4.3 Architecture.....	220
11.3.4.4 Implementation.....	221
11.3.4.5 Description.....	223
11.3.4.5.1 Piezo Module.....	223
11.3.4.5.2 Module Switching Electronics.....	223
11.3.4.5.3 Module Control Electronics.....	224
11.3.4.5.4 Electronics Enclosures and Electronics Mounting.....	225
11.3.4.5.5 Power Supply and Power Control.....	226
11.3.4.6 Camera Systems.....	226
11.3.4.7 Control Computer System.....	228
11.3.4.8 Interfaces.....	228
11.3.4.9 Issues.....	228
11.3.4.9.1 Back Illumination Control.....	228
11.3.4.9.2 Instrument Interlocks.....	229
11.3.4.9.3 Piezo Switching Methodology.....	229
11.3.4.9.4 Prototyping.....	229
11.3.4.9.5 Electronics Cooling.....	229
11.3.4.9.6 Power.....	229
11.3.4.9.7 Observatory Electronics Design Requirements.....	229
11.3.4.9.8 Environmental Requirements.....	230
11.3.4.9.9 Electro-Magnetic Compatibility (EMC).....	230
<i>11.3.5 Instrument Rotator Electronics Design.....</i>	<i>230</i>
11.3.5.1 Scope.....	230
11.3.5.2 Description.....	230
11.3.5.3 Interfaces.....	231
11.3.5.4 Issues.....	232
11.3.5.4.1 Instrument Interlocks.....	232
11.3.5.4.2 Servo Mechanisms.....	232
11.3.5.4.3 Prototyping.....	232
11.3.5.4.4 Electronics Cooling.....	232
11.3.5.4.5 Power.....	232
11.3.5.4.6 Observatory Electronics Design Requirements.....	232
11.3.5.4.7 Environmental Requirements.....	232
11.3.5.4.8 Electro-Magnetic Compatibility (EMC).....	233
<i>11.3.6 Software Design.....</i>	<i>233</i>
11.3.6.1 Scalability.....	233
11.3.6.2 STRIP vs XY Gantry FPI.....	234
11.3.6.3 Fiber to Object Allocation software.....	234
11.3.6.4 Telescope Optical Distortion Model.....	235
11.3.6.5 Impact of changed hardware on the software.....	235
11.3.6.6 Command Interface.....	236

11.3.6.7 Engineering GUI.....	236
11.3.6.8 Operating System issues.....	236
11.3.6.9 Miscellaneous.....	236
11.4 THE GUIDE SYSTEM.....	237
11.4.1 Overview.....	237
11.4.2 Design parameters for GFB re-imaging system.....	237
11.4.3 Strawman design of the GFB re-imaging system.....	238
11.4.3.1 GFB connector.....	238
11.4.3.2 Curved object plane.....	240
11.4.3.3 Back-illumination for guide spines.....	240
11.5 TARGET ALLOCATION ISSUES.....	240
11.5.1 Field configuration time.....	240
11.5.2 Field coverage and target selection constraints.....	242
11.6 COST FORECAST.....	242
CHAPTER 12 FIBER CABLE.....	245
12.1 SUMMARY OF STRAWMAN SPECIFICATION.....	245
12.2 TERMINOLOGY.....	245
12.3 GENERAL DESIGN CONCEPT.....	245
12.3.1 Fiber type and specification.....	245
12.3.2 Expected fiber throughput & FRD performance.....	246
12.3.3 Robot to Spectrograph mapping.....	248
12.3.4 Fiber environment.....	248
12.3.5 Fiber housing.....	249
12.3.6 Top end rotation unit.....	249
12.3.7 Cable Assembly, testing and quality assurance.....	249
12.3.8 Interlocks and safety management.....	250
12.3.9 Fiber cable health monitoring.....	251
12.3.9.1 Design overview.....	251
12.3.9.2 Set limits.....	251
12.3.9.3 Description of the optical system.....	251
12.3.9.4 Fiber health monitoring electronics.....	251
12.3.9.4.1 Interfaces.....	252
12.3.9.4.2 Issues.....	252
12.3.9.4.3 Electronics Cooling.....	253
12.3.9.4.4 Power.....	254
12.3.9.4.5 Observatory Electronics Design Requirements.....	254
12.3.9.4.6 Environmental Requirements.....	254
12.3.9.4.7 Electro-Magnetic Compatibility (EMC).....	254
12.3.10 Operation, repair and maintenance requirements.....	254
12.3.11 Fiber slit units.....	255
12.4 SUBARU ISSUES.....	255
12.4.1 Spectrograph interface and location for Subaru.....	255
12.4.2 Fiber positioner opto-mechanical fiber interface for Subaru.....	256
12.4.3 Connector interface and location.....	256
12.4.4 Subaru Operational issues	257
12.4.5 Subaru fiber run from connectors to the spectrographs.....	257
12.4.6 Fiber cable design Subaru	258
12.4.7 Fiber cable integration Subaru.....	259
12.4.8 Fiber cable risks for Subaru.....	259
12.4.9 Counter weights and cable to telescope loading.....	260
12.4.10 Guide fiber requirements - Subaru.....	260
12.4.11 Fiber cable hanging loop.....	260

12.5 GEMINI RELATED ISSUES.....	263
12.5.1 Spectrograph interface and location for Gemini.....	263
12.5.2 Corrector/robot opto-mechanical fiber interface for Gemini	263
12.5.3 Fiber parameters Gemini.....	264
12.5.4 Connector interface and location.....	264
12.5.5 Gemini Operational Issues	264
12.5.6 Gemini fiber run.....	264
12.5.7 Fiber cable design Gemini.....	265
12.5.8 Fiber cable integration.....	265
12.5.9 Fiber cable risks for Gemini.....	265
12.5.10 Guide fiber requirements Gemini.....	266
12.6 COST TRADES.....	266
12.7 COST FORECAST.....	266
CHAPTER 13 FIBER CONNECTOR.....	267
13.1 SUMMARY OF STRAWMAN SPECIFICATION.....	267
13.2 DESIGN CONCEPT.....	267
13.3 OPTICAL DESIGN.....	268
13.3.1 FMOS-type connectors.....	272
13.3.2 Optimisation.....	274
13.3.3 Microlens array connectors.....	274
13.3.4 Gradient index lenses.....	276
13.3.5 No lenses in the connectors.....	276
13.4 MECHANICAL DESIGN.....	276
13.4.1 FMOS-type connectors.....	277
13.4.2 Microlens array connectors.....	278
13.5 COST TRADES.....	279
13.5.1 Cost/performance options.....	279
13.6 REFERENCES.....	280
CHAPTER 14 LOW DISPERSION SPECTROGRAPH.....	281
14.1 SUMMARY OF STRAWMAN SPECIFICATION.....	281
14.2 SPECTROGRAPH DESIGN BASED UPON JHU SLOAN DIGITAL SKY SURVEY DESIGN.....	281
14.2.1 Optical Design.....	281
14.2.1.1 Overview.....	281
14.2.1.2 Slithead.....	283
14.2.1.3 Collimator.....	285
14.2.1.4 Beamsplitter.....	285
14.2.1.5 Gratings.....	285
14.2.1.6 Cameras.....	287
14.2.1.7 Detectors.....	288
14.2.2 Optical Performance.....	289
14.2.2.1 Image Quality.....	289
14.2.2.2 Spectral Resolution.....	289
14.2.2.3 Throughput.....	293
14.2.3 Mechanical Design.....	299
14.2.3.1 Overview.....	299
14.2.3.2 Optical Bench.....	299
14.2.3.3 Slithead.....	301
14.2.3.4 Collimator.....	302
14.2.3.5 Hartmann Doors.....	303
14.2.3.6 Shutter.....	304
14.2.3.7 Central Optics.....	304

14.2.3.8 Camera Optomechanics.....	306
14.2.3.9 Fiber Back Illumination.....	309
14.2.4 <i>Electrical System</i>	310
14.2.4.1 Collimator Tip/Tilt and Piston.....	310
14.2.4.2 Fiber Back-Illumination.....	310
14.2.4.3 Hartmann Doors.....	311
14.2.4.4 Shutter Doors.....	312
14.2.5 <i>Software Design</i>	312
14.2.5.1 Command Interpretation.....	313
14.2.5.2 Telemetry Status.....	313
14.2.5.3 Instrument Control.....	313
14.2.5.4 Health and Safety.....	313
14.3 SUBARU VS GEMINI	313
14.4 COST TRADES.....	313
14.4.1 <i>Component Costs</i>	313
14.4.1.1 Optical Components.....	314
14.4.1.2 Mechanical Components.....	314
14.4.2 <i>Cost/Performance Options</i>	315
CHAPTER 15 HIGH DISPERSION SPECTROGRAPH.....	316
15.1 SUMMARY OF STRAWMAN SPECIFICATION.....	316
15.2 SPECTROGRAPH STRAWMAN DESIGN.....	316
15.2.1 <i>Disperser Options</i>	316
15.2.1.1 Echelle Gratings.....	316
15.2.1.2 Volume-Phase Holographic Gratings.....	318
15.2.2 <i>System Overview</i>	319
15.2.3 <i>Optical Design</i>	320
15.2.3.1 Beam Diameter.....	320
15.2.3.2 Detector Influence.....	320
15.2.3.3 Demagnification (Camera Focal Ratio).....	320
15.2.3.4 Filters.....	321
15.2.3.5 Shutter.....	321
15.2.3.6 Collimator	321
15.2.3.7 Camera Options.....	321
15.2.3.8 Number of Spectrographs Required.....	322
15.2.3.9 Strawman Optical Design.....	322
15.2.4 <i>Mechanical Design</i>	324
15.2.5 <i>Electronics Design</i>	326
15.2.5.1 Scope.....	326
15.2.5.2 Approach.....	326
15.2.5.3 Interfaces.....	328
15.2.5.4 Issues.....	329
15.2.5.4.1 Back Illumination Control.....	329
15.2.5.4.2 Instrument Interlocks.....	329
15.2.5.4.3 Servo Mechanisms.....	329
15.2.5.4.4 Prototyping.....	329
15.2.5.4.5 Electronics Cooling.....	329
15.2.5.4.6 Power.....	330
15.2.5.4.7 Observatory Electronics Design Requirements.....	330
15.2.5.4.8 Environmental Requirements.....	330
15.2.5.4.9 Electro-Magnetic Compatibility (EMC).....	330
15.2.6 <i>Software Design</i>	330
15.3 SUBARU VS GEMINI.....	330

15.4 COST DRIVERS.....	330
CHAPTER 16 “DO-ALL” SPECTROGRAPH.....	331
16.1 SUMMARY OF STRAWMAN SPECIFICATION.....	331
16.2 SPECTROGRAPH STRAWMAN DESIGN	331
16.2.1 <i>General considerations</i>	332
16.2.2 <i>Beam size options</i>	333
16.2.3 <i>Detector acreage</i>	334
16.2.4 <i>Numbers and sizes of spectrographs</i>	335
16.3 OPTICAL DESIGN.....	336
16.3.1 <i>Overview</i>	336
16.3.2 <i>Optical layout and performance – high dispersion</i>	337
16.3.3 <i>Optical layout and performance - low dispersion</i>	338
16.4 OPTICAL COMPONENTS.....	341
16.4.1 <i>Lenses</i>	341
16.4.2 <i>Gratings</i>	341
16.4.2.1 <i>VPH gratings as dispersers</i>	341
16.4.2.2 <i>High dispersion grating set</i>	342
16.4.2.3 <i>Low dispersion gratings</i>	343
16.4.3 <i>Beamsplitter</i>	343
16.4.3.1 <i>Low dispersion</i>	343
16.4.3.2 <i>High dispersion</i>	344
16.4.4 <i>Coatings</i>	344
16.4.4.1 <i>Transmissive surfaces</i>	344
16.4.4.2 <i>Reflective surfaces</i>	344
16.4.5 <i>Detectors</i>	344
16.4.6 <i>Efficiency</i>	344
16.4.7 <i>Resolution</i>	345
16.4.7.1 <i>High resolution</i>	345
16.4.7.2 <i>Low resolution</i>	346
16.4.8 <i>Mechanical and thermal stability</i>	346
16.4.9 <i>Mechanisms</i>	346
16.4.10 <i>Cooling</i>	346
CHAPTER 17 NEAR-INFRARED SPECTROGRAPH OPTION.....	347
17.1 INTRODUCTION.....	347
17.2 SUMMARY OF STRAWMAN SPECIFICATION.....	347
17.3 SPECTROGRAPH STRAWMAN DESIGN.....	348
17.3.1 <i>Thermal Design</i>	348
17.3.2 <i>Optical Design</i>	350
17.3.2.1 <i>General Description</i>	350
17.3.2.2 <i>Optical Performance</i>	351
17.3.3 <i>Calibration Issues</i>	352
17.3.3.1 <i>Dithering</i>	352
17.3.3.2 <i>Fiber-Fiber Throughput Calibration</i>	353
17.3.3.3 <i>Wavelength Calibration</i>	353
17.3.3.4 <i>Sky Subtraction</i>	353
17.3.4 <i>Spectrograph Mechanical Design</i>	353
17.3.4.1 <i>Base Frame</i>	353
17.3.4.2 <i>Support legs</i>	354
17.3.4.3 <i>Optical bench</i>	355
17.3.4.4 <i>Collimator mounting</i>	355
17.3.4.5 <i>Slit and mask mirror unit</i>	357

17.3.4.6 Fold mirror, corrector and grating	358
17.3.4.7 Corrector (S2) mounting.....	359
17.3.4.8 VPH mounting.....	359
17.3.4.9 Dark slide arrangement.....	360
17.3.4.10 Camera articulation.....	361
17.3.4.11 Thermal Enclosure.....	361
17.3.4.12 Structural Analysis.....	363
17.3.5 Camera Mechanical Design.....	364
17.3.6 Control System Design.....	366
17.3.6.1 Mechanism Design & Control.....	366
17.3.6.2 Camera Temperature Control.....	367
17.3.6.3 Detector Control.....	367
17.3.6.4 Spectrograph Environmental Control.....	368
17.4 SOFTWARE.....	369
17.5 WF MOS-IR DESIGN MODIFICATIONS & TRADE-OFFS.....	369
17.5.1 Parameters of the modified FMOS design.....	370
17.5.2 Next-Generation IR Detectors.....	371
17.5.3 Bragg-grating Fibers.....	371
17.6 COST FORECAST.....	372
17.7 RISKS	372
CHAPTER 18 DETECTOR SYSTEMS.....	373
18.1 INTRODUCTION.....	373
18.2 DETECTORS.....	373
18.3 CRYOSTATS.....	375
18.4 DETECTOR CONTROLLERS.....	375
18.4.1 Optical detectors.....	376
18.4.2 IR detectors.....	377
18.5 DETECTOR TEMPERATURE CONTROL AND VACUUM MONITORING.....	377
18.6 SOFTWARE AND DETECTOR CONTROLLER CONFIGURATION.....	378
18.7 DATA FLOW.....	378
18.8 COST ESTIMATES.....	379
18.8.1 Optical detector systems.....	380
18.8.2 IR detector system.....	380
18.9 PROMISING NEW TECHNOLOGIES IN DETECTORS.....	381
18.10 CONCLUSIONS.....	381
18.11 REFERENCES.....	381
CHAPTER 19 ACQUISITION AND GUIDING.....	383
19.1 SUMMARY OF STRAWMAN SPECIFICATION.....	383
19.2 ACQUISITION DESIGN CONCEPT.....	383
19.2.1 Strawman Design.....	383
19.3 GUIDING SYSTEM CONCEPT OVERVIEW.....	384
19.3.1 Software.....	384
19.3.1.1 Guider Image Offset Calculation Process.....	386
19.3.1.2 Accounting for Refraction/Dispersion Effects.....	386
19.3.1.3 Validation of the individual centroid result.....	386
19.3.1.4 Calculating Rotation.....	387
19.3.1.5 Use of a FIFO to validate results.....	387
CHAPTER 20 WF MOS WAVEFRONT SENSORS SUBSYSTEM DESIGN CONCEPT.	388
20.1 INTRODUCTION.....	388

20.2 WIDE-FIELD CURVATURE SENSORS (LOCS).....	388
20.2.1 Terminology.....	388
20.2.1.1 LOCS.....	388
20.2.1.2 SDSU.....	388
20.2.2 LOCS System Overview.....	389
20.2.3 LOCS/AG Unit Design.....	390
20.2.3.1 LOCS/AG Requirements.....	390
20.2.3.2 CCD Selection.....	391
20.2.3.3 Validation of AG FOV.....	391
20.2.3.4 Validation of LOCS FOV.....	391
20.2.3.5 Operation after sunset.....	392
20.2.3.6 Sensor location.....	392
20.2.3.7 LOCS/AG Optical Design.....	392
20.2.3.8 LOCS/AG Filter Selection.....	393
20.2.3.9 Alignment Sensitivity.....	395
20.2.3.10 Mechanical Design.....	395
20.2.3.11 LOCS Thermal Design.....	397
20.2.3.12 LOCS/AG Unit Mass.....	398
20.2.3.13 LOCS Predicted Accuracy.....	398
20.2.3.14 LOCS Processor Requirements	398
20.2.3.15 LOCS Software.....	398
20.3 PWFS/AG.....	399
20.4 DESIGN TRADES.....	399
20.5 POTENTIAL DESCOPE.....	400
20.6 SENSITIVITY SPREADSHEETS.....	401
20.6.1 AG.....	401
20.6.2 LOCS.....	403
CHAPTER 21 CALIBRATION.....	406
21.1 CALIBRATION REQUIREMENTS.....	406
21.1.1 Determination of bias level.....	406
21.1.2 Pixel-to-pixel variation	406
21.1.3 Spectrum mapping	406
21.1.4 Scattered light subtraction.....	407
21.1.5 Fibre-to-fibre spectral variation	407
21.1.6 Fibre-to-fibre throughput variation	407
21.1.7 Spectral calibration requirements.....	408
21.1.8 Spectrophotometric calibration requirements.....	408
21.2 CALIBRATION SYSTEM DESIGN AND PERFORMANCE.....	408
21.2.1 Arc lamps and mounting.....	408
21.2.2 Arc lamp selection.....	410
21.2.3 Quartz-halogen lamps and mounting.....	412
21.2.4 Bias determination.....	413
21.2.5 Pixel-to-pixel flat-fielding.....	413
21.3 DATA REDUCTION CALIBRATION STEPS.....	415
21.4 ELECTRONICS.....	416
21.4.1 Scope.....	416
21.4.2 Description.....	416
21.4.3 Interfaces.....	418
21.4.4 Issues.....	418
21.4.4.1 Power Supply Number, Size and Weight.....	418
21.4.4.2 Prototyping.....	418
21.4.4.3 Electronics Cooling.....	418

21.4.4.4 Power.....	418
21.4.4.5 Observatory Electronics Design Requirements.....	418
21.4.4.6 Environmental Requirements.....	419
21.4.4.7 Electro-Magnetic Compatibility (EMC).....	419
CHAPTER 22 TELESCOPE INFRASTRUCTURE UPGRADE.....	420
22.1 TELESCOPE INFRASTRUCTURE UPGRADE – SUBARU.....	420
22.1.1 <i>Summary of Strawman specification</i>	420
22.1.2 <i>Design concept</i>	420
22.1.3 <i>Cost Forecast</i>	422
22.2 TELESCOPE INFRASTRUCTURE UPGRADE – GEMINI.....	422
22.2.1 <i>Summary of Strawman specification</i>	423
22.2.2 <i>Design concept</i>	423
22.2.3 <i>Cost Trades</i>	425
22.2.4 <i>Cost Forecast</i>	425
CHAPTER 23 DATA ANALYSIS AND HANDLING	426
23.1 OVERVIEW.....	426
23.2 SOFTWARE REQUIREMENTS.....	426
23.3 SOFTWARE PACKAGES	426
23.4 SOFTWARE SYSTEMS.....	427
23.4.1 <i>Data Retrieval and Analysis Environment</i>	427
23.4.2 <i>Data Analysis Components</i>	429
23.4.3 <i>Post-Processing Tasks</i>	431
23.5 PACKAGE B SOFTWARE.....	433
23.6 TESTING AND COMMISSIONING MILESTONES.....	434
23.7 COST MITIGATION.....	434
23.8 POTENTIAL RISKS.....	435
CHAPTER 24 OPERATIONS.....	437
24.1 SITE SELECTION NORTH VERSUS SOUTH.....	437
24.1.1 <i>Scientific considerations</i>	437
24.1.1.1 Dark Energy.....	437
24.1.1.2 Galactic Archeology.....	437
24.1.1.3 Input catalogues.....	437
24.1.2 <i>Resulting instrument complement</i>	439
24.2 SUPPORT REQUIREMENTS FOR INSTRUMENT OPERATION.....	440
24.2.1 <i>Instrument change</i>	440
24.2.1.1 Top end change.....	440
24.2.1.2 Spectrograph configurations.....	441
24.2.1.3 Fiber cable.....	442
24.2.2 <i>Maintenance</i>	442
24.2.3 <i>Software</i>	443
24.2.3.1 Data reduction packages.....	443
24.2.3.2 Reduction pipeline.....	443
24.3 OBSERVING SCENARIOS/STRATEGIES.....	443
24.4 SCHEDULING OF OBSERVATIONS.....	443
24.5 TIME ALLOCATION SELECTION.....	443
24.6 INTERLEAVING WFMOS SCIENCE CAMPAIGNS	445
24.7 DISTRIBUTION OF DATA PRODUCTS FOR MAXIMUM SCIENCE IMPACT.....	445

SECTION V: WFMOS PROJECT ORGANISATION AND MANAGEMENT..... 446

CHAPTER 25 ORGANISATION AND MANAGEMENT.....447

25.1 INTRODUCTION..... 447

25.2 ORGANISATION..... 447

 25.2.1 *Proposed Organisation Structure*..... 448

25.3 MANAGEMENT..... 449

 25.3.1 *Key Management Issues*..... 449

25.4 MANAGEMENT ARRANGEMENTS..... 450

 25.4.1 *Contracting Arrangements*..... 450

 25.4.2 *Management Arrangements and Focus*..... 451

 25.4.3 *Management arrangements for control of work*..... 452

 25.4.3.1 *Quality Management*..... 452

 25.4.3.2 *Schedule Management*..... 452

 25.4.3.3 *Cost Management*..... 452

 25.4.4 *Grouping of work scope components*..... 453

 25.4.5 *Management aspects of logistics issues*..... 454

25.5 PROJECT DOCUMENTATION..... 455

 25.5.1 *Configuration Management*..... 455

 25.5.2 *Configuration Item Data*..... 456

 25.5.3 *Definition of Hardware / Software*..... 458

 25.5.3.1 *List of Manufacturing Drawings*..... 458

 25.5.3.2 *Analysis Documentation*..... 458

 25.5.3.3 *Design Documentation*..... 458

 25.5.3.4 *ICDs and Data List*..... 459

 25.5.3.5 *I/F Control Drawings*..... 459

 25.5.3.6 *Drawings*..... 459

CHAPTER 26 WORK BREAKDOWN STRUCTURE AND DEVELOPMENT SCHEDULE.....460

26.1 TOP-LEVEL WORK BREAKDOWN STRUCTURE (WBS)..... 460

 26.1.1 *Overview*..... 460

 26.1.2 *Top Level WBS Diagram*..... 461

26.2 TOP-LEVEL DEVELOPMENT SCHEDULE..... 462

 26.2.1 *Overview*..... 462

 26.2.2 *Top-level development schedule*..... 462

 26.2.3 *Summary of Key Delivery Milestones*..... 462

 26.2.4 *Planning assumptions*..... 463

 26.2.5 *Commissioning schedules*..... 464

26.3 TOP LEVEL WBS – WFMOS PROJECT..... 465

26.4 TOP LEVEL WBS – CONCEPT PHASE (1)..... 466

26.5 TOP LEVEL WBS – CONCEPT PHASE (2)..... 466

26.6 TOP LEVEL WBS – CONCEPT PHASE (3)..... 467

26.7 TOP LEVEL WBS – DESIGN/MANUFACTURE PHASE (1)..... 468

26.8 TOP LEVEL WBS - DESIGN/MANUFACTURE PHASE (2)..... 468

26.9 TOP LEVEL WBS - DESIGN/MANUFACTURE PHASE (3)..... 470

26.10 HIGH LEVEL SCHEDULE (1)..... 471

26.11 HIGH LEVEL SCHEDULE – SHOWING DETAIL OF MAJOR DESIGN & BUILD PHASES..... 472

CHAPTER 27 COSTS STRUCTURE & COST ESTIMATES.....473

27.1 INTRODUCTION..... 473

27.2 COST STRUCTURE.....	473
27.2.1 <i>Basis of Derived costs</i>	473
27.2.2 <i>Quality of estimates</i>	473
27.2.3 <i>Labour rates</i>	474
27.2.4 <i>Exchange rates</i>	475
27.2.5 <i>Basis for calculating the estimates</i>	475
27.2.5.1 <i>Baseline estimates</i>	475
27.2.5.2 <i>Estimates for options</i>	475
27.2.6 <i>Cost component details</i>	476
27.3 COST ESTIMATES.....	476
27.3.1 <i>Estimated Baseline Cost</i>	476
27.3.2 <i>Summary of baseline cost estimates</i>	477
27.3.2.1 <i>Corrector</i>	477
27.3.2.2 <i>Top End modifications to existing central hub on Subaru</i>	477
27.3.2.3 <i>WF MOS positioner</i>	478
27.3.2.4 <i>WF MOS fiber cable</i>	478
27.3.2.5 <i>WF MOS fiber connector</i>	479
27.3.2.6 <i>WF MOS Low Resolution Spectrographs (10 off)</i>	479
27.3.2.7 <i>WF MOS High Resolution Spectrograph (double unit)</i>	480
27.3.2.8 <i>WF MOS Acquisition and Guiding System Software (other costs in Positioner)</i>	480
27.3.2.9 <i>WF MOS Wavefront Sensing System (mirror control)</i>	481
27.3.2.10 <i>WF MOS Calibration Systems</i>	481
27.3.2.11 <i>WF MOS System Software</i>	481
27.3.2.12 <i>WF MOS Data Reduction Pipeline Software – Package A</i>	482
27.3.2.13 <i>Subaru Infrastructure required for WF MOS instrument</i>	482
27.3.2.14 <i>Management and logistics for WF MOS baseline instrument</i>	483
27.3.2.15 <i>Process costs</i>	484
27.3.3 <i>Options</i>	484
27.3.3.1 <i>IR Spectrograph</i>	485
27.3.3.2 <i>Top End – Gemini CFRP</i>	485
27.3.3.3 <i>Top End – Steel Gemini</i>	486
27.3.3.4 <i>Do-All Spectrograph</i>	486
27.3.3.5 <i>Gemini Infrastructure required for WF MOS instrument</i>	487
27.3.3.6 <i>Data Reduction Science Analysis software - Package B</i>	487
27.3.3.7 <i>Gemini Implementation</i>	488
27.3.3.8 <i>2 degree field</i>	489
27.4 COSTING MODEL.....	489
27.5 COST MANAGEMENT.....	491
27.5.1 <i>Overview</i>	491
27.5.2 <i>Application of Cost Management</i>	492
27.5.3 <i>Cost Control</i>	492
CHAPTER 28 RISK MANAGEMENT & COST MITIGATION.....	494
28.1 INTRODUCTION.....	494
28.2 RISK MANAGEMENT.....	494
28.2.1 <i>Approach to Risk Management</i>	494
28.2.2 <i>Application of Risk Management</i>	496
28.3 RISK MITIGATION.....	496
28.3.1 <i>Identification of Key Risks</i>	496
28.3.1.1 <i>General</i>	496
28.3.1.2 <i>Management and Logistics</i>	497
28.3.1.3 <i>Science</i>	497

28.3.1.4 Electronics.....	497
28.3.1.5 Detectors.....	498
28.3.1.6 Software	498
28.3.1.7 Product Specific Risk Comments.....	498
28.3.1.7.1 Corrector.....	498
28.3.1.7.2 Top End.....	499
28.3.1.7.3 Fiber Positioner.....	499
28.3.1.7.4 Fiber Cable.....	499
28.3.1.7.5 Fiber Connector.....	499
28.3.1.7.6 LoRes Spectrograph.....	499
28.3.1.7.7 HiRes Spectrograph.....	499
28.3.1.7.8 Acquisition & Guiding.....	500
28.3.1.7.9 Wave Front Sensing.....	500
28.3.1.7.10 Calibration Systems.....	500
28.3.1.7.11 Wobble Plate.....	500
28.3.1.7.12 Subaru Infrastructure.....	500
28.3.2 Risk Management Plan.....	500
28.3.3 Insurance.....	501
28.4 COST MITIGATION.....	501
28.4.1 Cost risks.....	501
28.4.2 Cost mitigation approach.....	502
28.4.3 Logistics Risks.....	502
28.4.4 Technical Risks.....	503
28.5 EXAMPLE RISK REGISTER FORMAT.....	503
28.6 RISK PRIORITY RATINGS.....	504
28.7 LIKELIHOOD RATINGS.....	504
28.8 EXAMPLE OF RISK REGISTER – CFRC TOP RING FOR GEMINI.....	505
CHAPTER 29 LOGISTICS	506
29.1 INTRODUCTION.....	506
29.2 LOGISTICS.....	506
29.2.1 Importance of logistics for WFMOS.....	506
29.2.2 Logistics planning.....	506
29.2.3 Protection and Packing requirements.....	507
29.2.3.1 Standards for packing.....	507
29.2.3.2 Vacuum packs and moisture control agents where required.....	507
29.2.3.3 Number of crates.....	507
29.2.3.4 Likely inter-organisation movements for QA and integration checks.....	507
29.3 COMPONENT AND EQUIPMENT HANDLING.....	507
29.3.1 Approach.....	507
29.3.2 Special Tools.....	508
29.4 TRANSPORT.....	508
29.4.1 Approach.....	508
29.4.2 Freight arrangements.....	508
29.4.3 Air and Ocean freight movements to Hawaii.....	509
29.4.3.1 Air movements to Hawaii.....	509
29.4.3.2 Ocean movements to Hawaii.....	509
29.4.4 Ground Transport - Hawaii	509
29.4.5 Timing of Transport to Hawaii.....	509
29.5 COST ESTIMATE.....	510
29.5.1 Transport and packing costs.....	510
29.5.2 Other associated costs.....	510
29.5.3 Typical ocean transport costs.....	510

29.5.4 Typical air transport costs.....	511
29.6 GROUPING AND MOVEMENT OF COMPONENTS	511
CHAPTER 30 APPLICABLE DOCUMENTATION.....	513
30.1 DOCUMENTATION.....	513
30.1.1 AURA Contract No. 0084699-GEM00385 – Design Study for the Wide Field Fiber-Fed Optical MOS (WFMOS).....	513
30.1.2 Statement of Work.....	513
30.1.3 The KAOS Purple Book.....	514
30.1.4 Gemini WFMOS – Proposal Document in Response to RfP N231804.....	514
30.1.5 Guidelines for Designing Gemini Aspen Instrument Software – AspenSoft- 03072004-6.....	514
30.1.6 Interface Control Documents.....	514
30.1.7 Drawings.....	517
30.2 OPERATIONAL CONCEPT DEFINITION DOCUMENT.....	518
30.3 FUNCTIONAL AND PERFORMANCE REQUIREMENTS DOCUMENT.....	518
<u>SECTION V: ACKNOWLEDGEMENT OF CONTRIBUTORS.....</u>	519
CHAPTER 31 PEOPLE INVOLVED.....	520

SECTION I: INTRODUCTION TO THE WFMOS FEASIBILITY STUDY

Chapter 1 Glossary of Terms

Acronym/term	Meaning
2dF	The AAT's multi-object spectrographic facility – a multi-object, fibre-fed spectrograph covering a 2 degree field.
2dFGRS	2dF Galaxy Redshift Survey. A major cosmological survey undertaken by the 2dF multi-object spectrographic facility at the AAT.
A&G	Acquisition and Guiding.
AAO	Anglo-Australian Observatory.
AAT	Anglo-Australian Telescope. The 3.9-metre telescope operated by the AAO at Siding Springs Observatory in New South Wales.
ADC	Atmospheric Dispersion Compensator (or Corrector).
AG	Auto Guider.
AIT	Acceptance, Integration and Test.
aO	Active Optics – deformation/figure control of major optical elements to maintain their figure in response to slow deformations due, e.g., to varying gravity vector during tracking.
AO	Adaptive Optics – high frequency wavefront correction in an optical system to correct for distortions introduced by atmospheric refractive turbulence.
API	Application Programmer Interface. A set of well-defined interfaces supported by a software development environment.
Aspen Process	Was an extensive effort to canvas the Gemini user community to determine which scientific avenues of research the Observatory's instrument program should support over the next 5-10 years. It is a key step in the strategic planning for the Observatory and, in collaboration with Gemini's partner National Offices, involved hundreds of astronomers worldwide during late 2002 and much of 2003.
ATEUI	Engineering interface for operating a software system with fine, engineering level control.
AURA	Association of Universities for Research in Astronomy.
CADC	Canadian Astronomical Data Centre.
CC	Components Controller. Part of ICS.
CCD	Charge Coupled Device (optical image sensor).
Components Controller	Software and hardware used to control components of an instrument.
CORBA	A standardised communications protocol facilitating communications between separate software components.
CS	Curvature Sensor/sensing (a form of wavefront sensor).
CTE	Charge Transfer Efficiency. A performance measure of a CCD.
DC	Detector Control – software, which controls a detector. Part of ICS.
DHE	Detector Head Electronics. MONSOON CCD-controller terminology for a component of the CCD support electronics.
DHS	Data Handling System – the Gemini Software Scheme for moving and archiving instrument data.
EAC	Estimate at completion.
EEV42	A particular model of CCD with a 4k by 2k format, manufactured by EEV (Marconi).
EPICS	Experimental Physics and Industrial Control System . A software system used by Gemini to help implement its instrument control system.
ESO	European Southern Observatory.
ETC	Estimate to complete.
FITS	The standard data file format used in astronomy.
FLAMES	Multi-object fiber-fed spectrograph facility implemented on the VLT.
FOV	Field of View.

Acronym/term	Meaning
FPA	Focal Plane Array.
FPI	Focal Plane Imager – a system capable of collecting an image (or set of images) of the telescope’s focal surface within the Echidna fiber positioner. Used to provide spine tip position feedback to the fiber positioner.
FPRD	Functional Performance and Requirements Document. Gives the requirements of the instrument.
FRD	Focal Ratio Degradation. The degradation by fiber optics that result in a loss of throughput resolution product or etendue. It causes an increase in the fiber input cone angle at the fiber output, and is made significantly worse by localised stressing (micro-bending) of the fiber.
FSR	Feasibility Study Report. A document detailing the technical issues addressed during the study etc. See SoW Section 4.3 Not to be confused with Free Spectral Range.
FT	Frame Transfer (CCD).
GDSN	Gemini Data Storage Network.
Gemini	Gemini is an international partnership managed by the Association of Universities for Research in Astronomy under a cooperative agreement with the National Science Foundation . Partner countries include the United States, United Kingdom, Canada, Chile, Australia, Argentina, and Brazil.
GFB	Guide Fiber Bundle. A close-packed bundle of small-core fibers carried in a spine in the Echidna fiber positioner. Star images are be maintained centred on the bundle for telescope guiding.
GIS	The Gemini Interlock System. An Alan-Bradley PLC-based safety system with components mounted on the telescope structure that monitors aspects of the system from a safety standpoint. The intent of the GIS is to provide a way of locking out systems when the reason the lockout originates from outside that system.
GSA	Gemini Science Archive.
GUI	Graphical User Interface. An operator interface to a computer system, based on graphics such as pictures and menus instead of text. Uses a pointing device such as a mouse as well as a keyboard for input.
HSCam	Hyper-SuprimeCam, a wide field (2 degree) optical imager proposed for Subaru.
ICD	Interface Control Document. Gemini has a set of interface control documents we are required to obey. These are listed in the statement of work.
ICS	Instrument Control System – the instrument specific software.
IFPRD	Initial Functional Performance and Requirements Document. See FPRD and SoW Section 4.2.
Instrument Sequencer	The software, which sequences operations of various parts of an instrument and its associated detector system.
IOCDD	Initial Operational Concept Definition document. See OCDD and SoW section 4.1.
IP	Intellectual Property.
IR	Infrared.
IS	Instrument Sequencer. Part of ICS.
IS/ADC	Image Stabiliser and Atmospheric Dispersion Corrector, a combination wobble plate and ADC.
IRAF	A library of astronomical data reduction software.
Java	Environment-portable programming language.
JavaSpace	A Jini concept facilitating simultaneous processing of a single data archive by multiple independent computers.
JHU	Johns Hopkins University.
Jini	A programming technology, underlying the Gemini OLDP. This is a Java based connection technology which makes it possible for various devices to form a very dynamic local area network and offer services to each other

Acronym/term	Meaning
KAOS	Kilo-Aperture Optical Spectrograph. The name of the instrument concept developed for consideration in the ASPEN discussions.
Leach controller	See SDSU Controller.
LN2	Liquid Nitrogen.
LOCS	Low Order Curvature Sensor.
LOWFS	Low Order Wavefront Sensor.
MONSOON	NOAO's new generation CCD controller.
N&S	Nod and Shuffle. A beam switch mode of observation in which the CCD charge is shuffled in coordination with a nodding of the telescope.
NA	Numerical Aperture.
NIMO	Non-Inverted Mode Operation (CCD).
NOAO	National Optical Astronomy Observatory.
NSF	National Science Foundation.
OBCP	Observation Block Control Program. This is how instrument software is integrated into the Subaru telescope control software. It is the rough equivalent of the Gemini ICS
OCDD	Operational Concept Definition document. Describes how the instrument will be used.
OCS	Observatory Control System – the software that runs the Gemini telescope. The instrument software is a component of this system.
OH	Hydroxyl-radical. This molecular component present in the atmosphere contributes significant contaminating light, particularly towards the red end of the spectrum and in the near-infrared. It takes the form of a large number of narrow emission lines.
OIWFS	On Instrument Wave Front Sensor. A high rate guider, which can correct for seeing effects.
OLDP	On-Line Data Processing – Gemini's automated data reduction software.
OT	Observing Tool – used by observers to prepare (P2PP stage) and execute observations.
P2PP	Phase 2 Proposal Preparation. When an observer, having been allocated time on a telescope, prepares for the observation. Also see OT.
Package A & Package B	Terminology referring to the bundling of WFMOS data reduction pipeline software into separate packages. Package A provides core functionality, while Package B is a set of extensions in support of scientific analysis.
PAN	Pixel Acquisition Node. MONSOON CCD-controller terminology for a component of the CCD support electronics.
PCB	Printed Circuit Board.
PCI	Peripheral Component Interface (computer interface Data Bus standard).
PFU	Prime Focus Unit. A module that is fitted to the upper side of the Subaru top end central hub. It includes the fiber positioner, its rotator, cable/fiber wrap, related support structures and electronics, and the pointing mechanism required to maintain alignment of these components.
PIT	Gemini Phase 1 Proposal Tool. Used by observers to apply for time on the Gemini Telescopes. http://www.gemini.edu/sciops/P1help/p1Index.html .
PSD	Power Spectral Density (of measured image motion)
PMC	PCI Mezzanine Card.
PWFS	Peripheral Wavefront Sensor.
PWFS2	Gemini Peripheral Wavefront Sensor No. 2.
QE	Quantum efficiency. A measure of the sensitivity of a detector.
RC	Resistor Capacitor (electronic load).
RfP	Request for Proposal.
RMS	Root Mean Square.

Acronym/term	Meaning
ROM	Rough Order of Magnitude as in ROM Cost, which is a costing based upon preliminary information, guesses, and extrapolation from prior experience and is typically uncertain by up to +/-50%.
RON	Readout Noise. A performance measure of a CCD system.
SDSS	Sloan Digital Sky Survey. See http://www.sdss.org/sdss.html
SDSU Controller	San Diego State University Controller. A CCD controller . These are the main and recommended controller used by Gemini. Also known as the "leach" controller after the prime designer.
SFR	Star Formation Region.
SH	Shack-Hartmann – a commonly used type of wavefront sensor.
Sloan	Normally refers to the Sloan Survey Telescope used to conduct the SDSS.
SoW	Statement of Work.
Starlink	A library of astronomical data reduction software provided by the U.K astronomy community and the organization which supports that library..
STRIP	Spine Tip Reimaging in Primary. A form of FPI where a camera images the focal plane by its reflection in the telescope primary mirror. Used to provide position feedback for the Echidna unit to control its spine positions.
T&Cs	Terms and Conditions (of contract).
TCS	Telescope Control System – the software system used to control the telescope itself.
TE Cooling	Thermo-electric cooling.
Tweaking	A process where the positions of objects on the focal surface are fine-tuned for a given observation time.
VLT	Very Large Telescope. ESO's major optical telescope facility.
VME	Versa Module Europa – 19" rack data bus standard.
VO	Virtual Observatory. A programme aiming to maximise international sharing of astronomical data through the use of standardised formats.
VPH Grating	Volume Phase Holographic Grating. A diffraction grating based upon index of refraction modulations to disperse the light.
WBS	Work Breakdown Structure – a deliverable oriented grouping of project elements that organises and defines the total scope of the project.
WFC	Wide-Field Corrector.
WF MOS	Wide-Field Fiber-Fed Optical Multi-Object Spectrograph.
WFS	Wavefront sensor.
Work Package	A deliverable at the lowest level of the WBS.
ZEMAX	Optical design software package.

Chapter 2 Introduction and Purpose

2.1 *Gemini WFMOS Feasibility Study*

This document, the WFMOS Feasibility Study Report, gives the conclusions derived from a feasibility study commissioned by the Gemini Observatory (through contract GEM00385) to explore the technical feasibility/risk and cost for the development of a Wide-Field Fiber-Fed Optical Multi-Object Spectrograph (WFMOS). The WFMOS facility is an instrument concept that arose from the Gemini ASPEN Future Instrumentation Workshop held in Aspen, Colorado in June 2003. The facility will be one that implements a very high multiplex factor for seeing limited, spectroscopic surveys at low and high spectral dispersion in the optical (and possibly the near-infrared).

The Anglo-Australian Observatory (AAO) led the study team that also included the National Optical Astronomy Observatory (NOAO), University of Oxford (Oxford), University of Portsmouth (Portsmouth), University of Durham (Durham), Johns Hopkins University (JHU), and the Canadian Astronomical Data Centre (CADAC). With the experience gained through development of the original KAOS concept, in which the AAO, NOAO, JHU, and other team members were involved, the team was well suited to perform this Feasibility Study.

The overarching issues concerning WFMOS are the cost of the facility, the scientific reasons for deployment of WFMOS on Gemini, the technical feasibility of WFMOS, the expected performance level of the instrument, the operational impact and considerations for the facility, and the level of Gemini partner support for such a facility. The effort and results of the Feasibility Study described in this document focus on these issues.

The study entailed effort exploring the science, technical, data handling/archival, and operational aspects of the WFMOS facility. The KAOS concept served as the initial baseline upon which the technical study was based. The science study determined the aspects of the surveys required to explore the dark energy, galaxy formation, and dark matter topics. An assessment is made of the ability of the baseline concept to deliver the science out of such surveys. The science effort also indicates where the baseline concept must be changed in order to optimize the scientific return. The data handling effort explored what is required to turn the resultant spectral pixels into the scientific product and how such information will be archived and linked into the Virtual Observatory. The overall impact that the WFMOS facility will have on Gemini was explored to understand the change in operation required to accommodate such a facility and to allow timely realization of the end science.

After submission of the proposal to do the study, the study was expanded by Gemini to include a study of implementing WFMOS onto the Subaru telescope instead of the Gemini telescope. This added effort required an exploration of the top end interface issues, infrastructure issues, field of view, corrector design, etc. required for a Subaru implementation.

The AAO served as prime contractor for the overall study and was the leader on the technical studies with NOAO, Oxford, JHU, and Durham participating on various technical issues. NOAO led the science study with significant

participation from JHU, Portsmouth, Oxford, and Durham. Data Handling, or the “pixels to science” component was a joint study by Portsmouth and the CADC. Operational impact on Gemini was led by NOAO with Oxford participating.

WF MOS will implement a very wide field of view (1.5 to 2.0 degree diameter) at the prime focus of either one of the two Gemini telescopes or the Subaru telescope on Mauna Kea (pending an agreed upon arrangement for sharing Gemini and Subaru facilities between the Gemini partners and Subaru user community and to be decided prior to the onset of a concept design study). A high density of apertures (~4500 to 6000) will be implemented by using fiber optics to relay target light into an array of spectrographs. The operable wavelength regime will range from at least 0.39-1.0 micron with a possible extension to 1.8 microns in the near-infrared. Two spectral resolution regimes are required at a minimum, $R \sim 3000$ and $R = 40000$, in order to carry out the two major surveys that arose out of the ASPEN process.

The feasibility study was asked to explore technical design trades, feasibility, and costing for implementation on either Gemini or Subaru. As such, many of the technical requirements may be difficult to firmly define until the telescope platform is chosen, but best estimates were made in such areas of uncertainty to carry out the current study.

2.1.1 Aspen Process

The Gemini ASPEN process (<http://www.gemini.edu/science/Aspen/general-announce.html>) determined that a wide-field, fiber-fed, optical multi-object spectrograph (WF MOS) was needed in order to pursue scientific questions relating to the nature of the dark energy that is accelerating the expansion of the Universe, the formation process of galaxies, and the nature of dark matter on galactic scales.

2.1.2 Strawman Concept

The Gemini RfP for WF MOS (#N231804, Exhibit A to Schedule B, Statement of Work) identified the top level design guidelines to include the following (based upon the KAOS concept http://www.noao.edu/kaos/KAOS_Final.pdf):

- Wavelength Range: 0.39 – 1.0 μm .
- Field of View: ~ 1.5 degree diameter.
- Spatial Sampling: ~ 1 arc-second fiber aperture.
- Spectral Resolution: $R \sim 1000 - 30000$.
- One-shot wavelength coverage: $\sim 0.4 \mu\text{m}$ for the lowest resolution mode and undefined for the highest resolution mode.
- Simultaneous stellar targets: 4000 – 5000
- A cost goal of US\$32M for the total WF MOS facility.

- Full compatibility with the latest Gemini Interface Control Documents with waivers as required.
- Implementation, where practical, of existing Gemini instrument designs.

The addition of Subaru and additional changes in the requirements led to a change in the baseline concept from that in the Purple Book to the following:

Subaru telescope prime focus	
1.5 degree diameter field of view	
0.39-1.0 micron wavelength window	
1 arc-second diameter apertures	
4500 total fibers	3000 fibers to a set of 10 low-dispersion spectrographs 1500 fibers to a set of 2 high-dispersion spectrographs
Dual beam low-dispersion spectrographs for simultaneous and complete wavelength coverage from 0.39-1.0 micron	R=1800 in blue channel of low-dispersion spectrographs R=3500 in red channel of low-dispersion spectrographs Nod-Shuffle observing capability
Single channel high-dispersion spectrographs	R=40000 No nod-shuffle observing required

Possible optional implementations are the following (Note that these options will be resolved prior to or during the conceptual design phase.):

Gemini option	Gemini prime focus rather than Subaru All other aspects the same as baseline
Subaru 2 degree field	2 degree field rather than 1.5 degree 6000 total fibers 4000 low-dispersion 2000 high-dispersion All other aspects the same as baseline
Subaru NIR extension	0.39-1.8 micron total wavelength coverage for low-dispersion 1500 NIR fibers to a set of 5 to 8 NIR spectrographs 1500 low-dispersion optical fibers to a set of 5 low-dispersion spectrographs All other aspects the same as baseline

2.1.3 Purpose of the Feasibility Study

The following questions lead the primary issues regarding WFMOS feasibility at the Gemini observatory:

1. What is the cost of WFMOS?
 - Cost in dollars?
 - Cost in terms of number of telescope nights to do the science?
 - Cost in duration of the number of years to develop the instrument and get the science achieved.
2. What is the scientific strength of WFMOS science on Gemini?
 - What are the windows of opportunity for the proposed science?
 - What is the competition likely to achieve prior to the commissioning of WFMOS?
 - Is WFMOS competitively positioned?
 - Which site (Gemini North or South) is optimal for the scientific goals?
 - What are the value-added science objectives unique to WFMOS?
 - What is the WFMOS context with respect to synergistic facilities such as SNAP, WMAP, and GAIA?
3. Is WFMOS technically feasible?
 - What are the high risk technical areas?
 - What are possible avenues to mitigate risk and/or cost?
4. What performance level can be achieved with WFMOS?
 - Sky subtraction performance?
 - Radial velocity performance?
 - Spectrophotometric performance?
 - Blue performance?
 - Multiplex and target efficiency?
5. Is WFMOS operationally feasible in the Gemini/Subaru environment?
 - Is the Gemini/Subaru infrastructure able to support WFMOS?
 - Should WFMOS be scheduled in large (year/multi-year) blocks or small (monthly) blocks?
 - What impact does the operational mode have on the science objectives?
6. Is there broad support amongst the Gemini international partners and the Subaru community?

It was the objective of the Feasibility Study to evaluate and derive answers to these questions.

2.2 *Applicable Documentation*

The following documentation was utilized as input for the WFMOS Feasibility Study Report.

Document ID	Source	Title
Purple Book	NOAO	K.A.O.S. Kilo-Aperture Optical Spectrograph
Aspen report	GEMINI	Scientific Horizons at the Gemini Observatory: Exploring a Universe of Matter, Energy, and Life
GEM00385	GEMINI	WFMOS Feasibility Study Statement of Work
ICD 1.1.1/1.9	GEMINI	Telescope Structure to Science Instruments ICD
ICD 1.1.13/1.9	GEMINI	Interlock System to Science Instruments ICD
ICD 1.5.3/1.9	GEMINI	Instrument Support Structure to Science Instruments ICD
ICD 1.6/1.9	GEMINI	A&G System to Science Instruments
ICD 1.6/1.10	GEMINI	A&G to On-Instrument Wavefront Sensors
ICD 1.9	GEMINI	Science Instruments ICD Overview and Guide
ICD 1.9/1.10	GEMINI	Science Instruments to On Instrument WFS
ICD 1.9/2.7	GEMINI	Science and Facility Instruments to Facility Handling Equipment ICD
ICD 1.9/3.6	GEMINI	Science and Facility Instruments to System Services ICD
ICD 1.9/3.7	GEMINI	Science Instrument to Facility Thermal Electronics Enclosures
ICD 1.10	GEMINI	On-Instrument WFS
ICD G0013	GEMINI	Gemini Environmental Requirements
ICD G0014	GEMINI	Gemini Observatory Optomechanical Coordinate Systems
ICD G0015	GEMINI	Gemini Facility Handling Equipment and Procedures for Instrumentation
	GEMINI	Guidelines for Designing Gemini Aspen Instrument Software
GSCG.grp.005	GEMINI	Gemini System Interfaces
GSCG.grp.006	GEMINI	Overview of Gemini System Interfaces
SPE-ASA-G0008	GEMINI	Gemini Electronic Design Specification

SECTION II: WFMOS SCIENCE CASES

Chapter 3 Dark Energy and Cosmic Sound: A New Road to Cosmic Acceleration and the Equation of State from Giant Galaxy Redshift Surveys

3.1 Background

3.1.1 *Why dark energy is one of the most important problems in physics.*

The discovery that the expansion rate of the universe is accelerating is perhaps the most startling breakthrough in science since Hubble's demonstration of the expansion itself (Riess et al. 1998; Perlmutter et al. 1999). Such was the surprise at the acceleration of the universe that a leading string theorist exclaimed that the data were simply wrong. Instead the conclusion that the cosmos is accelerating has strengthened to a point where very few cosmologists doubt its accuracy (Knop et al. 2003; Tonry et al. 2003; Spergel et al. 2003; Riess et al. 2004).

Within the context of our current understanding of the cosmos, the acceleration unambiguously requires radically new physics: either gravity must be fundamentally different from the vision put forward by Einstein, or the cosmic energy budget must be dominated by a new form of matter which moreover has a negative pressure - dark energy (for a modest sample of the literature, see Ratra & Peebles 1988; Frieman et al. 1995; Caldwell et al. 1998; Wetterich 2002; Armendariz-Picon et al. 2000; Freese & Lewis 2002; Bilic et al. 2002; Deffayet et al. 2002). Both of these possibilities would have a profound impact on our understanding of the Universe and physics at the deepest levels.

Perhaps the simplest possibility is that the dark energy is just Einstein's cosmological constant. However, the tiny observed value of the cosmological constant is a total puzzle in the context of modern fundamental theories. Even finding stable accelerating solutions in superstring theory is proving extremely difficult.

Understanding the origin of the acceleration will almost certainly entail a major revolution in our understanding of the cosmos and physics in the realm of quantum gravity. Beyond this, the cosmic acceleration forces us to address our own position in the cosmos: why did the universe begin to accelerate just around the time when life formed? It appears that we live at a special time in the history of the universe and understanding this conundrum may have profound implications for cosmology.

To unravel the properties of dark energy will require going significantly beyond the current state-of-the-art, which to date has given us precious little information about the nature of dark energy. If the acceleration is due to a new particle, we would like to know its equation of state, its mass, its speed of sound and so on. Extracting this information will push dark energy surveys to the limit.

Current data slightly favor the Λ CDM model, which is attractive because of its simplicity. Nevertheless, more complex models with w (the ratio of pressure to the energy density of this component) differing from -1 are excellent fits to the data. Is there a point to probing arbitrarily close to $w = -1$? When should one stop?

One obvious argument in favor of probing w to as high a precision as possible is that, even if it cannot rule out Λ CDM, it will rule out many particle physics models of dark energy and hence tell us what the cosmos at high energy cannot be like. In this sense, a null result is still very useful for fundamental physics.

A more subtle argument is that different observational methods actually depend on different aspects of the acceleration of the expansion. A clue to the physics of dark energy might be found in a discrepancy between different probes. A prime example of this is that a change to gravity might well alter the connection between the kinematics of the expansion and the evolution of cosmic structure relative to the usual general relativity prediction. This would skew inferences from weak lensing or cluster counting relative to those from supernovae or acoustic oscillations. Hence, it is important to push multiple methods to high and comparable precision, not simply as a test against systematic errors, but also to be open to new surprises from dark energy.

3.1.2 *Acoustic oscillations as a standard ruler and probe of dark energy.*

The clustering of galaxies on large scales contains the fossil record of the growth of structure in the early universe. These can include signatures of the initial seeding of the perturbations, such as by an epoch of inflation, and of the processing of those fluctuations through the transition to matter domination and the epoch of recombination.

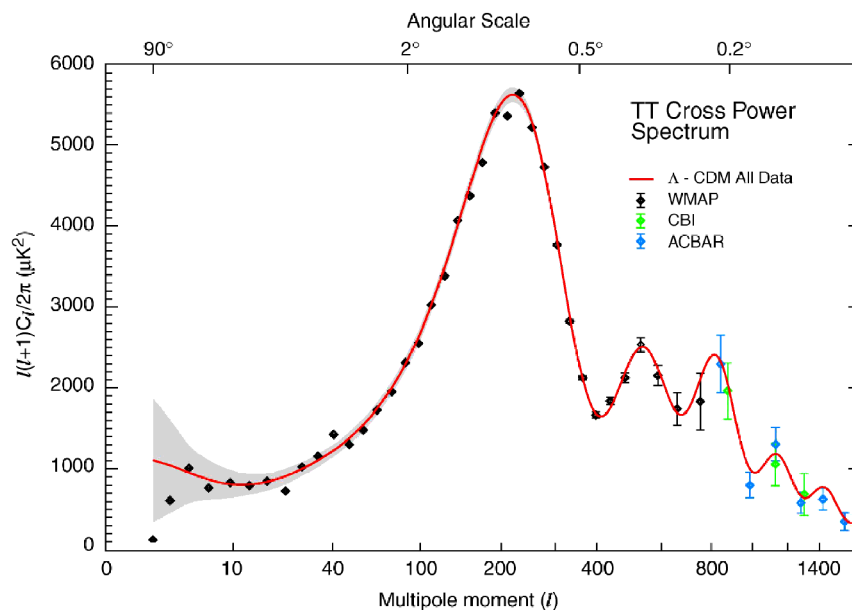


Figure 1: The state of experimental data on the anisotropies of the CMB as of February 2003 (WMAP; Bennett et al. 2003). Acoustic peaks have been clearly detected, and cold dark matter cosmologies are a great fit.

Here we will focus on the effect that has long been predicted and recently discovered to exist, namely the acoustic oscillations imprinted on the distribution of matter at the epoch of recombination (Peebles & Yu 1970; Sunyaev & Zel'dovich 1970; Holtzmann 1989; Hu & Sugiyama 1996). Prior to recombination,

the gas in the universe was locked to the photons of the cosmic microwave background, and the high pressure of this sea of photons caused the plasma to resist gravitational instability and instead to oscillate as a series of sound waves. After recombination, gas and light could separate, but the effects of the acoustic oscillations remain in their spatial structure. We are familiar with this signature as the now-famous Doppler peaks in the anisotropies of the cosmic microwave background (Figure 1). The same structure is also present in the late-time clustering of galaxies (see Figure 2) as a weak sinusoidal modulation of the amplitude of fluctuations as a function of scale. In both cases, the higher harmonics of the oscillation are suppressed by Silk damping and by the non-zero thickness of the last-scattering surface.

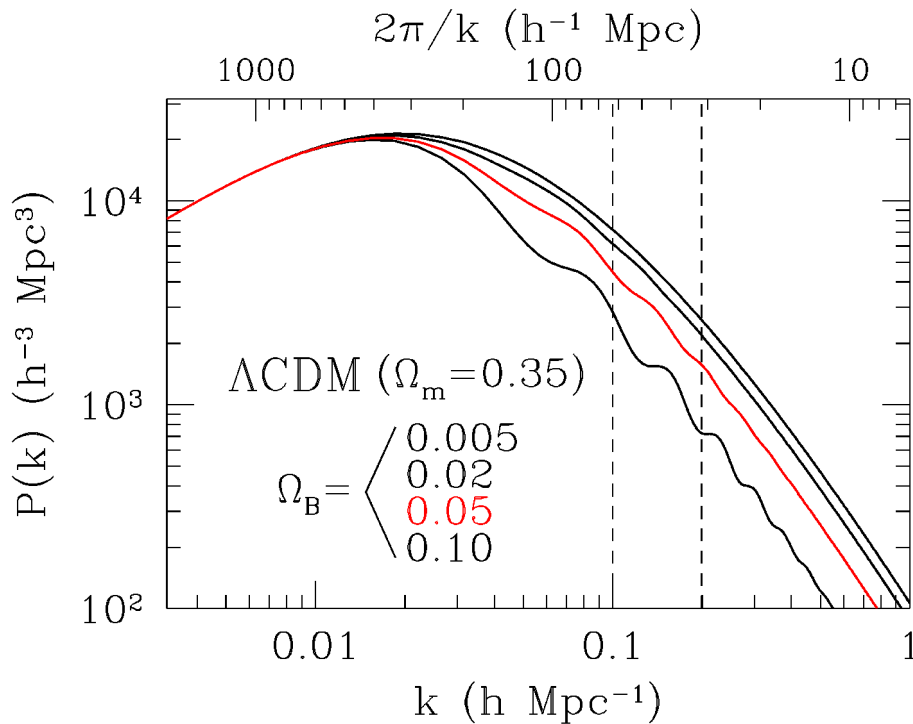


Figure 2: Power spectra for four different cosmologies, with an increasing baryon fraction from top to bottom. Note the appearance of the acoustic oscillations as the baryon fraction increases. From Eisenstein et al. (1998).

The oscillatory pattern in the power spectrum has a characteristic scale, known as the ‘sound horizon’, which is the distance that a sound wave can travel between the Big Bang and the epoch of recombination. The essential physics is very simple. A given localized adiabatic fluctuation is overdense in dark matter, baryons, and photons. The photon overdensity corresponds to an overpressure, and the drive to equalize this results in launching a spherical sound wave that carries the baryon and photon perturbation outward at the speed of sound (Bashlinsky & Bertschinger 2001). When the universe recombines, the photons separate from the baryons, and the baryon perturbation is left as a spherical shell 150 comoving Mpc in radius. Both the baryonic shell and the dark matter perturbation, much larger but still localized near the initial location, seed the late-time gravitational instability and the formation of galaxies. This results in a preferred separation of galaxies of 150 Mpc (a single acoustic peak in the correlation function). Alternatively, if one prefers to work in Fourier space, the crest of an initial plane wave perturbation launches a planar sound wave that travels away from the crest

for a distance of 150 Mpc. If the wavelength of the plane wave is such that this baryonic sheet falls onto the dark matter perturbation in any subsequent crest, then one has constructive interference, resulting in a peak in the power spectrum. If it falls in a trough, then one has a deficit in the power spectrum.

The key point is that this sound horizon depends only on properties of the early universe, namely the sound speed and the amount of time available prior to recombination. These ingredients are well measured by the CMB. WMAP presents a 3% measurement of the sound horizon (Spergel et al. 2003), and future CMB data should improve this to better than 1%. Hence, this scale is effectively a standard ruler (Eisenstein & Hu 1998; Eisenstein 2003).

As we will see, the scale of the oscillation can be measured to high precision in large redshift surveys. These surveys require not only large numbers of galaxies but also large volumes and hence large sky coverage. No existing spectrographs can efficiently achieve the depth and breadth required for these surveys. WFMOS could execute galaxy redshift surveys that would measure the acoustic scale at a variety of redshifts, thereby measuring the expansion of the universe as a function of time to high precision and providing useful constraints on $w(z)$.

3.1.3 *Theoretical Uncertainties in the Acoustic Oscillation Method.*

As discussed in Eisenstein & White (2004), the production of the acoustic oscillation and the calibration of its scale are robust aspects of $z=1000$ physics. The scale is generated in the redshift range 10^3 to 10^5 , with the implication that most known effects that would disturb the acoustic scale - e.g., admixtures of isocurvature fluctuations, decays of particles near $z=1000$, generation of cosmic perturbations at $z < 10^5$, etc. - create strong visible discrepancies in the CMB. Other effects, such as alterations to the relativistic energy density of the universe, introduce scale errors in *both* the CMB and low-redshift measurements that would cause our inference of the Hubble constant H_0 to be wrong but would leave our inferences of Ω_m and dark energy unchanged.

Once produced, the acoustic scale is expected to be unchanged by the formation of structure at $z < 1000$. We will present tests of this in the context of standard cosmology in Section 3.2.2, but even in the face of exotica, the robustness of the acoustic scale is simply that it is a preferred scale of 150 Mpc, and that it is implausible that a physical mechanism for gravitational evolution or galaxy formation would act in a way to select any large scale rather than treating 120, 150, and 180 Mpc equivalently.

3.1.4 *January 2005: Acoustic oscillations discovered*

In January 2005, independent groups from the Sloan Digital Sky Survey (SDSS) and 2dF Galaxy Redshift Survey (2dFGRS) announced the detection of the acoustic signature in their data sets (Eisenstein et al. 2005; Cole et al. 2005). These teams used different types of galaxies, different volumes of space, and different analysis methods, yet both provide compelling matches to the standard cosmological model with acoustic features (Figure 3). In the case of the SDSS, the acoustic peak was explicitly interpreted as a standard ruler, giving a 5% distance measurement to $z=0.35$ and, with the CMB acoustic scale, a 4% geometric measurement of the ratio of the distance to $z=0.35$ to the distance to $z=1089$. The latter constraint, along with the measurement of $\Omega_m h^2$ from the shape of the

acoustic peak, produced a 1% measurement of the curvature of the universe, taking the dark energy to be a cosmological constant (Figure 4).

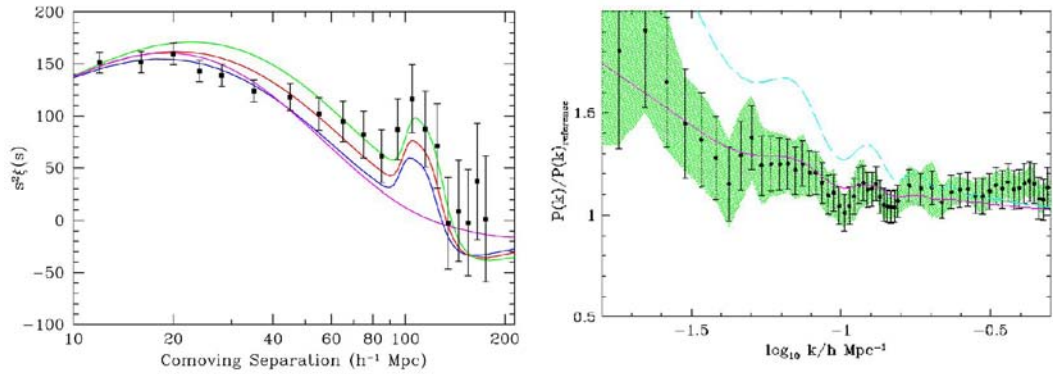


Figure 3 (Left) The correlation function $\xi(s)$ of luminous red galaxies from the SDSS, times the square of the separation s (Eisenstein et al. 2005). The peak at $100 h^{-1}$ Mpc scale is the acoustic feature at the expected location for the standard cosmology. The true scale of this feature is computed to be 150 Mpc from the physics of the early universe. The lines with peaks show cosmological models of different values of $\Omega_m h^2$; the one line without a peak shows the prediction of a pure cold dark matter model. (Right) The power spectrum of galaxies from the 2dF galaxy redshift survey, divided by a smooth reference power spectrum (Cole et al. 2005). The data points are correlated, but show evidence for oscillations to match the theory. The cyan line is the best-fit theory; the magenta line is the best-fit theory convolved by the window function of the 2dFGRS.

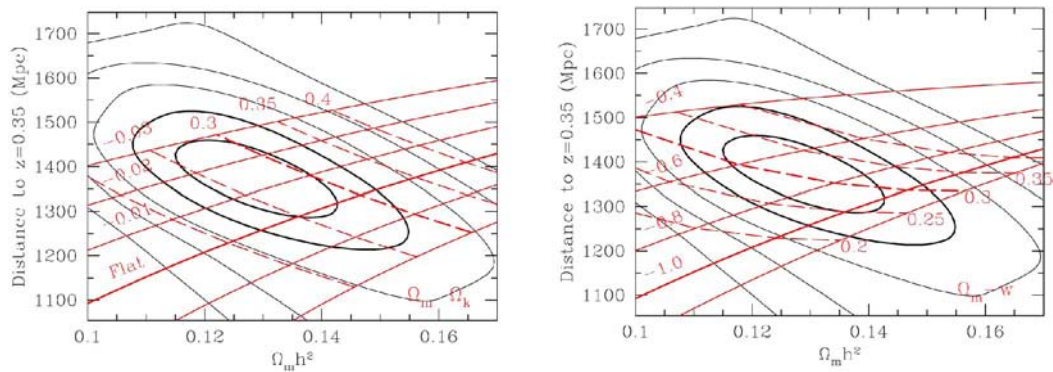


Figure 4: (Left) Constraints from the SDSS LRG sample on the matter density of the Universe $\Omega_m h^2$ and the distance to $z=0.35$. Overlaid are the predictions for these quantities for a grid of cosmologies with varying Ω_m (dashed lines) and non-zero curvature (solid lines), assuming a cosmological constant ($w=-1$). One sees that the data require a model that is very close to flat; a Markov chain analysis found $\Omega_\kappa = -0.010 \pm 0.009$. (Right) Same, but the overlaid grid is for a space of flat models with constant w . The constraints on w are currently limited by imperfect knowledge of $\Omega_m h^2$. With improvements there from Planck, the w constraints from this data will improve from of order $\sigma(w) \sim 0.2$ to about 0.1. Extending this method to give simultaneous leverage on $w(z)$ and spatial curvature will require precision measurements at other redshifts.

3.2 Galaxy redshift surveys for acoustic oscillations.

In a galaxy redshift survey, the fundamental observables are the angular separations and redshifts of the galaxies. We require a cosmological model to translate these angles and redshifts into physical distances. If we imagine observing a standard ruler at a particular redshift, then alterations in the dark energy model will distort the apparent radial and transverse size of the ruler. Here, instead of using a single object of known size, we use the distribution of separations between pairs of objects. The acoustic oscillations imply a preferred separation of 150 Mpc. Since we know the true size, we can use the observed radial clustering to recover the Hubble parameter $H(z)$ and the observed transverse clustering to recover the distance $DA(z)$. It is worth noting that this discussion differs from the familiar Alcock and Paczynski (1979) test in that we are working with a known length scale and therefore can extract $H(z)$ and $DA(z)$ separately, rather than merely their ratio.

Figure 5 shows the ratio of the radial and transverse distances between two cosmological models and a reference model as a function of redshift. The reference model is a cosmological constant model with $\Omega_m=0.3$, $\Omega_w=0.7$ and $w=-1$. The first variation model has $w=-0.9$. We pick $\Omega_m=0.329$ and adjust the Hubble constant to hold the value of $\Omega_m h^2$ fixed. This leaves the location and shape of the acoustic peaks in the CMB unchanged. A second model shows $w=-0.8$ and $\Omega_m=0.361$.

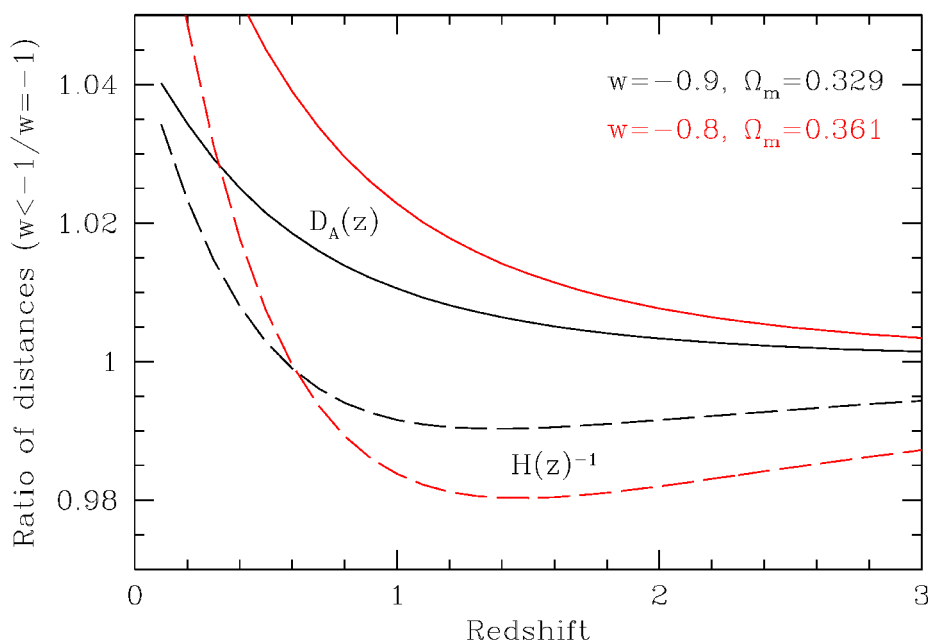


Figure 5: The length distortion of a rod as a function of redshift, supposing the true cosmology is $\Omega_m=0.3$, $w=-1$ and the assumed cosmology is either $\Omega_m=0.329$, $w=-0.9$ or $\Omega_m=0.361$, $w=-0.8$, all at constant $\Omega_m h^2$. These two models are indistinguishable in the CMB but, as shown by the figure, disagree in their low-redshift cosmography. The dashed and solid lines illustrate respectively the distortion if the rod is oriented radially (which depends on the ratios of $H(z)^{-1}$) and tangentially (which depends on the ratios of angular diameter distances). Thus it can be seen that the primary effect of assuming the incorrect cosmology is a re-scaling of distances away from their true values.

Clearly, the effect of changing w in this manner makes only a small impact on the distance scale. One must measure the distances to of order 1% at $z \sim 1$ in order to distinguish between these models. Given this requirement, we can proceed to calculate the necessary size of the redshift survey.

3.2.1 Analytic assessments of performance.

The statistical errors on the power spectrum resulting from a redshift survey can be approximated as (Tegmark 1997a):

$$\frac{\sigma_P}{P} = 2\pi \sqrt{\frac{1}{Vk^2 \Delta k}} \left(\frac{1 + nP}{nP} \right)$$

where V is the comoving volume of the survey, n is the comoving number density of galaxies in the survey, and P is the comoving power at the central wavenumber. This formula has a simple origin: the errors scale inversely with the square root of the number of Fourier modes measured, where the unit of volume in Fourier space is $(2\pi)^3/V$, and each mode is measured to order unity in the power with a penalty for shot noise. The shot-noise penalty occurs when the white noise from the Poisson sampling of the density field exceeds the true clustering power. This happens when the product of the number density and power, nP , is less than unity. Note that this product is wavenumber dependent.

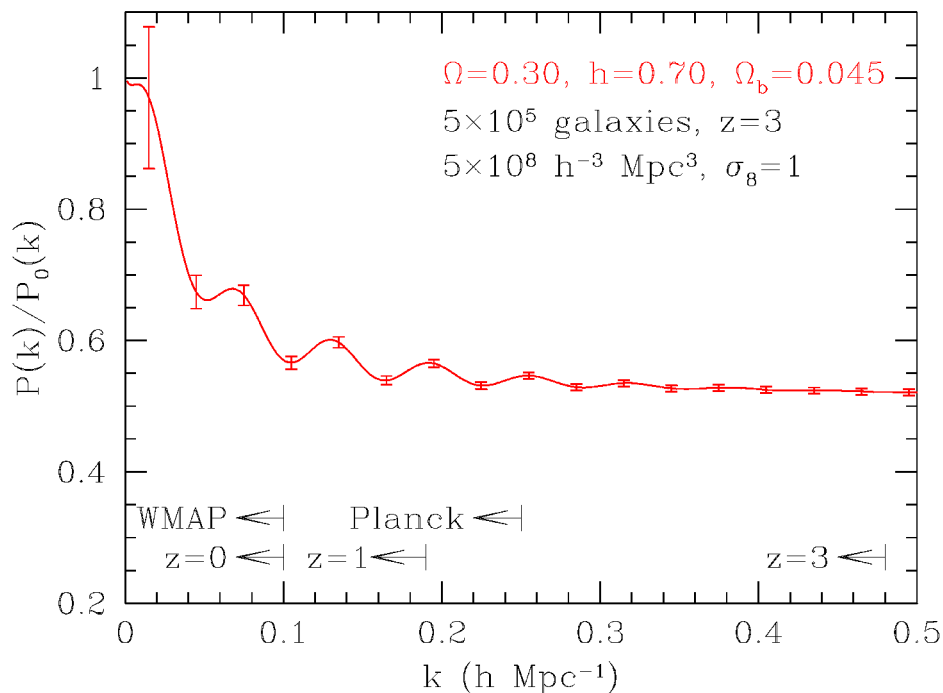


Figure 6: The forecast errors on the power spectrum of a large redshift survey at $z=3$. The power spectrum has been divided by that of a zero-baryon model to show the oscillations more clearly. The model itself is consistent with WMAP. This hypothesized redshift survey would be 500,000 galaxies over 150 square degrees and $0.5 h^3 \text{ Gpc}^3$. The approximate extent of the linear regime coverage at various redshifts is shown along the bottom. Also shown is the wavenumber range probed by the CMB missions, WMAP and Planck.

For the power spectrum measurement, if observational resources scale strictly with the number of survey objects (and not, e.g., with field of view), there is an optimal sampling density where $n = 1/P$ (Kaiser 1986). In other words, were our

only goal to measure the power at a particular wavenumber, we would be most efficient by choosing the number density so that $nP=1$. However, like all optimizations, the utility is a slow function of the controlling parameter near the maximum. In this case, $nP=3$ or $nP=1/3$ increases the errors by only 15%. Performance degrades more steeply as one moves further from the optimum.

An example of the errors that could be produced in a large high-redshift survey is displayed in Figure 6. This represents a sky coverage of about 150 square degrees with 1 target per square arcminute over a redshift depth of 1. Clearly, the acoustic signature would be easily detectable. Measuring the acoustic scale means that we want to measure the spatial frequency of the oscillation. Note that this is best done with higher harmonics, since a 10% shift in the fundamental mode would, e.g., shift the third overtone by 40%. However, the higher harmonics are smaller in amplitude, and there is a sweet spot around $k=0.2 h \text{ Mpc}^{-1}$.

Several authors (Blake & Glazebrook 2003; Hu & Haiman 2003; Seo & Eisenstein 2003; Amendola et al. 2004; Matsubara 2004) have used the sampling error formula above (eqn 1) to predict the performance on measuring the distance from the acoustic oscillation method. These calculations differ in their methods but agree in their conclusions.

Hu & Haiman (2003), Seo & Eisenstein (2003), Amendola et al. (2004) and Matsubara (2004) use Fisher matrix methods to propagate the assumed statistical error in the measurement of each mode through to constraints on the distance scales and then to dark energy parameters. The details vary somewhat: Seo & Eisenstein (2003) treat each redshift shell independently before combining to constraints on w and dw/dz ; Hu & Haiman (2003) focus on cluster surveys as a means to measure w ; Amendola et al. (2004) add the constraints from the evolution in the amplitude of clustering assuming that redshift distortions can be removed; and Matsubara (2004) treats the problem in real-space rather than Fourier-space. All of these methods assume that the shape of the power spectrum is as predicted by the standard microwave background theory; this is a good assumption given that alterations to the theory produce large deviations in the CMB anisotropy spectrum, particularly with Planck-quality data.

The fundamental constraints can be seen in Figure 7 (Seo & Eisenstein 2005). This shows the 1σ constraints on the Hubble parameter and angular diameter distance as a function of redshift for various hypothetical large redshift surveys. The low redshift points are representative of the SDSS Luminous Red Galaxy sample; the higher redshift points are 2000 (300) square degree surveys at $z=1$ (3) such as could be performed with WFMOS. Performance improves at higher redshift because the non-linear scale is smaller, allowing more acoustic peaks to be used.

Blake & Glazebrook (2003) used a more model-independent approach, in which they generated simulated point sets with the input power spectra and shot noise, measured the power spectra, and then fit a simple damped sinusoid after high-pass filtering, thereby determine a scale. This method is more aggressive about projecting away possible contamination from scale-dependent bias, unmodeled broadband tilts such as from massive neutrinos, and redshift distortions. The recovered precision is necessarily worse, but only by a small amount, reinforcing the robustness of the acoustic signal.

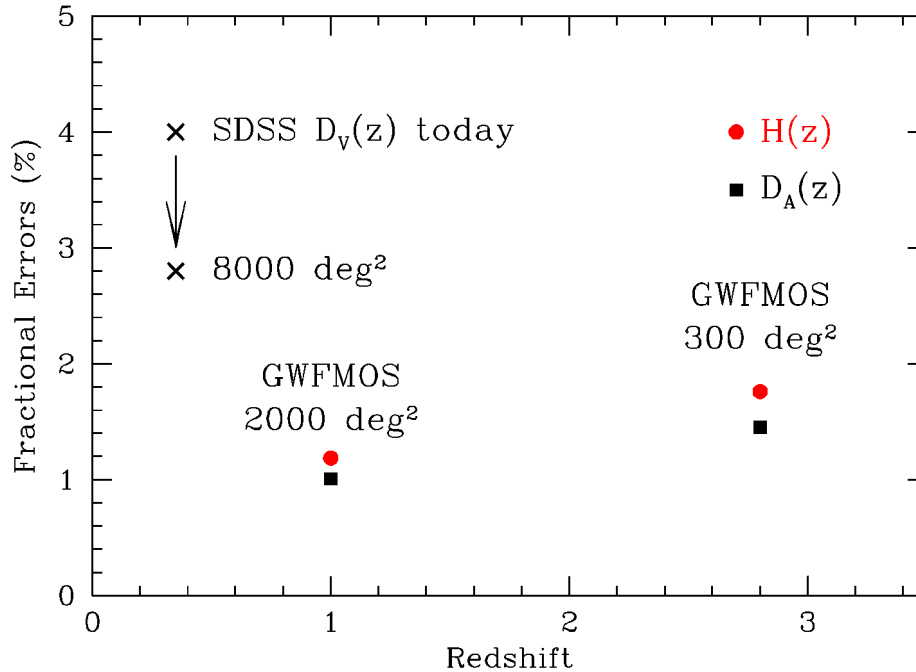


Figure 7: The $1-\sigma$ errors on the Hubble parameter and the angular diameter distance for the baseline WFMOS surveys as well as the SDSS LRG sample. One WFMOS survey is 2 million galaxies covering 2000 square degrees from $z=0.5$ to $z=1.3$. The other survey is a half million galaxies at $z=2.3$ to 3.3 covering 300 square degrees. The performance on the Hubble parameter is slightly worse than on the angular diameter distance because there are more tangential modes than radial modes. These forecasts are based on the Fisher method of Seo & Eisenstein (2003), but with revisions in the non-linear scale appropriate to the numerical investigation of Seo & Eisenstein (2004), and with a correlation length of $4h^{-1}\text{Mpc}$ for the galaxies. The left-most points are the measurement from the SDSS LRG sample Eisenstein et al. (2005) at $z=0.35$ (assuming an improvement in $\Omega_m h^2$ from Planck data) and what the extended SDSS will do.

In addition to the studies listed above, there have been studies of angular correlations by Dolney, Jain & Takada (2004) and Blake & Bridle (2004). The first of these is particularly notable for its inclusion of bispectrum information as an extension into the quasi-linear regime. The utility of the bispectrum would also extend to redshift surveys, but it has not been calculated in this context. Note, however, that the acoustic information itself is carried in the two-point function; the higher-point functions are used only to break degeneracies in the quasi-linear regime.

3.2.2 **Numerical validation of analytic computations.**

Because of the subtle yet important nature of the acoustic signature in the late-time correlations of matter, we have undertaken extensive studies of N-body simulations in connection with this report.

The correlations of galaxies on these scales are affected by a number of non-linear processes that do routinely cause the clustering of galaxies to deviate from the predictions from linear perturbation theory. These effects might obscure or distort the acoustic signature in such a way as to confuse the dark energy inferences. However, in our N-body investigations we find that the acoustic scale is robust to these complications, in a manner consistent with what was assumed for the analytic estimates.

There are three major sources of distortion in the galaxy clustering. (1) As structure grows by gravitational instability, the small-scale perturbations become of order unity, leading to runaway collapse into dark matter halos. This process causes a significant boost in the small-scale clustering of the matter, but it also leads to coupling between Fourier modes near the non-linear scale that cause the acoustic oscillation signature to be washed out (Meiksen et al. 1999). (2) Redshift distortions alter the correlations due to the coherent role of peculiar velocities (Kaiser 1986; Hamilton 1998; Scoccimarro 2004). The Finger-of-God effect on small scales manifestly mixes scales, but even on large scales the convergence to the classical Kaiser (1986) linear-theory form is slow. (3) Galaxies and dark matter halos exhibit a clustering bias relative to the full dark matter distribution. This bias is expected to be scale-independent on large scales (Coles 1993; Scherrer & Weinberg 1998) but is generically scale-dependent on small-scales.

Seo & Eisenstein (2005) have run 51 P³M N-body simulations, each 512 h^{-1} Mpc on a side with 256^3 particles with outputs at various redshifts of interest. They have analyzed the power spectra in real-space and redshift-space and included simple halo-mass-threshold bias schemes. The onset of non-linearity is obvious, but the very large collective volume of the simulation set allows one to recover even the weak power spectrum features.

One finds that the non-linearities do erase the acoustic oscillations on small scales, but that this is negligible at $z=3$, as expected, and matches the analytic assumptions at $z=1$. At $z=0.3$, the numerical performance is a little better than assumed. These results are shown in Figure 8 and Figure 9.

The Durham group has looked at these same questions with two simulations whose far higher mass resolution allows a more realistic inclusion of galaxies (albeit over less total volume). They have modelled the accuracy with which the acoustic oscillations can be reproduced using different tracers. They combine the high resolution, large volume N-body simulations with the Durham group's semi-analytic model of galaxy formation (see Benson et al. 2000 for a discussion of the implementation of the semi-analytic model in N-body simulations). The semi-analytic code predicts the star formation history of the galaxy population at different redshifts. Dust extinction is applied by computing an optical depth from the size of the galaxy and its metal content, as derived from a chemical evolution model. The N-body simulations that they have used are from the Virgo Consortium, and include the Millennium Simulation (a 500 h^{-1} Mpc box with 10 billion particles; Springel et al. 2005) and the ICC1000 (a 1000 h^{-1} Mpc box with one-eighth the number of particles used in the Millennium).

The advantage of this latter work is that it goes beyond a simple halo mass cut to include galaxies in a manner that matches our detailed understanding of the distribution of galaxy properties. Despite these additional complications, the acoustic signature is preserved at the expected level, as shown in Figure 10 for $z=1$.

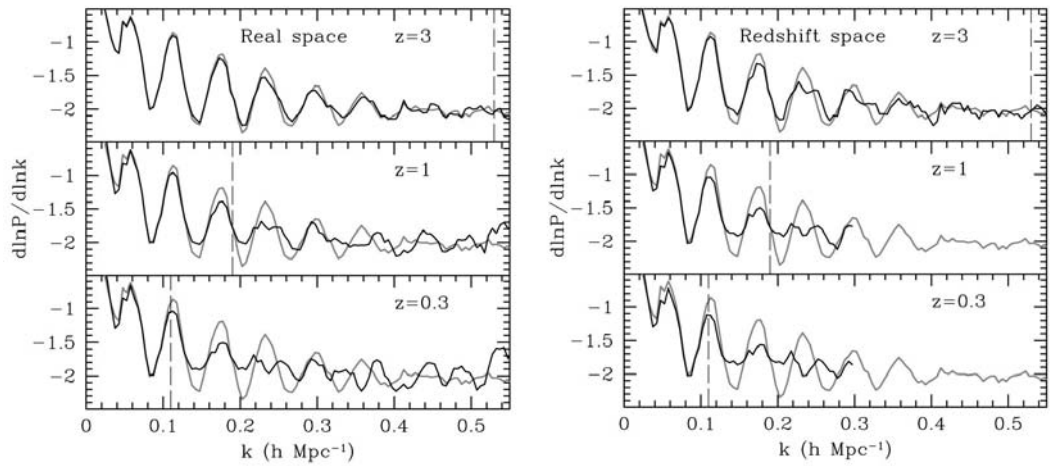


Figure 8: The logarithmic derivative of the matter power spectra from the N-body simulations of Seo & Eisenstein (2005). Taking the derivative focuses attention on the acoustic oscillations, but it should be remembered that the oscillations at $k > \sim 0.3 h \text{ Mpc}^{-1}$ are very weak and that most of the standard ruler constraints come from $k \sim 0.1-0.2 h \text{ Mpc}^{-1}$. The left panel shows the real-space power spectra at redshifts of 3, 1, and 0.3; the right panel shows the redshift-space power spectra at the same redshifts. The dashed lines show the nominal non-linear scale used in Seo & Eisenstein (2003). A very smooth function has been subtracted from power spectra to remove the effects of shot noise and restore the slope of the linear power spectrum. One sees that the acoustic oscillations do survive the effects of non-linearity and redshift distortions, although they are mildly degraded by both.

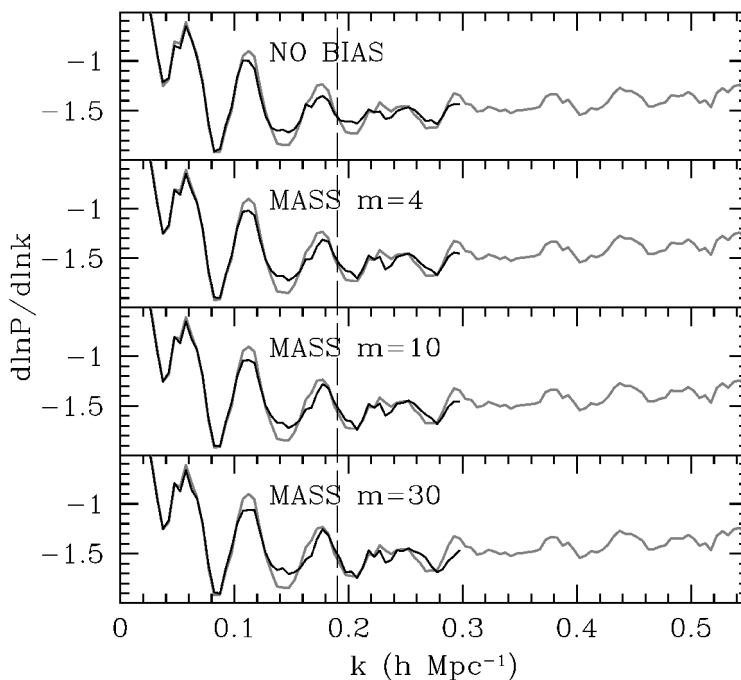


Figure 9: The logarithmic derivatives of biased power spectra at $z=1$ using different halo mass thresholds (Seo & Eisenstein 2005). In all panels, the grey line shows the real-space matter power spectrum. The black line in the top panel shows the redshift-space matter power spectrum, and the black lines in the bottom three panels show the redshift space of increasing the mass threshold (up to about 2.5×10^{13} solar masses and a bias of 3). A very smooth curve has been subtracted from the $P(k)$ to force the black lines to match the mean slope of the grey line; this represents the effects of shot noise and other smooth alterations. The degradation of the acoustic oscillations is minimal.

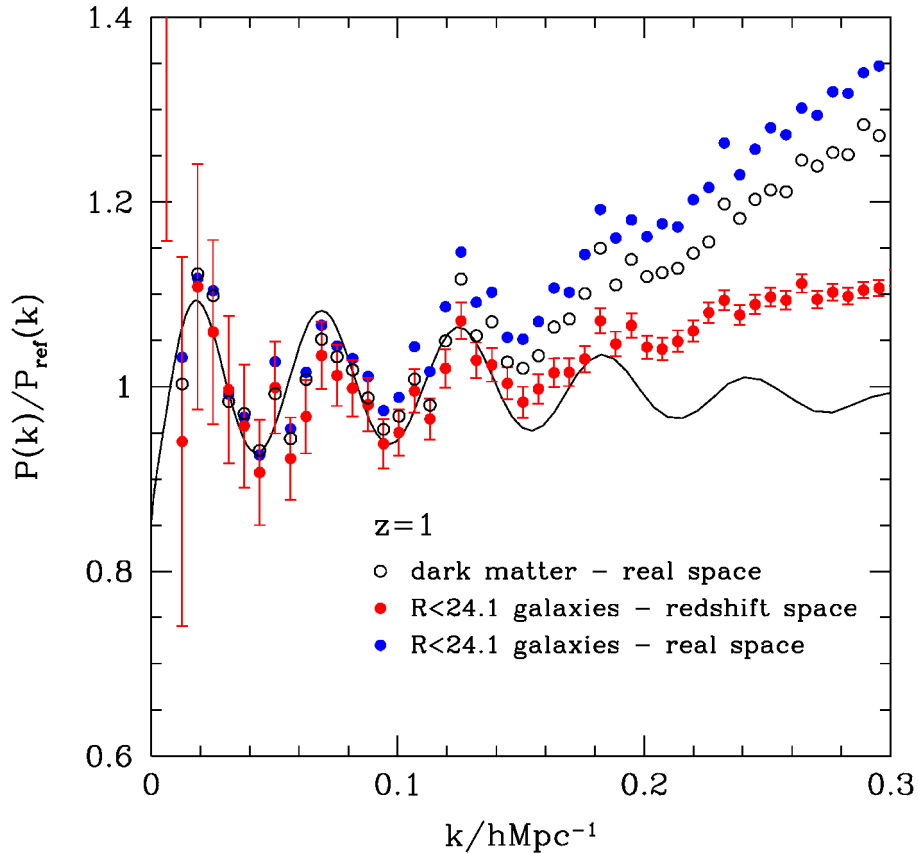


Figure 10: The power spectrum of galaxies and dark matter at $z=1$. The spectra have been divided by a smooth reference spectrum, which does not contain any acoustic oscillations. The solid curve shows the linear perturbation theory power spectrum divided by the same reference spectrum. The open black circles show the power spectrum of the dark matter in real space. The other points show spectra for galaxies selected to be brighter than $R=24.1$ at $z=1$. The blue points show the power spectrum in real space and the red points show how the spectrum changes when redshift space distortions are included. The errorbars are computed for the redshift space galaxy power spectrum and are based on the number of modes in the simulation box, the power spectrum amplitude and the number density of galaxies.

Both sets of simulations find that scale-dependent bias and redshift distortions have only mild effects on the detectability and utility of the acoustic oscillations. We see small degradations in redshift space (Figure 9). Very high mass thresholds leading to biases much larger than assumed can create enough noise that it is hard to determine whether the higher multipoles of the acoustic oscillations are being preserved.

Generically, the numerical galaxy power spectra have some extra contributions above the matter spectra. This is in part simply shot noise, but small-scale non-linearities enter as well. Seo & Eisenstein (2005) show that one can subtract smooth functions of power to restore the appropriate slope of the power spectrum and then recover the oscillations without a bias in the scale.

Finally, Seo & Eisenstein (2005) show that fits to the acoustic scale in the power spectra of the simulations have a scatter that matches the analytically estimated performance to within about 20%, thereby showing that non-Gaussianity in the power spectrum is not degrading the results in the linear regime. Indeed, at $z=0.3$, the performance is somewhat better than predicted in Seo & Eisenstein (2003),

due to the smaller non-linear scale. With this change, the observed performance from SDSS matches the predicted performance to good accuracy.

3.2.3 *Estimated performance as a function of survey size/redshift.*

The analytic methods give an easy way to forecast the ability of surveys of different sizes to use the acoustic scale to constrain $D_A(z)$ and $H(z)$. For example, Figure 7 presents the results for the results from Seo & Eisenstein (2003) for the baseline WFMOS surveys at $z=1$ and $z=3$. The analytic forecasts from various different authors (Blake & Glazebrook 2003; Hu & Haiman 2003; Seo & Eisenstein 2003; Amendola et al. 2003) seem to be in reasonable agreement despite their minor differences in methodology. In short, samples of order a million galaxies covering $1h^3\text{Gpc}^3$ are necessary to reach the levels of precision required to advance the state of the art on our understanding of dark energy.

We have investigated whether breaking the survey region into several or many pieces mattered for the constraints. The analytic estimate is that because of the spacing of the peaks in Fourier space, one must have a survey that is at least $300 h^{-1}\text{Mpc}$ on a side and preferably $500 h^{-1}\text{Mpc}$. $500 h^{-1}\text{Mpc}$ at $z=1$ is 15 degrees; at $z=3$, it is 7 degrees. This would still permit one to have several (2 - 4) separate regions spread out around the sky if desired. However, much smaller subsurveys would cause significant blurring in Fourier space that would degrade the acoustic signature. Numerical simulations of using large numbers of smaller survey regions bore out this argument.

Small holes in the survey, e.g., bright stars or even missing WFMOS pointings, do not matter, as has been borne out in many previous large-scale structure surveys.

3.2.4 *Comparing and Constrasting the Acoustic Oscillation Method with Others*

The acoustic oscillation method allows one to measure $H(z)$ and $D_A(z)$ to various redshifts and to do so on the same distance scale as the CMB measurement of the distance to $z=1089$. The $D_A(z)$ measurement is degenerate with the supernovae inferences of $D_L(z)$ unless photons are disappearing or being scattered en route.

The only non-linear effect for the acoustic oscillation method is the issue of galaxy bias. However, as long as some correlations exist between the galaxy density and the matter perturbation (which has basically been shown by SDSS and 2dF) then we only require linear perturbation theory. The success of the CMB measurements shows that this works and provides extremely clean data. All other approaches have to deal with (and understand) highly non-linear issues like exploding stars and the clustering of all forms of energy densities. When we just fit the oscillations there is no dependence on any unknown physics in order to produce the data points. The unknown physics only enters afterwards, when we try to fit them with models.

However, it is interesting to remember that the supernova method measures only distance ratios; it does not measure the absolute distance scale any better than the usual distance ladder. In particular, this means that it cannot be compared directly with the CMB. This is a disadvantage when trying to exclude the possibility of a small spatial curvature. Figure 11 shows the degeneracy that opens in the supernova inferences.

The acoustic peak method is the only current one that can probe dark energy at $z > 2$. This is because one is measuring the distance to some high redshift, say $z_{\text{survey}} = 3$, and comparing it directly to the distance to the last scattering surface, $z \sim 1000$, using the same physical feature. In a flat cosmology, the difference between these two distances depends only on the Hubble constant in the redshift range $z_{\text{survey}} < z < 1000$ (Eisenstein & White 2004). While the cosmological constant model predicts that dark energy is negligible at $z > 3$, other models could easily be different, and the acoustic peak method allows a 1% measurement of this distance. This is particularly important if the dark energy equation of state makes a transition from $w > -1$ towards $w = -1$ around some redshift. The acoustic peak method is very sensitive to such shifts, even if the residual density of dark energy is only $\sim 1\%$.

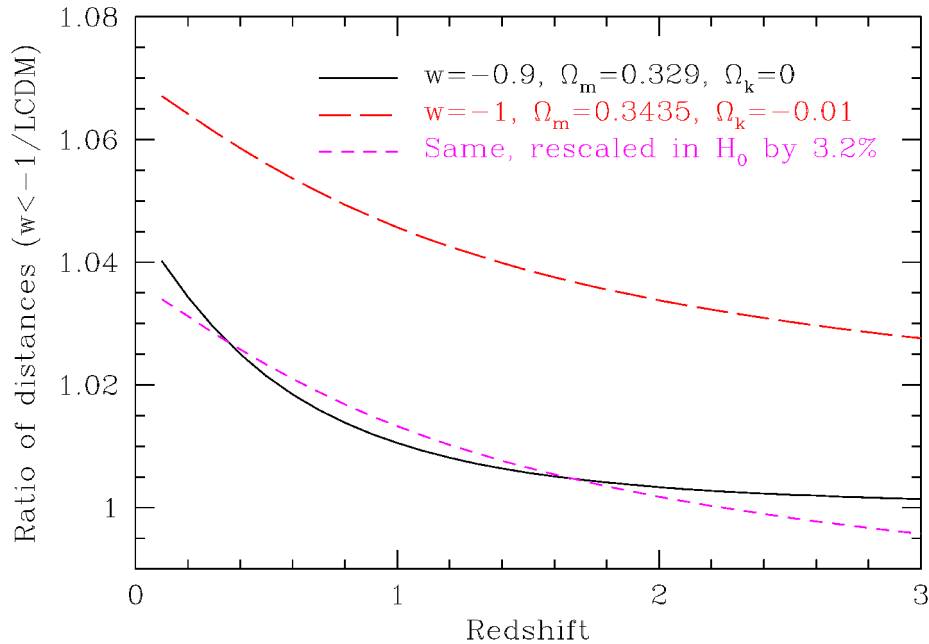


Figure 11: The ratio in angular diameter distance between two cosmologies and a fiducial $\Omega_m = 0.3$, $w = -1$ flat cosmology. All three cosmologies are chosen to have the same $\Omega_m h^2$ and distance to $z = 1000$; therefore the CMB anisotropy spectrum is essentially invariant. One cosmology has $w = -0.9$ and no spatial curvature; the other has $w = -1$ and a small spatial curvature. Both would be easily distinguishable from the baseline model. However, because the supernova method measures only distance ratios, one could imagine shifting the curved model by 3% in distance, thereby showing that the two models have nearly degenerate distance ratios out to $z \sim 1.5$. Proving w is not equal to -1 , while marginalizing over a curvature is difficult for the supernova method alone (this point is courtesy of Ned Wright at the Wide-field Imaging from Space conference). Acoustic oscillations break the degeneracy because they can relate their distances to the CMB, where curvature has a much larger effect.

Weak lensing promises great precision on dark energy through various methods. One method, now known as cross-correlation cosmography, compares the shear signal using sources at different redshifts (Jain & Taylor 2003; Bernstein & Jain 2004). The ratio of the signal between two different source planes isolates a ratio of distances independent of the lens properties. This removes much of the uncertainty in mass modeling and some of the uncertainties in coherent shear errors, but it requires enormous accuracy (0.001) in photometric redshifts that are unlikely to be achieved this decade over wide fields and it requires that there be no redshift-dependent biases in the PSF depolarization correction. These are very

difficult challenges. Indeed, calibrating the photometric redshifts required by cross-correlation cosmography will require enormous spectroscopic surveys such as what WFMOS would enable.

The more classical method of constraining w by weak lensing is to measure the shear power spectrum or to search for mass peaks (i.e., cluster counting). These are difficult methods, particularly the shear power spectrum, but regardless of one's assessment of their prospects for the next decade, it is important to note that there exist dark energy models that change gravity on large scales and therefore likely change the growth of structure differently than the expansion of the universe. Cluster counting by X-ray or Sunyaev-Zel'dovich surveys similarly rely on growth functions. We regard it as very important to measure dark energy properties by both the expansion history and the growth function of structure, because there is the possibility of distinguishing between models that create new gravitating fields and those that alter gravity itself.

Compared to the weak lensing, supernova, and cluster methods, the acoustic peak method appears to us to be more robust to systematic errors. Weak-lensing measurements rely on very subtle distortions that must be accurately modeled, particularly for small galaxies in ground-based seeing. Surveys of 1000's of square degrees will require these systematic errors to be controlled over 10 times better than the current state of the art. Next-generation supernova measurements will require control over the evolution of supernovae to 1%, which will be difficult to prove. Cluster methods require exquisite calibration of the mass scale.

The acoustic peak method, on the other hand, just requires a redshift factory. Each measurement is relatively easy and the observational and theoretical systematics appear to be comparatively straight-forward to handle.

3.3 Possible Targets for the Acoustic Oscillation Surveys

The original KAOS Purple Book study advocated studying galaxies in two redshift ranges. The first was 'normal' galaxies, i.e., the regular mix of spirals and ellipticals, at $0.5 < z < 1.3$, and the second was Lyman-Break Galaxies (LBGs), a starbursting young galaxy population at $z \sim 3$ (Steidel et al. 1996). The motivation for this choice is that both populations have been extensively studied in ground-based redshift surveys and hence were already known to be amenable to obtaining redshifts from low-resolution optical spectra in only a few hours exposure on an 8m telescope.

Below, we discuss in more detail these choices and also discuss the more difficult issue of covering the redshift gap $1.3 < z < 2.5$ known as the 'redshift desert,' which historically has been much harder to study in the optical and has only recently seen progress (Abraham et al. 2004, Fontana et al. 2004, Steidel et al. 2004). These redshift ranges are a natural breakdown, as they involve qualitative changes in observing approach, so we will discuss them individually.

For studying acoustic oscillations we don't care what types of galaxies we use, since we expect that on large scales (>20 Mpc) all galaxy types will be faithful tracers of large-scale structure. Thus we have the freedom to pick objects which are maximally convenient for getting redshifts in the shortest possible exposure time.

In our discussion here, we will focus on using measured properties of known galaxies in the various redshift ranges from existing surveys to constrain numbers, luminosity and clustering. This leaves us relatively immune from evolutionary corrections. We can also use existing surveys to estimate exposure time by aperture scaling, as well as making *ab initio* estimates using our WFMOS S/N calculator.

One general constraint is that targets must be pre-selected from broad-band imaging data. This for example makes it somewhat harder to pick out objects with strong emission lines, which would be very easy to get redshifts for. Techniques exist for directly selecting emission line galaxies (e.g., surveys with narrow band filters or slitless spectroscopy), but it is not currently feasible for a ground-based instrument to cover the required sky areas *and redshift ranges* using them.

3.3.1 **Redshift range $0.5 < z < 1.3$**

This redshift range corresponds to a lookback time of 5-9 Gyr¹ and has been well studied by surveys such as CFRS and LDSS2 with exposures of ~4 hours on 4m telescopes. It is being heavily targeted by large on-going DEEP2 redshift survey (several thousand $z \sim 1$ galaxies now down, ~50,000 planned) using one hour exposures on Keck. A mixture of red and blue galaxies are observed corresponding to the classical elliptical and spiral types (confirmed by HST morphologies). However there has been considerable evolution since $z=0$, the UV luminosity density has risen with increasing SFR as $\propto (1+z)^3$ in the blue population, and more luminous, blue and morphologically peculiar galaxies are seen. The red population is more luminous from passive evolution but reduced in number.

The initial question of course is red vs blue sequence or a mixture of both? It makes sense to frame the discussion in this sense as both sequences are distinctly resolved, i.e. the galaxy distribution is bimodal in color.

We will base our $z \sim 1$ estimates on data kindly provided by the DEEP2 redshift survey team for this purpose (total of 1463 galaxies). This uses a BRI color cut to select galaxies with $0.7 < z < 1.5$ and $R_{AB} < 24.1$ mag (=23.8 mag Vega). The DEEP2 selection delivers 25000 galaxies deg⁻². The efficiency of the color cut is about 87% (i.e. 13% of targets are $z < 0.7$ interlopers), so one strategy for WFMOS would be to simply duplicate this selection function.

As discussed in Section 3.2.1, the ability to extract acoustic oscillations from a given volume of space depends on the sampling density of the survey. At high number densities, the amount of extracted information saturates. For the acoustic oscillations, this threshold of declining returns is roughly a comoving density of $0.0007 \sigma_{8,gal}^{-2} h^3 \text{Mpc}^{-3}$ ($nP=2$ at $k=0.2 \text{ h Mpc}^{-1}$ at $z=1$). Here, $\sigma_{8,gal} = (r_0/5 \text{ Mpc})$ is the amplitude of the galaxy clustering on $8h^{-1} \text{Mpc}$ scales, and r_0 is the cross-correlation length in comoving units. Note $r_0 \propto$ galaxy bias.

However, while $nP=1$ is the optimal density for a survey with a fixed number of objects, it is not necessarily optimal for a survey with a fixed amount of telescope time and a particular fiber density. We generally expect that somewhat lower number densities will be better: although one is extracting less information per

¹ We will use a cosmology of $\Omega_m=0.3$, $\Omega_\Lambda=0.7$, $H_0 = 100 h \text{ km/s/Mpc}$ favored by WMAP (Spergel et al. 2003) in which the Universe is 13.5 Gyr old for $h=0.7$ (the value we use for timescales).

unit volume, the required exposure times are sufficiently shorter that one can cover more than enough extra volume to compensate. It is not the purpose of this section to lay out this optimization, but rather to discuss the observational options in some detail.

3.3.1.1 Red Sequence Galaxies at $z \sim 1$

The red sequence galaxies are expected to have more *linear bias*, which reduces the number density required for acoustic oscillations and means we can work with brighter objects. Coil et al. (2004) for DEEP2 calculate a correlation length of $4.3 h^{-1}$ Mpc for galaxies redder than the median (rest-frame $U_{AB}-B_{AB}>0.7$) at $z=1$ corresponding to a bias $b=1.3$. However the break between red/blue sequences is closer to $U_{AB}-B_{AB}=1$. Coil et al. quote correlation lengths of $6.6 h^{-1}$ Mpc for “absorption line galaxies” but these are not likely to be pure red sequence galaxies either. Brown et al. (2003), using photometric redshifts in the NOAO Deep Wide-Field Survey (NDWFS), quote $8.4 h^{-1}$ Mpc for red sequence galaxies at $z=0.9$. We will adopt $7 h^{-1}$ Mpc as a reasonable value, which gives $b=2$. This is similar to the bias of the SDSS Luminous Red Galaxies at $z=0.35$. This gives us $n = 0.0003 h^3 \text{Mpc}^{-3}$.

First if we just consider the low redshift end, $0.7 < z < 1$, then we need to reach a sky density of 350 deg^{-2} . For DEEP2 galaxies with $U_{AB}-B_{AB}>1$ this is reached in this redshift range at $R_{AB}<22.1$. Similarly for $1 < z < 1.3$ the density is 465 deg^{-2} . For DEEP2 galaxies with $U_{AB}-B_{AB}>1$ this is reached in this redshift range at $R_{AB}<23.6$. We are of course fighting a rapidly declining tail: there are NO red sequence galaxies in our DEEP2 sample with $z>1.3$.

Thus it seems likely that a DEEP2-like selection of red galaxies (the cut corresponds to an *observed* frame $R_{AB}-I_{AB}>1$ at $z=1$) with $R_{AB}<23.6$ would do the trick. Assuming one could refine the photometric redshifts more accurately to maintain constant space density one would need $800 \text{ fibers deg}^{-2}$, well less than the WFMOS fiber density.

3.3.1.2 Blue Sequence Galaxies at $z \sim 1$

Again adopting DEEP2, the correlation length of blue galaxies at $z \sim 1$ is $3.9 h^{-1}$ Mpc. This gives us $n = 0.001 h^3 \text{Mpc}^{-3}$. The following table gives the corresponding sky densities and DEEP2 magnitude limit in redshift bins (for rest frame $U_{AB}-B_{AB}<1$ galaxies). The total for $0.7 < z < 1.5$ reaches 2300 deg^{-2} , which is comparable to the WFMOS fiber density. Note that the baseline survey in Section 3.4.2 uses half this number density, which would make the magnitude limits brighter by about 0.6 mag.

Redshift	Targets NEEDED deg^{-2}	Mag limit
0.7 – 0.9	444	$R_{AB}<21.9$
0.9 – 1.1	553	$R_{AB}<22.5$
1.1 – 1.3	640	$R_{AB}<23.0$
1.3 – 1.5	706	$R_{AB}<23.6$

Note there are insufficient numbers of objects in DEEP2 at $z>1.5$; this simply reflects wavelength and flux limits as [OII] is contained within the DEEP2 wavelength range for $z<1.44$. We explore below what is required to access this ‘redshift desert’.

3.3.1.3 Exposure Times for $z \sim 1$ Samples

We note we only need to select $R_{AB} < 23.6$ to meet the number density constraint, 0.5 mags *brighter* than the DEEP2 limit. Interestingly, similar magnitude limits are required for red and blue galaxies, albeit with the blue galaxies probing to slightly higher redshift.

DEEP2 using one hour exposures on Keck had a 75% spectroscopic completeness. Simple scaling brighter then gives an exposure time of ~ 40 minutes on Gemini (for the same instrument efficiency). A S/N calculation with the Purple Book efficiency gives $S/N=6$ in 40 mins in the continuum, adequate for absorption line redshifts. The $z \sim 1$ blue galaxies in DEEP2 typically have $[OII] > 3 \times 10^{-17}$ ergs $cm^{-2} s^{-1}$, for this flux we calculate a line $S/N = 20$. It would be expected that most redshifts would come from a combination of the emission line and continuum shape.

If one was relying on red-sequence galaxies, one would be more conservative and target $S/N=10$ requiring a 4x longer exposure. There appears to be a stand-off: blue sequence galaxies probably require 4x as many fibers, but only a quarter of the exposure time. The exact trade would require test observations. Of course, if one is devoting the entire WFMOS to $z \sim 1$ galaxies, then one would pick the blue galaxies: since the red galaxies underfill the fiber budget, one would prefer to reduce the exposure time. However, one could imagine that combinations with other programs might alter the trade. The key conclusion is that a $z=1$ survey is eminently feasible in 1–2 hour exposure times on an 8m telescope and no more than one WFMOS pointing is required per field.

These exposure times and S/N values do not include the effects of using a nod-&-shuffle observing mode, which is discussed below. The baseline $z \sim 1$ survey of blue galaxies would reach $R=22.7$ at $z=1.3$, which would decrease the exposure times by 6. Even with off-source time, 30 minutes total would clearly be satisfactory.

3.3.2 Redshift range $2.3 < z < 3.5$

Here, the obvious population to probe are the LBGs. These are strongly star-forming objects with blue spectra longward of the Lyman break (912 \AA). Shortwards of the break all light is absorbed by neutral HI – at $2.5 < z < 3.5$ they are thus selected by very red $U-B$ colors combined with very blue $B-R$ colors.

LBGs cluster on a scale of $4.0 h^{-1} \text{ Mpc}$ (Adelberger et al. 1998), suggesting a target density of $n = 0.001 \text{ Mpc}^{-3}$, which yields 4000 galaxies deg^{-2} per unit redshift. The correlation scale is almost identical to $z \sim 1$ blue galaxies in DEEP2, this implies that a reasonable model for blue galaxies is constant clustering in comoving space, an idea that is also supported by galaxy formation models.

Using the luminosity function of Steidel (1999), Table 3a shows that $n = 0.0017 \text{ Mpc}^{-3}$ is reached at $R_{AB} < 25$. A brighter cut of 24.5 yields $n = 0.0007 h^3 \text{ Mpc}^{-3}$.

Steidel's 2003 paper on the $z \sim 3$ sample quotes "S/N \sim few in the region 4000-6500 \AA " to get redshifts. Steidel quotes 2-3 hours in 1" seeing – for $V=25.5$ (assuming $V - R_{AB} \sim 0$) and 30% LRIS-R efficiency. We calculate using our tools $S/N = 4.3$

at 5000 Å in 3 hours for Keck/LRIS,² demonstrating that our S/N tool predicts sensible numbers. For the WFMOS Purple Book throughput, we have 17% throughput at 5000 Å and 60% of the collecting area of Keck, so the exposure time is now 3x longer = 9 hours. At V=24.5 we only need one hour to reach S/N=3.6.

At a number density of 4000 deg⁻², we would require 2 WFMOS configurations per region of sky. However, we find that the acoustic oscillation performance from half the number density is sufficiently good that one would prefer to work with the brighter galaxies. Therefore, we establish R=24.5 as the baseline survey. With a nod-&-shuffle observing mode, this would require 4 hours to reach the required S/N ratio.

Alternatively, one could plan to survey a larger number of galaxies and use only the 25% with strong emission lines, thereby requiring far smaller exposure times (and failing on 75% of the redshifts). Returning to V=25.5 and picking the 1/4th of galaxies with Lyα emission rest EW's > 20Å, then the line flux is 3×10⁻¹⁷ ergs cm⁻² s⁻¹. We calculate that 1800 sec yields S/N=10 in the line, probably the limit for reliable single line identifications. These emission line galaxies would again have $n = 0.0009 h^3 \text{Mpc}^{-3}$ and a sky density of 3600 deg⁻². If single line identifications were robust this would appear to be a more attractive option. This idea of targeting line emitters is similar to the VIRUS/IFU concept, except it is more efficient to put fibers on known objects rather than on random sky. This trade remains to be done in detail, and will require simulations of actual redshift recovery.

3.3.3 **Redshift desert 1.3<z<2.3**

As we have seen, the red sequence is disappearing rapidly over this redshift range, so the only hope for efficient redshifts is to chase the star-forming blue population. The problem is that for *normal galaxies* there are no strong emission line features between Lyα (1216Å) and [OII] (3727Å). One is therefore driven towards the UV to reach Lyα, or to the red to reach [OII], or into the IR to use Hα.

Unfortunately, none of these strategies opens this full redshift range. Our study of the constraints on dark energy allowed by different redshift ranges suggests that there is no compelling reason to push the redshift range by a small amount; if one does well at z=1.3 and z=2.3, the gains from closing the gap are small, and completely closing it would require pursuing both a UV and a red/IR strategy.

If we assume 4.0 h⁻¹ Mpc over 1.3<z<2.5 as at the neighboring redshifts, then the nominal target density of $n = 0.001 h^3 \text{Mpc}^{-3}$ produces a surface density of roughly 400 galaxies per deg² per δz=0.1 bin. Hence, covering the full range requires 4800 deg⁻², about twice the WFMOS fiber density. One could of course trim this by halving the redshift range or the number density.

² Assumptions: 70% of light in slit, dark sky, 4 electrons RBN, 2 pixels = 10Å = spectral resolution, 2 pixels = 1 arcsec aperture, not accounting for N&S beamswitching time or sqrt(2) factors, it's pretty much background limited so one can scale in the usual way.

3.3.3.1 A red-optimized strategy

The rest-frame optical emission lines ([OII], [OIII], H β , H α) are redshifted beyond 8000Å where they are in the bright forest of night-sky OH emission lines. Beyond 10000Å near-IR detectors are required and the OH gets worse. A landmark is $z=1.7$ where [OII] redshifts beyond the CCD cutoff *and* H α redshifts off the edge of the H-band into the water hole. High-resolution in the red and near-IR can help in allowing us to see galaxy lines in between the OH lines where the sky continuum is still relatively dark. Aided by nod & shuffle, the GDDS observed [OII] lines right through this redshift range.

We can use the [OII] luminosities in the DEEP2 $R_{AB}<24.1$ sample to guide us in a modest extrapolation from $z=1$ to $z\sim 1.5-2$. If we take the blue sequence galaxies ($U_{AB}-B_{AB}<1$) in a redshift shell ($0.9<z<1.1$) we find that 89% of them have $L[\text{OII}] > 10^{41} h^{-3}$ ergs/s. The number density per unit volume of these emitters is about $3.5 \times$ that required for acoustic oscillations. The corresponding line flux limit is 4×10^{-17} ergs $\text{cm}^{-2} \text{s}^{-1}$.

An immediate question is how good is the correlation between $L[\text{OII}]$ and UV luminosity? A good correlation would imply one could select brighter line emitters with broadband cuts. Unfortunately, there is a *lot* of scatter. We explored cuts in $U-B$ and M_B but failed to come up with a convincing method that did not sacrifice the 89% completeness.

If we take the $L[\text{OII}] = 10^{41} h^{-3}$ ergs/s limit, then at $z=1.7$ we need to reach a flux of 1×10^{-17} ergs $\text{cm}^{-2} \text{s}^{-1}$. The WFMOS S/N calculator indicates that this is a S/N=3 line detection in one hour for $R=3000$ in between the OH lines, suggesting an exposure times of 2–3 hours.

We note that a $z\sim 1.5$ analog of the DEEP2 survey could be defined by $z_{AB}<25.3$ and using VIz color cuts. Over $1.3<z<1.7$ this would select ~ 26000 galaxies deg^{-2} . If we again adopt $n = 0.001 h^3 \text{Mpc}^{-3}$ then we only need 1460 galaxies deg^{-2} , *so there may be considerable room for improvement in exposure times through multi-color selection.*

3.3.3.2 A near-IR strategy

Instead, one could observe these galaxies using H α in the 1–1.8 μm region. This line is 2–3 times brighter than [OII], we will assume an average value of $H\alpha / [\text{OII}] = 2$. Our S/N calculation for H α at $z=1.7$ gives $S/N = 9$ in one hour. This is viable for $R=4000$ or OH suppressed near-IR spectrographs.

There is an interesting open question regarding target selection. It is possible that a lot of the scatter between [OII] and UV may be due to metallicity effects. If so, then there *could* be considerably less scatter between H α and UV and then one *might* pull out the bright H α with clever multi-color selection. This would bring considerable benefit: if we ignore continuum luminosities and just consider the H α luminosity function from $z>1$ NICMOS slitless surveys then we get to the right space density at a line flux of $\sim 10^{-16}$ ergs $\text{cm}^{-2} \text{s}^{-1}$, a factor of ten gain!

3.3.3.3 *A blue-optimized strategy*

An alternate approach is to explore the UV around the 3200-4000Å region. Here the sky is very dark and there are no bright emission lines; however, one is fighting increasing attenuation at the atmospheric cutoff. Steidel et al. (2004) has shown that color selection can indeed successfully pull $z \sim 2$ star-forming objects out. Unfortunately, one needs to see the continuum because Ly- α is usually weak or in absorption.

Steidel et al. (2004) defines two-color selections in UGR (\sim UBR). The ‘BM’ selection ($1.3 < z < 2.1$) has about 14000 galaxies deg^{-2} with $R < 25.3$. The ‘BX’ selection ($1.9 < z < 2.5$) has about 19000 galaxies deg^{-2} with $R < 25.3$. Redshifts were obtained for 64% of candidates in 1.5hr exposures on Keck with 3200Å – 7000Å wavelength coverage. The bluest channel (3200–4000Å) was critical in identifying the $z < 2$ galaxies.

If a similarly efficient UV channel could be built for WFMOS, then the exposure times would be 2.5 hours. Indeed, this is very conservative, because the required target densities are well lower and so one could use brighter objects.

A key issue is fiber transmission. For reference a 50m run of high-OH silica fiber transmits 35% of the light at 3500Å (90 dB/km absorption). Low-OH fiber is opaque. Fiber lengths of $< 10\text{--}20\text{m}$ are preferred.

None of the low-resolution spectrograph designs considered in the Purple Book or here has significant performance at 3500Å. The best is the JHU design which achieves 5% (c.f. 20% for LRIS-B). However, the designs have not been optimized for this wavelength regime, which is beyond the scope of this study. Although improvements may be possible it would likely require a radically different approach.

3.3.3.4 *Number of redshift desert fibers*

It can be seen that ample targets exist within the redshift ‘desert’. For the red/IR strategies one would select at $z_{\text{AB}} < 25.3$ and try to use color cuts and/or photometric redshifts to maintain constant space density. It would be necessary to only observe 1 in 5 galaxies but there do not appear to be clever selection criteria to select the bright [OII] emitters. Thus one needs to reach the $10^{-17} \text{ ergs cm}^{-2} \text{ s}^{-1}$ line flux regime. A similar flux level is required for H α in the near-IR although there are more uncertainties about possible improvements.

3.3.4 **Nod & Shuffle and Exposure time**

Nominally nod & shuffle requires a sky exposure and thereby results in $\sqrt{2}$ more noise. This would result in us having to multiply the quoted exposure times by 4 to reach a given S/N. Of course, the gain from nod & shuffle is the considerable reduction in systematic errors from the sky subtraction. With clean spectra, lower S/N can be acceptable.

Figure 12 helps to demonstrate this power of nod & shuffle. Nod & shuffle is routinely used for faint fiber spectroscopy with fibers on the AAT. Spectra from a 13.5 hour integration using 2dF with nod & shuffle are shown in the figure. Poisson limited sky subtraction (red curve shows the location of sky lines) is obtained with fibers. Galaxies as faint as $R \sim 23$ have clean spectra and reliable

acceptable theoretical guidance, it seems very unwise to limit oneself to parameterized models that assume simplicity at higher redshift.

WMOS surveys at $z\sim 1$ and $z\sim 3$ would probe dark energy in three different and distinguishable redshift ranges: $0 < z < 1$, $1 < z < 3$, and $3 < z < 1000$. Moreover, it does this with both $D_A(z)$ and $H(z)$ constraints. This represents a considerable discovery space. Other methods (SNe, weak lensing, cluster counting) focus almost entirely at $z < \sim 1.5$. Even if WMOS and other methods were able to show that the dark energy obeys some simple model out to $z\sim 2$, WMOS would be able to test that nothing exotic happens out to $z=1000$.

There are many possible mechanisms that would cause deviations at higher redshift. Here we discuss only a few representative ones. A simple one would be that w is making a transition from 0 to -1 in the recent past. This can leave a small residual amount of dark energy at high redshift while making w close to -1 today. The high-redshift anomaly will disturb the distance ratio between $z=3$ and $z=1000$ and will affect structure formation.

We currently have no data at $z>3$ and the constraints on $w(z)$, even for quintessence-type models, are consequently very weak there. One interesting possibility is that there may have been a significant amount of entropy generated at $z>2$ due to the radiation from the decay of dark matter. This might have led to a modification of the expansion rate (the extreme limit being a brief radiation-dominated phase) that WMOS would be able to detect. The ability of the acoustic peak method to use a survey at $z=3$ to probe the effects of dark energy at $z>3$ while separating them from those at $z<3$ is very powerful in constraining such possibilities.

In standard quintessence models of dark energy, the Compton wavelength of the dark energy is very large (greater than 100 Mpc) so the dark energy does not cluster and has a speed of sound equal to the speed of light. However, dark energy may be more complex, with a time-dependent speed of sound and Compton wavelength or may show coupling to dark matter. Alternatively the cosmic acceleration may be due to a deformation of Einsteinian gravity at large scales (e.g., the graviton leaking into a 5th dimension as in Deffayet et al. 2002) in which case perturbation dynamics will not be that of General Relativity. All of these will alter the way clustering and structure formation take place. As a result interesting 'anomalies' marking new dark energy results may be lurking in the matter power spectrum (to be detected by WMOS surveys) or in the amplitude of the correlations (to be probed by weak lensing, clusters, and perhaps WMOS).

Typically we assume that $w(z)$ is monotonic. This is a strong assumption and probing it will directly probe the slope and curvature of the effective potential of the dark energy. However, any oscillations in $w(z)$ are suppressed in their effects on $H(z)$ and even more suppressed in $D_A(z)$. Because WMOS probes $H(z)$ directly, it will be able to address such issues better than methods that probe only $D_A(z)$.

In summary, WMOS surveys for acoustic oscillations offer important and unique avenues for probing dark energy, while still providing competitive limits on the more conventional parameterizations.

3.4.2 Two Baseline Surveys

Here we describe two basic surveys, along the lines of Seo and Eisenstein (2003). These are not fully optimized but should help to get a feel for the numbers.

First, we consider a survey of emission-line galaxies at $0.5 < z < 1.3$. A number density of $5 \times 10^{-4} h^3 \text{ Mpc}^{-3}$ would require 1000 targets per square degree. A hexagonal pattern of WFMOS field centers with full coverage but minimal overlap yields 1 pointing per 1.46 square degrees, and hence a nominal number of 1500 targets per WFMOS configuration. This underfills the WFMOS low-res fiber budget by about 40%, but this contingency could serve to insure against imperfect photometric redshifts or imperfect spectroscopic success rates. This number density only requires one to target blue galaxies down to $R=22.7$ even at $z=1.3$. 1400 such pointings would yield 2000 square degrees, which would survey $4h^{-3} \text{ Gpc}^3$ and 2 million galaxies. For a correlation length of $4h^{-1} \text{ Mpc}$, the performance is predicted with Fisher matrix techniques to be 1.0% on $D_A(z)$ and 1.2% on $H(z)$ (1σ). Numerical simulations suggest that the $H(z)$ performance is slightly overestimated (say, 1.3–1.4%), but that the $D_A(z)$ performance would match expectations.

Selecting such a survey is a straight-forward photometric redshift application, since the Balmer and 4000Å breaks are below 1 micron and hence accessible with CCDs.

The exposure time for such targets ($R < 22.7$ emission-line galaxies) are expected to be about half an hour. We'll budget 40 minutes to include overheads. That implies 900 hours of exposure for the survey, which is about 115 clear nights. The key wavelengths are around 8000Å, so the time need not be particularly dark.

Second, a survey at $2.3 < z < 3.3$ with a number density of $5 \times 10^{-4} h^3 \text{ Mpc}^{-3}$ would require 2000 targets per square degree. This is well-matched to the WFMOS fiber density, and would thus require one WFMOS configurations per point on the sky. Surveying $1.0h^{-3} \text{ Gpc}^3$ would require a survey of 300 square degrees (600,000 galaxies), which is 200 pointings. We predict that this would yield 1.5% performance on $D_A(z)$ and 1.8% performance on $H(z)$ based on Seo & Eisenstein (2003) and including the revisions from the numerical simulation performance as well as a decrease of the correlation length to $4h^{-1} \text{ Mpc}$.

These are the usual Lyman-break galaxies and the required densities are similar to those quoted by Steidel et al. (1996), once one accounts for the broader redshift range. Hence, the flux limit is $R < 24.5$. We expect exposure times of 4 hours, so this survey would require 800 hours of exposure, which is 100 clear dark nights. An alternative strategy, in which one takes short exposures of 4 times more objects, in order to find the 25% of strong line emitters (i.e., failing to get a redshift 75% of the time), gives a similar amount of exposure time, although such a strategy might benefit from more optimization.

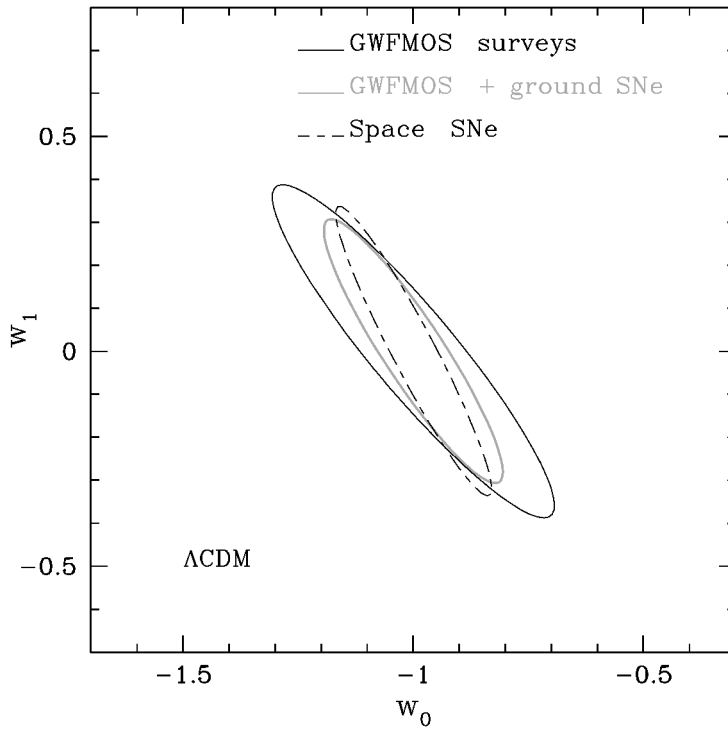


Figure 13: The performance on a model space of $w(z)=w_0 + w_1z$ from the baseline WFMOS surveys of 2000 square degrees at $z\sim 1$ and 300 square degrees at $z\sim 3$, including final SDSS and Planck constraints. We then combine the WFMOS constraints with aggressive ground-based supernova performance: 1% in distance for $9\Delta z=0.1$ bins up to $z=1$ (note that this differs in detail from that in Figure 14, but the effective leverage is similar). Were w_1 held at 0, then the error on w would be 5%. However, w_1 opens a difficult degeneracy for all methods. We compare the result to a mock JDEM satellite mission, with 16 1% distance bins up to $z=1.7$. This gives similar performance.

Together with Planck and the SDSS LRG sample, these surveys yield excellent performance on dark energy. Perturbing around $w=-1$ in a flat cosmology, we would measure w to within 8% for a constant w and would measure w_1 to 25% (1σ). This is shown in Figure 13. Including a ground-based supernovae program that measures 1% distances per $\Delta z=0.1$ bin out to $z=1$ drops the errors to 5% and 20%. If one extends this SNe sample out to $z=1.7$ as a Joint Dark Energy Mission (JDEM) might do, then one finds 3.5% and 22% performance ignoring WFMOS. In other words, the WFMOS surveys with ground-based supernovae does well compared to a space-based supernova program. These numbers are actually conservative regarding the impact of acoustic oscillation surveys on dark energy because the $w=-1$ fiducial model is a choice that favors low-redshift methods.

Figure 14 shows how the constraints in the model space of constant w and spatial curvature would be improved by WFMOS. Here, the degeneracy directions between the acoustic peak and supernova methods are very complementary. Together, the two can measure w to 5% precision while controlling the possibility of a small spatial curvature. This is very important: if SNe were to find a small deviation from $w=-1$ when interpreting as a flat universe, we would want to know if this ruled out a cosmological constant or simply was the effect of spatial curvature. WFMOS can distinguish these.

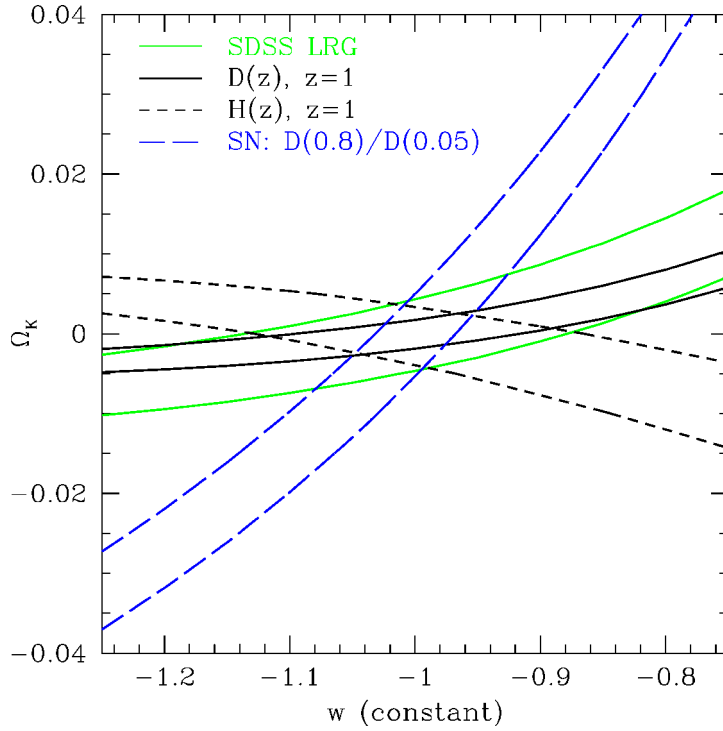


Figure 14: Constraints from various data sets in the model plane of spatial curvature and constant w . This would be an appropriate space if one wanted to show that w is not equal to -1 , while marginalizing over spatial curvature. Each pair of lines bracket a 1σ measurement in this space and assume that $\Omega_m h^2$ and the distance to $z=1000$ are known from the CMB. The green lines are a 3% measurement of the distance to $z=0.35$ from the final SDSS survey. The black solid lines are a 1% measurement of $D_A(z)$ from the $z=1$ baseline WFMOS survey. The black dashed lines are a 1.2% measurement of $H(z)$ from that survey. The blue dashed lines are a 1% measurement of the distance ratio between $z=0.8$ and $z=0$, as would be appropriate to an aggressive ground-based supernovae survey. Changing the upper redshift of the supernovae rotates these contours slowly; adding a $z=1.7$ constraint does not close the degeneracy well. One sees that supernovae and acoustic oscillations are very complementary in this model space. WFMOS plus the ground-based measurements would yield an error of about 5% on w .

In practice, the $z=1$ survey yields the more interesting constraints on "standard" dark energy models, i.e., those close to Λ CDM with bland redshift evolution, while the $z=2.8$ survey has the ability to detect the effects of dark energy at higher redshift.

Table 3. Summary of Baseline Survey Parameters. Note that the survey time is for clear, on-sky integration time. Actual telescope time will be about 1.7 times more to account for weather.

Redshift Range	R_{lim} (AB mag)	Number Density ($h^3 \text{ Mpc}^{-3}$)	Target Surface Density (deg^{-2})	Total Volume ($h^3 \text{ Gpc}^3$)	Total Area (deg^2)	Total Sample Size	Total Survey Time (hrs)
0.5 – 1.3	22.7	5×10^{-4}	1000	4	2000	2×10^6	900
2.3 – 3.3	24.5	5×10^{-4}	2000	1	300	6×10^5	800

3.4.3 *A Program for Optimization of the Experimental Design*

3.4.3.1 *Overview*

We are currently in the process of developing a full end-to-end program for the optimization of the experimental design. This program is intended to eventually allow a principled investigation of the optimum WFMOS survey configurations for dark energy science, once we enter the planning phase for the survey project. Our analysis is based on the Integrated Parameter Space Optimization (IPSO) methodology outlined in Bassett (2004; see also Bassett, Parkinson and Nichol 2004). Specifically, this framework will allow us to optimize between a large range of survey configurations, varying redshift binning, survey depths and areal target densities, and areal coverage; integrate over all possible dark energy models rather than assuming the single fiducial case of Λ CDM; and include the constraints from complementary datasets from other existing and planned surveys (e.g., SNAP, Planck).

We describe the current status of this effort in more detail below, but stress that this work is on-going and would be an important input for decisions taken during the design / survey definition phase of WFMOS.

3.4.3.2 *Testing analytical predictions of dark energy measurements for a fiducial Λ CDM model*

As discussed in Section 3.2.1, we have analytical assessments of the expected scientific performance of some default WFMOS dark energy surveys (e.g., see Figure 6). However, the default survey configuration of section 3.2 made little attempt to optimize WFMOS performance *for a fixed total survey duration*. There are a plethora of observational trade-offs: for example between the relative areal coverages of different redshift bins, in the context of realistic models for exposure times, and the evolution of the galaxy populations (as discussed in Section 3.3). The program currently includes the following features:

- We incorporate realistic exposure time calculations based on the updated WFMOS calculator.
- We include a better model for the expected number of strong emission - line galaxies as a function of redshift. This is obtained using the observed evolution of the COMBO-17 luminosity functions (Wolf et al. 2003), in conjunction with models for the observed change in the star formation rate density with redshift (Hopkins 2004). We use the scaling of Hippelein et al. (2003) to convert between broadband UV luminosities and [OII] emission - line fluxes.
- Given a trial survey volume and number of galaxies, we use the methodology of Blake & Glazebrook (2003) to generate many Monte Carlo realizations of the fiducial model power spectrum and thereby recover the statistical variation in the fitted baryon oscillation scales in the tangential and radial directions (i.e., the accuracy of measurement of the angular diameter distance and Hubble constant for this redshift bin). We include the convolving effects of the survey window function. We note that *this method only utilizes the oscillatory component of the power spectrum* rather than its overall shape, which is divided out prior to fitting of the acoustic scales. The

power spectrum shape does contain useful cosmological information, but is susceptible to a range of systematic effects such as galaxy biasing, redshift-space distortions, primordial tilts and non-linear structure growth. Neglecting the shape information implies that our results are conservative and robust.

- We combine our results for the angular diameter distance and Hubble constant (measured in a series of redshift bins) with other cosmological observations, including the recent SDSS measurement of the baryon oscillations at $z = 0.35$ (Eisenstein et al. 2005), and realistic priors on Ω_m and H_0 based on future Cosmic Microwave Background observations and other experiments.
- We compute marginalized errors on the dark energy parameters, as well as a Figure of Merit (FoM) for the survey configurations, using an Monte Carlo Markov Chain (MCMC) approach. We currently use the determinant of the sample covariance matrix as the FoM (see Bassett 2004).

This machinery can be used to perform a Monte Carlo Markov Chain (MCMC) search for the optimal redshift bins, i.e. the range of survey redshifts that, given a fixed amount of observing time, produce the smallest errors on the dark energy parameters. This approach naturally explores the trade-offs between going deeper, to obtain higher-redshift galaxies and a correspondingly longer redshift baseline for probing dark energy, versus areal coverage.

These questions have already been addressed in a general context and presented in Bassett, Parkinson & Nichol (2004), where it was discovered that the errors on the dark energy parameters were relatively insensitive to the position and number of redshift bins chosen; the general dark energy models considered did not prefer any particular redshift shell but slightly favored well-separated redshift bins to maximize the largest redshift leverage of the survey. This result can be readily understood: in the large parameter space inhabited by general dark energy models there cannot be a redshift configuration that is optimal for every model. In other words, for the testing of one particular dark energy model (such as a cosmological constant) there is an optimal set of redshift bins, but that particular configuration would likely not be optimal if the true dark energy model was not a cosmological constant.

The analysis of Bassett, Parkinson & Nichol (2004) was a full MCMC analysis of $H(z)$ constraints, including integration over the dark energy parameter space, but with a significantly simplified treatment of the assumed errors. Using the machinery discussed above we are in the process of revising our initial MCMC analysis to include a more detailed simulation of realistic errors as well as observational inputs such as the number of galaxies we expect to obtain per unit telescope time.

Initial tests suggest that our baseline survey strategy is sound, at least in its broad outline. We are continuing to work on our optimization calculations and will present the results from our analyses at a future date. The next improvements in our analysis will include:

- Extending the modeling of the galaxy population to $z > 1.5$ by incorporating realistic luminosity functions and exposure time estimates for galaxies in the

'redshift desert' ($1.5 < z < 2.5$) and Lyman Break Galaxies ($2.5 < z < 3.5$). This will enable us to investigate the worth of extending WFMOS surveys into the redshift desert, together with observational trade-offs between $z \sim 1$ and $z \sim 3$.

- Extending the modeling of the WFMOS instrument to permit multiple surveys to share the same configurations and to include overhead times.
- Exploring other parameterizations of dark energy models (e.g., Corasaniti et al. 2002), as well as integrating over a wider dark energy model space than presented above (see Bassett et al. 2004; Bassett 2004).
- Including information encoded in the shape of the power spectrum, which provides additional constraints on the cosmological model: including the parameter combinations $\Omega_m h$ and Ω_b/Ω_m together with the growth of structure with redshift (dg/dz). This latter has the potential to provide powerful constraints on dark energy (see Cooray, Huterer & Baumann 2003) if it can be untangled from the complexities of galaxy bias.

3.4.4 Trade-off of exposure time versus science gain

For the regime of WFMOS surveys, the precision on the distance measurements scales as the square root of the survey time. However, significantly smaller surveys would suffer worse than just the square root, for two reasons: 1) the survey areas would be too small to avoid blurring in Fourier space due to the survey boundaries, and 2) the survey volume would be insufficient to detect the small contrast of the acoustic signature.

3.5 Flow-down to instrument requirements, given optimisation.

3.5.1 Wavelength coverage and areal density

Target densities of order 2000 per square degree are required for surveys at $z=1$ and $z=3$ at the necessary number densities. Hence, 2000 fibers per square degree (as measured for a minimally overlapping full-coverage set of pointings, i.e., 1.46 deg² per 1.5 degree diameter field) is the desired sample.

The galaxies for such surveys will require of order 1 hour of exposure time for reasonable spectrograph design. Surveys for the acoustic oscillations are severely volume limited. At $z=1$, we must cover at least 1000 square degrees (and the baseline calls for 2000 deg²). As the exposures and overheads will surely be of order 0.5 hours or more, this pushes the field of view to be large so as to minimize the number of pointings. A WFMOS field of 1.5 degrees would require 1400 pointings, which is of order 90 clear nights at 40 minutes per pointing. This is already a very large project, so one should not drop the field of view below this.

It is important to push the throughput to the best possible out to 1 micron. Surveys of galaxies at $z \sim 1$ are central to the WFMOS $w(z)$ program and high throughput in the range of 8000-9500Å is critical. Accessing galaxies at $z \sim 2.5$ is best done in the blue with the Lyman alpha line. This requires high throughput at 4000Å. Extending this throughput into the UV (i.e., 3500Å) would allow one to study $z=2$, but is not seen as a critical requirement.

We do not see a compelling reason to push to $1.3 < z < 1.7$, where a IR spectrograph might do better than a silicon detector. Even if the dark energy equation of state varies quickly, the response in the Hubble parameter is always of order the Hubble time. This means that precision measurements at $z=1$ and $z=2.5$ can pick up the change; we do not need to monitor each and every redshift.

3.5.2 **Fiber allocation (given a clustered target set and multiple spectrographs)**

The WFMOS design does not permit an arbitrary distribution of the fibers within the focal plane. This means that for a realistic galaxy distribution, one would not be able to place a fiber on every (or even nearly all) targets unless one is willing to underfill each pointing and thereby incur large numbers of “filler” targets.

However, sparse sampling is acceptable in the study of large-scale structure so long as one knows exactly what the sampling fractions are at every point in the sky. Hence, the challenge for using WFMOS is *not* to achieve high total completeness but rather how to allocate the fibers in such a way that the sampling fractions don't develop significant uncertainties that are correlated over large angles on the sky. That is, one doesn't want a cluster of objects at one location to draw in the fibers and create an undersampling a large distance away, because that would appear as a large-scale density fluctuation. Our scales of interest are $10h^{-1}$ Mpc, which is about 20' on the sky at $z=1$ and 10' at $z=3$. This is considerably larger than the inter-fiber spacing or the fiber patrol radius.

It is easy to see that there is a trivial solution that would keep large-scale statistics unbiased. One divides the focal plane into disjoint regions that can each be served by a single fiber (i.e., we neglect the fact that some points could be served by multiple fibers and instead assign every point to a single fiber). If a region contains more than one target, a random target is chosen and assigned to the fiber. Then in the clustering analysis, every target that got a fiber is weighted by the ratio of the number of targets in its region (i.e., if a region has two targets, the one that is picked gets a weight of two).

To see that this scheme is unbiased in the large-angle correlation function, consider two regions A and B, the first of which has two galaxies. In a complete survey, one would count the pairs A1 - B and A2 - B into their respective separation bins. However, in our incomplete survey, 50% of the time one would count the A1 - B pair with double weight and skip the A2 - B pair; in the other 50%, one would do the opposite. Hence, averaged over many examples, the correlations are unbiased ($50\% \times 2 = 1$). The noise is higher, but this is exactly the familiar shot noise. The only error from the sparse sampling is that the pair A1 - A2 is never counted in the incomplete survey and hence the correlations at that separation are biased. However, so long as this separation is small compared to the physical scale of interest, this is acceptable.

The above trivial scheme works well when the target density is considerably higher than the fiber density, but it is suboptimal when the target density gets low enough that many regions are empty. It is very likely that there are better algorithms that would take advantage of the larger patrol radii to handle cases of comparable target and fiber densities while maintaining control over the selection function. For example, one could attempt to assign the fiber from an empty region to a randomly selected neighbouring region with multiple targets, and if this fails,

use the fiber for sky. However, the trivial algorithm isn't *that* bad, and so we have not yet pursued simulations of more clever schemes.

3.5.3 Fiber rearrangement time, accuracy requirements

The required surveys are large, and hence overheads must be minimized. Being able to rearrange fibers at any elevation angle, so as to avoid slewing the telescope to zenith or a lock position, is highly desirable to avoid overhead.

Minimizing aperture losses is crucial and so fibers must be positioned to 0".1 accuracy. This also places requirements on the astrometry of the input target catalogs and the relative astrometry of these catalogs to the guide stars (which may saturate the deep imaging data sets).

3.5.4 Acquisition and guiding requirements

Strong line emitters at $z=1$ or even $z=3$ do not take particularly long for WFMOS to get a successful redshift. While we have not called for it in our baseline, due to uncertainties of exactly what nature will provide and imaging surveys will isolate, it seems appropriate to retain the capability for efficient use of the telescope with exposure times of only 30 minutes. This means that one would like to be able to rearrange the fibers, slew, and acquire the target field in of order 5 minutes, preferably doing some of these tasks simultaneously. Of course, an appropriate precursor imaging survey would allow us to be completely prescriptive about where the acquisition and guide stars are.

Being able to rearrange a portion of the fibers while keeping the same pointing center without incurring significant additional overheads, such as being forced to reacquire the field, is a desirable goal.

It is worth mention that the dark energy science case (and most science cases with such a wide field instrument that we can imagine) do *not* require that a guiding solution be available for every single pointing center on the sky. If one has to move the nominal center by a few arcminutes to find a guide star, this is acceptable. Of course this search would occur in the planning stages not on-the-fly at the telescope!

3.5.5 Resolution and calibration requirements, including sky subtraction

For the dark energy science case, redshifts need only be accurate to about 600 km/s to resolve the acoustic oscillations along the line of sight. However, auxiliary science with the same data set at $z\sim 1$ would likely desire 100 km/s to resolve galaxy groups and map the small-scale redshift distortions. It is essentially impossible to measure a spectroscopic redshift worse than this using optical lines by noise alone. Keeping the wavelength solution stable to better than 100 km/s would be strongly desirable, but this will not be challenging particularly for bench-mounted spectrographs. The SDSS currently achieves 10 times better calibration than this.

At $z>2$, the Lyman-alpha line itself has velocity offsets of order 300 km/s. This is not a problem for the acoustic oscillations, but again it is pointless not to map the wavelength solution much better than this.

The need for 600 km/s accuracy redshifts means that one only needs rather modest resolution. $R=500$ would be fine. However, the redshift range $0.7 < z < 1.5$ is central to the science case, and this places the [OII] line beyond 7000\AA , where the sky is thick with OH lines. By working at higher resolution, one can work between the sky lines. One also resolves the [OII] doublet, thereby assuring a secure line identification. A resolution of $R=3000$ is the goal here, and the returned performance is a smooth function up to that point.

Sky subtraction is critical, as the targets are faint. While one might hope that for some applications it would be possible to use sky fibers to build and subtract a model for the sky, we think that the nod-&-shuffle technique will be the default mode. The spectrographs and control systems must be required to support this mode. Note that doing nod & shuffle does not lessen the interest in working between the sky lines: even if the sky subtraction is perfect, one still wishes to reduce the Poisson noise and minimize the blending of the sky lines.

If the high-resolution spectrographs do not have detector space to shuffle the charge, then they should be enabled to close their shutters while the telescope is nodding off-source. At least, this would preserve half the exposure time for parallel science.

3.5.6 Data reduction requirements

Reducing an exposure to assess the signal-to-noise ratio (SNR) in less than the time required to complete the next exposure is a requirement. This has been used very successfully in the SDSS to monitor the accumulated SNR so that one can integrate to a target SNR rather than a simple exposure time. The SDSS has been doing this for several years on a single workstation handling about 15% of the WFMOS data rate. Hence, we expect that it will be straight-forward to achieve this capability.

Searching the reduced coadded spectra for secure redshifts in the time required for the next exposure would permit a mode of operation in which one integrated for some period of time (say, 30 minutes) and then reassigned fibers that had yielded easy redshifts in a fraction of that time (say, 20 minutes). This is not a requirement, but it could lead to more efficient surveys.

3.6 Discussion of the availability of the required imaging data.

Targeting WFMOS of course will require deep, wide-field multicolor imaging surveys. However, several such projects are well underway. PanSTARRS and the Dark Energy Camera/Survey will provide thousands of square degrees of sufficiently deep multi-color optical data. Existing facilities, such as the CFHT Megacam and the NOAO Mosaic camera, could also map large regions. By 2010, it seems a certainty that at least 1000 square degrees of sufficient imaging will exist in either hemisphere.

There are several near-infrared ground-based options as well. UKIDSS, NEWFIRM, and VISTA will all be in operation in the next couple years and are planning to cover large amounts of sky. While these maps will not be deep enough to detect blue galaxies at $z > 1$, they would be good for detecting red galaxies at $z \sim 1$, if that were the choice, and discriminate low-redshift interlopers from the high-redshift selections.

For $z \sim 3$ surveys, deep U band data is important. This is a challenge because the next generation of major CCD cameras, e.g., PanSTARRS, DEC, and perhaps LSST, have generally compromised away from U band. However, the WFMOS surveys at $z \sim 3$ are only hundreds of square degrees, not thousands. A concerted effort on existing blue sensitive cameras, e.g., CFHT-MegaCam, NOAO-MOSAIC, or LBT/LBC-blue, should be sufficient.

It is worth mention that the $z=1$ emission-line galaxies might be efficiently selected as dropouts from the far-UV channel (1350–1750Å) of GALEX. The medium-depth imaging survey (MIS) is using 2 months of GALEX time to cover 1000 square degrees to a depth of 23 mag (AB) in the two channels. From the 1500Å luminosity function of Arnouts et al. (2005) this depth is about that required at $z=1.3$ to reach the desired number density. Of course, ground-based optical data to about 24 mag would still be required for careful interpretation of the GALEX catalogs. We have not investigated this possibility in detail.

3.7 Telescope impact on science.

3.7.1 Gemini North vs. Gemini South vs. Subaru.

The dark energy science case is agnostic as to hemisphere. We expect that good imaging data sets (in optical, NIR, and UV) will exist in both hemispheres and along the celestial equator.

Similarly, the dark energy science case does not depend on the question of Gemini-N versus Subaru, save in the availability of telescope time and speed of deployment.

3.7.2 Constraints on observatory operations.

The dark energy survey regions must be at least 15 degrees across at $z=1$ and 5-7 degrees at $z=3$. Hence, there will not be many of them across the sky. This means that there is some risk that one could be forced to observe at higher than desirable airmass. This is particularly a problem for the $z=3$ survey which relies on Lyman-alpha lines in the blue.

One could imagine mitigating this risk by pool-scheduling the telescope with other observing programs, by clustering the dark energy fields in right ascension and then focusing observations into a small number of months, or by placing the dark energy fields off the equator so as to stretch the airmass.

3.8 Opportunities for additional simultaneous, independent science programs

There is a tremendous opportunity for simultaneous science with a WFMOS dark energy survey, as this is a simple chance to acquire an hour of integration on a 8-meter telescope on thousands of targets spread over a thousand square degrees. Rare objects that would otherwise be impractical to survey in large numbers become a small overhead on the dark energy survey.

One could imagine a mode in which one team specifies the survey area, exposure time, and spectrograph configuration and is granted N% of the fibers and then the

remaining fibers are assigned to other targets, possibly by a time-allocation panel. These targets are observed with some priority, which would have to be investigated to ensure that it didn't cause artifacts in the spatial correlations.

The number of “parallel” science targets need not be small. For example, the $z=1$ baseline survey only calls for 1000 targets per square degree, which leaves something like 40% of the low-resolution fibers available for other programs.

This style of small survey has been immensely successful in the SDSS. The SDSS has over 30 categories of target selection, with the result that rare classes of stars and quasars that would otherwise have been impossible to survey in any multi-object way now have tens of thousands of high-quality spectra. To not enable small amounts of rare object science with WFMOS would be a severe error!

The obvious example here is the high-resolution fibers. Any pointing for a galaxy redshift survey would want to assign the high-resolution fibers to bright stars in the field. This would acquire a large set of high-resolution spectra at high galactic latitude, albeit not one that samples the full galaxy well (since the extragalactic surveys will need to concentrate on a few fields). While the exposure times for the baseline $z=1$ survey are shorter than what is needed to get chemical abundances on faint stars, one could get good velocities on faint stars and abundances on brighter stars. At 18th mag, there are roughly 400 stars per WFMOS field. Even if only 200 of these are available to a high-resolution fiber, this would still yield over a quarter-million high-resolution spectra.

3.9 Other facilities

3.9.1 Complementary Facilities

The cosmic microwave background is important for the low-redshift acoustic oscillation method because it is the CMB's measurement of $\Omega_m h^2$ and $\Omega_b h^2$ that provides the distance scale. Current CMB measurements constrain $\Omega_m h^2$ only to 10% accuracy, which is not quite enough to support WFMOS-type surveys. Future WMAP data and improvements in ground-based measurements at 10' scales and below will considerably improve the situation, as will improved modeling of intermediate-scale galaxy correlations (as discussed in Eisenstein et al. 2005). The Planck satellite, scheduled for launch in 2007, will take $\Omega_m h^2$ to 1% precision, which makes the error in $\Omega_m h^2$ subdominant for WFMOS acoustic measurements.

As we will describe below, we regard most dark energy probes as complementary, although the tendency is to see them as competing since they all quote errors on w .

3.9.2 Competing Facilities, both spectroscopic surveys and photometric redshift surveys.

In the next decade, there will be a number of state-of-the-art projects studying supernovae, weak lensing, and cluster counting. For supernovae, we list the *Essence* project, the CFHT Legacy survey, and PanSTARRS. For lensing, we list PanSTARRS and the Dark Energy Survey (using the Dark Energy Camera to be built for the CTIO Blanco telescope). Cluster counting will be advanced by these lensing surveys as well as by the South Pole Telescope Sunyaev-Zel'dovich map.

However, it is not obvious that one should count other dark energy methods as “competing”. It is possible that new physics required to explain the acceleration of the expansion changes the growth of structure, so that precision weak lensing and cluster counting probe dark energy in a different manner. It is important to have precision measurements of dark energy from both kinematics and structure formation, so as to be able to test for deviations from general relativity.

While supernova distances are probing the same quantities as acoustic oscillations, even this can be complementary: SNe are higher precision for D_L but are limited in that they can only measure relative distances. This is a disadvantage in constraining spatial curvature or any model that puts significant dark energy at $z > 2$, since it means that one cannot directly compare to the CMB. The acoustic peak method allows one to compare to the distance to $z=1000$ very robustly.

Indeed, we find that combining the acoustic method with supernovae yields powerful complementarity, particularly if one wishes to exclude the possibility that a small but non-zero spatial curvature is affecting one's inference for the dark energy equation of state.

3.9.3 A Road-Map for Acoustic oscillation surveys over the next decade

We divide the coming surveys into four generations, of which WFMOS is the third.

The first generation surveys are the SDSS and 2dFGRS. These have already detected the acoustic signature and used it to place cosmological constraints. The SDSS is currently applying for an extended survey to 2008. If funded, then the final sample will be twice the published sample, enabling the distance measurement to reach 3% precision to $z=0.35$.

The second generation surveys may be carried out using AAT/AAOmega and Subaru/FMOS. These are both wide-field fiber-fed spectrographs. Given the recent SDSS and 2dFGRS results, it is likely that $w(z)$ surveys will be undertaken with these instruments.

AAOmega is an upgrade to the 2dF spectrographs, using the 2dF fiber positioning system on the 3.9m Anglo-Australian telescope. An example of a survey that could be performed with AAOmega would be to survey luminous red galaxies at $0.5 < z < 0.9$ to a number density of $2 \times 10^{-4} h^3 \text{ Mpc}^{-3}$. This would require 150 galaxies per square degree, thereby filling the fibers, and would survey $0.75 h^3 \text{ Gpc}^3$ comoving in 1000 square degrees. We estimate that this would yield similar performance to the final SDSS sample, about 3% precision, but at a higher redshift $z=0.7$. However, it will require about 200 clear nights, perhaps 400 assigned, which is obviously a major project. There has been no commitment from the AAO or its community that such a project will occur.

FMOS is a 400-fiber system with a 0.5 degree field of view feeding OH-suppressed IR spectrographs on the 8m Subaru telescope. Its primary goal is to survey $z \sim 1.5$ galaxies using the $H\alpha$ emission line. A survey at $1.0 < z < 1.7$ with a number density of $10^{-3} h^3 \text{ Mpc}^{-3}$ would require 2400 targets per square degree, which is well-matched to the fiber density of the instrument. The exposure times are expected to be of order 1 hour for targets of this density, although determining which galaxies have the strong $H\alpha$ lines is not yet a solved problem. If this can be

done efficiently, then one can do 1000 pointings in 1000 hours (roughly 100 nights) and cover 160 square degrees and $0.4h^{-3}\text{Gpc}^3$. This would yield 1.5% precision on $D_A(z)$ and 2.0% precision on $H(z)$. Such a survey would nicely complement WFMOS. WFMOS is higher precision but at interestingly different redshifts.

LAMOST is a Chinese project to use a 6-meter Schmidt telescope (4-meter effective aperture) with a 5 degree field of view and 4000 fibers. Nominally, this is 10 times faster than the AAOmega system, although the instrument and telescope performance are unknown. It is unlikely that the performance beyond 8000\AA will be good enough to justify surveys at $z>1$, in which case an acoustic oscillation survey would not fully fill the fibers, decreasing the effective advantage. It seems possible that LAMOST could match the SDSS performance in of order 50 clear dark nights, i.e., with a few years of surveying, it could halve the errors to $\sim 1.5\%$ at $z=0.6$. This would complement WFMOS in redshift range.

The third generation would include WFMOS. Another possibility is the VIRUS concept for the Hobby-Eberly Telescope. This is a large set of UV-sensitive IFU spectrographs. The intent is to do blank sky pointings so as detect Ly α - emitting galaxies at $1.8<z<3.5$. At this time, it is not clear what the density of such strong line emitters are, and so the time required for a significant project is not known. However, we know that the frequency of such objects is small enough that the HET/VIRUS will detect at most 1000 per hour, which is a similar but slightly smaller rate than WFMOS working on Lyman-break galaxies. Hence, the two may be reasonably matched. VIRUS has no capability at $z<1.8$.

It is possible that other instruments or even new telescopes could appear in this generation, given the long lead time for building WFMOS.

It is also conceivable that existing wide-field multiobject spectrographs might attempt such a $w(z)$ survey. However, they would be very inefficient at doing so, and as of yet, there are no such surveys even in the planning stages. For example, Magellan/IMACS, which has the largest field of view of the current beam-fed (and therefore efficient) spectrographs on a large aperture telescope, has a survey speed (defined as $[\text{Aperture}]^2 \text{FOV } \eta$), where η is the spectrograph efficiency) which is $\sim 10\text{--}15$ times slower than WFMOS (e.g., see the Purple Book). Even the $z\sim 1$ survey described here would therefore take over a 1000 clear nights, even if we assume instrument overheads comparable to those required for WFMOS, making the survey almost infeasible.

A wider field instrument, like MMT/Hectospec, with a field of view of 0.78 sq deg, would be able to cover the requisite area more quickly, but has a much lower fiber density, requiring multiple pointings per sky position to build up the target density. Also, the lower efficiency and longer overheads of Hectospec work against it. Again, one projects very long surveys, over 1000 nights.

Wide-angle photometric surveys should also be weighing in on this time scale. A photometric survey with good photometric redshifts can achieve similar performance on $D_A(z)$ (but not $H(z)$) if it covers a factor of 10 more area than the spectroscopic survey (Seo and Eisenstein 2003; Blake and Bridle 2004). Hence, competing with these WFMOS surveys would require imaging half the sky for $z=1$ galaxies and about 3000 deg^2 for $z=3$ galaxies. Projects such as PanSTARRS may approach the first of these on a ten-year time scale, but it is a challenging

measurement requiring excellent calibration. Our feeling is that any photometric detection of the oscillation signal at $z \sim 1$ will not come before WFMOS is operational and would likely require spectroscopic confirmation.

The fourth generation would be much larger surveys. One possibility is the Baryon Oscillation Probe, a MIDEX-level satellite that could survey 10,000 square degrees at $z < 2$ (Glazebrook et al. 2004). Giant redshift surveys have also been put forward as a major project for the Square Kilometer Array. Some implementations of the SKA would permit 21-cm surveys over the entire visible sky out to $z = 1.5$, thereby mapping the oscillations with tremendous accuracy out to that redshift (Blake et al. 2004). However, the SKA is on a much longer timescale than WFMOS (2020?), with costs of order 1 billion, and only one of the several implementation strategies permit the wide-field survey.

3.10 Key risks to science goals.

3.10.1 Competition in 2012: How big a survey will be required?

There will surely be many dark energy focused projects in 2012. Some will have stronger statistical precision on w than the WFMOS surveys, particularly if the dark energy is close to a cosmological constant. However, as stated above, it is a mistake to think about this purely as a numbers game. Different methods probe dark energy in different ways and discrepancies could reveal important differences in the physics of the acceleration of the universe. Moreover, different methods will differ in their systematic errors. The acoustic oscillation method is thought to be the most straight-forward of the methods.

Hence, the issue is not “who has the best w error bar”, but rather insuring that different methods have similar w error bars so that they can be cross-compared with full leverage. We think that 1–1.5% errors on distances are appropriate for 2012. This corresponds to 2-3% flux uncertainties in the supernovae, likely similar to the systematic errors there. It is a 4% volume change, so equivalent to a 2% change in the mass threshold of a cluster sample, which would be a healthy goal for cluster methods in the next ten years. It is harder to compare directly to a weak lensing figure of merit, but we note that most estimates in the literature neglect systematic errors that are clearly present in today's analyses at a level that would not be acceptable in 2012.

These other methods will improve from today only by significant improvements in the control of their systematic errors. As such, it is difficult to predict what the exact ratio of performances with WFMOS will be. We expect that WFMOS will be fully competitive, but that it is wiser to focus on the complementarity between different methods.

3.10.2 Competition in 2012: Spectroscopic redshift surveys.

Rival spectroscopic surveys to measure the acoustic oscillations using methods similar to those outlined here would indeed be a risk. No extant multiobject spectrograph can really compete with WFMOS (cf. the Purple Book). Also, we are not aware of any funded instrumentation that would compete with WFMOS. Nevertheless, if WFMOS is slow to acquire funding, be late in deployment or in completing its survey, then it is possible that some currently unproposed

instrument could beat it to the punch. We believe that Gemini has a significant advantage, given its early entry into planning the future of multiobject spectroscopy. We are also aiming to mitigate this risk (i.e., of other competitors), by incorporating the (international) astronomical community interested in the dark energy science into a coherent and funded scientific collaboration, following a road map such as the one outlined in Section 3.9.3.

3.10.3 Competition in 2012: Photometric redshift surveys.

A deep multicolor photometric survey of most of the sky (say 20,000 square degrees) would, in principle, be able to detect the signature of the acoustic oscillations in the angular power spectrum of galaxies. A prerequisite for such a survey would be accurate photometric redshifts (to $\sigma_z/(1+z) < 0.04$) and no significant systematic errors (e.g., due to spatial variations in photometric calibration) across the survey area. For accurate and robust photometric redshifts and clean selection of samples in specific photo- z bins, such a survey would have to obtain observations in a large number of filters. Hence, although such a survey is in principle feasible and capable of yielding a precision similar to WFMOS for $D(z)$ at $z=1$, it is unlikely to be available until the culmination of the LSST surveys (circa 2015 at the earliest). The PanSTARRS survey has chosen to cover smaller areas of sky to greater depth, and is therefore unlikely to provide the data set required for a comparable $w(z)$ constraint by this method. It is also worth noting that such a survey would be more risky than our proposed spectroscopic survey; it has at least been experimentally determined that we can observe the acoustic oscillations using our proposed method.

3.10.4 Exposure time estimates

We have estimated 40 minutes per configuration for the $z=1$ baseline survey and 4 hours per configuration for the $z=3$ survey. These estimates reflect our understanding of the galaxy populations and the instrument throughputs. Indeed, if the spectrograph throughput can be improved, then the times will be conservative. However, if instrument performance lags or if the galaxy populations or color selection proves more difficult, then the required number of nights to reach a given survey size may increase.

3.10.5 The cosmological constant null result, i.e. would it be a failure if we just found $w=-1$?

If WFMOS were to provide the first convincing evidence that $w=-1$ to high precision that would not be a failure any more than the BOOMERanG or WMAP results that the cosmos is flat to high precision were a failure. In reality, proving anything to high precision provides a firm foundation for future progress, informing future theories and providing rigorous standards that must be met by new candidate theories.

And while the flatness of the cosmos has a natural explanation - inflation - the existence of a tiny cosmological constant is a thorny issue for quantum gravity and would stimulate and motivate theoretical work for years and perhaps decades to come.

Also, since it will be impossible to show $w=-1$ with infinite precision there will remain classes of dynamical models which can fluctuate either in space or time that are not ruled out. This will stimulate new experiments to search for new distinguishing features.

3.10.6 Failure of the Planck mission

Our $w(z)$ estimates have been based on the assumed performance of the Planck CMB satellite. At the base level, Planck should measure $\Omega_m h^2$ and the distance to $z=1089$ very accurately. However, the 3 years of WMAP data that already exists will measure the angular acoustic scale very accurately and will yield 1% measurements of the sound horizon. In other words, existing data is roughly what is required for WFMOS complementarity.

The more serious loss is that the superb precision of the Planck mission is useful for excluding more exotic models, such as minor admixtures of isocurvature modes and $z=10^4$ particle decays, that could bias the acoustic signatures.

The relevant data from Planck is at $l=1000-2000$, not large angles, so it can be done in part from the ground. Ground-based groups have been avoiding such projects simply because Planck is around the corner. Were Planck to fail, one would surely see a major ground-based effort to try to recover some fraction of the mission. One would also likely see a future CMB satellite: the cosmological opportunity of the CMB is far too great to ignore.

Hence, while the loss of Planck would be a moderate impairment of the immediate interpretation of the WFMOS data, it is neither severe nor permanent.

3.10.7 Telescope access

A major risk to the science goal is that the telescope allocation committees might not wish to invest in so large a project (several hundred nights) or might spread the time out over such a long period of time that the result is not competitive when it arrives. This is not a situation in which dividing the time into 10 similar but disjoint projects, each with different experimental design and in different parts of the sky, will yield a similar or greater body of knowledge at the end. The survey requires a homogeneous design in a few contiguous patches of sky. The formation of a key project team with guaranteed access and allocated time is critical to the success of this project.

3.10.8 Imaging surveys for photometric pre-selection

As discussed in Section 3.6, multicolor imaging surveys are required to select targets in the desired redshift ranges. While these surveys are clearly feasible (and several are being started, see Section 3.6) they need to be designed and performed in a manner consistent with the WFMOS survey. For example, the survey regions at $z=1$ ($z=3$) should be at least 15 degrees (7 degrees) on a side to eliminate aliasing, and U -band imaging may need to be added to surveys such as DES or PanSTARRS. A WFMOS key project team needs to begin coordinating these efforts soon after WFMOS is funded.

3.11 **References**

- Alam U., Sahni V., Saini T.D., Starobinsky A.A., 2003, MNRAS, 344, 1057
- Alcock, C., & Paczynski, B., 1979, Nature, 281, 358
- Amendola, L., Quercellini, C., & Giallongo, E., 2004, MNRAS, 357, 429
- Armendariz-Picon, C., Mukhanov, V. & Steinhardt, P.J., 2000, PRL, 85, 4438
- Arnouts, S., et al., 2005, ApJl, 619, L43
- Bashinsky, S., & Bertschinger, E., 2001, PRL, 87, 1301
- Bassett, B.A., 2004, astro-ph/0407201
- Bassett, B.A., Parkinson, D., & Nichol, R.C., 2004, astro-ph/0409266
- Bennett, C. et al., 2003, ApJS, 148, 1
- Bennett, C. et al., 2003, ApJ, 583, 1
- Benson, A., et al., 2000, MNRAS, 311, 793
- Bernstein, G., & Jain, B. 2004, ApJ, 600, 17
- Bilic N., Tupper G.B., Viollier R.D., 2002, Phys.Lett. B, 535 17
- Blake, C., & Bridle, S., 2004, MNRAS, submitted; astro-ph/0411713
- Blake, C., & Glazebrook, K., 2003, ApJ, 594, 665
- Blake, C., Abdalla, F., Bridle, S., & Rawlings, S., 2004, New Astron. Rev., 48, 1063
- Broadhurst, T.J., Ellis, R.S., Koo, D.C., & Szalay, A.S. 1990, Nature, 343, 726
- Caldwell, R.R., Dave, R. & Steinhardt, P.J., 1998, PRL, 80, 1582
- Cole, S., et al., 2005, MNRAS, submitted; astro-ph/0501174
- Coles, P. 1993, MNRAS, 262, 1065
- Cooray, A., Hu, W., Huterer, D., & Joffre, M., 2001, ApJ, 557, L7
- Deffayet, C., Dvali, G., & Gabadadze, G., 2002, PRD, 65, 044023
- Dolney, D., Jain, B., & Takada, M., 2004, MNRAS, 352, 1019
- Eisenstein, D. J., Hu, W., & Tegmark, M., 1998, ApJl, 504, L57
- Eisenstein, D. J., Hu, W., & Tegmark, M., 1999, ApJ, 518, 2
- Eisenstein, D.J., & White, M., 2004, PRD, in press

Eisenstein, D.J., 2003, in "Wide-field Multi-Object Spectroscopy", ASP Conference Series, ed. A. Dey

Eisenstein, D.J., et al., 2001, AJ, 122, 2267

Eisenstein, D.J., et al., 2005, ApJ, submitted; astro-ph/0501171

Freese K., & Lewis M., 2002, Phys.Lett., B, 540, 1

Frieman, J.A., Hill, C.T., Stebbins, A., & Waga, I., 1995, PRL, 75, 2077

Glazebrook, K., et al. 2004, Nature, 430, 181; astro-ph/0410037

Hamilton, A.J.S., 1998, "The Evolving Universe", ed. Hamilton (Kluwer Academic), p. 185; astro-ph/9708102

Hippelein, H., et al., 2003, A&A, 402, 65

Holtzmann, J.A. 1989, ApJs, 71,1

Hopkins, A. 2004, ApJ, 615, 209

Hu, W. & Haiman, Z., 2003, PRD, 68, 3004

Hu, W., & Sugiyama, N. 1996, ApJ, 471, 542

Jain, B., & Taylor, A., 2003, PRL, 91, 1302

Kaiser, N., 1986, MNRAS, 219, 785

Knop, R. A., et al., 2003, ApJ, 598, 102

Linder, E.V., 2003, PRD, 68, 3504

Matsubara, T., 2004, ApJ, 615, 573

Meiksin, A., White, M., & Peacock, J.A., 1999, MNRAS, 304, 851

Peebles, P.J.E. & Yu, J.T. 1970, ApJ, 162, 815

Percival, W.J. et al. 2002, MNRAS, 337, 1068

Percival, W.J., et al., 2001, MNRAS, 327, 1297

Perlmutter, S., Turner, M.S., & White, M. 1999, PRL, 83, 670

Perlmutter, S., et al. 1999, ApJ, 517, 565

Ratra, B. & Peebles, P.J.E., 1988, PRD, 37, 3406

Riess, A. G., et al., 2004, ApJ, 607, 665

Riess, A.G., et al., 1998, AJ, 116, 1009

Scherrer, R.J., & Weinberg, D.H. 1998, ApJ, 504, 607

Scoccimarro, R., 2004, PRD, 70, 3007

Seo, H., & Eisenstein, D.J., 2003, ApJ, 598, 720

Seo, H., & Eisenstein, D.J., 2005, in preparation

Spergel, D.N., et al., 2003, ApJS, 148, 175

Springel, V., et al., 2005, Nature, submitted

Steidel, C.C., Adelberger, K.L, Dickinson, M., Giavalisco, M., Pettini, M., & Kellogg, M., 1998, ApJ, 492, 428

Steidel, C.C., Giavalisco, M., Pettini, M., Dickinson, M., & Adelberger, K.L., 1996, ApJ, 462, L17

Steinhardt, P.J., 1997, in "Critical Dialogues in Cosmology", ed. N. Turok (World Scientific)

Sunyaev, R.A., & Zel'dovich, Ya.B., 1970, APSS, 7, 3

Tegmark, M. 1997, PRL, 79,3806

Tegmark, M., Hamilton, A.J.S., Strauss, M.A., Vogeley, M.S., & Szalay, A.S., 1998, ApJ, 499, 555

Tegmark, M., Taylor, A.N., & Heavens, A.F. 1997, ApJ, 480, 22

Tonry, J.L., et al., 2003, ApJ, 594, 1

Turner, M.S., & White, M., 1997, PRD, 56, 4439

Wetterich C., 2002, Space Science Reviews, 100, 195

Wolf, C. et al., 2003, A&A, 401, 73

Chapter 4 Stellar Archaeology and Galaxy Genesis

4.1 Science Case – How do galaxies form?

The main science goal is to use the fossil record contained in individual stars in nearby galaxies to decipher the history of star formation, chemical evolution and mass assembly in representative samples of the different morphological types of galaxies. This involves the acquisition and analysis of radial velocities and chemical elemental abundance data for large samples of individual stars. The origins and evolution of galaxies, such as our own Milky Way, and of their associated dark matter haloes are among the major outstanding questions of astrophysics. Detailed study of the zero-redshift Universe provides complementary constraints on models of galaxy formation to those obtained from direct study of high-redshift objects (Bland-Hawthorn & Freeman 2000).

Stars of mass similar to that of the Sun live for essentially the present age of the Universe and nearby low-mass stars can be used to trace conditions in the high-redshift Universe when they formed, perhaps even the ‘First Light’ that ended the Cosmological Dark Ages. While these stars may well not have formed in the galaxy in which they now reside (especially if the CDM paradigm is valid), several important observable quantities are largely conserved over a star’s lifetime - these include surface chemical elemental abundances (modulo effects associated with mass transfer in binaries) and orbital angular momentum (modulo the effects of torques and rapidly changing gravitational potentials). Excavating the fossil record of galaxy evolution from old stars nearby allows us to do Cosmology locally, and is possible to some extent throughout the Local Group, with the most detailed information available from the Milky Way Galaxy.

How might one trace galaxy evolution using the fossil record in stars nearby? To quote Binney & May (1986) ‘Galaxies, like elephants, have long memories.’ Since the seminal paper of Eggen, Lynden-Bell & Sandage (1962), the importance of the joint distributions of kinematics and chemical abundances has been recognised. A second lasting influence of that work was the emphasis on the importance of identifying (approximately) conserved quantities. A third was the subsequent realization of the importance of being able to understand and correct for sample selection effects and the limitations of small samples. WFMOS’s proposed dataset is unprecedented.

We advocate a two-pronged approach, the first obtaining high-resolution ($R = 40,000$) spectra for Galactic stars in order to analyse the internal kinematics of substructure and derive individual elemental abundances for ‘chemical tagging’ (Freeman and Bland-Hawthorn 2002), the second obtaining low-resolution ($R = 1800$) spectra for large samples of stars in the Galaxy and nearby galaxies in order to identify the presence of substructure, to define the distributions of metallicity and radial velocities for the dominant stellar populations, and to map the extent of the massive halo of the Milky Way.

Armed with these data, we should be able to identify stars now in the Milky Way that were not born there, and derive the merging history of the Milky Way in some detail. The merger history depends on the primordial power spectrum, which in turn depends on the nature of dark matter. A complementary and more direct

approach to dark matter is to use the kinematics to map the dynamics; the low resolution survey in particular will provide line-of-sight velocities for hundreds of stars at the furthest regions of the Milky Way (the Sloan Digital Sky Survey has detected RR Lyrae stars out to 100 kpc, in the regime where previously only dwarf galaxies were used as probes).

4.1.1 The High-Spectral-Resolution Survey

4.1.1.1 Identification of Distinct Stellar Populations

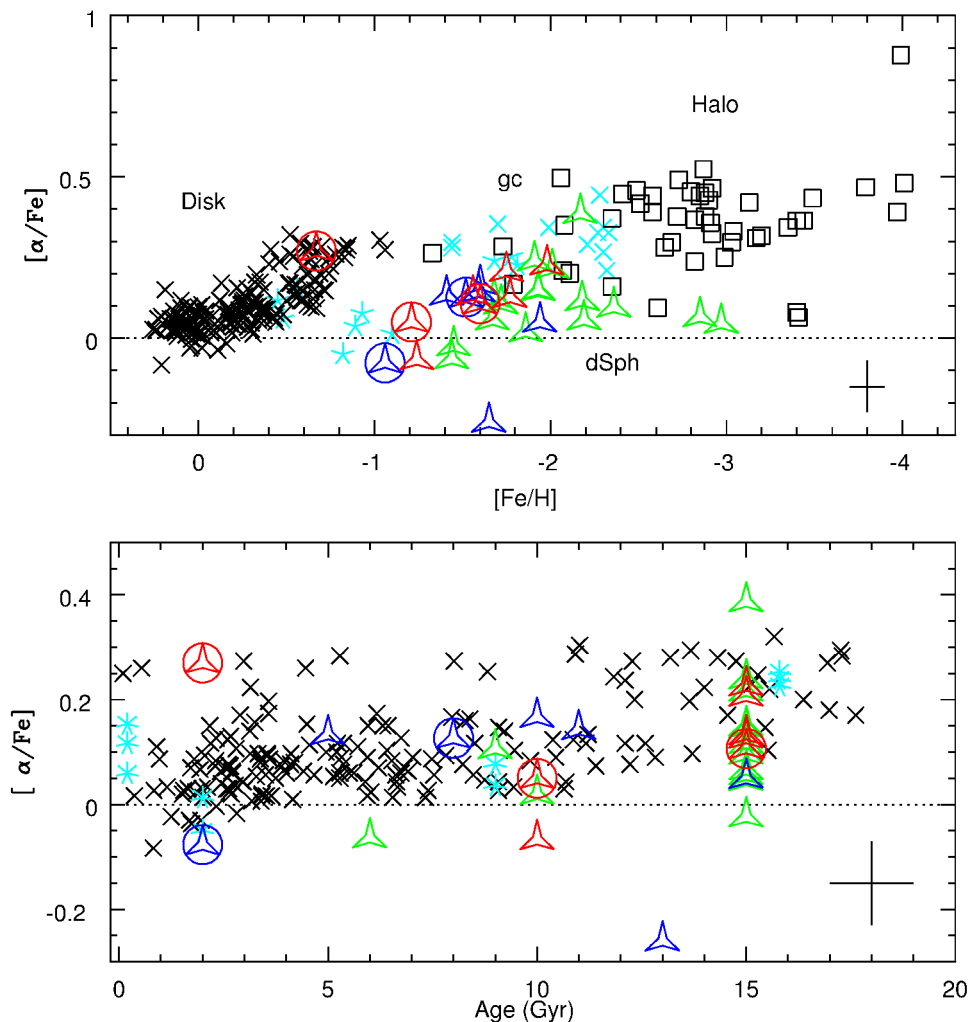


Figure 15. Taken from Tolstoy et al. (2003). The open coloured symbols are for stars in dwarf satellite companion galaxies to the Milky Way, while the small black squares and crosses are Galactic stars. They are clearly differentiated in the upper panel. The lower panel shows that as a function of age, they are not so differentiated, reflecting the same stellar IMF and Type Ia frequency. The lower panel also emphasises the large range of ages in the dSph, unlike the stellar halo.

Obtaining the elemental abundances and highly precise kinematics for large samples of Galactic stars is a unique capability of WFMOS. The elemental abundance pattern of a self-enriching star-forming region reflects the stellar IMF, and the past and present star-formation rates (see e.g. Wyse 1998). Thus one expects a very different pattern in, say, the Magellanic Clouds than in the local disk (see Gilmore & Wyse 1991) and this is indeed observed (Smith et al. 2003). Indeed, elemental abundances have been used to demonstrate that the stellar halo of the Milky Way could not be formed by disruption of systems like the present-

day retinue of satellites (see Figure 15 and Venn et al. 2004); again, this reflects the different star formation histories and age distributions of the satellites and the stellar halo (Unavane, Wyse & Gilmore 1996).

Elemental abundances can also be used to discriminate between thick disk and thin disk, since we now understand that they show different patterns, again reflecting the different star-formation histories (see Figure 16).

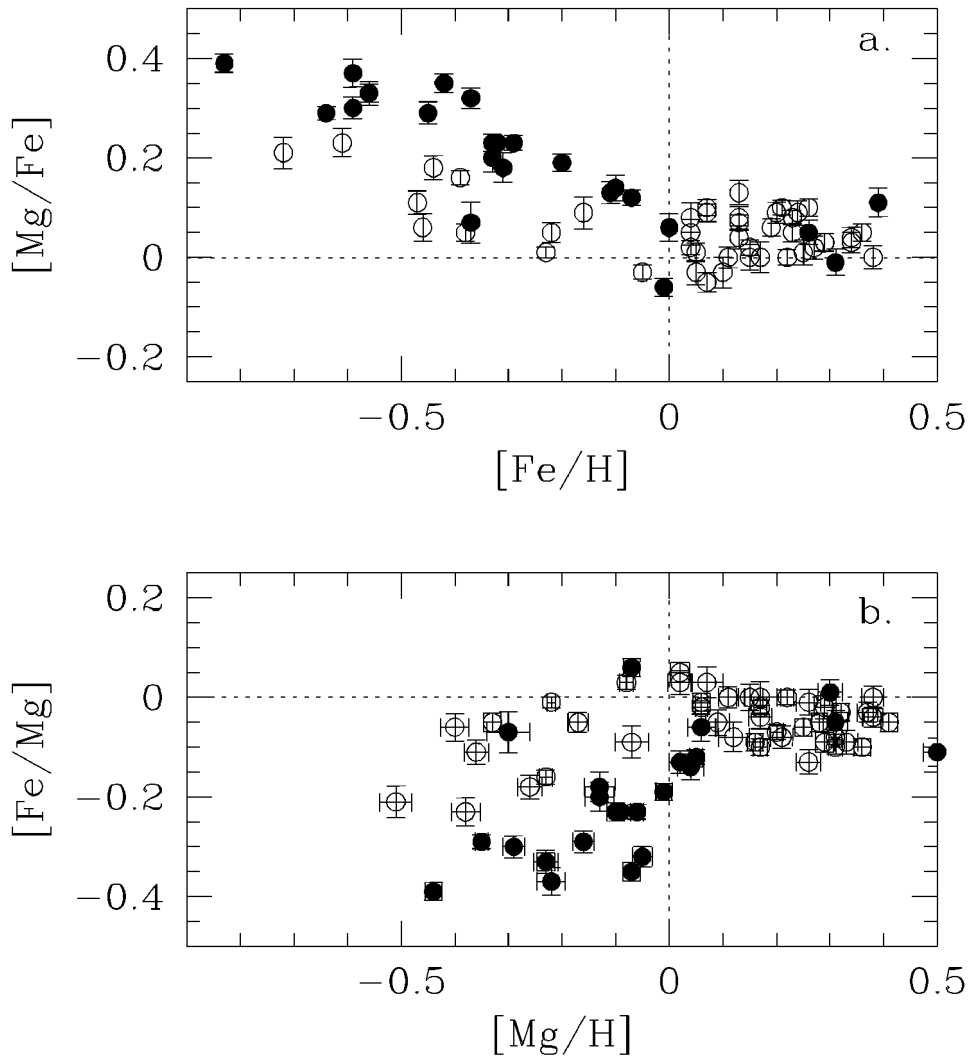


Figure 16. Taken from Feltzing et al. 2003, their Figure 2. Filled symbols represent stars whose kinematics are consistent with membership of the thick disk, while open symbols represent thin disk stars. The uncertainties in Mg abundance are indicated by the error bars; uncertainties in Fe are smaller than the symbol sizes. At a given value of $[Fe/H]$, the thick and thin disk stars are separated, with thick disk stars having higher $[Mg/Fe]$. At the typical thick disk metallicity, $[Fe/H] \sim -0.5$ dex, the value of $[Mg/Fe]$ in thick disk stars is equal to that seen in the stellar halo, and consistent with enrichment by Type II supernovae. More metal-rich thick disk stars show some enrichment by iron-dominated ejecta from Type Ia supernovae.

High-resolution spectroscopy of faint stars in relatively distant populations is now possible with 8 to 10-meter class telescopes. Chemical abundances can be derived from such stellar spectra and these abundances can be used to study chemical evolution in a variety of populations. Within a given stellar population in a galaxy, chemical evolution is driven by nucleosynthesis averaged over the stellar mass

range and subsequent dispersal of this processed material back into the galactic interstellar medium (ISM). This heavy-element enrichment over time depends on such processes as star formation history, internal stellar evolution and nucleosynthesis as a function of mass, how stars return their processed ejecta back into the ISM, and whether some of the stellar ejecta can be lost from the galaxy by galactic winds. Abundances derived from spectra are a powerful tool in probing all of the above processes that shape the chemical environment in a galaxy.

The ability to now conduct high-resolution spectroscopy with the new generation of big telescopes and their instruments is opening a new window into our ability to study chemical evolution, along with stellar evolution and nucleosynthesis, in a range of environments outside of the more traditional high-resolution spectroscopic studies that have been conducted primarily on small numbers of relatively bright stars.

The various types of red giants residing in different populations present excellent targets to the discerning spectroscopist. Because they are common (all stars below $M \leq 8M_{\text{Sol}}$ evolve onto the red giant branch) and fairly luminous, the red giants present us with a number of opportunities. Red giants are particularly good targets for studies of chemical evolution, as a range of masses are funnelled onto the red giant branch (RGB), thus red giant samples can be chosen to span a range of ages and metallicities. Hot stars, such as B stars, or A to F supergiants are almost exclusively massive stars (save for rare instances of post-AGB stars), with short lifetimes, and thus sample only the youngest (and usually most metal-rich) populations in a given galaxy. This is not to say that massive stars are not represented in cool giant or supergiant samples; many massive stars evolve into red supergiants and such stars can also be studied in young populations using the same techniques as those used on old, lower-mass red giants.

Main sequence stars, particularly F/G spectral types, are also good targets and have been extensively used to study the Galactic thin and thick disks (cf. Edvardsson et al. 1993; Nissen 2004).

Visual spectra at resolutions from $R=18,000$ up to $R=50,000$ contain measurable spectral transitions from upwards of 25 elements, whose nucleosynthetic origins sample the range of stellar sources, from SN II, SN Ia, or AGB stars. The α -elements, the Fe-peak, or the s- and r-process elements can be isolated and studied. The derived abundances can be studied as total abundance relative to hydrogen, or as abundance ratios (such as $[\text{O}/\text{Fe}]$), and can be studied versus age (from isochrones), or metallicity indicator (such as $[\text{Fe}/\text{H}]$ or $[\text{O}/\text{H}]$).

4.1.1.2 *Chemical Tagging*

In order to follow the sequence of events involved in the dissipation of gas to form the proto-disk of the Galaxy, we propose that the critical components which need to be re-assembled are the individual star clusters which formed at each stage. Since most stars are born in dense clusters, the formation and evolution of galaxies today must involve millions of discrete cluster events throughout their history. We would like to establish the evolving mass function of star clusters, their chemical composition, formation and survival rate as a function of cosmic time. Galaxy-wide enrichment from the fall-out of nuclear winds or mergers would be evident in the fossil record of reconstructed star clusters, assuming these

provide an unbiased sampling of cosmic time regardless of the star formation history.

But how are we to reconstruct star clusters which have long since dispersed? It will be necessary to tag individual stars to their parent cloud through unique chemical signatures shared by these stars, assuming these exist.

High resolution spectroscopy at high signal-to-noise ratio of many stellar types reveals an extraordinarily complex pattern of spectral lines. The spectral lines carry key information on element abundances that make up the stellar atmosphere. Many of these elements cannot arise through normal stellar evolution, and therefore must reflect conditions in the progenitor cloud at the time of its formation.

4.1.1.3 *Primary requirements of chemical tagging.*

Our long-term goal is to chemically tag stars into coeval groups, i.e. to identify individual members of star clusters which have long since dispersed. For unique chemical signatures to exist, there are several key requirements (see Bland-Hawthorn & Freeman 2004 – see the Appendix for a more detailed discussion):

1. Most stars must be born in dense star clusters.
2. Most dense star clusters must be chemically uniform in key elements.
3. Key chemical elements must reflect the cloud composition of the progenitor cloud.
4. Key chemical elements must not be rigidly coupled (i.e. vary in lock step), and there must be sufficient abundance dispersion in key elements to allow for unique groups (reflecting unique sites of formation) to be readily identified.
5. There must be a contiguous spectral window which contains the necessary information on key elements for chemical tagging.

Conditions 1, 2, 3 and 5 appear to be supported by observation. Condition 4 is the most uncertain largely because stellar abundance surveys to date target either too few stars or too few chemical elements.

Condition 2 is well demonstrated in Figure 17 where we show the chemical homogeneity of the Hyades star cluster, taken from De Silva et al. (2005); more than 50 stars in the Hyades have identical abundances in most measured elements, and all heavy ones above iron. Further, stars which show the largest scatter have the lowest membership probability (open circles in the figure); Hipparcos reveals these stars to be kinematic outliers. Figure 17 shows the rich potential for chemical tagging as an important diagnostic tool in large stellar surveys.

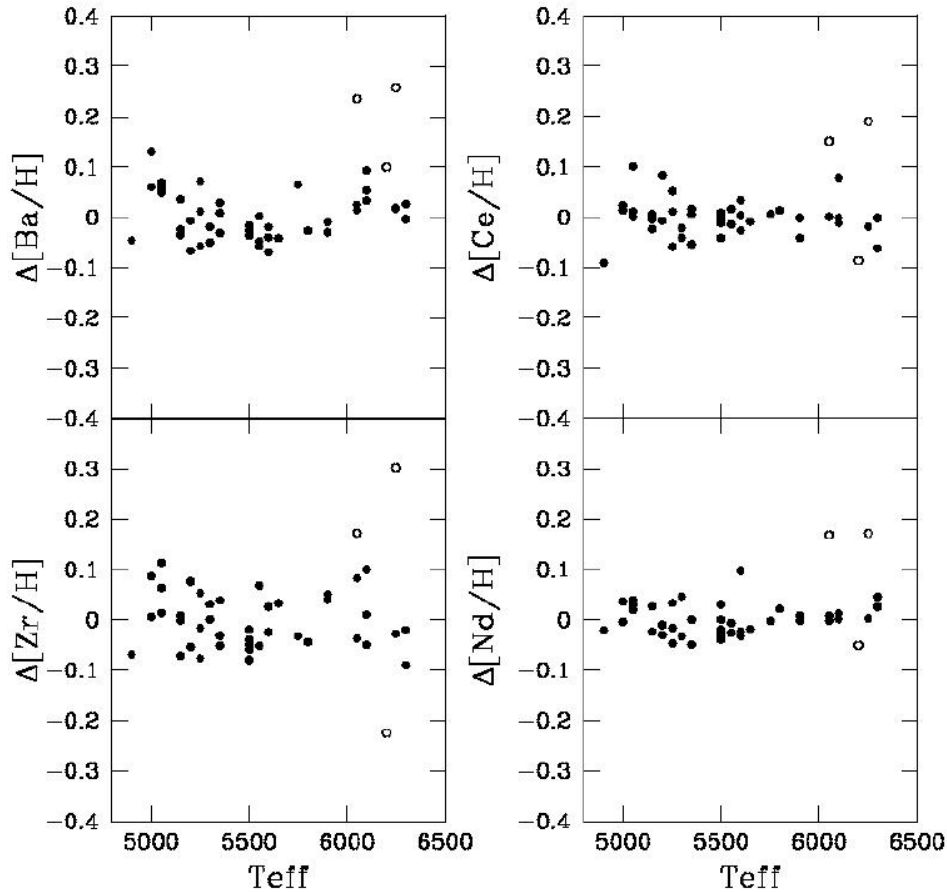


Figure 17. From De Silva et al. (2005). Differential Abundances vs Effective Temperature for a sample of F-K Hyades dwarfs. Abundances were derived using an LTE line analysis code and interpolated stellar model atmospheres based on the ATLAS9 code. The open symbols represent stars with low cluster membership probability (i.e. kinematic outliers). The Hyades members have uniform abundances within the 0.04 dex level.

The overall goal is to reconstruct ancient star groups from unique chemical signatures. The abundance dispersion in α and heavy elements provides a route forward for tagging groups of stars to common sites of formation. With sufficiently detailed spectral line information, it is feasible that ‘chemical tagging’ will allow temporal sequencing of a large fraction of stars in a manner analogous to building a family tree through DNA sequencing.

Consider the (extraordinary) possibility that we could put many coeval star groups back together over the entire age of the Galaxy. This would provide an accurate age for the star groups either through the color-magnitude diagram, or through association with those stars within each group that have $[n\text{-capture}/\text{Fe}] \gg 0$, and can therefore be radioactively dated. This would provide key information on the chemical evolution history for each of the main components of the Galaxy.

There is no known age-metallicity relation that operates over a useful dynamic range in age and/or metallicity. (This effect is only seen in a small subset of hot metal-rich stars; Nordstrom et al. 2004). Such a relation would require the metals to be well mixed over large volumes of the ISM. For the foreseeable future, it seems that only a small fraction of stars can be dated directly (Freeman & Bland-Hawthorn 2002).

Ideally, we would like to tag a large sample of representative stars with a precise time and a precise site of formation. Can we identify the formation site? The kinematic signatures will identify which component of the Galaxy the reconstructed star group belongs, but not specifically where in the Galactic component (e.g. radius) the star group came into existence. For stars in the thin disk and bulge, the stellar kinematics will have been much affected by the bar and spiral waves; it will no longer be possible to estimate their birthplace from their kinematics. Our expectation is that the derived family tree will severely restrict the possible scenarios involved in the dissipation process. In this respect, a sufficiently detailed model may be able to locate each star group within the simulated time sequence.

Our ability to detect structure in elemental-abundance-space depends on how precisely we can measure abundance differences between stars. It may be possible to construct a large database of differential abundances from echelle spectra, with a precision of 0.05 dex or better; differential abundances are preferred here to reduce the effects of systematic error. We discuss the requirements further below.

4.1.1.4 *Analysis of substructure in kinematic and elemental abundances*

The exquisite velocity accuracy provided by high resolution spectra will allow us to determine - and model - kinematic gradients along any substructure. Complementary to the research on the disk of the previous subsection, tidal debris in the halo can (at least in principle - it is a complex dynamics problem) be used to constrain the overall symmetries and lumpiness of the dark halo (cf. Helmi 2004; Johnston, Spergel & Haydn 2002)

4.1.2 **The Low-Spectral-Resolution Survey**

For the second approach, a low-resolution survey, WFMOS will target stars in the magnitude range $17 \leq V \leq 22.5$ and be exactly complementary to RAVE (southern hemisphere) and to GAIA (all-sky). GAIA will obtain moderate-resolution ($R = 11,500$) spectra, and hence radial velocities and metallicity information, only for stars brighter than $V=17$ (e.g. Perryman et al. 2001; Katz et al. 2004). RAVE, using the 6dF spectrograph on the UK Schmidt telescope, will concentrate on the brightest stars for which GAIA may saturate, $V < 12$ (Steinmetz, 2003). Competition for at least some of the science comes from projects which have similar ‘big picture’ science goals, such as the Sloan Digital Sky Survey extension SEGUE (northern hemisphere), and from possible surveys using AAOmega on the 4m AAT, FLAMES on the VLT and IMACS on Magellan (all southern hemisphere) and from DEIMOS on Keck (Northern hemisphere). The southern hemisphere telescopes cannot access a significant fraction of the outer Galactic disk where we have at present woefully limited information and much interest (e.g. Martin et al. 2004a). AAOmega and SDSS/SEGUE will be most effective at the brighter end of the WFMOS target range. DEIMOS utilises a slit-mask rather than being a fiber-fed spectrograph and so can go fainter than WFMOS, but this is of most interest for extra-Galactic stars (at $V=22.5$, a giant with $M_V = 1$ is at 200 kpc and a dwarf with $M_V = +5$ is at 32 kpc). While there is no record of large Galactic surveys with Keck or with the VLT, we may assume some effort there, but it is unlikely that more than a few times 10^4 stars would be observed by any one PI-project (this is the size of the DEIMOS M31 survey discussed below). As we discuss below, sample sizes orders of magnitude larger is required for reaching the next level in understanding.

We need to map both the large-scale and the small-scale structure of the Galaxy in kinematics and metallicity. This involves determining the full joint distribution function for the major stellar components of the Milky Way - and as many external galaxies as possible – as well as identifying the important deviations away from a smooth characterization. The metallicity of a star is largely conserved over its lifetime, modulo dredge-up on the AGB and possible mass transfer in close binaries, which preferentially affect s-process elements and perhaps some α -elements. Orbital angular momentum is approximately conserved in many models of the Galactic potential, even time-dependent models, and so lines of sight in which the radial velocity is most sensitive to rotational streaming should be targeted first.

4.1.2.1 *The stellar halo - thick disk interface*

Consider what we know now, from samples sizes of a few thousand stars. We know that the Milky Way Galaxy, once apparently satisfactorily described by Population I and Population II, is clearly a very complex system (Gilmore, Wyse & Norris 2002; Freeman & Bland-Hawthorn 2002). Particularly at faint magnitudes, $V \geq 18$, surface density enhancements in the outer halo - and disk? (Ibata et al. 2003) – are common (Yanny et al. 2000; Newberg et al. 2002; Vivas et al. 2001). Most structure is apparently tidal debris disassociated from the Sagittarius dwarf (Ibata, Gilmore & Irwin 1994, Ibata et al. 1997; Majewski et al. 2003) but our data that trace beyond the solar circle remain limited to a few thousand of those high-velocity and/or metal-poor stars (each selection with its own bias) passing through the solar neighbourhood and a few thousand more stars in selected lines of sight at distances of a few kpc (dwarf stars used as tracers) or a few tens of kpc (giants used as tracers). From these we have identified a few ‘moving groups’ with low confidence, and for the dominant populations, have derived only the mean and first moments of the distribution functions of metallicity and kinematics; this is not sufficient to interpret the observations. For example two recent analyses of samples of metal-poor stars (selection bias) in the solar neighbourhood have come to opposite conclusions, Chiba & Beers (2000) find only a one-component stellar halo, and a distinct thick disk, where as Gratton et al. (2003) conclude that there is a two-component halo, and no distinct thick disk. Further, while both samples contain stars on similar high-eccentricity orbits, contradictory conclusions are drawn: these stars are either the remnants of an early Eggen-Lynden-Bell-Sandage collapse (Chiba & Beers 2000) or belonged to an accreted structure (Gratton et al. 2003).

Dynamical times are longest in the outer Galaxy, and with the significant multiplexing capability of WFMOS we will be able to identify and quantify substructure. Is the entire outer halo debris from the Sagittarius dwarf? Is all sub structure due to the Sagittarius dwarf? Where are all the disrupted dwarfs predicted by even ‘pre-reionization only’ models of dwarf galaxy star formation (cf. Bullock, Kravtsov & Weinberg 2001)?

4.1.2.2 *The thick disk - thin disk interface*

As another example of our ignorance, consider the thin disk – thick disk interface. The thick disk plausibly arose from heating of a pre-existing thin disk by a minor merger; in this case, how did the thin disk re-form? Important constraints on this would come from the extreme low-metallicity tail of the thin disk, but we are hampered by the difficulty of assigning individual stars to thin disk or thick disk -

hence one reason for the continuing discussion of the existence or otherwise of a metal-weak thick disk; we need the joint distributions of kinematics and chemistry for large samples to be able to determine the 3σ tails. With the requirement of even 100 stars in this tail region, the main sample must be $\sim 10^5$ stars. Another aspect is the need to understand what fraction of stars more than 1 kpc above the disk plane are stars born in the thin disk that have been scattered into the thick disk regime by more prosaic, but still rare, events such as supernova explosions of a binary partner. This has implications for the observed age distribution of ‘thick disk’ stars, which has been used to constrain the mass assembly history of the Milky Way (e.g. Wyse 2001). Again, this requires study of the 3σ tails in kinematics of thin and thick disks.

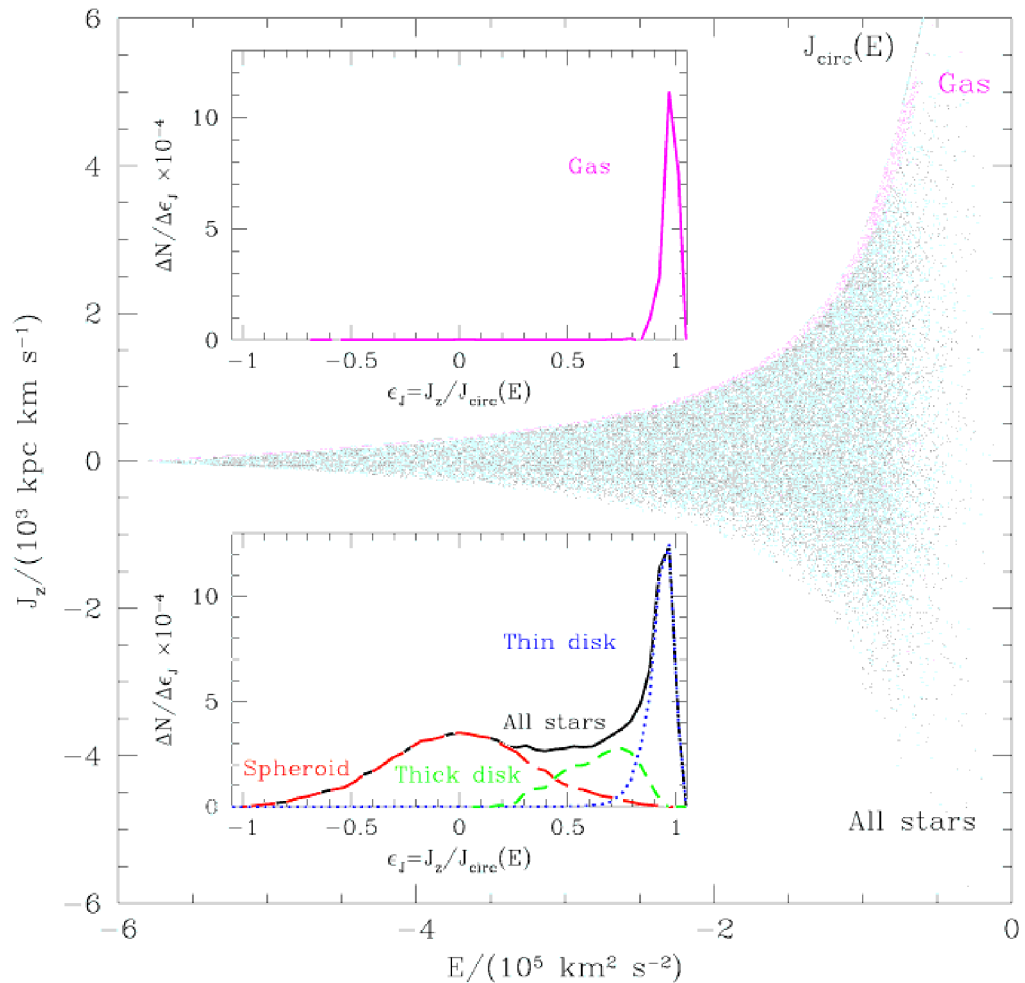


Figure 18. Taken from the simulation of the formation of an early-type spiral galaxy by Abadi et al. (2003). J_z , the z-component of the specific angular momentum of all ‘stars’ and gas particles within the radius of the central baryonic galaxy is plotted versus the specific binding energy of each ‘star’, E . The small inserts show the distribution of the normalized angular momentum (as a fraction of circular orbit value) or gas and for stars, together with a possible decomposition of the stars into different components.

Further, not only are observational capabilities maturing, models of disk galaxy formation and evolution are now reaching high enough resolution to be able to make predictions for stellar populations. Integrals of the motion, such as the z-component of orbital angular momentum (for axisymmetric potentials) are the most robust quantities to predict, together with the other conserved quantities such as stellar chemical composition and age. Figure 18 shows the angular momentum distribution predicted from the state-of-the-art simulation of the formation of a

disk galaxy (in the Λ CDM framework) by Abadi et al. (2003). These simulations further predict that a significant fraction of *each* of the stellar components of a disk galaxy, *even the thin disk*, consists of tidal debris from merged former companion galaxies. This is the answer, within these models, to the fact that there are old stars at the solar circle, some 2–3 disk scale-lengths from the Galactic Center, with ages that correspond to formation redshift of 1–2, despite the predictions of these models that extended disks cannot start to form until after a redshift of unity (Navarro & Steinmetz 1997; Weil, Eke & Efstathiou 1998).

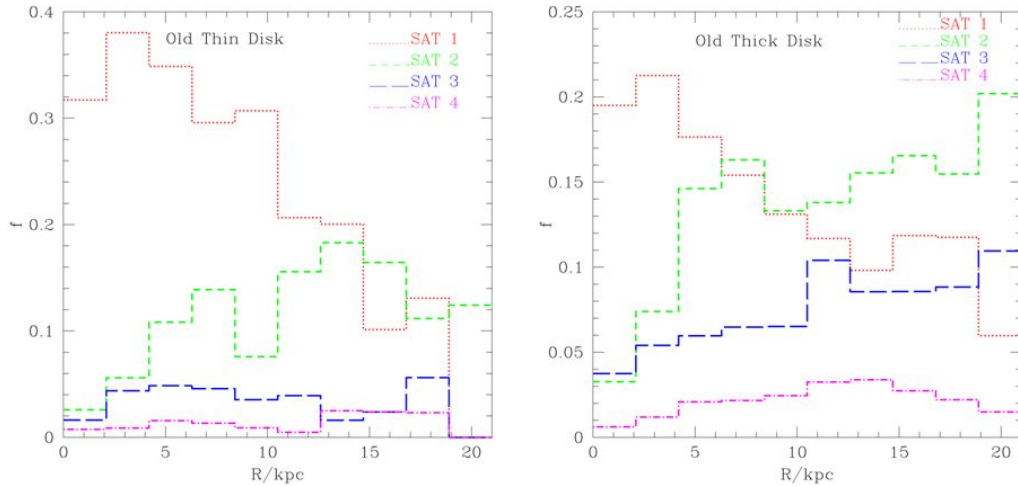


Figure 19. Taken from Abadi et al.'s (2003) simulation of the formation of an early-type disk galaxy in Λ CDM cosmology. The figure shows the radial variation of the contributions – as the fraction, f , of stars – to the old thin and thick disks (age > 10 Gyr) from each of the four satellite galaxies accreted by the main disk system since a redshift of unity.

For example, Figure 19 shows the predicted contributions to the old thin and thick disks (old is ages greater than 10 Gyr), in a model of a disk galaxy (Abadi et al. 2003), from the four tidally disrupted satellites that are accreted after a redshift $z = 1$. Clearly substructure should be seen in even the thin and thick disks. Kinematic and chemical signatures remain longer than do spatial overdensities, and the spectral survey is crucial. Dynamical times are longer in the outer Galaxy, and indeed recent observations of the outer disk, both photometric and spectroscopic, have been interpreted as evidence for an accreted galaxy (Newberg et al. 2002; Ibata et al. 2003; Helmi et al. 2003; Bellazzini et al. 2004) at Galactocentric distances of ~ 15 kpc. However, the observations may more simply reflect our ignorance of structure in the outer disk, which has a well established warp in the gas, and probably in stars (e.g. Carney & Seitzer 1993; Djorgovski & Sosin 1989). The recent detection of structure in HI, interpreted as a newly identified spiral arm, at just this distance (McClure-Griffiths et al. 2004) is intriguing. Indeed it has been suggested that most of the ‘accreted galaxy’ is simply an artefact of a stellar warp (Momany et al. 2004), though this has been disputed (Martin et al. 2004b). Given the complexity of the structure of outer disks, comprehensive colour-magnitude data plus metallicity distributions plus kinematics will be needed to understand what is going on.

4.1.2.3 The central bulge–bar–inner disk

In CDM models the bulge and inner Galaxy are the repository of much of the first star formation (cf. Moore 2001). This is also the location of the supermassive

black hole that apparently is closely connected to bulge/galaxy formation, at least as far as we can understand given the correlations between black hole mass and bulge properties (cf. Magorrian et al. 1998; Ferrarese & Merritt 2000). The Milky Way is one of the most discrepant galaxies (Tremaine et al. 2002) and again our understanding of the inner disk - bar - bulge - central regions is woefully inadequate.

4.1.2.4 *The extent of the dark halo*

The low-resolution survey will also provide radial velocities for many distant stars with which to re-analyse the still-unresolved question of the extent and mass of the dark matter halo of the Milky Way. Analyses are presently limited essentially by the small-number statistics of the satellite galaxies and globular clusters, which were the only tracers beyond ~ 30 kpc (e.g. Little & Tremaine, 1987; Kochanek 1996; Zaritsky 1999). With WFMOS we will rather be limited by the much larger statistics of stars. We note that the SDSS imaging survey has identified RR Lyrae stars beyond Galactocentric distances of 60 kpc (Ivezic et al. 2004). Even at these distances these stars are smoothly distributed.

As discussed below, competing facilities will address these issues, but only WFMOS can provide the large samples required in a feasible time.

4.1.3 **Investigations for requirements analysis**

4.1.3.1 *Detailed Simulations of the Merging of Substructure*

As noted above, we do not have enough information at present to understand even the basic roles of dissipation vs accretion in the formation of the stellar halo. The low-resolution spectral survey will detect and characterize kinematic and metallicity substructure, allowing a firm quantification of the role of merging and accretion of stellar systems. The high-resolution spectral survey will allow us to analyse the details of the substructure and will allow us to identify new substructure which cannot be identified kinematically, but has distinct elemental abundances.

To understand the capabilities required, we “observe” a model of a stellar halo built entirely from accretion events, from a location 8 kpc from the center of the galaxy (i.e. to mimic Solar perspective). The halo contains debris from N-body simulations of over one hundred such events, whose accretion times, masses and orbits are generated from a cosmological model. The dark matter particles in the simulation are subsequently painted with stars so that the metallicity and luminosity (in the range $10^5 - 10^9 L_{\text{Sol}}$) distributions of the satellites accreted most recently mimic those of the Local Group dwarf galaxies. The stellar halo produced is similar in size (of order $10^9 L_{\text{Sol}}$) and profile (density fall as r^{-3}) as the Milky Way's stellar halo. In the model, over 90% of the halo comes from roughly the 10 most luminous events (see Figure 20).

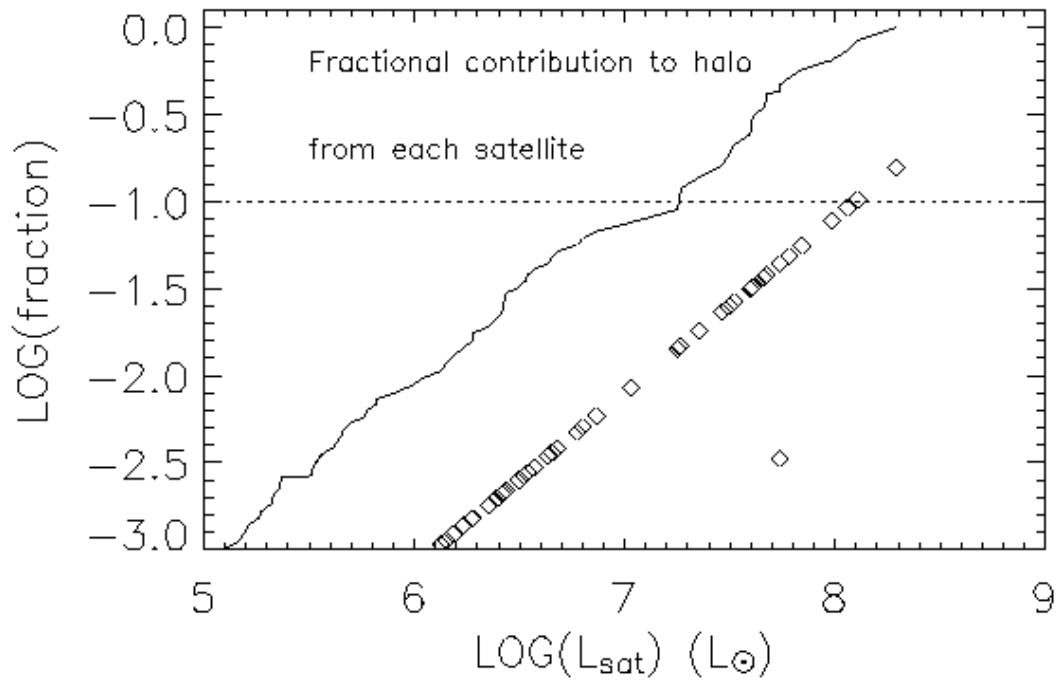


Figure 20. Symbols show the fractional contribution of stars to the stellar halo from each accreted satellite, as a function of satellite luminosity. Symbols falling below the straight-line trend are from satellites not yet fully disrupted. The solid line shows the cumulative distribution and the dotted line indicates the 10% level.

4.1.3.1.1 Observing the Milky Way

We convolve our model with the luminosity function of the globular cluster M12 (Hargis, Sandquist & Bolte 2004), and examine what we might expect to find in a 400 degree-squared survey area, randomly placed with a centre at $|b| > 30$ degrees and observing all stars brighter than $V=17$. We expect such a survey would contain of order 3×10^4 halo stars, 90% within 20kpc of the Sun and 10% beyond. In both regions, we expect of order 10 satellites, to contribute significantly (at the $> 1\%$ level) to such a survey (see left-hand panels of Figure 21 and Figure 22). The debris from these satellites is well-mixed in the inner (< 20 kpc) halo and smooth in both position (l, b, r) (where r is the distance from the Sun) and line-of-sight velocity v_r , on the resolution-scale of the simulations (see middle and right-hand panels of Figure 21). Nevertheless, previous studies of dark matter alone (Helmi, White & Springel 2003) suggest that high-precision radial velocities (i.e. of order 1 km/s) might distinguish some of the debris even in these regions into separate velocity groupings. The outer halo is more sparsely populated, and debris from individual satellites could be separated in these regions with much lower precision observations (of order 10km/s or even greater - see right-hand panels of Figure 22).

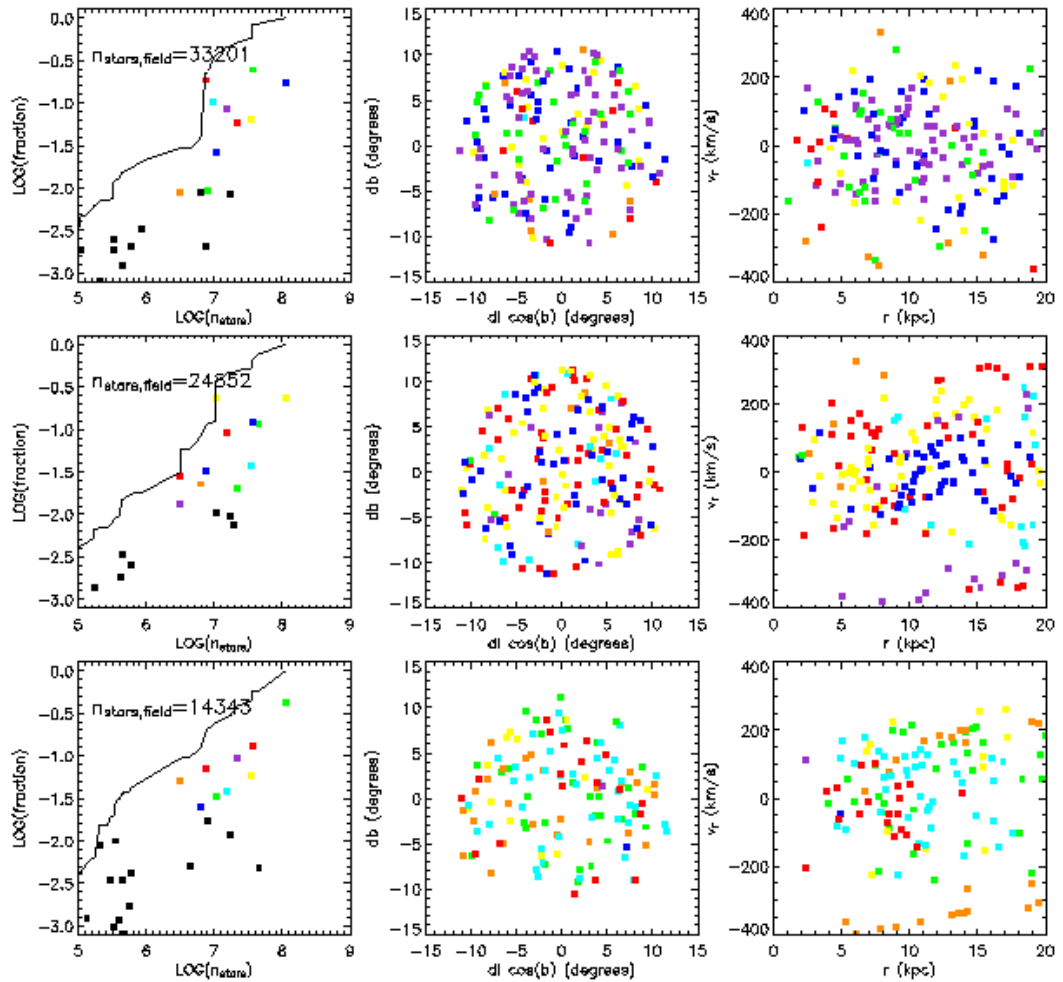


Figure 21. Left hand panels shows the fractional contribution of stars brighter than $V=17$, at distances $<20\text{kpc}$ to three 400 degree-squared randomly selected patches of the sky. Middle panels shows galactic latitude and longitude relative to the field center for all particles from each simulated satellite which contributes more than 300 stars to the region. The particles are colour coded with the satellite from which they came. Note that the particles are NOT equally weighted in luminosity, and should be used to indicate the location of the debris only. Right hand panels show the distance and line-of-sight velocity from a Solar perspective, in the Galactic rest frame.

Increasing the magnitude limit to $V>21$ and using some photometric system to select giants would allow us to probe deeper into the halo (of order 10^5 sources with $r > 20\text{ kpc}$ and 1000 sources $r > 60\text{ kpc}$), with the mean halo background dropping to zero at the larger radii and the contrast of debris becoming more apparent. Debris features in these regions typically cover many tens to hundreds of square degrees, and should be easily apparent.

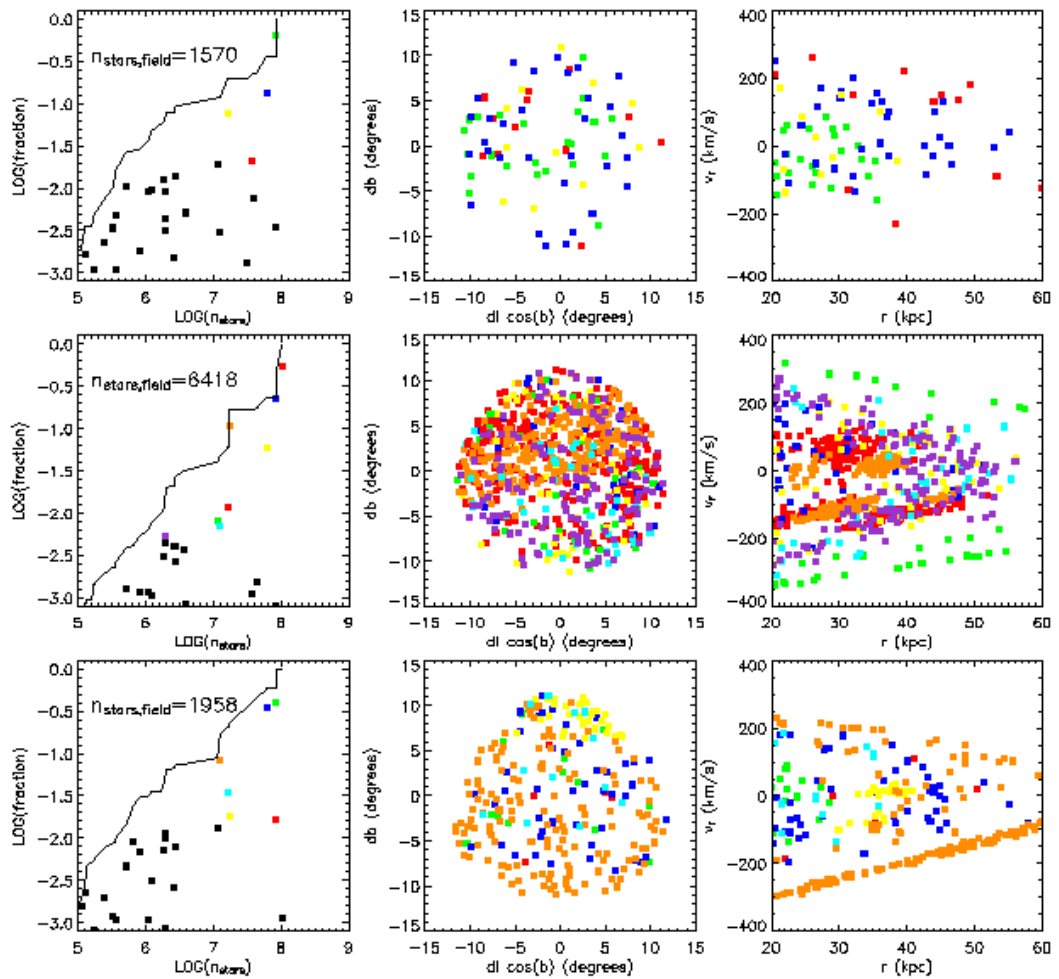


Figure 22. – As Figure 21, but for debris in the region 20-60kpc. Points are plotted for all satellites contributing more than 30 stars to the survey.

Figure 23 shows the average metallicity as a function of satellite luminosity.

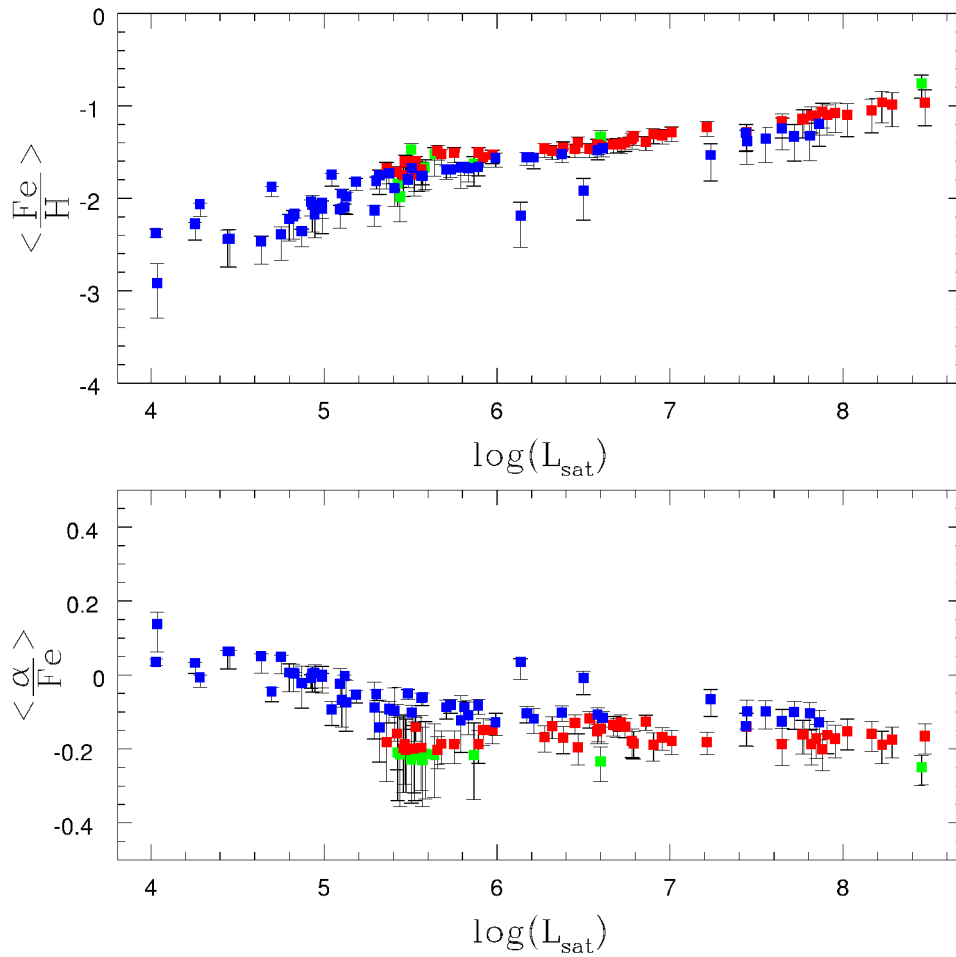


Figure 23. Average $[Fe/H]$ and $[Mg/Fe]$ at the time of accretion as a function of satellite luminosity. Green/red/blue points are for accretions events $< 4 / 4 - 8 / > 8$ G years ago and the error bars indicate the spread (25th-75th percentile) in the metallicity distribution within each satellite.

4.1.3.1.3 *Observing another galaxy*

Figure 24, Figure 25 and Figure 26 show the external view of the galaxy.

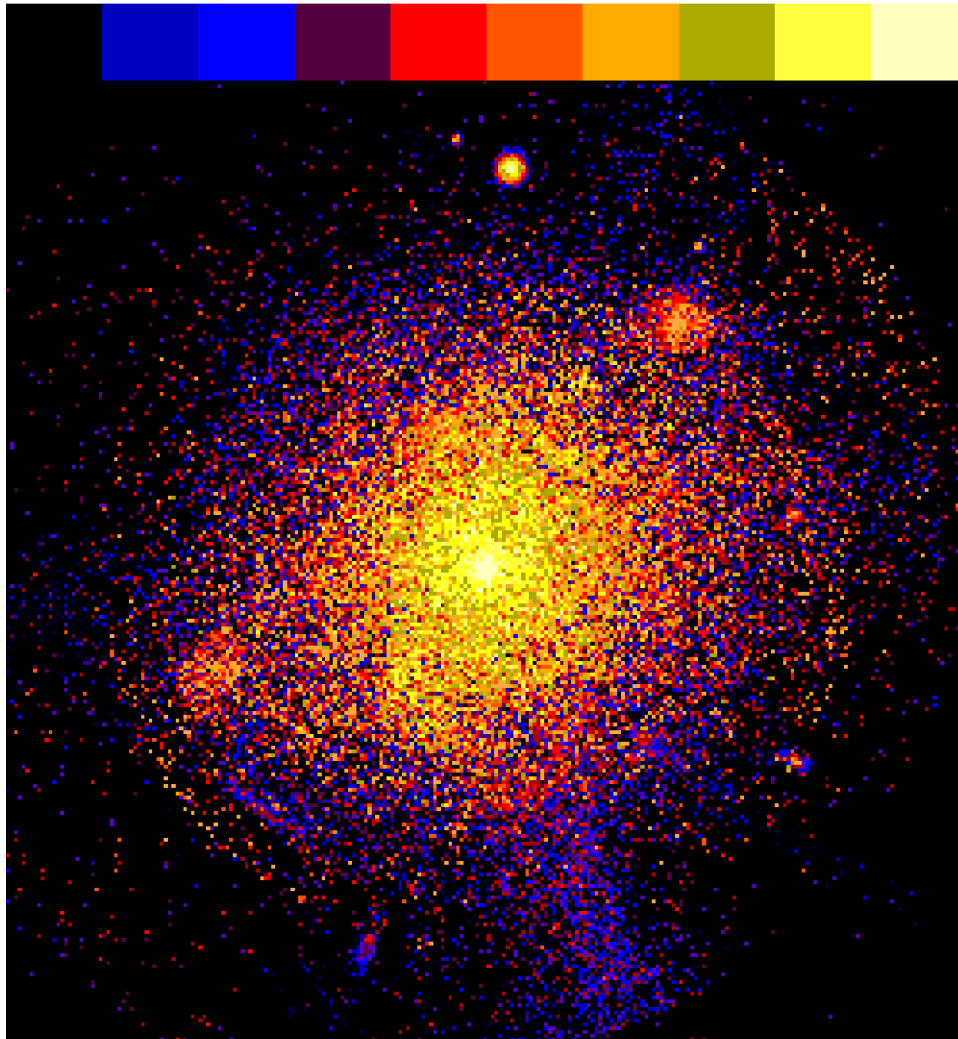


Figure 24. External view of the halo. Box is 200kpc on each side. Colour bar is 35-25 mag/arcsec2.

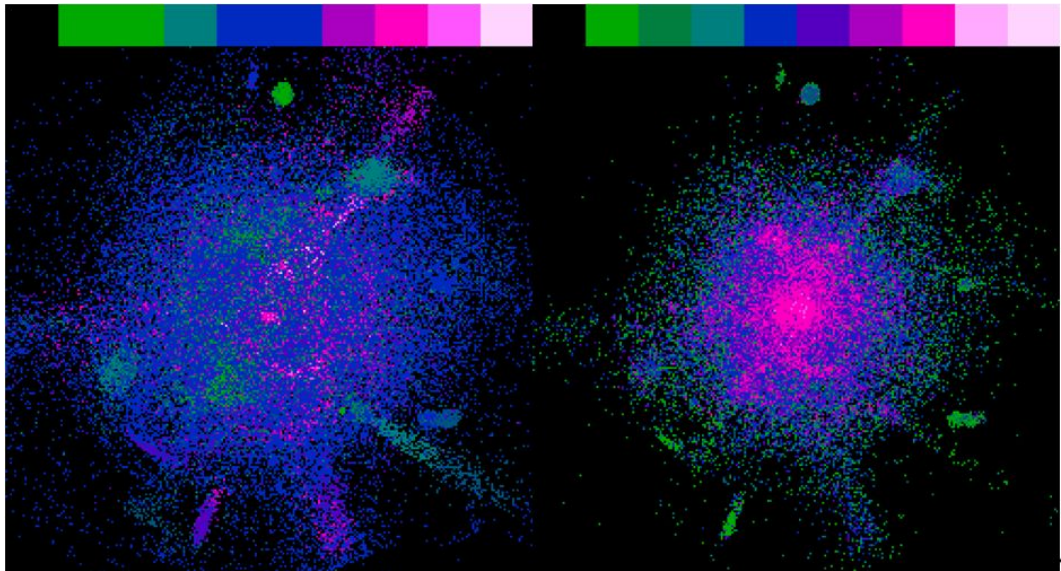


Figure 25. Line of sight velocities (left hand panels, color bar is -300km/s to 300 km/s) and velocity dispersion (right hand panel, color bar is logarithmic 10km/s to 1000km/s) for same external view as Figure 24.

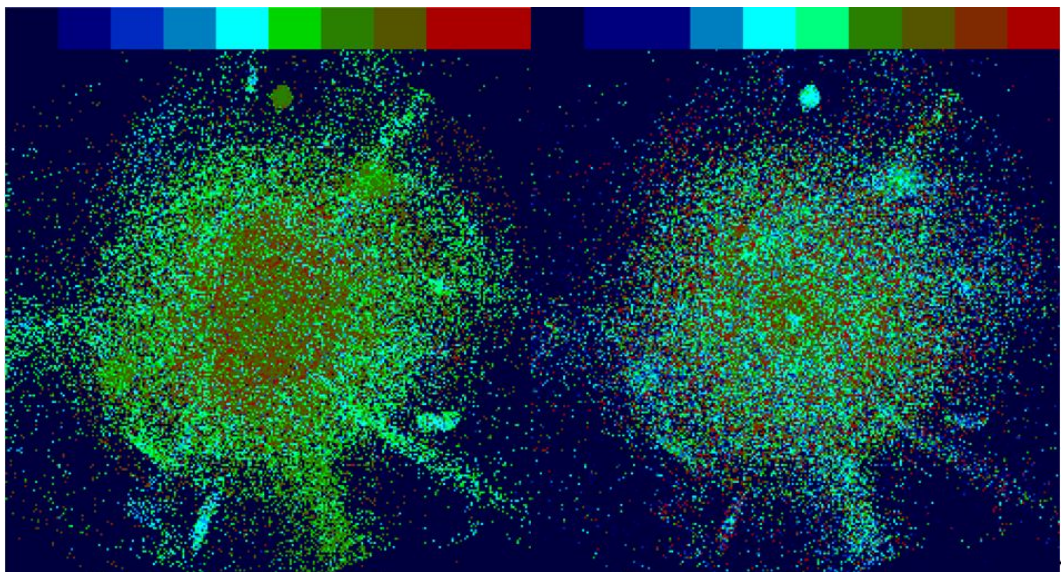


Figure 26. [Fe/H] (left hand panels, colour bar is -2.5 to -0.5) and [Mg/Fe] (right hand panel, colour bar is -0.1 to 0.2) for same external view as Figure 24.

4.1.3.2 Sky Coverage, Velocity Accuracy to Detect Streams

To detect streamers in the Milky Way halo from radial velocity data, plus positions, and perhaps distance data, one ideally wants full-sky coverage and as deep as one can get. Failing that, large fields of sky should be preferred over narrow strips, since a large field is more likely to catch a sizable fraction of a streamer than a narrow strip. That is, even though a narrow strip may touch more streamers, these touches are not very useful and significant. In other words, streamers are sizable objects and to find them you need a sizable field of view. We suggest to map a broad band on the sky, including a pole (where existing data can

be used to compare our findings) and perhaps looking both towards the outer and the inner Galaxy.

In order to detect a streamer, the uncertainty in velocity must be significantly less than the line-of-sight velocity dispersion of the background population, i.e. in the halo about 100–150 km/s. This goal should easily be met by the expected velocity uncertainty of ~ 10 km/s, achievable in the $R=1800$ low-dispersion ‘Sloan Spectrographs’. Note that the published velocity accuracy of the SDSS set-up is more like ~ 20 km/s (Yanny et al. 2004), at least for early-type A/F stars with moderate-to-low S/N. However, standard techniques usually provide an accuracy of 0.1 velocity pixel, and at $S/N > 10$ we would expect ~ 10 km/s (see e.g. Munari et al. 2003). Indeed Majewski et al. (2004) state an achieved accuracy of 1/20th of a resolution element with careful cross-correlation techniques. In this case these spectrographs should be able to attain an observational radial velocity uncertainty that approaches the intrinsic velocity width of the stream, ≤ 5 km/s, which is the ideal situation.

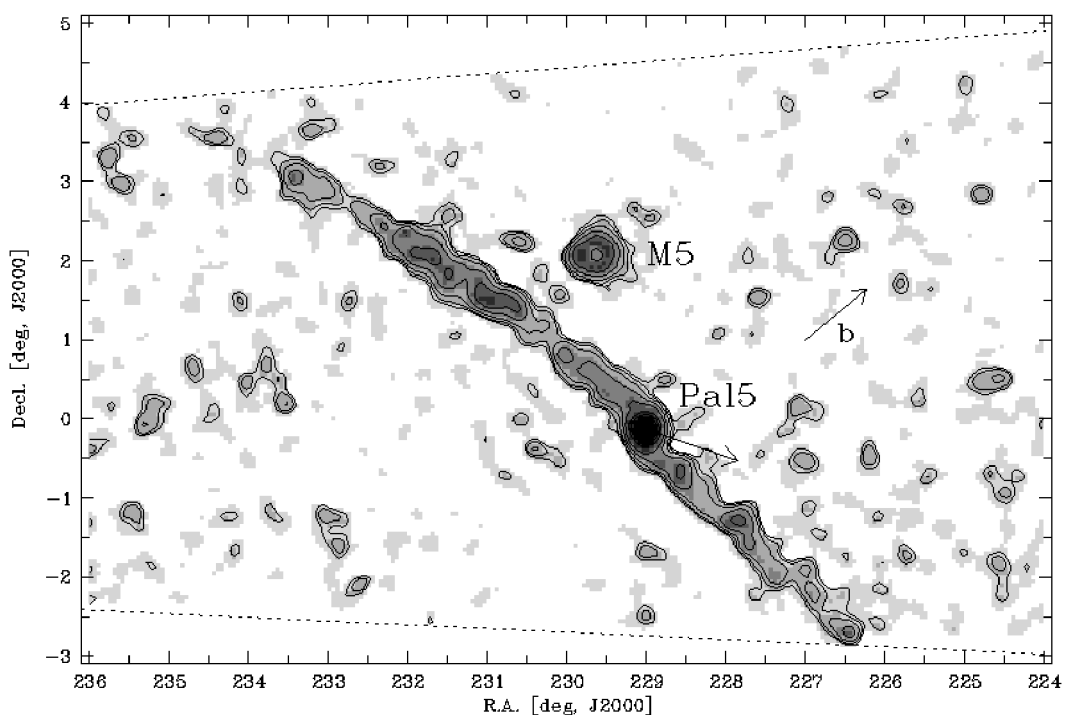


Figure 27. Taken from Odenkirchen et al.(2003), their Figure 3. The contours show the surface density of stars that are selected from their photometry to be members of Pal 5. There are clearly streams associated with this globular cluster. The arrow extending from the core of Pal 5 indicates the estimated direction of its orbit.

More problematic is the question of tiling and sampling density. Clearly, any sampling *must* be done in a way avoiding any velocity (or other unwanted) biases. Without radial velocities, streamers are *very* hard to detect, because of their very low surface density; e.g. the tidal tails of Pal5 were only identified through photometry with the use of prior photometric information allowing the technique of matched filters isolating member stars (Odenkirchen et al. 2002). Similarly the most comprehensive search of the SDSS photometry has revealed at most one new feature (Willman et al. 2004).

While this may point to the (very interesting) absence of physical substructure, with the addition of radial velocity data, the contrast is enhanced by about the ratio

of the velocity dispersion in the background halo (~ 150 km/s) to that in the stream (which ever is the higher of the actual stream dispersion of ~ 5 km/s or the observational errors), or even more if the stream is at an unusual radial velocity. This last could occur if the line-of-sight probed the angular momentum of the stream and this was different from the average background halo. Thus, the number density of objects required to detect the streamer is reduced by a factor of $\sim (\sigma_{halo} / \sigma_{stream})^2$ (assuming Poisson noise), which is of the order of 100 - 1000. Preselecting against disk-foreground stars using colour information avoids a significant amount of objects.

Similar gains are to be made for substructure in the thick disk, so that even the low dispersion spectrographs will detect significant structure, if it exists.

For the Galactic thin disk, the high-resolution mode is preferred even to detect substructure, since there will exist many cold systems from disruption of open clusters etc., unrelated to any merging activity.

The known, reasonably well-mapped, streams in the Milky Way halo are from the Palomar 5 globular cluster and from the Sagittarius dwarf. The Pal 5 streams are thin, less than 1 degree wide, but stretch across 10 degrees (note the thinness constrains dark matter substructure, Johnston et al 2002). The streams from the Sgr dSph are now traced across the sky (Majewski et al 2003). Tiling that ensures these would not be missed is essential.

4.1.4 What will have been achieved for M31?

Will WFMOS be uniquely capable of deciphering the history of M31 and other Local Group satellites? What is the complementarity to other ground-based capabilities?

As our nearest giant neighbour, M31 offers the opportunity to extend the picture of galaxy assembly inferred from the Milky Way. Over the past two decades, the field stellar population of M31 has been studied through colour-magnitude diagrams (both ground-based and from the Hubble Space Telescope) of its evolved stars and spectroscopy of bright red giant branch stars. All photometric studies, following the pioneering work of Mould & Kristian, find that the dominant field population probed down the southern minor axis has a mean metallicity³ of around ~ -0.6 dex, from projected distances of about 5 kpc out to 30 kpc. The metallicity distribution is asymmetric, and can be fit by the superposition of two populations, metal-poor and metal-rich, with the bulk of the stars, even out at 30 kpc, in the metal-rich population (cf. Durrell, Harris & Pritchett 2004). It should be remembered that these field stars are members of Baade's 'Population II', raising the issues of which stars in the Milky Way should have been identified as 'Pop II' - perhaps (Wyse & Gilmore 1988) the members of the Milky Way thick disk, whose mean metallicity is comparable to that of the dominant population in M31's 'halo'. Indeed, perhaps the 'halo' in M31, which is rather flattened with an axial ratio of ~ 0.6 , is actually a thick disk (cf. Wyse & Gilmore 1988).

Of interest are recent wide-field imaging surveys of M31, as well as the lower mass galaxy M33, which are yielding constraints on the amount and nature of stellar substructure in their outer regions (Ibata et al 2001, Ferguson et al 2002,

³ These metallicities are based on the colour of the red giant branch and are subject to calibration uncertainties including the elemental abundance mix.

Zucker et al 2004a,b, Irwin et al in prep, Ferguson et al 2005, in prep). In particular, the INT Wide Field Camera Survey of M31 has a depth sufficient to resolve individual red giant branch stars down to ~ 3 magnitudes below the tip of the red giant branch ($I \sim 23.5$) and covers more than 40 square degrees. The resulting star count map has revealed significant stellar substructure in the outer disk and halo. Many of the detected overdensities have effective surface brightness equal to, or fainter than, 27.5 magnitudes per square arcsec in the V-band, and would thus have been almost impossible to detect via traditional surface brightness photometry techniques. A particularly intriguing feature is the giant stellar stream which can be traced to more than 70 kpc in projection from the center of M31. Additional prominent stellar overdensities are observed along both sides of the major axis at radii of 25-35 kpc. While the existence of significant clumpiness in the halo stellar distribution strongly suggests that M31 has recently accreted one or more small satellites, additional data beyond wide-field imagery are needed in order to address the precise history of the accretions - what was/is being accreted and when was the epoch of most accretion?

Spectroscopic measurements of individual red giant branch stars provide key constraints on the origin of the substructure through radial velocities and metallicities (Ibata et al 2004, Guhathakurta et al 2004, Font 2004, Ferguson et al 2004). Recent studies with Keck/DEIMOS have measured radial velocities at several locations along the giant stellar stream, and used these in conjunction with line-of-sight distance estimates (e.g. McConnachie et al 2003) to constrain possible progenitor orbits. Somewhat surprisingly, the observed velocities appear to rule out any simple connection between the giant stream and M31's closest and most luminous satellite companions, M32 and NGC205. Both these systems have radial velocities which differ by several hundred km/s from the expectations (in the current orbital phase) of the stream at those locations. Instead, the stream velocities are best fit by an orbit which connects the feature to the moderate stellar overdensity located in the north-west quadrant, dubbed the "northern shelf". This connection is further supported by deep HST/ACS colour-magnitude diagrams of these regions (Ferguson et al 2005, submitted). Variations in line-of-sight velocity dispersion are observed along the stream and provide constraints on the likely locations of the progenitor's apo- and peri-centre.

At least two groups (one led by Chapman & Ibata and the other by Guhathakurta & Rich) are currently pursuing large spectroscopic surveys of the M31 halo and disk using Keck/DEIMOS. These programs exploit not only the standard DEIMOS multi-slit masks (~ 100 targets) but also a custom-built narrow-band filter to limit wavelength coverage and increase multiplexing in high density regions, allowing up to ~ 500 targets over the 16×5 arcmin FOV. The primary goals of the Chapman/Ibata survey include mapping the kinematics of all major stellar overdensities, and characterizing the kinematic structure and substructure of the field populations in the inner halo and outer (thick?) disk. A final sample of 10,000-15,000 radial velocities is envisioned, with a significant fraction of the data already in hand. The fields are indicated in Figure 28.

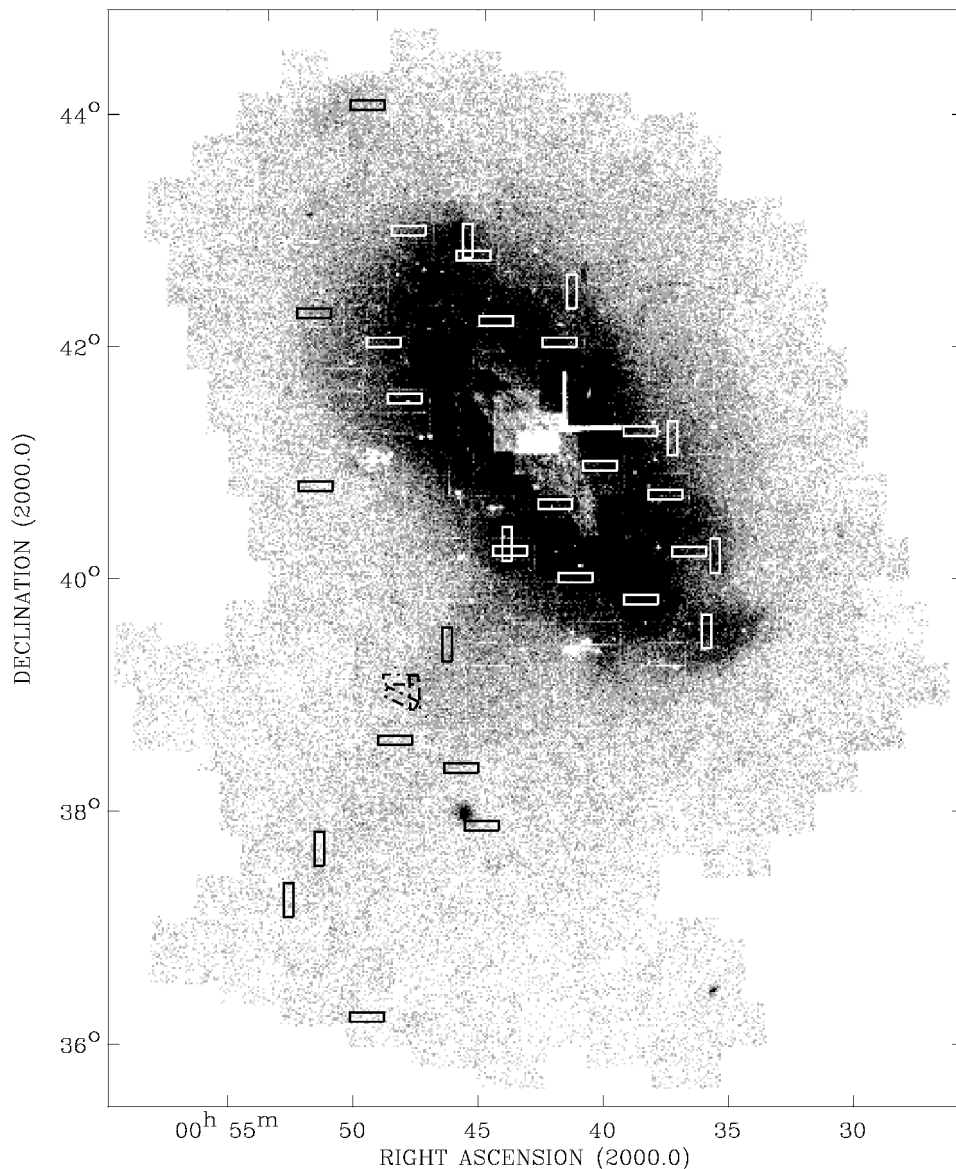


Figure 28. From Ferguson et al. (2004). The distribution of “blue” red giant branch stars (from the INT survey of Ibata et al, see Ferguson et al. (2002)) in a ≈ 40 square degree (125×95 kpc) area centred on M31, as mapped with the INT WFC. Overlaid are the 30 Keck/DEIMOS pointings observed as of September 2003; these mainly target major regions of stellar substructure and a few locations in the far outer disk/inner halo. The three DEIMOS fields of Guhathakurta et al (2004) are shown as dashed rectangles.

Wide-field imagery of M33 provides an interesting contrast to M31. Stellar density maps reaching the same limiting absolute magnitude as those of M31 reveal no stellar overdensities whatsoever in the halo (Ferguson et al in prep). Analysis of the stellar density distribution as a function of radius indicates a sharp steepening of the profile at roughly 4.5 exponential disk scale lengths; the steeper outer profile can be traced to an effective surface brightness of approximately 32 magnitudes per square arcsec in the V-band (this is very likely the deepest surface brightness profile of any galaxy obtained to date). While the lack of obvious stellar overdensities suggests M33 has not experienced a recent significant accretion event, the smooth steep outer profile limits the luminosity of any existing $r^{1/4}$ stellar halo to be less than a few percent that of the disk. Spectroscopic measurement of red giant branch in the outer regions of M33 will provide more rigorous constraints on the presence/absence of a smooth halo component. A Keck/DEIMOS survey has begun on this system, with the goal of characterizing

the metallicities and kinematics of roughly 2000 stars in fields located along the major and minor axes (Smecker-Hane/Ferguson).

The potential role of WFMOS: Most of the M31 stellar substructure discovered to date is large-scale and well-suited to the 1 degree FOV of WFMOS. The average stellar density of bright ($I = 20.5 - 21.25$) RGB stars in the low density regions of the M31 halo varies with radius and with local overdensity. Prominent stellar substructures such as the stream, the northern spur, the G1 clump and NGC205 loop have 4000-8000 ‘stellar’ sources per square degree in the range $20.5 < I < 21.25$ (note that typically 50% of these are foreground contaminants, with this fraction increasing at larger radius). The faintest stellar overdensities discovered to date have densities as low as 3500 sources per square degree, whereas regions of the diffuse outer halo (30-50 kpc in projection) drop to below 2000 sources in the same area. M33 stellar densities span a similar range. These estimates of target density are also well-suited to study with WFMOS.

An important factor is spectral resolution. DEIMOS work has focused on medium resolution (1-2 Angstrom) spectroscopy around the CaII triplet, which provides velocities accurate to typically 10 km/s and metallicities to 0.1 - 0.2 dex (using the most up-to-date empirical calibrations). At $R \sim 2000$, delivered by the proposed WFMOS low-dispersion/SDSS spectrographs, an exposure time of 2500s (the mean in the Mauna Kea simulations shown in Fig 19 below) with WFMOS on Gemini for $V = 21.5$ provides a S/N per pixel of 18.

Given that several programs are already underway on both M31 and M33 with DEIMOS, it is likely that a significant fraction of the key science, particularly focussing on substructure, will have been addressed by the time WFMOS comes into routine use at Gemini. The area where WFMOS could play the biggest role is in the characterization of the smooth halo, thick disk and outer thin disk components. WFMOS's high multiplexing capability means more targets can be observed over more area, thus providing much better samples with which to define in detail the dominant structure of the inner halo and outer disk.

4.2 Telescope impact on science

4.2.1 Hemisphere Impact

Different parts of the Galaxy are observed more efficiently from different hemispheres: the outer Galactic disk, particularly in the anti-centre, is better studied from the North, while the Galactic central regions are better studied from the South.

The science for M31 and M33 discussed here is, of course, only feasible if WFMOS has northern hemisphere access. If WFMOS is limited to the southern hemisphere, the case for using it to explore the fossil record in large galaxies is substantially diminished. The next nearby galaxy group in the south is the Sculptor Group, which contains 5 moderately-sized disk galaxies. Located at 2.5-3.5 Mpc, the most luminous red giant branch stars in these systems have magnitudes of $I \sim 23-24$, putting them essentially out of range for detailed spectroscopy with 8-m class telescopes.

The satellite galaxies of the Milky Way are distributed such that the gas rich Magellanic Clouds are Southern objects, while the gas-poor dwarfs are

approximately equally divided. Many of these systems will be targets of other 6 - 8m class facilities, particularly in the South e.g. VLT/FLAMES; Magellan/MIKE.

On balance, we favour the Northern Hemisphere.

4.2.2 *Field of View*

The large sample sizes required argue for a field-of-view of at least 1 degree. The proposed WFMOS field of 1.5 deg diameter is sufficient. We note that the speed of the surveys proposed here scale linearly with the areal field of view.

4.3 *Instrument Requirements*

4.3.1 *Basic Parameters*

4.3.1.1 *What Resolution and Wavelength Coverage are Required?*

4.3.1.1.1 *High-resolution survey*

4.3.1.1.1.1 *Spectral resolution*

A spectral resolution of $R = 40,000$ is the minimum requirement; see Figure 29 and Figure 30 for two independent analyses.

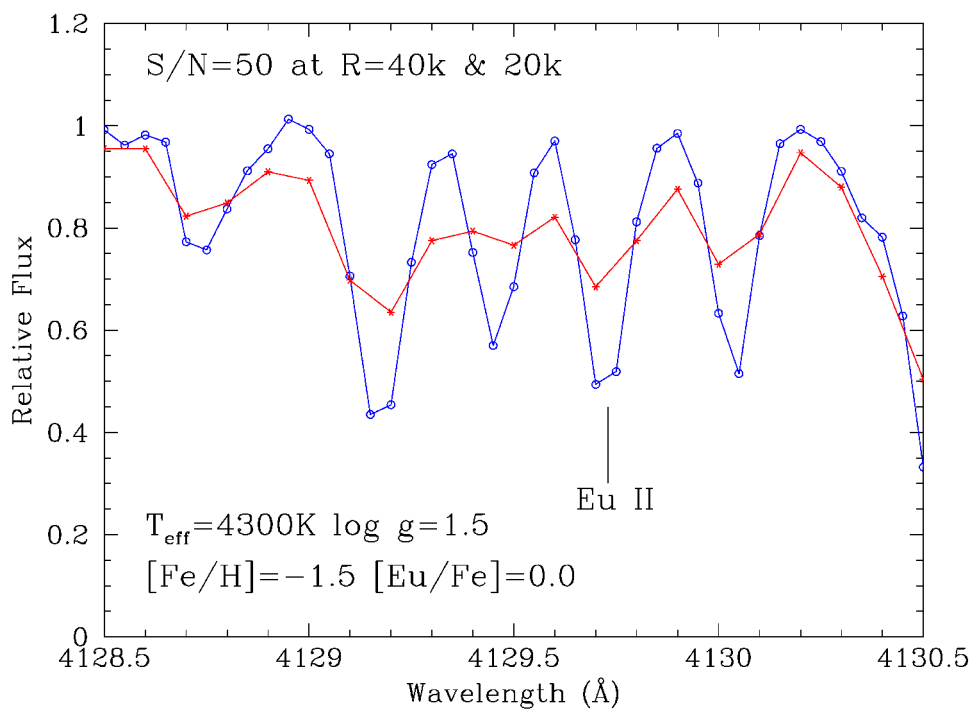


Figure 29. This figure shows two synthetic spectra of the strong Eu II line at 4129.7Å. These are done for S/N=50 and R = 20,000 (red curve) and 40,000 (blue curve).

Figure 29 shows two synthetic spectra of the strong Eu II line at 4129.7Å. These are done for S/N=50 and R = 20,000 and 40,000. The accuracy with which the Eu abundance can be determined will depend on how well the total area of the line profile is mapped and there are simple expressions for Gaussian-like line profiles

(e.g. Cayrel 1988). This would only hold for weak lines, but the uncertainty in the total area of the line is

$$\Delta W = [1.6 * (w * dx)^{0.5}] / SN$$

where w = FWHM of the line-profile, dx = pixel size, and SN = signal-to-noise. In K-giants the typical turbulent broadening is 5-8 km/s, which is nicely matched to an $R = 40,000$ spectrum. In contrast, with $R = 20,000$, the line-width, w , is set by the spectrograph, so we would lose by about a factor of 2 in w , plus if we have a coarser pixel scale, dx , that is another factor of 2. Thus for the same SN, the lower resolution lose a factor of $2(\sqrt{2 * 2})$ in accuracy in defining the line-area (equivalent width). For weak lines, the abundance is directly proportional to w , so the uncertainty would again then be about of factor of 2 bigger for $R = 20,000$ compared to 40,000. Having a higher signal-to-noise (same exposure time) would help at $R = 20,000$; for twice as many counts/pixel the SN improves by 1.4. The accuracy would still be about 40% better at $R = 40,000$ compared to $R = 20,000$.

A more crucial issue is the need to measure the stellar continuum level directly which is very difficult to do in the blue at $R < 40,000$ (Cayrel 1988). Given the choice between higher SNR at $R=20,000$ or lower SNR at $R=40,000$, a large body of literature over many years shows that higher resolution almost always yields more reliable abundances (see section 4.4.2). This is because the measurement errors are dominated by systematics, in particular, the uncertainty in the stellar continuum.

Finally, in Figure 30, we show how the fraction of resolved lines in the Sun increases dramatically to blue wavelengths with resolving power. Bland-Hawthorn & Freeman (2004) – see Appendix – have undertaken a detailed analysis of many thousands of absorption lines for the Sun ($[Fe/H]=0.0$ dwarf) and for Arcturus ($[Fe/H]=-0.6$ giant). They show that α elements and Fe lines are available in one or more ionisation states across the entire optical spectrum. However there is a dramatic rise in the occurrence of s-process and r-process lines below 5000\AA , and a slower rise for iron-peak elements. There are increasingly more heavy element signatures as one goes to shorter wavelengths all the way down to 4000\AA .

The number of chemical signatures required depends on the component of the Galaxy under study, and the number of formation sites which make up that component. This is discussed in the Appendix (e.g. Table 1). When considered with the kinematic information, we estimate that we will need to measure at least ten heavy element abundances to obtain a useful signature. Bland-Hawthorn & Freeman (2004) find that a return of 80% or better ($R=40,000$ down to 4000\AA) is needed to reach ten or more heavy element lines given that, at lower resolutions, most of the resolvable lines arise from Fe and α elements. This underscores the importance of high resolution spectroscopy at blue wavelengths for detailed abundance work of both dwarfs and giants.

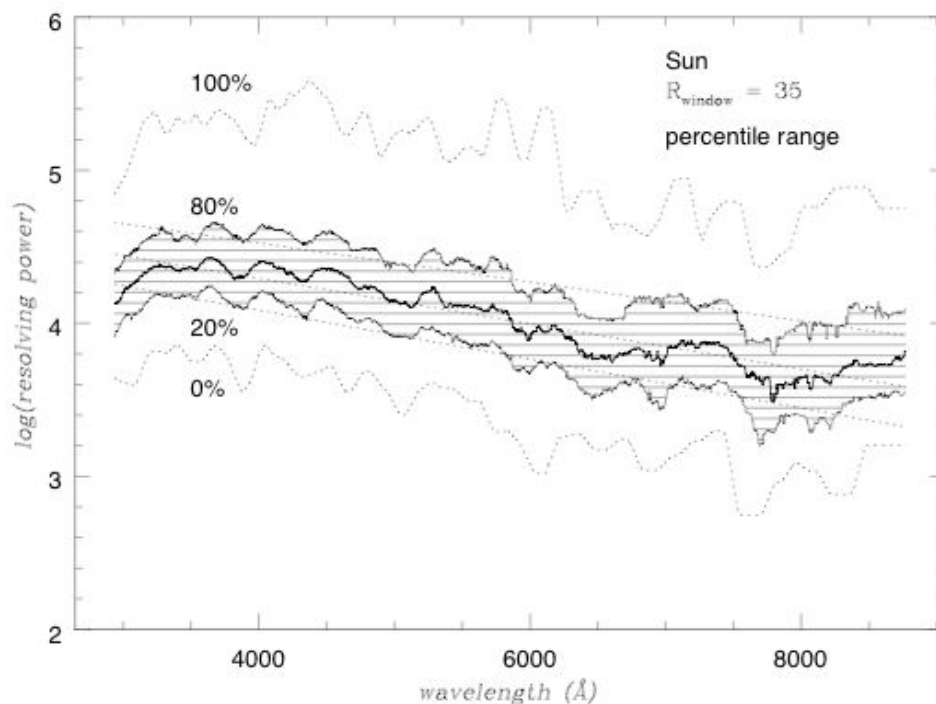


Figure 30. Taken from Bland-Hawthorn & Freeman 2004. The y-axis is the log of the spectral resolution, while the lines are contours of percentage of spectral lines that are resolved, as a function of wavelength. While this is shown for the Sun, a study of the spectral lines in the metal poor giant Arcturus gives a remarkably similar distribution. In order to reach the heavy element lines, our goal is 80% or better down to 4000Å, requiring a minimum of $R = 40,000$.

4.3.1.1.2 Wavelength Coverage

The required wavelength coverage depends on the target elements. Defining a useful set of elements to analyse in large samples of stars must include nuclei from a variety of nucleosynthetic sources in order to characterize the program stars in as much chemical detail as possible. This is analogous to DNA analysis in biological systems; the chemical abundance distribution that characterizes a star reveals much about its stellar ancestry, and comparisons of abundance distributions can yield possible links between different populations. A minimum set of elements to examine over a limited spectral range (that can be observed with one setting per star at high resolution) would include the following:

- O, Mg: products of massive SN II. These can probe contributions from the very massive core collapse supernovae ($M \geq 20M_{Sol}$)
- Si, Ca, Ti, Cr: also products of SN II, but with yields not as strongly weighted towards the more massive SN II, as are O and Mg. Combining O and Mg with this subset of even-Z nuclei can provide information on IMF's.
- Mn, Co: from SN II, these elements have metallicity dependant yields, such that ratios such as Mn/O or Co/O can probe chemical enrichment time scales in populations. The ratio Co/Mn may also be a useful probe of contributions from very energetic SN II, referred to as “hypernovae”.

- Eu: the best r-process indicator in stars. The r-process site has not been identified uniquely, but is almost certainly associated with SN II. There are some arguments that the r-process is driven most efficiently in lower-mass SN II ($M \sim 10 - 11M_{\text{Sol}}$).
- Y, Zr, Ba, La: mostly s-process elements, associated with synthesis in lower-mass AGB stars (evolving on Gyr-type timescales). In some metal-poor populations, these elements may actually be dominated by an r-process, but their abundance ratios, relative to Eu, can be used to quantify r- and s-process relative contributions.
- Fe, Ni: fiducial elements used to establish “metallicity”, largely because of numerous spectral lines. Both are useful in tracking contributions from SN Ia, which are expected to begin contributing to chemical enrichment on timescales of ~ 1 Gyr. Fe is also useful in checking, or in defining, stellar parameters, i.e. effective temperature and surface gravity.

Assuming red giant targets with metallicities from roughly solar, down to $[\text{Fe}/\text{H}] \sim -2.5$, then one red setting can be used to sample all of the above elements, as well as many others. This metallicity range covers the bulk of the stellar populations of the Milky Way; however, it misses an important population, possibly the “first star” which contain crucial information about the primordial IMF. The wavelength range will be set by the bluest and reddest lines required to sample the suite of defined elements: in this case, it will be Mn I at 6013\AA and 6021\AA and Eu II at 6645\AA -about 650\AA . If we midrange our discussion of resolutions and take $R = 40,000$ for 2-pixels, this would require $0.10\text{\AA}/\text{pixel}$, or 6500 pixels to sample the wavelength range. Hence cannot be achieved in one go. Other lines that fall in this wavelength interval “for free” include measurable lines from: Na I, Al I, Sc II, V I, Nd II. Notable elements we miss are Cu and Zn.

At the lowest metallicities defined by stars in the Galaxy, say $[\text{Fe}/\text{H}] < -2.5$, many of the red lines will become too weak, and we would have to shift wavelength regions to the violet, around $4100\text{-}4600\text{\AA}$, but we would be able to cover the same set of elements. In red giants, at the higher metallicities, these lines are too strong to be reliable abundance indicators and the violet spectral region is heavily blended. The lowest metallicity stars, candidates for which will be identified from the low-resolution survey, require the blue spectral region, and may well show patterns of elemental abundances consistent with enrichment from pair-instability supernovae from primordial, Population III stars (Heger & Woosley 2002).

Coverage of all metallicities would require two different data sets, but a suitable sample of stars at some intermediate/overlapping metallicity could be observed at both settings in order to calibrate the two different wavelength regions and thus to remove any abundance offsets.

The bottom line is that we would like to sample something like 650\AA at high resolution...the higher the better, but we are limited but what can be designed and built. As we are forced to restrict wavelength, we will lose information from the range of elements we can sample. We also want a flexible instrument that can observe at other wavelengths covering the visual part of the spectrum.

With $R = 40,000$, and a 2-pixel resolution element, at 5000\AA we have about $0.1\text{\AA}/\text{pixel}$. A 4K (6K) chip then would yield 400\AA (600\AA), which is acceptable for one-shot.

4.3.1.1.2 Low resolution survey

The requirements are to provide kinematics good enough to assign, in a statistical sense, a star to a given stellar population (e.g. thin disk, thick disk or halo); this is then an accuracy of ≤ 20 km/s. Similar requirements for metallicity imply an accuracy of ≤ 0.3 dex. Both requirements are met by $R \sim 2000$, as provided by the Sloan Sky Survey spectrograph design.

The radial velocity measurements use cross-correlation techniques and are not demanding on wavelength coverage provided spectral features are present. Metallicity measurements of low-metallicity stars are facilitated with blue coverage, extending if possible to the Ca II H & K lines at $\sim 3900\text{\AA}$ (cf. Beers et al. 1999).

4.3.2 Data Reduction Requirements

The survey will need automated radial velocity determinations (done as for RAVE; Steinmetz 2003) and also automated determination of stellar parameters such as gravity, effective temperature and metallicity and/or elemental abundances. For the low-resolution survey, which has a large wavelength coverage, the stellar parameters may be estimated by fitting lots of templates to the spectra and finding best fit $\log g$, T_{eff} and $[\text{Fe}/\text{H}]$ template. This has been started for RAVE and for SDSS (e.g. Allende-Prieto et al. 2004). Note that the technique is not a simple case of finding the highest value of the Tonry-Davis cross-correlation R -parameter, but rather one needs to compare the template spectrum and target spectrum using a minimum distance scheme which is sensitive to equivalent widths of absorption lines (Zwitter, Munari & Siebert 2004; Thevenin & Foy, 1983). Verne Smith has been developing an automated technique for chemical abundance analysis. Preliminary results are shown in Figure 31.

Table 4. Desired elements and lines, red wavelength range.

Element	Species	Approx. wavelength
Zinc	Znl	4800 \AA ; 6362 \AA
Sulphur	Sl	8694 \AA ; 9220 \AA
Iron	Fel	Lots
Iron	Fell	Lots
Oxygen	[OI]	6300 \AA
Magnesium	Mgl	6320 \AA
Silicon	Sil	6125 \AA
Calcium	Cal	6170 \AA ; 6455 \AA
Titanium	Til	6260 \AA
Nickel	Nil	6175 \AA
Europium	Eull	6645 \AA

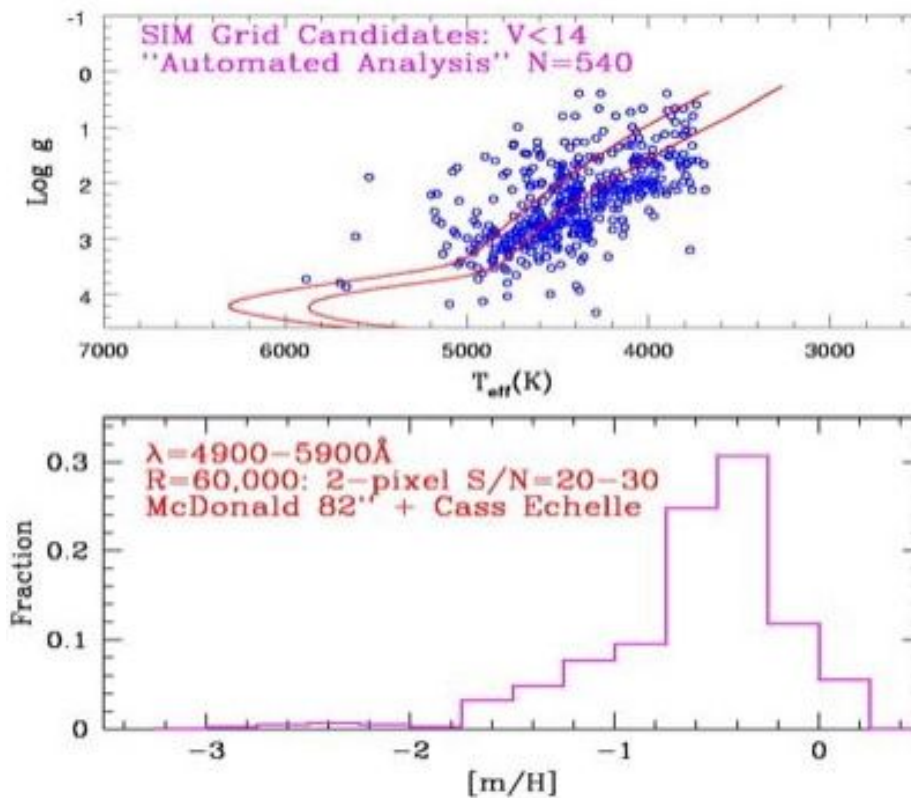


Figure 31. An example of a simple ‘automated’ abundance analysis using SIM grid stars as a test. The top panel shows derived stellar parameters plotted as Log g versus T_{eff} (a stellar atmosphere version of an HR diagram) along with sample isochrones. The bottom panel shows a ‘metallicity’ distribution derived from these giants by matching, via least squares, the observed spectrum to a synthetic one. In this case ‘metallicity’ includes all heavy elements and the abundances were changed by scaling solar abundances, i.e. no alpha-element enriched models. The data reduction and matching of observed to synthetic spectra was done totally ‘hands-off’. The SIM grid candidates are typically 1-3 kpc away and are probably dominated by thick disk stars, so this metallicity distribution would be determined largely by the thick disk population.

Sky subtraction has to be optimized; nod-and-shuffle will clearly help, but we can also limit the magnitude range within any one spectrograph to ~ 3 magnitudes to reduce the effects of scattered light in the instrument (cf. Wyse & Gilmore 1992).

4.3.3 Acquisition Requirements

The main requirement here is that the acquisition overheads be low in order to carry out the surveys in an efficient manner. The low-resolution survey will have typical exposure times of 30-60 min per pointing, and therefore acquisition overheads need to be short (~ 5 min) for efficiency. In addition, we require that the fiber repositioning be possible in situ at any sky / telescope position, and that the telescope not have to return to a stow or reference position for each fiber repositioning.

4.3.4 Calibration Requirements

We will need repeat observations, for both internal consistency checks and for the identification of binary systems. We also require radial velocity standards and metallicity standards. Twilight sky frames are extremely useful to understand

systematics across the slit. Note that for the few km/s velocity precision we require the standard HeNeAr arc lamps suffice; we do not need e.g. an iodine cell as required for the planet-detection m/s precision.

We require that the instrument be stable enough that usable calibration frames can be obtained during the daytime for a given night's observations. It would be even preferable if an entire campaign can be adequately calibrated using a set of afternoon calibrations (wavelength, flat-field, flux) taken during intermittently during the campaign. This would greatly reduce the time lost during the night for calibration, and greatly improve the efficiency of the instrument. This is crucial since the surveys proposed here are large and require significant amounts of telescope time, even for very low instrumental and telescope overheads. Every attempt needs to be made to minimize these overheads.

4.4 *Observing scenarios*

4.4.1 *Survey Parameters*

The primary targets are Galactic stars; from Gilmore's star-count model, as quoted in *Astrophysical Quantities* (table 19.11), there are 2×10^8 stars over the entire sky down to $V=18$ and an order of magnitude more down to $V=22$ (see Table 5).

Table 5. Predicted Log star counts per square degree in the V-band

V	$ b = 20^\circ$	30°	60°	90°
17	3.36	3.12	2.67	2.55
18	3.61	3.35	2.87	2.74
19	3.85	3.56	3.05	2.92
20	4.06	3.75	3.23	3.09
21	4.24	3.91	3.39	3.25
22	4.38	4.05	3.54	3.38

Fields at intermediate latitude, $|b| \sim 45^\circ$, are optimal for studies of the thick disk and halo, with thin disk stars dominating number counts below this. A stripe at fixed longitude allows the transitions between these main components to be studied (and again constrains substructure). The choice of longitude determines the ability to discriminate between the various stellar components by their mean azimuthal streaming (cf. Gilmore, Wyse & Norris 2002). The cardinal directions of $l = 0^\circ, 90^\circ, 180^\circ$ and 270° are obvious high priorities, particularly with the (future) prospects of proper motion data. The 'rotation' directions of $l = 90^\circ, 270^\circ$ are highest priority. Obviously the hemisphere of the telescope puts further constraints, as discussed in section 4.4.5 below.

4.4.2 *The High-Resolution Survey*

For the high resolution survey limit of $B \sim 18, V \sim 17$, in a 2 square degree (1.5 degree diameter) field there are ~ 1400 stars per field at $|b| = 45^\circ$. The current WFMOS concept devotes 1500 of 4500 fibers to the high-resolution spectrographs, extremely well-matched to the stellar surface density at these magnitudes. In order to target a large enough volume of the thick disk and halo, we need to reach to an apparent mag $V = 17$ (equivalent to $I \sim 16.5$).

If we adopt Gilmore's model (Gilmore, Reid & Hewett 1985) of the Galaxy (see also Robin et al. 2003), within our magnitude range towards the Galactic poles,

there are about 230 stars deg^{-2} with the following breakdown: 140 thin disk main sequence (MS), 45 thick disk MS, 10 halo MS, 15 evolved (subgiant or red giant) thick disk, 15 evolved halo, 5 halo horizontal branch. Along a cardinal sight line of ($l = 90^\circ$, $b = 30^\circ$), these numbers increase to 820 stars deg^{-2} , with the following breakdown: 660 thin disk main sequence (MS), 80 thick disk MS, 10 halo MS, 4 evolved thin disk, 43 evolved (subgiant or red giant) thick disk, 15 evolved halo, 5 halo horizontal branch. This amounts to 60 thick disk stars towards the poles, and 120 stars at the lower latitude; we observe about 30 halo stars along either sight line.

In summary, for a 2 square degree field, for the high-resolution survey we detect 100,000 thick disk stars in 500 - 1000 fields (depending on coordinates), and 30,000 halo stars in about 1000 fields (less dependent on exact coordinates). These are the required sample sizes for chemical tagging as discussed in Section 3 of the Appendix. For comparison, the number of thick disk and halo stars currently with high resolution spectra and detailed elemental abundances number in the hundreds (Cayrel et al. 2004; Nissen 2004; Feltzing et al. 2003; Bensby et al. 2004; Honda et al. 2004).

Table 6. Distance limit in log(parsecs) for different stars as a function of apparent V magnitude: metal poor giants (MPG), metal rich giants (MRG), clump giants (CG), blue horizontal branch halo (BHB), and main sequence dwarfs. The second column is the absolute V magnitude of the star. Brackets help to delineate the transition between 1 - 10 - 100 kpc. Note that the Solar Circle provides an extra 8 kpc in radial extent such that surveys which reach the Galactic Center also reach the outer disk.

	V	13	14	15	16	17	18	19	20
MPG	-2.0	(4.0)	4.2	4.4	4.6	4.8	(5.0)	5.2	5.4
	-1.5	3.9	4.1	4.3	4.5	4.7	4.9	5.1	5.3
MRG	-1.0	3.8	(4.0)	4.2	4.4	4.6	4.8	(5.0)	5.2
	-0.5	3.7	3.9	4.1	4.3	4.5	4.7	4.9	5.1
	0.0	3.6	3.8	(4.0)	4.2	4.4	4.6	4.8	(5.0)
CG/BHB	0.5	3.5	3.7	3.9	4.1	4.3	4.5	4.7	4.9
	1.0	3.4	3.6	3.8	(4.0)	4.2	4.4	4.6	4.8
	1.5	3.3	3.5	3.7	3.9	4.1	4.3	4.5	4.7
A	2.0	3.2	3.4	3.6	3.8	(4.0)	4.2	4.4	4.6
	2.5	3.1	3.3	3.5	3.7	3.9	4.1	4.3	4.5
	3.0	(3.0)	3.2	3.4	3.6	3.8	(4.0)	4.2	4.4
F	3.5	2.9	3.1	3.3	3.5	3.7	3.9	4.1	4.3
	4.0	2.8	(3.0)	3.2	3.4	3.6	3.8	(4.0)	4.2
	4.5	2.7	2.9	3.1	3.3	3.5	3.7	3.9	4.1
G	5.0	2.6	2.8	(3.0)	3.2	3.4	3.6	3.8	(4.0)
	5.5	2.5	2.7	2.9	3.1	3.3	3.5	3.7	3.9
	6.0	2.4	2.6	2.8	(3.0)	3.2	3.4	3.6	3.8
	6.5	2.3	2.5	2.7	2.9	3.1	3.3	3.5	3.7
K	7.0	2.2	2.4	2.6	2.8	(3.0)	3.2	3.4	3.6
	7.5	2.1	2.3	2.5	2.7	2.9	3.1	3.3	3.5

4.4.3 Low-Resolution Survey

For the low-resolution survey of the Milky Way Galaxy, there are 1500 stars per square degree even at the poles, and so selection by colour is desirable. A simple red colour cut would act to remove nearby faint red disk stars, but we have to be careful that distant red giants not also be removed; horizontal branch stars are

easier to retain. By the time of an operating WFMOS there will be publicly available many photometric surveys in several bandpasses, sufficient to use sophisticated multi-colour cuts to ensure selection of e.g. metal-poor red giants (for example, SDSS filters, Helmi et al. 2003). Note that the Galactic surveys cannot share fibers with $\omega(z)$ project, but will need to be done in series.

For the low-resolution survey, a minimum of 400 square degrees (the basis for the investigations of section 4.1.3.1) is required to detect streams, or place a meaningful limit on their importance. The survey ‘footprint’ can be chosen in a way to be optimal also for the determination of the joint kinematic-metallicity distribution functions of the dominant stellar populations. For the latter, as noted above, we wish to target constant longitude stripes at cardinal directions (coverage will depend on hemisphere of telescope!). In the model survey below, we observe as much of the high-latitude sky is accessible in 10 degree stripes about the four cardinal longitudes, giving a sample size of around a million stars, over more than a thousand degrees.

4.4.4 Required support for observation preparation

4.4.4.1 Precursor Surveys

Photometric surveys are required for target selection. At present, 2MASS is all-sky and for point sources at latitudes $|b| > 10^\circ$ has limiting magnitude (S/N > 10) of $K_s = 14.3$. The southern sky has DENIS to $I \sim 18.5$ and Schmidt Plate scans (e.g. SUPERCOSMOS) to $B_r \sim 23$ (Hambly et al. 2001). The northern sky has SDSS, soon hopefully to be extended, plus several smaller deep surveys e.g. NOAO Deep, wide survey. There are several photometric surveys that will be undertaken prior to the commissioning of WFMOS e.g. UKIDSS (using UKIRT) doing an IR survey to complement SDSS, to $K = 18.5$ in the north, the CFHT Legacy Survey also in the North, and two dedicated telescopes in the south, VST (a 2.5m telescope like the SDSS), and VISTA, a 4m IR survey. Further, several wide-field imagers such as SuprimeCam etc will have been working for years and should have built up databases.

In any case, one can do precursor surveys as required with 4m telescopes, if need e.g. DDO or Washington photometry for excellent dwarf/giant separation.

At the faintest limits, star-galaxy separation is an unavoidable issue, with galaxies out-numbering stars. The spectra of course will make a mis-identification immediately obvious, and this is where having the large multiplexing capability is extremely useful.

4.4.5 End-to-End observing cycle

4.4.5.1 Operational model

The requirements in terms of telescope time for the working scientific requirements described above can be modelled by specifying a field distribution of 10-degree-wide stripes in the directions of $l = 0^\circ, 90^\circ, 180^\circ, \text{ and } 270^\circ$ with $|b| > 45^\circ$, where the sign of b depends on the telescope site. How much telescope time do we need to observe the ~ 1200 fields? Do we prefer Mauna Kea or Cerro Pachon? A number of variables affect this calculation:

1. The telescope site.
2. The distribution of weather and atmospheric statistics: cloud cover and image quality.
3. The phase and location of the Moon with respect to the fields.
4. The length of the WFMOS observing blocks, including overhead for instrument installation.
5. Observing time including overheads: slew time, fiber setup time, exposure time, readout time.
6. The inclusion of smaller-scale "P.I." science projects running concurrently with the main surveys.

With the goal of minimizing the time required to complete the Galactic survey, we have developed a model that attempts to find the optimum order in which to observe each of the fields. Currently, the model takes as input the list of targets, the target brightness's, the desired S/N of the spectra, the average seeing and transparency of the Gemini sites, and the observing overheads. For each of the fields, it then calculates on an hourly basis the air masses and sky brightness's (including the contribution from the Moon) for every time at which those fields could be observed. The model attempts to find the order of observations that minimizes the total amount of time needed for the survey. It begins with an order set by the criterion that the telescope always observe the field closest to the zenith at a particular time, so-called "greedy optimization". It then uses the algorithm of simulated annealing in an attempt to further optimize this order. (In practice, we found that both optimization algorithms gave very similar results; while we will continue to attempt to find an order that minimizes the amount of telescope time used, for now we report only the results of the greedy optimization). The merit function uses the results of the KAOS exposure time calculator with parameters set by the fixed inputs and the combination of time-variable inputs (e.g. airmass, sky brightness) appropriate for the particular field order being tested. We have used this model and its inputs to address the questions of telescope time needed for the survey, the preferred lengths of the instrument blocks, and the preferred telescope site.

To begin, Figure 32 illustrates the fraction of the year that our proposed survey fields are visible at Mauna Kea and at Cerro Pachon. The field distribution, outlined by the cross, is projected onto the celestial sphere. The colour scheme indicates the fraction of nights over the course of the year that a piece of sky is more than 30° above the horizon. If the main evaluation criterion for the telescope site is flexibility of scheduling, then the fact that we can observe some of our fields for a larger portion of the year at Cerro Pachon than at Mauna Kea gives Cerro Pachon an advantage.

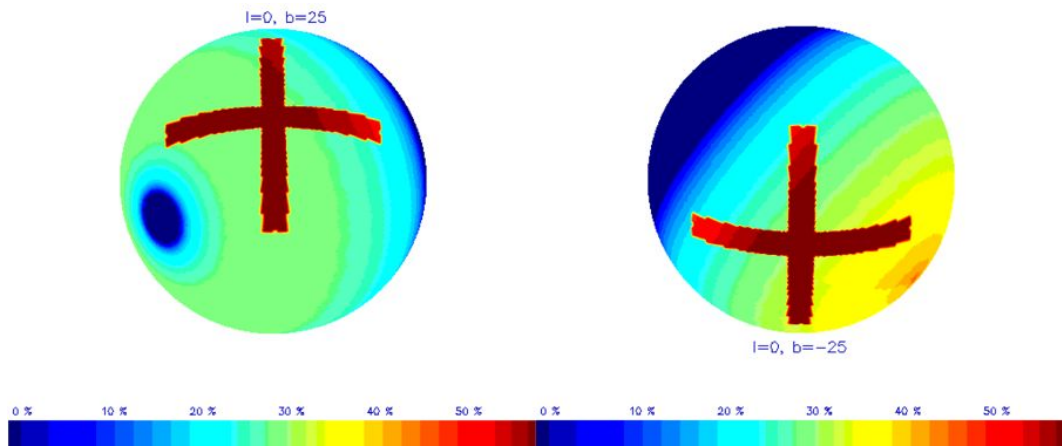


Figure 32. Visibility of our survey area from Mauna Kea (left) and Cerro Pachon (right). The survey area has been projected onto the celestial sphere. On the left, the sphere is aligned such that the Galactic coordinate $l = 0$, $b = 25$ lies on top of the sphere; on the right, $l = 0$, $b = -25$ lies on the bottom. The colour-coding represents the fraction of the available observing time in a given year that a point on the sphere rises at least 30° above the horizon, quantified by the scale at bottom. The interior of our survey area has arbitrarily been coloured red to distinguish it from the surroundings.

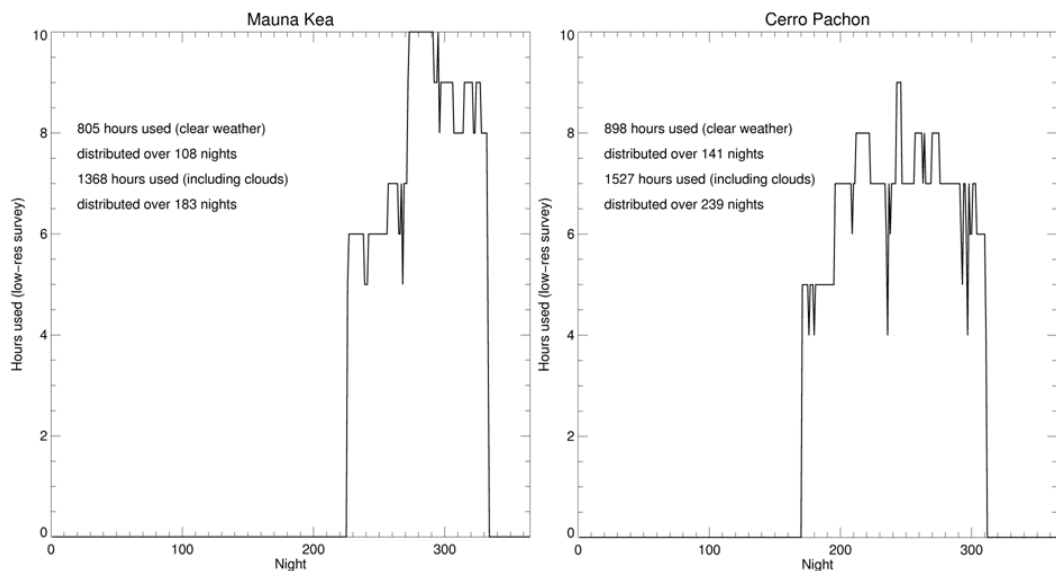


Figure 33. Results from runs of our operational model. The model simulates the time needed to observe our 1188 target fields at low resolution, assuming a central wavelength of $\lambda = 6100\text{\AA}$, $S/N=30$ at $V=20$, $0.8''$ seeing, and clear weather. At Mauna Kea, we begin observations on August 13, 2010, while at Cerro Pachon we begin on June 19, 2010. We find that at Mauna Kea, our survey requires 805 hours of time distributed over 108 nights; at Cerro Pachon, we require 898 hours distributed over 141 nights. Folding in the effects of clouds, we find that we require a factor ~ 1.7 more time than in clear weather.

Siting the telescope at Cerro Pachon, however, comes at considerable cost in telescope time. Figure 33 shows the time needed to complete the low-resolution survey proposed here, assuming completely clear weather and seeing of $\sim 0.8''$. We have adopted a minimum goal of S/N per pixel of 30 at $V=20$; this requires an exposure time of 30min. In the simulations the average exposure time was 45min and this also provides S/N per pixel of ~ 5 for $V=22.5$, sufficient for velocities. Although the period of time during which our fields may be efficiently observed at Mauna Kea is relatively short compared to Cerro Pachon, the minimum airmass of the fields is, on average, smaller at Mauna Kea, reducing the total observing time by 10% compared to Cerro Pachon. Moreover, the observing efficiency is higher,

such that a span of 108 clear nights completes the low-resolution survey at Mauna Kea, versus 141 clear nights are needed at Cerro Pachon. We thus prefer Mauna Kea over Cerro Pachon from an operational point of view.

What will be the effect of weather on the survey time? Figure 34 shows the cumulative distribution of cloud cover published on the Gemini website in units of magnitudes of extinction; also shown is the derivative of the cumulative distribution. Using the differential distribution of cloud cover, we can calculate the average extinction by clouds for a given fraction of the available time that is used by the survey. We see that if we use 100% of the time that the telescope is open, the effect on the survey is to add ~ 0.5 magnitudes to the length of the survey. For the low-resolution survey, we thus account for weather losses simply by scaling the amount of time needed to complete the survey in perfectly clear weather by a factor 1.7. Thus, we estimate that we need 1368 hours of time to complete the low-resolution survey, distributed over ~ 183 nights, assuming the instrument is sited at Mauna Kea.

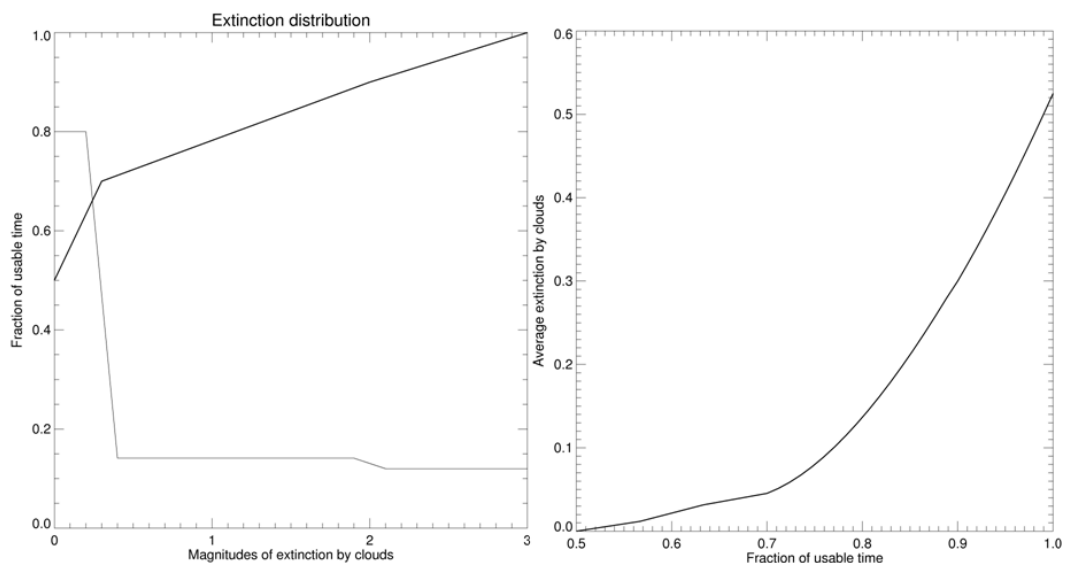


Figure 34. Gemini weather statistics. Left: the thick black line shows the cumulative distribution of cloud cover in units of magnitudes of extinction, as published on the Gemini web site. The thin line shows the differential cloud cover distribution. Right: The average extinction by clouds for a given fraction of time that is deemed usable, as derived from the distributions on the left. By observing 100% of the time that the telescope is open, we effectively add ~ 0.5 magnitudes of extinction to our targets, resulting in ~ 1.7 times more time used.

The limited observability of the fields at Mauna Kea immediately suggests a natural length of the observing blocks of ~ 110 days over the months of August to December. Shorter observing blocks can of course be accommodated, at a cost in instrument switching time. Longer observing blocks force our survey to use less than $\sim 70\%$ of the available time on a given night, as is evident in Figure 35.

To calculate the time needed for the high-resolution survey, we simply scale the time needed by the ratio of the typical exposure times. Assuming $\sim 15\%$ total system throughput for the echelle spectrograph setups, we find we need 1.75 hours to produce $S/N=50$ over a three-pixel resolution element at for the target $V=17$ K giant. This number is very similar to the published sensitivity limit of the UVES spectrograph ($V=19.5$ in 1.5 hour for $S/N=10$, $R = 62,000$, seeing $0.7''$). This exposure time is typically ~ 3.2 x longer than that for the low-resolution survey.

We thus conclude that the high-resolution survey requires ~ 4900 hours of observing time distributed over 765 nights, or $\sim 7 \times 110$ -night observing blocks.

There are two ways in which smaller-scale “PI” projects could be incorporated into the Galactic survey. As seen in Figure 35, the survey is almost never able to use 100% of a given night given the desired field distribution. In every 110-night block, ~ 200 hours, or 20% of the available time, is left open for other uses. This time could either be used by the dark energy survey or by smaller projects. The other way to assign time to smaller-scale projects is through the unassigned fibers in any given field, with the constraint that the spectrograph setup and exposure time will be fixed by our survey needs.

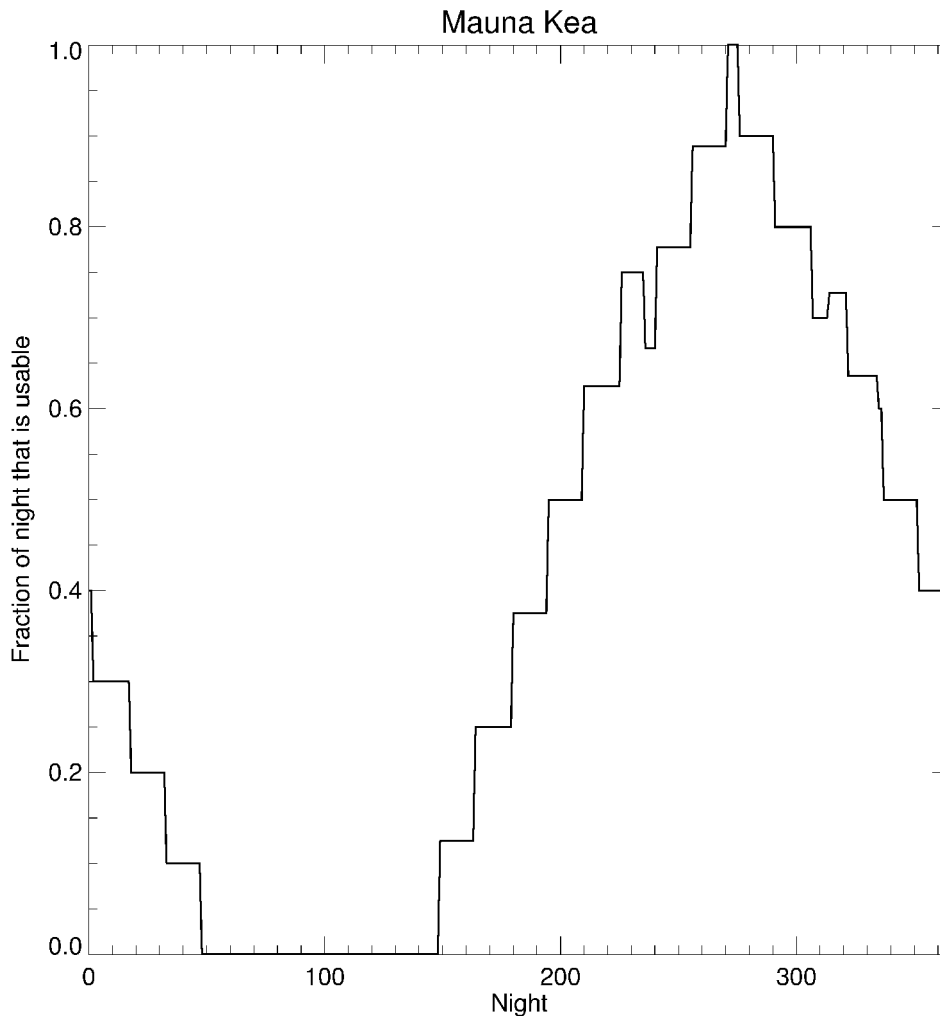


Figure 35. The fraction of time on a given night that is useful to our survey, given our field distribution. There is a ~ 110 -day window in August - December where we are able to use $>70\%$ of every night.

4.4.5.2 Fiber assignment

The WFMOS instrument design assigns $1/3$ of the full fiber set to the high resolution spectrographs, with the remainder to the low resolution spectrographs and infrared spectrographs. The high resolution fibers will be distributed in a hexagonal pattern, with each fiber able to access a circular patch of sky $80''$ in radius. The placement of the fibers is such that that any point on the field is

accessible to a fiber, but only a small fraction of the field is accessible to more than one fiber.

Figure 36 demonstrates the fraction of our targets to which we will typically be able to assign fibers in our high resolution survey. In this example, we consider a field at $l = 90$, $b = 55$, which contains an intermediate density of stellar targets. Using the SDSS DR3 source catalogue, we first selected as possible high resolution targets all sources with $r' < 18$ and $0 < g' - r' < 2$. Of the 613 available fibers, we found we could assign 484 (or 79% of the full set) to targets, of which there were 893 within the 1-degree diameter field. Thus, roughly half of our targets have assigned fibers. However, we may choose to exclude the reddest stars, as these are likely foreground thin disk dwarfs. Using a stricter colour selection criterion of $0 < g' - r' < 0.8$, we found that we were able to assign fibers to 74% of the 479 objects, using 58% of the full fiber set. We thus expect to be able to observe ~ 50 -75% of our target list at high resolution, using ~ 50 -75% of the available fibers. For the low-resolution survey, both the target assignment rate and the fiber usage rate will be larger owing to the larger target density and the larger number of fibers.

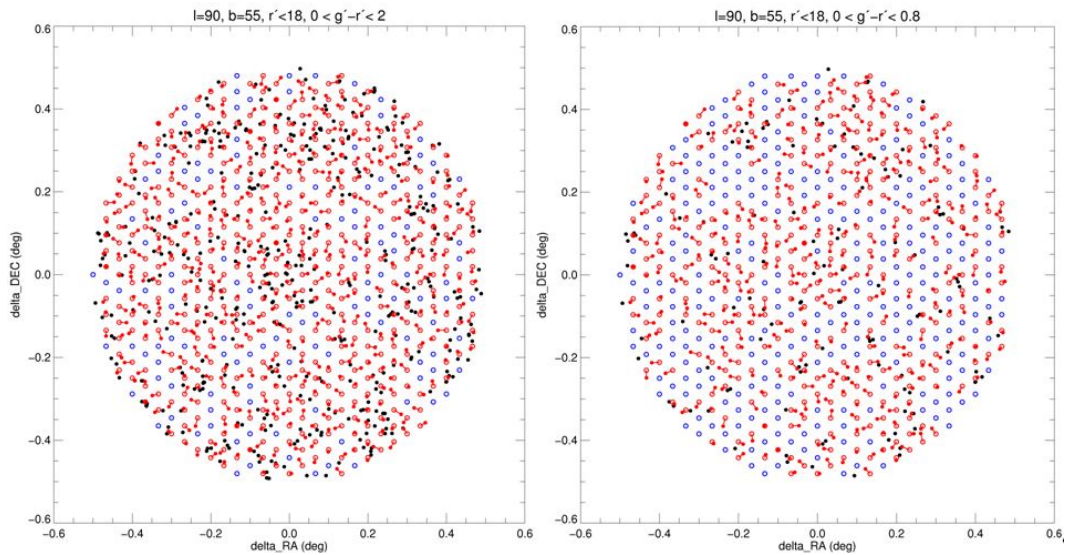


Figure 36. Trial high-resolution fiber assignments for a field at Galactic coordinate $l = 90$, $b = 55$. Filled circles are target stars from the SDSS DR3 catalogue, while open circles represent the fiducial positions of the fibers. Assigned star-fiber pairs are coloured red, with red lines joining the pairs. Black filled circles are stars with no fibers assigned to them. Blue open circles are unassigned fibers. On the left, the criteria $r' < 18$ and $0 < g' - r' < 2$ have been used to select targets. On the right, we select only those stars with $r' < 18$ and $0 < g' - r' < 0.8$, so as to weed out thin disk red dwarfs.

4.5 Other Facilities

4.5.1 Complementary

Ground-based complementary projects are discussed earlier.

The Yale Southern Proper Motion survey will provide data for stars in a significant fraction of the Southern sky ($-22 < \delta < -45$), to $V < 17.5$, nicely complementing the high-resolution survey (provided the instrument is sited at Gemini South).

The ESA Cornerstone mission GAIA (expected launch date mid-2011) will provide at mission end (launch + 5 years) unprecedented astrometric and photometric data to $V=20$. The Radial Velocity Spectrometer will also provide multi-epoch radial velocities at moderate resolution ($R = 11,500$ over $8480\text{\AA} - 8740\text{\AA}$) for around 10^8 stars to $V = 17$ (see e.g. Katz et al. 2005).

Deep imaging of selected Galactic targets and extra Galactic targets with HST to obtain colour-magnitude diagrams will aid determination of e.g. reddening and ages.

4.5.2 Competition

For the low-resolution survey, WFMOS will target stars in the magnitude range $17 \leq V \leq 22$ and be exactly complementary to RAVE (southern hemisphere) and to GAIA (all-sky). GAIA will obtain moderate-resolution ($R = 11,500$) spectra, and hence radial velocities, only for stars brighter than $V=17$ (e.g. Perryman et al. 2001; Katz et al. 2004). RAVE, using the 6dF spectrograph on the UK Schmidt telescope, will concentrate on the brightest stars for which GAIA may saturate, $V < 12$ (Steinmetz, 2003).

Competition comes from SDSS/SEGUE plus possible surveys using AAOmega on the 4m AAT, FLAMES/GIRAFFE on the VLT and IMACS on Magellan (all southern hemisphere) and from DEIMOS on Keck (Northern hemisphere). The southern hemisphere telescopes cannot access a significant fraction of the outer Galactic disk where we have at present woefully limited information and much interest. SDSS/SEGUE and AAOmega will be most effective at the brighter end of the WFMOS target range and is not competitive for the bulk of the WFMOS low-resolution targets. The planned SDSS/SEGUE survey will be sparse-sampled whereas our much greater multiplexing capability allows much larger samples of fainter stars in a given line-of-sight, and dense packing. Our fainter limits probe the halo efficiently and effectively. DEIMOS utilises a slit-mask rather than being a fiber-fed spectrograph and so can go fainter than WFMOS, but this is of most interest for extra-Galactic stars (at $V = 22$, a giant with $M_V = 1$ is at 158 kpc and a dwarf with $M_V = +5$ is at 25 kpc). While there is no record of large Galactic surveys with Keck or with the VLT, we may assume some effort there; Indeed a modest effort using time with poor seeing has been initiated, again limited to the brighter stars $V \leq 19$. It is unlikely that more than a few times 10^4 stars would be observed by any one PI-project (this is the size of the DEIMOS M31 survey discussed below). As we discussed, sample sizes orders of magnitude larger is required for reaching the next level in understanding.

Competition for the high-resolution survey comes from the MIKE single-object echelle spectrograph on Magellan; a significant target will be the southern dwarf spheroidal galaxies (Mateo, PI). We have not discussed them as science targets, since they are now being studied by two large surveys (PIs Tolstoy and Gilmore respectively) with the VLT with FLAMES/GIRAFFE and FLAMES/UVES and will certainly be largely completed by the time of WFMOS. Note that FLAMES/UVES provides resolutions of 47,000 but is limited to only 8 fibers while FLAMES/GIRAFFE is limited to resolutions $\leq 25,000$ with 130 fibers. These are also not competitive in terms of time-to-completion for the large surveys conceived here.

With the (favoured) northern hemisphere, Keck does not offer a competitive multi-object high-resolution spectrograph.

4.6 Risks to the Science

The main risk to the science is that the instrumental set-up fails to deliver the required multiplexing and field-of-view to provide the orders-of-magnitude leap in sample size that makes these surveys feasible.

Some of the science will be addressed by competitors but the full surveys are highly unlikely to be achieved.

The spectral resolution for the high-resolution survey is critical; as discussed above the elemental abundances will be compromised if $R = 40,000$ is not achieved. Some compensation can be made by the higher S/N for a given exposure time, at lower resolution, (also discussed above) but more likely an increased exposure time will be required, still with accompanying loss of precision due to line blending.

4.7 References

- Beers, T. et al. 1999, AJ, 117, 981
- Bensby, T., Feltzing, S. & Lundstrom, I. 2004 A&A, 415, 155
- Bland-Hawthorn, J. & Freeman, K.C. 2000, Science, 287, 79
- Bland-Hawthorn, J. & Freeman, K.C. 2004, PASA, 21, 110
- Bullock, J., Kravtsov, A. & Weinberg, D. 2001 ApJ, 548, 33
- Carney, B. & Seitzer, P. 1993, AJ, 105, 2127
- Cayrel, R. 1988, In The Impact of Very High SNR Spectroscopy on Stellar Physics, 1988, IAU Symp. 132, 353
- Dehnen, W. & Binney, J. 1998, MNRAS, 298, 387
- De Silva, G., Sneden, C., Paulson, D., Asplund, MA, Bland-Hawthorn, J., Bessell, MS, Freeman KC 2005, ApJ, in prep.
- Djorgovski, G. & Sosin, C. 1989 ApJ, 341, L13
- Feltzing, S., Bensby, T. & Lundstrom, I. 2003 A&A, 397, L1
- Ferguson, A. et al 2002, AJ, 124, 1452
- Ferguson, A. et al 2004, astro-ph/0408058
- Ferrarese, L. & Merritt, D. 2000, ApJ, L9
- Font et al 2004, astro-ph/0406146
- Freeman, K. & Bland-Hawthorn, J. 2002, ARAA, 40, 487

Gilmore, G., Wyse, R.F.G. & Norris, J, 2002, ApJL, 574, L39

Guhathakurta, R. et al 2004, astro-ph/0406145 (AJ submitted)

Hargis, J.R., Sandquist, E.L., & Bolte, M. 2004, ApJ, 608, 243

Helmi, A., White, S.D.M., & Springel, V. 2003, MNRAS, 339, 834

Helmi, A. et al.2003, ApJS, 152, 113

Honda, S. et al.2004, ApJS, 152, 113

Ibata, R. et al., 2001 Nature, 412, 49

Ibata, R. et al., 2004 MNRAS, 351, 117

Ibata, R., Chapman, S., Ferguson, A. et al., 2004, MNRAS 351, 117

Ivezic, Z. et al. (SDSS collaboration), 2004, in Milky Way Surveys, ASP Conf series vol 317, eds D. Clemens, R. Shah & T. Brainerd, p179

Johnston, K. 1998 ApJ 495, 297

Johnston, K., Hernquist, L. & Bolte, M. 1996, ApJ, 465, 278

Johnston, K., Sackett, P. & Bullock, J. 2001, ApJ 557, 137

Johnston, K., Spergel, D. & Haydn, C. 2002, ApJ, 570, 656

Johnston, K., Zhao, H.-S., Spergel, D. & Hernquist, L. 1999 A&A, 348, L49

Katz, D. et al.2004, MNRAS, 354, 1223

Kochanek, C. 1996, ApJ, 457, 228

Little, B. & Tremaine, S. 1987, ApJ, 320, L493

Magorrian, J., et al.1998, AJ, 115, 2285

Majewski, S., Strutskie, M., Weinberg, M. & Ostheimer, J. 2003, ApJ, 599, 1082

Majewski, S. et al. 2004, AJ, 128, 245

Martin, N., Ibata, R., Bellazzini, M., Irwin, M., Lewis, G. & Dehnen, W. 2004a MNRAS 348 12

Martin, N. et al. 2004b MNRAS 355, L33

McClure-Griffiths, N., Dickey, J., Gaensler, B. & Green, A. 2004, ApJ, 607, L127

McConnachie, A. et al.2003, MNRAS, 343, 1335

Momany, Y. et al. 2004, A&A, 421, L29

Moore, B. 2001, in 20th Texas Symposium, AIP conference proc.vol 586 (eds C. Wheeler & H. Martel) p73

- Munari, U. et al. 2003, GAIA Spectroscopy, ASP Conf series vol 298 (ed Munari) p275
- Nissen, P. 2004, in `Origin & Evolution of the Elements', eds A. McWilliam & M. Rauch (CUP, Cambridge) p156
- Nordstrom, B. et al. 2004, A&A 418, 989
- Odenkirchen, M., Grebel, E., Dehnen, W. et al. 2003, AJ 126, 2385
- Olsen, K., Blum, B. & Rigaut, F. 2003, AJ, 126, 452
- Perryman, M. et al. 2001, A&A, 369, 339
- Steinmetz, M., 2003, GAIA Spectroscopy, ASP Conf series vol 298 (ed Munnari) p381
- Willman, B. et al, 2004, astro-ph/0410416
- Wyse, RFG 2001, In Galaxy Disks and Disk Galaxies, ASP Conf series vol 230 (ed Funes & Corsini) p71
- Yanny, B. et al. 2004, ApJ 605, 575
- Zucker, D. et al 2004a, ApJ, 612, L117
- Zucker, D. et al 2004b, ApJ, 612 L121

Chapter 5 Other Science Enabled by WFMOS

5.1 Background

In addition to the two main science surveys (Dark Energy and Galaxy Genesis), WFMOS will provide a host “value-added” science. We briefly summarize some of these “value-added” science products below and split them into two main categories; archival science done with existing WFMOS data in the GSA and new observations using WFMOS as a facility instrument. We also present a few extended science cases in the attachment of this feasibility study titled “ATTACHMENT 3: Extended Value-added Science Cases” (these are marked with an *).

5.2 Value Added Science

Archival science that will be possible with existing WFMOS data in GSA, includes:

1. Probing dark energy regardless of the acoustic oscillations. Redshift space distortions will help break key degeneracy's and allow one to use the Alcock-Paczynski test to tightly constrain dark energy models (see Yamamoto, Bassett, Nishiota 2004)
2. Constraining the shape of the primordial power spectrum to a few %, as well as placing tight constraints on the neutrino masses.
3. Constraining dark energy and the growth of structure using cluster counts as a function of velocity dispersion and optical luminosity (see Newman et al. 2002; Davis, Gerke & Newman 2004).
4. Spectroscopic detection of thousands of high redshift SNe Ia (Madgwick et al. 2002; Dahlen et al. 2004). The present SDSS spectroscopic survey detects one SNe Ia per ~2000 galaxies, with the expected $z \sim 1$ SNe Ia rate being a factor of 3 to 5 greater (Dahlen et al. 2004).
5. By combining of WFMOS with other surveys, which test the luminosity distance (e.g. SNAP), we can test distance-duality (the reciprocity relation) to high significance. This constraints General Relativity (or any metric theory of gravity), photon number conservation (possible axion-photon interactions) and systematic uncertainties like magnification bias for distant SNe Ia (see Bassett & Kunz 2004).
6. Provide accurate calibration of the errors on multi-color photometric redshift estimates (see Padmanabhan et al. 2004). Such calibrations are essential to extract science (e.g. weak lensing and clustering studies) from the next generation of large imaging surveys (see Blake & Bridle 2004)
7. Determination of the evolution in the comoving space density of the global average galaxy star-formation rate. Out to $z \sim 1$, there remains a factor of 5 scatter in the different measurements of this quantity, with greater uncertainty above this redshift (see Hopkins et al. 2004). This science would greatly benefit from an NIR channel on WFMOS to observe $H\alpha$ to high redshift.

8. Provide precision measurements of the density of star-formation as a function of environment, luminosity, stellar mass and redshift. The local SDSS and 2dFGRS samples have been extensively mined for data on these topics (e.g. Balogh et al., 2004, Kauffmann et al. 2003, Gomez et al. 2003). Also studies of the bimodality of the galaxy population as a function of redshift, luminosity and environment (see Baldry et al. 2004).
9. Studies of rare but important subpopulations of galaxies such as ‘k+a’ galaxies and ‘anemic spirals’ (see Goto et al. 2003; Blake et al. 2004).
10. The study of chemical abundance of millions of high redshift galaxies and compare these to local SDSS samples (see Tremonti et al. 2004)
11. Precision measurements of the shape and amplitude of the high redshift power spectrum and correlation functions. These can be used to study the growth of structure with redshift, as well as constrain the relative biasing of galaxies as a function of redshift and scale (see Zehavi et al. 2004).
12. Measurement of the higher-order correlation functions (or bi- and tri-spectra) of high redshift galaxies. Large volumes are essential to minimize cosmic variance (see Baugh et al. 2004) and can be used to determine scale-dependent bias (see Kayo et al. 2004) as well as test assumptions of Gaussianity (Baugh et al. 2004).
13. Identification and classification of tens of thousands of Active Galactic Nuclei (AGNs), thus providing large samples for studies of their clustering (Wake et al. 2004) and host galaxy properties (Miller et al. 2003). These can be compared to lower redshift surveys (see Kauffmann et al. 2003) and used to study the growth of Black Holes.
14. Accurate determination of the high redshift luminosity function of galaxies. Present surveys from VVDS, COMBO-17 and DEEP2 are still limited by cosmic variance and small number statistics (when considering volume-limited surveys).
15. The WFMOS fields and targets will provide an important foundation for a host of follow-up multi-wavelength studies, including space-based observatories like Constellation-X, JWST, Spitzer etc.
16. Discovery of serendipitous objects and events. For example, WFMOS will yield a very large spectroscopic survey of ‘blank’ sky, resulting in a high potential for the discoveries of very high redshift galaxies e.g. Jarvis, van Breukelen & Wilman (2004)

5.3 Science Cases Enabled by WFMOS as designed

In addition to the above archival research, WFMOS will also deliver a unique new capability for targeted observations on Gemini or Subaru. We illustrate below a selection of major new studies that will be possible with this instrument; we provide extended science cases for some of these new observations and studies in the Attachment 3 (these are marked with an *). There are further examples of possible WFMOS observations presented in the KAOS Purple Book (see <http://www.noao.edu/KAOS>).

1. New studies of the local distribution of faint galaxies. For example, WFMOS provides for the first time both the field-of-view and aperture to

gain thousands of redshifts for the faintest galaxies detectable in local cluster of galaxies ($M_R \sim -11$; Bernstein et al. 1995), voids and filaments. Mapping such low luminosity galaxies will be a major observational constraint on emerging models of galaxy formation.

2. Formation and evolution of the highest redshift galaxies in the Universe. In addition to the archival galaxy evolutionary studies with the WFMOS dark energy study discussed above, WFMOS can provide new targeted observations of $z \sim 4$ galaxies over a large area of sky (A1 in Attachment 3).
3. Understand the physics of AGN by obtaining a large sample of faint quasars out to $z < 6.5$. This sample will facilitate the study of hierarchical models of QSO formation, the evolution of black holes from $z = 6.5$, and the contribution of AGNs to the UV ionizing background (A2 in Attachment 3).
4. Quantifying the relation between the Intergalactic Medium (IGM) and the associated large-scale structures as traced by galaxies. This can be achieved via a simultaneous survey of both galaxies and quasars in the same field-of-view with WFMOS (with different spectral resolutions), which will provide over an order of magnitude improvement on the sampling of the structure of the IGM at high redshifts (A3 in Attachment 3)
5. New stellar population studies of local galaxies. For example, new targeted observations of the M31 and M33 will provide a host of kinematical and chemical abundance information of stars in the bulges and disks of these galaxies to help determine the likelihood of any recent merger activity.
6. In addition to the Galaxy Genesis survey, similar study of the disk of the Large Magellanic Cloud (LMC) will allow us to study disk formation in a galaxy with mass and age close to that of the primordial galaxy building blocks. The main goal of the experiment would be to identify, through abundances and kinematics, the population of disrupted low-mass star clusters that accompanied the formation of the LMC's existing globular clusters (A4 in the Attachment 3)

5.4 **References**

- Newman et al. (2002), PASP, 114, 29N
- Madgwick, et al. (2003), ApJL, 599, 33
- Dahlen et al. (2004), astro-ph/0406547
- Bassett & Kunz (2004), Phys.Rev. D69
- Padmanabhan et al. (2004), astro-ph/0407594
- Balogh et al., (2004), MNRAS 348, 1355,
- Kauffmann et al. (2003), MNRAS, 341, 54
- Blake et al. (2004), MNRAS, 355, 713
- Hopkins, A., (2004), astro-ph/0407170

Zehavi, I., (2004), submitted

Baldry et al. (2004), astro-ph/0410603

Baugh et al. (2004), MNRAS, 351, L44

Kayo, I., et al. (2004), PASJ, 56, 415, 2004

Termoniti et al. (2004), astro-ph/0405537

Yamamoto, Bassett, Nishiota (2005), Phys.Rev.Lett., 94, 051301

Blake & Bridle (2004), MNRAS, astro-ph/0411713

Jarvis, van Breukelen & Wilman, (2004), MNRAS, astro-ph/0412600

SECTION III: WFMOS TECHNICAL STUDY

Chapter 6 WFMOS Summary Instrument Description

6.1 Primary Description

The Wide-Field Multi-Fiber Multi-Object Spectrograph (WFMOS) is an optical spectrograph for very high multiplex observing over a very wide field of view. The baseline instrument is described as follows:

Subaru telescope prime focus	
1.5 degree diameter field of view	
0.39-1.0 micron wavelength window	
1 arc-second diameter apertures	
4500 total fibers	3000 fibers to a set of 10 low-dispersion spectrographs 1500 fibers to a set of 2 high-dispersion spectrographs
Dual beam low-dispersion spectrographs for simultaneous and complete wavelength coverage from 0.39-1.0 micron	R=1800 in blue channel of low-dispersion spectrographs R=3500 in red channel of low-dispersion spectrographs Nod-Shuffle observing capability
Single channel high-dispersion spectrographs	R=40000 No nod-shuffle observing required

Possible optional implementations are the following (Note that these options will be resolved prior to or during the conceptual design phase.):

Gemini option	Gemini prime focus rather than Subaru All other aspects the same as baseline
Subaru 2 degree field	2 degree field rather than 1.5 degree 6000 total fibers 4000 low-dispersion 2000 high-dispersion All other aspects the same as baseline
Subaru NIR extension	0.39-1.8 micron total wavelength coverage for low-dispersion 1500 NIR fibers to a set of 5 to 8 NIR spectrographs 1500 low-dispersion optical fibers to a set of 5 low-dispersion spectrographs All other aspects the same as baseline

6.2 System Components

The instrument system includes the following major subassemblies:

- Top end
- Wide-field corrector (WFC)
- Atmospheric dispersion compensator (ADC)

- [Gemini option: Image stabilizer (Wobble Plate)]
- Acquisition and guiding system (A&G Unit)
- Wavefront sensing system (OIWFS)
- Calibration system
- Fiber positioner
- Instrument rotator
- Flexure compensator
- Fiber cable
- Fiber connector
- Low dispersion spectrographs
- High dispersion spectrographs
- Detector systems
- Instrument control computers and software
- Instrument handling facilities
- Observing preparation software
- Data pipeline software

6.2.1 Top End

The top end of the instrument serves the following purposes:

- Holds the corrector assembly in alignment with the telescope
- Holds the instrument package in alignment with the corrector
- Holds the calibration system along the vanes
- Allows the WFMOS instrument to be removed and replaced with other Subaru prime-focus correctors, instruments, and secondary mirrors [Gemini option does not have this requirement]
- [Gemini option: Interface to the Gemini telescope]

On Subaru, the top end is the existing top end structure with hardware modifications to the central mounting ring to allow the WFMOS and HyperSuprime Camera to be mounted without causing significant vignetting of the light.

6.2.2 *Wide-Field Corrector*

The WFC is an assembly of large optics that minimize image aberrations across the full field of view. It must serve the following purposes:

- Maintain self alignment with the primary mirror and amongst the lenses to keep image aberrations at a minimum
- Provide a well-defined focal surface that interfaces to the instrument
- Contain the ADC assembly
- Provide focus
- [Gemini option: Contain an image stabilizer]
- Interface to both the WFMOS and HSCam instruments.

6.2.3 *Atmospheric Dispersion Compensator*

The ADC serves the purpose of correcting the spatial spread in wavelength due to the wavelength dependence of atmospheric refraction. It is typically a set of counter-rotating prisms that mimic the dispersive characteristics of the atmosphere in order to reverse the dispersion introduced by the atmosphere. The amount of dispersion is a function of the elevation angle (or Zenith distance) with zero dispersion at the Zenith and maximum dispersion at the horizon.

The ADC will need to provide the following:

- Cancel atmospheric dispersion over the range of typical Zenith angles over the wavelength band of the WFMOS instrument
- Be an integral component of the WFC
- Not introduce significant field distortion that is a function of ADC rotation
- Maintain optical alignment with the WFC
- Not introduce significant image degradation to the images

6.2.4 *[Gemini Option: Image Stabilizer]*

WFMOS on Gemini will require a mechanism for stabilizing the telescope images against motion induced by wind buffeting the telescope structure. The image stabilizer will need to provide the following capabilities:

- Stabilize the images across the field of view against wind induced image motion
- Not significantly degrade the images produced by the WFC
- Not introduce vibration into the telescope

6.2.5 Acquisition and Guiding System

The A&G Unit must provide the following capabilities:

- Acquire the target field and align the telescope and instrument to the targets
- Provide closed-loop tracking of the target field
- [Gemini option: the A&G may be the component providing tip-tilt correction signals for the image stabilization system, but certainly must interface with the functionality of that particular unit]

6.2.6 Wavefront Sensing System

The On-Instrument Wave Front Sensing (OIWFS) System must provide the following:

- Evaluate wavefront performance of the primary mirror
- Provide error signals to correct the wavefront errors of the primary mirror through the active mirror support system

6.2.7 Calibration System

The Calibration System must do the following:

- Provide a flat-field illumination for CCD pixel-to-pixel and fiber-to-fiber photometric correction
- Provide an appropriate wavelength calibration for all spectroscopic modes of operation

6.2.8 Fiber Positioner

The fiber positioner will perform the following:

- Interface to the WFC and Top End
- Align properly to the image surface in focus, tilt, and rotation
- Must rotationally track the target field
- Position the fiber probes onto the targets
- Maintain proper target position as a function of telescope orientation
- Interface to the A&G and OIWFS systems

6.2.9 Instrument Rotator

The instrument rotator must have the following capabilities:

- Interface the fiber positioner to the WFC and Top End assemblies

- Rotate the fiber positioner in response to guide signals and lookup tables to keep the instrument package rotationally aligned
- Allow the fiber cable to rotate and exit the instrument package

6.2.10 Flexure Compensator

The Flexure Compensator is a system that keeps the instrument package aligned to the telescope optical axis. It must do the following:

- Maintain axial alignment of the instrument package (WFC and Fiber positioner) to the optical axis

6.2.11 Fiber Cable

The fiber cable must do the following:

- Interface to the fiber positioner
- Interface to the instrument rotator
- Match to the input aperture of each fiber spine
- Transmit light to the spectrographs
 - With appropriate level of transmission efficiency
 - With minimal level of focal ratio degradation
- Interface to the telescope structure
- Must not hinder telescope motion and performance
- Interface to the spectrograph room
- Interface to the spectrographs

6.2.12 Fiber Connector

The Fiber Connector relays light from the fiber positioner spines to a larger core fiber for transmittal to the spectrographs. The Fiber Connector must perform the following:

- Interface the fibers connected to the fiber positioner with the fibers that feed into the spectrographs
- Allow routine disconnection and reconnection of the fiber cable
- Maintain alignment to minimize loss of efficiency
- Introduce minimal loss of efficiency
- Transform the focal ratio of the light to be appropriate for fiber transmission.

6.2.13 Low Dispersion and High Dispersion Spectrographs

The set of low and high dispersion spectrographs must perform the following:

- Interface to the spectrograph room and utilities
- Interface to the fiber cable
- Interface to the detector controller
- Interface to the instrument controller
- Provide the required spectral coverage
- Provide the required spectral resolution
- Provide the required stability

In addition, the low dispersion spectrographs must do the following:

- Image spectra to allow for nod&shuffle observing mode

6.2.14 Detector Systems

The Detector Systems must do the following:

- Interface to the spectrograph cryostats
- Meet the required level of performance for sensitivity, stability, and cosmetics
- Interface to the Data Handling system
- Incorporate a nod&shuffle observing mode

6.2.15 Instrument Control Computers/Software

The Instrument Control Computers and Software must be capable of the following:

- Operation of the Fiber Positioner
- Operation of the Calibration System
- Operation of the WFC and ADC
- [Gemini option: Operation of the Image Stabilizer]
- Operation of the A&G Unit
- Operation of the Wave Front Sensors
- Operation of the Instrument Rotator

- Operation of the Flexure Compensator
- Operation of the spectrograph control
- Operation of the Detector Systems
- Operation of other ancillary equipment as required

6.2.16 Instrument Handling Facilities

The Instrument Handling Facilities must do the following:

- Store the WFMOS related hardware and related equipment
- Interface with the observatory infrastructure
- Enable safe and routine installation and removal of WFMOS to the telescope
- Allow on and off telescope maintenance operation of the WFMOS subsystems

6.2.17 Observing Preparation Software

The Observing Preparation Software must do the following:

- Extract the desired target astrometric positions from input databases
- Optimally allocated the fibers to target coordinates
- Provide a user interface for user interaction in the assignment process
- Archive the assignment information
- Interface with the fiber positioner and other necessary instrument components for alignment of the instrument onto the target field

6.2.18 Data Pipeline

The Data Pipeline must do the following:

- Collect the data from the detector controllers
- Store the data
- Allow quick look examination
- Calibrate and remove instrumental signatures in the data
- Provide the reduced data in a standard format for further data analysis and archival

A second phase of the data pipeline, related to scientific analysis of the data must be able to do the following [Note that this piece of software may or may not be developed as part of the WFMOS instrument development.]:

- Provide required batch analysis software

6.3 System Performance

The Purple Book gives an overview of how the Gemini implementation of WFMOS might perform. Analysis of the modified system shows that the previous analysis is still relatively correct. A few areas in which the performance might differ would be in the spectrograph, choice of grating technology (VPH vs Echelle), and the fiber cable length (36 meters for Subaru, 60 meters for Gemini). Specific component efficiencies, where applicable, are given in the related chapters. The Purple Book estimates are repeated here for completeness.

The left panel of Figure 37 shows the predicted system efficiency for WFMOS as a function of fraction of detected photons that are incident on the telescope primary mirror. This includes all known sources of losses, except for the seeing loss on the circular aperture. Data from the right panel of Figure 37 (showing the aperture efficiency as a function of image quality) should be utilized to scale the left panel as a function of input seeing.

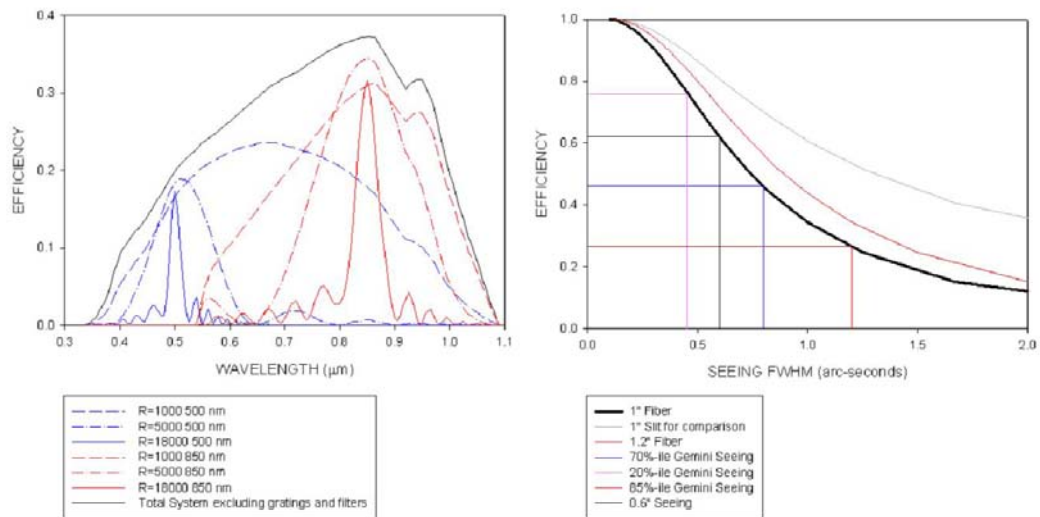


Figure 37. Left: Total system efficiency for WFMOS inclusive of telescope, fibers, and detector. Six different grating configurations are displayed along with the efficiency exclusive of the gratings. Right: Aperture coupling efficiency for a 1" fiber as a function of seeing FWHM. A 1.2" fiber and slit are also shown for comparison. 20%, 70%, and 85% seeing cases are shown along with that for 0.6" seeing FWHM.

Figure 38 shows the breakdown of assumptions for each component in the WFMOS system. The majority of components were appropriately modelled for efficiency as a function of wavelength. The anti-reflection coatings, however, were assumed to be flat over wavelength at a level of 1% reflective loss per air/glass surface. This assumption was used due to the wide variety of options available for AR coatings. The most likely favoured coatings for the majority of surfaces are the combination of MgF2 and SolGel. Such coatings can have excellent broadband performance with the peak being well under the 1% level. It is assumed that such coatings on different elements would have their peak shifted

across wavelength in order to optimize the broadband nature of the system rather than focus on a specific peak wavelength. That assumption led to the flat 1% average performance. The conceptual design studies should fold in a more realistic AR coating behaviour.

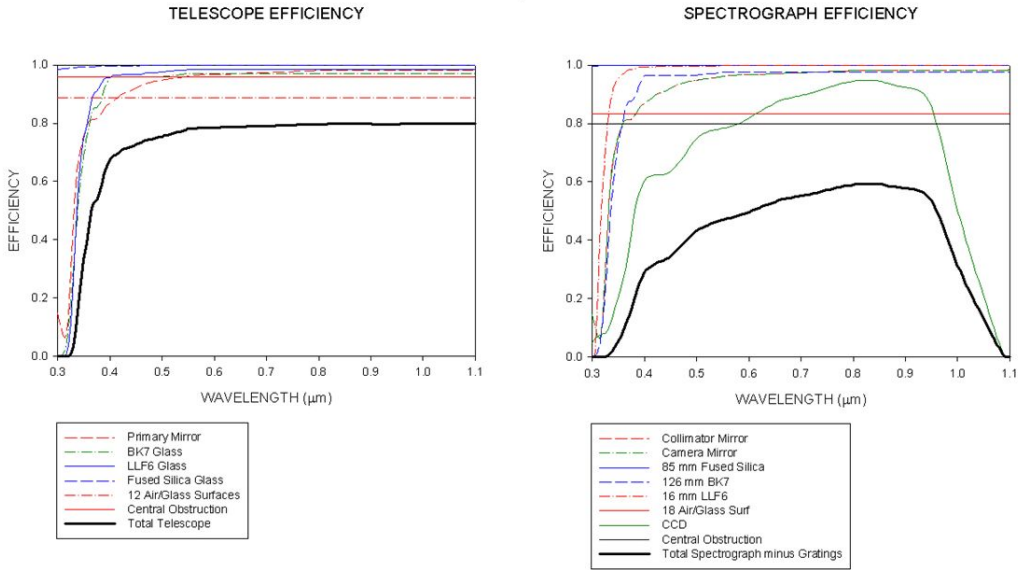


Figure 38. Efficiency of components in the telescope and wide field corrector (left) and in the spectrograph (right).

Chapter 7 Systems Engineering

7.1 Systems approach

A committed systems approach in the WFMOS development is essential to ensure cost-effective success in instrument delivery, maximising performance and containing costs. Strong connections must be forged and maintained between the science goals of the instrument and the engineering detail. Systems engineering is a ‘big picture’ approach that considers the needs and existing modes of operation of the observatory and the astronomical community, with the goal of providing a quality product on time, on budget, that meets the science aims of the instrument.

This involves an interdisciplinary process of understanding operational needs and translating them into a full set of capabilities. Delivery involves concept definition, design, development, implementation and testing and validation of the system as a whole as well as its subsystems. Flexible and expandable architectures must be developed, integrating proven technology into workable solutions that incorporate WFMOS into the observatory to answer the science questions.

Some of the major WFMOS subsystems defined, discussed and costed separately in this feasibility study, are tightly integrated from a systems perspective. Design trades in one subsystem immediately impact cost or feasibility of another, and complex interfaces existing between subsystems can dominate the subsystems’ designs. To manage this level of systems complexity, certain subsystems should be managed tightly as a single work package, with design teams interacting closely and even sharing members.

A complex instrument system with as many subcomponents as WFMOS requires special care to coordinate disjoint development teams. The return on this effort is maximised performance, constrained costs and a delivered instrument supportable for its lifetime in the observatory environment. Common components, common mechanism design, common software components, and reuse of design elements in existing instruments are mandated for the separate development teams system-wide.

This approach is inherent in the work breakdown structure of this study, where it will be seen that the development and operating environment of the WFMOS system is considered explicitly – not only telescope systems interfaces but also operational health and safety, EMC and other direct environmental considerations, and the operational lifecycle from source selection to science delivery. Explicit consideration is also given to the required coordination between partners in the consortium executing the contract.

The systems engineering philosophy is to be maintained throughout the WFMOS project by ensuring that the assigned instrument scientists have strong backgrounds in both science and engineering, and by an architecture-driven approach to planning. Technology developments are not to be permitted to drive project planning, but rather to provide tools to implement carefully thought-out system architectures.

7.2 *Architectural and Telescope constraint issues*

Depicted in Figure 39 below, the WFMOS system is highly modular, and the approach chosen is to analyse the feasibility and cost of implementation of each subsystem to allow a ‘pick and choose’ selection to match available funding to desired science goals. In this section, we describe how architectural decisions are made by balancing the cost and risk of subsystem options with the overall system performance, particularly focussing on aspects where the cost and/or risk and/or performance of one component affects the cost/risk/performance of another component with implications for the WFMOS system.

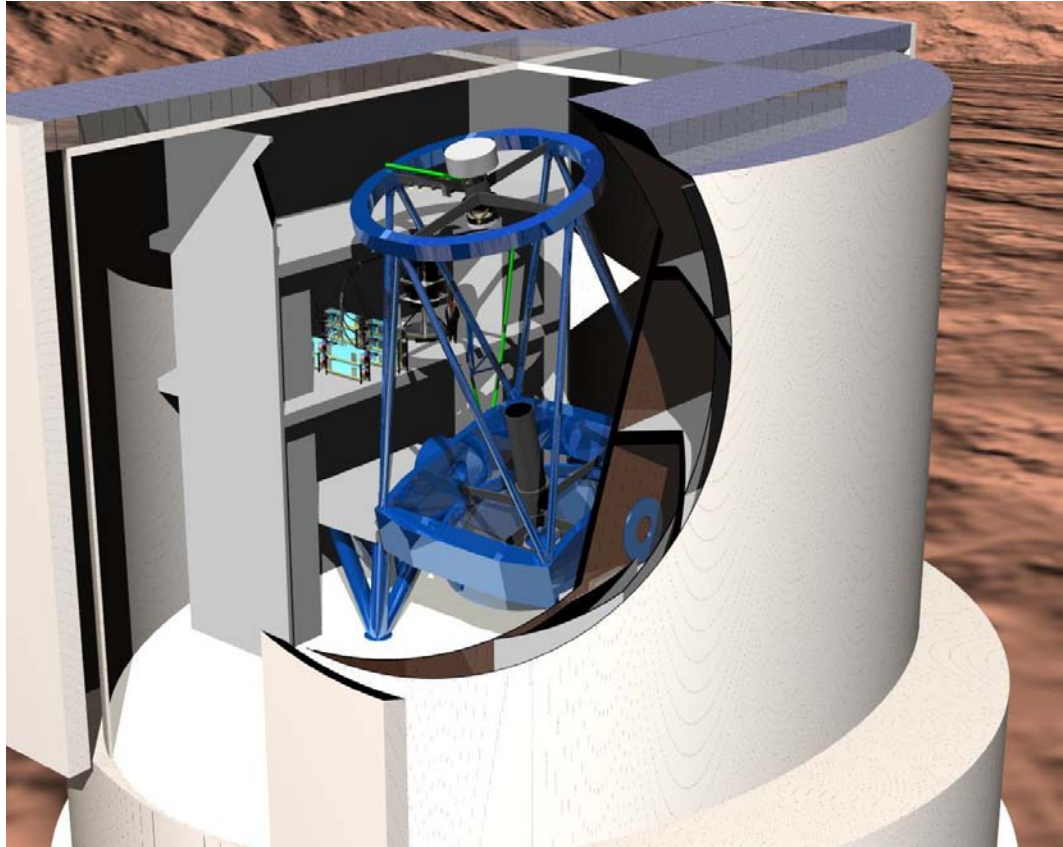


Figure 39. Baseline WFMOS system. The fiber positioner and wide field corrector are mounted to the central hub at the Subaru top end. The fiber cable (shown here in green) loops to a room above the nasmyth platform, which houses a suite of low resolution and high resolution spectrographs.

Part of a full consideration of the system architecture is a Failure Mode Effect Analysis, undertaken to identify and prevent system and process problems.

In order to provide a basis for discussion, a ‘baseline’ strawman architecture is adopted, assuming an overall system architecture regarded as a likely implementation. Discussion of alternative architectures can then be regarded as perturbations from this baseline.

The strawman architecture selected is summarised in Table 7 below. Note that although Subaru is selected as the subject instrument platform for this feasibility study, no infrared spectrographs are considered. Detector costs make such spectrographs an expensive component of a WFMOS implementation, and a requirement to allocate a fraction of the fibers to infrared spectrographs impacts the multiplex advantage of WFMOS for its primary cosmological mission. For the

purposes of this feasibility study, we will assume that wide-field infrared multi-object capability for Subaru is enabled by preservation of the 400-fiber FMOS system.

Table 7. Baseline WMOS configuration.

Target telescope	Subaru
Corrector	1.5-degree, spherical focal surface ~520mm in diameter with radius of curvature near 5 metres. ADC to accommodate observations from 400nm to 1 micron.
Spectrograph location	'Upper Nasmyth room', on the 'optical side' of the dome (the space between the top-end instrument store and the Nasmyth platform, equivalent to the FMOS spectrograph room on the infrared side of the dome).
Positioner	~4500-fiber echidna unit, with ~44 modules each bearing 140 spines. Position feedback via a STRIP system employing four cameras with 2k detectors.
Fiber	100-micron core in spines, 200-micron core for long run to spectrographs
Fiber routing	Minimise the fiber length by running the cable in a free loop from the telescope top-end to the spectrograph room. This loop will hang alongside the 'Great Wall'.
Fiber connectors	Connectors should be as close as reasonable to the spines to allow early focal ratio conversion. No backillumination capability is required at the connector. Easy fiber interchange is not a strong driver, although replacement of a spine should be possible in some manner.
Spine-spectrograph allocation	Every third spine allocated to high-resolution (~40,000) spectrographs; remaining 2/3 allocated to low-resolution spectrographs.
High resolution spectrographs	White-pupil design as described elsewhere in this document. The proposed design allows two spectrographs, each accommodating approximately 800 fibers, to save significant space by sharing a single primary mirror.
Low resolution spectrographs	The Sloan spectrographs are adopted for the strawman WMOS architecture.
Wavefront sensors	Sensors are required for sensing the primary mirror form, field acquisition and guiding. Guiding may be accomplished through the use of spine-mounted fiber bundles incorporated into the fiber positioner.
Calibration system	Illumination of spines by calibration lamps placed in the telescope pupil.

Certain deviations from the baseline architecture are considered on a subsystem basis. These are indicated in Table 8 below.

Table 8. Optional additions or modifications to baseline WMOS configuration.

Gemini implementation – top end	A Gemini implementation of WMOS requires construction of a new top end for the telescope. We consider two designs; a steel top end similar to the existing one, and a lighter, carbon-fiber version. The composite top end is expected to be more expensive, but lighter, potentially saving difficulty and cost if excessive counterweight is required for telescope balance.
Gemini implementation – spectrograph location	The pier lab, beneath the telescope’s azimuth bearing and azimuth cable wrap.
Gemini implementation – fiber routing	The fiber cable needs to be led through an elevation cable wrap and then can run through a ‘chimney’ running down the centre of the pier.
Gemini implementation – infrastructure	Gemini infrastructure requirements are likely to differ from Subaru requirements.
Infrared spectrographs	For Subaru implementation only, a design based on the FMOS spectrographs is considered, to take one third of the science fibers (~1500 fibers, reducing the number of fibers feeding the low-resolution optical spectrographs to ~1500 too).
Do-all spectrograph	A single reconfigurable spectrograph design based on the AAO’s AAOmega design, able to perform high- or low-dispersion measurements, is considered as an alternative to the low-resolution and high-resolution spectrographs.

7.3 **Software systems overview**

In this section we discuss the overall system architecture from a software perspective.

Although WMOS is an ambitious instrument, its control software does not present any particular software challenges. The spectrographs are relatively simple to control, the detectors are almost off the shelf items, and the various top-end systems such as the ADC, rotator, etc. are also relatively straightforward. The Fiber positioner may seem at first glance to be a complex system, but from a control perspective it is merely a very large Echidna unit and the AAO is already close to commissioning such a system for Subaru.

The control software has, of course, to mesh in seamlessly with the observatory infrastructure, and this often presents as many challenges as the actual instrument control. However, this is to a large extent simply a question of understanding the philosophy behind the observatory software structure and working with it. For Gemini this has recently been simplified by the recent 'thin client' approach described in the Gemini Document - “Guidelines for designing Aspen Instrument Software, Gillies, May 13, 2004”. This gives instrument suppliers rather more freedom in choosing the internal details of their control software. The following description of the software structure is targeted at a version of WMOS installed at a Gemini telescope, but this would be essentially unchanged were the system to be installed at Subaru as envisaged in the Strawman design. The details and terminology would be different in a Subaru system, but the overall structure would be similar. Many of the requirements are similar in concept to those of the OzPoz fiber positioner, which AAO integrated successfully into the ESO VLT system - so long as the target system is known and documented, working with it is straightforward enough. This is not to say that the control software design is not

deeply influenced by the target system, and changing once the project is started from Gemini to Subaru, for example, would require a very significant redesign.

7.3.1 **Strawman Design**

7.3.1.1 *Top-level description of software functionality required to support science case*

A large suite of software is required to support the WFMOS science case and to integrate the instrument into Gemini or Subaru observatory systems. There are seven stages to consider.

1. Observing teams must be able to efficiently select large groups of targets appropriate for survey work from existing catalogue and break those targets into survey sets to be observed. Doing as little as eight different fields a night will require 36000 targets be selected. Software support will be required to make this practical. This is detailed in *Chapter 23, Data Analysis and Handling*. (But it is part of the optional package B described therein. This helps indicate that package B should be funded to make best use of the instrument).
2. The teams must apply for time. For the Gemini case, this would normally be done using the PIT application. Gemini should consider if this is appropriate for the type of Survey work to be done with the WFMOS. If large blocks of time are to be allocated to WFMOS then an alternative block allocation process might be more efficient. For the Subaru case, similar requirements apply. It is also noted that the current implementation of PIT requires the selection of guide stars. We believe Gemini will need to drop this requirement in PIT, for WFMOS, as allocation of guide fibers is part of the fiber to object allocation process. Otherwise, PIT will be forcing a complex early fiber allocation on observers when applying for time.
3. Once given time, the Phase II stage is entered. There are two parts to this. First, fiber allocation software to be provided, as part of the WFMOS project, must be run on the target lists to produce a fiber to object allocation for each field to be observed. Having produced an allocation, the Gemini Phase II tool – OT, can be run to specify the observation. It will be necessary to combine the fiber allocation result with the OT and some integration between the two is appropriate.
4. The observation must be performed. A large suite of instrument control software is involved, the requirements of which are dictated by the combination of the instrument itself and telescope requirements and which is the prime concern of this section.
5. On line data reduction and archiving. Detailed in Section 23.3 in *Chapter 23, Data Analysis and Handling*, this software works with the instrument control software. It is responsible for removing “the instrument” from the data, producing quality spectrum for archiving.
6. Detailed in Section 23.5, this software is responsible for detailed processing of the data to achieve the science results.

7. Acceptance, Maintenance and commissioning software. This software is required to help test and maintain the instrument and to assist in commissioning the instrument.

7.3.1.2 *Block diagram level illustrations of major subsystems*

Figure 40 shows a very high-level block diagram of the major sub-systems of the instrument software. Boxes with double borders are complex collections explained with later diagrams (Figure 42, Figure 43, Figure 44 and Figure 45). Note that data processing is presented in minimal detail in these diagrams. Figure 41 is the legend for these diagrams.

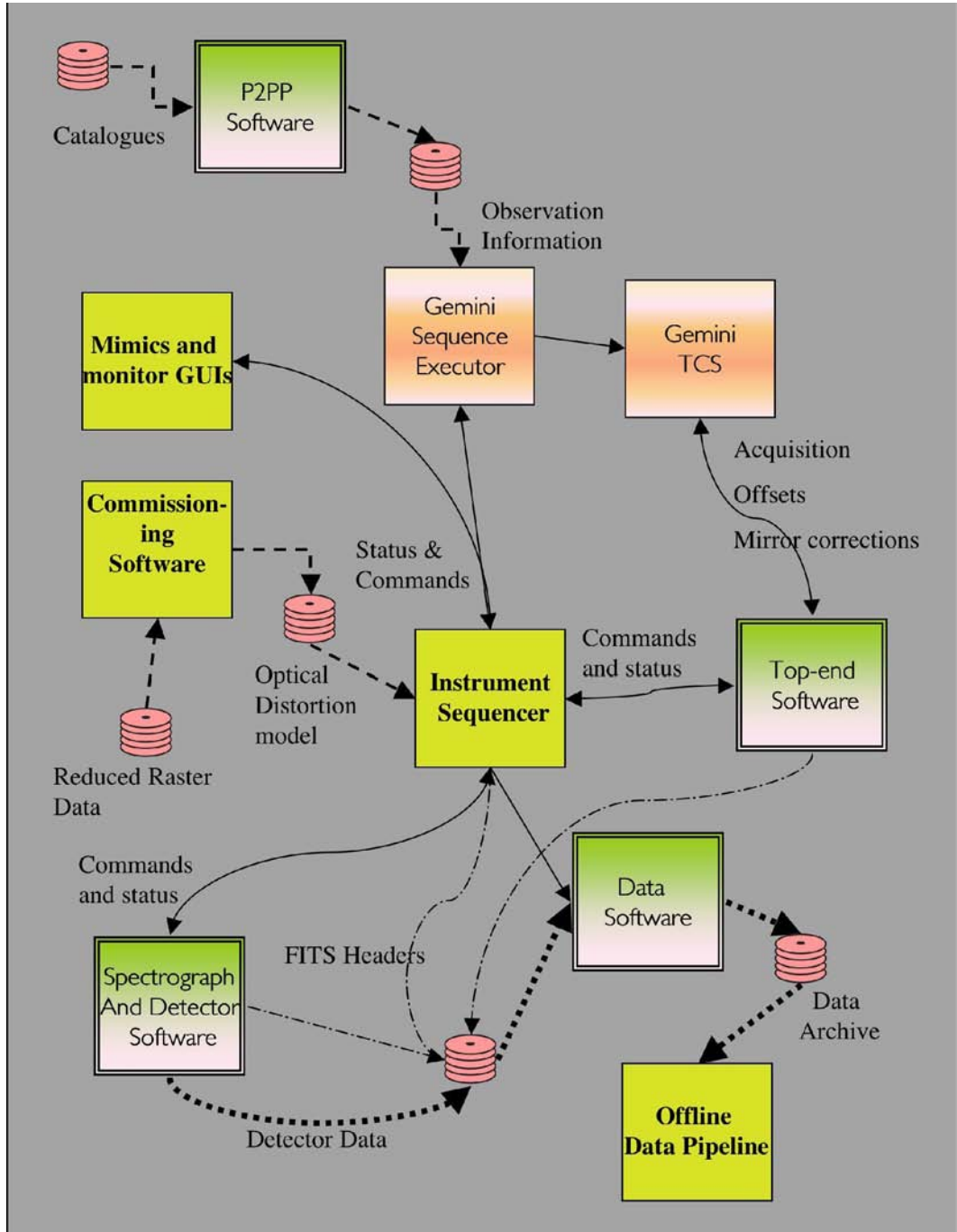


Figure 40: Instrument Software Block Diagram

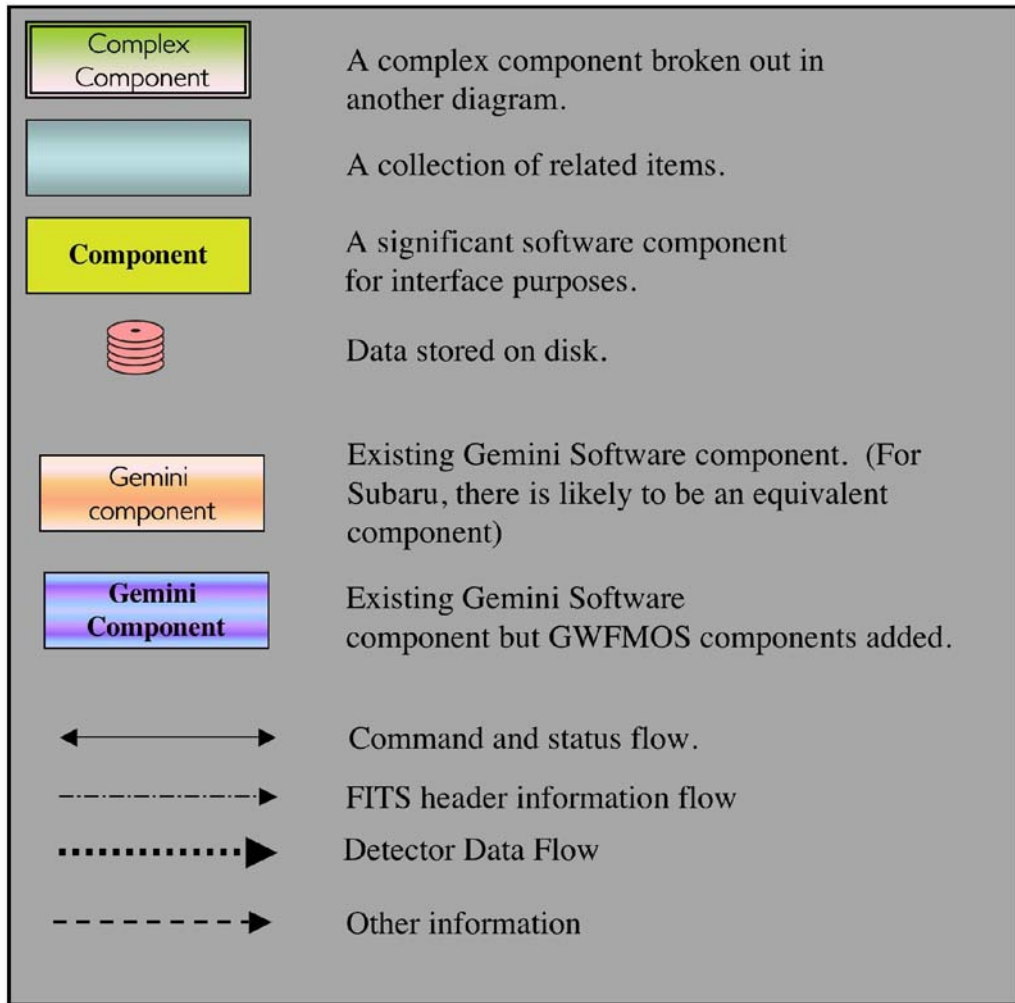


Figure 41. Block Diagram Legend.

This design is consistent with the Gemini Document [Guidelines for designing Aspen Instrument Software] and would also be largely suitable for Subaru, where the “Instrument Sequencer” becomes an Observation Block Control Program (OBCP). The following points are noted.

- The addition of fiber to object allocation to the “Phase 2 Proposal Preparation” (P2PP) stage (Figure 42) will impact existing Gemini P2PP stage software. There will need to be some way of importing a fiber allocation into the Observing Tool and storing that allocation with the relevant observing information. We will supply the tool to do the actual fiber allocation.
- The term “Instrument Control Software” (ICS) refers to all the software in Figure 40 except the P2PP software block and the “Offline Data Pipeline”.
- The “Instrument Sequencer” (IS) is the main component of the instrument software seen by Gemini systems. As per [Guidelines for designing Aspen Instrument Software], the IS accepts commands/configurations from the OCS and controls the ICS subsystems and detector controllers. It is responsible for the required sequencing operations of the WFMOS

instrument. The IS implements the WFMOS instrument “Gemini Command Status Interface”.

- Details for TCS interaction are still to be determined in detail and are significant due to a rotator, OIWFS, ADC and Shack-Hartmann all being part of the WFMOS top end. None of this impacts feasibility. But there may be some impact on existing Gemini systems, which should be determined in detail in the Conceptual and Preliminary design stages of the project in conjunction with Gemini staff. *Changes to the Gemini TCS software may be required. We presume that if such changes are needed, Gemini staff will make the required changes.* Changes for a Subaru implementation are less significant due to that telescope already supporting instruments with their own rotator, Shack-Hartmann system, etc. (e.g. FMOS).
- According to [Guidelines for designing Aspen Instrument Software], A Gemini ICS traditionally has just one “Components Controller” (CC). The complexity of WFMOS will require a considerable number of such units, corresponding to each significant top-end component and each spectrograph. Regardless, the IS will ensure that only one instrument will be seen by the Gemini OCS. Each CC will hide any complexity of the unit concerned, ensuring for example that complex movements are presented as one operation and that no unnecessary motion is performed.
- The number of spectrographs and number of spectrograph designs is still to be decided. All will be designed to respond to the same basic command set, for example, “INITIALISE”, “CONFIGURE”, “WRITE_FITS”, “TEST”, “ABORT” and “PARK” cover most of the spectrograph requirements, presuming the “CONFIGURE” command takes a configuration file which may be different for each spectrograph type. This command set is also sufficient to implement the required Gemini Sequence commands. As a result, the IS will see all spectrographs as being the same. An expanded and spectrograph type specific command set will be available for debugging and test purposes, but would only be used by the engineering level software. See Figure 43 for a breakdown of this box.
- The number of detector control systems is still to be decided. All controllers of a given type (Optical/Infrared) will be identical and it should be possible to have the same basic command set on both Optical and Infrared controllers. As a result, the IS will see all “Detector Controllers” (DC) as being the same. See Figure 43.
- FITS header information will be written using the HEASARC CFITSIO library as required by [Guidelines for designing Aspen Instrument Software]. It is possible this information will be collected by the IS, which will then write it disk. Alternatively, the individual software components may write the headers when a command is received from the IS. Details will be determined when full information on the “Gemini Data Storage Network” (GDSN) becomes available. A FITS table or binary table extension will be used to store fiber allocation information. This table will be different for each spectrograph, with only the fibers allocated to that spectrograph included (to avoid having details for 4500 fibers in every data file). All information used to position the fibers will be written to the binary table or its header.

- The commissioning software is to calibrate the optical distortion model used by the fiber allocation and positioning software. It uses reduced data files from spectroscopic rasters, from which it obtains the flux for each fiber. This software produces a new optimised optical model, which is then fed back to instrument sequencer. It will be based on software from FMOS/Echidna project (itself a derivative of software developed for the VLT FLAMES/OzPoz instrument).
- Various engineering interfaces (ATEUIs) and instrument mimics will be provided, allowing independent development and testing of components. These may be integrated into the one interface if this proves appropriate. It is expected the mimics will prove useful during operations to check that status of the instrument – showing spectrograph light paths, fiber configuration etc.
- Details of software associated with each hardware component are described in that component's section of this document, where that software component is significant.
- The top-end support software includes environment control (if needed) Top end Focus (and x/y motion for Subaru (i.e. Hexapod)) control and fiber cable status monitoring.

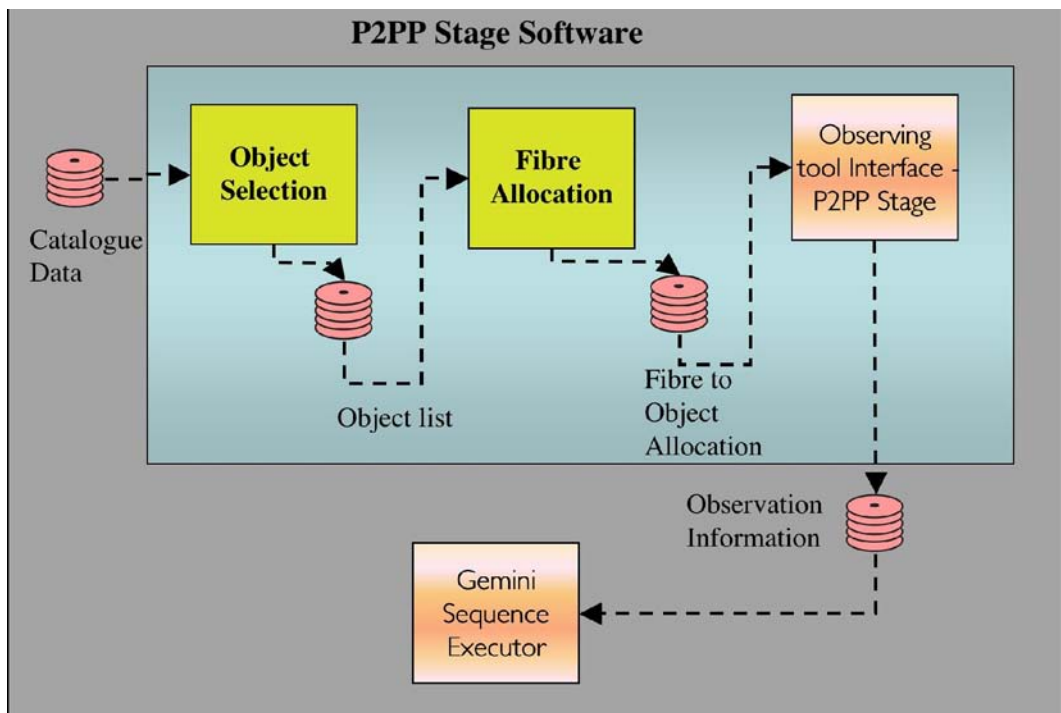


Figure 42. Phase 2 Preparation (P2PP) Stage Software

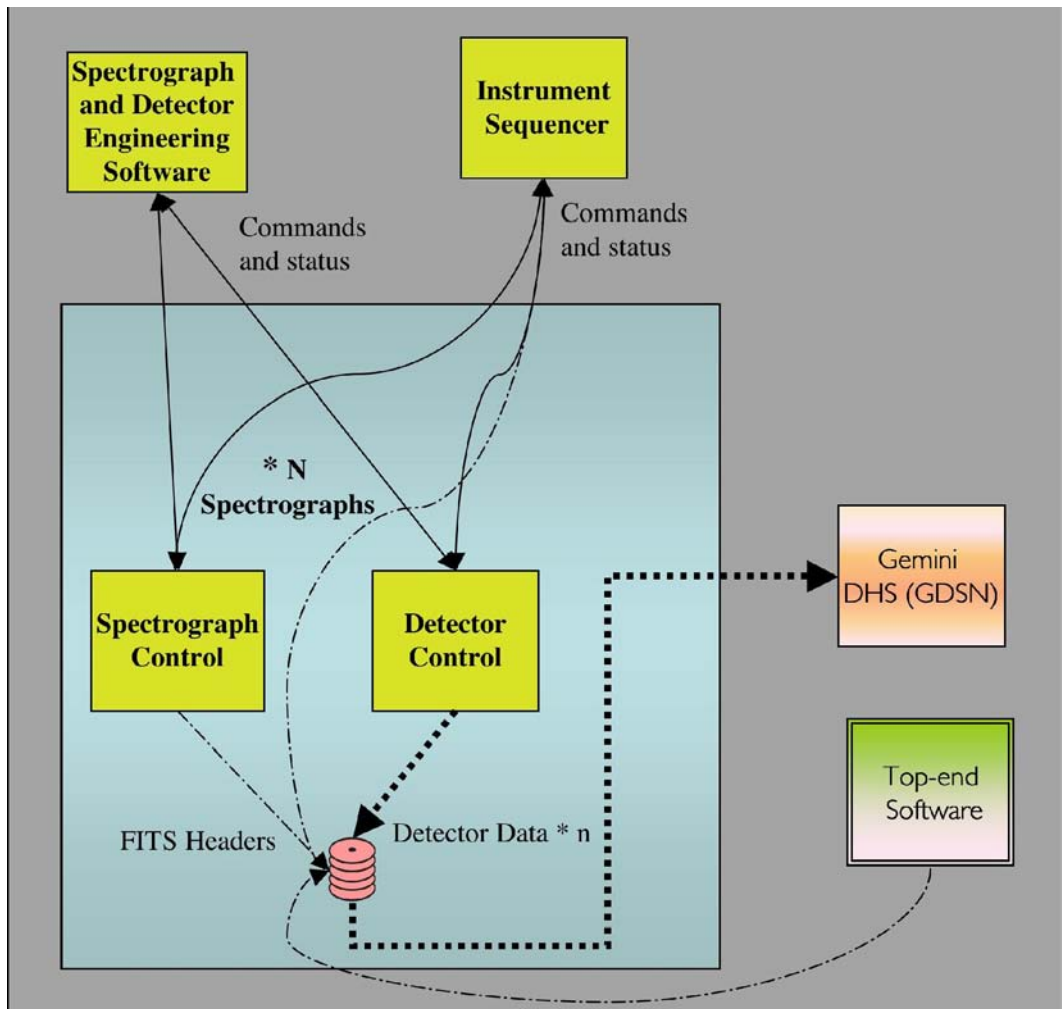


Figure 43. Spectrograph and Detector Control Software

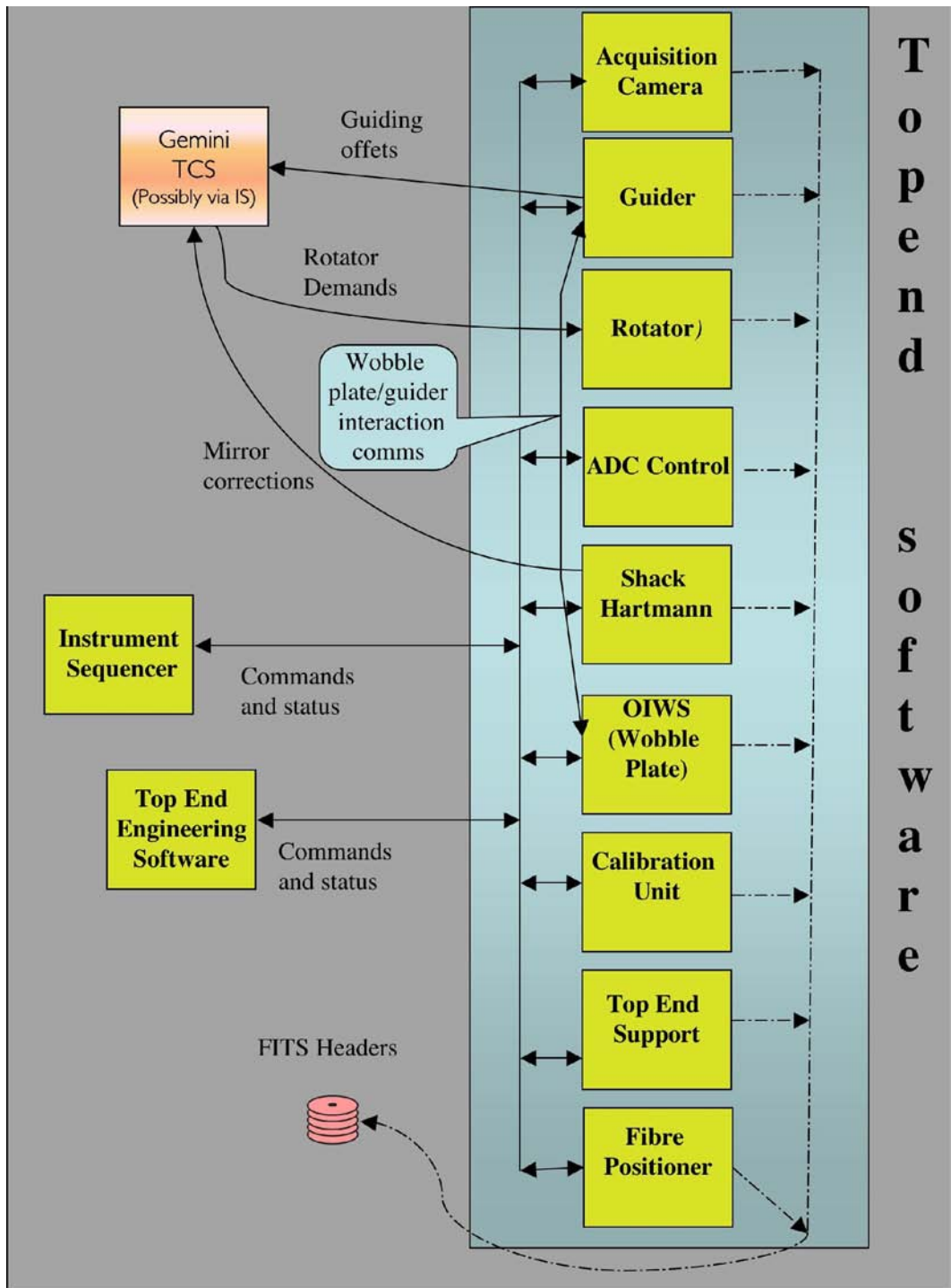


Figure 44. Top end component software

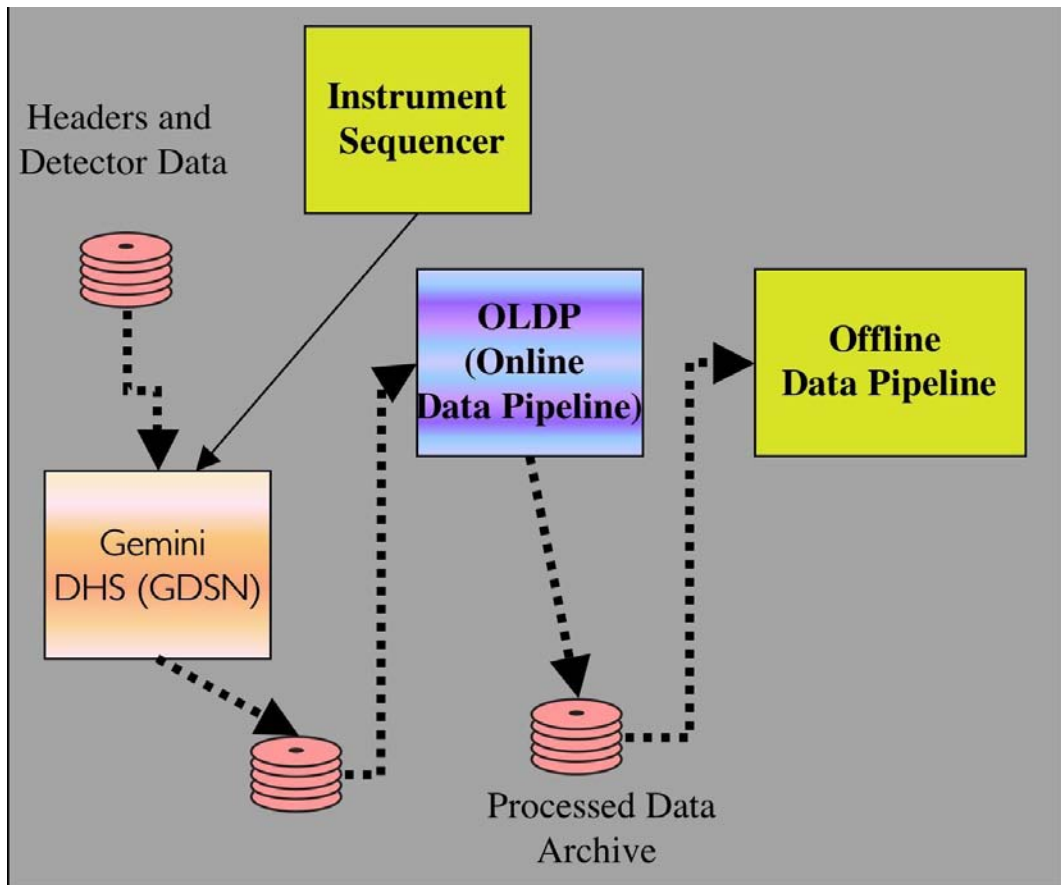


Figure 45. Data Handling Software

The various figures (Figure 40 through to Figure 45) indicate the interfaces to existing Gemini systems. In summary these are:

- The “Gemini Observing Tool” interface, in particular, the association of a fiber to object allocation file with each observation. This is likely to require modifications to the Observing Tool by Gemini, details to be determined.
- The interface between the WFMOS “Instrument Sequencer” and the “Gemini Sequence Executor”. This will use the “Gemini Command Status Interface”.
- The interface between the “WFMOS” instrument and the “Gemini Data Storage Network” - GDSN. This will use the defined Gemini Interface.
- The interface between the “WFMOS” on-line data processing software and the “Gemini OLDP”. This will be handled by implementing the “WFMOS” processing software to be compatible with “OLDP”.
- The interface between the “WFMOS” instrument and the “Gemini TCS”. This is likely to require modifications to the Gemini TCS or Gemini Sequence Executor by Gemini, details to be determined.

Figure 46 and Figure 47 show a flowchart of a typical observing sequence. The legend for this diagram is found in Figure 48.

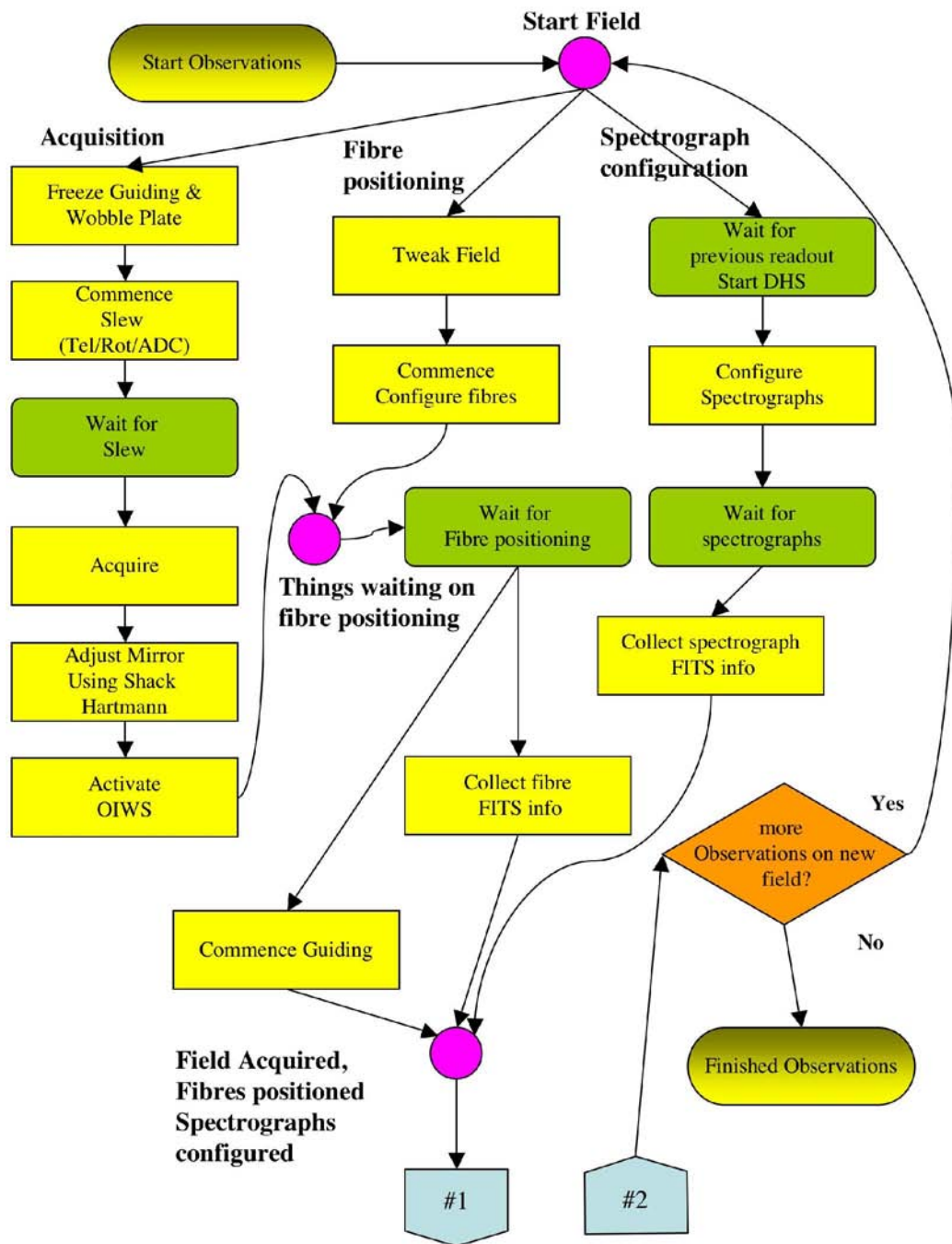


Figure 46. Observing Flowchart - Instrument Control Perspective. Part A (Acquisition)

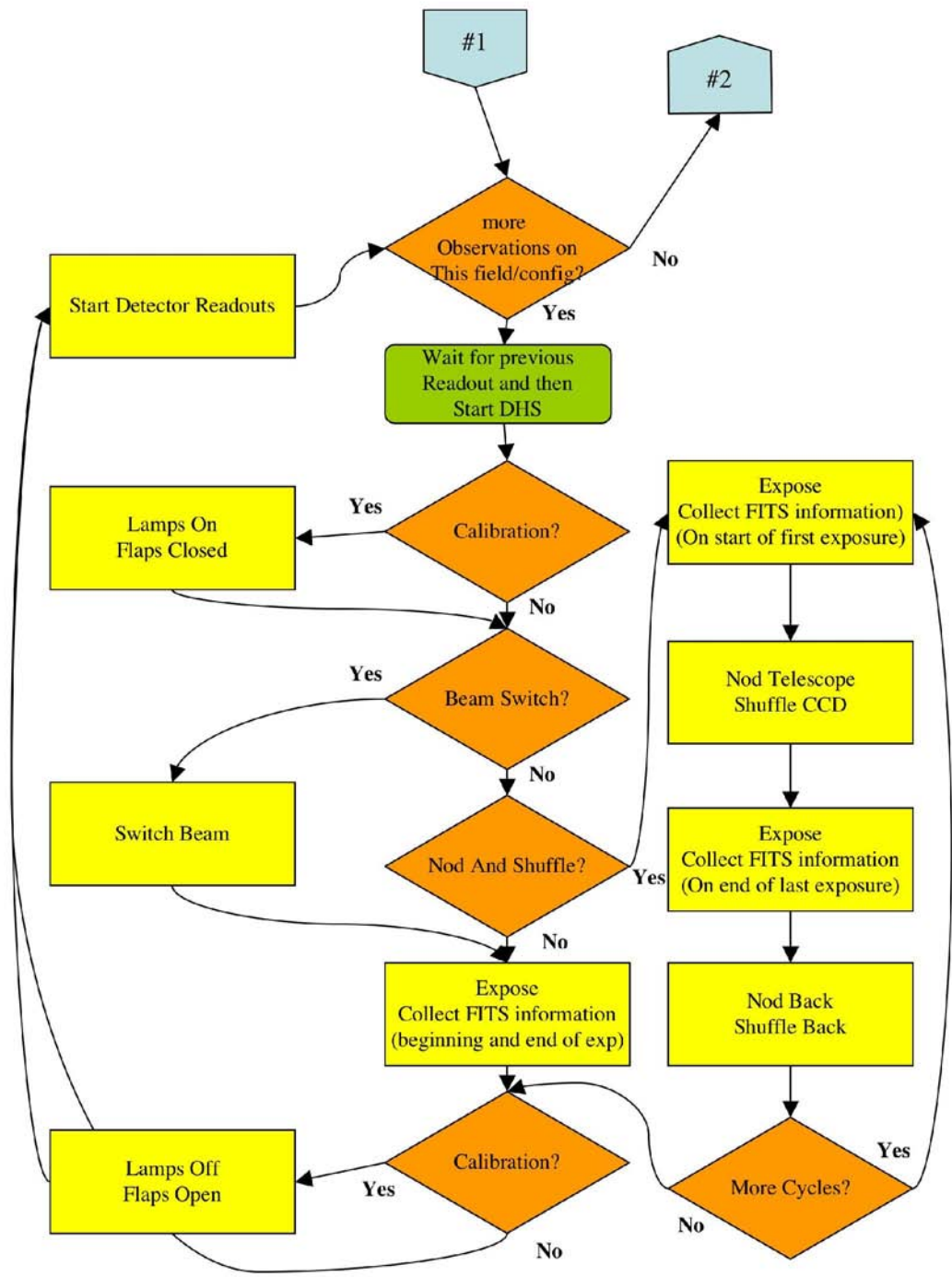


Figure 47. Observing Flowchart - Instrument Control Perspective. Part B (Observation)

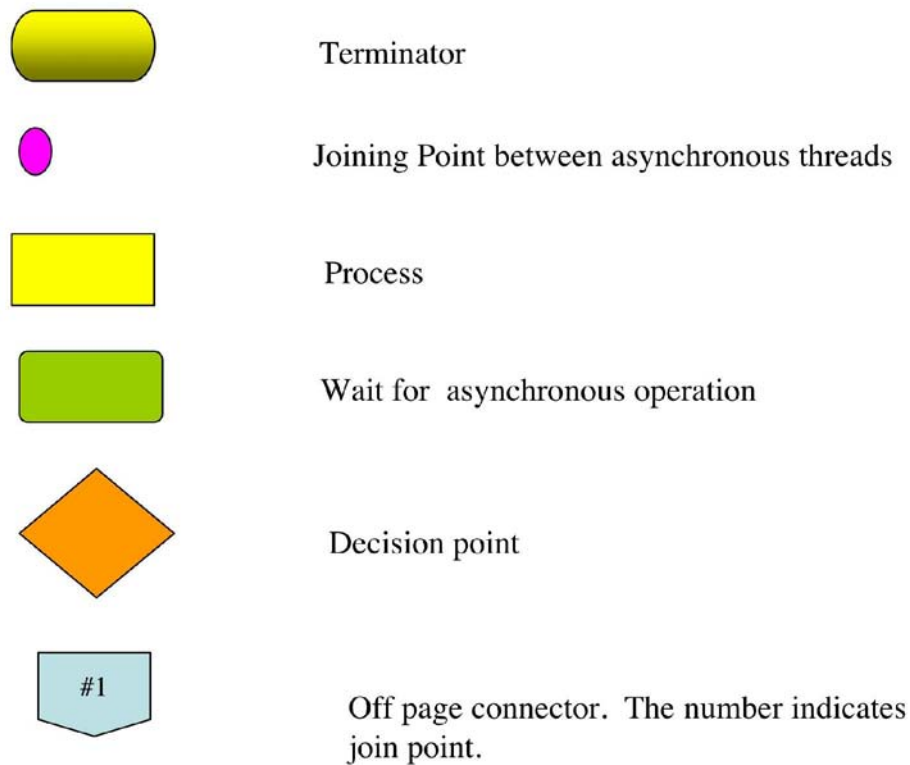


Figure 48. Flow chart Legend

7.3.1.3 *Communications pathways*

Figure 40 and the related figures show the communications pathways involved in the instrument control software.

7.3.1.4 *Data flows*

The data flow in the instrument control system can be seen in Figure 40 through Figure 45, and understood with reference to Figure 42. An outline follows:

- Targets are selected, producing a list of objects to be observed.
- The target list is fed into the fiber allocation software, which produces an allocation of objects to fibers.
- The fiber allocation is fed into the Gemini Observing tool with other information to produce the observation information.
- The observing information is used to configure the fiber positioner, spectrographs and point the telescope.
- Start of observation FITS information is collected from instrument components.
- The image data is read from the detectors and end of observation FITS information is collected.

- A observation event is used to notify the Gemini DHS of the existence of new Image data and FITS header information.
- On-line data processing is performed to remove instrument details and produce science quality data. Quick look is available.
- The data is submitted for archiving.
- Data is retrieved from the archive for use with off line science-level data processing software.

Beam switching and nod & shuffle operations modify the flow a little, but not significantly. The peculiarities of fiber instruments mean that the sky subtractions required with this data must be done in the OLDP, rather than in the DC as only after significant processing has occurred are the sky fiber locations on an individual frame known.

7.3.1.5 *Instrument Control Software Implementation notes.*

The WFMOS software must integrate appropriately with existing Gemini or Subaru systems to allow for queue scheduled observing via standard interfaces, telescope interaction and data archiving – as well as other Telescope specific requirements. For Gemini, the current reference document is [Guidelines for designing Aspen Instrument Software]. The same basic design is also appropriate for Subaru, where the “Instrument Sequencer” becomes an OBCP program. We have not addressed the Subaru design in as much detail as the Gemini design, due to requirements for this document to primarily address Gemini, but deployment on Subaru this would not significantly impact the project and we are somewhat familiar with Subaru software requirements from our FMOS project.

The main interfaces to Gemini software will be via the Instrument Sequencer, which will obey the “Gemini Command Status Interface” and interactions with the GDSN. Some components of the instrument software already exist in part, due to the use of existing hardware designs. The instrument is likely to be built by several teams in various countries, few of who are familiar with the Gemini EPICS environment. The software will run on a large set of Linux machines using Intel compatible CPUs.

It is felt that maximum productivity can be obtained by using CORBA as the communication protocol between the internal parts of the WFMOS software. The reasons being:

- CORBA is a well-defined standard that is now mature enough to use in such an application.
- Use of CORBA should allow the “buying in” of software engineers. Those software engineers who must learn it for the project will feel the skills they acquire can be used elsewhere, so they will develop the skill-set further.
- Quality Open Source implementations of CORBA available.
- E.g. omniORB - <http://omniorb.sourceforge.net/>

- CORBA seems to be tool of choice for this type of job at the moment and in the near future. This was seen at for example the SPIE 2004 “ASTRONOMICAL TELESCOPES AND INSTRUMENTATION 2004” conference, where many ongoing and new projects were reported as using CORBA.

Since existing software components are being used in some cases, our approach will be to use CORBA as the glue software for such components. The Instrument Sequencer and Engineering Interfaces will talk via CORBA to the various software components.

We will in the Conceptual and Preliminary design stages of the project define the CORBA level interfaces in detail. The use of CORBA makes the use of C++ preferred (through not essential⁴) as our lower level software development language. This might be an issue for Subaru deployment where C is preferred⁵. Additionally, Subaru requires sockets to be used for communications – and it is currently unclear if using CORBA meets this requirement (as it is a wrapper around a socket interface). We will have to address these issues fully in the Conceptual design stage of the project.

For scripting and GUI development, we intend to use Python. Python has a good interface to CORBA and is now in heavy use in the astronomy community. It is likely we will use the wxPython GUI toolkit, through this is not certain at this stage as that toolkit is still a touch immature (Python/Tk is an alternative). This decision will be made during the Conceptual or Preliminary design phase of the project. For Subaru, use of Python/Tk is required.

Our project schedule relies on the early delivery of software simulators. Each component development team will be required to provide early delivery of software that obeys the designed CORBA level interface for that component and works in a simulation mode, without the hardware. This will ensure that testing and development of the Instrument Sequencer can progress quickly. When delivered in this fashion, Gemini staff will be able to start testing the software suite quite early in the build phase of the project. Of course the use of simulators does not remove the need for testing against the hardware and ample time had been scheduled for this.

The instrument control software design and costing presumes development on Unix style operating systems, in particular, Linux. No need for a particular version of Linux is foreseen at this stage, through a need for a low-latency or real-time variant may become necessary as the hardware design advances. This should present no significant development problems.

No particular development platform will be required, the simulators can be written on almost any Unix style operating system (For example, Linux/Solaris/Mac OS X). Hardware control requiring special drivers will require computing hardware approximating the deployment computing hardware such that drivers can written

⁴ CORBA has well defined interfaces for most modern programming languages. But because uses a strongly object-oriented approach, an object-oriented language would be preferred. C and C++ are the two most commonly known programming languages amongst programmers with the required skill sets – as a result, C++ would be the preferred language for us to use with CORBA.

⁵ From communications at an FMOS meeting between AAO Staff and Subaru software staff - Subaru has a preference for using Python with the Tk toolkit for GUI development, Sockets for communications and prefers limited use of C++ features likely to result in hard to maintain code.

if needed, tested and the software developed. Appropriate hardware simulators, prototypes, test jigs etc. will be required, to be determined during the design stages of the project.

With this approach, the actual number of CPUs and their allocation evolves out of the electronic and software design process. There will be at least one significant central machine that will run the Instrument Sequencer and other software not directly associated with hardware components (known in the electronics design as the “Top Level Instrument Computer”). Sets of related or associated hardware components are likely to have individual CPUs, such as to allow separate development, testing etc. Some components, in particular the fiber positioner, may use a number of CPUs in order to provide the required processing power and locate it appropriately. The use of CORBA as the internal communications protocol will hide the details of CPU allocation.

7.3.2 Interfaces

7.4 Electrical/Electronic systems overview

In this section we discuss the overall system architecture from an electronic systems and services perspective.

7.4.1 Strawman Design

The WMOS system consists of a considerable number of sub-systems. These are summarised in the block diagram shown in Figure 49. This diagram is applicable to WMOS implementations on either the Gemini or Subaru Telescopes. The only sub-system that is specific to Gemini is the Wobble Plate Controller. The sub-systems that are specific to Subaru are the Corrector Pointing and Focus controller, and the PFU Instrument and Corrector Hub Clamp systems.

The system is highly modular, with most sub-systems requiring only LAN and power connections, and some sub-systems requiring connection telescope time information and to the telescope interlock system.

While the notion of a Control LAN, Data LAN, Time Bus and Telescope Interlock System are derived from Gemini Telescope terminology, they are generic enough to be equally applicable to the equivalent Subaru Telescope functions.

The WMOS system consists of a number of telescope top-end sub-systems, and a number of “off telescope” sub-systems:

7.4.1.1 Top End Sub Systems

Calibration Lamp Controller – provides remote control of calibration lamps mounted on top end. Probably a network enabled microcontroller.

Fiber Positioner Control Computer – controls the Echidna fiber positioner, the FPI STRIP camera system, the Acquisition Camera system and the Guide camera system. The Fiber Positioner control computer also manages the Fiber Cable Health Monitoring system, which has a light source unit mounted at the spectrograph end of the fiber cable.

PFU Instrument Rotator Controller – provides remote control of the Prime Focus Unit Instrument rotator. Likely to be computer based, but could be implemented with an intelligent, network enabled motor drive.

PFU Instrument Pointing and Focus Controller – provides remote control for focusing and pointing correction of the Prime Focus Unit instrument. Likely to be a network enabled controller (e.g. for a hexapod).

Corrector Pointing and Focus Controller – provides remote control for focusing and pointing correction of the corrector. Only required for the Subaru implementation. Likely to be a network enabled controller (e.g. for a hexapod).

ADC Controller – provides remote control of the Atmospheric Distortion Compensator. May be computer based or an intelligent network enabled motor drive.

Wobble Plate Controller – provides remote control of the Prime Focus wobble plate. Likely to be a network enabled controller. The wobble plate controller is only required for the Gemini Telescope.

Wavefront Sensor Control Computer – provides access to the Wavefront Sensor Detector System.

Fiber Connector – the fiber connector is a manually operated device, but it does have an interface to the Telescope Interlock System to prevent Gemini Top End or Subaru PFU removal if the fiber cable remains connected.

Hub Clamp Control – on the Subaru telescope, these control units provide the means for telescope staff to control the attachment mechanisms for the Prime Focus Unit and corrector on the top end hub. These controllers each have interfaces to the Telescope Interlock System (i.e. to prevent telescope operation if the PFU or corrector are not correctly attached). These systems are only used during instrument change operations, and are not remotely controllable. The Gemini Telescope does not require these systems.

7.4.1.2 Off Telescope Sub-systems

Low Resolution Spectrograph Control Computer – provides remote control access to the ten Low Resolution Spectrograph controllers.

High Resolution Spectrograph Controller – a computer based controller providing remote control of the two High Resolution Spectrographs.

Detector Control Systems – Twelve separate Detector Head Electronics systems, each with their own Pixel Acquisition Node computers. All systems are controlled by a Supervisory Node, and send their data to a Data Handling System. Each Detector Head Electronics has a hardware connection to the shutter in its corresponding spectrograph.

7.4.1.3 Top Level Control Computer

The top-level control computer interfaces to both the Telescope Control LAN and the Data LAN. It provides the platform for the Gemini Instrument Sequencer, which interfaces the WFMOS system to the Gemini OCS.

7.4.1.4 Block diagram level illustrations of major subsystems

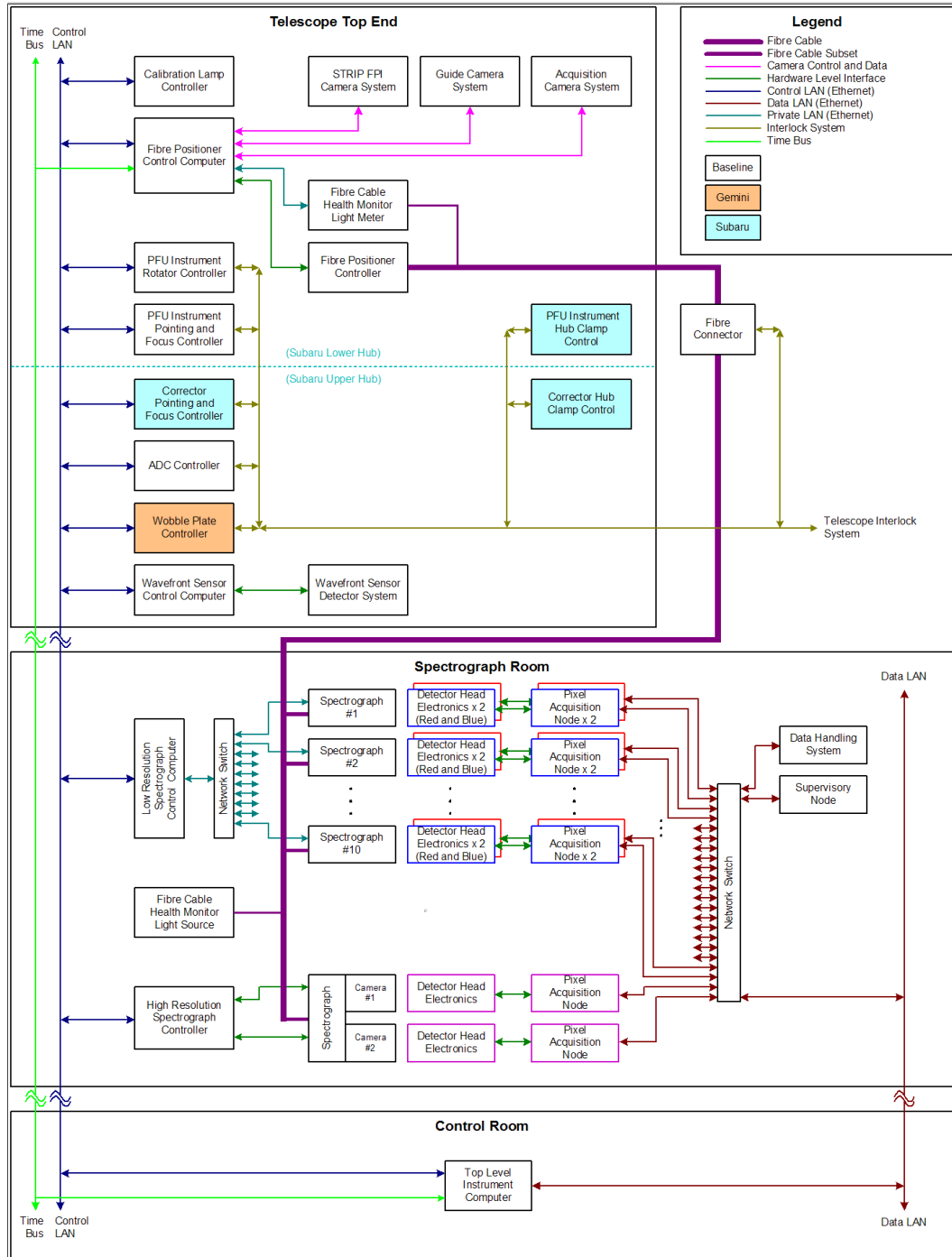


Figure 49: WMOS System Level Diagram

7.4.2 Conformance with Gemini Aspen Instrument Architecture

The Gemini document [Guidelines for designing Aspen Instrument Software], defines the computing architecture of Gemini Aspen instruments. One of the stated goals of this document is to minimise the number of computers involved in an instrument. As such, the design presented here is a “worst case” scenario and is considered to be a “devalued approach”. However, given an instrument the size of WMOS, which consists of a collection of disparate and physically distributed instruments and systems, it is clearly not possible to have a top level instrument

computer providing component control for all of the WMOS sub-systems. The Gemini Aspen instrument guidelines identified a number of reasons why this approach is undesirable. While these are perfectly reasonable for small “traditional” instruments (e.g. a spectrograph and a detector system), in the WMOS context they are less applicable, as follows:

The top-level computer is wasted and adds more complexity to the system while contributing to generated heat and power use.	The top-level computer provides a single point of access to the full WMOS system. Power use and heat dissipation are negligible compared to the full WMOS system.
The approach inevitably introduces a number of new protocols that must be provided by the builder, documented and tested.	An unavoidable consequence. However, this does allow each WMOS sub-system to be independently developed and tested, on and off the telescope.
The cost of the instrument hardware is increased.	The cost of a top-level computer is a fraction of the overall WMOS instrument cost.
The overall performance of the instrument to commands and status is inevitably reduced.	An unavoidable consequence, but will be offset by the availability of fast processors and fast network speed, particularly given the WMOS project time scale.

7.4.3 Interfaces

The WMOS system consists of a number of sub-systems. These have both external hardware level interfaces (i.e. to the Telescope) and hardware level interfaces to each other. Table 9 summarises these hardware level interfaces.

Table 9: WMOS Sub-system Hardware Interfaces.

Sub-system	Sub-system external hardware interfaces	Sub-system internal hardware interfaces
Calibration Lamp Controller	Mains Power Control LAN	
Guide Camera System	Mains Power (via Fiber Positioner power control)	
Fiber Positioner Control Computer	Mains Power (via Fiber Positioner power control) Control LAN Time Bus	STRIP FPI Camera System control and power Acquisition Camera System control and power Guide Camera System control Fiber Cable Health Monitor Light Meter (Private LAN) Fiber Positioner Controller (Private LANs or other high speed serial links to fiber positioner quadrant controllers)
Fiber Positioner Controller (power controller)	Mains Power	Switched Mains Power to Fiber Positioner Control Computer and Guide Camera System DC power to fiber positioner quadrant controllers
PFU Instrument Rotator Controller	Mains Power Control LAN Telescope Interlock System	

Sub-system	Sub-system external hardware interfaces	Sub-system internal hardware interfaces
PFU Instrument Pointing and Focus Controller	Mains Power Control LAN Telescope Interlock System	
PFU Instrument Hub Clamp Control (Subaru Telescope only)	Mains Power Telescope Interlock System	
Corrector Hub Clamp Control (Subaru Telescope only)	Mains Power Telescope Interlock System	
Corrector Pointing and Focus Controller (Subaru Telescope only)	Mains Power Control LAN Telescope Interlock System	
ADC Controller	Mains Power Control LAN Telescope Interlock System	
Wobble Plate Controller (Gemini Telescope only)	Mains Power Control LAN Telescope Interlock System	
Wavefront Sensor Control Computer	Mains Power Control LAN	Wavefront Sensor Detector System
Fiber Connector	Telescope Interlock System	
Low Resolution Spectrograph Control Computer	Mains Power Control LAN	Low resolution spectrograph controllers (ten) via private LANs Note – spectrograph shutters are controlled by detector controllers
High Resolution Spectrograph Controller	Mains Power Control LAN	Note – spectrograph shutters are controlled by detector controllers
Fiber Cable Health Monitor Light Source	Mains Power	
Detector Controller Pixel Acquisition Node (one for each Detector Head Electronics)	Mains Power Data LAN	Detector Head Electronics
Detector Head Electronics (one for each Spectrograph Camera)	Mains Power	Spectrograph shutter
Detector System Supervisory Node	Mains Power Data LAN	

Sub-system	Sub-system external hardware interfaces	Sub-system internal hardware interfaces
Top Level Instrument Computer	Mains Power Control LAN Data LAN Time Bus	

7.4.4 General Electronics System Engineering

7.4.4.1 Equipment and Component Standardisation

In any complex system, it is desirable to limit the number of different types of electronic components used. However, for a project as large as WFMOS with numerous development teams and their differing requirements, and given that Gemini has, to some extent, relaxed its own standards with regards to computer hardware and operating system selection, attempting to enforce a strict hardware standard will be very difficult. Nevertheless, the potential savings in capital costs (e.g. by minimising spares purchases) and in operational costs (spares replacement, staff training etc.), makes it worthwhile attempting to achieve some agreement within the team on a set of standard components. It is recognised that some sub-systems of WFMOS are of such a size and/or development status that they already have defined and selected components, for example the Low Resolution Spectrograph instrument controllers and the Detector Systems.

In particular, the choice of computer hardware and operating system would be a key area that could be somewhat standardised. Sub-system control computers will need to be of a type that provides sufficient processing power and input/output capability to meet the requirements for that sub-system. It should be possible for most if not all sub-systems to use a non real-time system such as Linux running on an x86 (IA32) processor. A control computer generally requires an open bus structure to support the addition of interface boards. A high performance Pentium 4 class single board computer, with at least 1 Gbyte of memory capacity, and multiple Gigabit Ethernet interfaces in either VMEbus (VME64/VME64x), CompactPCI (PICMG 2.0) or PCI-ISA (PICMG 1.0) format would be suitable for most tasks and would provide all the necessary features identified in [Guidelines for designing Aspen Instrument Software]. Some control computers are likely to be mounted on the telescope, and it may be desirable for those systems to be able to operate without a local hard disk.

Similarly, it would be hoped that standardisation on such components as computer interface boards, motion controllers, servo motor drives (amplifiers), motors, encoders, limit and home sensors etc., could be also be attempted.

It is proposed that the WFMOS team members and the Observatory agree a set of standard components during the concept or preliminary design stages. This set of standards will be driven by the Instrument Hardware Design Document, which will be developed during the concept design.

7.4.4.2 Prototyping

Prototyping of circuits or systems regarded as “high risk” because they involve the use of new technology or techniques or they have a high level of complexity, will

be carried out in the concept or preliminary design phases in order to provide “proof of concept”.

7.4.4.3 Electronics Cooling

If any WF MOS electronics sub-systems are located in an area in which the optical environment can be degraded by the effects of heating, it is likely that it will be necessary to provide active cooling of the control electronics enclosures to minimise the heating effects of the electronics equipment. This will be achieved using appropriate cooling systems that extract the heat generated in the electronics enclosure and transfer it to the Telescope coolant system. Such cooling systems maintain a small temperature differential between the outside surface of the electronics enclosure and the ambient air. It is expected that a thermal analysis will be carried out during concept design to determine the cooling requirements for all electronics mounted on the telescope top end and in the spectrograph room.

7.4.4.4 Power

In general, it is assumed that all equipment will be supplied with protected mains power (i.e. from the Observatory Uninterruptible Power System).

7.4.4.5 Observatory Electronics Design Requirements

As far as possible, the design of the WF MOS electronics sub-systems will comply with any requirements defined in the relevant electronics design specifications and standards relating to Observatory instrumentation. The concept design will identify the relevant specifications and standards.

7.4.4.6 Safety

The design of the WF MOS electronics sub-systems will be designed to comply with any Observatory requirements defined in the relevant electronics design specifications and standards for Occupational Health and Safety. The concept design will identify the relevant specifications and standards.

7.4.4.7 Environmental Requirements

The selection and design of electronics components for the WF MOS electronics sub-systems will take into consideration the environmental requirements and operating conditions of the Observatory. The concept design will identify the relevant environmental requirements.

7.4.4.8 Electro-Magnetic Compatibility (EMC)

The design of the WF MOS electronics sub-systems will meet all the relevant requirements for Electro-Magnetic Compatibility for Observatory instrumentation. Achievement of EMC requires an understanding of interference coupling mechanisms, consideration of EMC in equipment layout, grounding and circuit design, application of appropriate filtering and shielding of interfaces and the testing and evaluation for EMC continuously through the project. Observatory EMC requirements will be identified during the concept design.

7.5 Failure Mode Effect Analysis (FMEA)

7.5.1 Introduction

An FMEA is a systematic method of identifying and preventing system and process problems before they occur. FMEA differ from risk assessments as they are focused on preventing defects and enhancing safety of the system under design, as against looking at the project as a whole.

The FMEA techniques used are based on the recommendations of ‘The Basics of FMEA’ written by McDermot, Mikulak and Beauregard. The first step in the process is to review the designs in detail for potential failure modes and potential failure effects. Each failure thus identified is then scored on two criteria:

- **Severity** – the consequences of the failure should it occur
- **Occurrence** – the probability or frequency of the failure occurring.

At the feasibility study stage the FMEA is very basic and can only highlight the major potential failure modes seen with the feasibility proposal; and suggest some methods that might be used to reduce the potential result of the failure.

7.5.2 FMEA approach

Each of the criteria (Severity and Occurrence) is allocated a score between 1 and 5, with 5 being the most severe. The two criteria are multiplied together to give the **Risk Priority Number (RPN)**. The higher the RPN value the more serious the failure and hence the greater should be the effort expended in reducing the risk of it occurring.

An individual who is very familiar with the overall design such as the Project Engineer normally does the initial assessment. The preliminary FMEA produced is then taken to a meeting of the FMEA Team, normally made up of the key designers and other experienced individuals. This team run through the FMEA and agrees the Potential failure modes etc.; other potential failure modes may also be added at this time. The meeting also suggests actions that might be taken to reduce the effects of the failure and a team member is charged with seeing that the recommended actions are taken.

Periodically during the design process the FMEA Team meet to follow up on the actions defined at the preliminary meeting. As the actions are discharged the severity and Occurrence are reassessed and a resulting RPN is given. Generally with the agreement of the FMEA Team an RPN value is chosen as a cut off, all efforts are made to ensure that any resulting RPN value is lower than the cut off value. The FMEA process generally operates from the early design stage through to the approving of the maintenance schedules as these have a large outcome on the overall failure rate of the system.

7.5.3 Failure Mode Effect Analysis Rating Scales

The tables given below give criteria for selecting the severity and occurrence values are assigned to a potential failure

Table 10. Failure mode analysis severity rating scale.

Rating	Description	Definition
5	Catastrophic	Failure could cause serious injury, or cause severe damage to system or other systems. (More than 1 month to repair)
4	Major	Failure could cause minor injury, or cause major damage to system or other systems. (More than 1 week to repair but less than 1 month)
3	Moderate	Failure could cause moderate damage to system or other systems. (More than next nights observing run to repair but less than 1 week)
2	Minor	Failure would cause minor nuisance, but could be repaired before next nights observing run
1	Very Minor	Failure would be an irritant but could be repaired in less than 30 minutes

Table 11. Failure Mode Analysis Occurrence Rating Scale

Rating	Description	Definition
5	Almost certain	Very high probability of occurrence could occur several times (more than 10) during the life of the system.
4	Likely	High probability, may arise (6 to 9 times) during the life of the system
3	Moderate	Possible, reasonable probability that it may arise (2 to 5) during the life of the system
2	Unlikely	Plausible, probability that 1 failure may occur during the life of the system
1	Rare	Very low likelihood, but not impossible, unlikely to occur during the life of the instrument

7.5.4 Results of Feasibility Study FMEA

At this early project stage, where the system design is still largely undetermined, an FMEA can highlight broad areas to attract particular attention because of the high impact of later design deficiencies in those areas.

We undertook an FMEA of the baseline WFMOS configuration. Any potential failure that was allocated an RPN value of greater than 20 would be defined as a very serious failure mode and would require significant attention throughout the design process. As a general rule all failures with an RPN value of greater than 10 would normally be defined as serious and warrant some attention. It should be noted that this analysis has been done with no design in place, thus in many cases it is assumed that no design provision has been made and the occurrence rating is then set to 5 (certain).

For the top end the integrity of any fasteners used in the structure was seen as critical as a loose fastener could fall and damage the primary mirror. The stiffness of the top end was also seen as critical as any major flexure issues could make the fiber fed system inoperable. Lastly the overall mass of the top end could also render the system inoperable if it exceeds telescope load and balance limitations.

For the fiber cable, a number of catastrophic failure modes can be identified, and this emphasises that the routing and handling of the fiber cables will have to be thoroughly investigated. Special handling procedures will have to be written and adhered to.

Fiber connectors are also seen as a critical area where failures to align the fibers for instance could lead to very serious throughput losses. It does suggest that fiber connectors should be well prototyped to ensure the expected performance can be met reliably.

Chapter 8 Wide Field Corrector

8.1 Summary

A very wide field of view on a classically built 8-meter class telescope requires a large corrector. Investigation of a number of possible designs led to the selection of the corrector depicted in Figure 50, taken from the KAOS Purple Book study. Our study of alternative designs for the Subaru telescope shows that they have comparable form to the Purple Book design. For the purposes of tolerancing and costing, this is the design adopted as the baseline for this feasibility study. We note that the Subaru design will not require the wobble plate and that the ADC prisms will likely be incorporated into powered elements of the corrector.

8.1.1 Baseline Corrector Design

The baseline corrector has an unvignetted 1.5 degree diameter field of view with very good image quality across the field. Although challenging, it is feasible to build at reasonable cost using standard glasses and current grinding and polishing techniques. The design includes an Atmospheric Dispersion Compensator (ADC) part of which is also actively controlled in tilt to cancel out telescope wind shake.

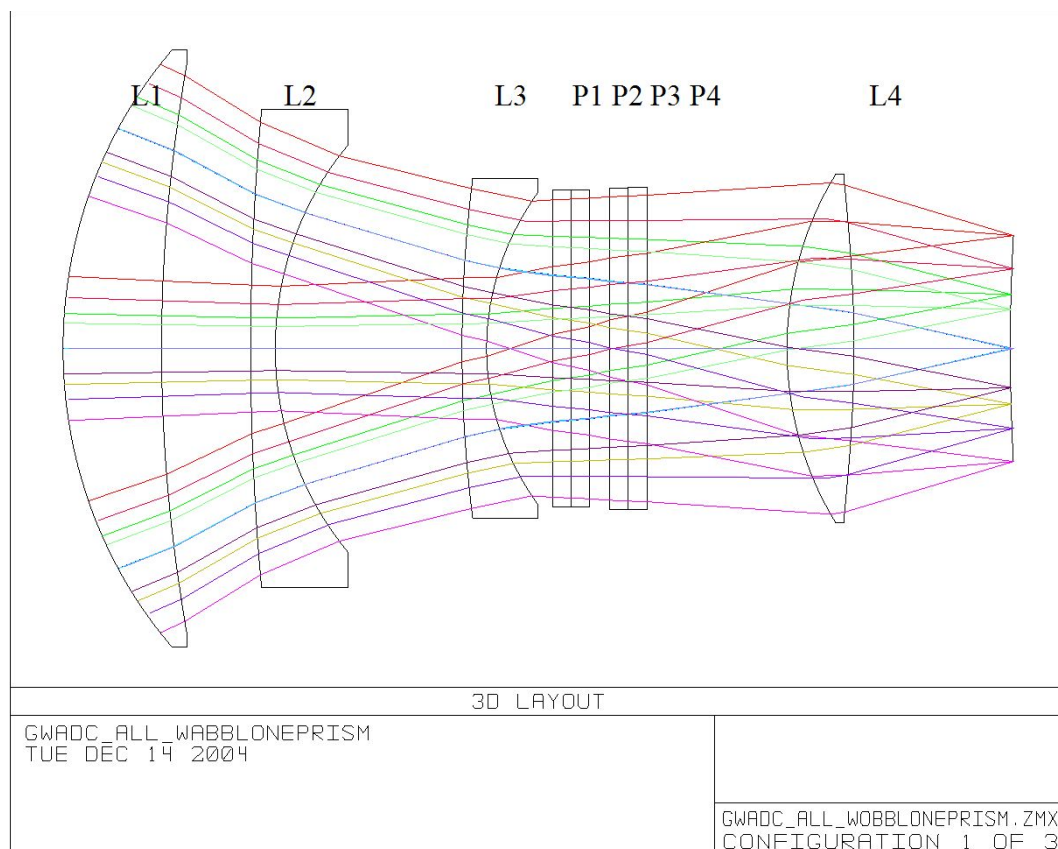


Figure 50. Ray trace of baseline Gemini 1.5df design.

Table 12 gives a summary of the specifications for the baseline design of the Gemini corrector.

Table 12. Baseline WFMOS corrector specifications. From KAOS Purple Book.

Parameter	Specification
Field of view diameter	1.5 deg
Focal length	19,187 mm
Plate scale	0.093 mm/arcsecond
Focal ratio	f/2.4
Focal surface shape	Spherical, Convex facing incoming beam
Focal surface curvature	4,382 mm radius
Exit pupil	Concentric with curved field
Vignetting	None
Physical diameter, largest element	1,428 mm
Physical length, optical system	2,305 mm
Physical diameter, housing	1,825 mm
Physical length, housing	3,050 mm
ADC design	Plane-parallel dispersion prisms
Aspheric surfaces	3

Figure 50 shows a ray trace of the baseline design. It is a four-element corrector made from Fused Silica and BK7. The ADC prisms are composed of LLF6 and BK7 prism pairs. The aspheric surfaces in this design are on the concave (rear) surfaces of L1 and L2 and on the convex front surface of L4. These surfaces were forced to be conic in order to simplify their fabrication and testing. Overall focus is achieved by translating the fiber positioner towards or away from L4. Field derotation is accomplished by rotating the fiber positioner with respect to the optical corrector.

The front element has a total clear aperture diameter of 1.29 meters. Although the size of this element will introduce some risk, it is within the current state-of-the-art for current optical fabrication techniques, and two vendors provided bids for its fabrication (see below). Actually, the major challenge presently appears to be obtaining the LLF6 for the ADC prisms in sufficient size.

Overall image quality is quite good. The rms spot size across the full field of view is less than 40 microns diameter (or less than 0.43 arcseconds projected on the sky) with the telescope pointed to Zenith and no wobble plate displacement. At a Zenith angle of 70 degrees and a wobble plate image displacement of 1 arcsecond, the rms spot size is still less than 60 microns (0.65 arcseconds) across the field. Both spot sizes are based on integrated light across the spectral window from 0.38 to 1 micron in wavelength.

8.1.2 **Optical design exploration – Subaru and Hyper-SuprimeCam**

The KAOS Purple Book considered only a Gemini implementation of WFMOS. With the inclusion of Subaru as a potential platform, the possibility was opened for sharing the wide field corrector with a proposed future Subaru instrument, Hyper-SuprimeCam. This instrument would be a 2-degree field-of-view imager, with significant overlap with WFMOS in corrector requirements. Sharing the expensive corrector components is therefore an attractive option for both instrument programmes.

The attachment “Comparison of suitability of Subaru and Gemini for wide field prime focus multi-fiber feeds” by Peter Gillingham compares the Purple Book and published Hyper-SuprimeCam corrector concepts.

As part of this feasibility study, an astronomical optical designer, Damien Jones, was contracted to undertake a further exploration of corrector design, and he worked with the AAO to refine designs with the Subaru telescope and a shared application in mind. His detailed report forms an attachment to this report (Wide-Field Prime Focus Correctors for WFMOS and Direct-Imaging on SUBARU. “Tomorrow’s Technology”). Damien’s designs pursued an unvignetted approach requiring large front elements (1.6 meters in diameter) and very likely a redesigned top end hub and spider assembly. Peter Gillingham, of the AAO, took Damien’s designs and pursued vignetted solutions that fit within the existing Subaru top end constraints (see the additional attachment by Peter, Wide Field PF Correctors for WFMOS and Direct Imaging).

Mechanical constraints at the Subaru top end, and a desire to minimize risk in component manufacture, impose significant constraints on a corrector design of a Subaru implementation of WFMOS. Various corrector options have been investigated, but the requirements tend to force the designs to be broadly similar in optical configuration. Figure 51 shows the tight fit of the corrector design into the mounting hub at the telescope top end.

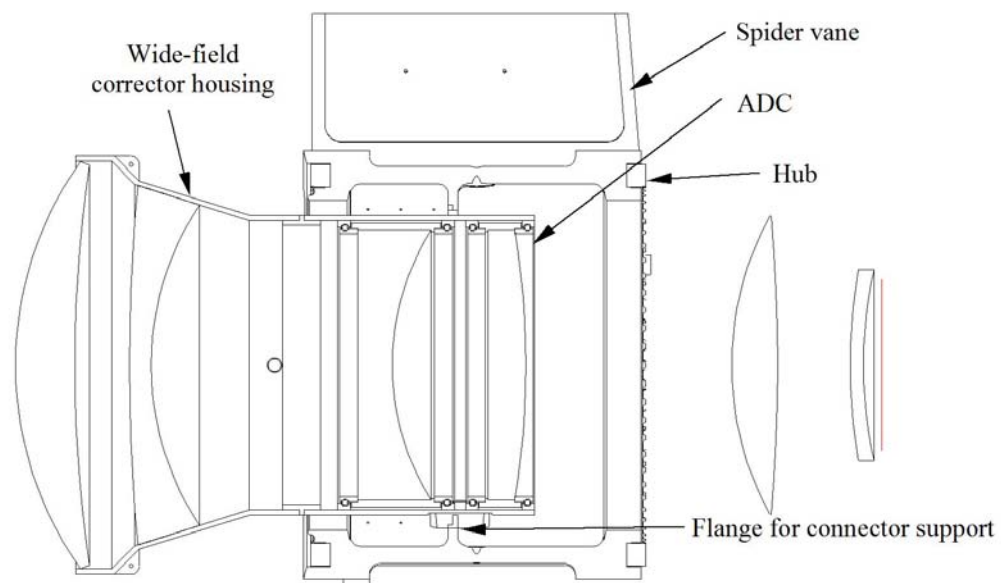


Figure 51. Central hub and corrector optics. Note the small mechanical clearances throughout, and possible interference with the flange near the middle of the hub. Note also the need to mount the corrector in two sub-units, from opposite sides of the hub.

A natural configuration for implementation of this and similar corrector designs is to construct the corrector from two sub-units, one of which mounts from one side of the central hub, and one from the other. This leads further to a design where the first corrector elements (those mounted from below the central hub) are shared between wide field instruments, while the final corrector elements are carried with the instrument package on its own Prime Focus Unit. This arrangement means that the final corrector elements can be of varying designs customized for specific instruments, thereby optimizing the focal surface parameters for the application.

Draft designs were laid out confirming this approach for WMOS and Hyper-SuprimeCam.

In order to fit within the existing central hub dimensions, the light will be vignetted, especially if the front element must be kept at a 1.2 meter diameter. Design explorations show that the typical vignetting across the field will be 17% at the edge of the 1.5 degree field and 23% at the edge of the 2 degree field (see Peter Gillingham's attachment Wide Field PF Correctors for WMOS and Direct Imaging for further details).

8.1.3 Potential IR Performance

Figure 52 shows the encircled energy for the 1.2-1.8 micron wavelength regime for one of the designs explored. The performance is quite good, but does require a refocus from the visible wavelength setting.

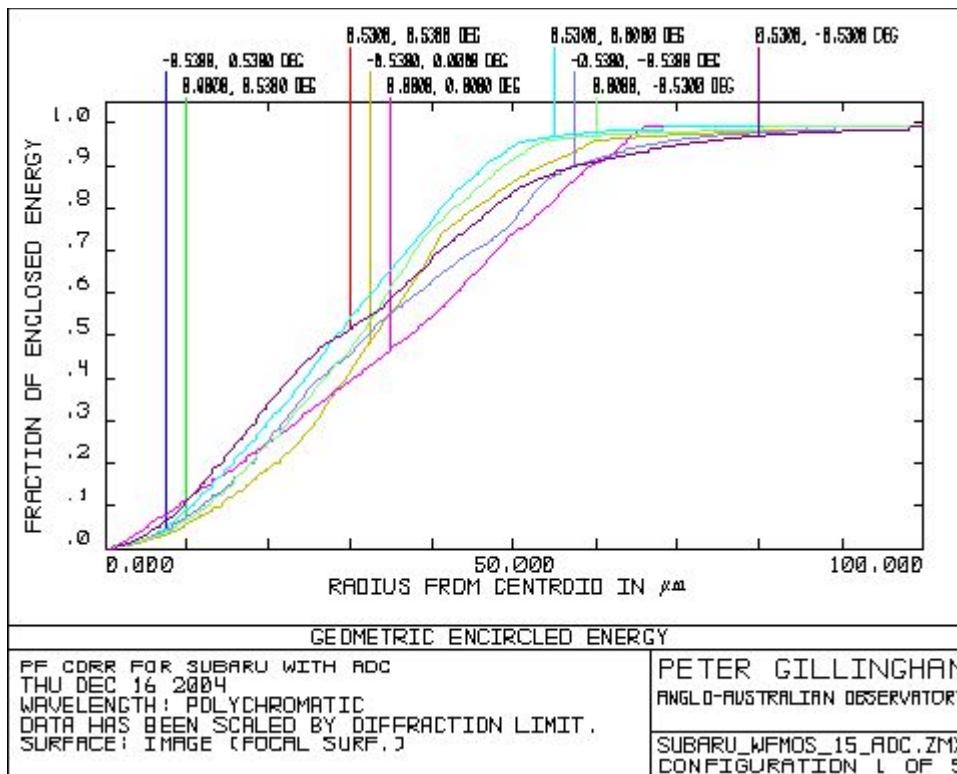


Figure 52: Encircled energy for combined wavelengths 1.2 + 1.5 + 1.8 μ m with corrector design Subaru_WMOS_15_adc, multi-fiber feed configuration with refocus from visible range setting (by 0.185 mm).

8.2 Optical Tolerancing

Preliminary optical tolerances were examined. If one assumes that the optics are mounted and pre-aligned in sub-assemblies, then individual lens decenters of 100 microns are acceptable for all components with the front element giving the worst case image degradation of 1.6%. Tilts of 0.003 degrees are acceptable for L1 and L2, and even larger tilts for L3 and L4. The front element is also the most sensitive to tilt errors, giving worst case image degradation of 3.4%. For the corrector as a whole, solid body decenters and tilts of 100 microns and 0.002 degrees, respectively, are acceptable, yielding respective image degradations of 1.6% and 1.4%.

	Radius tolerance			Surface irregularity		
	Radius	Tolerance	Image degradation	Tolerance	Image degradation	
	mm	mm	%	Fringe	%	
Lens 1	1004.6	0.10	1.00	5.0	0.34	
	3304.5	1.00	0.62	5.0	0.43	
Lens 2	5595.7	1.00	0.60	5.0	0.41	
	696.26	0.10	0.89	5.0	0.27	
Lens 3	2883.9	1.00	0.50	5.0	0.28	
	546.45	0.10	0.49	5.0	0.25	
ADC 1	plane	3 fringe	0.75	5.0	0.22	
	plane	3 fringe	0.75	10.0	0.05	
	plane	3 fringe	0.75	5.0	0.21	
ADC 2	plane	3 fringe	0.75	5.0	0.19	
	plane	3 fringe	0.75	10.0	0.05	
	plane	3 fringe	0.75	5.0	0.18	
Lens 4	724.13	0.50	1.03	1.0	-0.48	
	-2547.3	1.00	0.08	1.0	0.05	
	4382.2			0.0	0.00	
Sub total			2.732		1.038	

	Thickness tolerance			TIR		Conic Constant			Glass refractive i	
	Thickness	Tolerance	Image degradation	Tolerance	Image degradation	Conic constant	Tolerance	Image degradation	glass	Tolerance
	mm	mm	%	mm	%			%		
Lens 1	239.73	0.30	1.4982	0.108	3.000	-4.7615	0.010	2.7783	SILICA	0.0001
Lens 2	60	0.10	0.6418	0.108	2.722				SILICA	0.0001
Lens 3	60	0.10	0.1449	0.113	2.276	-0.37239	0.001	4.949964	BK7	0.0005
ADC 1	45	0.20	0.2000	0.054	2.541				BK7	0.0010
	45	0.20	0.2000	0.054	2.145				LLF6	0.0010
ADC 2	45	0.20	0.2000	0.000	2.409				BK7	0.0010
	45	0.20	0.2000	0.000	1.966				LLF6	0.0010
Lens 4	163.24	0.50	0.5000	0.224	2.024	-41.6523	0.2	1.07996	SILICA	0.0001
Sub total			1.757		6.81			5.778		

	Group tolerance						
	Separation			Decenter		Tilt	
	Separation	Tolerance	Image degradation	Tolerance	Image degradation	Tolerance	Image degradation
			mm	%	Degree	%	
Group 1	12497	0.20	1.7605	0.1	1.6301	0.002	1.40
Sub total			1.761		1.630		1.404

	Lens separation			Lens decenter		Lens tilt	
	Separation	Tolerance	Image degradation	Tolerance	Image degradation	Tolerance	Image degradation
				mm	%	Degree	%
Lens 1	216.89	0.10	1.1169	0.1	1.64	0.003	3.41
Lens 2	454.36	0.20	0.3387	0.1	3.13	0.003	3.27
Lens 3	160	0.50	0.5000	0.1	3.01	0.005	1.09
ADC 1	50	0.50	0.6559	0.1	0.00	0	0.00
ADC 2	341.01	0.50	0.6560	0.1	0.00	0	0.00
Lens 4	380.39			0.1	0.05	0.007	0.03
Sub total			1.573		4.64		4.85

Total degradation in % 12.42

Figure 53. Preliminary error budget table. The whole instrument and focal plane positions are compensators. The blue colored tables show the element and whole package misalignment sensitivity. The degradation columns show the average image rms degradations.

8.3 Wobble Plate for Gemini implementation

The Gemini telescopes are prone to vibration by the wind causing the images to move by about an arc-second in amplitude at a frequency of a couple of Hertz. The KAOS Purple Book raised the suggestion of combining the function of the corrector's ADC prisms with that of a 'wobble plate' to provide tip-tilt image stabilization. Detailed consideration of the optical and mechanical implications of this option is given in *Chapter 9, Wobble Plate*.

8.4 Prime Focus Mounting Structure

For a Subaru implementation of WFMOS, with a two-component structure as outlined in Section 8.1.2, some of the corrector elements will be mounted with the positioner in the Prime Focus Unit, secured at the top of the mounting hub at the telescope top end (Figure 54). The larger elements and ADC are carried in the shared sub-unit mounted from below the hub.

A pointing and focus adjustment mechanism is required to maintain alignment of the corrector as the telescope distorts due to varying gravitational loads during tracking. A range of mechanical solutions is available to meet this requirement, and for costing and feasibility analysis as required for this study, a pair of hexapods is offered as baseline. Positioning accuracy specification of the hexapod design identified for the PFU support, detailed in the report attached to this study, is sufficient to maintain alignment of the two separate corrector assemblies (see also Section 11.3. in the positioner chapter for further discussion of the hexapod).

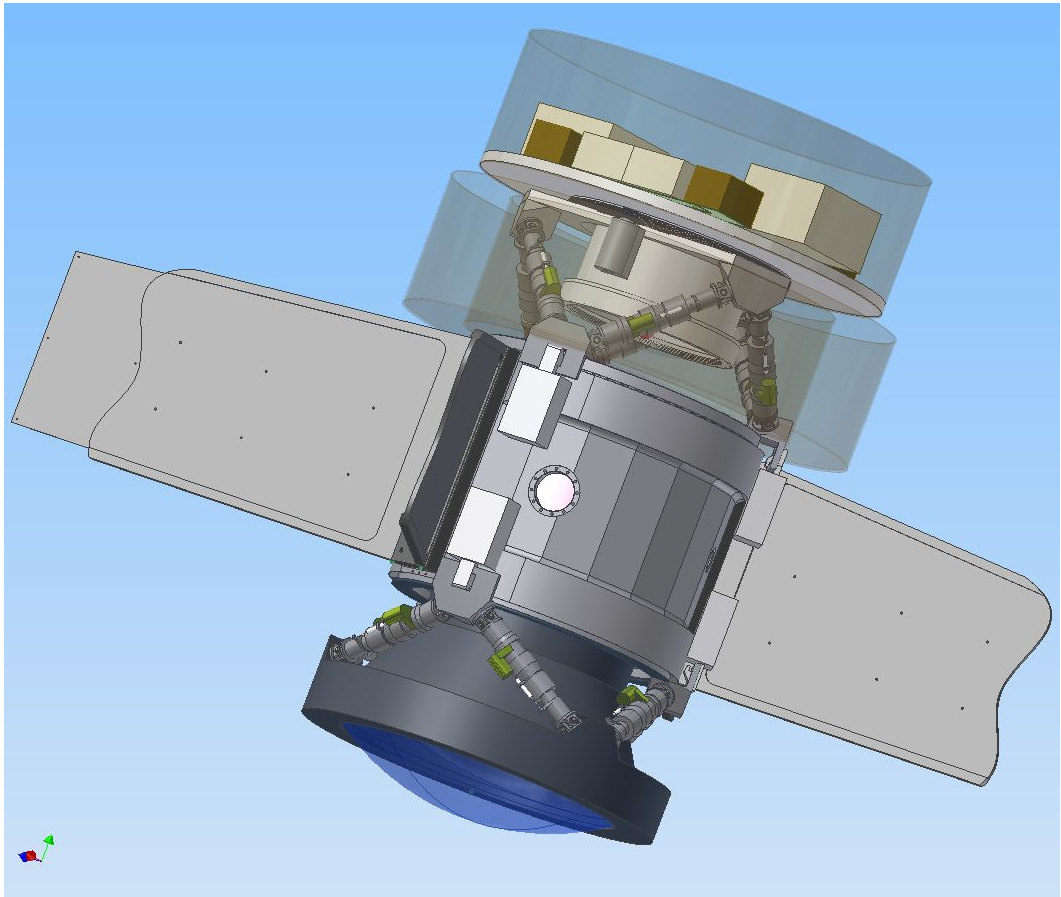


Figure 54. WF MOS corrector components mounted to the Subaru top end central hub. Two sub-units are shown, to be mounted from opposite sides of the hub. The upper component carries the final two elements of the corrector along with the fiber positioner. A pair of hexapods provides pointing and focus adjustment for both sub-units.

For a Gemini implementation of WF MOS, the KAOS Purple Book suggested a notional combined structure to house the corrector and positioner.

Figure 55 shows this support structure and housing for the wide field corrector and related components. The space envelope fits within that available at the top end of the Gemini telescopes. The volume of space allocated for the fiber positioner is a cylinder 1.3 meters in diameter and 0.88 meters in length. The overall diameter of the housing is less than 1.9 meters, resulting in a central shadow of 6%.

In this case, it is expected that a single hexapod will be able to maneuver the monolithic support structure for focus and pointing adjustment.

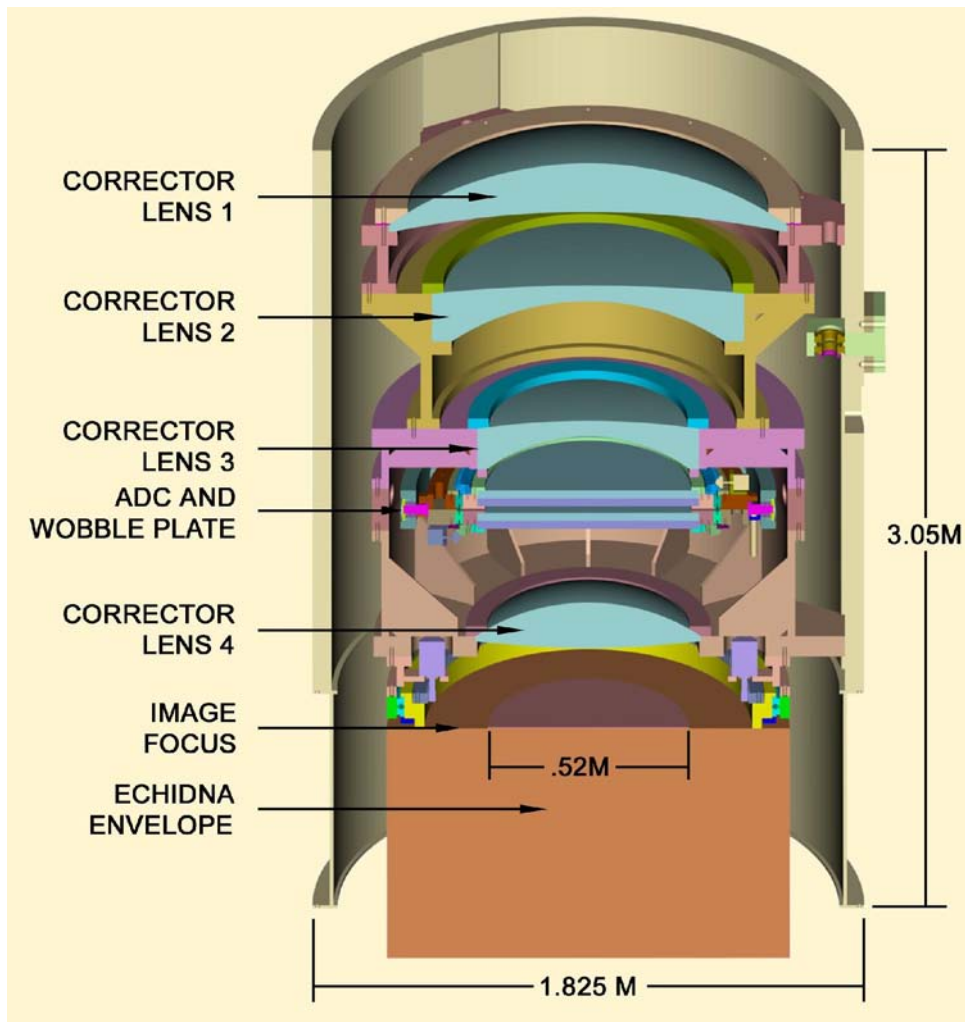


Figure 55. WF MOS prime focus corrector assembly for a Gemini implementation, showing various components.

8.5 Cost Trades

Clear cost trades arise in the design of a system component like the wide field corrector. In exploration of the optical design space, vignetting performance, imaging performance and field-of-view can clearly all be improved by allowing element size to grow. The cost of optical elements is a strong function of size, and the designs are already approaching what is regarded as feasible limits for the current state-of-the-art in manufacture. Availability of the raw materials in volumes with sufficient homogeneity and optical quality, formation of the blanks, achieving the surface figure and AR-coating the finished elements are all strong cost and feasibility drivers that increase cost and difficulty as the size of elements grow.

Further, the mechanical constraints imposed by the Subaru top end can be expected to drive a ‘step change’ in project cost as the corrector size grows to a point where it can no longer be accommodated within the existing central hub design. Replacement of the hub with a larger one has much greater implications for the telescope structure, extending to the spider vanes, the need for an interface adaptor for existing top end-mounted components, and possible impact on the designs of existing instruments (for example, cold stop designs will need to change if the pupil of the telescope is affected).

Mass of the corrector is a major fraction of the total mass of WFMOS top end components, and it is expected that the instrument’s mass budget will already be under pressure to remain within telescope balance limitations.

8.6 Cost and Feasibility

8.6.1 Optical elements

Fabrication cost quotations were solicited from four vendors, using the baselined Purple Book design described above. For competitive reasons, the vendors asked that they not be identified in any public documents, but all four are established companies with significant experience in the fabrication of large optical elements. All vendors were also asked to identify any issues with material availability, material cost, or other particular risks that might affect the feasibility of this design. All vendors received detailed drawings of each element, showing materials, tolerances and other pertinent information.

Two of the vendors expressly declined to quote after reviewing the drawings. Quotes from the remaining two vendors are summarized in Table 13. All amounts are in US Dollars.

Table 13. Received quotations from manufacturers for WFMOS corrector optics.

Element	Material	Vendor 1	Vendor 2
L1	Fused Silica	1,465,000	1,550,000
L2	Fused Silica	550,000	1,200,000
L3	BK7	220,000	390,000
P1	BK7	135,000	220,000
P2	LLF6	112,000	265,000
P3	BK7	135,000	220,000
P4	LLF6	114,000	270,000
L4	Fused Silica	400,000	790,000
A/R Coatings		700,000	Included in element prices
Total		3,831,000	4,905,000

The primary feasibility issue noted by both bidders is the availability and cost of LLF6 blanks in the size required for the ADC prisms. LLF6 in this size is available from Schott only by special order, and only when such orders total at least 5 metric tonnes. For reference, the finished P2 and P4 elements are predicted to weigh less than 20 kg each.

The largest differences in the quoted prices are on L2 and L4, which are also the elements with the largest aspheric departures. These differences in the quotes apparently reflect the vendors’ differing judgments about the difficulty of fabricating and testing these challenging surfaces.

No specific quotes were obtained for the mounting assembly depicted in Figure 55. The mounting assembly presents no special feasibility issues and is within the capabilities of the AAO or NOAO to fabricate. Based on experience from prior instruments and optical systems including prime focus units for the 4-meter AAT, Mayall, and Blanco telescopes, it is believed that the cost of the mounting assembly would not exceed \$1,500,000, excluding the Echidna fiber positioner, the drive and control system for the wobble plate, and the rotator.

A notional wide field corrector for the project baseline Subaru implementation was selected from the exploration of the optical design space, with consideration given to the cost and feasibility trades discussed above. In particular, a design with slightly smaller front element was selected (1.20 m) to provide enhanced confidence in the manufacture of this challenging element. Independent quotes were sought by the AAO for the blanks required for this component, and estimates were made for the optical element manufacture based on this design and the quotes shown in Table 13 above.

8.6.2 *Mechanical Structure*

In order to gain an understanding of the likely cost of the work, cost estimates for the corrector work package are derived from a schedule built around the work breakdown structure. Conceptual designs were undertaken to identify the required system components and to build a detailed schedule for design and manufacture. Work package components making these up were estimated by AAO staff and subject to internal review by the AAO WFMOS team.

Components considered included both optical and mechanical design, component manufacture, electronics and other components for the ADC, the hexapod pointing mechanism, integration, labour and software.

Chapter 9 Wobble Plate

The WFMOS system needs to deliver as high as possible a throughput to the fiber apertures. In the early KAOS studies it was realised that to achieve this with Gemini, some equivalent to the tip-tilt secondary was probably needed. For a prime focus instrument, this led naturally to the idea of a ‘wobble plate’ which could fulfil the same role. A promising location for such a wobble plate was identified as part of the ADC. For the current feasibility study, further work has been done on the mechanical properties of such a wobble plate. We have used the Gemini wind shake power spectrum as input, and performed a servo analysis for the combined WFS and wobble plate system. We have also performed an FEA analysis of the proposed wobble plate in order to confirm that such a system is practical and affordable. Specifications for the actuators needed have also been developed and their availability confirmed.

In the case of a Subaru implementation, it is likely that such a wobble plate will not be needed (due to the smaller windshake expected), although we have not investigated this in detail for this feasibility study.

Below we describe the windshake assumptions, the servo analysis, the mechanical solution for the wobble plate and its FEA analysis. At the end we detail the estimated costs and risks.

9.1 *Effect of Windshake on Gemini*

All ground-based telescopes exhibit image motion over a wide range of timescales. This motion stems from a number of sources, which include residual tracking errors, atmospheric tip-tilt, and windshake/wind-buffeting. In addition to its direct effect on the telescope orientation, windshake can excite resonances within the telescope structure, optics and instrumentation, with the nature and extent of such excitations typically dependent on the telescope zenith pointing and the precise wind direction. Gemini is no exception, and its cassegrain instrument feed includes servo systems designed to cancel the combined image motion effects encountered within Gemini’s operational limits. In order to deliver the required image quality this motion cancellation must be sufficiently complete and extend to sufficiently high frequencies. These requirements drive the specification of the Cassegrain/instrument sensors and the actuation capabilities of M2. The deployment of WFMOS would bypass M2 and the cassegrain sensors, and alternative systems must be substituted.

For the purposes of designing the WFMOS sensor and actuation systems, a measured image motion power spectral density (PSD) is adopted. This is illustrated in figure 1 and was provided by the Gemini observatory. The figure also includes the closed-loop corrected PSD for Cassegrain operation, and can be usefully compared with predictions for the design concepts described for Gemini implementation of WFMOS. The design concept for the prime focus actuation system (a “wobble plate”) is described in this section, whilst the feasibility of alternative concepts for the sensor is described in the related section on wavefront sensing.

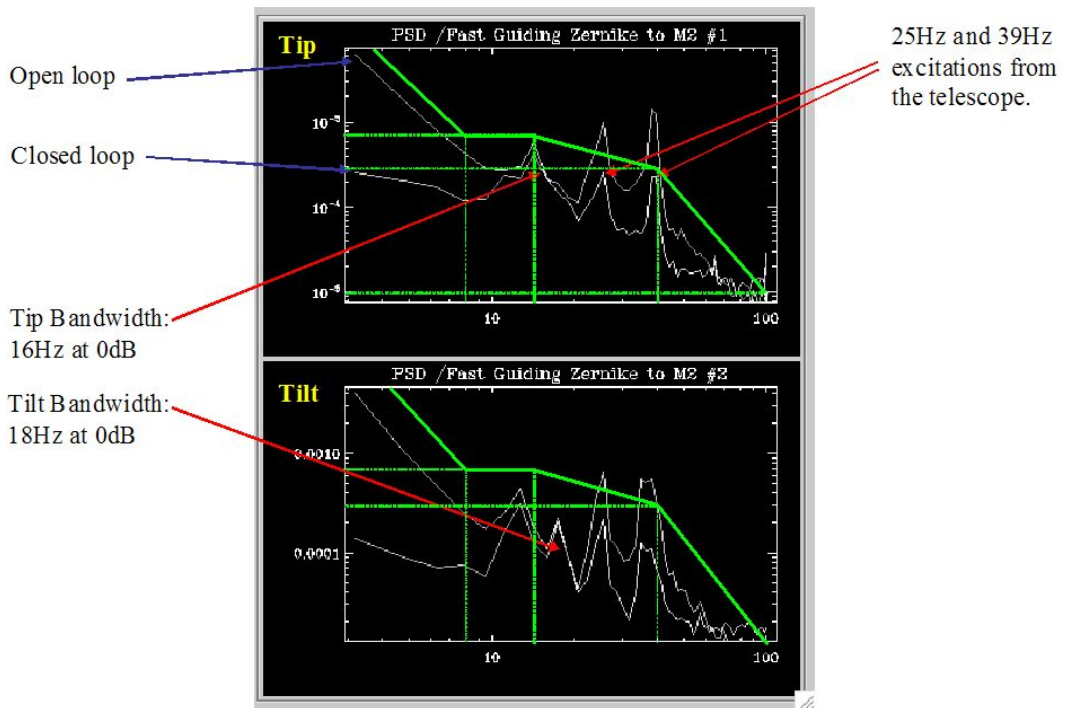


Figure 56. Open- and closed loop PSD of fast guide measurements done with Gemini Peripheral Wavefront Sensor No. 2 (PWFS2) in binning mode and operating at 200Hz on a bright star (9-10mag) - March 18, 2003. The vertical axis is in units of PWFS2 pixels²/Hz, where 1 PWFS2 pixel corresponds to 0.143 arcsec.

9.2 Wobble Plate Servo Concept

A first-order MATLAB/Simulink control system model is displayed in Figure 57. The estimated plant transfer function is based on the first two resonant frequencies of the wobble plate (derived in subsequent subsections) and the response of the proposed actuators. A short time delay has been introduced to the system to represent the RTCS latency.

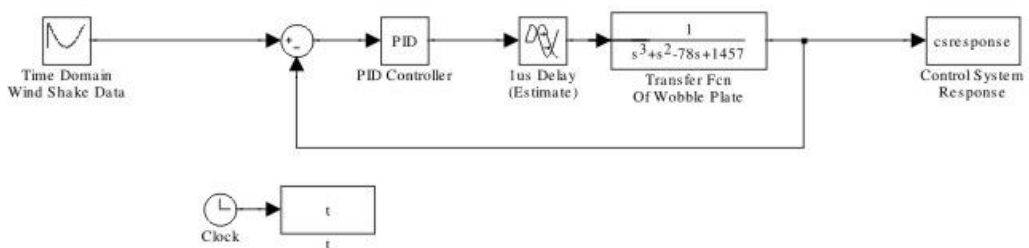


Figure 57. WFMOS Control System Simulink Model.

The windshake data supplied by Gemini and illustrated in Figure 56 was enveloped as described in subsequent subsections and fed into the control model as a time domain signal, with effective sensor sampling at 200Hz, which becomes the requirement for the wavefront sensor.

Although a PID controller was selected for control only the integral term was varied. The output signal was transformed back to a PSD. shows the results of $G_I = 1$ (red) and 10 (blue) plotted with the original Windshake PSD (blue).

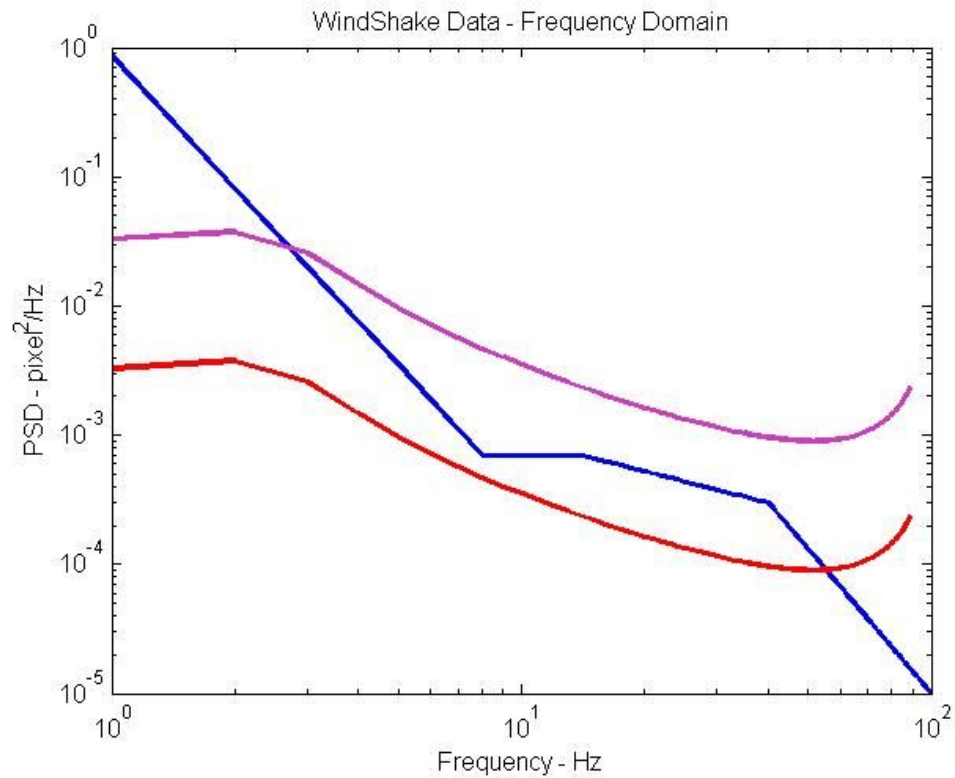


Figure 58. Control System Response to Windshake.

These simple model predictions may be compared with measured cassegrain closed-loop performance of Figure 56 and provide confidence that the wobble plate design concept can meet image quality requirements.

Proposed subsequent work packages include a full analysis with input phase information and a more refined model.

9.3 **Wobble Plate Solution**

9.3.1 **Mechanical Design**

The design of the Image Stabiliser and Atmospheric Dispersion Corrector (IS / ADC) is based on the wobble plate design presented in the KAOS Purple Book. It incorporates the optical design for the 1.5 degree field-of-view corrector for WFMOS on Gemini. The corrector specification is summarised in Table 14 below, and a schematic lay-out is shown in Figure 59.

Table 14: *Optical specification for the 1.5 degree field-of-view corrector for WMOS.*

Element name	Radius (mm)	Separation (mm)	Medium	Aperture radius (mm)	Conic constant	Surface tilt (degree)
Primary mirror	28800.000	12496.97	Mirror	4200.0	-1.00376	
Lens 1	1004.624	239.73	Silica	680.0		
	3304.460	216.89		653.1	-4.76153	
Lens 2	5595.693	60.00	Silica	544.8		
	696.262	454.36		464.2		
Lens 3	2883.939	60.00	BK7	386.6		
	546.455	160.00		356.0	-0.37239	
ADC prism	plane	45.00	BK7	358.6		
ADC prism	plane	45.00	LLF6	360.5		0.0265
	plane	50.00		361.8		0.0008
ADC prism	plane	45.00	BK7	364.6		
ADC prism	plane	45.00	LLF6	366.2		-0.0284
	plane	341.01		367.9		-0.0009
Lens 4	724.135	163.24	Silica	396.5		
	-2547.336	380.39		391.2	-41.65229	
Focus	4382.211			257.4		

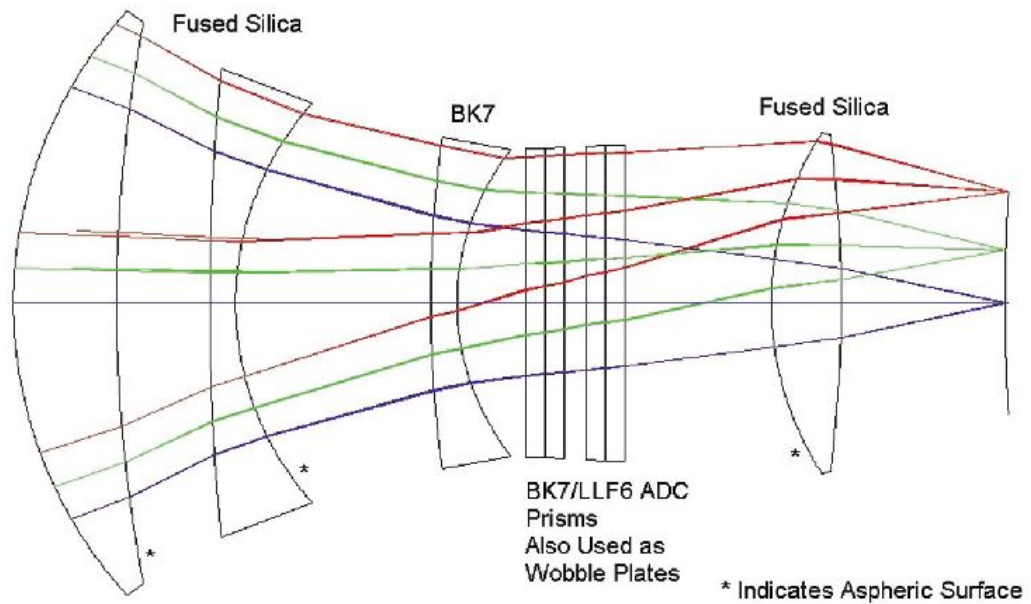


Figure 59: Zemax layout for the 1.5 degree field-of-view corrector for WMOS. The output is f/2.4 with 19,187 mm focal length. The total length of the system is 2,305 mm. The image surface is 1.5 deg (515 mm diameter) with a curvature radius of 4,382 mm.

The IS / ADC assembly consists of two pairs of prisms which, when counter-rotated around the optical axis, provide continuous compensation for the atmospheric dispersion on Mauna Kea up to a zenith angle of 70° across the 0.39 - 1.0 μm spectral window. Each of the two ADC elements contains two plane-parallel dispersion prisms made from Fused Silica (LLF6) and BK7 respectively.

One of the ADC elements acts as an image stabiliser (wobble plate) which can be actuated in tip-tilt to enable fast guiding to compensate for the wind buffeting of the telescope. This approach minimises the number of optical elements in the corrector and, more importantly, the total mass of the corrector. Figure 60

illustrates the image displacement and image quality as a function of the wobble angle for a single ADC element. The image stabiliser produces an image displacement of 3.6 arcsec per degree wobble angle (= 0.2 arcsec per mrad). The excellent image quality across the field is preserved for image displacements of several arc-seconds, i.e. for wobble angles less than 0.5° .

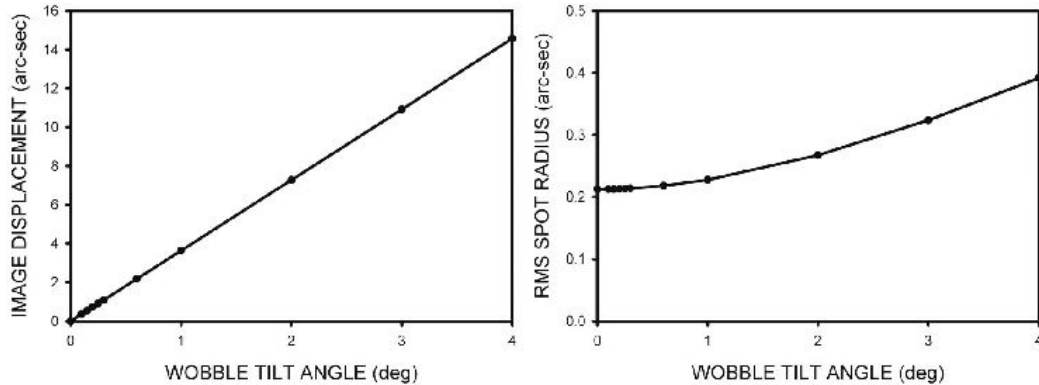


Figure 60: Image displacement and quality as a function of wobble plate tilt angle. Only one of the two ADC elements was tilted.

The separation between the two ADC elements is 50 mm, allowing some room for the mechanisms that rotate and wobble the ADC elements. The separation between Lens 3 and the first ADC element is very limited (28 mm), which restricts the envelope available for such mechanisms, and the structure required to support the ADC element (and the lens). No such restrictions are present for the space between the second ADC element and Lens 4.

Each set of prisms is mounted inside a prism holder, which is supported inside a mounting ring by means of a large diameter, small cross section 4-point contact bearing. The proposed bearing is a custom size Kaydon Reali-Slim KF-Series bearing with a 33 inch bore. The prisms can be rotated by means of a stepper motor driving a bevel gear. Their clear aperture is \varnothing 740 mm. Figure 61 shows the mounting arrangement for the fixed (i.e. non-wobbling) ADC element. The implementation of such a rotating mechanism (including the procurement of a suitable motor / gearbox combination) should be fairly straightforward and is not considered to incur any significant risks. The light-weighted mounting ring can also be effectively used to support the wobble plate actuators (not shown).

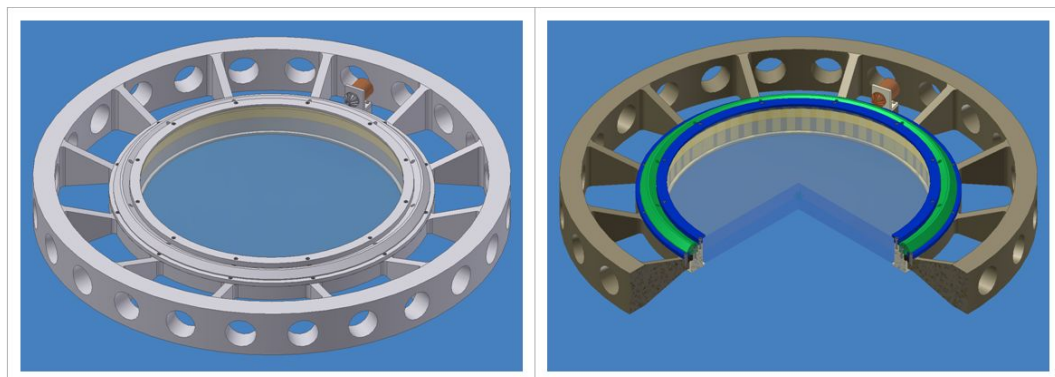


Figure 61: Mounting arrangement for the fixed (i.e. non-wobbling) ADC element.

Two concepts were investigated for mounting and actuating the wobble plate:

1. A double ring design as proposed in the KAOS Purple Book.
2. A hexapod-type arrangement, similar to e.g. the mounting arrangements for secondary mirrors.

The hexapod design offers the advantage of a smaller moving mass, as there is no requirement for a double ring to facilitate the tip-tilt motion. Also, the omission of the double ring produces a much stiffer design, with a significantly higher resonance frequency. However, the major drawback with this design is that the wobble plate actuators have to support the full weight of the ADC assembly under varying orientations of the gravity vector. As linear voice coil actuators are proposed for this application (see Section 9.3.3), this requires that the actuators are powered continuously to compensate for the gravity load. This would require significant input powers and induce prohibitive heat dissipation. It may be possible to devise a passive mechanism to compensate for the gravity load, but the design of such a mechanism was considered to be beyond the scope of this study. Furthermore, the implementation of such a mechanism would (to some extent) negate the advantage of a lower mass.

Consequently, the design approach that was selected for further investigation is the double-ring design concept as proposed in the KAOS Purple Book (see Figure 62). The inner ring which holds the prism pair is supported inside the outer ring by means of two pairs of angular contact ball bearings mounted in a tandem configuration. The outer ring, in turn, is mounted in the same way inside the mounting ring, which forms the main interface with the instrument. This arrangement enables the ADC element to be rotated about two axes (tip-tilt) with an amplitude of up to 1 degree and a frequency of a couple of Hertz to compensate for the rapid windshake motion.

A compensation mechanism is required to eliminate the reaction forces and torques on the telescope top end induced by actuation of the wobble plate. In order to minimise the required additional mass, the counter-balance mass should be implemented in such a way as to provide the largest possible inertia (i.e. a large diameter ring) and/or largest practical amplitude. The design of such a mechanism was considered to be beyond the scope of this study.

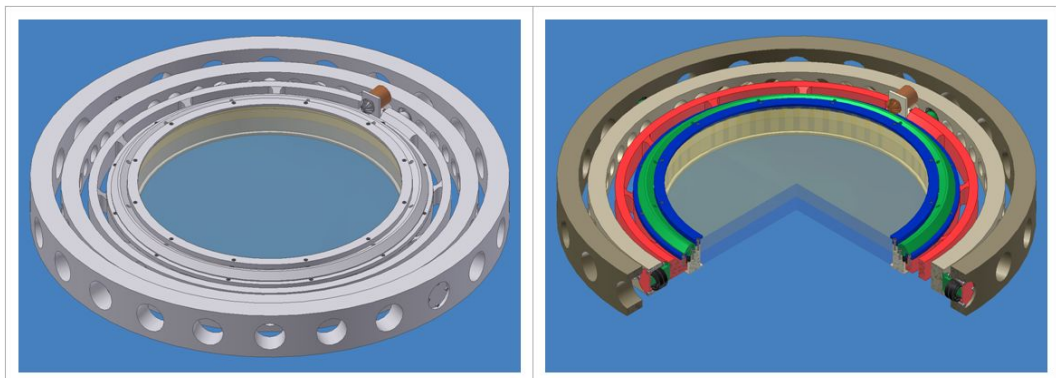


Figure 62: Mounting arrangement for the moving (i.e. wobbling) ADC element.

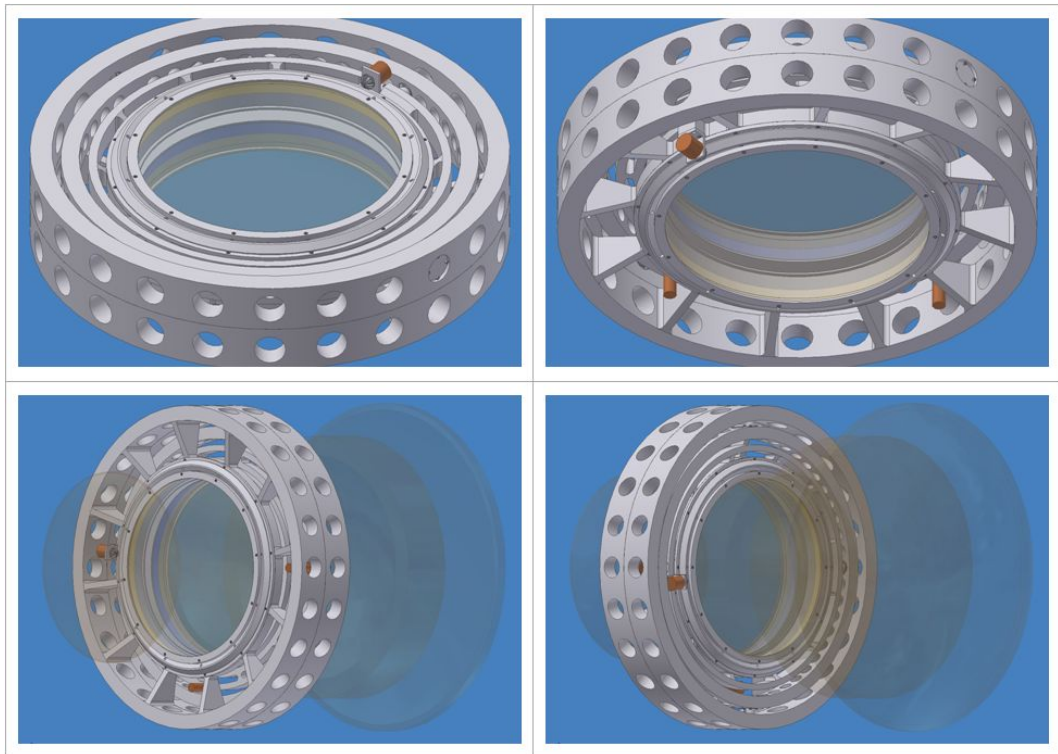


Figure 63: The Image Stabiliser and Atmospheric Dispersion Corrector (IS / ADC - top) and its implementation in WFMOS (bottom).

A schematic of the entire IS / ADC is given in Figure 63, with an overview of the implementation in the WFMOS instrument.

9.3.2 Mass and Inertia Estimates

The total mass estimate for the IS / ADC (*excluding* the reaction torque compensating mechanism) is 528.6 kg. This does *not* include any margins. The mass of the drive electronics is also not included. The mass breakdown is as follows:

Fixed ADC Element

ADC Prism Sub-Assembly		
ADC Prism (BK7)	51.2 kg	
ADC Prism (LLF6)	57.4 kg	
Prism Holder	21.1 kg	
Clamp Ring	3.1 kg	
Ring Gear	7.8 kg	
Bearing	6.5 kg	
Sub-Total		147.1 kg
Mounting Ring Sub-Assembly		
Mounting Ring	88.3 kg	
Bearing Clamp Ring	2.5 kg	
Stepper Motor Assembly	1.5 kg	
Wobble Plate Actuators and Sensors (4 off)	12.0 kg	
Sub-Total		104.3 kg
Total		251.4 kg

Wobble Plate

ADC Prism Sub-Assembly (see above)		147.1 kg
Inner Ring Sub-Assembly		
Inner Ring	23.2 kg	
Bearing Clamp Ring	2.5 kg	
Stepper Motor Assembly	1.5 kg	
Bearing Assembly (2 off)	1.3 kg	
Sub-Total		28.5kg
Outer Ring Sub-Assembly		
Outer Ring	30.1 kg	
Bearing Assembly (2 off)	1.3 kg	
Bearing Clamp Assembly (2 off)	0.3 kg	
Sub-Total		31.7 kg
Mounting Ring Sub-Assembly		
Mounting Ring	69.1 kg	
Bearing Clamp Assembly (2 off)	0.3 kg	
Sub-Total		69.4 kg
Total		276.7 kg

The estimates of the various moments of inertia, relevant to the dimensioning of the various actuators, are as follows:

- ADC Prism Sub-Assembly:

Mass: 147.1 kg

Moment of Inertia: 14.3 kg.m²

- Tip Sub-Assembly (i.e. ADC Prism Sub-Assembly *plus* Inner Ring Sub-Assembly):

Mass: 175.6 kg

Moment of Inertia: 10.1 kg.m²

- Tilt Sub-Assembly (i.e. Tip Sub-Assembly *plus* Outer Ring Sub-Assembly):

Mass: 207.6 kg

Moment of Inertia: 15.7 kg.m²

9.3.3 Actuator Selection

The actuators will be used to wobble the ADC element about two axes (tip and tilt) to compensate for the vibrations induced by wind buffeting.

Assuming a sinusoidal excitation, the actuator's minimum required stroke (s), velocity (v), force (F) and power (P) can be calculated as follows:

$$s = A \cdot r ,$$

$$v = (2\pi \cdot f) \cdot A \cdot r ,$$

$$F = \frac{(2\pi \cdot f)^2 \cdot A \cdot I}{r},$$

$$P = \frac{1}{2} \cdot (2\pi \cdot f)^3 \cdot A^2 \cdot I,$$

where: A is the required wobble plate amplitude [rad], f the frequency [Hz], I the moment of inertia [kg.m²] and r the actuator's moment arm about the rotation axis [m].

Assuming the following (preliminary) top-level requirements:

- wind shake amplitude: ~ 1 arcsec (which corresponds to a wobble plate amplitude (A) of 5 mrad, see Figure 60),
- wind shake frequency (f): ~ 4 Hz,

the actuator requirements are:

	Tip	Tilt
Stroke:	± 2.5 mm	± 2.8 mm
Velocity:	62 mm/s	70 mm/s
Force:	65 N	90 N
Power:	2.0 W	3.1 W

with $r = 495.3$, and $r = 558.8$ mm for the tip- and tilt mechanisms respectively.

The type of actuator considered to be most suitable to this application is a linear or rotary voice coil actuator.

Voice coil actuators are single phase, direct drive, limited motion electromagnet devices that utilise a permanent magnet field and coil winding (conductor) to produce a force that is proportional to the current applied to the coil. These non-commutated, hysteresis- and cog-free devices are used in linear and rotary motion applications that require linear force or torque output, and high acceleration or high-frequency actuation. They provide highly accurate linear and rotary motion, free from the backlash, irregularities and energy losses that result from converting rotary to linear motion. Originally used in radio loud speakers, voice coil actuators are ideally suited to applications where proportional or tight servo control is a necessity. They deliver infinite position sensitivity, limited only by the encoder used for feedback, and the force-versus-stroke curve is extremely smooth.

In its simplest configuration, the linear voice coil actuator consists of a cylindrical coil which is free to move axially within a radially oriented magnetic field. The field is produced by permanent magnets embedded on the inside diameter of a ferromagnetic cylinder, arranged so that the magnets facing the coil are all of the same polarity. An inner core of ferromagnetic material set along the centreline of the coil and joined at one end to the permanent magnet assembly, is used to complete the magnetic circuit. Application of a voltage across the two coil leads will generate a current in the coil, causing the coil to move axially along the air gap, provided the force is large enough to overcome friction, inertia, and any other forces from loads attached to the coil. The direction of movement is determined by the direction of current flow in the wire.

Depending upon the required operating stroke of the actuator, the axial lengths of the coil and magnet assemblies can be chosen such that the force vs. stroke curve is extremely flat. In some cases the axial length of the coil exceeds that of the magnet, by the required amount of coil travel, whereas in other cases the magnet is longer. The long-coil configuration provides a superior force-to-power ratio and dissipates heat better. The short coil however, has a lower electrical time constant, smaller mass, and produces less armature reaction. Neither arrangement provides a perfectly linear force-vs.-travel characteristic, but the degradation of force at the two travel extremes with respect to the mid-stroke force can often be kept below 5%. An armature reaction results from current in the coil and alters the level of flux in the air gap. Current through the coil in one direction decreases air gap flux, whereas current in the opposite direction increases it. Applications calling for a more linear force-vs.-position characteristic may use two actuators working in tandem. Here, one actuator pulls when the other pushes, and vice versa.

If one were to flatten the linear voice coil actuator from a round tube to a flat tube, then bend the two ends to form a planar arc, such as the sector of an annulus, one would have a rotary voice coil actuator. This device can also be referred to as a Limited Angle Torquer or a Sector Torquer. Its principle of operation and force generation is analogous to that of the linear counterpart; however, ratings are in units of torque, instead of force, because force is generated along the circumference of an arc.

The baseline actuator is an off-the-shelf BEI-Kimco Magnetics Division Linear Voice Coil Actuator, part no. LA25-42-000A, see Figure 64. The actuator has a ± 0.5 inch (± 12.7 mm) stroke and generates a peak force of 60 lb-f (266.9 N). The actuator characteristics are summarised below:

Characteristic	Value	Characteristic	Value
Stroke:	± 12.7 mm	Voltage at peak force:	30.0 V
Peak force:	266.9 N	Current at peak force:	12.5 A
Continuous stall force:	86.3 N	Power consumption at peak force:	375 W
Actuator constant:	13.8 N/ \sqrt{W}		
Force sensitivity:	21.35 N/A	DC resistance:	2.4 Ω
Electrical time constant:	1.04 ms	Inductance:	2.5 mH
Mechanical time constant:	2.86 ms	Back EMF constant:	21.36 V/m/s

The actuator performance (expressed in terms of the amplitude of a sinusoidal excitation of the WFMOS wobble plate as a function of frequency) is given in Figure 65 below. Up to the switch-over frequency (between 3 and 4 Hz), the performance is limited by the actuator stroke, whereas for higher frequencies the amplitude decreases with frequency in accordance with the following power law: $A \propto f^2$. The figure demonstrates that the actuator is capable of moving the wobble plate with the required amplitude (i.e. 5 mrad) for frequencies of up to 7 and 8 Hz in tip and tilt respectively. This simple analysis assumes that the wobble plate behaves like a rigid body.

where the summation is performed over all relevant frequency bands with $f_{1,n}$ and $f_{2,n}$ being the lower and upper cut-off frequencies for the n-th band (note that $f_{1,n}$ may be equal to the starting frequency f and $f_{2,n}$ may be equal to ∞).

Scaling the result by the ratio between image displacement and wobble angle, derived from Figure 60 (i.e. 0.2 arcsec per mrad), gives the wobble angles required to correct for the RMS- and 6- σ vibration levels induced by wind buffeting of the Gemini telescope. Note that Figure 65 indicates that, for high frequencies, the actuator performance drops below the requirement for 6- σ correction. This implies that for frequencies in excess of 20 - 30 Hz, the system will not provide full correction of the 6- σ vibration levels, and a reduced performance should be expected. This is more fully discussed in Section 9.2, where the wobble plate servo model analysis results are presented.

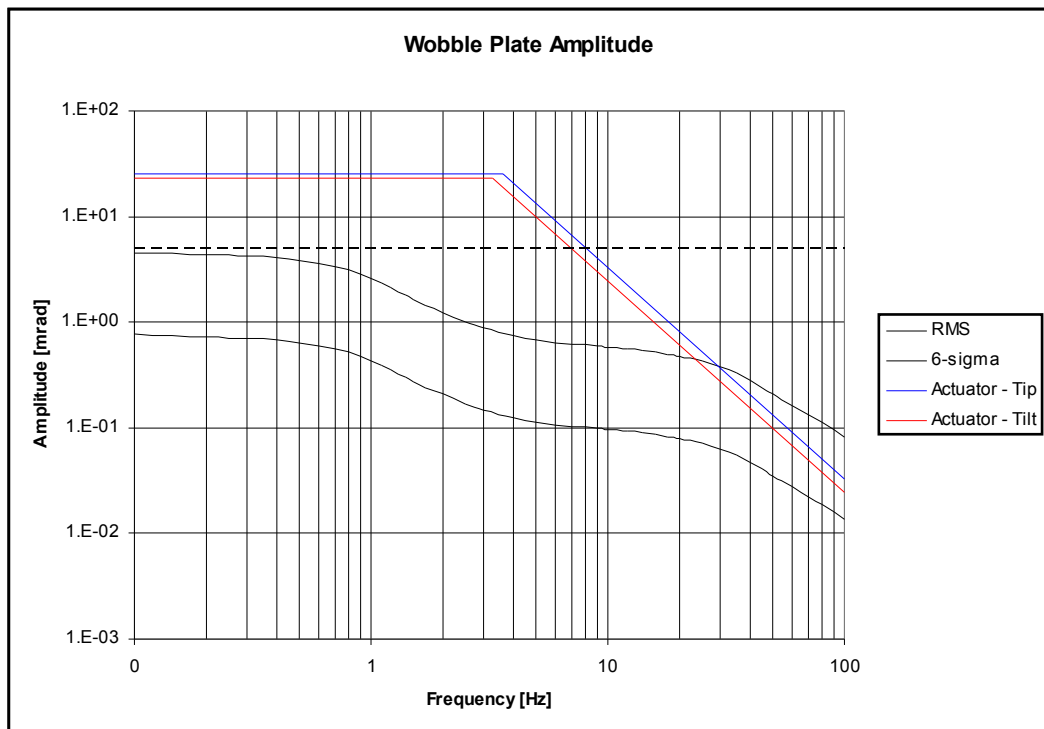


Figure 65: Performance of the BEI-Kimco Linear Voice Coil Actuator (part no. LA25-42-000A) compared with the angles required to correct for the RMS- and 6- σ vibration levels induced by wind buffeting of the Gemini telescope as a function of frequency for the WFMOS wobble plate.

The actuator requirements, necessary to provide full 6- σ correction, are presented in Figure 66. This figure shows that for frequencies in excess of ~ 10 Hz, the actuator force and power dissipation⁶ increase to very high levels. Consequently, the maximum permissible input power (heat dissipation!) may place a practical

⁶ The power dissipation in the actuator has been calculated using the following equation:

$$P = \left(\frac{F}{K} \right)^2 \cdot \Omega,$$

where: K_a is the actuator's force sensitivity (21.35 N/A), and Ω its DC resistance (2.4 Ω).

limit on the correction bandwidth that can be obtained, with an acceptable degradation of the wobble plate performance at higher frequencies.

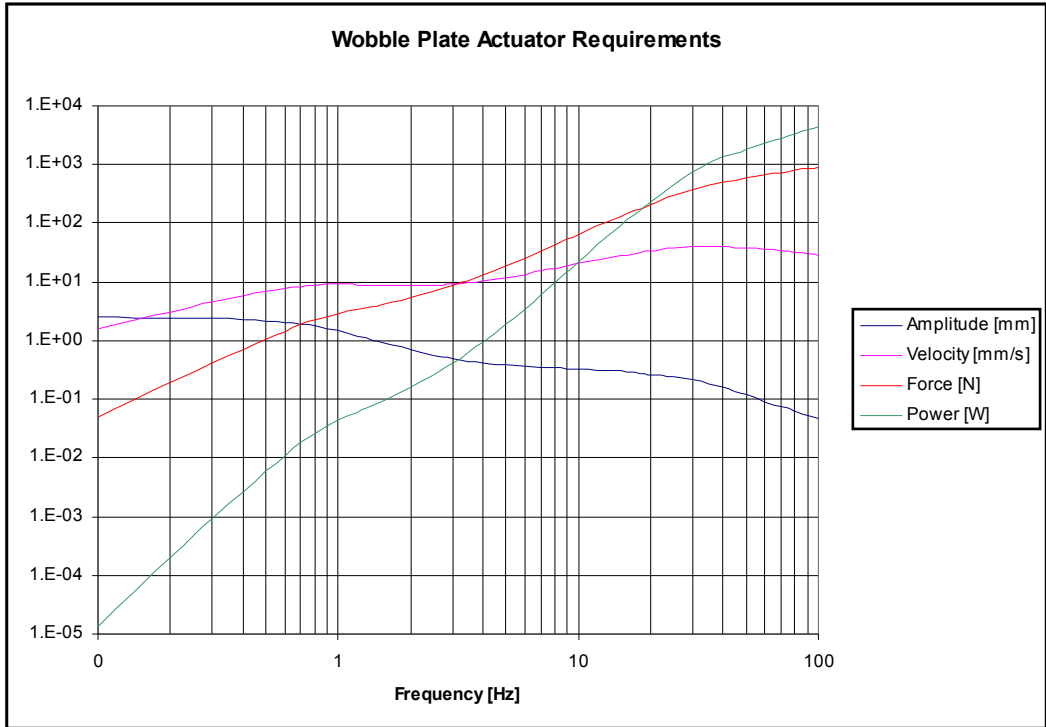


Figure 66: Amplitude, velocity, force and power requirements for correction of the 6- σ vibration levels induced by wind buffeting of the Gemini telescope as a function of frequency for the WFMOS wobble plate.

9.3.4 Finite Element Analysis

5
1
1

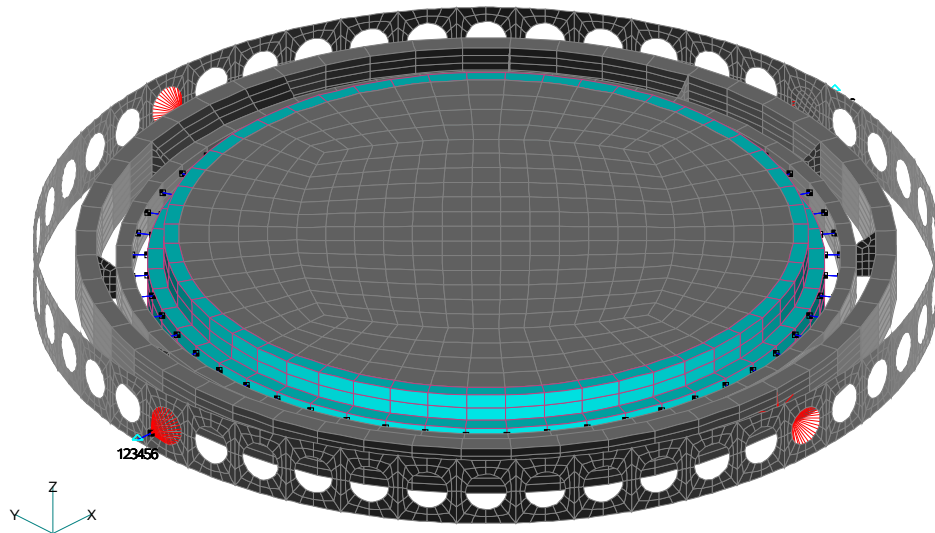


Figure 67: Finite element model for the WFMOS wobble plate.

A finite element model representing the wobble plate was developed to calculate the natural vibration frequencies and corresponding mode shapes. This model is

shown in Figure 67 below. The prism angles are extremely small and have been neglected for the purpose of the mechanical design and analysis. The prisms were modelled using parabolic hex elements. The prisms are cemented together and mounted inside the prism holder. It has been assumed that the adhesive used to cement the prisms together is rigid (i.e. does not shear) thus providing a rigid connection between the prisms. Also, the assumption is made that the prism elements are rigidly connected to the prism holder. The prism holder has also been modelled using parabolic hex elements.

The Kaydon Reali-Slim KF-Series large diameter, small cross section 4-point contact bearing, which holds the prisms inside the inner ring, has been modelled using 52 spring elements, with a combined stiffness of 2.0×10^9 N/m in both the axial- and radial directions, and a stiffness of 0.37×10^9 N.m/rad against out-of-plane bending. These values take into account the compliance of the bearing interface with the prism holder and inner ring. The assumption was made that the bearing will be pre-loaded to increase its stiffness. This will obviously increase the torque required to drive the bearing, but this can easily be accommodated by proper dimensioning of the stepper motor and bevel gears. The inner ring was modelled using parabolic hex elements, with parabolic plate elements to represent the thin webs.

The two tandem pairs of angular contact ball bearings which hold the inner ring in the outer ring, and the outer ring in the mounting ring, were modelled using a spring element with a stiffness of 200×10^6 N/m in both the axial- and radial directions, and a stiffness of 3.30×10^6 N.m/rad against out-of-plane bending. The spring elements were connected to the rings using rigid elements (see Figure 68), which represent the bearing shafts. The spring elements which represent the angular contact ball bearings which hold outer ring in the mounting ring were constrained in all degrees of freedom, thus effectively assuming that the mounting ring is rigid. The outer ring was modelled using parabolic plate elements.

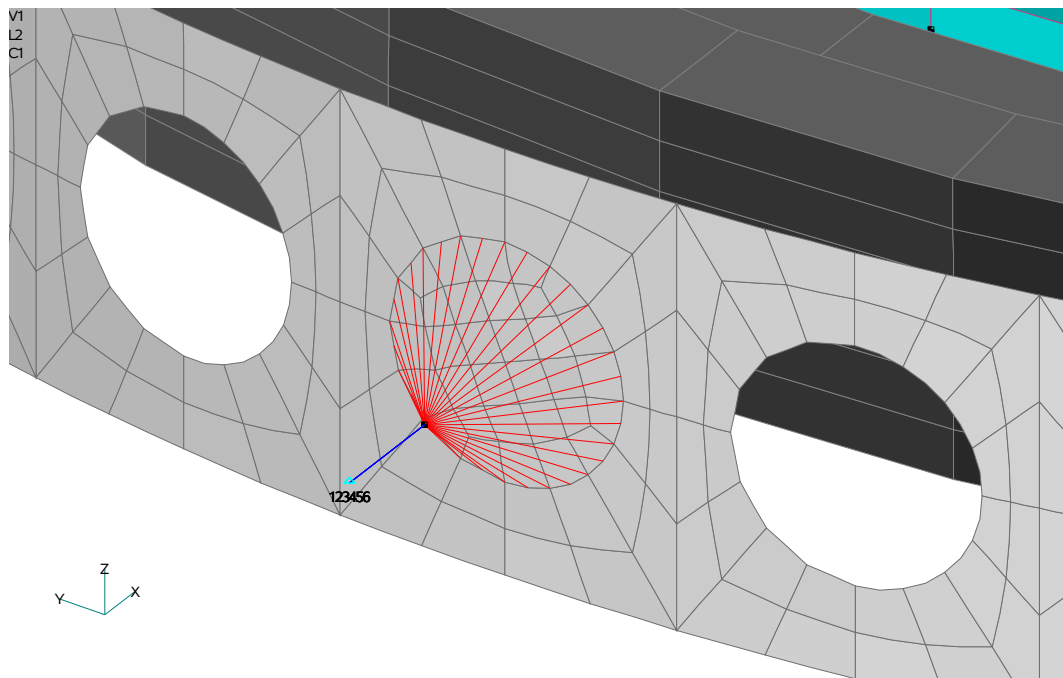


Figure 68: Detail of the implementation of the bearings in the finite element model for the WFMOS wobble plate.

Mass elements were added to represent the mass of non-structural elements, e.g. motors, etc.

All materials were assumed to be linear and isotropic.

The results of the normal modes analysis are given in Figure 69 to Figure 74. These figures show the mode shapes for the first six natural vibration modes, with frequency of up to 250 Hz. As the bearing assemblies which support the inner ring in the outer ring, and the outer ring in the mounting ring, have been assigned a zero stiffness about their respective rotation axes, the first two modes represent free-body modes, i.e. the rotation of the prisms about the tip- and tilt-axes. The natural frequencies up to 250 Hz are listed below:

first natural frequency:	31 Hz;
second:	48 Hz;
third:	53 Hz;
fourth:	79 Hz;
fifth:	91 Hz;
sixth:	225 Hz.

The figures show that the first five mode shapes appear to be dominated by motion of the Tip Sub-Assembly (consisting of the ADC Prism Sub-Assembly plus the Inner Ring Sub-Assembly) as a more or less rigid body inside the Outer Ring Sub-Assembly. Only for the sixth natural frequency, at 225 Hz, do the deformations of the Inner Ring appear to contribute significantly to the mode shape. This becomes particularly apparent when comparing the strain energy density distribution for e.g. the 1st and the 6th mode (see Figure 75): for the 1st vibration mode the Inner Ring appears to be virtually strain-free, whereas for the 6th mode significant strain levels are present. This suggests that the most effective way to increase the first natural frequency will be to increase the stiffness of the Outer Ring, e.g. by increasing its depth. This will obviously be at the expense of additional mass, and increased inertia about the tilt axis.

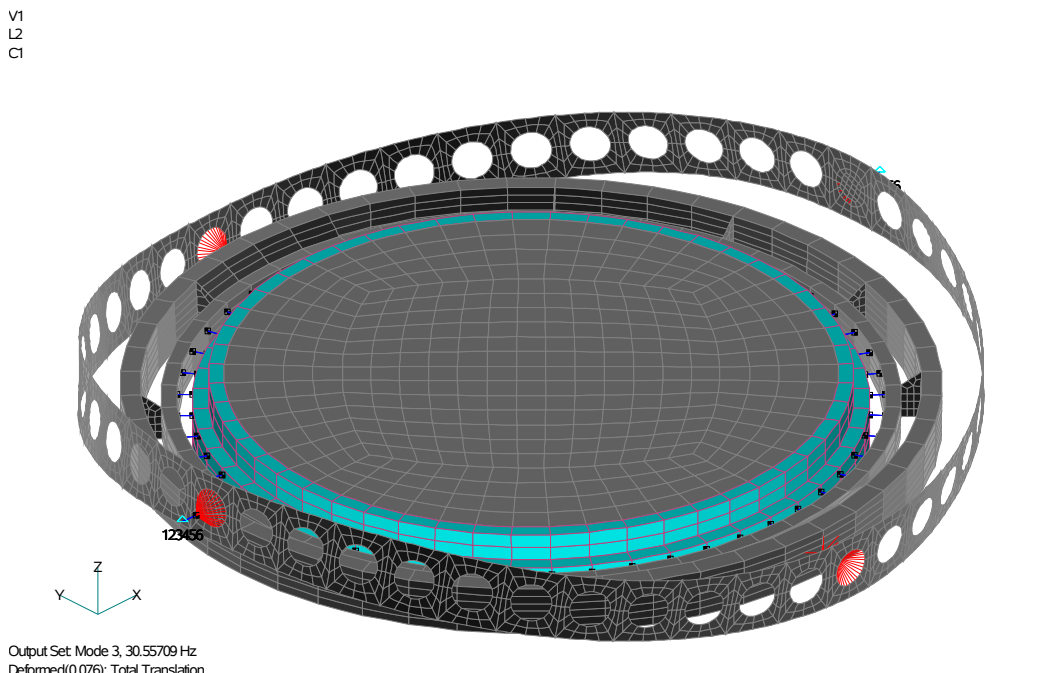
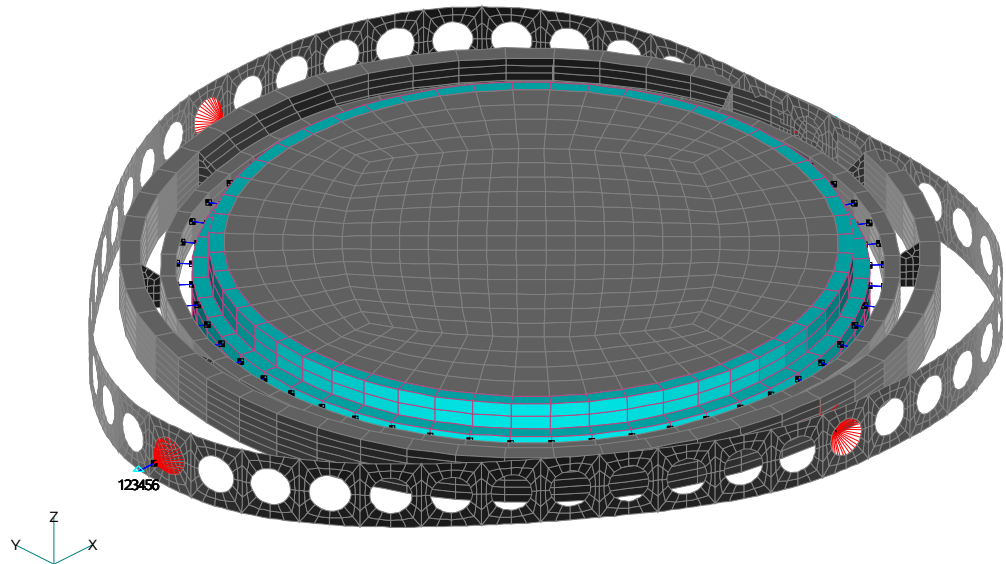


Figure 69: Mode shape for the first natural frequency (31 Hz) of the WF MOS wobble plate.

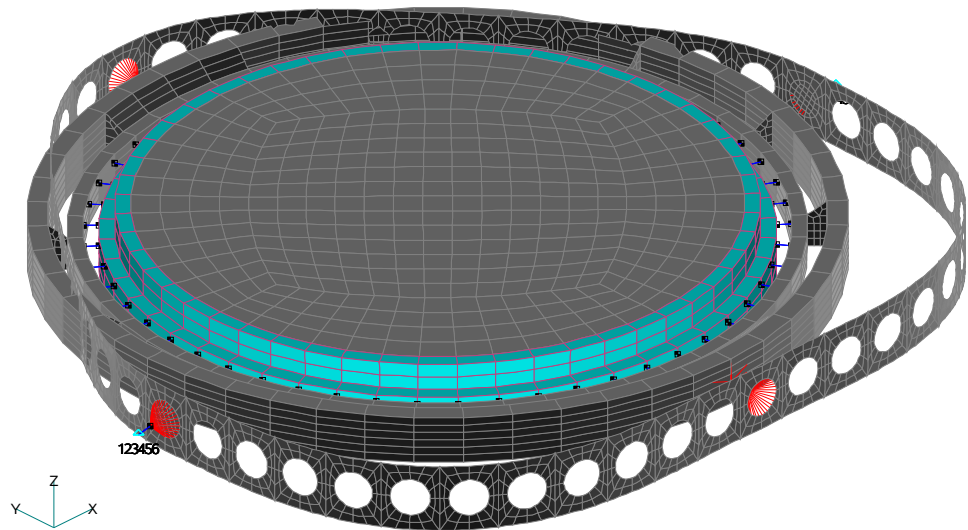
C
L
1



Output Set: Mode 4, 47.55095 Hz
Deformed(0.0812); Total Translation

Figure 70: Mode shape for the second natural frequency (48 Hz) of the WFMOS wobble plate.

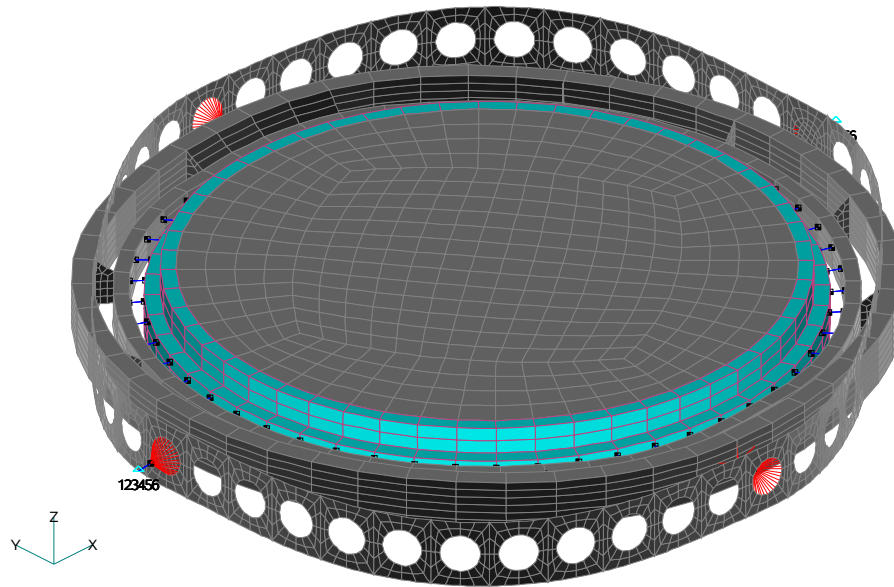
V1
C
L
2



Output Set: Mode 5, 53.41828 Hz
Deformed(0.0747); Total Translation

Figure 71: Mode shape for the third natural frequency (53 Hz) of the WFMOS wobble plate.

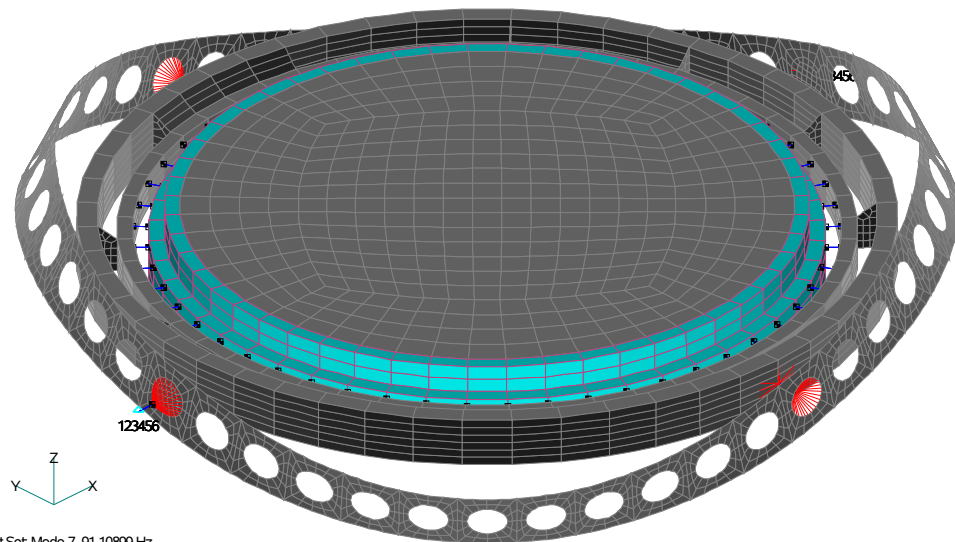
C1
L2
V1



Output Set: Mode 6, 79.21722 Hz
Deformed(0.113): Total Translation

Figure 72: Mode shape for the fourth natural frequency (79 Hz) of the WF MOS wobble plate.

C1
L2
V1



Output Set: Mode 7, 91.10899 Hz
Deformed(0.265): Total Translation

Figure 73: Mode shape for the fifth natural frequency (91 Hz) of the WF MOS wobble plate.

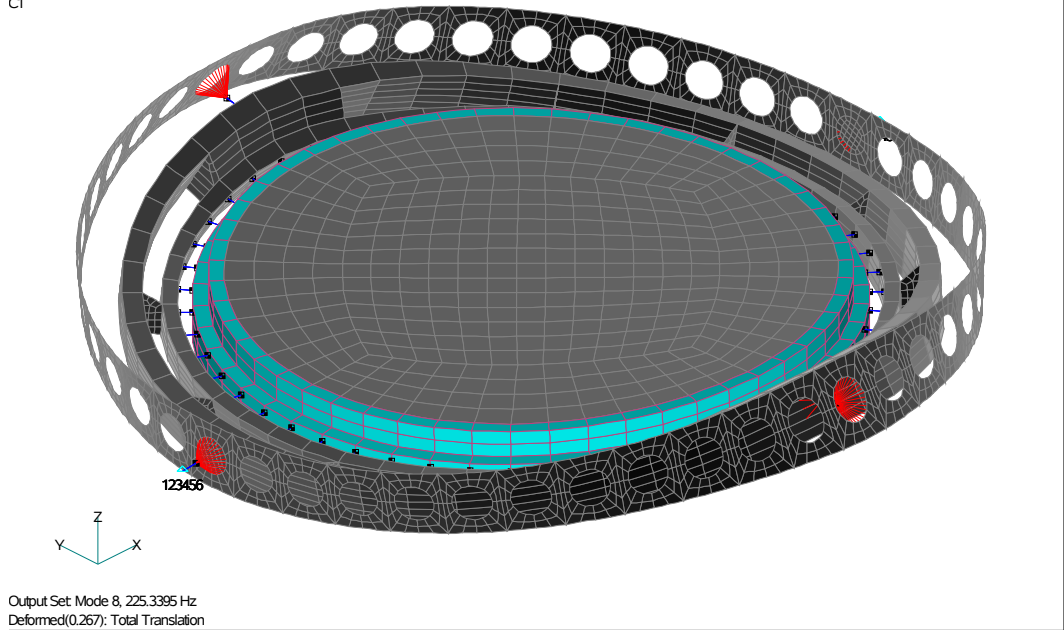


Figure 74: Mode shape for the sixth natural frequency (225 Hz) of the WFMOS wobble plate.

Limitations of the Model

For the purpose of the finite element analysis, some simplifying assumptions were made, which will be briefly reviewed below:

1. The adhesive used to cement the prisms together is assumed to be rigid thus providing a rigid connection between the prisms;
2. The prism elements are rigidly connected to the prism holder;
3. The ring gear was modelled as non structural mass elements (i.e. not adding to the stiffness of the assembly);
4. The bearing shafts were modelled using rigid elements;
5. The mounting ring, which provides the interface with the WFMOS instrument, is assumed to be rigid.

As was highlighted previously, the first five mode shapes are dominated by rigid-body motion of the Tip Sub-Assembly inside the Outer Ring Sub-Assembly, and strain levels in the Inner Ring and Prism Holder / ADC Prisms and very low. As a consequence, assumptions 1 to 3 are expected to have a marginal effect on the outcome of the analysis. Only for the sixth- and higher vibration modes, where significant strain levels appear inside these elements, would one expect a significant impact on the results.

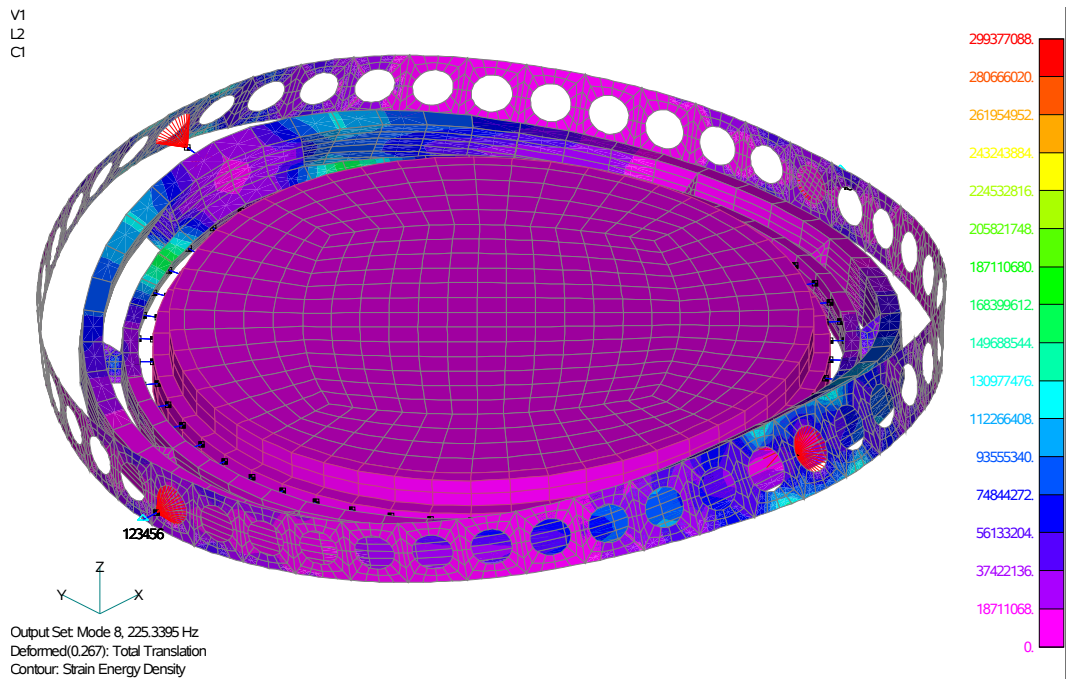
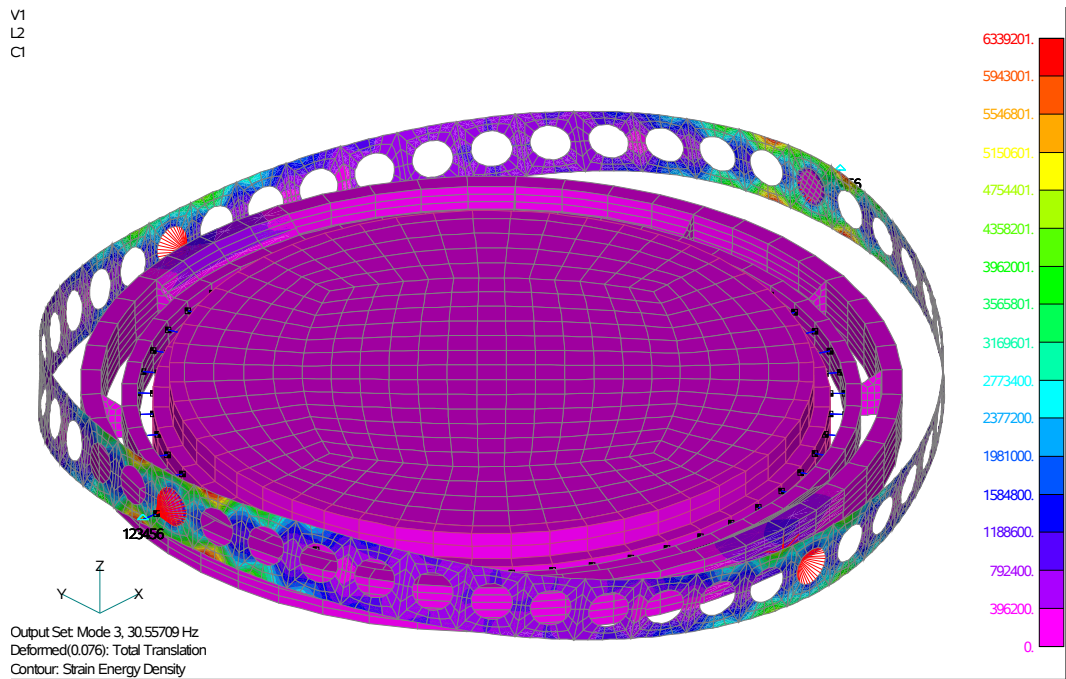


Figure 75: Strain energy intensity distribution for the first (top, 31 Hz) and sixth (bottom, 225 Hz) natural frequency of the WFMOS wobble plate. Note the virtual absence of strain from the Inner Ring for the first mode, compared to the high strain levels for the sixth mode.

Assumption 4 and 5 may have a more significant effect, as stress and strain levels around the bearing attachment points are high. The dominant contribution to the structural compliance, however, is the tandem pair of bearings, and any compliance in the mounting ring and bearing shafts will effectively act as some reduction in the bearing assembly's resistance to out-of-plane bending. Variation of the bearing stiffness by a factor of two only produces a change in the resulting vibration frequency of less than 1 Hz (the first natural frequency decreases from 30.6 Hz to 30.0 Hz when the bearing stiffness is reduced by a factor of two). The model consequently appears to be fairly insensitive to the precise value of the bearing stiffness.

During the next phase of the study, detailed analyses of the deformations and stresses under various gravity loads will be performed of such critical areas as e.g. the Prism Holder, Inner- and Outer Rings, bearing shafts, bearing shaft attachment points, etc.

9.3.5 Variations on a Theme

A number of variations on the corrector design were explored during the KAOS Conceptual Design Study. A number of these options will be briefly discussed in the following, as far as relevant for the wobble plate mechanical design and performance.

- The ADC is implemented as part of the powered optics, similar to the 2dF wide field corrector. This design would have similar dimensions to the baseline design presented in this report. It would not only reduce the total element count but would also significantly improve the image quality. A separate, independent wobble plate would be needed however, to act as an image stabiliser (see Figure 76).

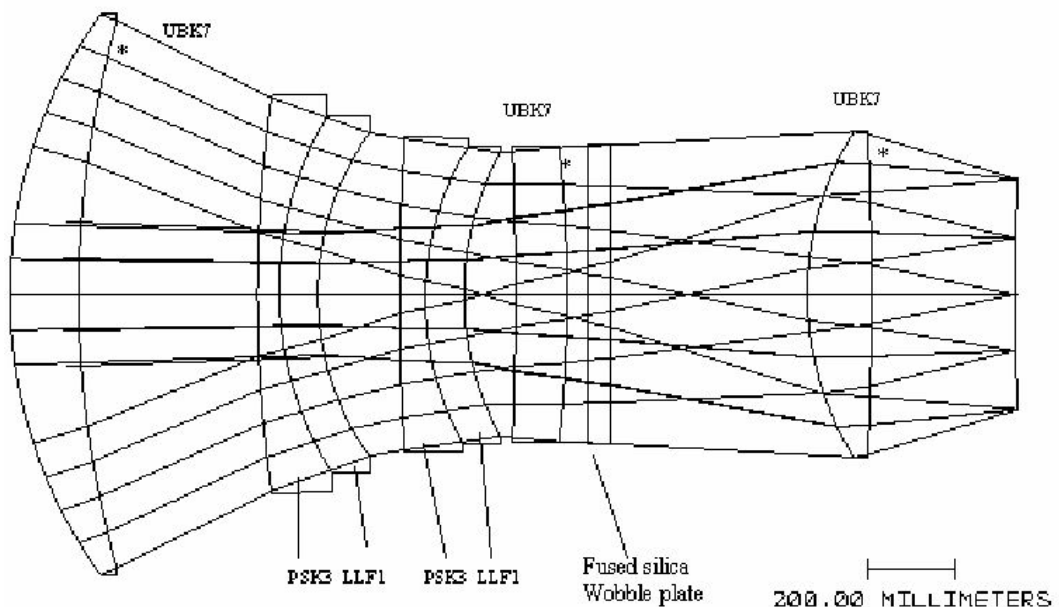


Figure 76: Zemax layout for the WFMOS corrector design using a lens-prism as the Atmospheric Dispersion Corrector. A separate wobble plate is incorporated to compensate for the windshake.

In addition to the obvious benefit of reduced number of optical components, and the resulting reduction in the mass of the instrument, the wobble plate design would also be simplified. As it will no longer be necessary to rotate the ADC prisms inside the inner ring, the wobble plate could be mounted directly inside this ring. This will reduce the mass and inertia of the wobble plate (reducing the force and power requirements of the actuators), but also allow for a stiffer construction, increasing the first natural resonance frequency.

- A further development based upon this concept would be to use the lens-prism (i.e. ADC element), which has very weak power, as the image

stabiliser. This would reduce even further the number of optical elements and allow for a very elegant design. The disadvantages of this design, however, are the possible high cost of materials and fabrication and their associated risks. In addition, the mechanical design advantages associated with the previous concept (i.e. reduced mass and increased stiffness of the wobble plate) would be lost.

- A third concept would be to actuate one ADC element in one direction (tip) and the second ADC element in the other (tilt). This means that would no longer be a need for an outer ring to facilitate rotation about a second axis, but the inner ring would attach directly to the mounting ring. This would reduce the mass and inertia of the wobbling elements (reducing the force and power requirements of the actuators). In addition, this would allow for a stiffer construction (as the deformations predominantly occur in the outer ring), increasing the resonance frequency. The only caveat is that the optical performance of this solution has not been investigated.
- Another option would be to mount both ADC elements inside the inner ring, and the entire tip sub-assembly inside a single outer ring, and wobble both ADC elements simultaneously. Whilst it may appear counter-intuitive, this would actually increase the natural frequencies of the design. Even though the mass supported by the outer ring would double, the outer ring's area moment of inertia (which is proportional to the depth of the ring) would increase 8-fold, assuming that the ring's depth is doubled. As the frequency is proportional to the square root of the area moment of inertia divided by the moving mass, the resonance frequency would actually double!

Furthermore, as a first approximation, the image displacement induced by wobbling both plates would be double the image displacement induced by wobbling a single plate, which means that the wobble plate amplitude requirement would be halved. As the required actuator force is proportional to the product of the amplitude and inertia (see Section 9.3.3) the force requirement would not change (as a first approximation), whereas the minimum required stroke and velocity (which are proportional to the amplitude) will be halved! This also implies that the reaction torques on the instrument, induced by the wobble plate, will not increase, thus not placing any additional demands on the reaction torque compensating mechanism.

Obviously, the bearing assemblies and bearing shafts will have to be re-sized to account for the increased mass.

- It may be possible to utilise the ADC elements for nod and shuffle observing, where the image is moved on and off the fibers on a timescale of about every 30 seconds, requiring image displacements of up to 10 or possibly 20 arcsec. In order to reduce the physical tilt angles, both ADC elements should be tilted simultaneously. This ideally lends itself to implementation of the previous concept, where both ADC elements reside in a single gimbal mechanism and are wobbled simultaneously. Assuming that the speed with which the beam switching is performed is not too critical (i.e. not much less than ~ 1 second) the only change required to effectively implement this observing mode would be an increase of the actuator stroke to some ± 25 to 50 mm. Whilst it should be possible to achieve this

requirement, it would require the customisation of an existing actuator design, which will have a significant impact on cost and delivery schedule.

- A final option would be to increase the instrument's field of view to 2 degrees. This would increase the required clear diameter of the ADC prisms to ~ 1.0 m, and double their mass, whilst significantly reducing their bending stiffness. It is expected that the total mass of the IS / ADC would also more than double, and as a consequence, achieving a sensible resonance frequency will become a significant challenge. In addition, the increasing top end mass will affect the telescope's stiffness, and deteriorate its resistance to wind buffeting thus increasing the demands on the image stabiliser performance. In balance, increasing the instrument's field of view to 2 degrees appears to be extremely ambitious and the associated risks appear to be prohibitive.

Choice of Materials

Aluminium has been selected as the baseline material for the main structural elements of the IS / ADC assembly. Fabricating these elements from a composite Carbon Graphite material, would enable us to either increase the stiffness (and thus the resonance frequencies) and / or reduce the structural mass of the IS / ADC. The total mass is a critical concern for a prime focus instrument such as WFMOS. A reduction in instrument mass would also help to reduce the telescope's susceptibility to windshake disturbances, thus reducing the performance requirements of the Image Stabiliser. An additional benefit of a composite structure would be the ability to fine tune the structural behaviour of the assembly through engineering analysis.

There are two considerable drawbacks to a composite structure that must be taken into consideration: 1) significantly higher cost than that of an aluminium structure, and 2) the sensitivity to temperature and humidity of the material. Assuming that the humidity sensitivity can be adequately controlled, it is anticipated that the cost of the composite structure will be more than offset by the advantage of its lower mass and higher stiffness compared to that of aluminium.

9.4 Wobble Plate Specification

The final specification for the wobble plate will be presented.

Requirement	Value (Gemini)	Comment
Correction range on sky	+/- 1.5 arcsec	Limited by delivered IQ
Optical clear aperture diameter	1000 mm	Assumes ADC element
Mechanical tilt angle range	+/- 0.5 deg	
Mechanical tilt angle resolution	1 arcmin (TBC)	0.05 arcsec on sky
Correction bandwidth	>15 Hz (TBC)	
Frequency response	>50Hz at -3dB	

9.5 Feasibility of Optical Elements

It should be noted that the wobble plate and ADC can be fully characterised and acceptance tested without the prisms in place; a dummy mass can be used during qualification. The prisms could then be mounted after delivery of the IS/ADC to the instrument prime contractor. This would minimise the risk of (accidental)

damage during shipping from the IS/ADC sub-contractor to the instrument prime contractor, etc.

The prisms require no unusual, special features and therefore the major risks associated with the procurement of the prisms are limited to the following:

- the size of the prisms (760 mm diameter), and
- the tolerances on the required wedge angle and flatness of the faces.

The size- and tolerance requirements may be beyond the (current) capabilities of industry. To mitigate these risks, potential suppliers should be involved in the design and specification of the ADC prisms from the earliest possible stage in the project. As the prisms are by no means the largest optical components in the corrector, the risks should be relatively benign compared to (some of) the other components. The finite element analysis demonstrates that the strain energy in the actual ADC prisms is very low; the risk of structural damage to the prisms as a result of wobble plate actuations is therefore considered to be negligible.

9.6 Cost and Feasibility of Mounting

The cost of the structural (i.e. mounting) hardware has been folded into the cost estimate for the Image Stabiliser and Atmospheric Dispersion Corrector (IS / ADC), as provided by Durham.

The IS/ADC has been designed with a view to facilitate integration with the other (optical) elements of the wide-field corrector. As the interfaces have not yet been frozen, a certain degree of flexibility has been maintained to facilitate adaptation of the design to the exact interface specification that may be defined during the detail design phase.

Although the size requirements may be beyond the capabilities of many suppliers, the mounting hardware does not require fabrication or integration to any particularly demanding tolerances, so the (technical) risks are considered minor. Any programmatic (i.e. schedule, cost) risks can be mitigated by identifying potential suppliers at an early stage in the project.

9.7 Cost and Feasibility of Control System

The basic servo analysis given at the start of this section indicates that the proposed design concepts for the wobble plate and actuators can be combined with an appropriately specified guide sensor in order to adequately suppress the measured image motion power spectra. The proposal is to couple the sensors and wobble plate actuators via the existing Gemini control system. This provides the required offloading of large, slow tip-tilt components to the Telescope Control System, as well as all the required control, status, diagnostic and logging functions. As the signals and required bandwidth are within the current specifications for the corresponding cassegrain systems, the servo controller implementation task is entirely one of electronic and software interfacing (dealt with in the next section).

The cost of the actuators and associated (development) risks can be minimised by using off-the-shelf hardware (i.e. standard linear voice coil actuators) where practical.

Should an escalation of the mass or inertia of the wobble plate necessitate the use of larger (non-standard) actuators, development risk can be minimised by means of the following:

- The selection of an off-the-shelf design, which would require only minor modifications will minimise technical and development risks.
- Selection of a competent sub-contractor, with a proven track record regarding the successful development of custom-built actuators to the required schedule and budget will minimise any programmatic risks.

A major concern relates to the power consumption of the actuators; the power dissipation could quite easily exceed several tens of Watts. No maximum power dissipation is currently specified and it is therefore impossible to assess whether this would be a potential issue. If this level of power consumption were unacceptable, a trade off between the maximum power consumption and system performance (particularly at high frequencies) may be necessary.

9.8 Cost and Feasibility of Electronics and Software

The electronics and software tasks of interfacing the control input and output signals to the existing Gemini controller are essentially without issues of risk or cost uncertainty. This is because the nature and bandwidth of the signals lies within existing specifications for cassegrain operation.

The cost of the electronics and associated (development) risks can be minimised by using off-the-shelf hardware (i.e. actuator drive electronics etc.) where practical. Any technical and programmatic risks can be minimised by employing the same mitigation strategy and controls as those employed to for the procurement of the actuators.

9.9 Final Cost and Risk Analysis

The major threats to the feasibility of the current concept are expected to occur during the (detail) design phase, and could arise through two conceivable mechanisms:

- The first eigenfrequency of the wobble plate needs to be increased to ensure adequate servo system performance. This may necessitate a (major) redesign of the mounting hardware and would almost certainly increase the subsystem mass.
- The wobble plate mass escalates (not necessarily as a result of the above), necessitating customisation of the off-the-shelf actuator.

These risks can be mitigated by:

- develop a robust and accurate model of the wobble plate servo mechanism in order to define the required first eigenfrequency, and

- dimension the actuators such that a “reasonable” increase of the wobble plate’s mass and inertia can be accommodated without necessitating a re-design of the servo mechanism. What should be called “reasonable” in this context will depend on the status of the detailed design (i.e. the accuracy of the mass estimate), and the margins applied (or acceptable).

An area which has thus far remained under-illuminated (and could therefore be considered a major to extreme risk) is the design of the counter-balance mechanism, which is required to eliminate the reaction forces and torques on the telescope top end induced by actuation of the wobble plate. The (conceptual) design of this mechanism should be kicked-off as soon as possible, with a view to minimise any possible impact on the corrector system design.

The servo analysis performed to date has been very basic and it is possible that a more elaborate model would give improved performance and/or immunity to changes in the eigenfrequencies. However it is not recommended that any optimistic assumptions in this respect are made at this stage.

Chapter 10 Top End Structure

10.1 Top End Structure – Subaru

10.1.1 Summary of Strawman specification

The top end of the Subaru telescope is designed to accommodate a suite of alternative secondary mirrors and several prime focus instruments. A fast exchange system allows top end components, stored in a room alongside the top end, to be securely and precisely fitted to and removed from a central hub in the telescope top end.



Figure 77. A central hub in the Subaru telescope top end allows fast exchange of top-end components.

The baseline approach for WFMOS is that the WFMOS top-end components should be similarly readily exchangeable, and that the exchange and mounting functionality for existing secondary mirrors and other top-end mounted instruments should not be significantly affected. A design goal is to minimise any modifications to the telescope to accommodate WFMOS. Mounting requirements for the proposed Hyper-SuprimeCam imager are likely to be similar to WFMOS, and a shared corrector component is envisioned, and so any top-end telescope modifications should be compatible with a Hyper-SuprimeCam or similar installation.

10.1.2 Design concepts

10.1.2.1 Existing top end

Figure 78 shows the central instrument mounting hub as it presently exists, supported by the Subaru top end spider vanes. Existing top end components mounting to the hub engage with the ‘castellations’ visible on the end face, and are clamped by actuators pressing against the inner, curved edge of the rim. Also visible in this figure is a flange on the interior of the hub, about halfway along its

length. This flange serves as a mounting point for panels carrying connectors for electrical cables. The dimensions of the central hub are shown in Figure 79.

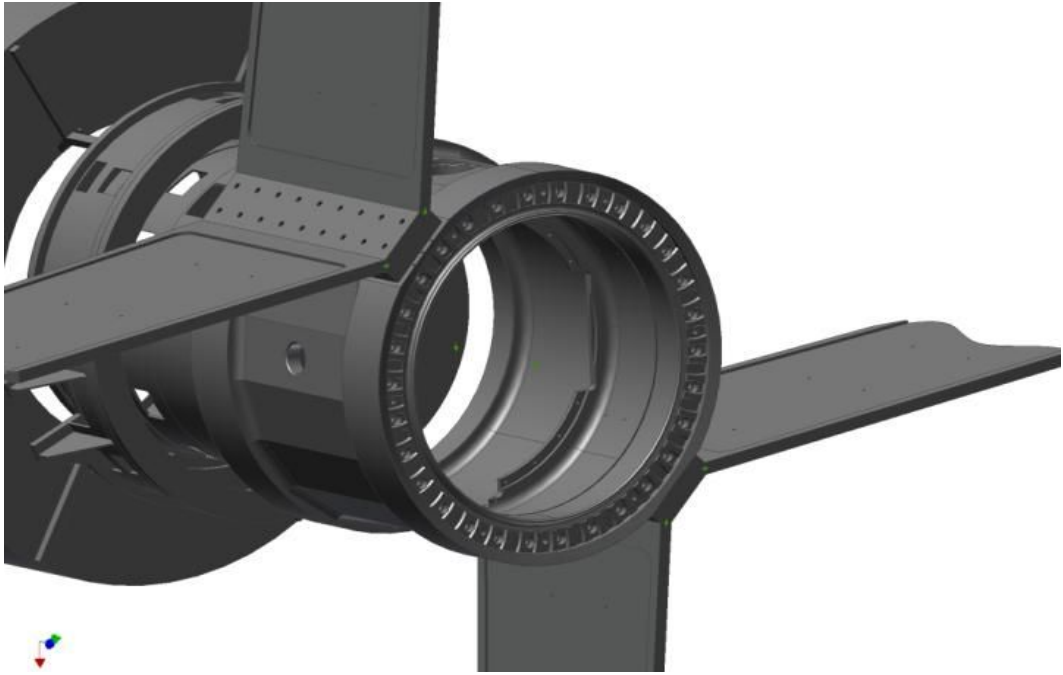


Figure 78. Existing Subaru top end central hub, stripped down to the main structure and still supported by the Subaru spider vanes. A flange to support cable connector panels is clearly visible on the inside of the hub, approximately halfway along its length. Castellations on the hub's end faces provide precise alignment of secured components.

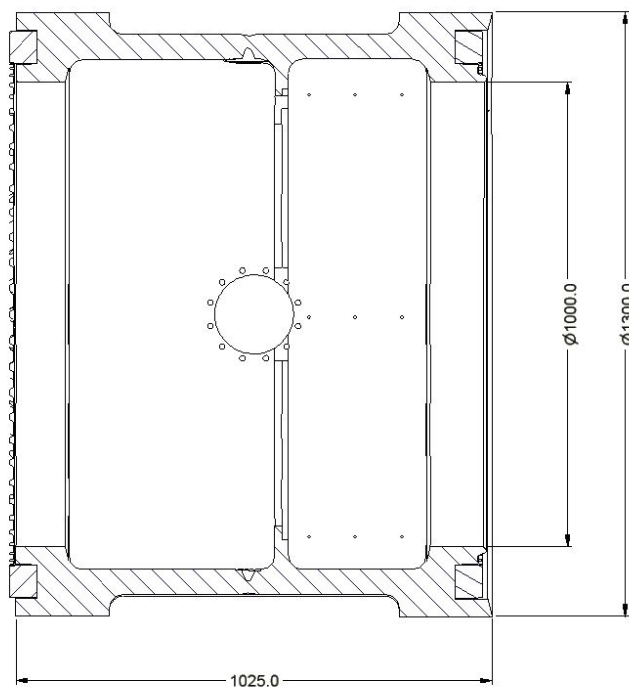


Figure 79. Dimensions of existing central hub (mm).

10.1.2.2.1 Allowing an Optimal Optical Design

Various optical designs have been considered for the wide field corrector critical to the successful implementation of WFMOS, and it has become clear that the central hub imposes very tight constraints on the optical design. To minimise vignetting losses, light paths must pass very close to the physical structure of the inside of the hub. Superimposing the corrector optics onto the hub, as in Figure 80, highlights the close fit and indicates a possible interference between the light path and the electrical cable connector support flange. Certainly, the connector panels secured to the flange will obstruct the light and interfere with corrector components. Discussions with Subaru suggest that there is no substantial impediment to relocating the connectors to the outside of the hub.

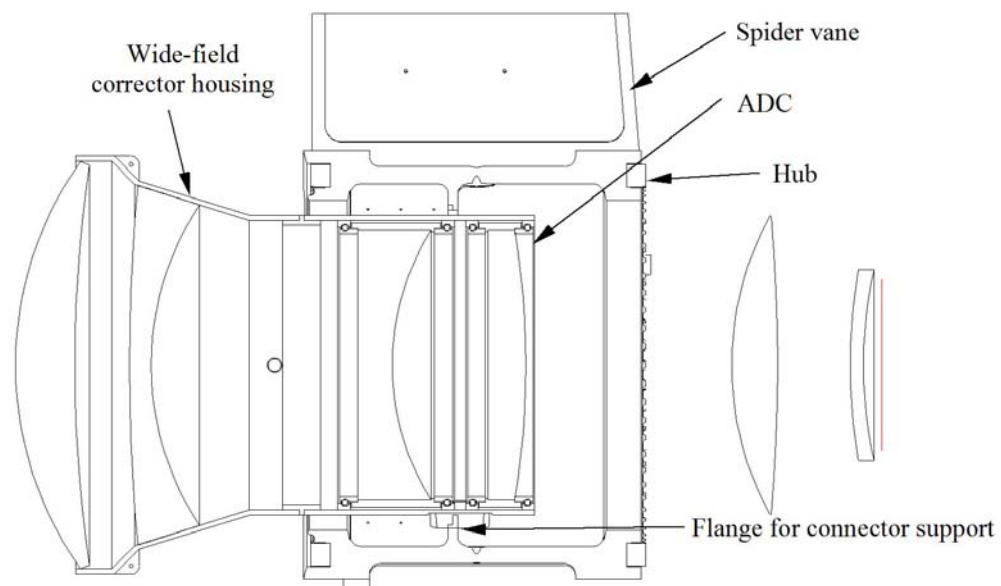


Figure 80. Central hub and corrector optics. Note the small mechanical clearances throughout, and possible interference with the flange near the middle of the hub. Note also the need to mount the corrector in two sub-units, from opposite sides of the hub.

Figure 80 also makes very clear the necessity of mounting the corrector in two sub-units, one from each side of the hub.

It should be noted that the corrector design depicted incurs a measure of vignetting towards the edges of the field. A larger corrector design raises manufacturing feasibility issues, and may be impossible to constrain to fit through the hub.

10.1.2.2.2 Mechanical Design

The tight mechanical clearances highlighted in Figure 80, especially in conjunction with the requirement to translate and tilt the corrector components, require removal of the connector support panels and the flange supporting them. Additionally, there is insufficient clearance to accommodate clamping actuators of the same design as used for existing top end components, which extend to press against the curved inside edge of the hub rim.

With regard to the above considerations, it is clear that some modifications are required to the central hub – to relocate the electrical cable connectors to the exterior of the hub, to remove the support flange from the inside of the hub, and to implement an additional clamping mechanism to secure the WMOS and Hyper-SuprimeCam components. Such a clamping mechanism must not interfere with the interface of present secondary mirrors or prime focus instruments.

The AAO has considered several design concepts for the instrument clamping mechanism, and Figure 81 shows a sample of these. This feasibility study does not extend to a detailed design of the securing mechanism, however the range of plausible options makes it quite clear that a solution can be found that can fulfil the functional requirements without needing excessive modification to the hub.

In all cases, the clamping interface comprises two parts. One part is bolted to the exterior of the hub in a way so as to avoid interference with the interface for existing components, and its mating part is on the removable WMOS (or Hyper-SuprimeCam) component. The castellations on the end faces of the hub can still be used with the WMOS components for precise location alignment.

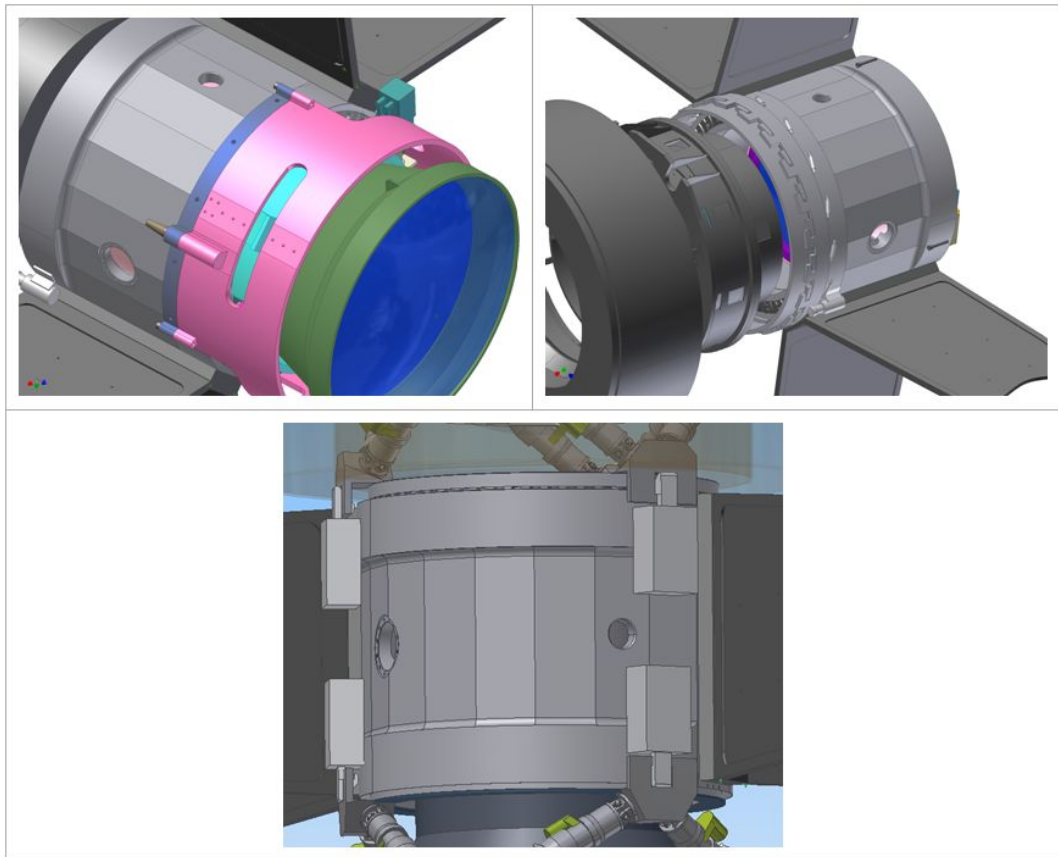


Figure 81. A selection of concepts for securing WMOS components to the central hub. All of these can provide precise location using the castellated interface on the end faces of the hub. All of them involve a component bolted to the outside of the hub.

10.1.2.2.3 *Electronics Design*

There are two aspects to the electrical/electronic impact of the proposed top end modifications. The first is simply the rewiring effort involved in relocating the existing cable connectors from the inside to the outside of the hub. The other is the switching and control electronics associated with the clamping mechanisms.

Regardless of the hub clamping mechanism selected to retain the instrument on the hub, there are likely to be a number of actuators and sensors required to drive the mechanisms and sense their positions. Further more, this is an operation that is carried out with close human interaction, rather than being under the control of a remote computer. Therefore it is highly likely that the hub clamping control system can be fully implemented using a suitable commercial off the shelf industrial controller (such as a PLC). Figure 82 provides a very generic diagram of such an electronics control system, showing a number of actuators and sensors connected to a controller that is operated via a push-button control panel. The controller would be connected to the telescope interlock system, to allow telescope movement when the instrument is clamped to the hub and to prevent the hub clamping system from operating when it is not safe to do so.

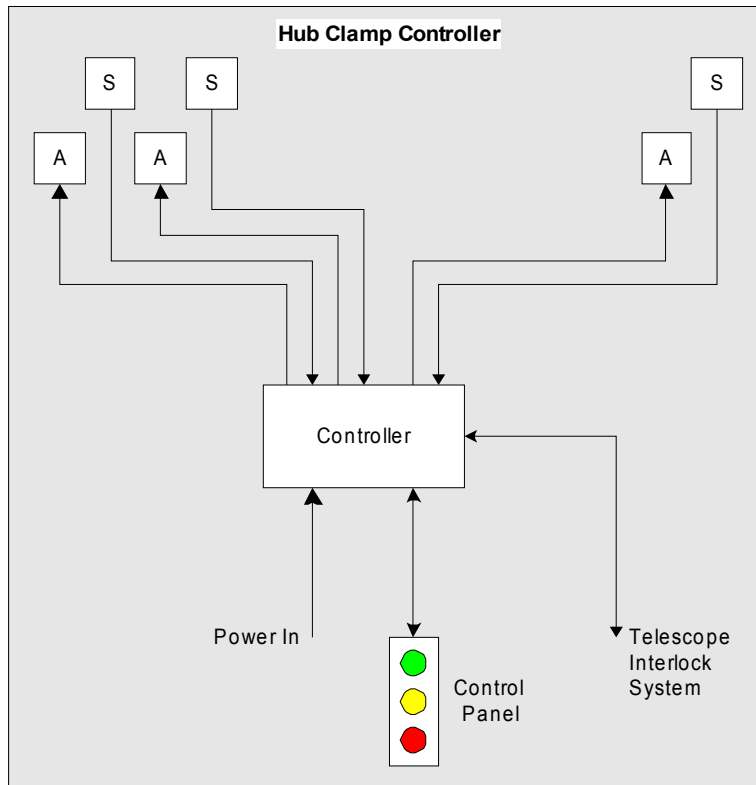


Figure 82: Hub Clamp Control

No aspect of the electronics design for the top end modifications is regarded as challenging.

10.1.2.2.4 Software Effort

A work package like the top end modifications does not involve very much software effort, being largely mechanical in nature. However, it is expected that there could be some related software effort required associated with interlocks, environmental monitoring, etc., as well as to provide engineering access to top end components and design acceptance tests.

10.1.3 Cost Trades

A primary cost trade that requires assessment for the Subaru top end modifications is the balance between modifying the existing hub and manufacturing a new one.

Removal, machining and refitting the existing hub will necessarily involve more telescope downtime than simply exchanging one hub for another. If the process cannot be achieved within a scheduled break in telescope operations then the cost of the additional downtime must be taken into consideration.

A further consideration is the requirement for assembly, integration and test of the WMOS top end components – the Prime Focus Unit and the wide field corrector. At the very least, a mechanical simulator for the hub interface will be required. If the implementation of the hub modifications is via construction of a new hub, then that hub can be used for subsystem integration, with a simple arrangement such as shown in Figure 83. Use of the ‘real’ hub for this purpose additionally reduces downstream risk of unanticipated incompatibilities.

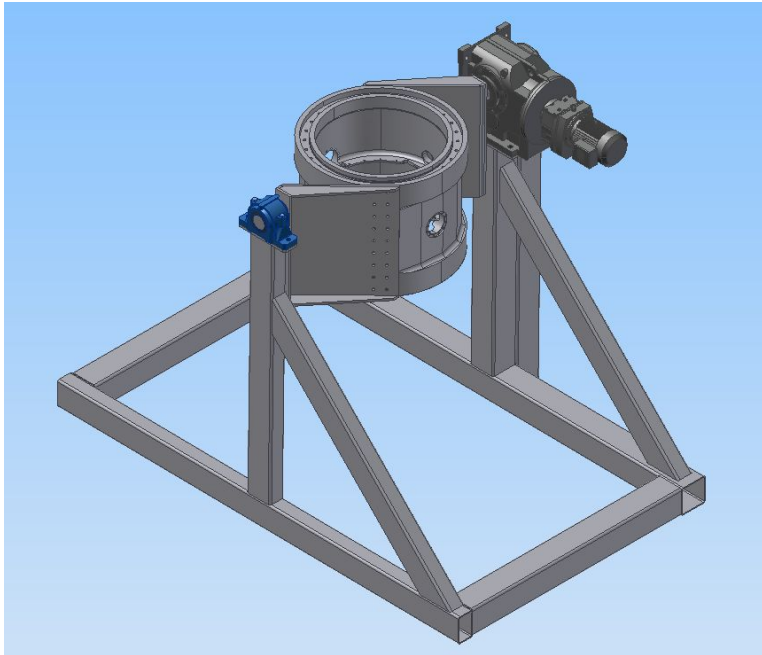


Figure 83. Assembly, test and integration jig. This allows the Prime Focus Unit and corrector to be assembled and tested with mounting hub and with each other. Its use argues in favour of manufacture of a new central hub for the telescope.

It is our assessment that the additional costs of manufacturing a replacement, near-identical hub rather than removing and modifying the present one are more than compensated by the benefits. Accordingly our cost estimates include the cost of manufacture of a new hub.

Note that this assessment is based on an assumption that the selected wide-field corrector design can be accommodated within the space envelope of the central hub. As discussed in Section 8.5, should the required space envelope for the corrector grow beyond this, a ‘step change’ in project cost is likely as replacement of the hub with a larger one has much greater implications for the telescope structure, extending to the spider vanes, the need for an interface adaptor for existing top end-mounted components, and possible impact on the designs of existing instruments (for example, cold stop designs will need to change if the pupil of the telescope is affected).

10.1.4 Cost Forecast

Input from Subaru is essential when considering modifications to the telescope as proposed in this section. In order to gain an understanding of the likely cost of the work, however, cost estimates for the top end modification work package are derived from a schedule built around the work breakdown structure. Components making these up were estimated by AAO staff and subject to internal review by the AAO WFMOS team.

Components considered included design, component manufacture (including a new hub), electronics, integration, labour and software.

10.2 Top End Structure – Gemini

This section discusses two approaches for implementing a new telescope top end to carry the WFMOS system components, should a non-baseline option of a Gemini installation be selected.

10.2.1 Summary

The original Gemini telescope concept included the ability to change top ends, particularly with a wide-field secondary. Although only one top end currently exists for each Gemini telescope, the as-built design of the telescopes includes this ability for relatively easy exchange of top end assemblies. In principle, the top end can be quickly and easily disengaged and installed with excellent mechanical alignment to within 100 microns.

The WFMOS-Gemini implementation will take advantage of this design feature and will utilize that interface for both the mechanical structure of the top end and for the location of a fiber cable interconnect.

The total mass of the top end is a critical concern for the WFMOS-Gemini implementation given the significant mass of the complete prime focus unit. Purple Book estimates of the entire mass to be suspended from the top end spider vanes were approximately 3,900 kg, including the wide-field corrector, the Echidna positioner, the wobble plate and its drive system, the rotator, and the mounting assembly. Feasibility study investigations into these subcomponents appear to be applying some upward pressure on that mass estimate, although it is still of the same order of magnitude. For the purposes of this section, the Purple Book mass estimates will be used.

If the top end ring and other structures are made from steel, the total mass of the complete assembly is estimated to be 10,100 kg or about 1.6 times that of the currently existing f/16 top end assembly. In order to balance the telescope for this assembly, an additional mass totaling of between 12,800 and 18,600 kg would be needed behind the primary mirror (depending on the location of its centre-of-gravity) over and above the currently existing mass of the ISS and mounted instruments.

If, on the other hand, the top end ring were to be made from a composite carbon fiber material, the mass of that component could be under 1,000 kg, reducing the

total mass of the complete assembly to less than that of the present f/16 top end assembly and eliminating additional counterbalance requirements.

10.2.2 Design Concepts

10.2.2.1 Steel Top End

The principal advantage of a steel top end is its low cost. A preliminary quote of USD 100,000 was obtained from one vendor for fabrication of the top end structure depicted in Figure 84, excluding the spider vanes and the prime focus mounting assembly. This price is essentially the same whether the ring itself is made from round tubing as shown, or from a rectangular box beam of roughly equivalent cross-sectional area. Preliminary FEA shows that the box-beam alternative has somewhat greater stiffness in the hoop, or radial, mode and so may be preferable. The total mass of the ring is estimated to be about 5,200 kg in either case.

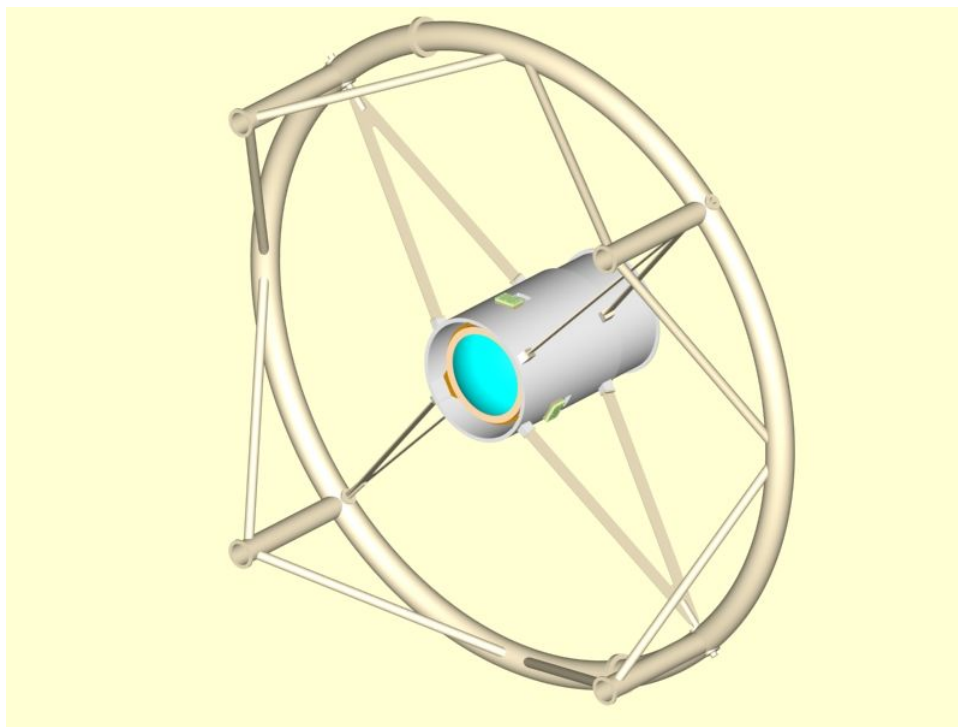


Figure 84. Solid model rendering of the WFMOs-Gemini top end structure, designed for fabrication in steel.

The principal disadvantage to steel is of course its weight. As noted above, the total mass added to the top end of the Gemini telescope is estimated to be about 10,100 kg, broken down as shown in Table 15.

Table 15. Mass budget of steel top end for Gemini-WFMOs

Assembly	Component Mass (kg)
Steel ring	5,200
Corrector + Echidna + mechanisms	3,900
Fiber Cable	730
Spider vanes	300
Total	10,130

The current f/16 top end has a total mass of 6,257 kg. Given the long moment arm from the elevation axis to the top end, the additional mass of the steel WF MOS top end will require adding 12,700 to 18,600 kg to the bottom end of the Gemini telescope as additional counterbalancing, over and above the present mass of the ISS and Cassegrain instruments (depending on the selected location for this additional mass). WF MOS with a steel top end would therefore increase the total telescope mass by about $(10,130 - 6,257) + 18,600 = 22,473$ kg. The significant increases in both top end and total telescope masses present issues relating to telescope performance, infrastructure adequacy, and operational practice.

10.2.2.1.1 Telescope Performance

Clearly the increases in top end and total mass will change the way the telescope structure responds to gradually varying loads such as changes in elevation angle and to impulse loads such as wind gusts. To help understand these changes, Gemini commissioned Quartus Engineering to perform an FEA of the telescope structure with the additional weight. Their report forms an attachment to the feasibility study documentation.

The analysis undertaken by Quartus shows the telescope structure retains acceptable performance when loaded with the additional top end and counterbalance mass.

10.2.2.1.2 Infrastructure Adequacy

Adding significant extra weight to the telescope raises a number of questions about whether various other observatory systems have adequate margins to work with the additional weight. Many different systems may be affected, from those that directly support and move the telescope to those that are needed during instrument and top end changes. In all these cases, the Gemini Observatory itself is the only entity with the expertise and institutional knowledge to thoroughly answer these questions; indeed, Gemini may be the only corporate body able even to identify all the questions. The following paragraphs attempt only to illustrate the types of issues that need to be addressed, but are not meant to be definitive. Resources, including access to knowledgeable Gemini staff, were simply not adequate to identify or address all relevant issues during this feasibility study. Clearly, further investigation will be needed during a conceptual design phase.

There are concerns about the capacity of the Hydrostatic Bearing System (HBS) which “floats” the telescope allowing it to move smoothly. How much will the pressure increase on each of the Azimuth and Elevation HBS pads due to the increased telescope weight? How much pressure can the HBS pumps supply? If the pumps can supply the extra pressure, will this have any effect on the pumps’ MTBF or overall lifetime? Can the hoses and plumbing carry the extra pressure, and how will their MTBF’s and lifetimes be affected? Will the extra work required from the pumps cause them to vibrate more, and if so will that vibration be “felt” or “seen” by the telescope and instruments?

Although the telescope will still be in balance, the telescope’s moments of inertia will increase substantially, increasing the work required to accelerate and decelerate the telescope during movements. There are concerns about the capacity of the telescope drive and brake systems to provide this additional acceleration and deceleration. How much will the Azimuth and Elevation moments of inertia

change with the extra weight on the telescope tube? How much torque will be required in each dimension to maintain current (or acceptable) accelerations and decelerations during slewing? Will the torque requirements in tracking mode change, and if so how much? Can the existing drive and brake systems supply sufficient torques to handle the extra weight? What will be the effects on their MTBF's and lifetimes? Will the extra loads increase drive or brake vibrations during operation?

10.2.2.2 Composite Top End

Identifying the extreme counterweight requirements implied by WMFOS components fitted to a new Gemini top end constructed from steel, the KAOS Purple Book noted the possibility of a much lighter top end constructed from composite materials. As part of this feasibility study, a company specializing in the design and manufacture of carbon-composite structures was contracted to undertake a concept design, analysis and costing of such a lightweight top end.

The detailed report from Quickstep Technologies Pty. Ltd. is attached as an appendix to this feasibility study. Their report concludes that a carbon fiber reinforced plastic top end structure as shown in Figure 85 can readily meet the stiffness and other requirements of a WMFOS top end structure, with a mass estimated at 940 kg and at a cost near USD 500,000. Design optimization of the structure and selection of higher modulus material is likely to further reduce weight while maintaining the required stiffness.

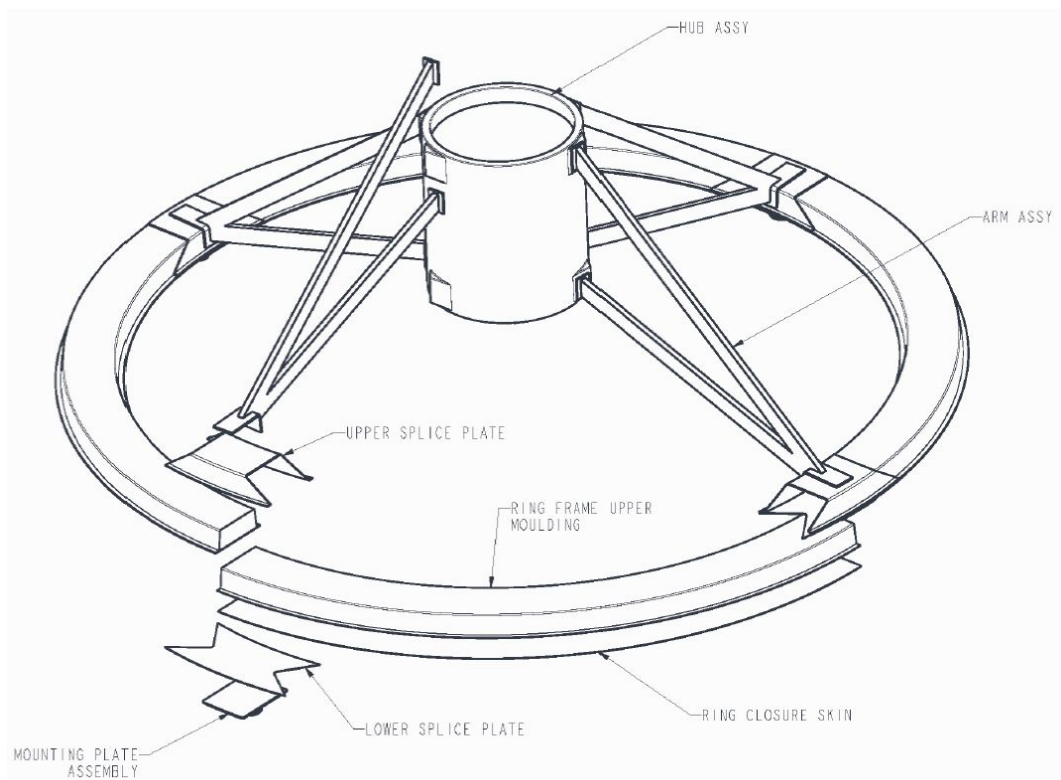


Figure 85. Carbon-fiber composite top end for Gemini-WFMOS, as proposed by Quickstep Technologies Pty. Ltd.

10.2.2.2.1 Telescope Performance

The mass of this conceived top end structure is approximately 4,260 kg lower than that of the steel one. Applying the same overheads in the instrument mass budget (Table 15) as the steel top end, we arrive at a total WF MOS top end mass of 5870 kg when implemented with a composite top end structure. Note that this is 387 kg less than the mass of the existing f/16 top end, eliminating the need for additional counterbalance weights and increasing the allowance of the mass budget of the top end-mounted components of WF MOS.

The aerodynamically ‘cleaner’ structure is unlikely to transmit greater wind loads to the telescope structure than the existing top end with secondary mirror, although modeling should confirm this in a later design phase should the option of a new composite top end be pursued for the Gemini telescope.

Possible concerns regarding the general application of fiber-based composites to telescope structure, such as humidity, temperature and other environmental considerations, are addressed in Quickstep’s report.

A Gemini implementation of WF MOS involving a composite top end similar to the one proposed here is therefore unlikely to adversely affect telescope performance.

10.2.2.2.2 Infrastructure Adequacy

The proposed composite top end design is of sufficiently different shape from the existing top end that it is likely that a custom handling cart will be required for top end exchange. This, and other infrastructure issues, are discussed in *Chapter 22, Telescope Infrastructure Upgrade*.

10.2.3 Operational Practices

The basic steps for changing top ends are fairly straightforward and are laid out in Table 16. Of course, most of the details are still to be worked out, most significantly including the number and type of personnel needed for each step.

Table 16. WF MOS top end exchange.

WF MOS Top End Change Steps
1. Move telescope to horizon and engage locking pins.
2. Disconnect services
3. Position top end storage cart to telescope.
4. Release motorized top end latches
5. Lower f/16 top end to basement, place on storage fixture.
6. Remove WF MOS top end from storage fixture and raise to telescope level.
7. Latch top end to telescope.
8. Connect services.
9. Connect fibers.
10. Install counterbalance.
11. Telescope is ready.

There are, however, no significant issues affecting the feasibility of the process, so any assessment of the operational burdens can be addressed during a later design phase.

One issue that has not been addressed is the placement and method of attachment for many tonnes of bottom-end counterweights required in the case of steel top end structure. To supply 18,600 kg of mass would require about 1.65 cubic meters of solid lead. It is not clear whether the existing ISS could carry that much extra mass, or whether there is sufficient room to attach that much volume. In the worst case it may be necessary to remove the Cassegrain instruments and the ISS and install a special counterbalance truss to carry the total mass needed. This would of course significantly increase the time, effort and care required to safely convert the Gemini telescope between f/16 + Cassegrain and WFMOS configurations. Even if the Cassegrain instruments and ISS can remain in place, adding the additional mass will require a great deal of labor and (probably) operation of the dome crane. Clearly, these issues can best be resolved by the instrument team and Gemini staff cooperating closely during the conceptual and preliminary design phases. The close involvement of the observatory staff is absolutely essential to ensure that the observatory infrastructure is protected and the operational considerations are safely addressed.

Issues regarding top end exchange, handling and storage are discussed in *Chapter 22, Telescope Infrastructure Upgrade*, on observatory infrastructure requirements.

10.2.4 Cost Trades

A primary cost trade that requires assessment for a Gemini top end is that of steel vs. composite structure. Although it is difficult to quantify, the cost of a >> 10 tonne counterweight and related handling equipment must run to a substantial figure. Especially if upgrades are also required to telescope bearings or drive systems, additional cost could be expected to exceed the USD 400,000 price difference between the basic structures.

10.2.5 Cost Forecast

Clearly, the cost of implementation of a major observatory system such as a new telescope top end is much more than simply the cost of fabrication of the bare structure.

For our costing estimates for the two top end options, in addition to the fabrication costs of the main structure, we have included consideration for design work, rerouting and connectorising existing cabling, integration, labour and other materials (e.g. cable ducting and services). Due to the large size and specialized requirements, we have also made allocation for logistics and transportation to the observatory.

Input from Gemini is essential when considering new major telescope components as proposed in this section. In order to gain an understanding of the likely cost of the work, however, cost estimates for the Gemini top end work package are derived from a schedule built around the work breakdown structure. Components making these up were obtained from the NOAO/steel fabrication contractor, the Quickstep composite design and fabrication contractors, and others estimated by AAO staff and subject to internal review by the AAO WFMOS team.

Chapter 11 Positioner

11.1 Introduction

In order to satisfy the science case for Gemini WFMOS, the fiber positioner must accurately and quickly position four thousand or more fibers in a focal surface over 500 mm in diameter. Until very recently, such a capability would have been quite inconceivable. Well known positioning robots like 2dF on the AAT or its evolutionary successor, OzPoz on the VLT, can accommodate focal surfaces of similar dimensions to WFMOS, but are limited to a few hundreds of fibers, and have long configuration times proportional to the number of fibers.

The AAO's revolutionary Echidna technology developed for FMOS on Subaru, in which the fibers are mounted on tilting spines, overcomes many of the traditional constraints of positioning robots (see Gillingham et al. 2003 Proc. SPIE 4841:985). It is this development that makes WFMOS possible as envisioned in the Purple Book. Growing out of the AAO's recognized expertise in fiber positioning, the technology enables high density of fibers, enhanced reliability due to the high level of redundancy, and fast configuration time (~couple of minutes) independent of the number of fibers.

Certain differences between the Subaru-FMOS application and WFMOS require further refinement of the Echidna technology. As part of the planning for this WFMOS Feasibility Study and from the development of the 'Ukidna' proposal for a 2250-fiber Echidna unit to enable the RAVE survey on the AAO's 1.2m UK Schmidt telescope that has similar design issues, the fiber positioner strawman design was already developed somewhat beyond the description in the Purple Book. This Feasibility Study has continued this refinement process, taking further advantage of other developments arising from the MOMFOS study for a fiber positioner for the GSMT 30 meter telescope, notably the use of a compact and fast imaging system for position encoding of the fibers (STRIP camera).

The proposed WFMOS positioner configuration is very similar to that of FMOS-Echidna. Certain application differences, including the curvature of the focal surface and the increased size of the focal surface have necessitated design changes. Full advantage has been taken of AAO's experience in the design and construction of FMOS-Echidna in order to refine design details to improve reliability and reduce cost. A change in the application of tolerances based on the FMOS experience has substantial impact on the assembly process and related costs.

The new developments allow implementation of a fiber positioner able to accommodate a flat or curved focal surface, concentric or non-concentric, with diameter in excess of half a meter, with a mean fiber pitch near 7mm, where each fiber can be arbitrarily positioned within 7mm of its nominal home position.

The fiber positioner for the WFMOS project is to be based on the AAO's Echidna design for FMOS on Subaru. This is a particularly elegant solution to the otherwise nearly intractable problem of precisely positioning thousands of fibers in a compact focal surface in a short time. It is the Echidna technology that makes WFMOS a feasible instrument concept.

At the top of the Subaru telescope, the baseline instrument configuration includes a ‘Prime Focus Unit’ (PFU), comprising the Echidna positioner, its support structure, rotator and cable/fiber wrap. This is clamped to the upper side of the telescope top end central hub via a pointing mechanism able to maintain the positioner’s alignment with the telescope’s optical axis while it shifts due to gravitational distortion during tracking. The PFU also accommodates the positioner control electronics, acquisition and guide systems and wavefront sensing systems required to maintain the form of the Subaru primary.

This chapter of the WFMOS feasibility study report discusses the elements mentioned above.

11.2 *Summary of Strawman specification*

At this feasibility study stage, many elements of the design of the WFMOS facility have not been finally determined. Design decisions and parameters of one subsystem have a ripple-on effect throughout the WFMOS system, and accordingly the detailed requirements for any one subsystem are not finalised. Required specifications for the fiber positioner are particularly subject to variation with target telescope choice and corrector design.

However, it is possible to establish representative requirements, and so the baseline positioner discussed in this study adopts some nominal specifications outlined in Table 17 below.

Table 17: Provisional requirements for Echidna fiber positioner for WFMOS baseline.

Number of fibers	4500
Fiber size	~1 arcsecond on sky, equates to 100µm core
Positioning accuracy	10% of fiber core diameter (nominally 100µm core, so 10µm positioning accuracy)
Focus accuracy	For 10% light loss due to defocus
Maximum spine tilt	For 10% light loss due to excessive cone angle
Reconfiguration time	< 10 minutes
Field rotation	+/- 110 degrees
Corrected field diameter (physical)	520 mm
Corrected field diameter (angular)	1.5 degrees
Focal surface radius of curvature	5 metres
Required fiber acceptance speed	f/1.9
Space envelope for positioner	Maximum height of 1.6m above upper rim of Subaru mounting hub, and remain within a radius of 1m of the optical axis (same constraints as the FMOS positioner).
Maximum mass for positioner, its support and pointing mechanism	2000 kg (this has not been provided as a hard limit, but an estimate from Subaru as to a mass that can be accommodated)
Required focus adjustment range	20 mm
Required focus tolerance	0.2 mm
Required decentre adjustment range	10 mm
Required decentre adjustment tolerance	0.1 mm
Required pointing adjustment range	0.1 degrees
Required pointing adjustment tolerance	0.002 degrees

11.3 Positioner Strawman design

The heart of the WF MOS facility is an Echidna-style fiber positioner. Echidna was developed for the FMOS instrument, also destined for the Subaru telescope (Figure 86). The Echidna positioner consists of an array of long spines (160 mm in the case of FMOS), with the optical fibers carried through to their tips, pivoted from mounts near their bases by very compact piezo electric actuators. This array is located such that the tips of all the spines lie in the focal surface of the telescope. It is then possible to simultaneously move all of the spines to position their ends anywhere within their own ‘patrol zone’. In this way, all objects in the field are accessible by one or more fibers.

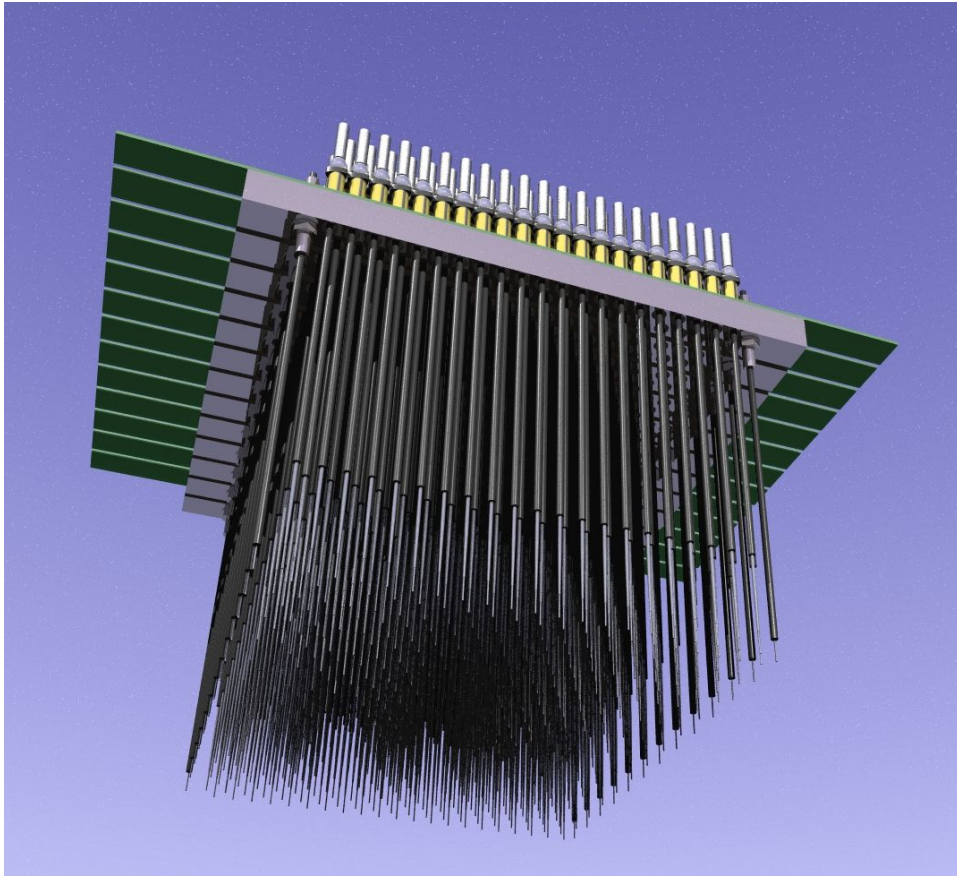


Figure 86: The FMOS-Echidna fiber positioner consists of a dense array of some 400 spines mounted on ball-pivots in piezoelectric actuators. Identical linear modules, each carrying a double row of actuators, make up the square array. Fibers are carried through to the tips of the spines to reach the telescope focal surface. The actuators can be operated simultaneously to position all fibers to 10 μ m accuracy.

For assembly and maintenance purposes, the spine actuators are mounted in long modules spanning the field. The AAO has undertaken a design to accommodate the strawman WF MOS positioner requirements through incremental development of the FMOS positioner. This will require approximately 42 or 44 modules each capable of carrying 140 spines (Figure 87). Modules are identical, giving a square array when assembled, although for WF MOS only the spine positions falling within the corrected field of view will be populated. The scale of the WF MOS focal surface is such that the required number of spines (~4500) is achieved with a similar spine density to that of the FMOS positioner – the focal surface and hence array size simply grows larger as shown in Figure 88.

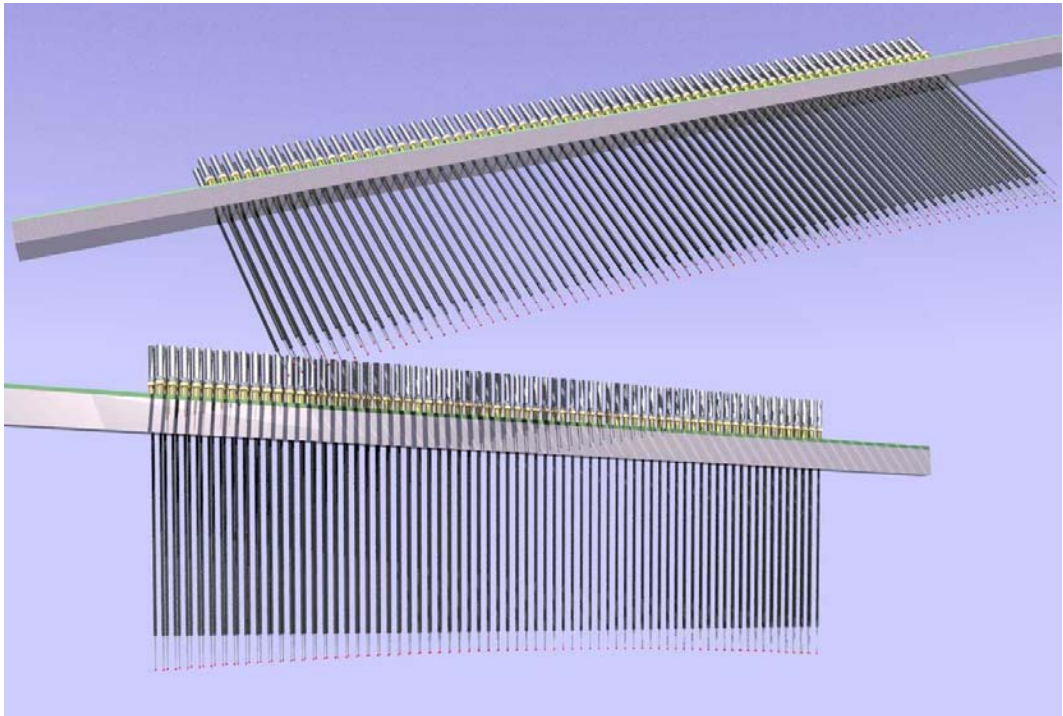


Figure 87: Early concept for the WF MOS spine modules. Each module carries 140 spines in two rows.

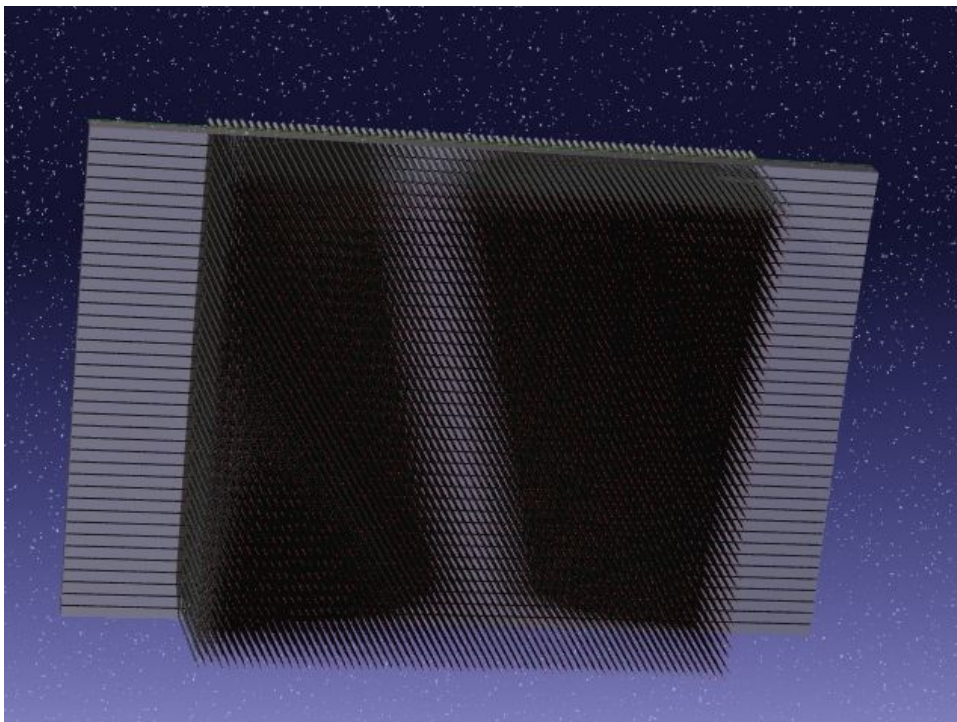


Figure 88: WF MOS-Echidna spine array, as viewed from below.

Control electronics for the positioner will be mounted in racks around the positioner, where a fiber-reinforced plastic cover protects the positioner and its aluminium support structure. This support structure forms the PFU and additionally houses the instrument rotator, A&G and wavefront sensing systems.

Owing to the design restrictions imposed by use of the existing Subaru top end central hub design, all optical elements of the baseline wide field corrector design

cannot be fitted to the telescope from just one side of the central hub – accordingly, the PFU housing the positioner is also required to carry the final two elements of the corrector. This design feature accords well with the proposed corrector concept of sharing the expensive corrector optics with the Hyper-SuPrimeCam imager, where the intent is to use different final corrector elements for the two instruments, to optimise the imaging parameters for each application.

Instrument pointing and focus control is by the use of a hexapod which secures to the Subaru top end central hub – space constraints in this area preclude the use of the standard Subaru instrument securing mechanisms, and so a new instrument clamp is required here.

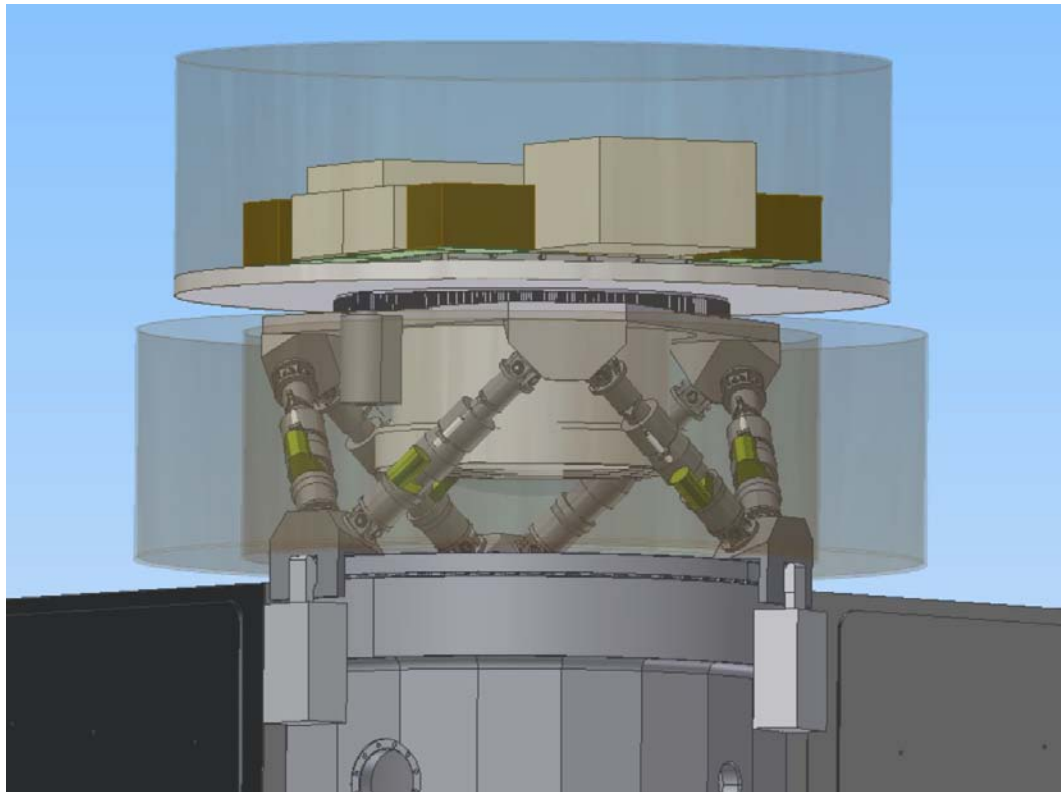


Figure 89. WF MOS positioner assembly mounted on the top end of the Subaru telescope. The Echidna ‘core’ of the positioner is mounted alongside its control electronics on a circular instrument mounting plate. The instrument rotator bearing is immediately below this, itself supported on a plate attached to the upper end of a hexapod providing pointing and focus adjustment for the instrument. The final two optical elements of the wide field corrector are also carried on this unit, surrounded by the hexapod actuators. An annular tray surrounding the hexapod carries the fiber/cable wrap (shown here as semi-transparent).

11.3.1 Positioner configuration

The KAOS Purple Book described an Echidna positioner for Gemini, however further work has resulted in numerous refinements to that concept. We now envision a design able to accommodate a curved focal surface, and have incorporated incremental refinements to the FMOS-Echidna positioner components and construction process.

Some basic parameters of the selected design are shown in Table 18 below.

single set of images – see Figure 90. The FPI subsystem is thereby enormously simplified compared with FMOS.

Similar to the scheme proposed for the MOMFOS fiber positioner for the GSMT 30-metre telescope, a camera with a suitably long lens, placed nearby to the fiber positioner and looking directly into the telescope's primary mirror, will image the spine tips when focused to infinity – hence the term 'Spine Tip Re-imaging In Primary', or STRIP used to describe the system. If the field of view is selected to match the WF MOS field of view, the positions of all of the fiber tips may be captured with a single image.

As the STRIP system samples the plane wavefront generated by the WF MOS corrector and telescope primary, the image quality will be determined by these optics and the STRIP camera, and this ensures that the spine tip images will essentially have the same image quality as star images at the corrected prime focus (actually better than this, because of the relatively short atmospheric path), convolved with the STRIP imager optics.

At times when the positioner is not fitted at the prime focus, closed loop operation is provided by a similar system with the cameras using either direct imaging or a fold mirror arrangement to view the array of spine tips, for engineering and maintenance purposes.

11.3.2.1 STRIP specifications

The specifications demanded of an imaging system for the STRIP position feedback system are quite straightforward to derive.

The baseline WF MOS field of view is 1.5 degrees, hence a camera imaging the focal plane from its reflection in the telescope primary must also have a field of view of 1.5 degrees.

Fiber positioning constraints similar to FMOS require spine position feedback accurate to ~ 0.1 arcseconds. Tests conducted for the Subaru-FMOS design show the software used for analysis of the focal plane images can locate the spine tips to an accuracy of $\sim 1/25$ image pixels, provided each image has a FWHM of approximately 4 pixels.

Given that the entire STRIP camera field of view is 1.5 degrees, that the positioning accuracy required is 0.1 arcseconds, and that the software provides positioning accuracy of $1/25$ pixels, we find that the STRIP field of view must subtend at least $1.5 \times 60 \times 60 \div 0.1 \times \frac{1}{25} \approx 2200$ pixels. Conservatively, we specify a $4k \times 4k$ imaging field, which may equally well be composed of a single camera of that format, or of a set of four, $2k \times 2k$ cameras of a type more conveniently available today.

A system imaging 1-arcsecond fibers in a 1.5-degree field resolved at 4000 pixels results in spine tip image sizes of less than a single pixel. To satisfy the centroiding software requirements, the images must therefore be defocused to reach a FWHM near 4 pixels. Since this defocusing changes the intensity profile of the images, tests were conducted with the Subaru-FMOS FPI prototype which confirmed that the software would correctly locate the spine tips when the images were defocused a similar proportion (to a FWHM of 40 pixels from a focused size

near 4 pixels). Detailed Zemax modelling will be required in the concept or preliminary design phase to include the effects of spine tilt, the off-axis aberrations of the primary/corrector imaging systems, and the specific characteristics of the STRIP camera optics.

Note that this imaging specification is unable to resolve spines at separations of less than 8 pixels, or 10 arcseconds. The mechanical design allows spine tip separations to approach approximately 3 arcseconds, however the WF MOS baseline configuration allows back-illumination of fibers from individual spectrographs allowing adjacent spines to be independently illuminated.

11.3.2.2 STRIP prototyping

In view of the novel nature of this FPI scheme, a measure of prototyping was seen as important for the Feasibility Study. We conducted this testing using a STRIP camera set up on the Anglo-Australian Telescope, to image a configured 2dF field plate. The geometry of this arrangement would be quite comparable with the proposed system for WF MOS.

An analog camera similar to the type used for the XY gantry FPI in FMOS-Echidna was fitted to a ~700-mm focal length lens, selected to match the image scale to the WF MOS STRIP specifications (Figure 91). The smaller-than-specified image format of this test camera means that it only images a portion of the 2dF focal surface.

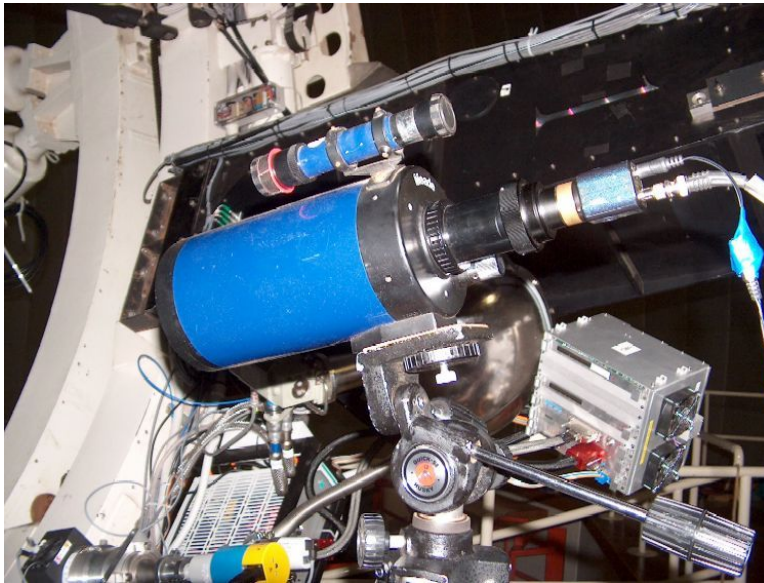


Figure 91. Prototype STRIP camera and lens, as used in tests on the AAT.

The 2dF instrument was fitted to the AAT 4-m telescope, and a known field configuration was set up. Fibers on the active plate were back-illuminated while the telescope was brought to ‘prime focus access’, where the prototype STRIP camera had visibility into the telescope aperture from near the prime focus (Figure 92). From here, it was used to image a portion of the focal plane reflected in the AAT primary (e.g., Figure 93).

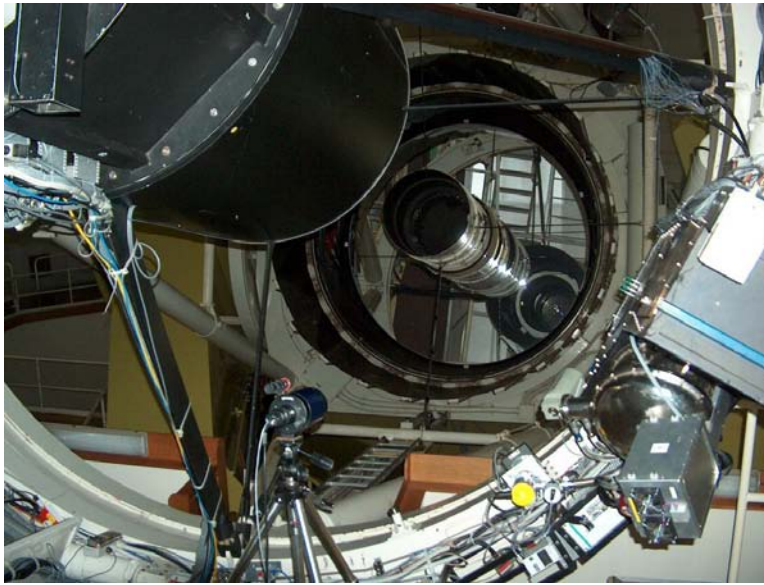


Figure 92. Prototype STRIP camera viewing into the AAT aperture, to image a portion of a configured and back-illuminated 2dF field.



Figure 93. Sample STRIP prototype image of backilluminated 2dF field.

FMOS-derived image processing software was applied to images collected in this way and matched to the known 2dF field target positions, demonstrating the feasibility of the concept. Centroids were readily obtained, showing that back-illumination intensity is suitable for this configuration and imposes no challenging sensitivity requirements. The target centroiding accuracy was not achieved, due to insufficient optical modelling of the various system components and noise in the analogue video signal capture hardware.

The WMOS baseline positioner design specifies a set of four, $2k \times 2k$ digital cameras for the STRIP system, which will virtually eliminate noise problems for this imaging. No impediment is seen to the successful implementation of the

concept for WFMOS, following detailed optical modelling of the final STRIP system design.

11.3.2.3 *Back-illumination requirements*

Back-illumination of the fibers is required for imaging with the STRIP system for position feedback. The strawman concept for WFMOS, with a relatively large number of spectrographs, provides a natural solution. Fibers are routed to spectrographs such that no adjacent spines are fed to the same spectrograph. Each spectrograph can be commanded independently to back illuminate its fiber slit, and so the positioner software will always be able to resolve all the spines. In addition, spine positions will in general be tracked very accurately and so confusion will normally not be a problem. If confusion were to occur, perhaps at the limits of spine travel where overlap between non-adjacent spines may be possible, differential movement of spines should readily resolve the issue (this approach is feasible because of the short time required to image the spines).

Clearly, a back illumination scheme must be incorporated into the spectrographs, and this will form part of the interface requirement for the spectrograph.

11.3.3 **Mechanical Design**

The mechanical design of the Echidna fiber positioner will incrementally build upon the successful design of FMOS-Echidna. Increased size and complexity of the positioner, as well as certain specific features such as field curvature, demands investigation of technologies to simplify the manufacturing and assembly process.

11.3.3.1 *Spherical Focal Plane implications*

While FMOS-Echidna has a flat focal surface, the baseline corrector for WFMOS delivers a spherical, concentric surface. Curvature of this surface is such that both the position and the orientation of the spines and their actuators must be matched to the surface – approximation to a flat or parallel focal surface yields unacceptable errors. The manufacturing techniques adopted for FMOS-Echidna are not directly applicable to a spherical focal surface, but the AAO can further take advantage of its FMOS experience to refine and improve the process. This allows the present concept design to accommodate the spherical surface, while at the same time streamlining the manufacture process to reduce tight manufacturing tolerances on several components. Rapid interchangeability of the modules is sacrificed in this approach, however a requirement for this is of doubtful value. Even in FMOS-Echidna, fiber constraints limit the extent to which module interchange is rapid.

The AAO's concept for WFMOS accommodates a spherical focal surface with a new module layout where the actuators are mounted concentric to the field curvature, and a refined spine design allowing achievement of the required dimensional tolerances by individually tuning each spine to the focal surface on assembly (Figure 94).

11.3.3.2 *Adjustable length spines*

Pre-prototypes of the adjustment mechanism have been produced and tested for spine-drive function with promising results. We have obtained quotations from

potential manufactures of the various components comprising the new design, and these have been used in the cost estimates.

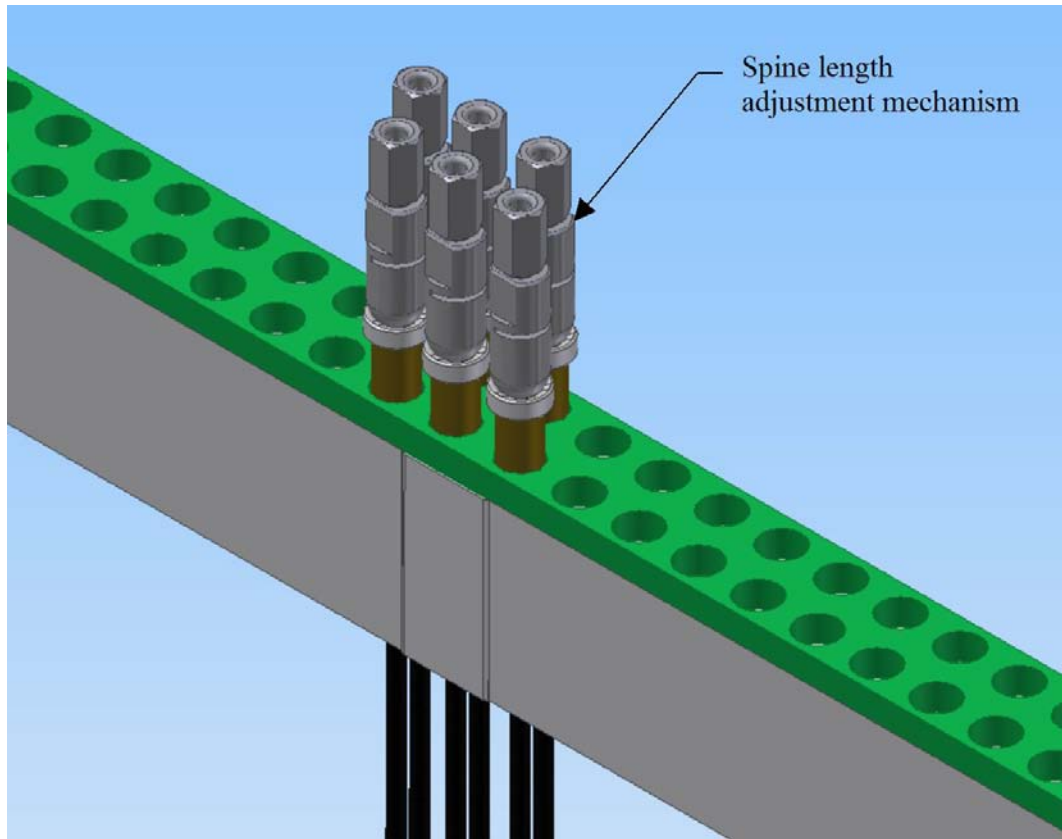


Figure 94. Adjustable length spines mounted on the Echidna module

11.3.3.3 *Reduced actuator size*

In order to provide sufficient clearance on the module PCB to route the tracks necessary for the large number of actuators per module, the actuators must have a smaller diameter than those used in FMOS-Echidna. Designs of the actuator and spine have been incrementally advanced to reduce the actuator footprint size as required, as well as supporting the concept developed to enable a curved focal surface with an adjustable length spine as described above.

11.3.3.4 *Streamlined design of spine drive actuators*

FMOS-Echidna experience has shown a high labour cost in assembly of the spine drive actuators. Accordingly, effort has been devoted to a refined design to reduce assembly labour and improve component accuracy and reliability. A simplified form is under development, with early prototyping work yielding promising results. Potential savings and improved reliability are forecast.

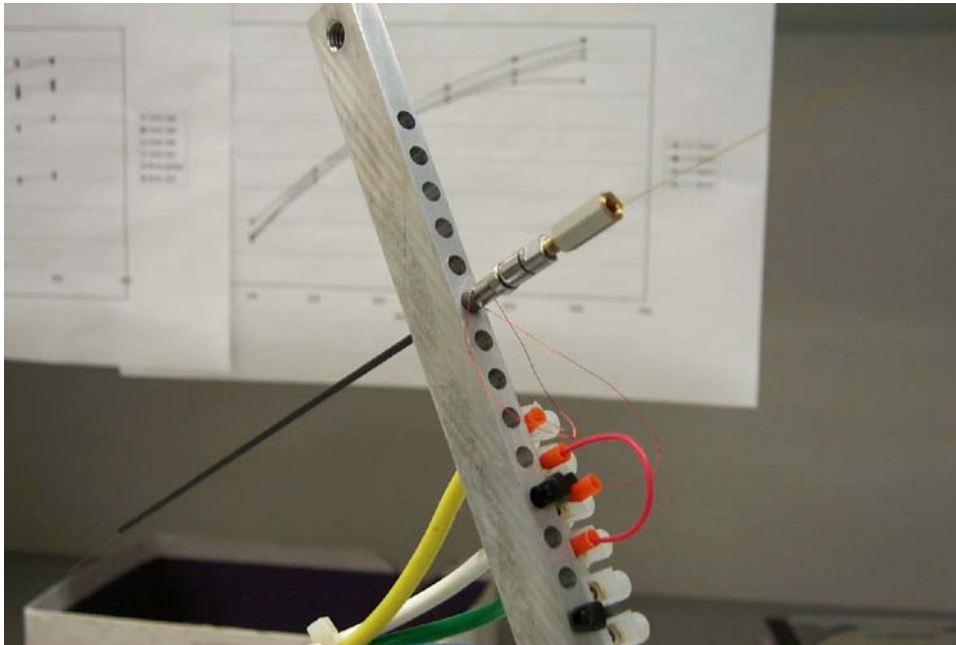


Figure 95. Pre-prototype WFMOS spine and actuator, featuring reduced diameter actuator, adjustable-length spine, and streamlined design of actuator and spine components.

11.3.3.5 Module base

Modules comprising the WFMOS-Echidna fiber positioner will necessarily be much longer than those built for FMOS, with an active length near 520 mm compared with 150 mm. The width of the modules is quite similar, and so the stiffness of the longer modules is clearly an important issue. Naively, the deflection of the module due to gravitational loading would increase as the square of the length, leading in WFMOS-Echidna to deflections an order of magnitude greater than those found in FMOS-Echidna. Such deflections would be quite unacceptable, purely from the effects of defocus variation across the focal surface, without further considering the likely effects of lower frequency vibrational modes. Module stiffness may be improved by increasing the thickness of the module base, and by using different materials. Preliminary finite element analysis (FEA) suggested that both approaches will be required for WFMOS-Echidna, but that a solution is achievable.

Various shapes and configurations of module bases have been investigated to meet the WFMOS requirements. Similar to FMOS-Echidna, a long module base with two rows of spines has proven to be most practical. As foreshadowed above, a challenging aspect of this configuration is the difficulty of obtaining satisfactorily low deflections of this slender, long span structure. Material solutions including thick ceramic coatings were tried, and although improvement in stiffness was confirmed by tests, none of them appeared to be technologically mature enough to be considered a reasonably low risk.

Correspondingly, a geometric solution employing conventional materials appears to be most promising. FEA simulations on Algor with a carefully considered geometry confirm that sufficiently low deflections of the slender module bases can be achieved without resorting to exotic materials. Our new design of the module bases can be machined from structural aluminium (*c.f.* steel for FMOS-Echidna) with the necessary tolerances at a reasonable cost.

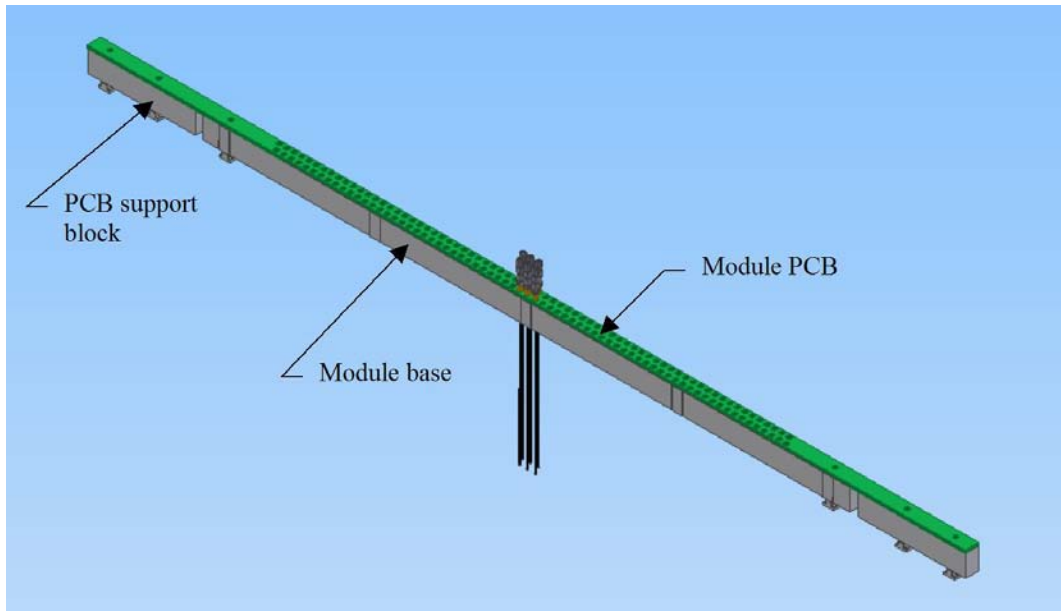


Figure 96. WF MOS-Echidna module base, with PCB and support blocks. Only 6 of the 140 actuators and spines are shown. The WF MOS module design is approximately 700mm in length.

11.3.3.6 Module Mounting Frame

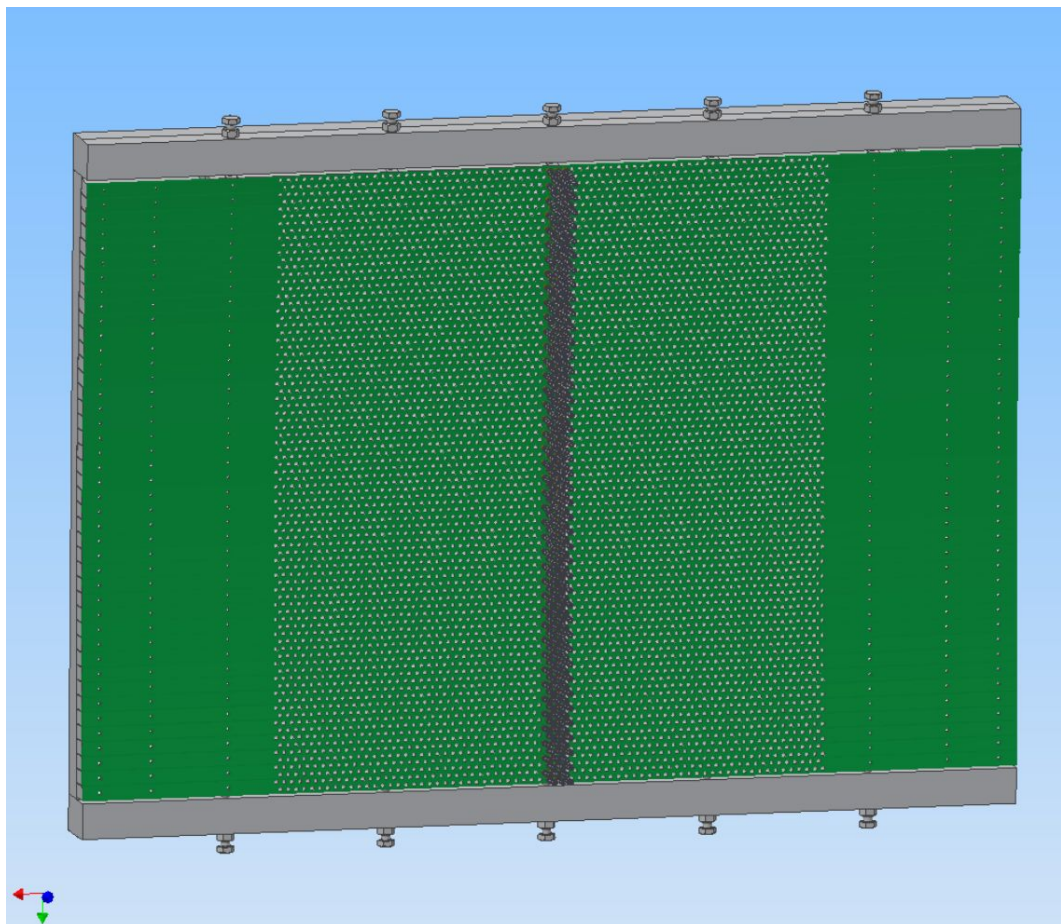


Figure 97. Echidna structure viewed from the PCB side

The modules comprising the WF MOS spine array require very dimensionally stable support. An aluminium frame serves this function, providing rigid support

to the module bases and the PCB support brackets. This frame is mounted on a thick aluminium plate, itself bolted to a large bearing serving as the instrument rotator. Figure 89, Figure 97 and Figure 98 show the arrangement.

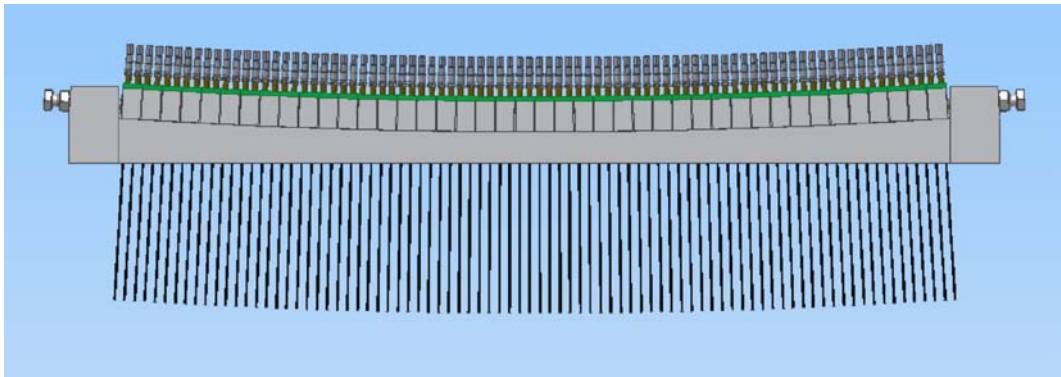


Figure 98. 4500-fiber Echidna positioner for WFMOS – accommodating spherical focal surface (side view).

11.3.3.7 *Fiber routing within the positioner*

Routing the fibers from the spines through the Echidna ‘core’ will follow a similar approach to that used for FMOS-Echidna. Gantry style conduit holders are mounted above the modules to support ‘mini-flex’ conduits, which will be fitted into the holders on assembly as spines are inserted into the actuators. From the top of the Echidna core, these flexible conduits will be guided back down through a slot in the instrument mounting plate into a fiber/cable wrap within a composite housing under the plate – Figure 89 shows this annular tray surrounding the hexapod pointing/focus mechanism.

11.3.3.8 *Instrument rotator*

As can be seen in Figure 89, the Echidna unit and its control electronics are mounted atop an instrument mounting plate, with field rotation capability provided by a precision wire-race bearing with an aluminium housing. The instrument mounting plate is attached to the outer race of the rotator bearing, and driven with a standard backlash-free drive such as a double servomotor. The inner race of the bearing will be supported by a triangular rotator support plate which also carries the rotator drive and three support blocks for the hexapod.

The instrument mounting plate will also support the last two elements of the corrector, for reasons discussed previously. Separate housings for these two elements will be secured to the instrument mounting plate beneath the fiber positioner core, contributing further to the stiffness of the module mounting frame of the Echidna unit.

11.3.3.9 *Pointing and focus adjustment mechanism*

Figure 99 depicts a hexapod employed as the instrument’s pointing and focus adjustment mechanism. It will allow necessary corrections for the gravitational deflections and thermal expansion of the telescope structure.

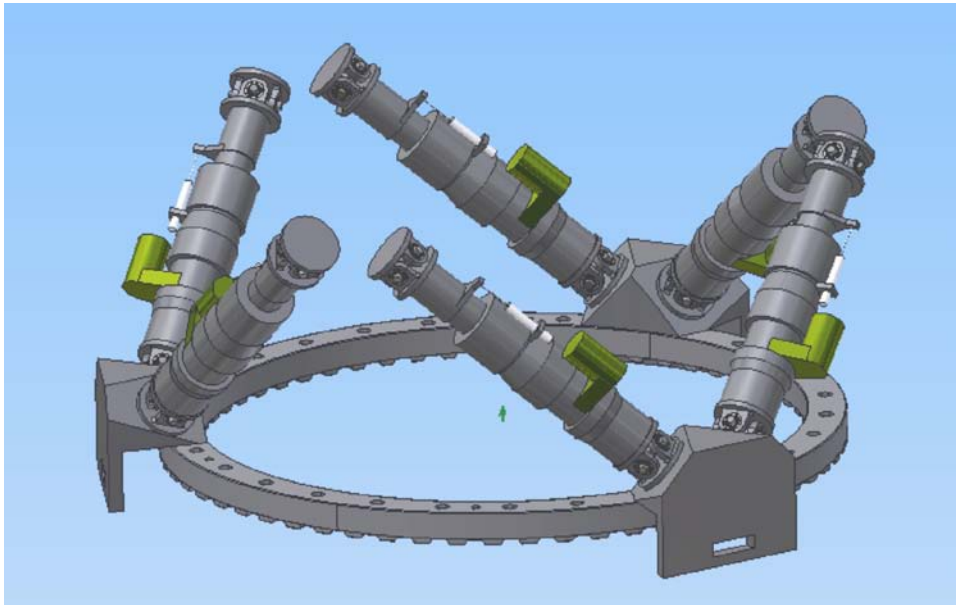


Figure 99. Hexapod with the instrument mounting hub interface. This provides instrument pointing and focus adjustment.

Discussions have been entered into with a commercial company (ADS International) regarding design and manufacture of a suitable hexapod structure, and their commercial-in-confidence report is attached to this document. Considering this report in the light of the manufacturer's experience, a high degree of confidence attaches to the feasibility, specifications, performance, delivery and cost of this system component.

Positioning tolerances and performance specified for the hexapod are sufficient to allow open-loop control using a look-up table to control the instrument pointing errors and maintain alignment to the telescope's optical axis. This hexapod will work in tandem with a similar unit installed on the opposite side of the instrument mounting hub to support the wide field corrector.

11.3.3.10 *Fiber and Cable Wrap*

Positioner components mounted on the rotating instrument mounting plate inside the PFU require servicing with a large number of optical fibers (~4500) and a quite small number of electrical cables. Derotation for these fibers and cables is planned using an energy chain with fiber bundles, folded within a composite enclosure surrounding the hexapod. One part of this annular enclosure is secured to the clamping arrangement to the top end of the central hub, while the other part is mounted to the rotating instrument mounting plate. The termination for the WF MOS fiber connector will be mounted at the bottom of this enclosure. The energy chain housing is shown in Figure 89 and Figure 100, where the energy chain itself is omitted for clarity of the structure behind it.

Based on the FMOS design with a 2-metre diameter cable wrap, this design incurs some minor vignetting of the telescope aperture. While this design as presently envisioned is regarded as quite conservative, the design and technology of energy chains is in continuous development. At later instrument design periods, reassessment will of course be made based on designs available at the time, to potentially reduce the wrap footprint. Within the available space envelope there should be a range of choices.

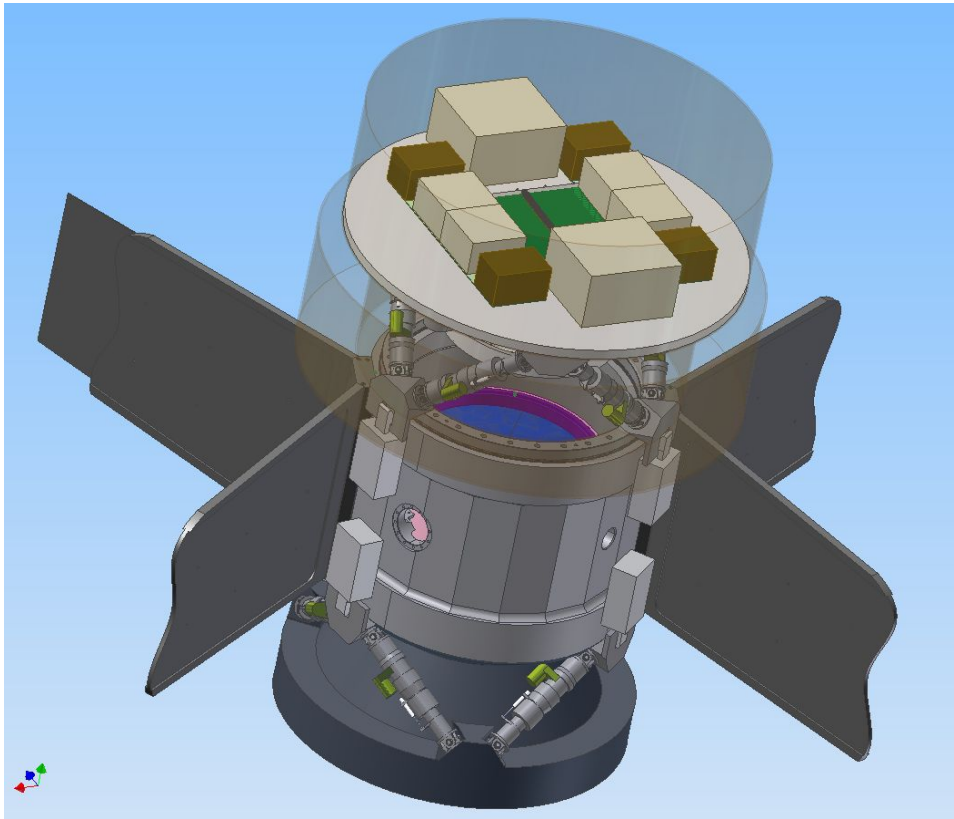


Figure 100. WF MOS positioner and other top end components on the Subaru top end central hub. Electronics enclosures are mounted around the Echidna 'core' of the positioner, while the fiber/cable wrap is carried in the annular tray surrounding the hexapod (shown semi-transparent in this view).

11.3.3.11 *Electronics enclosures and support structure*

Sections 11.3.4 and 11.3.5 detail electronics components and systems residing in the PFU, mounted to the telescope top end. These will be mounted in racks on either side of the Echidna core of the positioner, where they will be supported on the rotating instrument support plate as shown in Figure 100. FEA will demonstrate that the load from the electronics does not cause excessive deflections or vibrations to the positioner. If necessary, flexible extensions to the plate can be considered to control such issues.

11.3.3.12 *Electronics cooling system*

A small amount of heat dissipation from the electronics is expected. At a later design stage, should it prove necessary to limit this, there is sufficient space on the instrument mounting plate to install a heat exchanger-based cooling system. Coolant lines for such a system can be accommodated within the fiber/cable wrap. Thermally-controlled and insulated electronics sub-enclosures can further contain heat issues in this area.

11.3.3.13 *Positioner enclosure*

The positioner and associated electronics will be covered with a composite enclosure, to protect them from dust and damage during handling. This will be a simple cylindrical structure of less than 2 metres diameter and 0.5 meter high, as depicted in Figure 89.

11.3.3.14 *Assembly and alignment process*

Experience with the FMOS-Echidna positioner has shown that the process of assembly of the modules is a significant cost driver. Refining the process to minimise cost and enhance reliability has been an important part of the WFMOS Feasibility Study.

Adjustable spines and refinements to the spine-drive actuators as described in sections 11.3.3.2 and 11.3.3.3 may alleviate some of the costs and enhance manufacturability by relaxing the dimensional tolerances on the support framework, modules and spines. These considerations have been taken into account in developing an accurate cost estimate for these stages of the instrument manufacture.

Additionally, various process options have been identified to enable or facilitate assembly of the modules, based on particular difficulties identified during the build of FMOS-Echidna. Some of these relate to processes found to be challenging with FMOS which will be just as challenging for WFMOS, others result from scaling the FMOS-Echidna design. The schedule and cost estimates for the fiber positioner presented in this study include allowances for these aspects as well.

11.3.4 *Positioner Electronics Design*

11.3.4.1 *Introduction*

This section describes the control electronics for an Echidna style wide field fiber positioner for use on either the Gemini or Subaru Telescopes. From an electronics perspective, the telescope on which the fiber positioner is located makes little difference to the design. In the baseline positioner design for either case, the fiber positioner will control 44 modules, each with 140 spines.

11.3.4.2 *Approach*

The WFMOS fiber positioner electronics will be based heavily on the design used in the FMOS-Echidna fiber positioner. However, the increase in the number of spines by a factor greater than ten requires some modification to the architecture and some changes to the implementation.

11.3.4.3 *Architecture*

The FMOS-Echidna control system (shown in Figure 101) consists of three separate electronics assemblies – a computer (with an analog output board and a digital input/output interface), an intermediate set of control electronics and switch boards for each half of the spine/piezo actuator modules. The three units have several multi-core cable interconnections.

For the WFMOS fiber positioner it is proposed that all the electronics required to control the spines will be located as close as possible to the spine array to minimise cabling and cable connections.

For electronic control purposes, the array of spines is arranged in four identical quadrants. Each quadrant has independent control electronics that allow the quadrant to operate autonomously from the control computer and simultaneously

with the other three quadrants. The quadrant control electronics is divided into three groups – the piezo modules, the module switching electronics and the module control electronics. A diagram of the control system is shown in Figure 102.

The four sets of quadrant control electronics are connected to a single control computer via high-speed serial links. The control computer also operates the spine position feedback cameras (STRIP FPI system), the acquisition cameras and the guide camera.

11.3.4.4 Implementation

The FMOS-Echidna control computer uses an analog output board to generate the necessary piezo actuator drive waveforms under software control. Control of the piezo electrode switching is achieved using the digital input/output interface, also under software control.

Reconfiguration of a field consists of a number of iterative moves of the spines, each of which is typically followed by measurement of the spine tip positions with a single analog camera (mounted on an XY carriage – not shown in Figure 101). As part of the setup prior to an iteration, the software determines the number of waveform pulses that must be applied to each piezo electrode to achieve the desired length of travel of the associated spine tip for that iteration. During a position iteration, the software in effect counts the number of waveform pulses applied to each piezo electrode and stops further application of pulses to the piezo using the switching electronics when the required number of steps for that piezo have been made.

While this design has proved to be adequate for the FMOS-Echidna fiber positioner, it has a number of shortcomings that are likely to make it unacceptable for a WF MOS proportioned positioner.

- The start/stop nature of the piezo drive waveform caused by the software needing to switch off the application of the waveform to the piezo electrodes gives the waveform a variable mark space ratio that leads to uneven step movements in the spine. This contributes to positioning errors, which may cause additional configuration iterations to achieve an accurate final position. Additional configuration iterations contribute to the overall configuration time.
- The overheads of switching on and off the waveforms and controlling the piezo switches add significantly to the time required for each iteration, also affecting the total configuration time.
- Most of the overhead in positioning is through the use of a single focal plane imaging analog camera with a small field of view carried on an XY positioner that is used to measure the spine tip positioners.

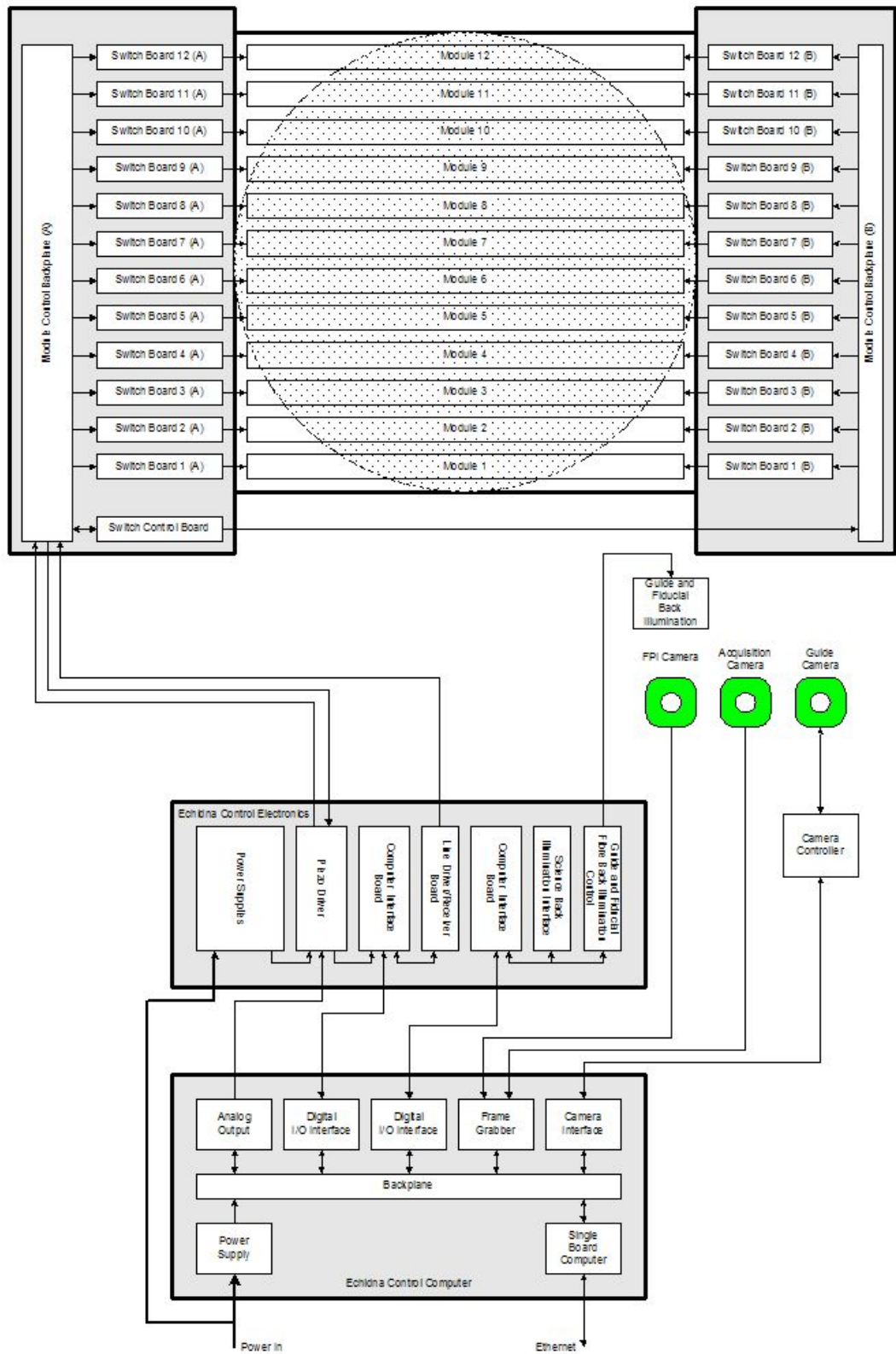


Figure 101: FMOS-Echidna Fiber Positioner Electronics

The waveform issues can be addressed by using a hardware counter to count down the number of waveform pulses applied to a piezo electrode (one counter per piezo), and having the output of the hardware counter control the switches that supply the waveform to the piezo electrode. This means that the software can preload all the counters, start the waveform and allow it to free run until all

counters have counted down their respective spine movements. This scheme would be prototyped and tested during the concept design phase.

The measurement of spine tip positions will be addressed by using the Spine Tip Re-imaging In Primary FPI technique, which replaces the single camera mounted on an XY carriage with four high resolution fixed cameras. The STRIP camera system is discussed in more detail elsewhere in this document.

11.3.4.5 *Description*

11.3.4.5.1 **Piezo Module**

The piezo module contains the quadrant piezo tube actuators and a means of providing signal connections to the piezo electrodes. The FMOS-Echidna module PCB with its 42-piezo actuators is approximately 380mm long including its connectors and mounting area. Using smaller sized actuators (to improve PCB track routing), on a 7.4mm pitch, the WFMS module PCB is more than 700mm long including connectors and mounting area. This length of PCB is beyond the manufacturing capabilities of local PCB manufacturers, so the 140-spine module needs to be made with two PCBs, each with 70 spines. Two identical half modules can be end-buttet together to produce a 140-spine module.

Two trial PCB layouts of half modules containing 70 piezo actuators have been carried out to demonstrate the feasibility of an Echidna-style positioner of this capacity. The first layout is based on the switching design used in the FMOS-Echidna system (referred to as “individual switching”). This design requires approximately 150 signals in three connectors. This half module is 12.8mm wide by about 500mm long, and has 26 layers for signal routing in a 3.5mm thick PCB. The second trial layout is based on a “matrix switching” design concept, needing approximately 80 signals in two connectors. This module is 12.8mm wide by about 380mm long, and is implemented using 18 layers in a 2.5mm thick PCB. In addition to using less space on the sides of the spine array, the shorter PCB with fewer layers has some cost savings in tooling and manufacture. The matrix switching design also saves components in the switching electronics, leading to cost savings and reduced power consumption during operation. However, the tradeoff is that the time to physically move the spines is doubled compared to the FMOS approach of individually switched piezos, as only one row of piezos per module can be driven at a time. As discussed in Section 11.5.1, this can have a significant effect on the overall field configuration time. The matrix switching module design needs to be prototyped and tested (during the concept design phase).

11.3.4.5.2 **Module Switching Electronics**

The module switching electronics consists of one switch board per piezo half module PCB. The switch boards are configured under software control to switch the piezo drive waveform to the electrodes of the spine piezos for the required number of movements. As previously noted, the switch board design is likely to be heavily based on the FMOS-Echidna fiber positioner design. However, the design will be enhanced to support hardware counting of piezo pulses.

The switch board design depends on the type of piezo switching used (individual or matrix). As previously noted, the matrix switching design uses half as many components as the individual switching design and so has savings in cost of

production and in operational power consumption. The matrix switch board design needs to be prototyped and tested (during the concept design phase).

As well as connecting to piezo half module PCBs, the module switch boards plug in to a common backplane that extends the length of one quadrant. As the half-module PCBs are the same on each side, the switch boards on one side of the spine array “face” the opposite direction to those on the other side. As the module control electronics connect to the outside ends of the module switch backplane, four versions of the backplane are required for each quadrant.

The module switch boards will have a means of providing mechanical assistance during their insertion and extraction into and out of the backplane/module PCBs. Rigid card guides to ensure good connector alignment as well as a board retention scheme will also be provided. PCB connectors will be of a high reliability pin and socket type.

11.3.4.5.3 *Module Control Electronics*

The module control electronics contains all those components needed to produce the piezo drive waveform and control the module switch boards. The module control electronics will be arranged as a number of circuit boards plugged in to a common backplane. These circuit boards would include:

Power Supply – generates the necessary supply voltages for the fiber positioner control electronics from a single DC supply input (e.g. 48VDC).

Module Control and Serial Interface – interfaces the module control electronics to the fiber positioner control computer using a high-speed bi-directional fiber optic serial link and provides local control of the quadrant electronics.

Back Illumination Control – provides a switchable, adjustable current source for an external LED board that provides back illumination for the guide and fiducial fibers.

Telemetry Interface – contains data acquisition electronics to monitor power supply voltages and various temperatures in the system, including electronics enclosure temperatures and piezo module temperatures.

Waveform Generator – generates several types of waveform depending on the type of positioning required (e.g. fine, course etc).

Piezo Driver – contains amplifiers to generate the voltages necessary to drive the piezo actuators, using the waveform from the waveform generator.

Switch Board Interface – interfaces the module control electronics backplane to the module switch backplane.

Module Control Backplane – distributes power and interconnects signals between the module control electronics boards. Four versions of the backplane are required, depending on the quadrant in which it is located.

The module control boards will have a means of providing mechanical assistance during their insertion and extraction into and out of the backplane. Rigid card guides to ensure good connector alignment as well as a board retention scheme

will also be provided. PCB connectors will be of a high reliability pin and socket type.

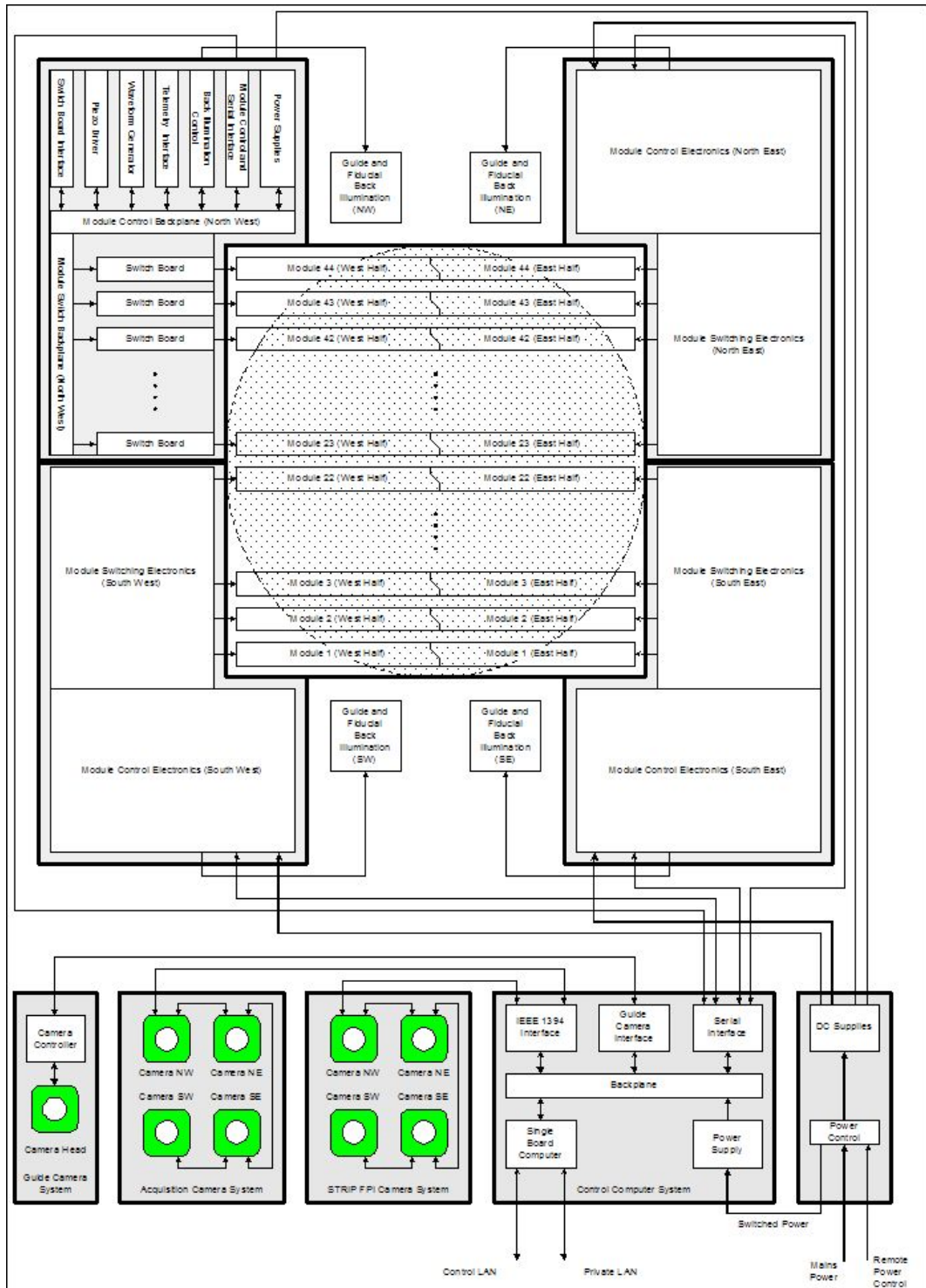


Figure 102: WFMOS Fiber Positioner Control Electronics

11.3.4.5.4 Electronics Enclosures and Electronics Mounting

A number of 482.6mm (19-inch) rack mount units will need to be located near to the fiber positioner, including chassis for the control computer (probably 3 rack units high), the DC power supply (3 rack units high), the mains power control (3 rack units high), the guide camera controller (2 rack units high) and possibly a network switch/hub (1 rack unit high). These chassis are likely to be mounted in

one or two enclosures, which may need to be actively cooled to minimise degradation of image quality in the telescope dome.

The positioner control electronics will require their own purpose designed enclosures, for each quadrant control electronics (possibly separated into an enclosure for each quadrant's module switching electronics and an enclosure for each quadrant's module control electronics). The enclosures may need to be actively cooled to minimise heat dissipation.

A thermal analysis of the heat generated by the positioner electronics will be carried out during the concept design.

11.3.4.5.5 *Power Supply and Power Control*

It is envisaged that power for the fiber positioner electronics would be derived from a single power supply. Low voltage power (48VDC) would be provided to power supply boards in each quadrant, which would then be regulated down to the required supply rails. This minimises the distribution of mains rated wiring and cabling in the fiber positioner area and electronics, and minimises the size (and weight) of power distribution cables.

Power to the fiber positioner control electronics and computer would be remotely controllable, due to the difficulty in accessing the central area of the top end whilst on the telescope. The remote control would be via easily accessible manual switches, or possibly by computer control over the network. The power control would also contain appropriate filtering, protection and isolation capability.

11.3.4.6 *Camera Systems*

There are three independent camera systems that are controlled by the fiber positioner computer. These are the acquisition camera system, the STRIP FPI camera system and the guide camera system. Both the acquisition and STRIP camera systems are likely to require multiple cameras to achieve optimal field coverage. The cameras used in these systems do not require the sensitivity provided by a cooled detector, but some control over the exposure time may be necessary. In the case of the STRIP cameras, high resolution is a requirement. The guide camera system requires high sensitivity, and therefore is likely to be a cooled camera.

There are several camera options that can be considered, largely depending on the camera interface.

In previous fiber positioner instruments, analog cameras have been used for position feedback and acquisition. Analog cameras produce interlaced video at TV frame rate (25 or 30 frames per second). They usually have limited resolution (< 1 Megapixels) to maintain compatibility with television standards, and are essentially “dumb”, with no control over exposure time or region of interest (ROI). Some cameras may have some switches or external digital inputs for automatic gain control, gamma correction and electronic shuttering.

Images from an analog camera are acquired using a bus level analog frame grabber, which is essentially synchronised to the camera video signal and performs analog to digital conversion of the camera analog data. Some frame grabbers may support windowing capability, and some frame grabbers can accept switchable

input from multiple cameras. Long cable lengths are possible and fiber optic video cable extenders are available.

These cameras suffer from several sources of error – noise pickup and signal reflections in the cable and aliasing between frame grabber “pixels” and camera pixels (pixel jitter). These errors complicate the task of determining the centroids of the fibers in the field.

It is proposed for the WFMOS instrument to use digital cameras for all vision tasks. A digital camera contains an on-board analog to digital converter, and sends digital data to the computer. These cameras are generally high resolution (up to 6 Mpixels), with programmable trade-offs between frame rate and resolution. The cameras usually have a number of programmable features, including exposure time, ROI, video format, frame rate etc. These cameras are available with a number of interfaces, including:

- Gigabit Ethernet – high bandwidth (1000 Mbits/second), peer to peer, 100m cable, no standard protocol for video.
- IEEE 1394 (Firewire) – high bandwidth (400 Mbits/second), peer to peer, 72m cable with hub, 200m with fiber optic interface, latching connectors, standardised protocols (DCAM/IIDC).
- USB2.0 – high bandwidth (480 Mbits/second), master to slave, limited cable length, non-industrial connectors, proprietary protocols.
- CameraLink – very high bandwidth (255 MBytes/second), point to point, 10m cable, fiber optic extenders available, requires CameraLink compatible frame grabber.
- Proprietary LVDS links – requires proprietary frame grabber.

A concept design phase will identify the most appropriate cameras and camera interfaces, but for the purposes of this study it is assumed that IEEE 1394 cameras will be used for the STRIP and acquisition functions, and either a CameraLink or IEEE 1394 camera will be used for the guiding function.

There are a number of manufacturers of Megapixel cameras with IEEE 1394 interfaces. One particular camera that has been identified as being suitable for both the STRIP and acquisition functions is the PixelINK PL-A780. This is a 6.6 Megapixel camera based on a 2210 x 3002, 3.5 μm^2 pixel CMOS sensor (IBIS4-6600).

It is assumed that the guide camera will need to be of a cooled type for minimal dark current and read noise and maximum full well and dynamic range. A possible camera for this application is the Hamamatsu ORCAII-BT-1024. This camera has a 1024 x 1024, 13 μm^2 pixel CCD (EEV47-10), is available with liquid cooling and has either an IEEE 1394 or a CameraLink interface.

The interfacing of potentially nine cameras to a single computer is unlikely to be a significant performance issue, unless all cameras were to be used simultaneously. However, use of the camera systems is unlikely to overlap significantly; while the FPI cameras are in use during field configuration, the guide camera will be idle.

The FPI cameras will be idle while observing when the guide camera is in use. Use of the acquisition cameras may overlap with the FPI cameras, but careful programming should ensure that this is minimised.

The effects of camera image acquisition and processing on the control computer would be investigated in the concept design. A fall back scenario is to offload some of the cameras (e.g. the acquisition and guiding cameras) to a second control computer.

11.3.4.7 Control Computer System

The control computer system will be of a type that provides sufficient processing power and input output capability to meet the requirements that are determined. There are no hard real-time constraints required for fiber positioner control, or for any of the camera systems, so it should be possible to use a non real-time system running on an x86 (IA32) processor, such as Linux. However, considerable processing power and memory is likely to be needed for the FPI function, to process the images from four cameras to determine spine centroids. The control computer must have an open bus structure to support the addition of interface boards. A high performance Pentium 4 class single board computer, with at least 1 Gbyte of memory capacity, and multiple Ethernet interfaces in either VMEbus (VME64/VME64x), CompactPCI (PICMG 2.0) or PCI-ISA (PICMG 1.0) format would be suitable for the task and would provide all the necessary features identified in [Guidelines for designing Aspen Instrument Software]. Ideally, all instrument control computers used in the WFMOS instrument should be of the same type. As the control computer system is likely to be mounted on the telescope, it may also be desirable for it to be a diskless system, capable of booting from solid state mass storage or from the network.

11.3.4.8 Interfaces

At this stage of the design, there appears to be no requirement to connect the fiber positioner control electronics to the Telescope Interlock System. This aspect of the design would be explored further in the concept design.

Assuming that back illumination control is performed at the software level, the electrical interfaces to the fiber positioner control electronics are as follows:

- Control LAN connection
- Mains power connection

11.3.4.9 Issues

11.3.4.9.1 Back Illumination Control

As previously noted, it is assumed for this study that back illumination control will be done at the software level via commands on the Control LAN. Software on the High Resolution Spectrograph control computer will receive commands from the instrument sequencer or fiber positioner control system to turn on or turn off the back illumination. However, this is a departure from previous fiber positioner systems where there has been a direct (non network) link between the fiber positioner controller and the spectrograph controller to control back illumination. The concept design study will identify if it is necessary to control back

illumination at the hardware level. A hardware level control would be implemented using a simple fiber optic connection.

11.3.4.9.2 Instrument Interlocks

It is unknown at this time if there are any significant interlocking requirements associated with the fiber positioner that prevent either harm to humans or damage to the instrument as a result of unplanned, unintended operation of mechanisms. The concept design will identify any such requirements.

11.3.4.9.3 Piezo Switching Methodology

As previously discussed, there are two possibilities for controlling the piezo actuators. The concept design will further examine the trade-offs between the two methods, and will propose the most suitable design for the WF MOS positioner. If necessary the concept design will demonstrate proof of concept of the matrix switching design through prototyping.

11.3.4.9.4 Prototyping

Prototyping of circuits or systems regarded as “high risk” because they involve the use of new technology or techniques or they have a high level of complexity, is usually carried out in the concept or preliminary design phases in order to provide “proof of concept”. The hardware counting of piezo pulses is a new technique that would be prototyped during the concept design. If it is established that the benefits of “matrix switching” the piezos are superior to individual switching, it will be necessary to prototype the matrix switching design. Again, this would be undertaken during the concept design.

It is expected that prototypes of all fiber positioner control electronics will be developed during the preliminary design phase of the project.

11.3.4.9.5 Electronics Cooling

It is likely that it will be necessary to minimise the heating effects of the electronics equipment on the Telescope environment. This will require a purpose designed enclosure for the fiber positioner electronics, and the provision of active cooling of the control electronics enclosure and control computer enclosures. This will be achieved using a cooling system that extracts the heat generated in the electronics enclosures and transfers it to the Telescope coolant system. The cooling system maintains a small temperature differential between the outside surface of the electronics enclosure and the ambient air. It is expected that a thermal analysis will be carried out during the concept design to determine the cooling requirements.

11.3.4.9.6 Power

The power requirements of the Fiber Positioner control electronics are not expected to be large (i.e. < 1000W). However, a more thorough estimate of power consumption will be carried out during the concept design.

11.3.4.9.7 Observatory Electronics Design Requirements

As far as possible, the design of the Fiber Positioner control electronics will comply with any requirements defined in the relevant electronics design

specifications and standards relating to Observatory instrumentation. The concept design will identify the relevant specifications and standards.

11.3.4.9.8 Environmental Requirements

The selection and design of electronics components for the Fiber Positioner control electronics will take into consideration the environmental requirements and operating conditions of the Observatory. The concept design will identify the relevant environmental requirements.

11.3.4.9.9 Electro-Magnetic Compatibility (EMC)

The design of the Fiber Positioner control electronics will be undertaken to meet all the relevant requirements for Electro-Magnetic Compatibility for Observatory instrumentation. Achievement of EMC requires an understanding of interference coupling mechanisms, consideration of EMC in equipment layout, grounding and circuit design, application of appropriate filtering and shielding of interfaces and the testing and evaluation for EMC continuously through the project. Observatory EMC requirements will be identified during the concept design.

11.3.5 Instrument Rotator Electronics Design

11.3.5.1 Scope

This section discusses the electronics associated with the Prime Focus Unit Instrument Rotator Controller.

11.3.5.2 Description

The PFU rotator controller is responsible for closed loop control of the PFU rotator drive motors, under command of the Telescope Control System. The PFU rotator drive consists of one or two motors and one or two encoders. The first motor and encoder provides closed loop control of the rotator, the second motor and or encoder provides a means to cancel backlash in the system. The most appropriate control scheme to cancel backlash would be determined during the concept design. The motors are likely to be DC brushless motors, each with their own servo amplifier. The rotator is allowed to rotate ± 110 degrees, and so requires end of travel limit switches. There is also likely to be a home position switch.

The rotator control system electronics will consist of two parts – the “instrument electronics” that includes all electronics associated with the actual rotator mechanism, such as cables and wiring, and the “control electronics” that includes the control computer and motion controller, interfaces to the servo axes, servo amplifiers and power supplies. The motion controller would need to be of a type that supports anti-backlash control, either through two motors or two encoders or both.

The control computer system will be of a type that provides a cost effective solution for the task at hand. There are no hard real-time constraints required for spectrograph control, so it should be possible to use a non-real-time system such as Linux, running on an x86 processor. In addition, the control computer must have an open bus structure to support the addition of interface boards. An x86 (IA32) architecture single board computer in VMEbus (VME64/VME64X), CompactPCI (PICMG 2.0) or PCI-ISA (PICMG 1.0) format would be suitable for

the task and would provide all the necessary features identified in [Guidelines for designing Aspen Instrument Software]. Ideally, this would be the same type of system as used in all instrument control computers in the WMOS instrument.

A block diagram of the rotator control system is shown in Figure 103.

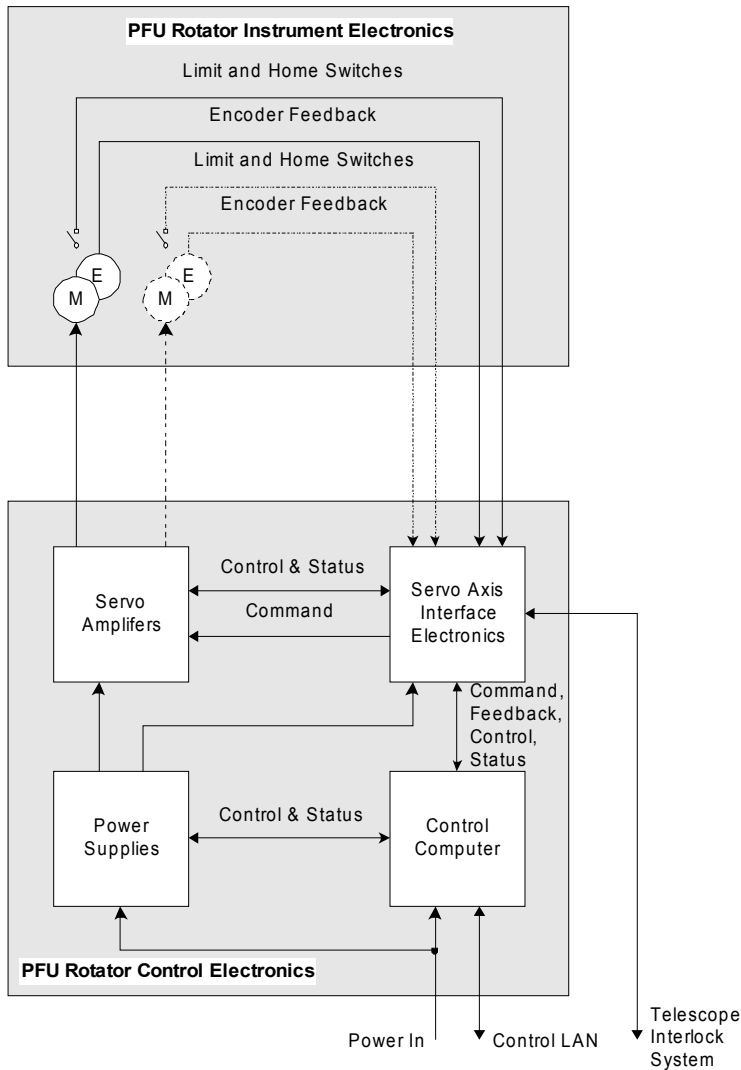


Figure 103: PFU Rotator Control Electronics

11.3.5.3 Interfaces

- Control LAN connection
- Mains power connection
- Telescope Interlock System

The instrument rotator requires a manual “lock-out” system to prevent accidental remote control of the rotator if it is unsafe to do so.

11.3.5.4 *Issues*

11.3.5.4.1 *Instrument Interlocks*

It is unknown at this time if there are any significant interlocking requirements associated within the spectrograph that prevent either harm to humans or damage to the instrument as a result of unplanned, unintended operation of mechanisms. The concept design will identify any such requirements.

11.3.5.4.2 *Servo Mechanisms*

The motion controller needs to be of a type that supports anti-backlash compensation.

11.3.5.4.3 *Prototyping*

Prototyping of circuits or systems regarded as “high risk” because they involve the use of new technology or techniques or they have a high level of complexity, is usually carried out in the concept or preliminary design phases in order to provide “proof of concept”. At this time, there do not appear to be any parts of the rotator control electronics control that require prototyping in any design phase.

11.3.5.4.4 *Electronics Cooling*

The PFU Instrument Rotator Control electronics are likely to be located on the Telescope Top End, it is likely that it will be necessary to provide active cooling of the control electronics enclosure to minimise the heating effects of the electronics equipment on the Telescope environment. This will be achieved using a cooling system that extracts the heat generated in the electronics enclosure and transfers it to the Telescope coolant system. The cooling system maintains a small temperature differential between the outside surface of the electronics enclosure and the ambient air. It is expected that a thermal analysis will be carried out during concept design to determine the cooling requirements.

11.3.5.4.5 *Power*

The power requirements of the PFU Instrument Rotator Control electronics are not expected to be large (i.e. < 750W). However, a more thorough estimate of power consumption will be carried out during the concept design.

11.3.5.4.6 *Observatory Electronics Design Requirements*

As far as possible, the design of the PFU Instrument Rotator Control electronics will comply with any requirements defined in the relevant electronics design specifications and standards relating to Observatory instrumentation. The concept design will identify the relevant specifications and standards.

11.3.5.4.7 *Environmental Requirements*

The selection and design of electronics components for the PFU Instrument Rotator Control electronics will take into consideration the environmental requirements and operating conditions of the Observatory. The concept design will identify the relevant environmental requirements.

The design of the PFU Instrument Rotator Control electronics will be undertaken to meet all the relevant requirements for Electro-Magnetic Compatibility for Observatory instrumentation. Achievement of EMC requires an understanding of interference coupling mechanisms, consideration of EMC in equipment layout, grounding and circuit design, application of appropriate filtering and shielding of interfaces and the testing and evaluation for EMC continuously through the project. Observatory EMC requirements will be identified during the concept design.

11.3.6 Software Design

Although it is clearly important, the software design for the positioner is not regarded as a technical feasibility issue, as it will be based on the existing FMOS instrument fiber positioner software design. The FMOS fiber positioner is currently being constructed at the AAO and soon to be deployed to the Subaru telescope.

From a software viewpoint, the WF MOS instrument fiber positioner is functionally similar to the FMOS instrument fiber positioner. Consequently, a large portion of the FMOS software should be reusable for the WF MOS system. This has been aided by the fact that, during development, the FMOS software has been designed with scalability in mind.

11.3.6.1 Scalability

Most of the scalability issues with the WF MOS system can be addressed simply by editing include file constants and recompiling. The relevant include file defines such constants as:

- Spine length.
- Spine pitch.
- Number of modules.
- Number of rows per module.
- Number of spines per module.
- Field physical diameter at the focus.
- Field of view,

The values are defined in the one include file, which is used by both the fiber positioner software and the fiber allocation software

The software differences between FMOS and the proposed WF MOS instrument, however, are different in more than just scale. By far the most significant difference is that the FMOS Focal Plane Imager (FPI) has been replaced with a Spine Tip Re-Imaging of Primary (STRIP) system in WF MOS.

11.3.6.2 *STRIP vs XY Gantry FPI*

While the removal of the XY gantry-based FPI used in FMOS greatly simplifies the overall design of the WFMOS instrument, it unfortunately creates a significant amount of additional software effort.

In effect, the existing software used to control the XY gantry-based FPI and perform its functions would be discarded and replaced with a new set of software modules developed entirely from scratch.

To analyse the impact of the removal of the XY gantry-based FPI it is prudent to identify the functions that it performs in the FMOS instrument and determine how they will be replaced in the WFMOS instrument.

Functions that the FPI performs in the FMOS system:

- Spine-position feedback
- Carries sky camera
 - Used during commissioning to calibrate telescope optical distortion model.
 - Find "lost" guide stars.
- Carries FPI subsystem:
 - Determine guide spine rotation.
 - Spine-to-slit mapping.
 - Test Autoguiding system.
 - Detect broken fibers?

New methods will likely be used to replace the above functionality. Consequently, software will need to be developed for them. A system to simulate the FPI STRIP camera will be needed for development and testing off the telescope.

11.3.6.3 *Fiber to Object Allocation software*

This component of the FMOS software should work almost verbatim for a WFMOS instrument. Only two major issues need be addressed:

- Spectrograph preference feature

An Astronomer requesting the use of the WFMOS instrument will likely want to be able to specify a preferred (possibly mandatory) spectrograph for some/all of their target objects.
- Performance

The scaling increase by an order of magnitude will likely affect the execution time of the allocation algorithms. The effect of an increase from 400 to ~4000 spines and a similar increase in target objects in the input catalogue needs to be quantified. This performance decrease will be offset by an increase in processor speeds between now and the estimated

instrument completion date. If processor speeds increase enough to compensate for the increase in scale, no modifications may be necessary.

The position of guide spines within the WFMOS instrument are staggered and as such the calculation of the "ring" of usable guide stars will need to be recalculated - this is trivial however.

11.3.6.4 *Telescope Optical Distortion Model*

This is a parameterised model used to determine the optical distortions across the focal plane. The basic FMOS telescope model software shouldn't require many modifications for use with the WFMOS instrument. The corrector distortion is modelled using a polynomial - higher-order terms maybe be required given the size of the corrector likely to be used for WFMOS. Extending the model is relatively trivial, however, the fitting software (used during commissioning operations) to determine the parameter values will likely be more complicated.

Getting the various calibration models right for FMOS has proved a time-consuming task. This includes the Spine camera distortion model - the parallel to this in the WFMOS instrument is the STRIP distortion model.

11.3.6.5 *Impact of changed hardware on the software.*

Much of the hardware detail will change for a WFMOS instrument. For example:

- The Guide Camera

A new cooled guiding camera is likely to have a different API. If this hardware is an off-the-shelf component (as expected), little software effort will be required. This should not impact the existing Echidna software too much (only a little software refactoring and other minor changes), as we only utilise basic features of this camera.

- Spine switching system

The spine switching electronics will be quite different and will lead to a new software interface. The existing FMOS modules dealing with spine switching should be easily modified to support what will be a simpler interface from a software viewpoint.

- FPI STRIP camera

The FMOS instrument uses a framegrabber/CCD camera system to image spines in the focal plane. WFMOS will likely have a purely digital FPI camera system, probably interfaced via IEEE 1394 (Firewire). A significant amount of software effort will be spent on the FPI system, as we tend to use the FPI camera in complicated ways. This will be done in the Conceptual and Preliminary design stages of the project.

- Spine Back Illumination system

Will likely be completely different. Again, the high-level software from FMOS should be easily modified. The low level software will likely be

quite different as currently it is intended to use a network control scheme rather than the hardware scheme used in FMOS.

- Guide/fiducial Back Illumination system

Won't be too dissimilar from a functional viewpoint.

11.3.6.6 *Command Interface*

The FMOS Fiber Positioner Software uses TCP/IP sockets to communicate with external systems. All communication is channelled through a piece of software called the OBCP, which roughly corresponds to the Instrument Sequencer in Gemini system. For the WFMOS instrument, the communication interface will be replaced with a CORBA implementation. (Please see *Chapter 7, System Engineering* for a discussion of this).

This should not prove too difficult as most of the code dealing with external communication is well modularised.

11.3.6.7 *Engineering GUI*

The FMOS engineering GUI is hardware-independent and utilises an "instrument description file" to achieve instrument-independence. Consequently it should be largely reusable with WFMOS with only minor changes. The FMOS GUI is written in Tcl/Tk. There is a suggestion to rewrite the GUI in Python. The GUI-to-ICS API is well documented so this should not prove difficult. Rewriting software in another language is always much easier than developing software from scratch (effectively the specification is very precise and there is a reference implementation to reduce development time) so this should not be overly time-consuming.

11.3.6.8 *Operating System issues.*

All of the FMOS software can be trivially ported to an up-to-date Linux distribution with the exception of the device drivers. But, with the current WFMOS, we will not require the FMOS device drivers anyway, but will instead use standard device drivers, such as IEEE 1394 (Firewire) drivers.

11.3.6.9 *Miscellaneous*

There are a number of other differences between FMOS and WFMOS. The effort required for software changes related to these items is negligible, but listed here to show that the issue has been considered:

- 200mm spine length (~40mm increase)

Will need to recalibrate differential spine deflection and update telescope model accordingly

- The Fiducial positions are non-linear.

The software to determine reference point will be different.

- Longer and different length modules.

Will probably affect the amount of defocus. Throughput/efficiency calculations will need to be modified.

- Curved focal plane

Recalculate efficiency throughput. Update telescope model? Determine optimal tilt position of each spine for allocation software.

- Back Illumination system.

Still only requires 3 different sequences. This is predicated upon spine travel distance \leq pitch.

11.4 The guide system

A similar guiding concept to that used in FMOS-Echidna is proposed for WMOS to correct telescope pointing throughout observations. A significant source of error for this type of fiber positioner is gravitational deflection of the Echidna spines as the telescope moves in zenith angle. If left uncorrected each of the fibers would gradually move away from the object under observation because of spine deflection. The proposed guide concept avoids this problem by using guide spines which have the same deflection characteristics as the science spines.

11.4.1 Overview

The guide system comprises some number (14-20) of guide spines occupying some of the available spine positions in the WMOS field. Each guide spine contains a 7-fiber bundle of 50 μ m diameter core fibers (compared to the 100 μ m core science fibers). Given each guide spine is virtually identical to a science spine (except for the nature of the fibers contained within) the relative deflection is similar enough to use the guide spines for guidance. With guide stars ($R \sim 16-18$) located on a subset of the available guide spines, movement of the images on the guide fiber bundles (GFBs) can be used to track the telescope during observation, implicitly correcting for spine deflection. The GFBs travel from the Echidna core of the positioner assembly to the guide re-imaging system located alongside, on the instrument mounting plate (the electronics and ancillary equipment units shown in that location in Figure 89).

11.4.2 Design parameters for GFB re-imaging system

The following was considered commencing the design of the Guide Fiber Bundle re-imaging system:

- The guide fiber core diameter is 50 μ m. The input beam F/ratio is approximately F/2.
- The optimal CCD pixel size is $\sim 20\mu$ m with 1:1 imaging if the guide fiber output is to be adequately sampled. The magnification must be scaled appropriately if the CCD pixel size of the selected guide camera differs from this value.

- To reduce the size of the re-imaging optics and CCD chip size (the latter is favourable but not essential) the GFB connector should be as compact as possible.
- The GFB connector must allow for removal of a single guide fiber bundle, preferably without affecting the others. This allows for a quick module interchange if required.
- The GFB connector must house a minimum of 14 GFBs. The light from each GFB must be successfully imaged onto the chip with adequate sampling.
- A filter blocking $\lambda < 600\text{nm}$ is to be located in between the GFBs and CCD.
- The back-illumination of the GFBs (for guide spine location during a field configuration) is to be incorporated into re-imaging system.
- As always the difficulty of manufacture, ease of assembly and cost should be considered at all times.

11.4.3 Strawman design of the GFB re-imaging system

A schematic of the GFB re-imaging system is shown in Figure 104. It comprises a GFB connector supporting the output ends of the guide bundles, reimaging optics, and a sensitive CCD camera.

As discussed in Section 11.3.4.6, a possible guide camera is the model *ORCA-IIBT* from Hamamatsu Photonics. Extensive analysis selected this camera for the same role in FMOS-Echidna, and the requirements are essentially the same for WFMOS.

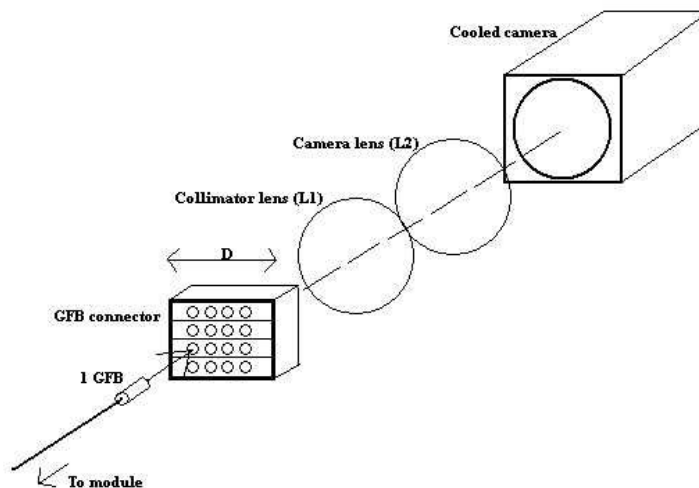


Figure 104. A schematic of the GFB re-imaging system.

11.4.3.1 GFB connector

Figure 105 shows a design for the GFB connector. The four layers are identical and each consists of a rectangular plate with 4 cylindrical sections removed. Each

of the cylindrical sections holds a GFB ferrule (OD 1.47mm). This plate is coloured white in Figure 105 and is shown with all components removed in Figure 106.

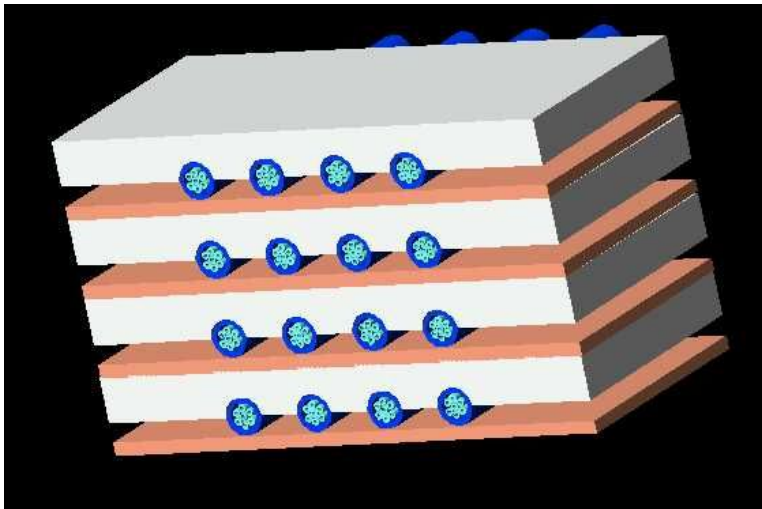


Figure 105. A concept design of the guide fiber bundle (GFB) connector (for schematic purposes only).

After each ferrule is placed in a corresponding cylindrical section, the plate is fastened to the layer below (fasteners are not shown in Figure 105). A section of compliant material (coloured orange in Figure 105) located in between each layer is compressed on fastening and locates the ferrules.

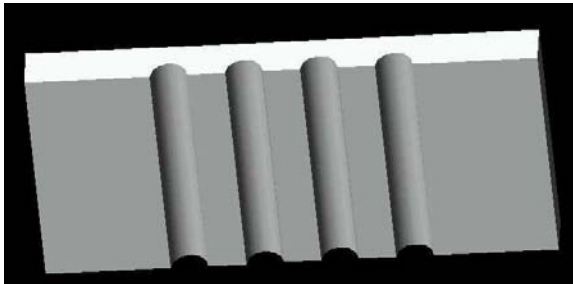


Figure 106. The ferrule plate.

Closer detail of the GFB ferrules is shown in Figure 107. The OD 1.47mm GFB ferrule (dark blue) houses 6 identical ferrules of OD 0.305mm (light blue). Cemented inside the latter ferrule is a single guide fiber. The spacing of the guide fibers in a single bundle prevents image crosstalk on the detector. Though 16 GFBs are shown in these figures, the precise number of bundles required for WF MOS is subject to final determination.

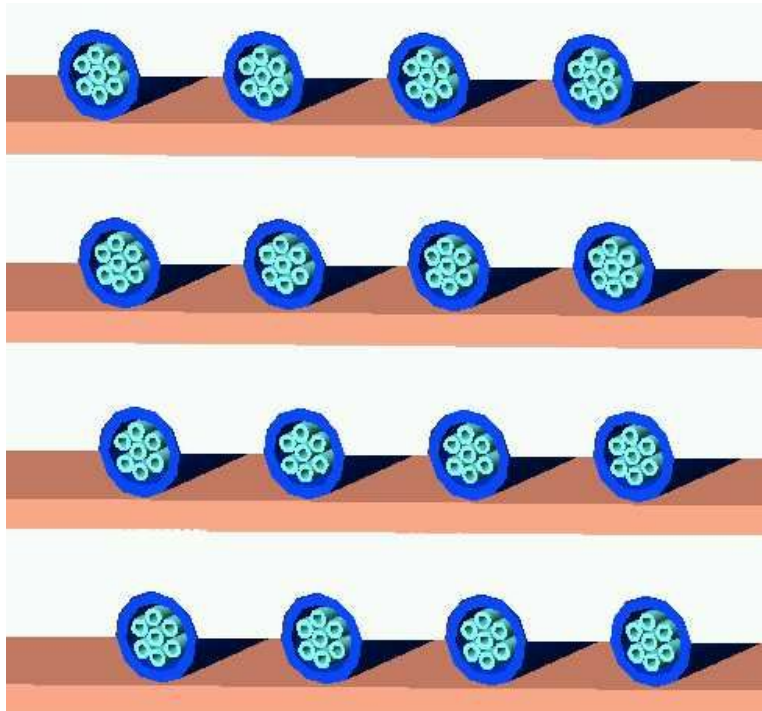


Figure 107. The fiber bundles inside the GFB ferrules.

11.4.3.2 *Curved object plane*

In order to use simple optics one requires the image or object plane be curved. We can achieve this for the object plane by:

- arranging the cylindrical sections in the ferrule plate such that they are non-parallel and
- using a curved reference surface to position the GFB ferrules before fastening the layers together.

Neither of the above requirements is considered challenging.

11.4.3.3 *Back-illumination for guide spines*

Clearly, the guide spines require back-illumination for position feedback in the same manner as the science spines, but this cannot be accomplished in the same way by slit illumination in the spectrograph. Following the FMOS-Echidna design, a relatively simple method of guide fiber bundle back-illumination can be implemented. This consists of 1-2 LEDs located in front of the guide camera providing uniform illumination simultaneously on all guide fiber bundles.

11.5 **Target allocation issues**

11.5.1 **Field configuration time**

FMOS-Echidna is able to reach any possible field configuration in a time under 10 minutes, and the target for WFMOS is to match this. However, the field configuration time in the FMOS system is dominated by the FPI system, which needs to raster its imaging camera on an x-y gantry across the field, collecting multiple subfield images for image processing. Experiments with the FMOS

development have shown that, within a dense pack of adjacent spines, approximately 5 measurement/movement iterations are required for all spines to reach their target destinations (). In this event, the overheads of the FPI dominate the configuration time.

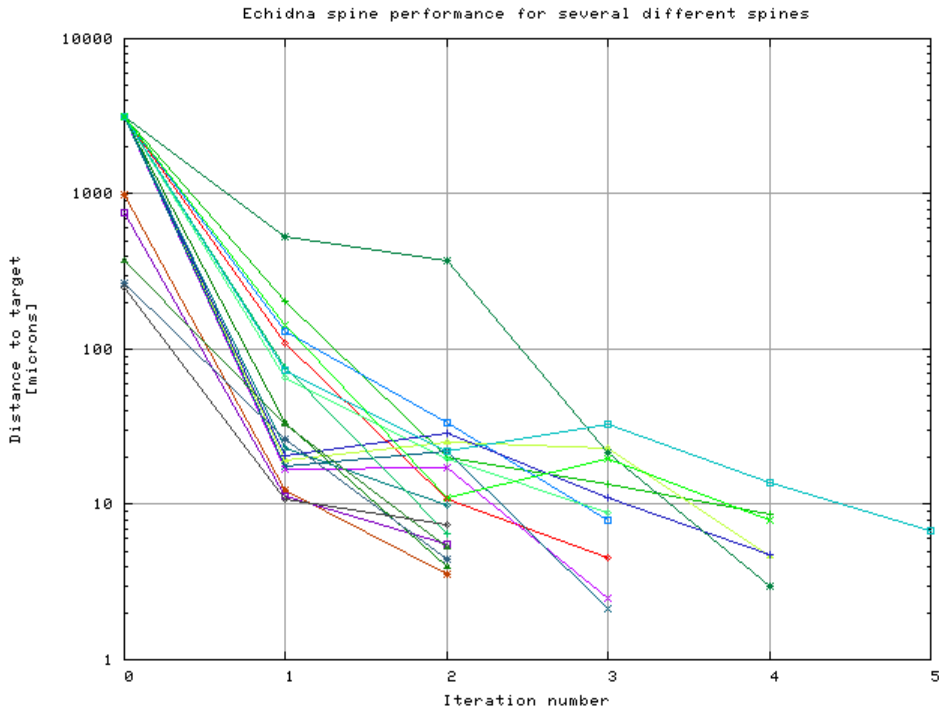


Figure 108. FMOS-Echidna test results showing movement performance of a close-packed set of spines. All spines reached target position within 5 measurement/movement iterations.

In WF MOS, this semi-mechanical FPI process is replaced by the STRIP system, and the FPI overhead should be significantly reduced. Offsetting this advantage is the greatly increased number of fibers to locate.

A time budget for field configuration yields an estimate for the WF MOS field configuration time of just two and a half minutes, as shown in Table 19.

Table 19. WF MOS field configuration time budget.

Collect images from STRIP camera	3 sets of images with differing backilluminated fiber sets (camera frame rate is high – allow one second for backillumination switching)	3 seconds
Analyse images	3 images from each of four, 2k by 2k quadrants; each image contains ~500 fiber images (estimate is ~52 seconds on FMOS 1GHz processor – use Moore’s Law to expect ten times speed improvement available for processor(s) procured in 2008).	5 seconds
Command positioner		2 seconds
Fibers move	Single movement iteration; assume smaller WF MOS actuators achieve 25% of FMOS spine tracking velocity	20 seconds
Total for a single movement iteration		30 seconds
Assume 5 iterations to reach final position	Total field configuration time	150 seconds

Note that the ‘matrix switching’ methodology described in Section 11.3.4.5 to reduce electronics costs and improve manufacturability of the module PCB potentially doubles the ‘spine movement’ periods in this estimate, consequently adding an extra 100 seconds to the configuration time.

11.5.2 Field coverage and target selection constraints

Although the positioner includes some 4500 fibers, there are significant constraints on how they may be allocated to targets. Each is able to patrol approximately to the ‘home position’ of its neighbours, which to a first order approximation means that any point in the target field can be allocated to any of three spines. This constraint alone imposes limits in the degree of clustering that can be accommodated.

Sky coverage and clustering capability is further limited by the allocation of spines to spectrographs as proposed in the Purple Book. On this model, one third of the spines are allocated to high-resolution spectrographs (predominantly for stellar work) and the remaining two-thirds to low-dispersion spectrographs for cosmological studies (distribution of dark energy). This significantly reduces ‘oversampling’ of the field. Allocation of a fraction of the spines to guide bundles and fiducials may further impact the target allocation capability, and should properly assess the impact of further erosion of field coverage that might be required should this study find that significant cost savings be available by modifying the present strawman positioner design in a way that affects sky coverage.

Individual science case studies will need to take account of the impact of available fibers and clustering capabilities for target allocation.

11.6 Cost forecast

The AAO’s experience in building the FMOS-Echidna fiber positioner is invaluable in reaching a robust cost forecast for a similar system component for WFMOS. The estimate offered is a synthesis of two approaches:

Firstly, detailed analysis of the FMOS-Echidna design and build data was used to construct an estimate for WFMOS-Echidna, by careful comparison, suitable adjustment, and scaling where appropriate. This estimate was undertaken by engineering staff largely responsible for design and manufacture of FMOS-Echidna and made extensive use of detailed records. A panel of AAO staff held an internal critical review of the estimate in conjunction with its originators and further reference to the estimate detail.

Secondly and quite independently, an estimate was constructed based on a product breakdown and schedule-building exercise. This approach takes better advantage of design innovations specifically proposed for the WFMOS incarnation of Echidna. The list below is indicative of the level of subcomponents that was considered – the full schedule developed extends to much greater detail for accurate estimation.

- Manufacture of module bases
- Module PCB

- Piezo elements
- Magnet/three-point-mounts
- Module assembly process
- Module magnetisation
- Carbon tubes
- Adaptor tube (=taper in FMOS)
- Counterweight
- Bullet-nosed pivot
- Spine assembly process
- Switch boards + connectors
- Support structure
- Fiber strain relief structures
- Positioner alignment tools
- Positioner core assembly and alignment process
- Control electronics package
- Instrument rotator
- Cable derotator
- Fiber derotator
- STRIP camera(s)
- STRIP camera lenses
- STRIP mount
- Positioner control software
- STRIP software
- Interface definition – mechanical
- Interface definition – electrical
- Interface definition – software/control
- Positioner set-to-work

- STRIP calibration
- Performance measurement
- Management overheads
- Other overheads (concept design, prototyping, travel, shipping, documentation)
- Contingency

A critical review panel of AAO staff synthesised the final estimates based on a point-by-point discussion of the two independent costings.

Chapter 12 Fiber Cable

12.1 Summary of Strawman specification

A summary of the strawman specification for the fiber cable is given below in Table 20. For this chapter the 1.5° corrector option with ~ 4500 spines (see *Chapter 8, Wide Field Corrector*) has been assumed for both the Subaru and Gemini implementations. The 2° corrector option for Subaru with ~ 6000 spines is not considered here.

Table 20 Strawman specification for the fiber cable.

	Subaru	Gemini
Number of “active” spine	4500	4500
Number of spine modules	44	44
Number of spine per module	140	140
Fiber per connector	140 (2 rows of 70 fibers)	140 (2 rows of 70 fibers)
Thin fiber core size	100 μ m	100 μ m
Thin fiber length	10m (Including Rotator)	10m (Including Rotator)
Thin fiber f/ratio	f/2	f/2
Thick fiber core size	200 μ m	200 μ m
Thick fiber length	30m (10 on telescope, 10 hung, 10m in spectrograph room)	50m
Thick fiber f/ratio	f/4	f/4
Spectrograph location	Upper Nasmyth room	Pier Lab
Fiber route	Free loop by “Great Wall”	Pier chimney via elevation wrap
Total fiber run	40m	60m
Fiber mapping	1/3 high res, 2/3 low res	1/3 high res, 2/3 low res
Wavelength of system	390-1000nm	390-1000nm

12.2 Terminology

Fiber Cable: The whole fiber assembly containing ~4500 fibers

Fiber Bundle: A sub-assembly of fiber cable containing ~34 fibers within kink resistant tubing

12.3 General design concept

12.3.1 Fiber type and specification

The fiber run may be regarded in two distinct sections; the first from the fiber positioner to the fiber connectors (“thin fiber”), requiring high numerical aperture optical fibers ($NA > 0.28$) to accommodate the fast input beam and spine tilt, and a second section from the fiber connectors to the spectrograph (thick fiber), only needing moderate NA optical fibers (an NA of 0.13 or greater). The f/4 beam speed is suitable for the standard high transmission multimode silica optical fibers as they typically have an NA of 0.22 ± 0.02 and would be used from connectors to the spectrographs. However, the higher NA optical fiber required for the fiber positioner to the fiber connector will be more specialised. The slower beam speed

(f/4) has been optimised to minimise FRD, maximise scrambling and suit the spectrograph collimator design.

The optical fiber thin core size of 100 μm at the input has been selected to provide ~ 1 arcsec aperture on the sky. In order to ensure good red performance, the optical fiber core-to-cladding ratio should be chosen such that the cladding is at least 10 μm thick, leading to a core:cladding ratio of 1:1.2 for the thin fiber and 1:1.1 for the thick fiber.

12.3.2 Expected fiber throughput & FRD performance

Historically, a choice between a red optimised (Ultra low OH) and blue optimised (High OH) “standard” (silica core and doped silica cladding) optical fiber has been necessary. In the KAOS purple book STU fiber was proposed that was a compromise between the high and low OH optical fiber. Since then a new type of broadband optical fiber has been developed, providing low attenuation characteristics over the whole optical window, see Figure 109.

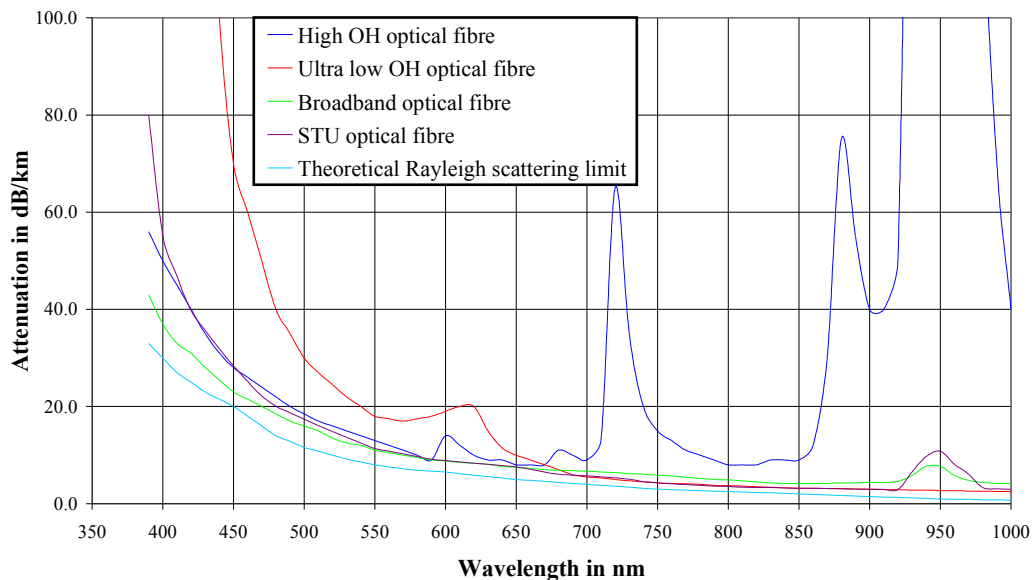


Figure 109: Attenuation data for low OH, High OH, STU and Broadband optical fiber types. The plots have been derived from the manufacturer’s data sheets and only include attenuation losses within the bulk material of the optical fiber.

In the blue, the new broadband optical fiber performs close the theoretical Rayleigh scattering limit for silica, having better than 60% transmission down to the 390nm specification for a length of 50m or less, however, minimising the optical fiber length is still desirable (see Figure 110 thick core fiber). Fiber with NA greater than >0.22 typically uses a polymer cladding material and has poorer “blue” performance than all-silica optical fibers. The transmission data for the higher NA thin core fiber over the wavelength range 390nm to 500nm is a model based on the manufactures data between 500nm to 700nm and follows the Rayleigh scattering limited performance that is typical of all silica optical fibers in the blue, however, the model does not account for unexpected absorption features introduced by the polymer cladding used in these fibers. Experimental data for the region between 390 –500nm is being sought from fiber manufacturers for the higher NA (“thin”) fiber.

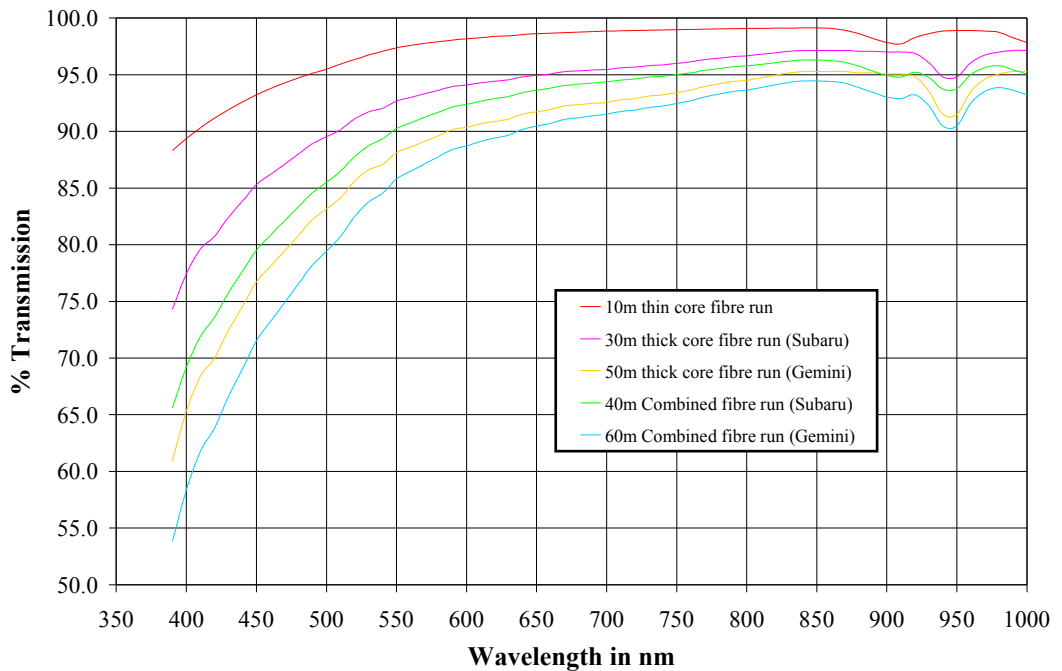


Figure 110: Bulk transmissions for the separate and combined sections of the optical fiber run for Subaru and Gemini WFMOS implementations. The “thin” core is a high NA (0.37) polymer clad optical fiber (NOTE: the data between 500nm and 390nm for this fiber has been modelled using a Rayleigh scattering assumption). The “thick” core is an all-silica broadband optical fiber. This data included material absorption losses in the fiber only, and does not include any sources of FRD or end reflection losses.

It is clear from Figure 110 that for optimal blue performance it is desirable to minimise the total length of the optical fiber run, however, even the 60m Gemini optical fiber run would have an estimated bulk transmission of around 54% at the most extreme blue wavelength (390nm) and greater than 80% for most of the wavelength range (i.e. 500nm and beyond).

Note: If the Subaru near infrared extension is considered, the performance of the broadband optical fiber from 1.0 – 1.8 μm is comparable with its performance beyond 500nm (i.e. below 20dB/km) with the exception of a significant absorption feature at $\sim 1400\text{nm}$ ($\sim 100\text{dB/km}$). The polymer clad optical fiber attenuation rises above 20dB/km beyond $\sim 1120\text{nm}$ as a result of a $\sim 70\text{dB/km}$ absorption feature at $\sim 1180\text{nm}$. The performance returns to below 20dB/km by $\sim 1270\text{nm}$; however, there is no manufacturer’s data available beyond 1300nm, further information is being sought.

The FRD performance of the broadband fiber is very good⁷ with the intrinsic fiber FRD performance expected to marginally degrade the input beam (for an $f/4$ input), such that more than 90% of the encircled energy would remain in an equivalent output beam (i.e. an $f/4$ output) over a fiber run of 50m or more. The FRD performance of the polymer-clad fiber has not been quantified, but is not expected to be significantly worse than the broadband fiber.

Losses in the fiber connectors and reflection losses have not been included in the previous analysis. Anti-reflection coating to all air/glass surfaces should reduce

⁷ Haynes, R.; Bland-Hawthorn, J.; Klein, K.; Large, M.; Nelson, G; “New age fibers: the children of the photonic revolution” *SPIE Proceedings, Astronomical Telescopes and Instrumentation 2004*, Vol. 5494-74, 2004.

reflection losses to $\sim 1\%$ per surface and the AR coating of optical fiber end faces is a rapidly maturing technology.

12.3.3 *Robot to Spectrograph mapping*

The fiber positioner-to-spectrograph mapping is unchanged from the KAOS Purple Book concept (see Figure 111), with 2/3 of the optical fibers for low-resolution work and 1/3 for high resolution. The optical fiber requirement for both resolution extremes is the same. Remapping of the module layout into groups of fibers relating to individual spectrographs will be carried out at the fiber connectors. The details of the specific spine-to-spectrograph mapping will be addressed in later phases of the project.

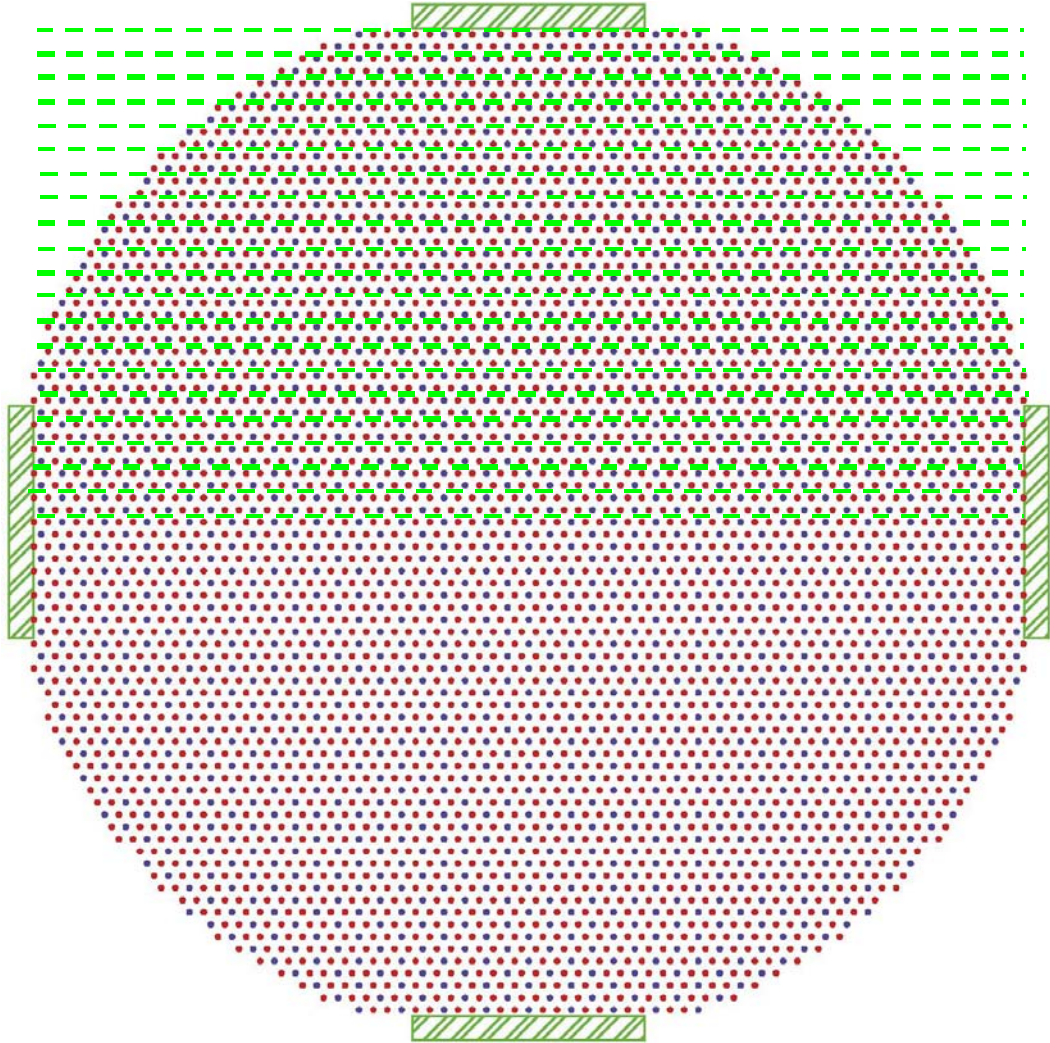


Figure 111: Schematic of the optical fiber arrangement for the low-resolution (red) and high-resolution (blue) spectrographs. Fiber positioner modules (shown in green) each carry a maximum of ~ 140 “active” optical fibers, although only those available positions within the corrected instrument field of view will be populated.

12.3.4 *Fiber environment*

The optical fiber cable has to be able to operate over temperature ranges of -5°C to 30°C and relative humidity of up to 95%. There are a number of mechanical considerations along the cable route and these are addressed in the telescope-

specific sections of this chapter, however, the top end rotation unit is similar in both implementations.

12.3.5 Fiber housing

Along virtually all of the cable's length, the fibers will be housed within a bend limiting, kink and crush resistant tubing used in the FMOS project. There will be ~135 of these bundles each containing ~34 optical fibers, to comprise the full cable assembly. The only places where the fibers will not be protected in this tubing are within the spine modules where fibers are distributed to the individual spines, within the fiber connectors (*Chapter 13, Fiber Connector*), and within the spectrograph slit assemblies, i.e. where the cable has to be distributed into individual fibers.

12.3.6 Top end rotation unit

The rotation unit, forming part of the PFU, is outlined in *Chapter 11, Positioner*. The fiber bundles (~34 fibers/bundle, housed within kink-resistant tubing), that make up the fiber cable, will be carried within an 'energy chain' folded within the enclosure surrounding the hexapod, in a fashion similar to a standard electrical cable wrap. Due to the potential risk to the fibers in the rotator, a section of the energy chain assembly will be prototyped to fully confirm the design. The location of the fiber connectors on Subaru will be close to the PFU, but in a Gemini implementation they would be located at the outer edge of the top end ring. The fiber connectors are where the 1:2 focal ratio conversion and fiber core size change will take place (see *Chapter 13, Fiber Connector*).

12.3.7 Cable Assembly, testing and quality assurance

The fiber cable for WFMOS would be amongst the largest fiber cables assembled for astronomy (the VIMOS IFU for the VLT has ~ 6400 fibers). For telescope counterbalance and drive load reasons (see section 12.4.9) the cable is designed to be lightweight, yet robust. Fiber assemblies of this size are uncommon in astronomy, but a fiber assembly of ~1 million fibers has been produced for CERN as part of their high-energy particle detector system, see Figure 112.



Figure 112: Picture of section the fiber assemblies for the CERN LHC detector system, courtesy of Gary Nelson and Prof. Karl Klein of Polymicro Technology LLC.

The general polishing, assembly, testing and quality assurance for the WMOS fiber cable could be carried out using standard techniques developed over the past 10-15 years. However, very large numbers of fibers and overall lengths do require particular consideration.

When assembling fiber cables, it is often necessary to lay the fiber tubing out straight in order to ease threading the optical fibers into the tube, this would require “dust free” areas of around 50m in length in which the fiber cables could be assembled.

Because of the number of optical fiber and length of the fiber cable it would be highly advisable to carry out testing and quality assurance during each step of the assembly process as remedial work after assembly is likely to involve a significant overhead. Particular attention should be paid to sources of FRD as the system performance penalties from severe FRD would be large.

12.3.8 Interlocks and safety management

The fiber cable on either telescope implementation follows a route that includes a number of potential hazards that could, if not properly managed, damage the fiber cable or the telescope systems. The overall design specifically minimises these risks through design, route and interlocks. Most of these issues are addressed within this chapter under the specific sections of the fiber cable, however, the distributed interlock and safety system is detailed below.

12.3.9 Fiber cable health monitoring

12.3.9.1 Design overview

There are two main aims of fiber cable health monitoring. The first is to prevent breakage of the fiber cable and the second is longer term monitoring of the cable, to ensure that the “as delivered” performance is maintained. The proposed design is based on monitoring the FRD of sample fibers, checking for significant changes that would indicate a change in the strain on the fiber.

12.3.9.2 Set limits

There are two distinct scenarios that should trigger action. The first is when the fiber cable appears to be in imminent danger of breakage, typified by a rapid increase in FRD over many fibers within the cable. This should precipitate an alarm and immediate emergency stop of all telescope and dome movement, followed by immediate investigation of the problem. The second scenario is longer term degradation in performance, which is below the limits set for an emergency stop. Such a scenario would indicate building up strain from possible kinking within the fiber cable and though it shouldn't require an emergency stop, but should be investigated at the earliest convenient time. The emergency limits could be set both for degree of FRD loss and rate of change of FRD. The precise details of the system will need to be carefully evaluated in the next phases of the project.

12.3.9.3 Description of the optical system

The optical layout of the fiber “health” system is shown in Figure 113. The light from a source LED is re-imaged onto the fiber input face using a small lens mounted close to the LED. The fiber output would be re-imaged onto the photodiode. The output aperture would vignette that part of the beam that has been degraded by the fiber FRD and this would be registered by the photodiode.

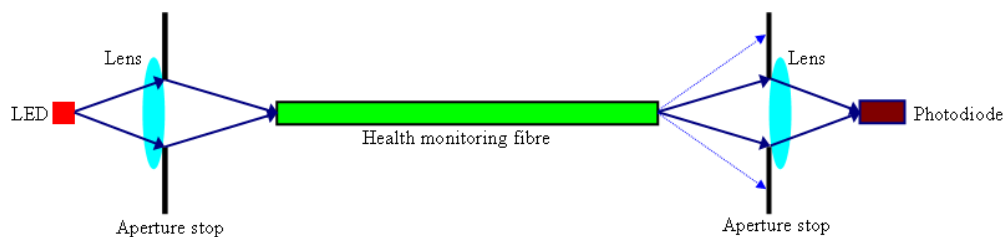


Figure 113: Schematic layout of the WF MOS cable fiber health monitoring system.

The science fibers could also be checked at regular intervals to monitor long term maintenance of their performance.

12.3.9.4 Fiber health monitoring electronics

The fiber cable “health” monitor system provides a quantitative indication of the integrity of the fibers in the fiber cable. The attenuation of light from a calibrated source by the cable is measured and can be made available for current cable quality. The data may also be recorded for long term trend analysis and indication.

A number of fibers in the cable (135 are currently envisaged) are available for this purpose. The system described is capable of accepting up to 136 fibers. The fiber cable health monitor consists of a launch system and a metering system.

The launch system consists of one LED source for each monitor fiber in the cable. The LEDs operate at 1300-1500 nanometers and are supplied from a continuously running (perhaps remotely controlled) stabilised power supply. The launch system would be located near the spectrograph end of the fiber cable, with appropriate connection to the fiber cable.

The metering system consists of a photodiode and preamplifier for each monitor fiber. The preamplifier outputs are input to analog to digital converters via an analog multiplexing arrangement. The analog multiplexer and analog to digital converters are controlled by a suitable microcontroller with a LAN interface. The metering system would be under the control of the fiber positioner control computer, via a private LAN connection, and would be located in the Prime Focus Unit near the fiber positioner, with appropriate connection to the fiber cable.

A block diagram of the system is shown in Figure 114. It is envisaged that the launch and metering systems could each be implemented in single 482.6mm wide, 3U rack mounted chassis.

12.3.9.4.1 Interfaces

- Private LAN connection (Metering System)
- Mains power connection (Source and Metering Systems)

12.3.9.4.2 Issues

If remote control of the launch system is desired, this could either be done using a microcontroller with a Control LAN interface, or a direct hardware link (e.g. using a Telescope infra-structure fiber). The concept design will identify any such requirement, and propose a suitable control method.

Prototyping of circuits or systems regarded as “high risk” because they involve the use of new technology or techniques or they have a high level of complexity, is usually carried out in the concept or preliminary design phases in order to provide “proof of concept”. Prototyping of the LED launch and photodiode metering electronics would be carried out during the concept design.

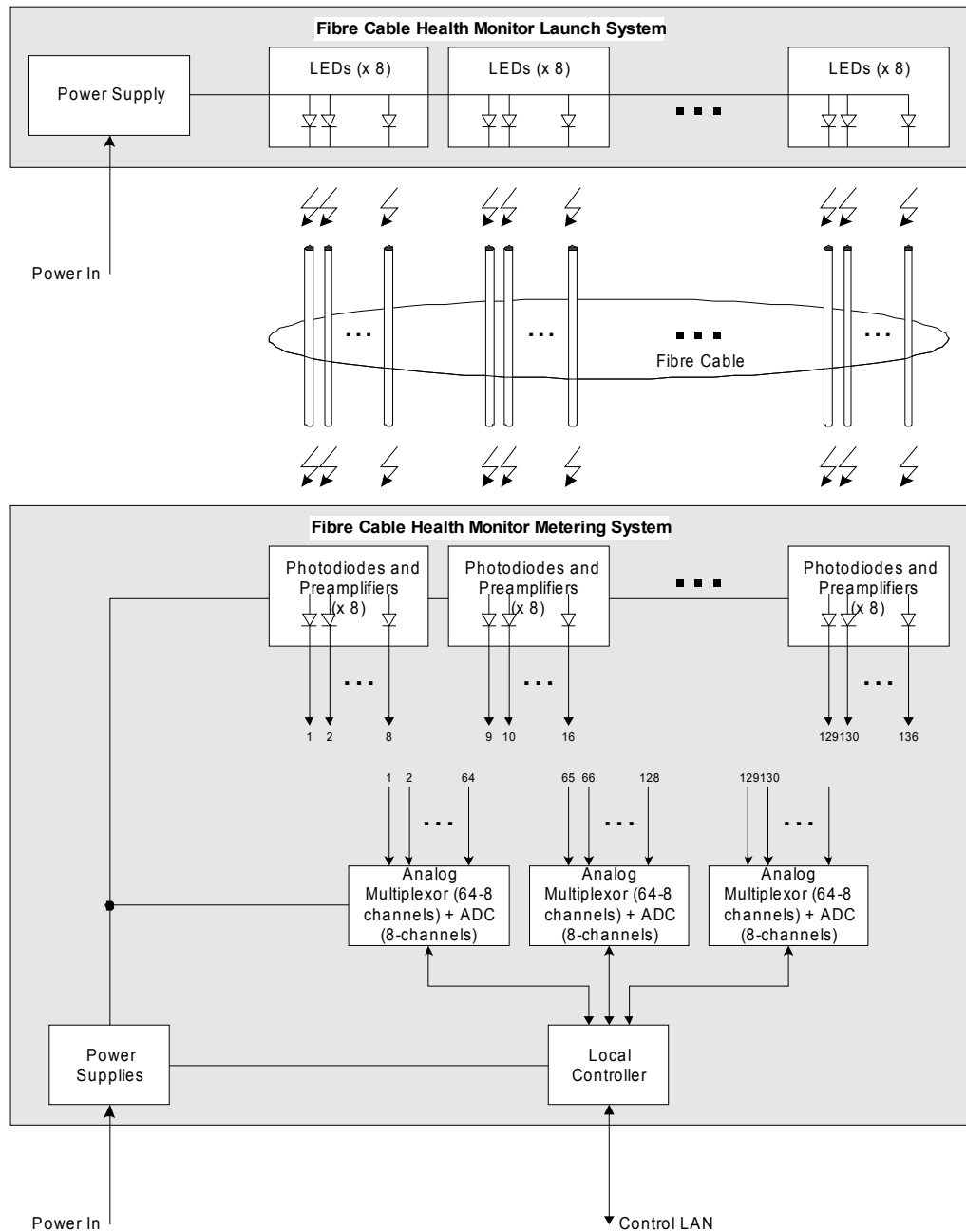


Figure 114: Fiber Cable Health Monitoring System

12.3.9.4.3 Electronics Cooling

The launch system electronics are likely to be located in the same room as the Spectrographs, which are of an open design. It may be necessary to provide active cooling of the control electronics enclosure to minimise the heating effects of the electronics equipment on the spectrograph room environment.

The metering electronics are likely to be located at the Prime Focus Unit, near to the fiber positioner electronics. As such, they are likely to be in the same cooled enclosure as the fiber positioner electronics.

It is expected that a thermal analysis will be carried out during concept design to determine the cooling requirements.

12.3.9.4.4 Power

The power requirements of the Fiber Cable Health Monitor electronics are not expected to be large (i.e. < 250W). However, a more thorough estimate of power consumption will be carried out during the concept design.

12.3.9.4.5 Observatory Electronics Design Requirements

As far as possible, the design of the Fiber Cable Health Monitor electronics will comply with any requirements defined in the relevant electronics design specifications and standards relating to Observatory instrumentation. The concept design will identify the relevant specifications and standards.

12.3.9.4.6 Environmental Requirements

The selection and design of electronics components for the Fiber Cable Health Monitor electronics will take into consideration the environmental requirements and operating conditions of the Observatory. The concept design will identify the relevant environmental requirements.

12.3.9.4.7 Electro-Magnetic Compatibility (EMC)

The design of the Fiber Cable Health Monitor electronics will be undertaken to meet all the relevant requirements for Electro-Magnetic Compatibility for Observatory instrumentation. Achievement of EMC requires an understanding of interference coupling mechanisms, consideration of EMC in equipment layout, grounding and circuit design, application of appropriate filtering and shielding of interfaces and the testing and evaluation for EMC continuously through the project. Observatory EMC requirements will be identified during the concept design.

12.3.10 Operation, repair and maintenance requirements

Both sections (thin and thick core) of the cable will be designed with a maintenance free approach, with the health monitoring in place to highlight any degradation in performance. In the unlikely event that repair is necessary for either the thin or thick core sections of the fiber cable, it is likely that the whole cable assembly would have to be removed from the telescope to allow the cable to be laid out straight, in order to run new fibers or bundles. Currently, because of the maintenance/repair free philosophy and in order to minimise mass and volume, it has been assumed that there will not be any level of redundancy within the fiber cable for the eventuality of repair. This would be reviewed in the next phase of the project. If deemed necessary at the later stage schemes with extra fibers in each bundle (as is implemented in FMOS) would be feasible. However, the re-mapping from positioner to spectrographs and the fiber connector scheme would necessitate a potentially complex and relatively costly design.

For a Subaru implementation of WMOS, the intention is that the entire cable run be taken off the telescope when the instrument is removed. Fibres will not be disconnected from the spectrographs, and accordingly the hanging loop section of cable can be stored hanging against the 'Great Wall', possibly behind a protective cover. An arrangement to bring it into the spectrograph room may be possible although this would be an additional complication.

The design philosophy for a Gemini implementation is to permanently house the thick core section of the fiber cable on the telescope, i.e. the whole fiber run from the top end fiber connectors through to the spectrographs. The only reason to remove this section of the fiber cable would be for an extreme case where the repair of a section of the telescope requires its removal or where damage to the fiber cable requires repair. Routine operation and maintenance of the telescope should be possible without disturbing the cable.

12.3.11 **Fiber slit units**

Bundles of fibers enter each spectrograph to make up the ‘slits’ feeding the spectrograph collimators. Slit units would of course be specific to each spectrograph design. However, they are expected to follow the same basic principle. Fiber slit technology is well developed and has been used on numerous fiber spectrographs such as 2dF, FLAMES, Hectospec and PMAS, where a number of small flat-ended slitlets containing a few fibers are mounted side by side to make up a large curved slit unit (see Figure 115 and *Chapters 14 and 15*). There should be little generic risk associated with these units.

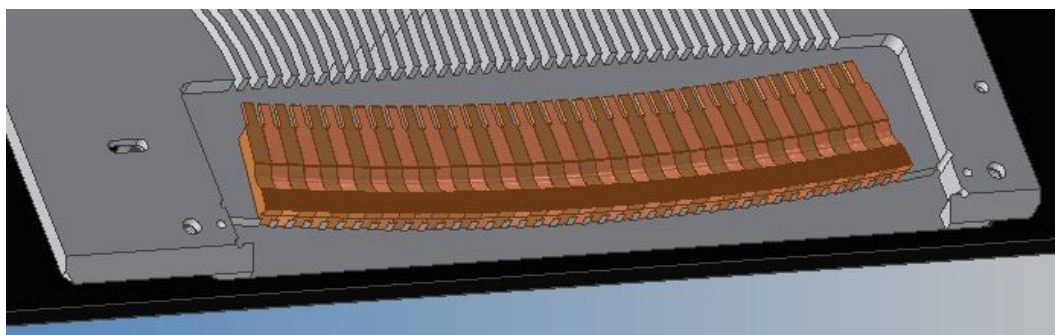


Figure 115: Diagram of the fiber slit unit for AAOmega. The slitlets are shown alternating brown and pink for clarity. Each slitlet contains 10 fibers, which are fed away from the slit along the channels shown behind the slitlets. Each slitlet is polished flat and arranged to form a curved pseudo-slit.

12.4 **Subaru issues**

This section concentrates on the Subaru-specific implementation and those areas where the fiber cable system for the Subaru telescope would differ significantly from those on Gemini. As previously stated, the thin-core section on the telescope top end will differ little between the two possible telescope implementations. From the fiber connectors onwards, the cable route differs greatly.

12.4.1 **Spectrograph interface and location for Subaru**

The baselined location of the spectrographs on Subaru is in the upper nasmyth room of the optical side of the dome (Figure 116). The main spectrograph cable interfaces are the fiber slit units (discussed above) and the field re-formatting that is to be carried out at the connectors. The location of the spectrographs in the upper nasmyth room allows a Subaru implementation to have a fiber cable 20m or more shorter than a Gemini system, reducing the expected fiber attenuation losses from ~42% to 30% at the extreme blue wavelengths. The nasmyth location also reduces the movement axes compared to Gemini by eliminating differential

azimuthal motion and allowing a different method to address the telescope elevation axis motion; see 12.4.11 (Fiber cable hanging loop).

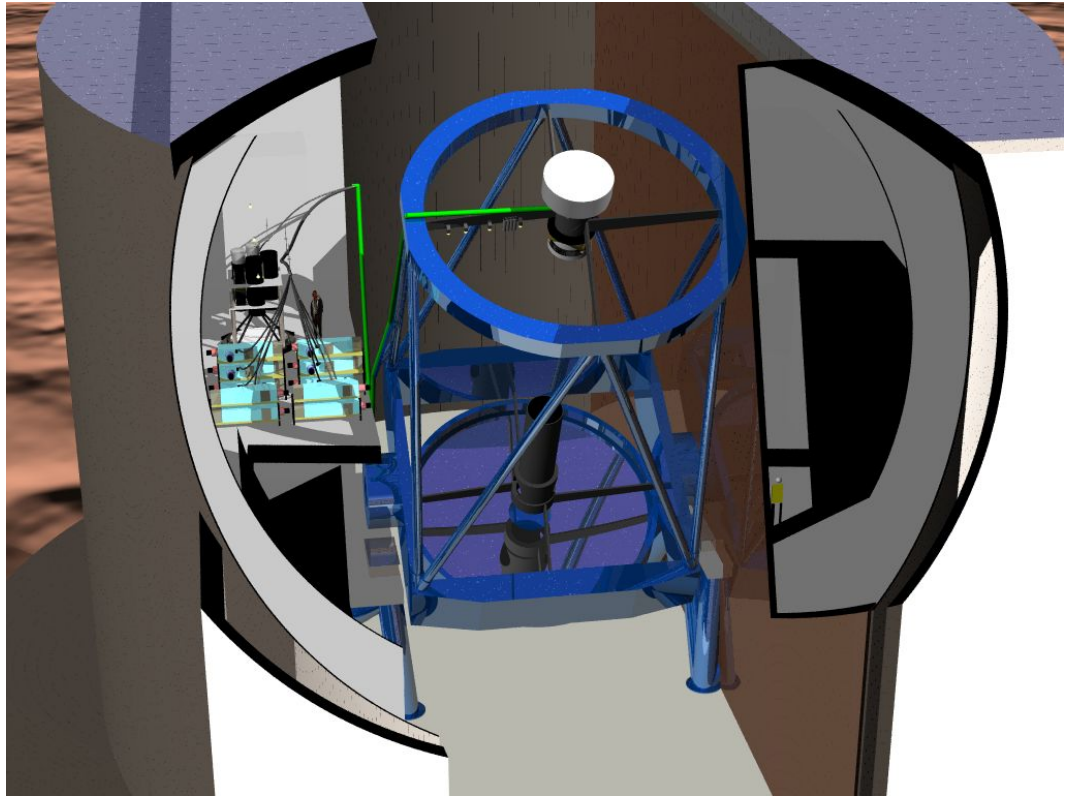


Figure 116: Proposed layout of the WFMOS system on Subaru, the fiber cable is green.

12.4.2 Fiber positioner opto-mechanical fiber interface for Subaru

The wide field corrector (see *Chapter 8, Wide Field Corrector*), nominally provides an $f/2.4$ beam, that when combined with the maximum spine tilt angle (see *Chapter 11, Positioner*) can give up to an $f/2.0$ input into the optical fibers. As previously discussed, this necessitates the use of high NA fibers between the spine tips and the fiber connectors. The route, strain relief and organisation of the fibers within the spine modules has been addressed for FMOS (see Figure 117) and a similar system could be used for WFMOS, but with up to 4 (the field centre with all the spines populated with fibers) kink resistant fiber bundles feeding from each module. These fiber bundles feed through the top end derotator and into the fiber connector mounted near the PFU.

12.4.3 Connector interface and location

The details and proposed location of the fiber connectors are addressed in more detail in *Chapter 13, Fiber Connector*. In order to prevent possible damage to the telescope or WFMOS it is recommended that an interlock system is developed for the fiber connectors to ensure that the PFU cannot be removed without releasing the fiber connectors. The details of this system will be developed in later phases of the project along with the details of the precise spine – fiber bundle – connector mapping.

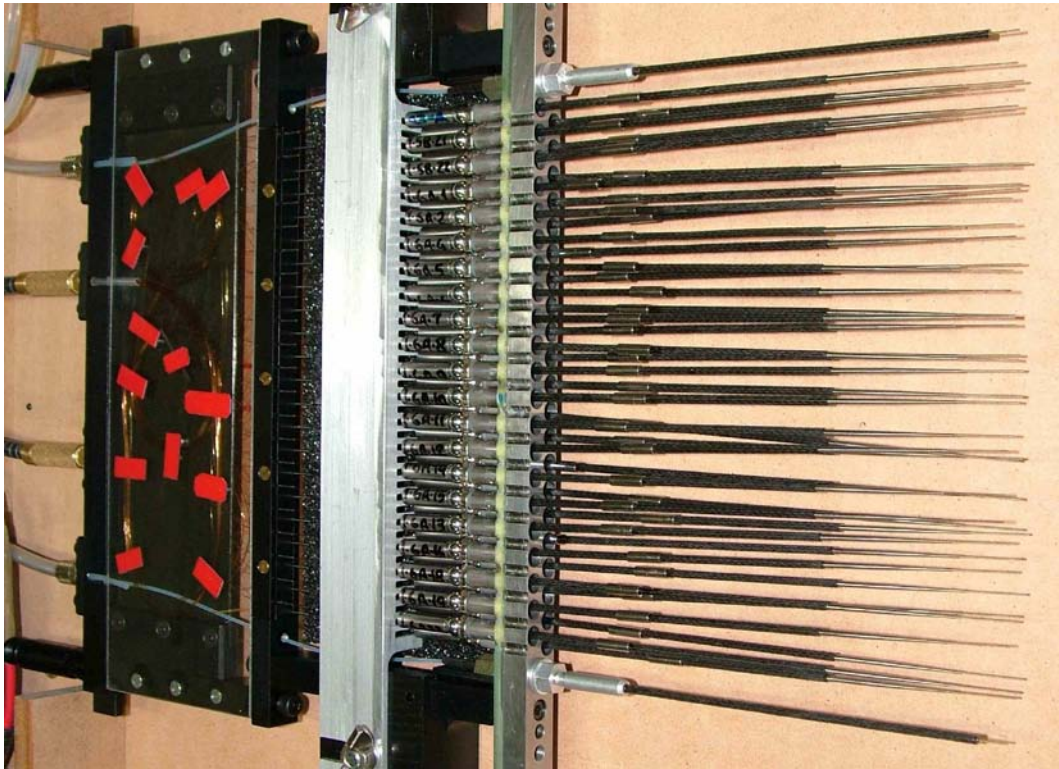


Figure 117: An FMOS spine unit packed for shipping with fiber distributions section at the left hand side (black with clear plastic cover). The science fibers are fed from the spines into two kink-resistant cables fixed to the module with brass ferrules (far left). The outer two cables contain fiducial fibers for position reference.

12.4.4 Subaru Operational issues

The most significant fiber cable operation issues for Subaru appear to be the top end rotator, the fiber health monitoring system and the fiber cable hanging loop. Further discussion and development of specific operational requirements and system design details must involve Subaru in the next phases of the project. The fiber cable is visualised to be a maintenance-free system, so it should only be interfaces with telescope systems that would impact operations.

12.4.5 Subaru fiber run from connectors to the spectrographs

The proposed route of the fiber cable from the connectors to the spectrographs is shown in Figure 118. Here, the fiber cable runs from the fiber connectors along a spider vane to the outer edge of the top end ring. A support frame mounted to the telescope truss structure guides it down from the top end to a point approximately 3 meters above the telescope elevation axis (see Figure 120). From there the cable hangs in a loop to an attachment point on the “Great Wall” outside the upper nasmyth spectrograph room (see section 12.4.11). Within the spectrograph room, fiber bundles are distributed to the various spectrographs, most likely using a simple cable tray system often used for electrical cable distribution.

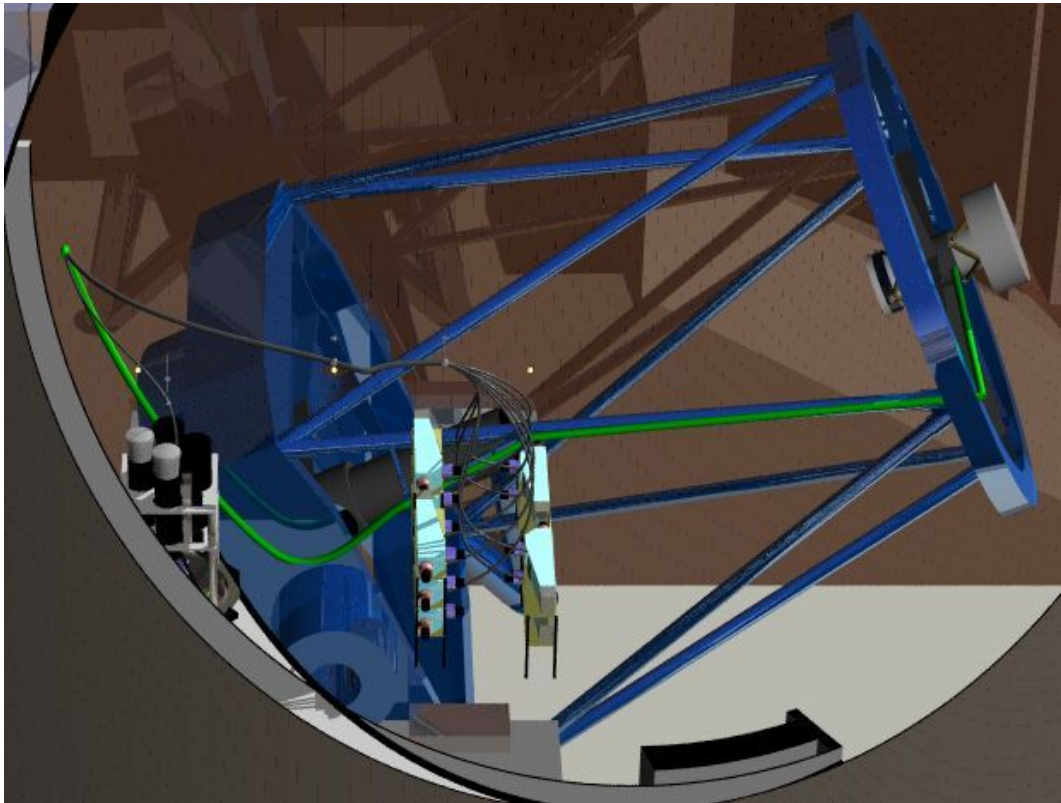


Figure 118: Diagram of the fiber cable route for the WFMOS system on the Subaru telescope. The fiber cable is marked in green inside the dome area and grey once it penetrates the “Great wall” into the upper Nasmyth spectrograph room.

12.4.6 *Fiber cable design Subaru*

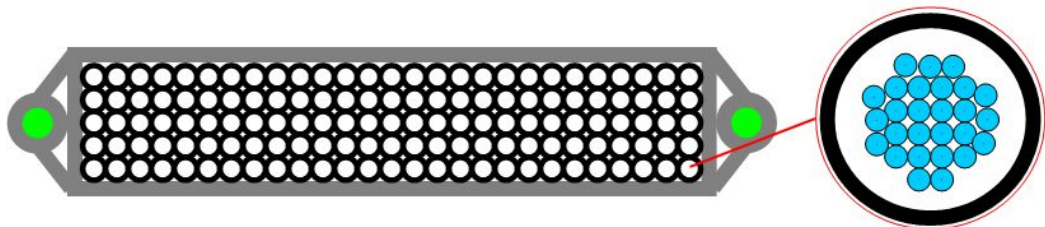


Figure 119: Schematic cross-section of the fiber cable for WFMOS on Subaru at one of the binding points. The black circles represent the kink-resistant tubing and the green is a re-enforcing steel cable. Shown in grey is the one of the binding clamps, which are spaced at regular intervals. Blue circles represent the fibers inside the kink-resistant tubing; this is purely schematic as they would take up much less room within the tubing, with 35 fibers filling less than 25% of the area of the tube cross-section.

The “thin” fiber cable is described previously (12.3.4). Beyond the fiber connectors it is proposed that the fiber cable be made up of ~135 fiber bundles each containing ~34 fibers (see Figure 119). These could be housed together in the fiber cable made up of 5 layers each containing 27 fiber bundles (OD ~ 6.5mm) within the kink-resistant tubing. The cross-sectional dimensions of such a fiber cable would be ~ 35mm by 200mm. The fiber packing fraction within the tubing is less than 25%, allowing the fibers to move freely inside. The cable of 135 tubes would be loosely bound at regular intervals to maintain the overall shape. Such a structure should allow for differential length changes as the fiber cable bends to accommodate the changes in telescope elevation angle. The design would provide

a light weight (<5kg/m) cable design that is robust and flexible enough in one plane to allow the telescope to move freely.

Binding clamps at regular intervals along the cable maintain the bundle shape also hold reinforcing steel cables – the steel cable length in each clamped segment will be slightly shorted than the fibre and tubing lengths, to minimise strain and allow for bending.

It will be vital to ensure the fiber cable design does not strain or over-bend the fibers, this leading to poor FRD performance (introducing possible severe light losses in the system) and in extreme cases to fiber breakages. Many techniques for minimising fiber strain have been developed over the past decade and more, some that may be suitable for WFMOS have been used in both the FMOS and AAOmega fiber cables. The choice of the most effective strain relief (to compensate for fiber movement and differential thermal expansion/contract of material along the cables length) techniques will become more apparent as the system design develops. Any strain relief would preferably be implemented within those sections of the cable that are reasonably well constrained, such as close to the positioner, along the top end support veins, down the telescope truss and inside the spectrograph room. Some prototyping of the higher risk section of the cable, particularly where telescope or positioner motion has to be accommodated would be highly advisable.

12.4.7 Fiber cable integration Subaru

The integration of the thick core section of fiber cable at the Subaru telescope should not provide any particular challenges, the most complex section being the hanging loop and routing into the spectrographs. The fiber slits units of two of the spectrograph designs (see *Chapters 14 and 15*) would be in the collimator beam, so minimising the cross-section area that could vignette the beam would be important. The small core section that feeds through the top end rotator would also require significant attention in order to minimise the problems of integrating the cable with the positioner, the rotator and the fiber connectors.

12.4.8 Fiber cable risks for Subaru

Since FRD can have such a big impact on the overall system performance it would be highly advisable to carry out some prototyping of all sections of the fiber cable, with particular attention on the top end rotator and hanging fiber loop. Once detailed discussions have taken place with Subaru, it may transpire that the perceived risk of damage to the fiber cable resulting from their operational requirements increases significantly. It therefore may be necessary add extra re-enforcement to the cable beyond that currently envisaged. However, at this stage it is deemed unnecessary and undesirable, also the re-enforcement would increase the working stiffness and weight of the cable impacting the load on the telescope elevation axis (see section 12.4.11). Other factors that need to be considered in the fiber cable design are differential thermal expansion/contraction, fiber creep, possible kink points, positioner to spectrograph mapping and any repair/maintenance requirements (though the current system has been envisaged as maintenance free).

12.4.9 Counter weights and cable to telescope loading

Some concerns have been expressed with regards to load the fiber cable will put on the telescope drives and structure. As currently envisaged the load introduced by the cable does not require the addition of a counterweight system (see section 12.4.11). However, a small trimming weight would reduce the moment to less than 10 Nm for most telescope elevations (see Figure 122).

12.4.10 Guide fiber requirements - Subaru

The guide fiber system requirements are discussed in *Chapter 11, Positioner* and has 14-20 guide spines each composed of a group of seven hexagonal close packed high NA (>0.25 in order to accept the maximum $f/2.0$ beam) and fiber core size $\sim 50\mu\text{m}$. Other than the higher NA fibers, the WF MOS guide system would be similar to the system already designed for FMOS and should not present any significant development concerns.

12.4.11 Fiber cable hanging loop

Concern has been raised regarding the capacity of the telescope elevation drive to accommodate the varying loads applied by a hanging length of fiber cable as the telescope tracks in elevation. This section provides a brief justification for the concept, showing that the applied loads are well within capabilities.

The routing requirement for the fiber cable is to deliver the fibers from the fiber positioner to the spectrographs with a minimum of cable length, a minimum of stress to the cable and a minimum of additional load to the telescope. The proposed route to accomplish these aims involves a hanging loop of cable between the telescope structure and the enclosure wall, close to the spectrographs.

In order to minimise loads on the telescope drive systems, it is clear that the fixed end of the hanging loop (*i.e.* the spectrograph end) should be attached as high as reasonable to the enclosure wall, and that the moving ('telescope' end) of the hanging loop should be attached low on the telescope structure. Minimising cable stress during telescope motion can be achieved by locating the telescope attachment point off of the centreline of the telescope so that its 90-degree arc of motion involves predominantly horizontal translation. With the fixed end of the hanging loop further away from the telescope's centreline, this arrangement ensures that the entire movement of the hanging cable is reduced to a gentle opening and closing of a loop, with no need for the cable to cross itself. The end points can be fixed in direction, eliminating the need for pivoting attachments. Figure 120 shows the proposed geometry, including initial guesses for the locations of the endpoints.

This loop is assumed to hang close to the enclosure wall to distance it as much as possible from the telescope structure and minimise the likelihood of snagging on any other equipment. The proposed structure of the cable itself (discussed in section 12.4.6) renders it inherently resistant to flexure in any plane except that of its loop.

The free loop of cable will hang approximately into a catenary form (modified slightly by the cable stiffness and the end-point direction fixed by the attachments). For ease of analysis, the cable shape is fitted to a parabolic form – a

parabola is probably closer to a true catenary than whatever shape a physical cable is likely to reach in practice.

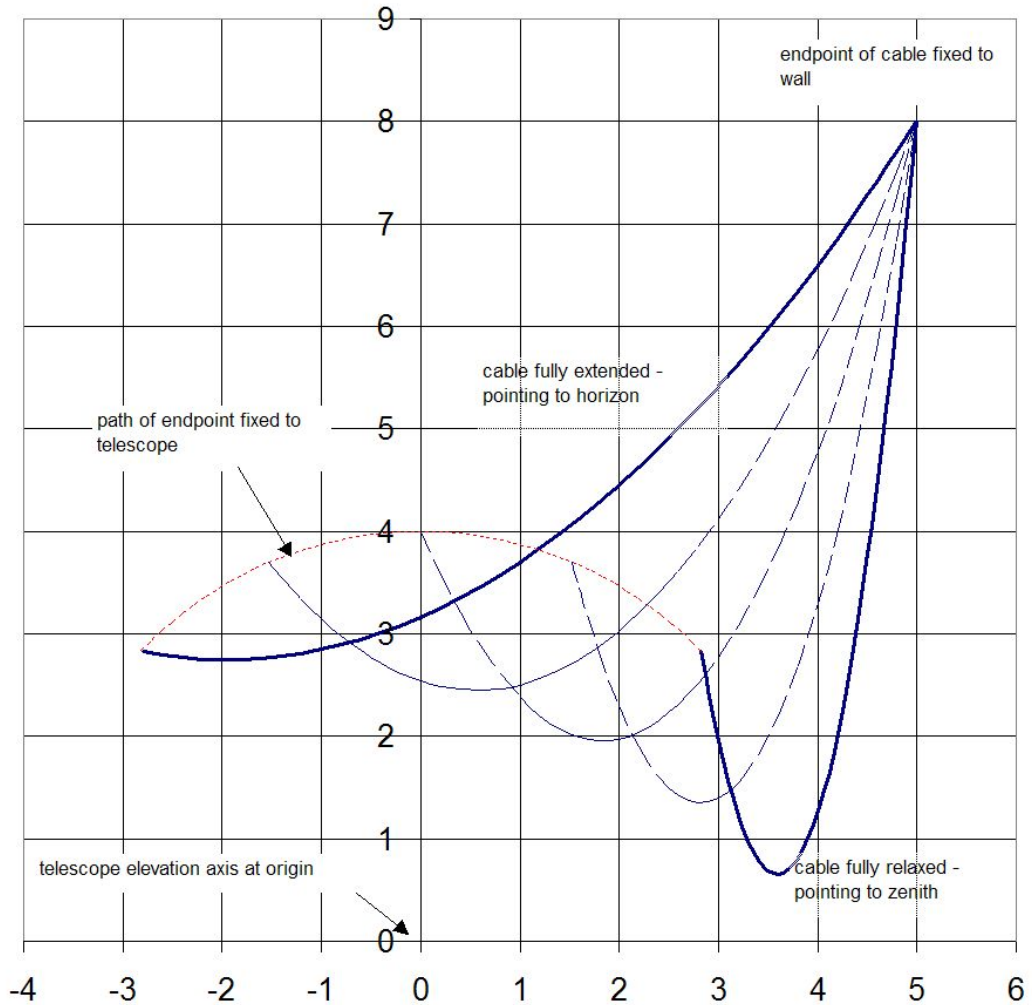


Figure 120: Possible geometry of hanging cable. Axis scales are metres, with the origin placed at the telescope's elevation axis. The cable end attached to the telescope traces a 90-degree arc as the telescope slews from zenith to horizon. Force analysis of the concept is based on this geometry.

The analysis was undertaken simply by fitting a parabola through the endpoints for a range of telescope elevations, constraining it such that the arc length along the hanging segment remains a constant 9.9 m (this figure was selected to minimise the hanging cable length without applying undue loads to the telescope when it points to the horizon). The mass per unit length of fiber cable was then used to calculate the cable tension at the telescope attachment point. The slope of the parabola at that point completes the applied force vector. These results are shown in Figure 121, along with the moment applied by the cable to the telescope about the elevation axis. As the telescope moves through the full range of elevation, the angle of the cable with respect to the moving telescope structure varies by only plus/minus 20 degrees about a mean. Since this amount of bending will be readily accommodated by the flexure of the cable, no pivoting mounting point will be required.

To partially compensate for the moment applied by the cable, a small mass (~8kg) acting as a trim weight was modelled mounted on the opposite side of the

telescope primary mirror cell, and the net moment applied to the telescope as a function of elevation angle is shown in Figure 122.

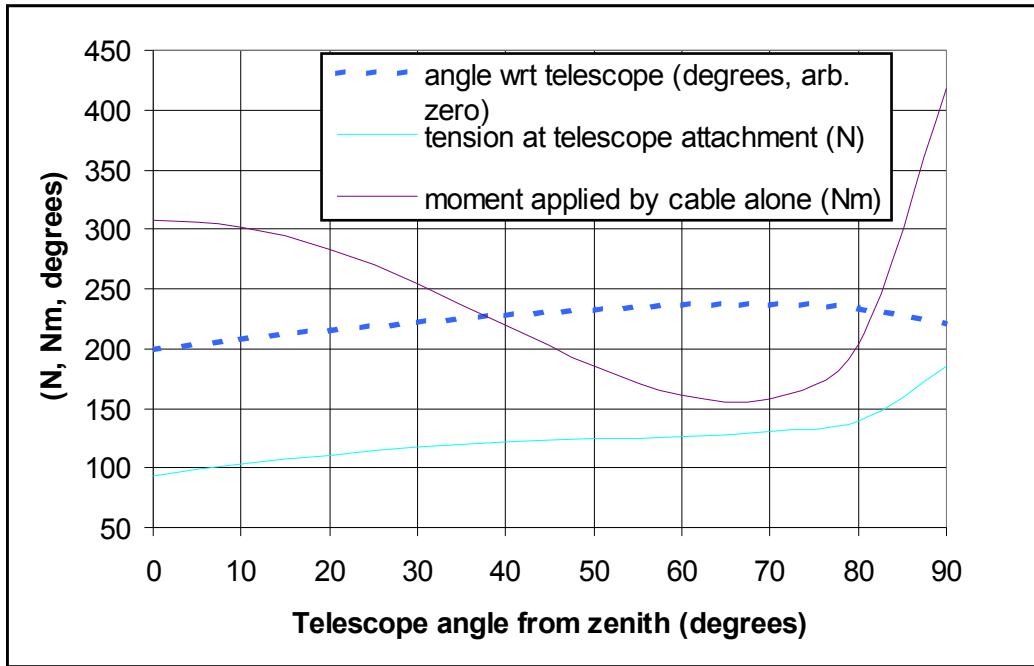


Figure 121: Results of calculations of loads transmitted to telescope structure by the hanging cable arrangement. The cable tension remains low throughout the telescope travel, increasing as the telescope approaches the horizon. The moment applied by the cable is also low. The dotted trace shows the change in angle relative to the moving telescope structure of the applied tension – this is less than 40 degrees throughout the entire travel, justifying a fixed attachment point.

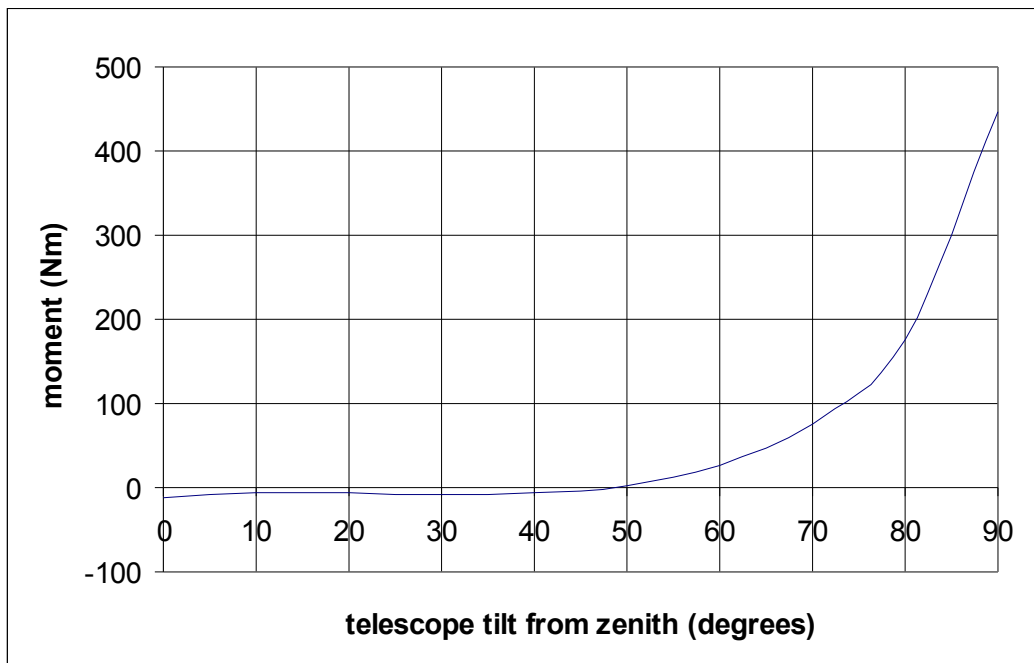


Figure 122: Net moment of cable and trim weight. The positive sense of this moment is to try to restore the telescope towards the zenith. Moment is negligible through almost all of the telescope's normal operating range.

It will be noted that this arrangement yields moments of less than about 10 Nm throughout most of the operating range of the telescope. If the telescope is taken all the way to horizon pointing, then a righting moment of ~450 Nm is applied as the hanging cable reaches its maximum extension.

No figure is available to the study authors for the capacity of the Subaru elevation drive, however it is clear that the estimated loads are insignificant for normal telescope operation.

12.5 Gemini Related Issues

12.5.1 Spectrograph interface and location for Gemini

The highly significant difference between the Gemini and Subaru WFMOS implementation is the location of the spectrographs in the pier lab (see Figure 123) and this has a large implication on the fiber cable route. However, the spectrograph interfaces should be essentially the same as Subaru, though the exact details of the fiber run to the spectrographs in the pier lab will differ somewhat.



Figure 123: Layout of the WFMOS spectrographs in the Gemini pier lab

12.5.2 Corrector/robot opto-mechanical fiber interface for Gemini

At this stage of the FWMOS design and from the perspective of the fiber cable, the Subaru and Gemini wide field corrector have been assumed to be identical, each producing an $f/2.0$ beam when combined with the maximum spine tilt angle. The top end interface does, however, differ in that for Subaru only the PFU unit is removed in a top end change, where as for Gemini, the whole top end including the outer ring would be removed. The most significant impact this has on the fiber cable is the likely location of the fiber connectors⁸, which would be located near the top end outer ring (see Figure 124). The top end rotator unit requirements will be similar to Subaru, though because of the different top end design, there will be some difference in the detailed that would need to be considered as the design develops.

⁸ Note: In the fiber performance discussions the thin core section of the fiber cable was assumed to be the same length for both Subaru and Gemini as the details of the location of the fiber connectors are not finalised. However, it is likely that this section of cable in the Subaru implementation would be slightly shorter, giving a small gain in system performance.

12.5.3 Fiber parameters Gemini

Other than the overall length of the fiber cable the fiber parameters for Subaru and Gemini are the same.

12.5.4 Connector interface and location

The fiber connectors for Gemini will be similar in design to Subaru, but as previously stated, the location of the fiber connector will differ, being located near the outer top end ring instead of near the PFU. However, the interface and interlock requirements are very similar.

12.5.5 Gemini Operational Issues

The overall operation issues for Gemini should for the most part be similar to Subaru. The main differences being the details of the top end exchange and the fiber routing issues as the Gemini implementation does not have the hanging loop and has additional telescope motion to accommodate.

12.5.6 Gemini fiber run

The fiber cable run between the positioner and connectors would be similar to Subaru, passing from the spine modules, through top end rotator, and out to the fiber connectors. However, the proposed cable run from the fiber connectors to the spectrograph differs significantly (see Figure 124), though it is intended to be permanently fixed to the telescope once initially installed. From the fiber connector, mounted on the telescope tube truss just below the top end outer ring, the fiber cable route runs down the telescope truss to a node above the primary mirror. From there a support structure would be installed to take the fiber from the node to a point just above the elevation axis structure. Then the cable would run above, but parallel to the telescope elevation axis. This section will need to accommodate the full elevation axis motion (0-90°) over a distance of ~1.5m. Designs currently exist that could accommodate this twist⁹.

From the elevation axis cable twister the cable will run down the telescope “legs” and across the floor¹⁰ to the centre of the azimuth axis. The cable would then feed down the pier chimney from the centre of the azimuth floor to the pier lab, accommodating the full telescope rotation range (~±270°) over roughly a 10m vertical section. With careful design the twist should be readily accommodated without increasing the fiber length significantly, either with a “Chinese lantern” (FMOS) or a long spiral (as used on OzPoz and 6dF electrical and pneumatic cabling system).

Once in the pier lab the fiber bundles can be distributed to each of the spectrographs in standard electrical cable tray structures.

⁹ The FMOS twister design is able to accommodate ±270° over a length of ~1m and more than 480 fibers.

¹⁰ This section will have to be carefully design to prevent crushing damage, also not interfere with telescope operation and maintenance such as bottom end instrument changes and mirror re-coating.

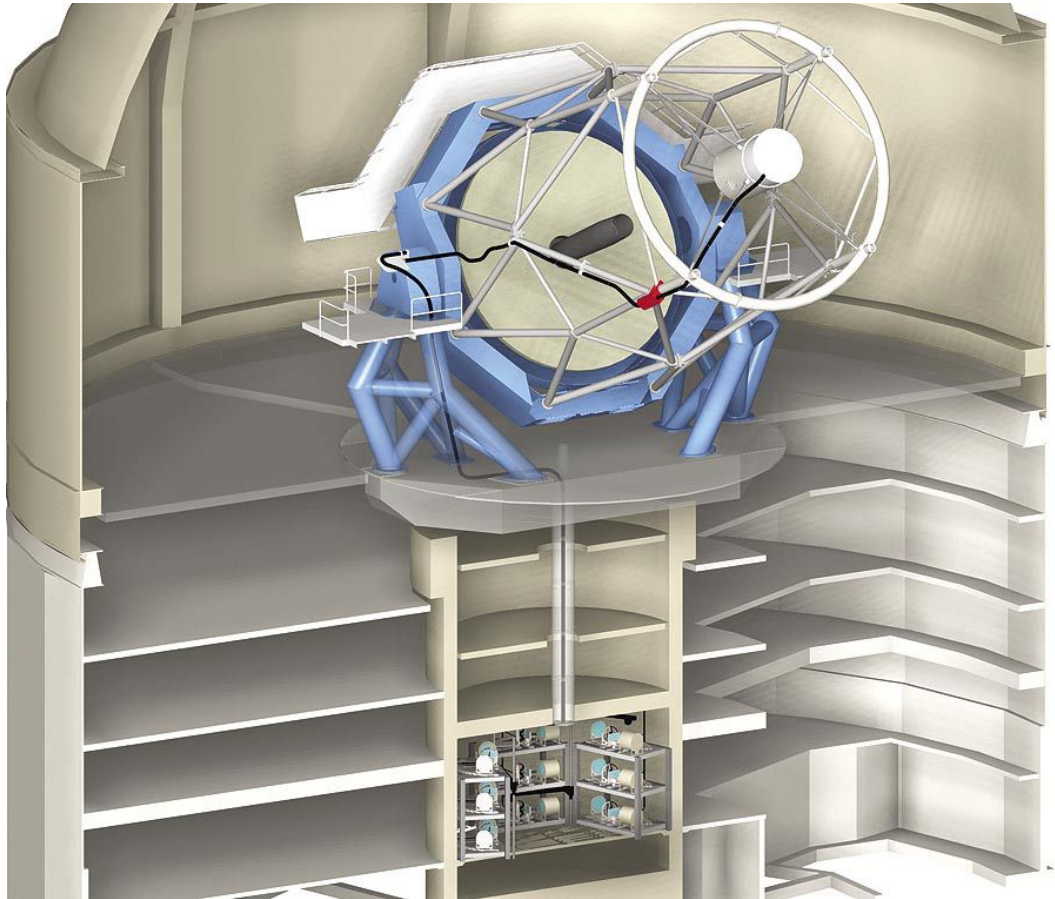


Figure 124: The KAOS concept on Gemini. The fiber positioner is located at the prime focus of the telescope. The fibers run down the truss, into the telescope mount, and drop down to the lower floor where the spectrographs reside. The fiber connector location is marked in red at the top end interface.

12.5.7 *Fiber cable design Gemini*

As for a Subaru implementation, the basic fiber cable design would be made up from ~ 135 bundles, each of ~34 fibers, in kink-resistant tubing. However, the additional cable twister units at the elevation axis and down to the pier lab, also the run across the telescope floor, make the route somewhat more vulnerable to potential damage during normal telescope operations. Therefore more reinforcement and protection of the cable run would be required, particularly in areas such as the telescope floor. As the cable does not have to accommodate the hanging loop a more circular or square profile (~80x80mm with extra reinforcement) for the cable may be preferred.

12.5.8 *Fiber cable integration*

Because of the more complex, integrated and convoluted fiber route, the integration of the cable onto Gemini would have a significant impact on the cable design. We do not foresee any significant issues, just the particular need for a careful consideration of all stages of design, manufacture and integration.

12.5.9 *Fiber cable risks for Gemini*

With the exception of the fiber hanging loop, a Gemini implementation shares most of the fiber cable risks with Subaru, however, a few extra areas of potential

risk present themselves. There are two additional fiber twisters in the Gemini fiber cable. Although design principles for these devices have been proven with other instruments, this particular configuration in combination with the large fiber numbers is unique. Prototyping sections of the cable, including fatigue testing, would be highly desirable to ensure fiber performance is not compromised. Also because of the much higher level with which the fiber cable integrates and interacts with the Gemini telescope, greater care must be taken to assess the impact of the permanently mounted cable on telescope operation and maintenance. The level of integration would also be likely to complicate any repair work that would be required, reinforcing the desire to have a repair- and maintenance-free cable design.

12.5.10 Guide fiber requirements Gemini

The guide fiber requirements for Gemini are essentially the same as for Subaru.

12.6 Cost Trades

Only one significant cost trade is associated with the fiber cable; that of the level of cable reinforcement and protection, against light-weighting and flexibility. The cable as envisaged has deliberately been made light-weight and flexible, yet robust. However, if further strengthening is demanded then the cost, weight and volume will go up rapidly. In addition, the flexibility of the cable would likely reduce significantly. Both the increased weight and volume along with reduced flexibility would have profound impacts on the all the sections of and interfaces with the fiber cable, particularly the telescope drives, fiber twisters, fiber connectors, strain relief points and attachment points.

12.7 Cost Forecast

In particular, both the AAO and Durham, but also other members of the WFMOS consortium, have extensive experience building fiber cables. Recently, FMOS and AAOmega fiber cables have been extensively prototyped, and are still under construction.

The cost estimate is a synthesis of two estimating processes. The first based on a detailed cost analysis of the numerous fiber cables assembled at and in association with the AAO. An appropriately scaled and adjusted estimate was derived from this analysis that was then reviewed by the WFMOS team along with the estimate originators. The second independent estimate was constructed based on a product breakdown and schedule-building exercise. This approach takes better advantage of design innovations specifically proposed for the WFMOS fiber cable.

A critical review panel of AAO staff then reviewed these estimates. The details of the final cost estimate derived from this process are given in the cost management section of *Chapter 25, Organisation and Management*.

Chapter 13 Fiber Connector

The fiber connector is a critical element in the fiber cable module. It provides a natural break in the cable so that the WF MOS top-end structure can be removed from the telescope without removing the entire cable down to the fixed spectrographs. It also provides a natural point for beam conversion from the fast focal ratio delivered by the prime focus corrector into a slower focal ratio required to feed the spectrograph collimator efficiently. This break in the cable run can also be used as the point at which to inject light up the fibers for back-illumination whilst a field is being configured, but this option is not considered in the baseline design for the connectors to reduce their complexity, cost and size. In principle the fiber connector could also be adapted to incorporate dichroic beamsplitters to multiplex the light from a single object into simultaneous optical and infrared spectrograph channels.

The connector must be robust and easy to mate together since it may be located on parts of the telescope structure which are difficult to access. A critical requirement of the connector is that it should minimise coupling losses and focal ratio degradation between the two sections of the fiber cable even after repeated use. Specific feasibility issues which will be addressed are: (i) space/mass/costs budgets, (ii) module maintenance/replacement schemes, (iii) location of connectors, (iv) simultaneous wavelength coverage.

13.1 Summary of Strawman Specification

The baseline specifications taken as inputs for the fiber connector design process are given in the following table. The effects of changes in these assumptions are discussed in section 13.5 on cost/performance trades.

Requirement	Value (Gemini)	Value (Subaru)	Comment
Number of channels (fibers)	4500	4500	Subaru option includes NIR extension
Nominal input f/ratio	f/2.4 (1.9)	f/2.2 (1.8)	Values in parentheses include FRD due to spine tilt & a corrector non-telecentricity of 0.8°
Nominal input fiber diameter	100 microns	100 microns	May be smaller for hi-res spectrograph
Nominal output f/ratio	f/4	f/4	
Nominal output fiber diameter	200 microns	200 microns	May be smaller for hi-res spectrograph
Spectral Window	390 – 1000 nm	390 – 1600 nm	Option for different connector designs for visible and NIR regions
Throughput	>85%	>85%	Goal for connector alone

13.2 Design Concept

Four different basic designs of fiber connector have been investigated based on experience in developing similar systems for other instruments. The first option is to use the same basic connector design as that used in the FMOS¹ near-infrared fiber-fed spectrograph, currently under construction for Subaru, but adapted for

the WMOS specifications. In this design, there are two lenses per connector, one on each side of the connector break (Figure 125). In the second option, the individual lenses are replaced by microlenses grouped in arrays which can offer potential reductions in volume and mass. In the third option, the lenses are replaced by gradient-index lenses. This does not change significantly the characteristics of the design but could have some advantages in achieving tolerances albeit with an associated cost penalty. In the fourth option, no lenses are used at the connector but this requires that the focal ratio of the spectrograph collimator is changed from $f/4$ to $f/2$ or that microlenses are added at the spectrograph slit. However, a faster focal ratio collimator would bring an increase in the spectrograph cost while the microlenses on the slit may introduce a large loss of light. The connector break incorporates both launch (Echidna-side) and receiver (spectrograph-side) fibers. The connector will be composed of sub-connector modules located in precision-machined holes to control alignment tolerances.

The design concept is based on two principles. First, if a change in focal ratio is necessary, a system of two lenses minimum is needed to correctly position the focal plane *and* the pupil image surface. It then becomes natural to have a break at this position with one lens on either side. Second, if lenses are not used, the required tolerances are very badly distributed between the position tolerances and the angular tolerances. Whilst the position tolerances are extremely tight, the angular tolerances are extremely loose. The lens system rebalances the two. This is done by having a pupil image formed between the two lenses which is much larger than the original fiber core diameter of $100\ \mu\text{m}$. For the same mechanical precision therefore, the losses due to position errors are then proportionally smaller. Conversely, the angular distribution of rays between the two lenses corresponds to a slower beam than the input focal ratio $\sim f/2.3$. The angular errors due to mechanical tolerances are therefore proportionally larger but this is less of a problem since the latter can be made very small. Note however that the position tolerances on each side of the connector separately remain tight, for example the position of the fiber core with respect to the lens is a critical area. It is the tolerances between both sides of the connectors that are rebalanced. Fortunately, it is much easier to achieve high tolerances between the fixed fiber and the lens of one half of a subconnector half than between the two sides of the connector.

All four basic designs will be investigated but with most analysis of the design based on FMOS and the design using microlens arrays.

13.3 Optical Design

The optical design has been done using a method developed initially for designing fiber-lenslet integral field units and subsequently adapted for the FMOS connectors². In this method, calculations are done of the transmission losses by vignetting at the output of the connectors, that is on the input fiber core on the spectrograph side. Transmission losses due to vignetting in the spectrographs are also evaluated. This is because a reduction of the vignetting losses at the connector outputs corresponds usually to an increase of the vignetting losses in the spectrographs. Optimization is done by maximizing the product of the two.

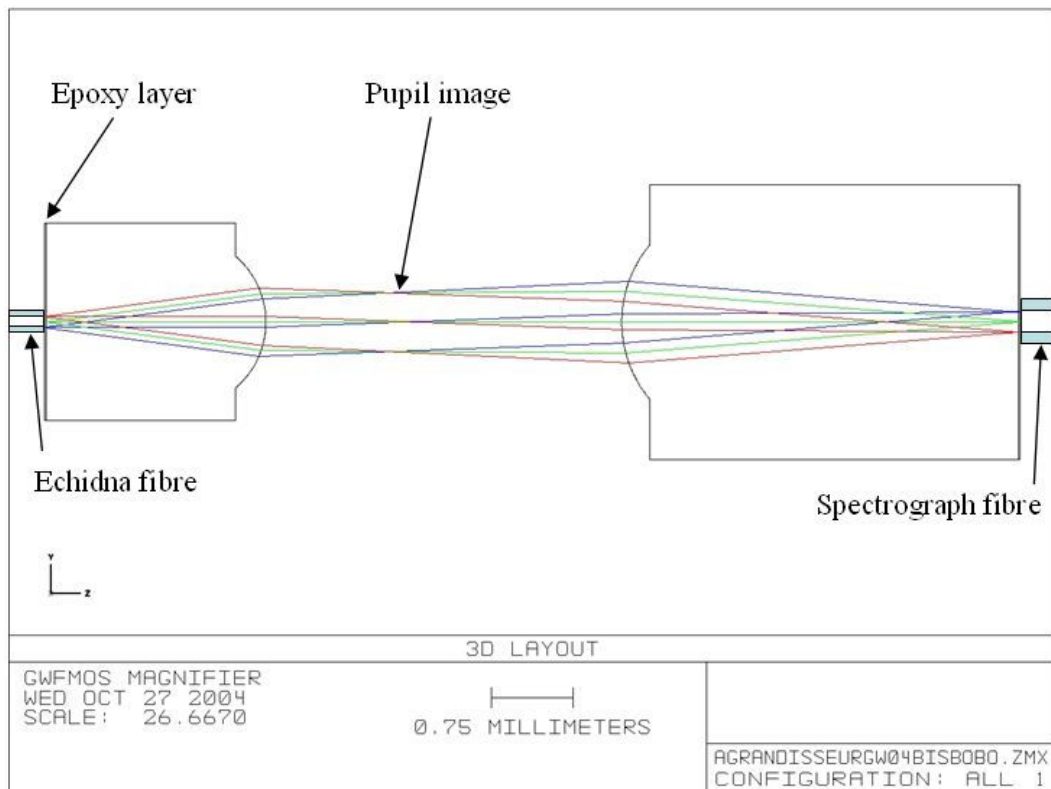


Figure 125. FMOS type design of the Gemini WMOS connectors.

The first step in the three basic designs using lenses is to obtain a rough design using ZEMAX. Some decisions have to be taken on what will be the number of surfaces and the characteristics of the glasses. Experience with the FMOS connectors has shown that it is possible to have a reasonable image quality with two plano-convex lenses glued on their flat side to their respective fiber core (Figure 125). This removes four air-glass surfaces including the two fiber cores where anti-reflection coatings are difficult (but not impossible) to put. This significantly reduces the losses in the connector.

The choice of glass must be done carefully for the best results. With spherical lenses of silica glass alone, aberrations in connectors are still quite large on the fiber core and the pupil image surfaces. A correct choice of glasses can significantly reduce the aberrations and hence the losses by vignetting at the spectrograph side fiber core. However, using other glasses than silica can cause some internal losses due to internal reflections between the silica fiber and the glass, and due to absorption. One must therefore choose the glasses to minimize the total losses, combining both internal losses and vignetting. The method we use includes this optimization combining the use of ZEMAX and our own programs iteratively.

The second step is a careful tolerance analysis. After making a preliminary estimate of each mechanical tolerance, a model is made of its effect on the fiber core PSF and on the pupil image, which corresponds to the focal ratio degradation (FRD). A large amount of information on mechanical tolerancing is now available following experience with FMOS, especially through discussions with manufacturers and the measurements made on the components they produced. Note that the design is not telecentric between the lenses i.e. the input fiber core image is not at infinity. This gives a better image quality but has a small effect on the tolerances. More generally, a change in the dimensions of the design, distances

and radii of curvature, would increase the aberrations but could decrease the effects of the tolerances resulting in less losses by vignetting. A study of this effect is beyond the scope of a feasibility study but should permit some small improvements in the final transmission.

The third step is the calculation of the transmission due to vignetting losses at the output of the connectors and in the spectrograph, and the optimization of the parameters to maximize this transmission. Of particular importance is the magnification of the connectors. A larger magnification will cause more vignetting at the fiber core but less at the stop of the spectrograph due to the slower beam entering the fiber. The calculations include the effects of the image quality (obtained with ZEMAX in the first step) on the connector output and in the spectrograph, the tolerances (modelled in the second step), the fiber FRD, diffraction, etc. The optimisation program also uses a model of the telescope input, including the central obscuration and another of the spectrograph in which the vignetting is modelled.

The fiber FRD will ultimately be obtained via measurements on the selected fibers but conservative values have been adopted for this study. The choice of numerical aperture (NA) for the WFMOs fibers in Echidna must be done carefully since existing measurements on fibers with larger NA, which are necessary on the Echidna side, suggest that they have much larger FRD than conventional step-index fibers. While a fiber with larger NA will have less internal losses, its larger FRD will cause some losses by vignetting in the spectrograph. For the calculations of transmission in this report, the FRD of the Echidna-side fibers is taken from the measurements done on the Echidna fibers of FMOS. This gives a value around 2° FWHM. The FRD of the spectrograph fibers was chosen via an “educated guess” and put as being a Gaussian of 3° FWHM at $f/5$. The values at other focal ratios are extrapolated from measurements done on similar fibers some years ago for fiber-lenslet IFUs. Better FRD values may well be possible depending on the length and path of the fibers at the telescope.

Another important design driver is the choice of focal ratio of the spectrograph collimator. If the fiber core size on the spectrograph side is changed in proportion to a change in focal ratio of the collimator, there will be no change to the design after the collimator, that is no change to the grating system and the camera. For example the collimator could be slowed from $f/4$ to $f/6$ while the fiber core size is changed from $200\ \mu\text{m}$ to $300\ \mu\text{m}$. The rest of the spectrograph remains unchanged. There is an optimal focal ratio that will minimize the total vignetting losses at the fiber core and in the spectrograph. Figure 126 and Figure 127 show the predicted transmission curves as a function of the spectrograph focal ratio for the Gemini and Subaru WFMOs connectors respectively. While the vignetting losses at the connector output (the fiber core) decreases with a slower focal ratio, the vignetting losses in the spectrograph increases. The total transmission due to vignetting has a maximum around $f/3.2$, which comes with a fiber core diameter of $160\ \mu\text{m}$. This is for a spectrograph stop that matches exactly the given focal ratio with no oversizing to account for tolerances.

Other considerations are for example the position of the pupil image at the output of the connectors (the exit pupil of the telescope-to-connector system). The present design puts it at infinity to avoid any additional FRD. At any other position, the rays would not enter the fiber parallel. The distribution of angles would then contribute an additional FRD. However, it may be possible to reduce

the PSF size on the fiber core by accepting some additional FRD. There is an optimum pupil image position where the transmission will be maximized.

An important issue during fabrication will be to develop a method of quality control that permits the design to be re-optimized using the measured tolerances rather than theoretical ones. This permits the design to be fine-tuned whilst avoiding significant losses if a component is worse or better than expected.

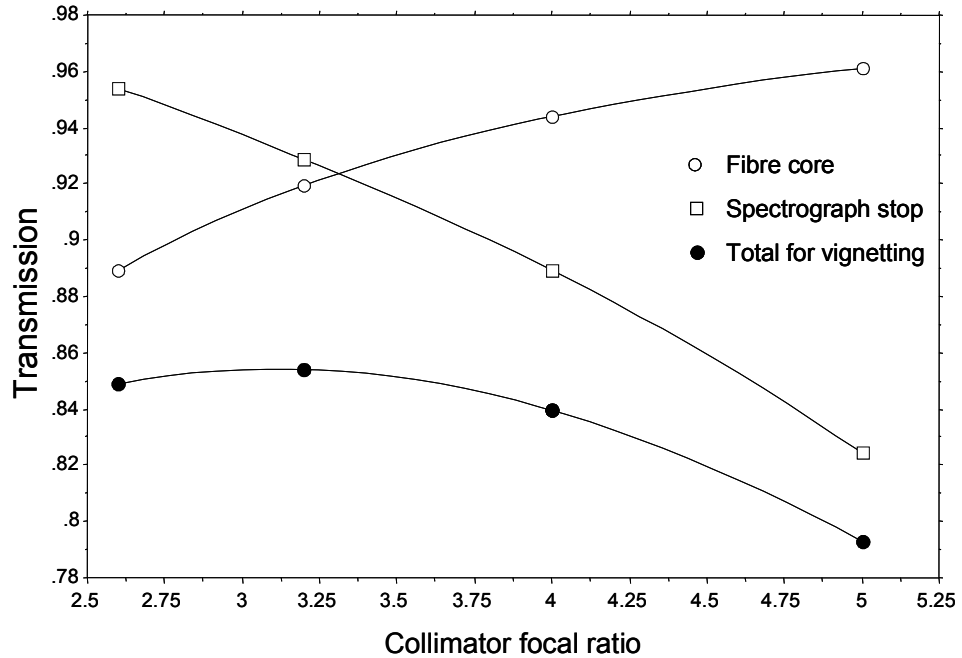


Figure 126. Transmission from vignetting losses for the output of the Gemini WFMOs connectors at the fiber core (open circles), at the spectrograph stop (open squares), and the product of the two which gives the total for vignetting (filled circles); the fiber core diameter in microns is 50 times the focal ratio

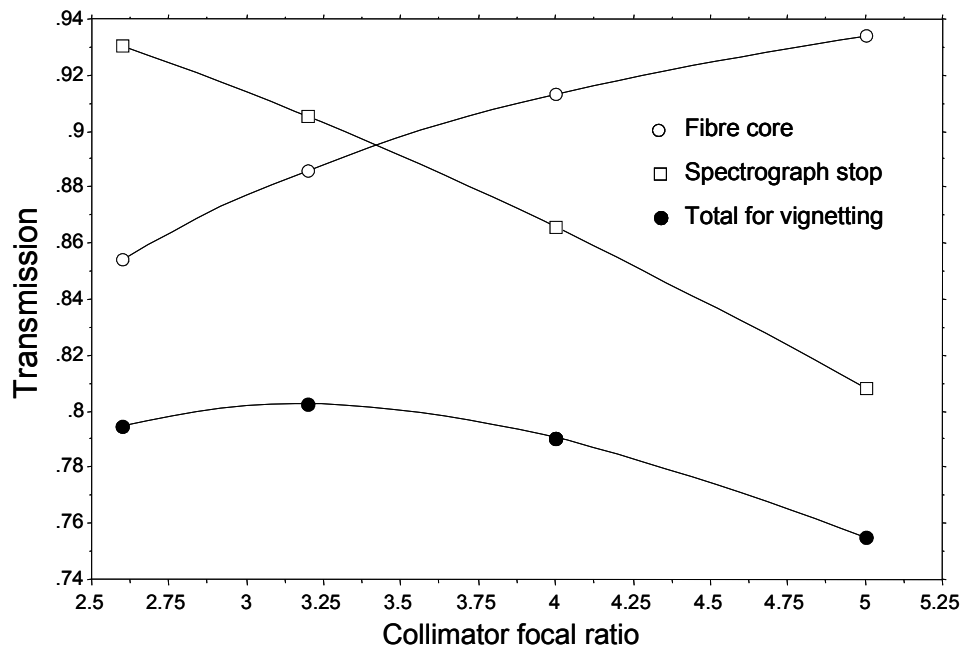


Figure 127. Transmission from vignetting losses for the output of the Subaru WFMOs connectors at the fiber core (open circles), at the spectrograph stop (open squares), and the product of the two which gives the total for vignetting (filled circles); the fiber core diameter in microns is 50 times the focal ratio.

13.3.1 FMOS-type connectors

Figure 125 shows the basic design of the FMOS-type connectors for WFMOS. The pupil image is visible between the lenses. The typical size of the lenses is 2-3 mm. This is the minimum size that is reasonably easy to manufacture for discrete lenses. The design is optimized to give the best image quality on the spectrograph fiber core and on the pupil image at the input of the spectrograph fiber. The characteristics of the optical design and the methods described above directly apply to this design. The lens materials are fused silica/Ohara S-BSM4 and all powered surfaces are spherical.

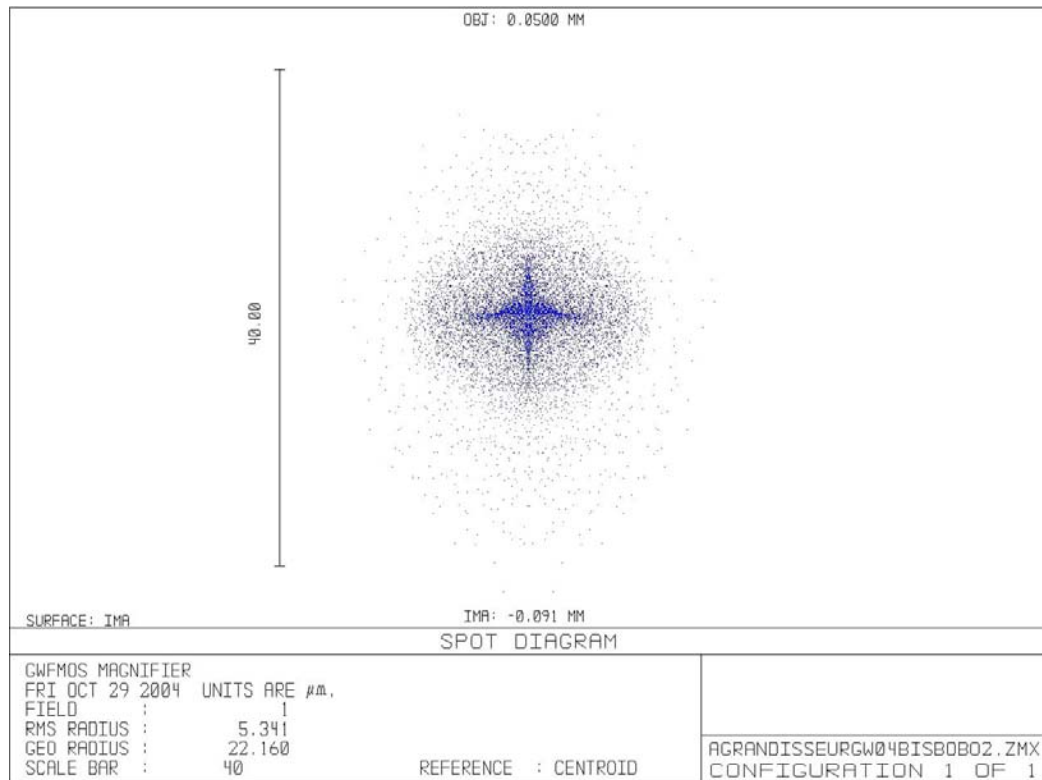


Figure 128. PSF on the fiber core of the FMOS type design for the Gemini WFMOS connectors.

Figure 128 gives a view of the PSF near the edge of the spectrograph fiber. Since this fiber has a $200\ \mu\text{m}$ core, the blurring at the image edge is small along the radial direction (vertical) and is responsible for only a small fraction of the losses due to vignetting. Most of the losses are due to the mechanical tolerances. The blurring in the tangential (horizontal) direction is larger but does not contribute to the loss of light by vignetting. Figure 129 shows the pupil image at the input of the spectrograph fiber. Again, the image quality is excellent in the radial direction and the edge is only slightly blurred.

The two main disadvantages of this design are the mechanical complexity and the size. The total surface area of the connector break for example would be about $1.5\ \text{m}^2$ extrapolating directly from the size of the FMOS connectors. However, if the facility to back-illuminate the Echidna-side fibers from the connector break is removed (this facility would then need to be provided at the spectrograph slit) it is possible to significantly reduce the size. An additional reduction in size and complexity would result if the ability to remove each Echidna fiber individually

from the connector was abandoned (replacing it with the ability to remove blocks of a few tens of fibers).

Table 21 shows the tolerances that were used in the calculations. They are derived from the tolerances of the FMOS connectors and are therefore securely based in what manufacturers are actually able to achieve.

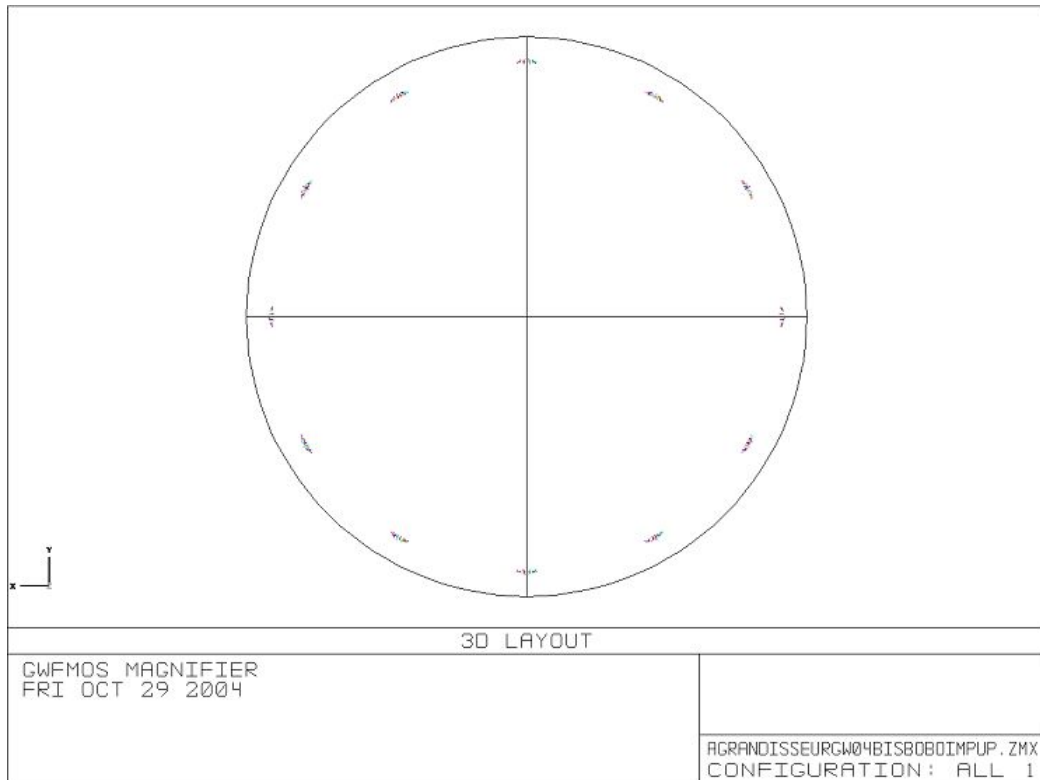


Figure 129. Pupil image at the entrance of the spectrograph fiber core for the Gemini WFMOS connectors.

Table 21. Tolerances for FMOS-type connectors.

Concentricity of fiber hole and ferrule	<1.4 μm
Diameter of fiber core :	
Echidna side	+/- 2 μm
Spectrograph side	+/- 5 μm
Decentering between buffer and fiber core	<2 μm
Decentering between cladding and fiber core	<1 μm
Diameter of lenses	+/- 5 μm
Difference in diameter between lens and tube :	
Echidna side	<8 μm
Spectrograph side	<10 μm
Decentering of lens surface wrt edge of lens	<10 μm
Thickness of lenses :	
Echidna side	+/- 20 μm
Spectrograph side	+/- 40 μm
Radius of curvature of lenses	+/- 1%
Angle of deviation of tubes	< 0.001°
Angle of deviation of fibers	<0.23°
Decentering between input and output of connector	<15 μm

13.3.2 Optimisation

An estimate of the total transmission of the FMOS-type connectors for the Gemini and Subaru WFMOS parameters is given in Table 22, assuming that the spectrographs are baffled at f/4 exactly without oversizing of their stop. A rough optimization was done to maximize the product of the transmission of the connectors and the transmission due to vignetting losses in the spectrograph (see above section on optical design). A complete optimization should give between one and a few percent more light. The lower transmission of the Subaru connectors comes mainly from its faster input focal ratio which gives a larger field in arcseconds on a fiber core of 100 μm . With a larger field but the same spectrograph and the same linear size of the fiber on the slit (200 μm) additional light must be lost by vignetting. A smaller part of the losses with Subaru is due to the increased wavelength coverage (visible and infrared) required for this design. Some small improvements could be made by optimising the optical and infrared designs separately, although this would lead to two different designs for the connectors, which is undesirable from a production viewpoint.

Table 22. Transmission of FMOS-type connectors.

Loss mechanism	Gemini WFMOS (%)	Subaru WFMOS (%)
Vignetting on fiber core	94.4	91.3
Internal reflections	99.8	99.8
Absorption	99.9	99.9
Anti-reflections coatings	97.6	96.0
Total connectors	91.9	87.4
<i>Vignetting by outside edge of spectrograph stop</i>	88.9	86.6

13.3.3 Microlens array connectors

For the FMOS spectrographs, with 2x200 fibers, the use of individual lens systems in the fiber connectors provides an efficient and cost-effective solution to the problem. However scaling this to the 5000 fiber channels required for WFMOS would obviously be a not insignificant challenge in process control, manufacture, assembly and test. Alternatively, it appears that the complexity of the above system could be considerably reduced if the individual lens assemblies were to be replaced by microlens arrays. The principal difficulty is in obtaining microlens arrays with sufficient image quality. Some manufacturers provide microlenses which have very poor surface roughness, others seem to have large aberrations near the edge and others have defects in the substrate. If only the centre regions of microlenses with large edge aberrations are used, it is in principle possible to obtain much better results. Moreover, progress in this field is very rapid and new techniques are being developed to produce high quality microlenses with low surface roughness for the telecommunications industry.

Figure 130 shows an optical design with microlenses that would significantly reduce the size of the connectors. The arrays are 1-D, and are matched to the input/output fibers using precision v-groove arrays. The pitch would be made larger than the diameter of the microlenses at around 1-1.5 mm. Whilst giving a better image quality and a smaller size than the FMOS-type design, the design in Figure 130 would be more sensitive to mechanical tolerances because of its smaller size. However, some manufacturers claim very high precision for their

components (position tolerances of the order of 1 μm or less) and the transmission could then be even better than for the FMOS type of design. A detailed design study will be required to determine the optimum transmission and array properties. A baseline design is discussed further below.

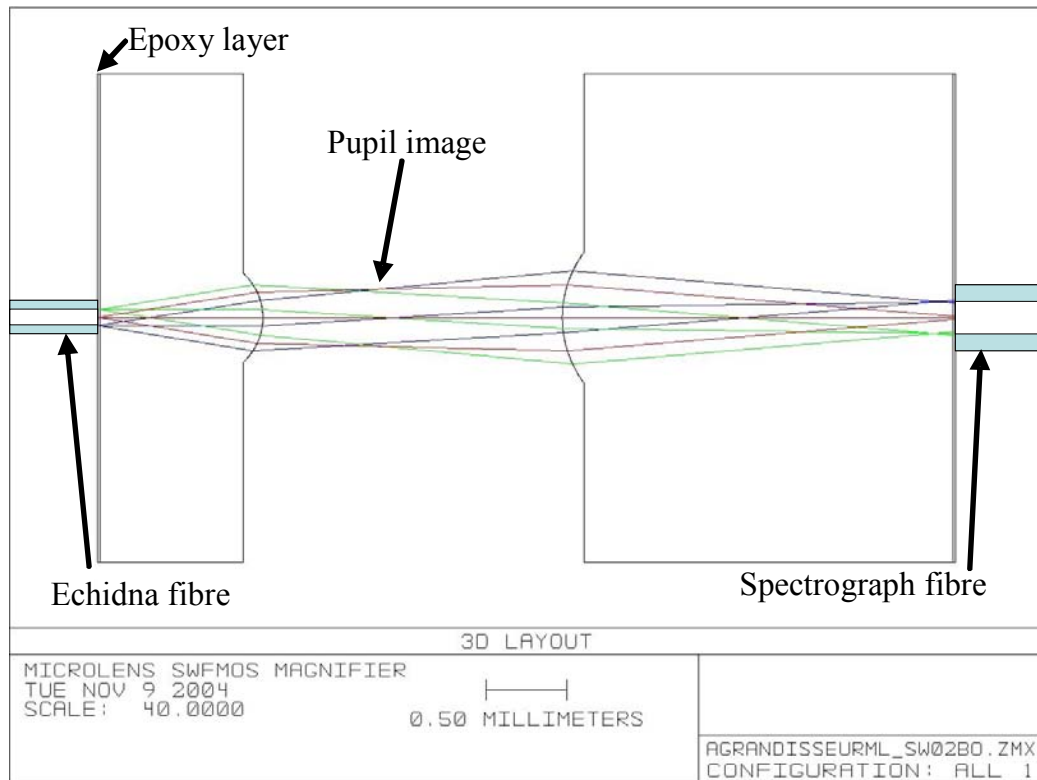


Figure 130. Optical design of microlens connector for the Subaru WFMOS

Table 23. Specification for a microlens array fiber connector.

	Echidna-side	Spectrograph-side
<i>Material</i>	Fused silica	Fused silica
<i>Diameter</i>	>0.55 mm	>0.80 mm
<i>Lens centre thickness</i>	1.000 +/- 0.015 mm	2.400 +/- 0.025 mm
<i>Substrate size</i>	10.0 x 100.0 (+/- 0,.2) mm	10.0 x 100.0 (+/- 0,.2) mm
<i>Pitch</i>	1.2500 +/- 0.0002 mm	1.2500 +/- 0.0002 mm
<i>Radius of curvature</i>	0.370 +/- 0.005 mm	0.670 +/- 0.008 mm
<i>Clear aperture</i>	>0.5 mm	>0.74 mm
<i>Spherical surface quality</i>	<0.15 μm P-V	<0.15 μm P-V
<i>Spherical surface roughness</i>	<3 nm RMS	<3 nm RMS
<i>Flat surface quality</i>	<5 μm P-V	<5 μm P-V
<i>Flat surface roughness</i>	<30 nm RMS	<30 nm RMS
<i>Flat surface angular error</i>	<0.5 degrees	<0.5 degrees

Table 23 shows the baseline specification for a microlens-array based connector which we have used for preliminary mechanical packaging estimates and ROM costings. The principle difficulty with this specification appears to be in the

required lens sag. Although the tolerance specification is relatively high, the manufacturers appear to be able to deliver these without difficulty using a photolithographic process. A solution to the lens sag problem appears to be achievable by either reducing the diameter of the launch & receiver lenslets or using a higher index substrate.

13.3.4 Gradient index lenses

There may be some advantages to replacing the lenses in the FMOS-type design by Gradient Index lenses (GRIN). These lenses have the advantage of easier handling properties because of their inherently cylindrical shape (GRIN lenses are flat-ended rods of custom glass or polymer which refract light by virtue of a radially varying refractive index profile). The use of GRIN lenses does not change much the basic optical design but may make assembly and maintainability (repair) easier. A more advanced option would be to have them polished with a spherical shape making each equivalent to two lenses which would in principle give a higher image quality. However, there are disadvantages in cost, in the control of length/profile characteristics and many are hygroscopic. A detailed analysis and comparison of samples with FMOS-type lenses will be required to determine if they can give any improvement. If they are better, it is likely this would be a marginal gain.

13.3.5 No lenses in the connectors

With no lenses in the connector, the light losses would be fully dependent on the mechanical precision. The alignment between the two sides would become very critical. The spectrograph collimator would also have to be made much faster at around $f/2$. There would still be some losses because the distance between the fiber cores on each side cannot be made exactly zero which will cause a defocus. The diameter of the spectrograph fiber can however be made slightly larger than $100\ \mu\text{m}$ to reduce the losses at the connector. As for the options with lenses, this comes with additional losses in the spectrograph by vignetting because the collimator must then be made slower. For example, the spectrograph fiber core could be increased to $105\ \mu\text{m}$ with a collimator slowed to $f/2.1$. This leaves unchanged the design of the rest of the spectrograph. Another problem is the anti-reflection coating of the fiber end faces which is a much more difficult task than coating lenses and may lead to additional light losses.

Alternatively, the spectrograph collimator could be maintained at $f/4$, or even made slower, and microlenses added at the output slit. This solution was rejected for FMOS because experience with small format microlenses (less than $0.5\ \text{mm}$) showed that they scatter a large part of the light and generally perform worse than the technology of the larger lenses discussed in the previous section.

13.4 Mechanical Design

The mechanical design of the WMOS fiber connector is based on that developed for the FMOS connectors. The connector is formatted as an array of sub-connectors, each of which is identical and contains the fibers from a fixed number of Echidna modules. The Echidna-side sub-connector array is housed in a rack enclosure which, for the baseline Subaru option, would be located on the Prime Focus Unit (PFU). The spectrograph-side consists of an array of individual self-

contained, discrete sub-connectors which are manually carried to the Echidna-side connector from a parking position at the interface between the spider arm and the PFU (Figure 131).

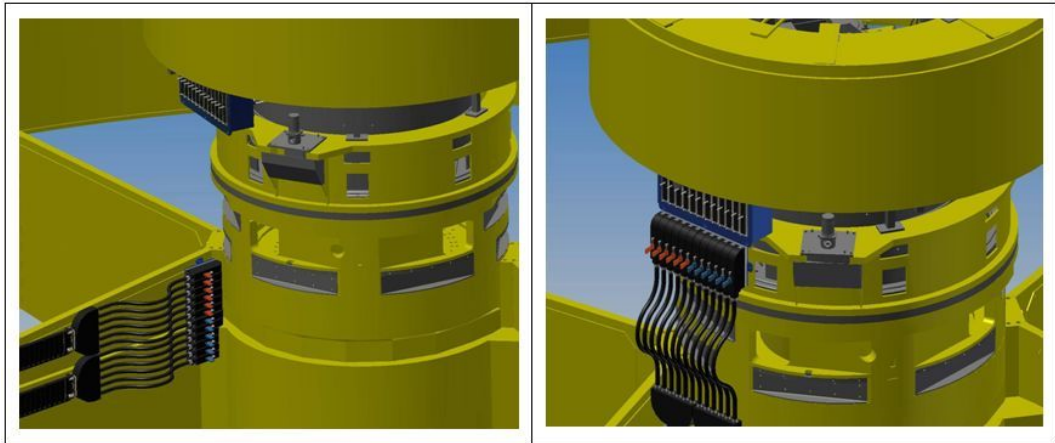


Figure 131. Fiber connector array configuration for Subaru WFMOS showing fibers in the park position (left) and after connection to the Echidna-side fibers (right).

For the Gemini option the fiber connector would most likely be located on the outside of the new prime focus top-end ring where it would not vignette the main telescope beam and would be in a convenient position for access.

13.4.1 **FMOS-type connectors**

For the FMOS-type connector option, each sub-connector contains the fibers from two Echidna modules or 140 fibers. These are arranged in two groups of $5 \times 14 = 70$ within the sub-connector head (Figure 132). Around 32 sub-connectors would therefore be required to deliver the required baseline specification (4500 fibers). An individual Echidna-side sub-connector consists of an accurately machined faceplate that carries 140 launch lenses, associated ferrules and fibers. The faceplate is made from vacuum-hardened ‘Stavax’, a highly stable machine steel, with holes cut by a wire electric-discharge process to achieve the high degree of mechanical precision required. Two dowels on the front of each faceplate serve as a precision location for the corresponding spectrograph-side sub-connectors. The spectrograph-side sub-connectors follow a similar pattern (Figure 132) but are ruggedised for more regular handling. Locking pins protruding from the Echidna-side sub-connectors engage with barrels in the spectrograph-side sub-connectors and are locked into position manually using a spring-loaded cylindrical cam. Both sides of the sub-connectors include aluminium connector shells and strain relief tubing to protect the delicate fibers and avoid mechanically-induced FRD. The overall dimensions of the fixed Echidna-side module (32 sub-connectors) is approximately 540 mm x 355 mm x 185 mm (L x W x D).

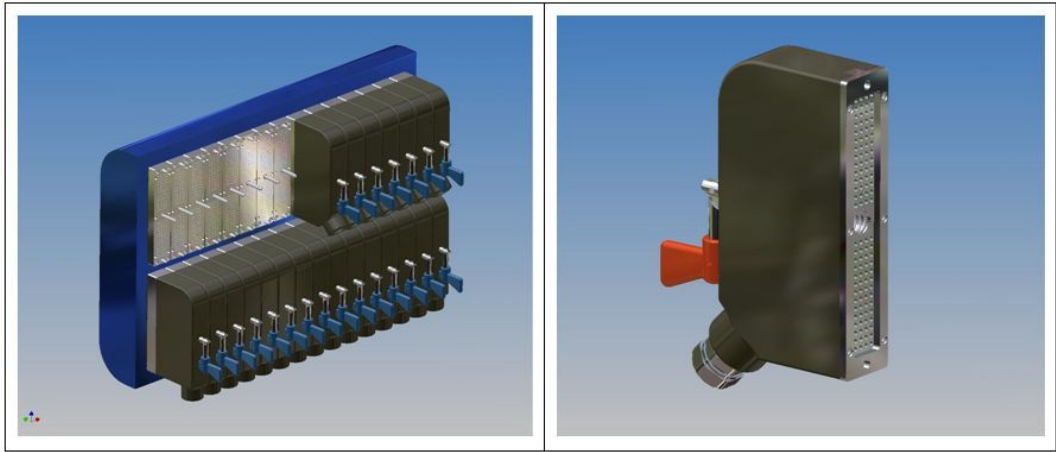


Figure 132. Array of fixed Echidna-side FMOS-type sub-connectors (left) and removable spectrograph-side sub-connector (right).

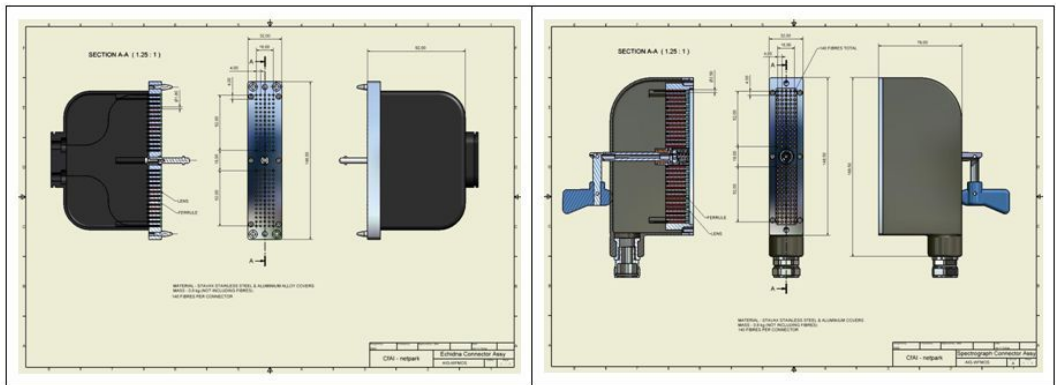


Figure 133. Dimensions of the FMOS-type 140-fiber sub-connector on the Echidna-side (left) and the spectrograph-side (right). Each Echidna-side connector has dimensions of 148.5x32x92 mm and an estimated mass of 0.6 kg excluding fibers. The spectrograph-side connector has dimensions of 148.5x32x79 mm and an estimated mass of 0.8 kg excluding fibers.

13.4.2 ***Microlens array connectors***

The microlens array connector is based around stacked linear arrays of 70 fibers bonded to linear 1D microlens arrays. The fibers are held in pairs of precision v-groove arrays in a sandwich arrangement which locate the fiber cores to extremely high precision ($<2\mu\text{m}$). The v-groove arrays would be made from pyrex or fused silica using an etching process to minimise any potential CTE mismatches with bonded MLAs. The array dimensions are approximately 100mm x 12mm x 3mm. This technology has been extensively used in fiber-lenslet integral-field units and the larger dimensions proposed here appear perfectly feasible from a manufacturing viewpoint. As an example, Figure 134 and Figure 135 show a fixed Echidna side sub-connector with 30 v-groove arrays (2100 fibers) interfaced to 2x1050 fiber sub-connectors on the spectrograph side. The packaging here is illustrative and the number of v-groove arrays (fibers) per sub-connector can be traded off against ease of use and modularity for ease of replacement/repair. The relatively compact nature of these connectors compared to the FMOS-type is clearly apparent, even though the design has not been optimised in this regard.

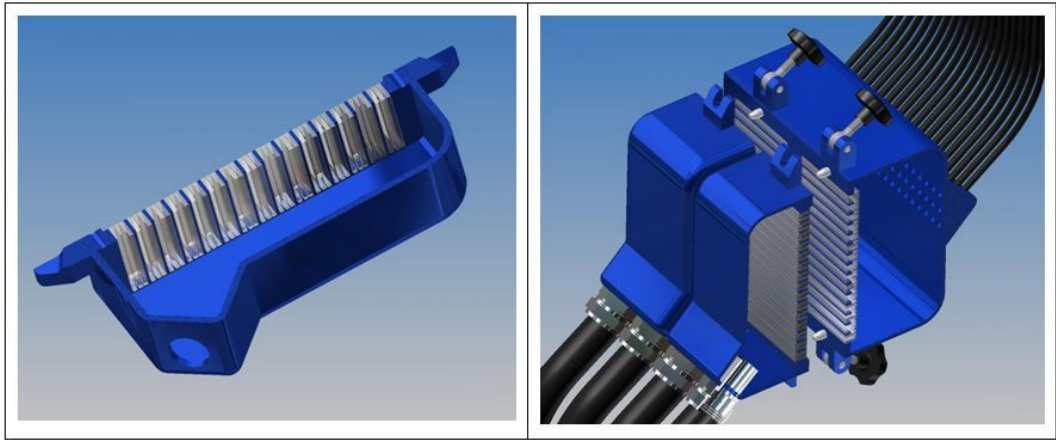


Figure 134. Cross-section through a spectrograph-side microlens array sub-connector (left) and complete connector head with 2x1050 fibers (right).

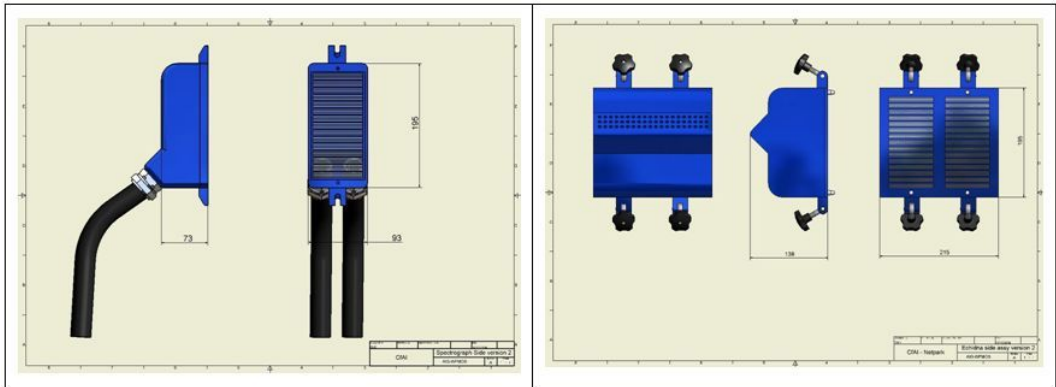


Figure 135. Dimensions of the microlens array 1050-fiber sub-connector on the Echidna-side (left) and the 2100-fiber fixed spectrograph-side (right). Each sub-connector has dimensions of 195x93x73 mm and has an estimated mass of 1.4kg excluding fiber & conduit. The spectrograph-side connector has dimensions of 195x215x138 mm and an estimated mass of 3.7 kg excluding fiber & conduit.

13.5 Cost Trades

13.5.1 Cost/performance options

The principle area for cost/performance trades is in the modularity of the connectors. Both the FMOS-type connector and the microlens-base connector appear to have similar performance levels, assuming that the specified tolerances can be reached. The tolerances specified in Table 21 imply a relatively low yield in manufacture and hence have a cost impact. However, reducing the tolerances has an immediate detrimental effect on throughput. Because of the monolithic processes used in their manufacture, the high tolerances required for the microlens-based connectors (Table 23) appear relatively easier to achieve.

The solutions presented for both connector types imply a minimum modularity at the several tens of fiber level. Each FMOS-type connector contains 140 fibers, the equivalent of two Echidna modules. Although in principle individual fiber/lens components could be replaced in such a connector (and this capability has been implemented in the connectors for FMOS) the desire to miniaturize the connectors for WF MOS makes such an approach impractical here. We envisage a maintenance routine where a complete connector and associated Echidna modules

would be replaced once the numbers of defective channels had reached a predefined level (10-20%) beyond which effective science operations had become significantly compromised. The mean failure rate of the Echidna-side fibers is currently hard to estimate but should become better defined once FMOS is in operation on Subaru (post 2006). Because the fibers are constrained throughout their length, however, we expect many fewer breakages than experienced with XY fiber positioners such as 2dF (Gemini) or OzPoz (VLT).

The microlens-array based connector has modularity at the 70-fiber (single) Echidna module level. Although the individual connector shells hold several pairs of v-groove arrays, the design proposed is configured to allow individual arrays to be replaced. The extent to which Echidna-side and spectrograph-side modules are interchangeable, or whether they are produced as matched pairs, is likely to be a cost driver, especially for the FMOS-type connector. The costings assume that both sides will be changed during the maintenance operation; this also required that the spectrograph slits are assembled in a similar modular fashion.

The optimisation of the Subaru design to cover both the optical and near-infrared spectral regions with the same connector was not considered to be a cost driver. However, the design presented assumes that the connector will be used to feed *either* an optical spectrograph *or* a near-infrared spectrograph, but not both simultaneously. Although a connector design which included a dichroic beamsplitter between the two sides is in principle possible, the increase in separation of the launch and receiver lenses would have a detrimental effect on performance. A similar issue arises if the connector is modified to allow back-illumination of the Echidna-side fibers from the connector.

13.6 **References**

1. Eto et al SPIE 5492, 1314-1318 (2004)
2. Murray et al SPIE 5492, 1383-1394 (2004)

Chapter 14 Low Dispersion Spectrograph

14.1 Summary of Strawman specification

The Dark Energy science case for WFMOS drives the requirements for the low dispersion spectrograph and are outlined in Table 24.

Table 24 Science requirements for the low dispersion spectrograph.

Requirement	Value	Comment
Spectral Resolving Power	$\lambda/\Delta\lambda = 1000$	Higher resolution (~4000) desired for OH suppression
Spectral Window	390 – 1000 nm	
Simultaneous Coverage	1 octave	
Number of Simultaneous Targets	~3000	2/3 of fibers
Nod & Shuffle Operation	Required	Alternatively, new low-read-noise, fast-read-out CCDs might be used in “Nod & Read” mode

Some additional implementation assumptions relevant to the low resolution spectrograph design are detailed in Table 25.

Table 25 Fiber and detector parameters for the low dispersion spectrograph design.

Parameter	Value
Fiber Diameter at Slit	200 μm
Fiber Output Focal Ratio	f/4
CCD Detector Format	4096 x 4096 pixels
CCD Pixel Size	15 μm

14.2 Spectrograph design based upon JHU Sloan Digital Sky Survey design

14.2.1 Optical Design

14.2.1.1 Overview

The optical design follows closely from the Sloan Digital Sky Survey (SDSS) spectrographs, which have been performing superbly in survey operation since early 2000, with record-breaking throughput for a fiber spectrograph. This performance results from the throughput-optimized optical design, using a single-surface reflecting collimator and all-refractive cameras containing only ten AR-coated air/glass surfaces and no beam obscuration. For WFMOS this throughput can be increased even further with improved gratings and newer CCDs, resulting in an impressive 70% peak instrumental efficiency.

Table 26 SDSS (as-built) and WFMOS low dispersion (baseline) spectrograph parameters.

Specification	SDSS Value	WFMOS Value
Spectral Window (simultaneous coverage)	390 – 910 nm (2 channels)	390 – 1000 nm (2 channels)
Fibers per Spectrograph	320	292 (N&S) 584 (non-N&S, upper limit)
Fiber Diameter	180 μm (3 arcsec on sky)	200 μm (1 arcsec on sky)
Fiber Spacing at Slit	360 μm center-to-center	560 μm ctr-to-ctr (N&S) 280 μm (non-N&S)
Fiber Output Focal Ratio	f/4	f/4
Beam Diameter	159 mm	159 mm
Camera Focal Ratio	f/1.5	f/1.5
CCD Detector Format	2048 x 2048 pixels	4096 x 4096 pixels
CCD Pixel Size	24 μm	15 μm
Spectrum Height on Detector	3 pixels	5 pixels
Spectrum Spacing on Detector	6 pixels center-to-center	14 pixels ctr-to-ctr (N&S) 7 pixels (non-N&S)

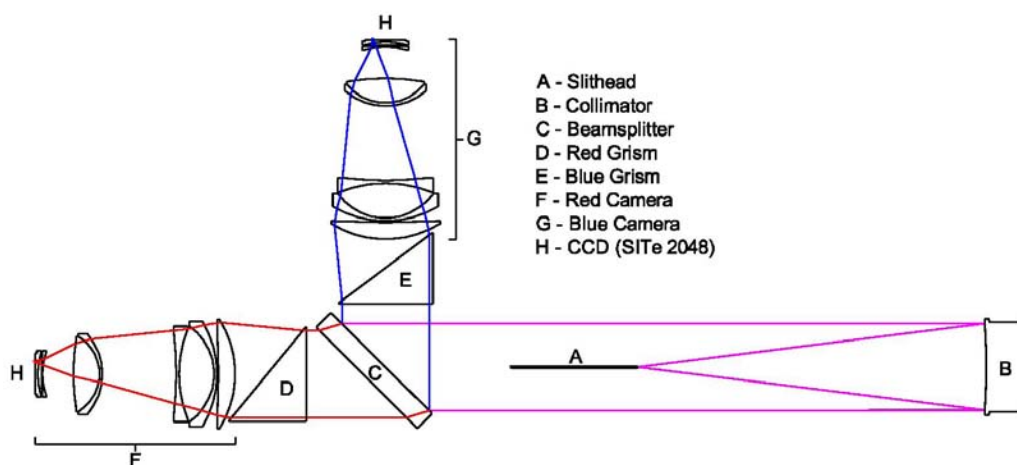


Figure 136: Optical schematic of the SDSS spectrograph.

Except for the total number of fibers, these twin spectrographs provide a close match to the low resolution requirements for WFMOS. Table 26 lists the parameters for the as-built SDSS spectrographs. The design employs two channels with a dichroic beamsplitter to divide the light between the red and blue sides. Figure 136 shows the optical layout of the SDSS spectrographs. A curved slithead positions the fibers on a radius concentric with the spherical collimating mirror, which transforms the f/4 output from the fibers to a 159 mm diameter collimated beam. The 45 degree dichroic beamsplitter reflects the blue portion of the bandpass ($\lambda < 600$ nm) and transmits the red wavelengths ($\lambda > 600$ nm). Immediately after the beamsplitter in each channel is a grism, containing a replicated ruled grating applied to the hypotenuse of a right prism whose incident face is normal to the optical axis. The dispersed light exits the gratings and enters all-refractive, eight-element, f/1.5 cameras. Each camera contains a single $2k^2$

CCD with 24 μm pixels, which records the 320 first-order, full-bandpass spectra simultaneously. The camera demagnification from f/4 to f/1.5 produces fiber images that are just under 3 pixels in diameter, resulting in spectra 3 pixels tall on the detector separated by 6 pixels center-to-center

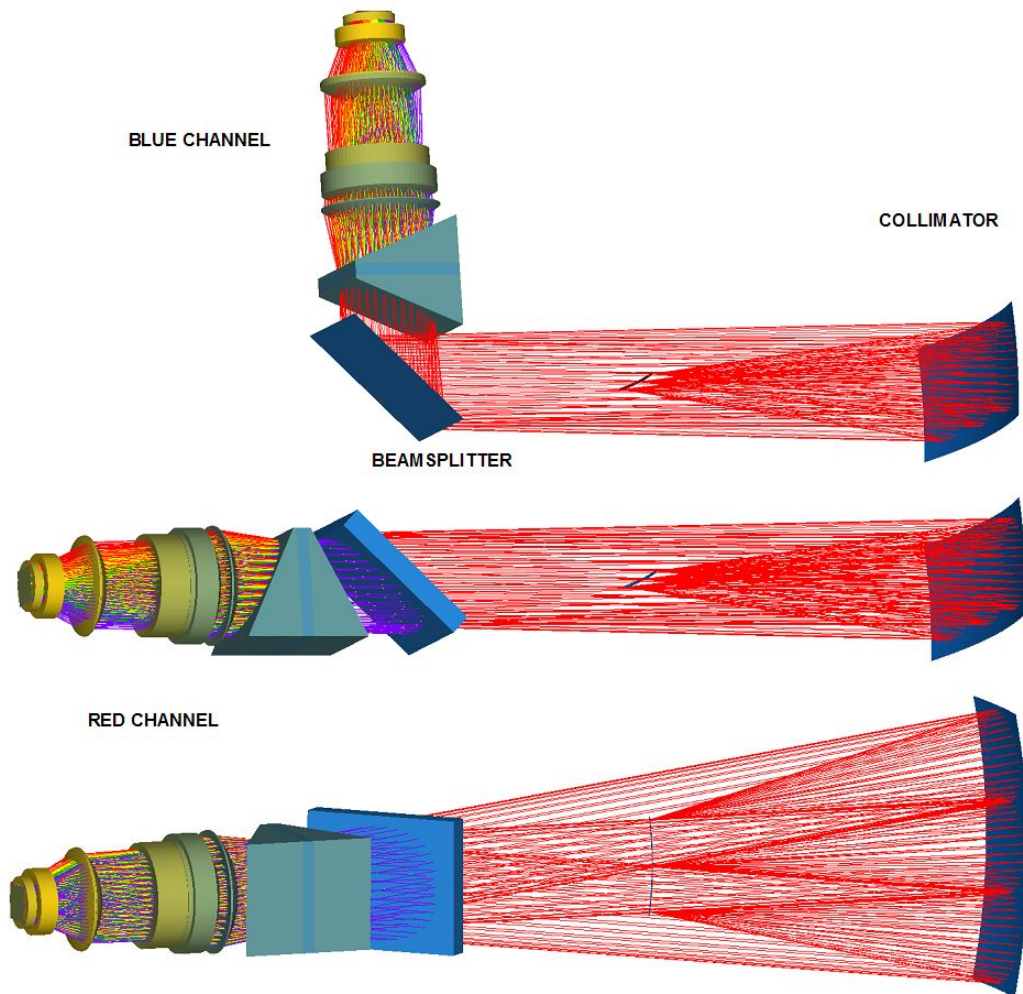


Figure 137: Optical layout of the WF MOS low resolution spectrographs. The red and blue channels are maintained in separate design files for more efficient optimization, so they appear separately above. The collimator mirror is to the right. *Top*: Top view of the blue channel, whose light is reflected by the dichroic beamsplitter. *Middle*: Top view of the red channel, whose light is transmitted through the beamsplitter. *Bottom*: Side view of the red channel, showing the long, curved slit with rays emanating from the center and both ends.

For WF MOS, minor changes to the optical design have been made, but the overall format of the spectrograph is very similar (see Figure 137 and Figure 138). The changes result from the use of physically larger detectors, broader wavelength coverage, and VPH gratings to maximize throughput. These are discussed in the following sections that detail the spectrograph optics.

14.2.1.2 Slithead

Light enters the spectrograph through fibers, which terminate at the slithead. For the purposes of this study, we have assumed 200 μm diameter fibers with an f/4 output cone. The fibers are stacked vertically to form a long slit and are placed on a radius whose center of curvature coincides with that of the collimator.

Additionally, the fibers are aimed in a fanlike pattern outward from the center of

curvature toward the collimator, so that the central (gut) ray from each fiber strikes the collimator normal to the surface. Thus, the slithead is at the focus of a one-dimensional Schmidt collimator. See Section 14.2.3.3 for more details on the slithead design. The assumed detector is larger for WFMOS than for SDSS by a factor of 1.25, and the slit length must increase by the same factor (assuming the same camera focal length) to fill the entire detector; the WFMOS slit will be 157.5 mm in length.

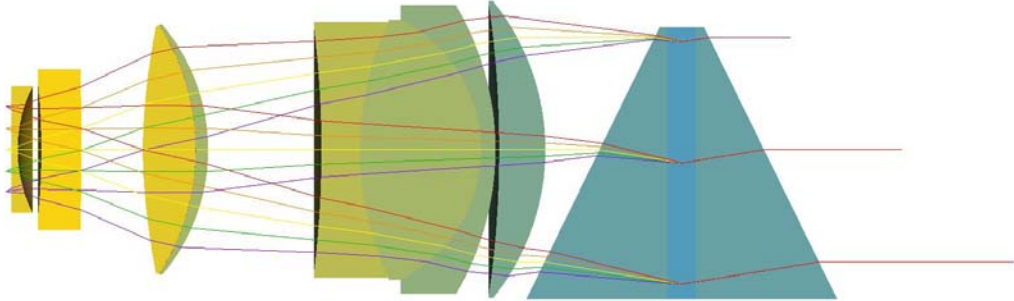


Figure 138: Red channel optical layout, with light incident from the right. The camera has eight elements in five groups (singlet-triplet-doublet-singlet-singlet).

The spacing of the fibers on the slit was determined from an analysis of the flux contamination due to crosstalk at the detector between adjacent spectra. Assuming an object four magnitudes fainter than the sky (e.g. a galaxy and sky with magnitudes 24 and 20, respectively), and using error functions to model the profile of the spectra in the spatial direction, we calculated the signal contamination from the adjacent sky spectra as a percentage of the galaxy flux. With a 14-pixel fiber-to-fiber spacing at the detector (the spectra are 5 pixels tall), and using SDSS camera PSFs, there is less than 1% contamination of the *galaxy's light* from the two adjacent nod & shuffled sky spectra. The WFMOS camera design discussed below has tighter PSFs than the SDSS cameras, so we feel very comfortable with this spacing. At the slithead, this results in 292 fibers on a 560 μm center-to-center spacing.

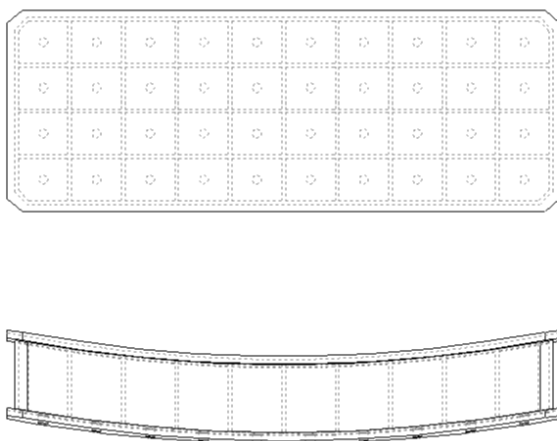


Figure 139: Drawing of the rectangular Hextek collimator mirror.

14.2.1.3 *Collimator*

In combination with the curved slithead, the spherical collimator mirror forms a corrector-less Schmidt collimator. The mirror itself is fabricated from a rectangular Hextek borosilicate blank, 175 mm wide, 483 mm tall, and 73 mm thick (see Figure 139). The planar blank is slumped by Hextek's gas-fusion process to near-net radius and then ground and polished to the final radius of 1264 mm. The collimator is the largest optic in the spectrograph and drives the overall height of the optical bench. The longer slit for WFMOS requires the collimator to be ~64 mm taller than in the SDSS design.

The collimator mount provides remote tip/tilt and focus adjustment (see Section 14.2.3.4). An initial focus adjustment can compensate for surface radius variation from nominal, allowing for less critical fabrication tolerances on the mirror and optomechanics. More frequent adjustments can compensate for seasonal temperature variations. A pair of Hartmann doors is located in front of the mirror (see Section 14.2.3.5) to allow shifts in the collimator focus to be measured rapidly. Tip/tilt adjustment allows the collimator to be precisely coaligned to the cameras, or at least to an average of the two camera axes. Thus, the center fiber can be positioned at the center of the detector in the spatial direction, and the central wavelength can be positioned at the center of the detector in the spectral direction.

The collimator forms a pupil at the center of curvature of the mirror, and this is where the gratings are located in each channel in order to minimize their required size.

14.2.1.4 *Beamsplitter*

A dichroic beamsplitter divides the incident collimated beam, reflecting the blue portion of the bandpass ($\lambda < 640$ nm) and transmitting red wavelengths ($\lambda > 640$ nm). Note this has been tweaked from SDSS's 600 nm dichroic split, due to the extended bandpass out to 1 μ m. It is fabricated from fused silica, 229 x 271 x 38 mm, with the dichroic coating applied to the incident surface. Based on the SDSS beamsplitters, the coating will reflect the blue light very efficiently ($R > 99\%$) and transmit the red light somewhat less efficiently ($T > 92\%$ average, including the reflection loss at the exit surface, which has a high performance broadband antireflection coating). The 10%–90% zone at the crossover wavelength is approximately 50 nm wide.

14.2.1.5 *Gratings*

In the Sloan spectrographs, a grism immediately follows the beamsplitter in each channel, consisting of a transmission grating applied to the hypotenuse of a right-angle BK7 prism. The gratings are replicated in a resin applied to the surface of the prism, using master gratings ruled specifically for SDSS by Hyperfine. Using a transmission grating allows the camera to be placed close to the system pupil (located about midway on the grating). Reflection gratings (e.g. in the 2dF instrument) require the camera to be located away from the grating/pupil to avoid interference with the incident beam, resulting in larger and more expensive camera designs. Additionally, the grisms avoid the geometric losses in plane transmission gratings used at high diffraction angles (the groove facets are foreshortened), resulting in higher grating efficiencies.

Hyperfine no longer exists in the same form as during the SDSS years, and the opticians who produced the SDSS gratings are gone. Even if we wanted to use the same master rulings, which we almost certainly would not (given the extended bandpass and different crossover wavelength), the company which now owns Hyperfine has shown no interest in locating the SDSS grating masters and has declined to quote this work. Therefore, it is certain we would need to have new master rulings produced, at some considerable expense. This situation, along with the promise of higher efficiency offered by VPH gratings, led us to abandon the SDSS approach using ruled gratings.

For WMOS, we believe VPH gratings will increase the throughput by more than 46% over that realized by the SDSS spectrographs (see Section 14.2.2.3), and our baseline design calls for their use. In order to preserve the straight-through SDSS form, we are proposing to use VPH gratings, consisting of a VPH grating sandwiched between two BK7 prisms (see Figure 140). On the incident side, the prism imparts a non-zero angle of incidence on the VPH grating, which is oriented normal to the incident collimated beam. On the output side, the prism returns the central wavelength to its original, undeviated path. Figure 140 shows a drawing of the red VPH grism, with a ruling density of 612 l/mm and a 26.8° apex angle. The blue grism is similar with 842 l/mm and a 23.3° apex angle. The gratings were designed independently at JHU (using the ZEMAX raytrace program) and at Kaiser Optical Systems, Inc. (KOSI), who also provided preliminary efficiency curves based on rigorous coupled wave analysis (RCWA). Recent measurements at JHU of the new VPH gratings for the LDSS-2 (Magellan), which are similar to the WMOS design, showed ~90% peak efficiencies and support our enthusiasm for using these gratings in WMOS.

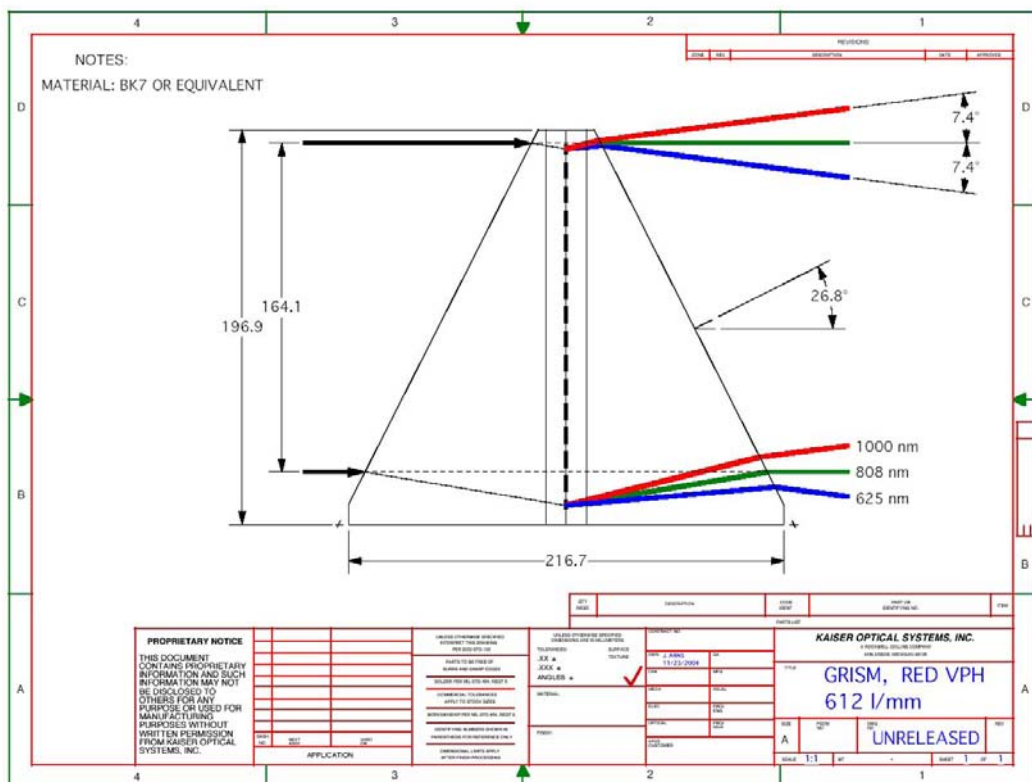


Figure 140: Preliminary design for the red channel VPH grism.

14.2.1.6 Cameras

The cameras are very similar to those used in the SDSS spectrographs, which were designed by Harland Epps (see Figure 141). The all-refractive approach was taken to maximize throughput, because placing the detector or a secondary mirror in the unobstructed beam produced by the fibers and collimator would result in significant light loss. The 2dF spectrographs, for example, use a modified Schmidt camera and the CCD detector does vignette the beam. The SDSS camera employs eight lens elements arranged in five groups, including a contact triplet, a contact doublet, and three singlets. All the surfaces are spherical except for the air side surface of the second element in the doublet, which is a relatively mild asphere. Careful attention was paid to glass selection in order to maximize throughput at 390 nm, with five of the eight elements being either calcium fluoride (CaF_2) or Ohara i-line glasses (which have >98% internal transmission at 365 nm). Dow Corning Q2-3067 optical coupling gel was used to join the elements in the doublet and triplet.

The WFMOS cameras present a more challenging design than SDSS, due to the significantly larger field of view (20.6° vs. 16.5°) and the extended wavelength coverage. A preliminary design has been identified, using the same glasses and element configuration as the SDSS cameras, but with a second aspheric surface (see Figure 142). The 240 mm focal length is preserved, the overall length of the camera is increased by 15 mm, and the diameter of the larger lenses has grown by about 6% (remember the longer slit produces significantly higher beam angles from the collimator). The second asphere is located on the rear surface of the first element, which is made of CaF_2 and could be diamond-turned and post-polished for a modest premium over a spherical surface.

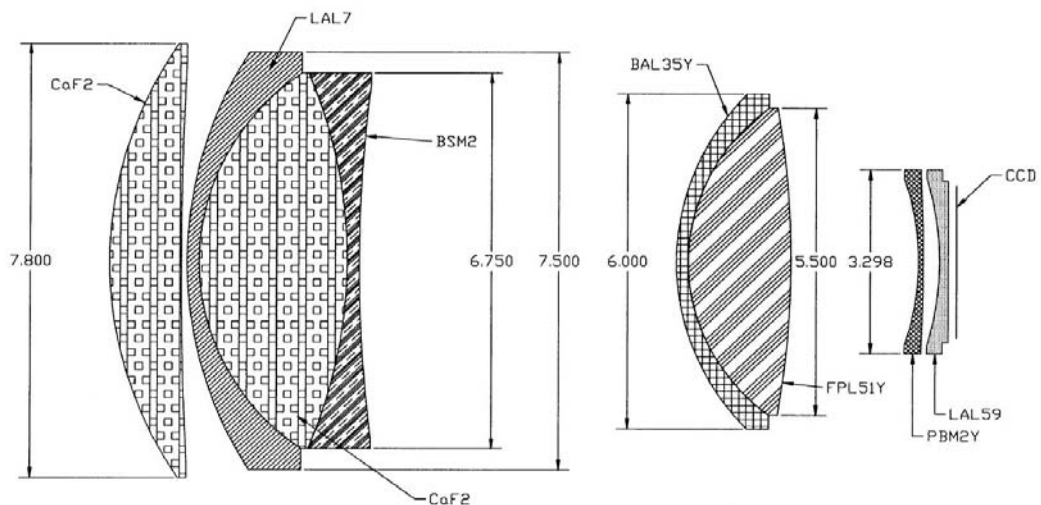


Figure 141: Layout of the SDSS spectrograph blue camera. The red camera is nearly identical.

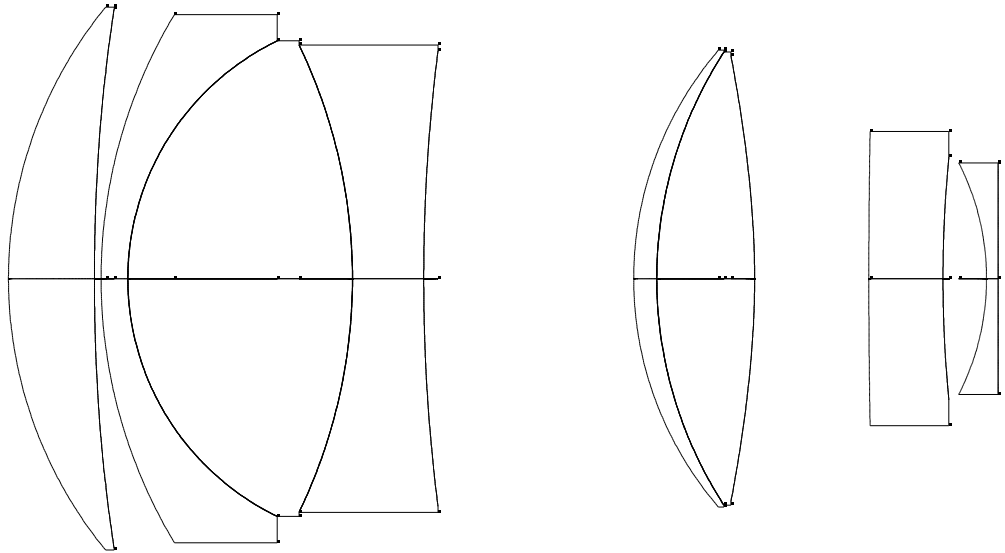


Figure 142: Layout of the preliminary red camera design for WFMOS.

Other camera designs could be explored during a design study; however, it is encouraging that a slightly modified version of the SDSS cameras could suffice for WFMOS.

14.2.1.7 Detectors

For the purposes of the low dispersion spectrograph study, we have assumed $4k^2$ CCDs with $15\ \mu\text{m}$ pixels. This represents a 25% increase in the physical extent of the CCDs over SDSS ($2k^2$ with $24\ \mu\text{m}$ pixels), and allows us to maintain ~ 300 fibers per spectrograph with nod and shuffle while preserving the basic design, layout, and resolution of the SDSS spectrographs. The $200\ \mu\text{m}$ fibers are imaged to $75\ \mu\text{m}$ by the cameras, which corresponds to 5 pixels on a $15\ \mu\text{m}$ pixel CCD.

The choice of particular CCD devices is most important from an instrument efficiency standpoint, and is discussed in Section 14.2.2.3. A commercial CCD, the e2v CCD44-82, is currently available and is a good match for the instrument. This device is a $2k \times 4k$ array in a 3-side buttable package. However, the recent acquisition of a larger “stepper” (here stepper refers to the lithographic equipment used to step-and-repeat the mask layout on the silicon die) now makes it possible for e2v to produce a $4k^2$ version of this device. No new technology development is required for the larger format. There are several reasons we prefer the $4k^2$ format over butted $2k \times 4k$ devices:

- The $4k^2$ device is available now with reasonable lead times. In quantities of 10–20, an order placed today would carry a lead time of 18-20 months. An order placed in mid-2005 would carry a reduced lead time of only 12-14 months.
- There will be no cost impact. In fact, the larger format would be slightly less expensive in quantity than double the number of $2k \times 4k$ devices.
- The monolithic detector will be quite a bit simpler to mount and align than a mosaic.

- The 4k² package promises to be more scalable to the L3 Vision technology than the 2k x 4k buttable device. L3 technology from e2v allows the CCD to be read out rapidly with very low read noise, thus potentially offering the advantages of the Nod & Shuffle technique without the large cost in detector real estate. However, L3 requires considerable real estate around the edge of the CCD, and it is not clear that a buttable 2k x 4k package with L3 is possible.

With the standard astronomy broadband AR coating, the CCD44-82 QE is excellent over the blue channel bandpass. For the red channel, deep depletion CCDs offer much improved response at 1 μm , but the inherent detector PSF degradation with a fast f/1.5 camera is an issue that needs to be studied. The CCD44-82 is available in a deep depletion version with an NIR coating, as would be the 4k² version of the device, and would be quite a good match for the red channel. Even better would be the fully depleted devices developed at Lawrence Berkeley National Laboratory, which have significantly better response beyond 8000 \AA than the e2v devices. Throughput curves assuming each of these devices are presented in Section 14.2.2.3.

14.2.2 **Optical Performance**

The following sections will describe the optical performance of the SDSS-based low dispersion spectrograph design for WFMOS, including image quality, spectral resolution, and instrumental throughput. Comparisons with the SDSS spectrograph performance will be shown, as well.

14.2.2.1 *Image Quality*

Spot diagrams for the red and blue channels, for both SDSS and WFMOS, are shown in Figure 143 and Figure 144. The spots are shown within a 75 μm diameter circle, representing the imaged fiber diameter on the WFMOS detector. Each diagram covers the full respective bandpass of the channel, and field points covering the full length of the respective slits (note the WFMOS slit is 30.5 mm longer than the SDSS slit). It is apparent that the WFMOS camera design produces smaller spots in general than the SDSS design, and indicates there will be some performance headroom available for fabrication and alignment tolerances, or perhaps for other cost reduction (e.g., matching of vendor test plates).

14.2.2.2 *Spectral Resolution*

To analyze the spectral resolution, defined as $\lambda/\Delta\lambda$, where $\Delta\lambda$ is taken to be the spectral FWHM of the slit image on the detector, the following procedure was used for both the SDSS and WFMOS designs. In ZEMAX, a circular source the diameter of the fiber was placed at the slit location having the largest RMS spot size for the wavelength under consideration. Many thousands of rays were launched from this circular source with a uniform distribution, and the resulting image recorded on a simulated detector with pixels $\frac{1}{4}$ the size of the assumed 15 μm CCD pixels (in order to better sample the image). The simulated image data was exported and analyzed to determine the FWHM, *without* collapsing the image. The FWHM thus determined was taken to be $\Delta\lambda$, and the results are plotted in Figure 145 for both SDSS and WFMOS. For a given wavelength, the spectral FWHMs of the two designs are very similar, and thus, so are the resolutions.

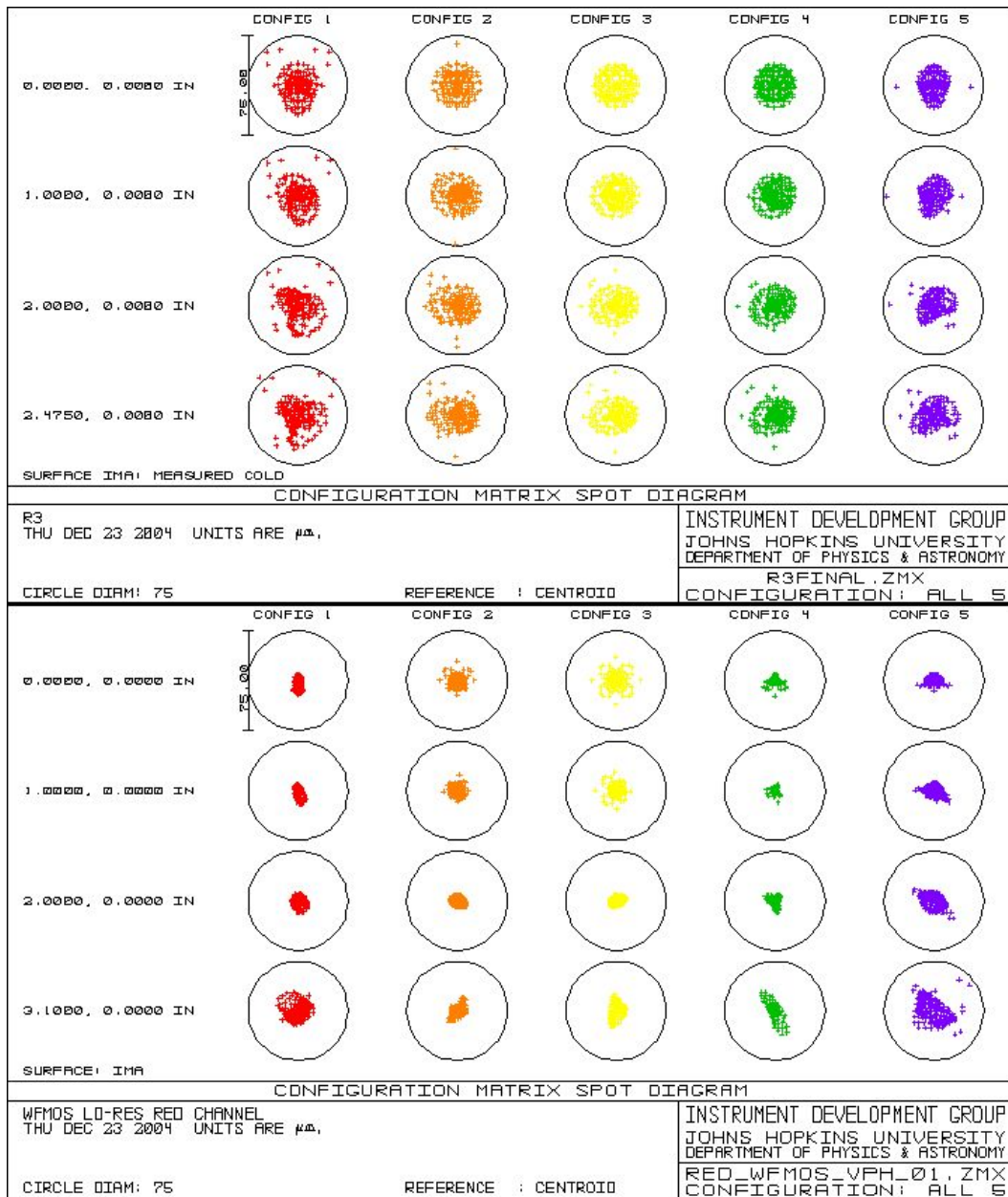


Figure 143: Spot diagrams for SDSS (top) and WFMOs (bottom) red channels. The circles are 75 μm in diameter, corresponding to the size of the fiber image on the WFMOs detector (SDSS has 68 μm fiber images). Rows represent a particular position along the slit, from center (top row) to end (bottom row), indicated by labels to the left of each row. For WFMOs, the bottom row represents the end of a longer slit than in SDSS. Each column represents a particular wavelength. For SDSS, the wavelengths are (left to right): 910, 800, 740, 700, 600 nm. For WFMOs: 1000, 900, 806, 710, 625 nm.

Figure 146 shows simulated images of two lines separated by the spectral FWHM determined by the above procedure, at both the short and long wavelength ends of the WFMOs bandpass. Also shown is a plot of the collapsed spectrum, showing that the lines are easily resolved. In reality, the resolution of the instrument will be determined using collapsed spectra, so the resolution as reported here is on the low side. However, the ZEMAX analysis assumes perfect optics and alignment, so it is prudent to be conservative at this stage. It is worth noting that the SDSS cameras were reported to perform exactly as predicted by raytrace using the as-built prescriptions.

Higher resolution than the SDSS design is beneficial in the red channel for OH line suppression. By pushing the dichroic cutoff to ~690 nm and increasing the speed of the cameras to f/1.4 and f/1.2 in the blue and red channels, respectively, we can increase the resolution in the red channel to ~3 Å ($R = 3300$ at $\lambda = 1 \mu\text{m}$) while maintaining the SDSS resolution in the blue channel. These changes would come at a modest cost compared to the overall instrument budget. Pushing the resolution higher would involve a reduction in simultaneous wavelength coverage and the addition of rotating grism mounts, or major changes to the design to maintain full simultaneous coverage of the bandpass.

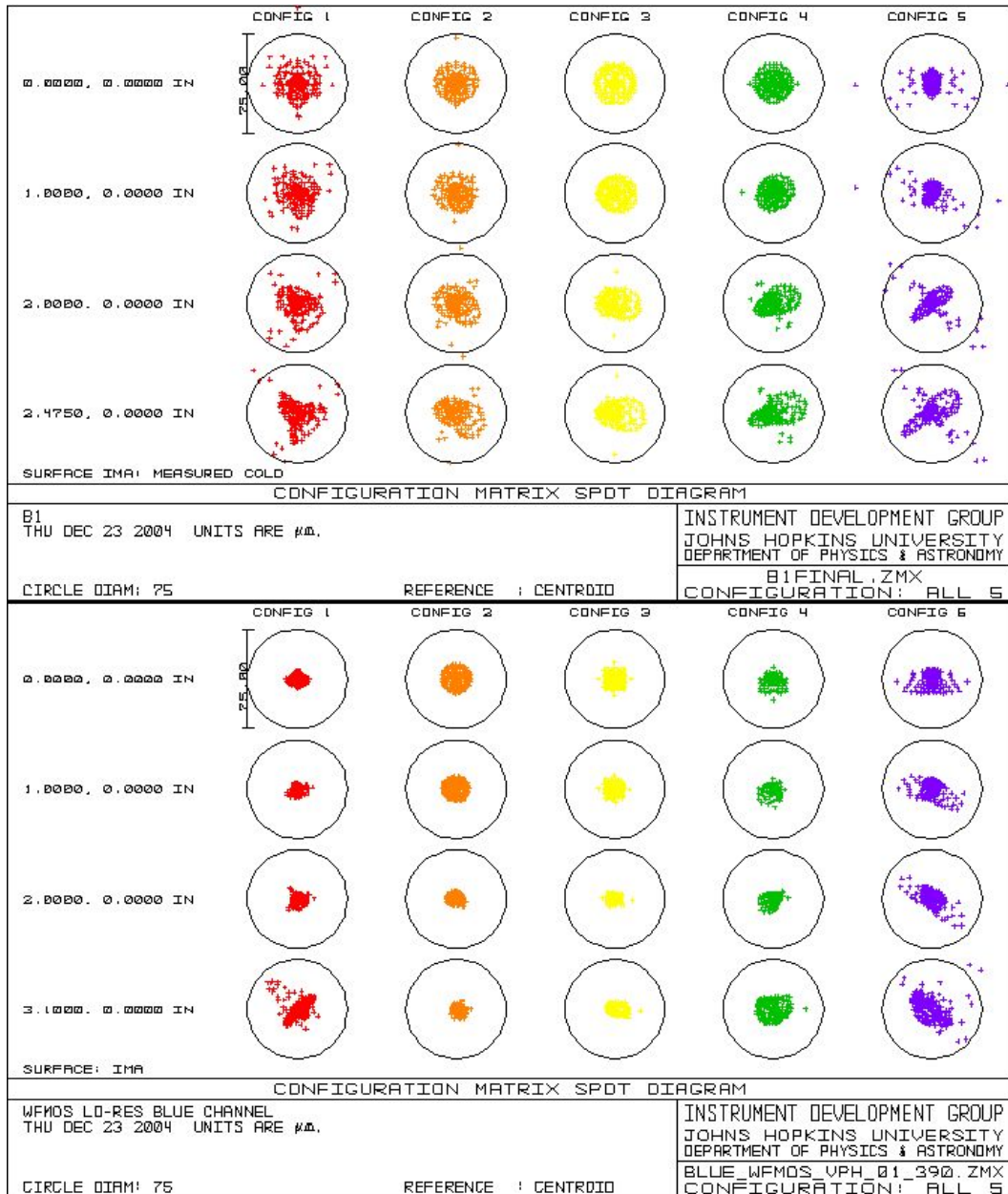


Figure 144: Spot diagrams for SDSS (top) and WFMOs (bottom) blue channels. For SDSS, the wavelengths are (right to left): 610, 555, 500, 440, 390 nm. For WFMOs: 655, 586, 516, 460, 390 nm. Circles are again representative of the size of the fiber image on the detector.

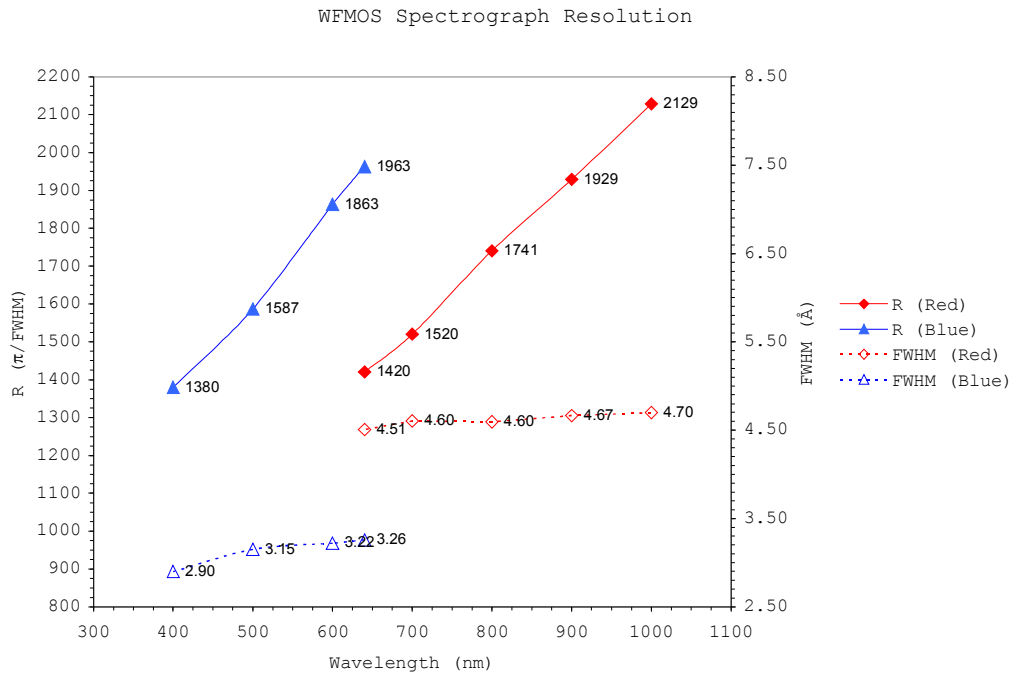
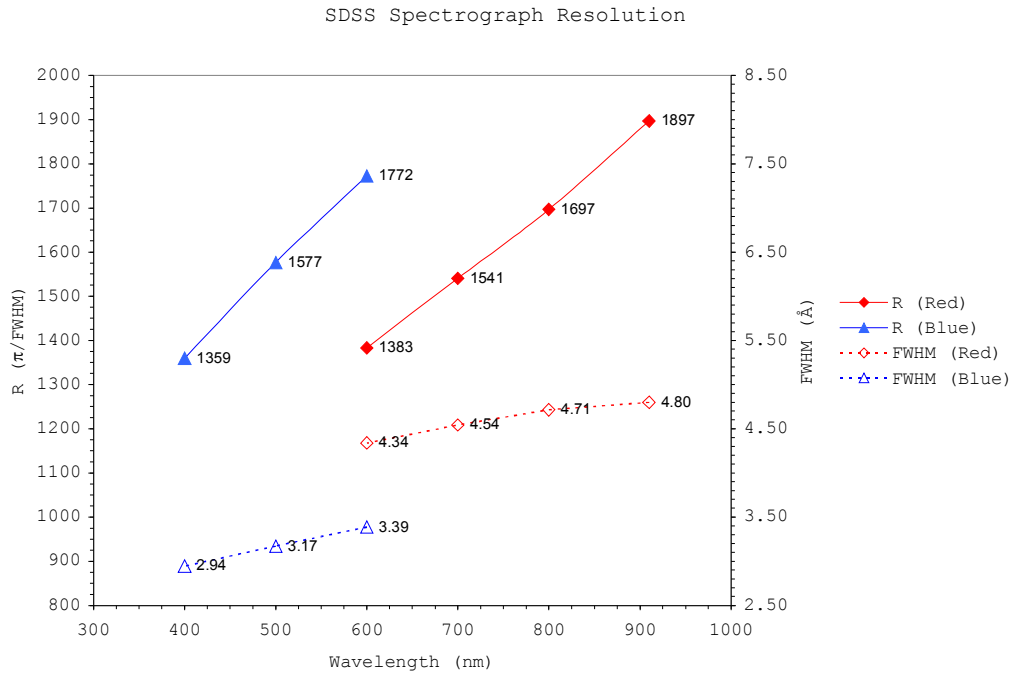


Figure 145: Plots of resolution and spectral FWHM for the SDSS (top) and WFOS (bottom) spectrograph designs.

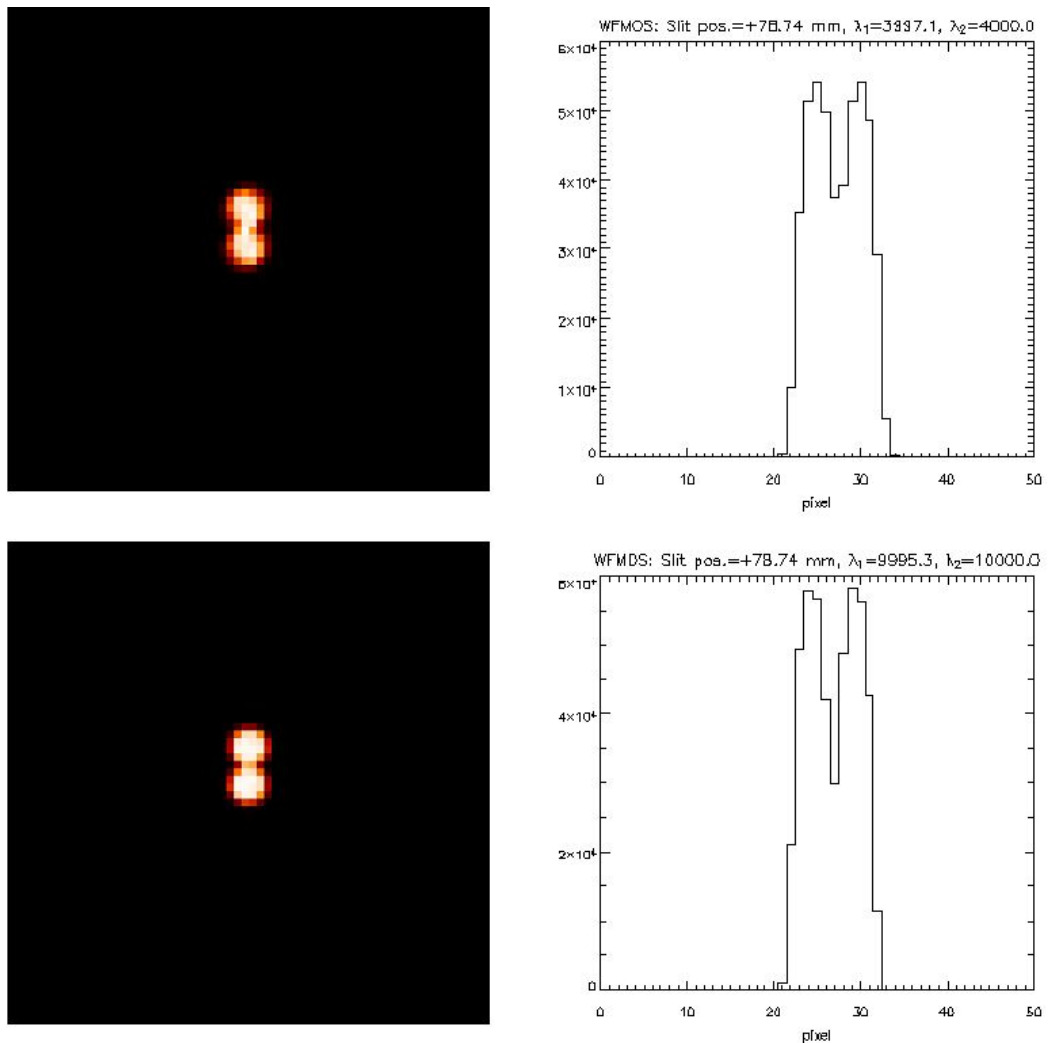


Figure 146: Simulated WF MOS images of two lines separated spectrally by $\Delta\lambda$ as reported in Figure 145, along with a plot of the collapsed spectrum. The lines are well resolved. The top row is at 400 nm; the bottom row is at 1000 nm. For both, the image was placed at the end of the WF MOS slit, where the RMS spot size was largest.

14.2.2.3 Throughput

The SDSS spectrographs form the basis for the efficiency model developed for the WF MOS low dispersion spectrographs. The model for SDSS consists of component efficiencies as a function of wavelength for the following: atmospheric extinction, telescope, fibers, collimator, dichroic, grism, camera, and CCD. *Measured curves* were used for the collimator, dichroic, grism, camera coatings, and CCD QE. Internal transmission curves for the camera glasses were obtained from the manufacturer's data sheets. The telescope and fiber efficiencies came from the SDSS spectrograph purple book (www.astro.princeton.edu/PBOOK/spectro/spectro.htm). Figure 147 shows the individual component efficiencies used for this model. The ripples in the dichroic curve ("ringing" due to the sharp edge) could be a concern, but practical experience with SDSS has shown that such variations are well corrected in the flux calibration.

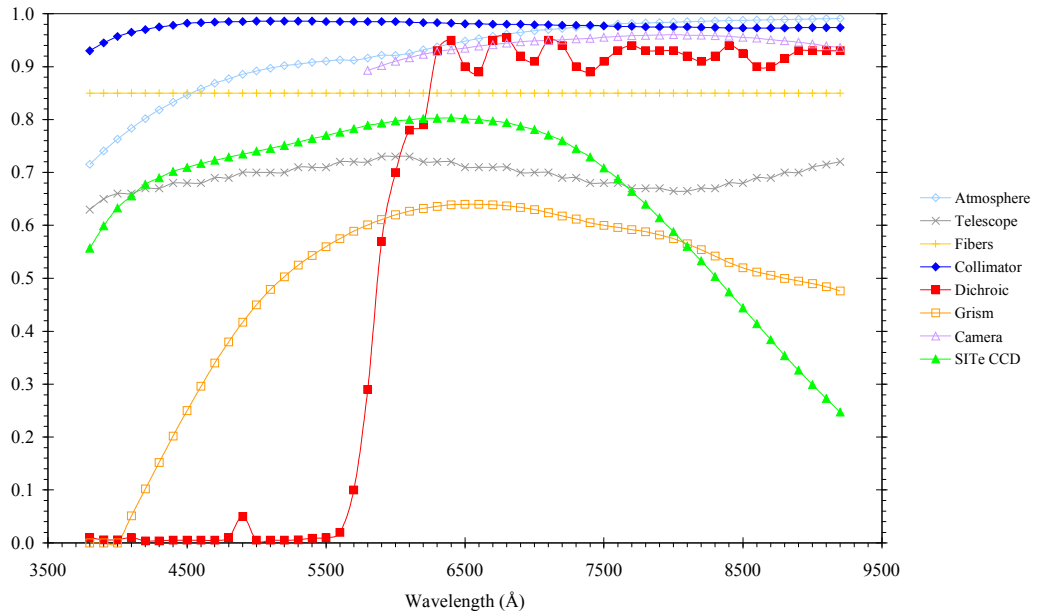
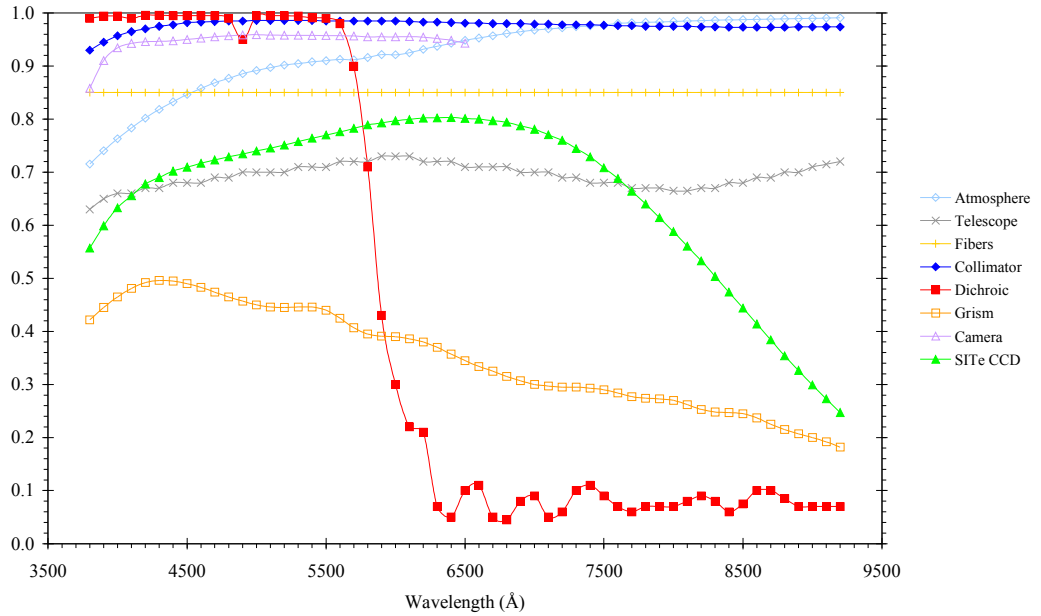


Figure 147: Component efficiencies for the SDSS spectrograph model: blue channel (top) and red channel (bottom).

Figure 148 shows end-to-end throughput curves for the SDSS spectrographs. The measured curves are taken from the JHU SDSS web site (<http://www.jhu.edu/~sdss/Spectrographs/Throughput.html>) and the model curve is derived from the component efficiency model described above. The agreement between the model and measured curves is very good.

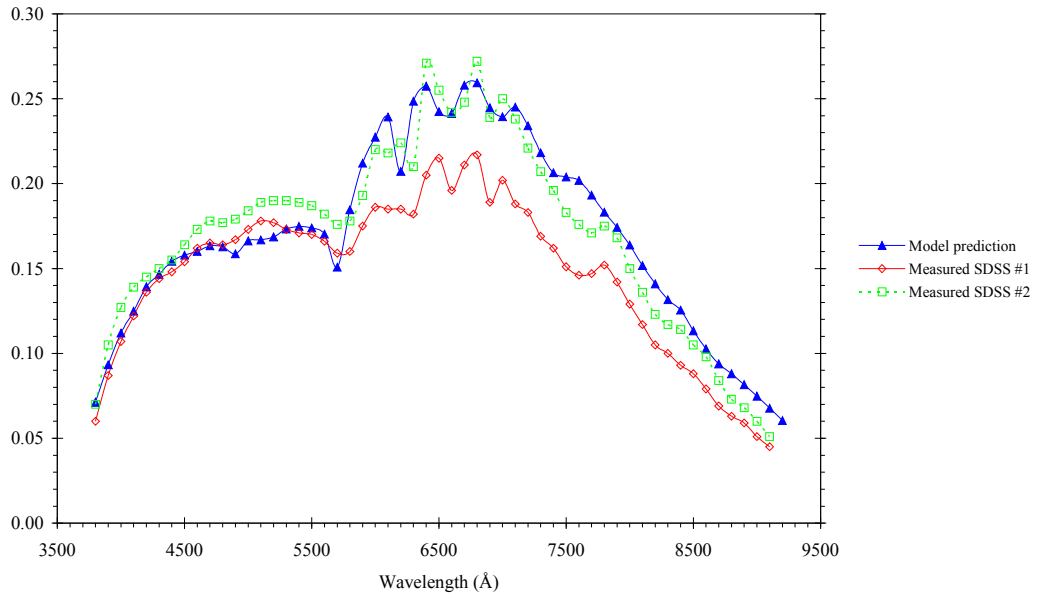


Figure 148: Component model throughput prediction and measured end-to-end throughput for the as-built SDSS spectrographs.

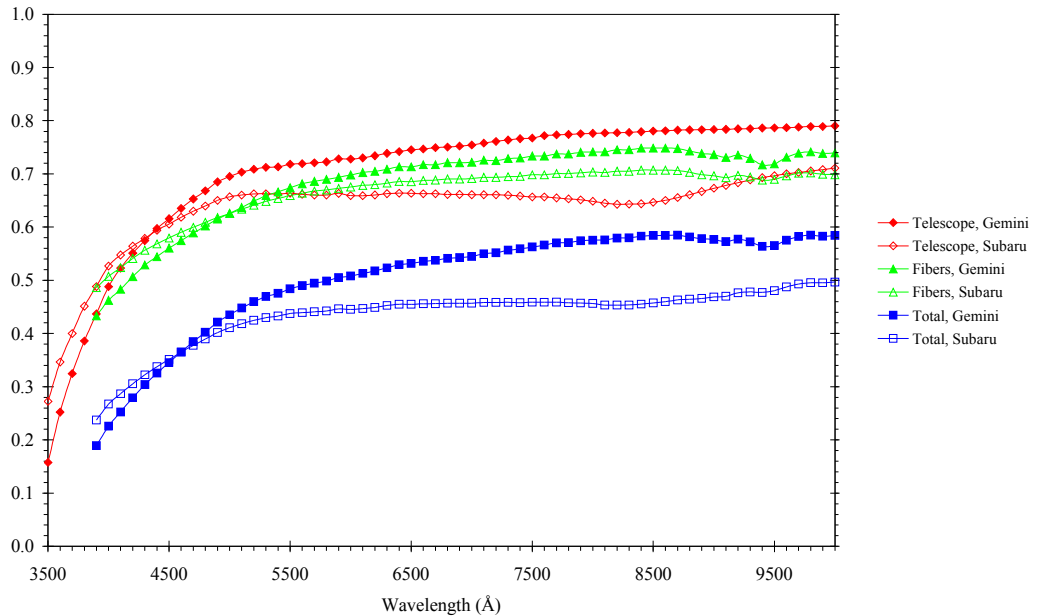


Figure 149: Front-end (i.e., non-spectrograph) efficiencies used in the WFMOS model for both the Gemini and Subaru telescopes. The telescope curves include atmosphere, primary, and corrector; the fiber curves include transmission (both 100 and 200 μm fiber runs), air/glass interfaces, fiber connector, and vignetting loss.

Having thus validated the component efficiency model with real measurements from the actual instrument, we can apply the same model with confidence to predict the efficiency of the WFMOS low dispersion spectrographs based on the SDSS instrument design. shows the modelled efficiencies for everything prior to the spectrographs. The 4-layer protected silver coating was used for the Gemini primary, while for Subaru an aluminum coating was assumed. Fiber lengths of 60 m and 40 m were assumed for Gemini and Subaru, respectively. Due to the aluminum coating and shorter fiber run, Subaru is more efficient below ~ 460 nm. Figure 150 shows the spectrograph component efficiencies for both channels..Two

curves are shown for VPH gratings for each channel. One is the RCWA prediction from KOSI for a preliminary, unoptimized grating design, derated by a hefty 10% from the theoretical curve. The other is from very recent measurements of the new LDSS-2 (Magellan) VPH gratings performed at JHU. The LDSS-2 gratings are similar in design to the WF MOS gratings, with the gratings manufactured by Wasatch Photonics (WP) and bonded to prisms at JHU. We have chosen to use the measured LDSS-2 efficiencies for the throughput predictions presented here.

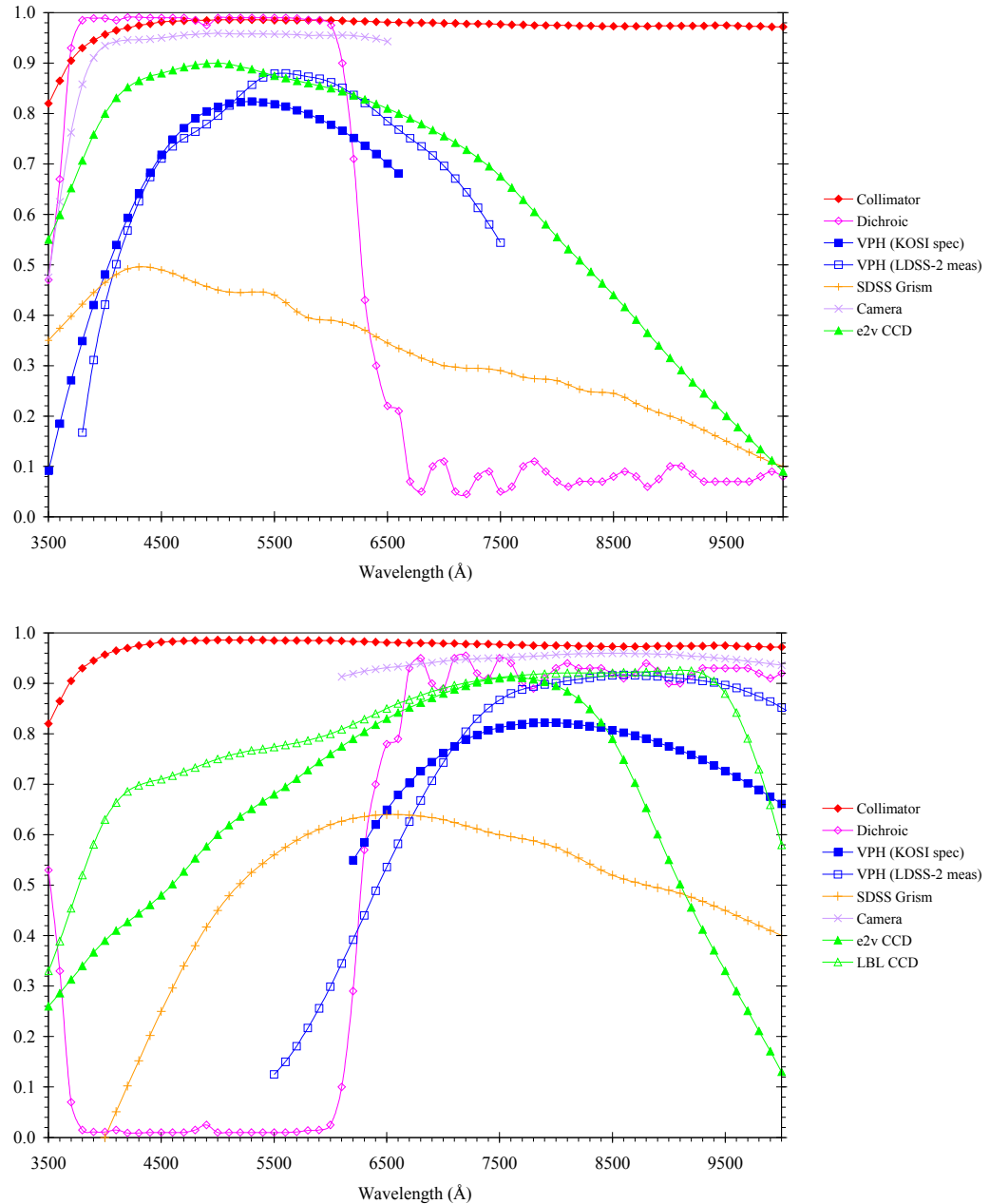


Figure 150: WF MOS spectrograph component efficiencies used in the model: (top) blue channel and (bottom) red channel.

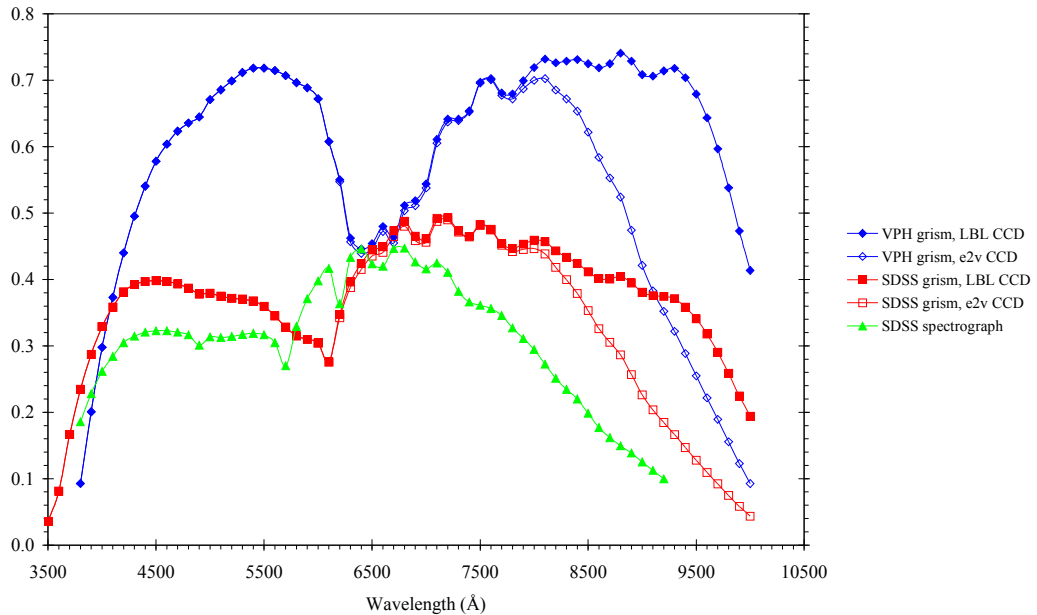


Figure 151: Instrumental efficiency predictions for the WFMOS low dispersion spectrographs.

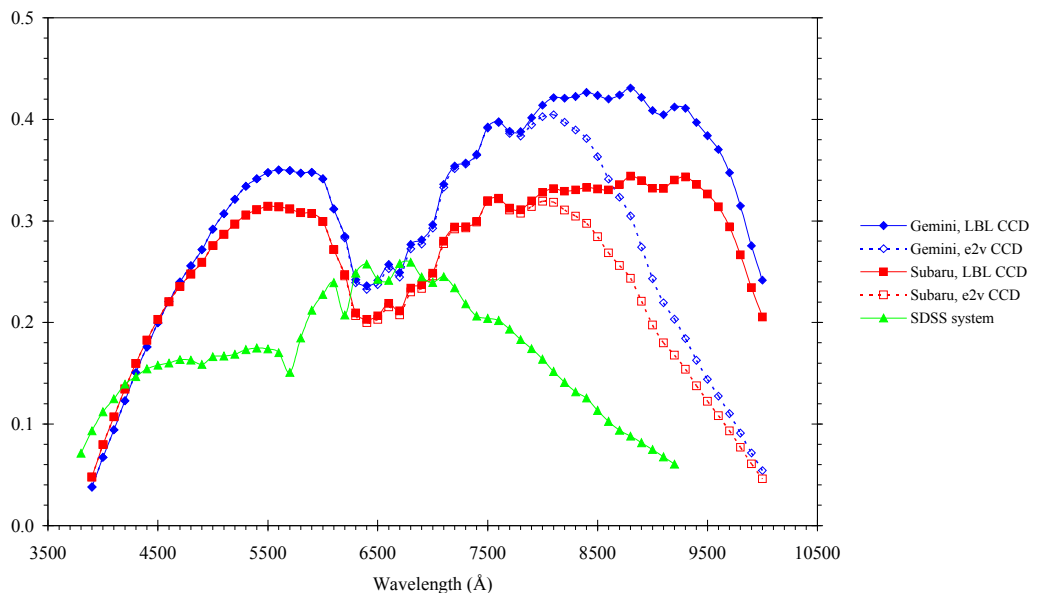


Figure 152: End-to-end throughput predictions for the WFMOS low dispersion spectrographs. Aperture/seeing losses are not included here.

Figure 151 shows the instrumental efficiency prediction for the WFMOS low dispersion spectrographs based on the SDSS design. Curves are shown using the VPH gratings as well as exact replicas of the SDSS gratings. Clearly the use of VPH gratings will enhance the efficiency of these spectrographs significantly over that realized by SDSS, so much so that VPH gratings are now the baseline and we are no longer considering the use of conventionally ruled and replicated surface-relief gratings. KOSI and WP (formerly Ralcon) gratings are now used in spectrographs at many observatories.

Another enhancement to the SDSS spectrograph efficiency comes from improved CCD response. The SITe CCD used for SDSS had excellent QE as seen in Figure

, but employed a broadband AR coating that peaked just longward of 6000 Å and fell rather rapidly beyond 7000 Å. With AR coatings better matched to the two bandpasses and enhanced red sensitivity offered by high-resistivity deep depletion devices, significant gains in efficiency will be realized in both channels, but especially in the red, for WFMOS. Figure 150 shows curves employing two possible CCDs for the red channel: e2v's deep depletion NIR device and Lawrence Berkeley Lab's high-resistivity, fully depleted device, which has significantly better response longward of 8000 Å. For the blue channel, an e2v device with the astronomy BBAR coating was assumed for all four WFMOS curves shown.

The combination of VPH gratings and better CCDs provides an increase in peak instrumental efficiency from 49% for SDSS to 74% for WFMOS (using LBL CCDs for the red channel; the peak is 70% using the e2v CCDs). *This factor of 1.5 improvement in throughput comes entirely from two demonstrated technologies and thus we feel our numbers are extremely robust.* shows the predicted end-to-end throughput from the model on both Gemini and Subaru, with the SDSS curve included for comparison. The peak throughput of the WFMOS spectrographs on Gemini with LBL CCDs is 43%, a factor of 1.65 increase in performance over SDSS at 26%. On Subaru, with an aluminium coating on the primary, the peak throughput is 34%, still a factor of 1.3 higher than SDSS. And Subaru is slightly better than Gemini below 460 nm.

This throughput performance compares with the baseline Purple Book peak of 23% for single channel low-resolution gratings (Fig 3.1.29), and represents almost a doubling of the integrated photon flux between 400 and 1000 nm. Table 27 gives the integrated flux relative to the Purple Book prediction for both telescopes and choice of red channel CCD.

Table 27 Relative integrated photon flux from 400 – 1000 nm.

Purple Book Fig. 3.1.29	Gemini LBL CCDs	Gemini e2v CCDs	Subaru LBL CCDs	Subaru e2v CCDs
1.00	1.92	1.63	1.64	1.40

We re-emphasize that while these results are spectacular, they are based on well-tested component efficiencies.

14.2.3 Mechanical Design

14.2.3.1 Overview

The mechanical design, like the optical, follows closely from that of the SDSS spectrographs, which have performed very reliably over the past seven years. For SDSS, the twin spectrographs were mounted on the telescope. This was done to minimize the repeated bending of the fibers that would occur with floor-mounted spectrographs, as well as minimizing the length of the fibers. With telescope-mounted spectrographs, flexure in the optical bench was critical, and it was also important to protect the optics from dust and condensation. The mechanical design thus incorporates a closed, stiff optical bench. While not as strictly necessary for the WFMOS spectrographs, this proven heritage does have the advantages of protecting the optics environmentally, as well as protecting the optics mechanically and maintaining alignment during handling. Hence, given the proven on-sky performance, reliability, and design heritage of the SDSS spectrographs, we have chosen to maintain the overall mechanical design and simply scale it to meet the WFMOS requirements.

Figure 153 shows the WFMOS low resolution spectrograph. The mechanical layout of the instrument is identical to the SDSS spectrographs and the size and mass differ only slightly. The main difference is a slight increase in height. Instrument height is driven by the size of the collimator, which is slightly taller for WFMOS in order to utilize the full height of the detector and to maximize the number of fibers at the slit. The overall length, width, and height of the instrument is ~ 2230 mm x 1000 mm x 570 mm, respectively. The instrument mass is 318 kg. Like the SDSS design, all optical subassemblies (i.e. the slit assembly, collimator, central optics, and cameras) interface to a common, enclosed optical bench. Each of these subassemblies is described in more detail below.

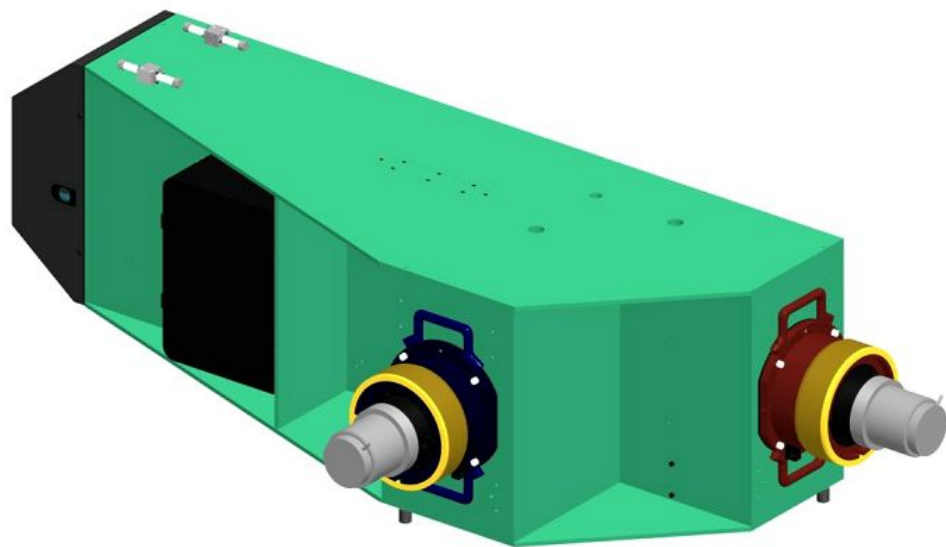


Figure 153: Rendering of the WFMOS low resolution spectrographs. The design has been scaled from the SDSS spectrographs to meet the WFMOS requirements.

14.2.3.2 Optical Bench

One of the primary design goals during the development of the SDSS spectrographs was to simplify alignment of optical components mounted to the

optical bench. To achieve this goal, it was decided that, wherever possible, adjustments would be eliminated in favor of precision machined interfaces that would guarantee accurate and repeatable component placement. This objective, combined with the flexure and environmental requirements, led to the enclosed optical bench design shown in Figure 153. Though the flexure and environmental requirements for WFMOS are far less stringent, the nicety of being able to assemble the instrument without time-consuming adjustments, as well as design heritage and robustness, make the SDSS bench design a logical choice for WFMOS.

The WFMOS low-resolution spectrograph layout, depicted in Figure 154, shows the optical bench and the optomechanical subassemblies that interface to it. As shown in the figure, the dual-channel optical design naturally leads to a T-shaped bench design. In this configuration, the red and blue channel cameras, as well as the collimator assembly, mount to exterior faces of the bench; one at the end of each leg of the “T”. The fiber slithead and the central optics assembly, which contains the dichroic and grisms, are mounted internally. At all of these subassembly interfaces the bench surfaces are precision machined to guarantee optical alignment. Instrument control electronics and CCD controllers (not shown) mount to exterior walls of the bench.

The SDSS optical bench was constructed as a weldment from 6061-T6 plate stock. Each plate was machined for dimensional control and features were machined into the plates to create an interlocking, snap-together, structure that minimized plate displacement during welding. Subsequent to welding the structure was heat treated, stress relieved, and then machined. This method of fabrication was successful and was economical for the quantity of two required for SDSS. And for this study we have based the cost of the bench on this fabrication approach. However, for the larger quantities which are required for WFMOS, there may be some benefit to using a casting instead of a weldment. This option should be investigated as part of a design study.

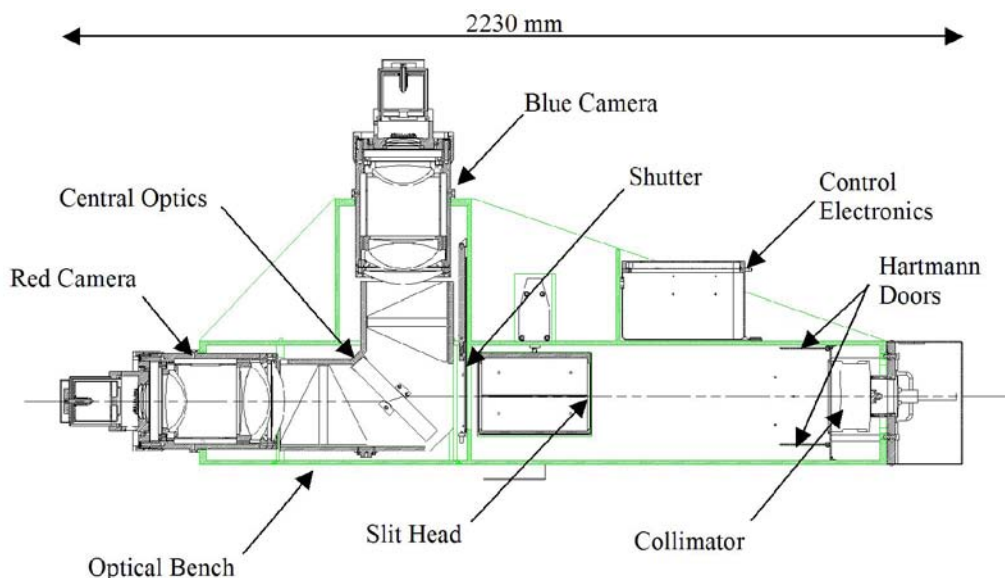


Figure 154: WFMOS low resolution spectrograph optomechanical layout. Optomechanical subassemblies interface to the optical bench at machined interfaces dramatically reducing the number and complexity of adjustments. The central optics subassembly contains the dichroic and the grisms.

14.2.3.3 Slithead

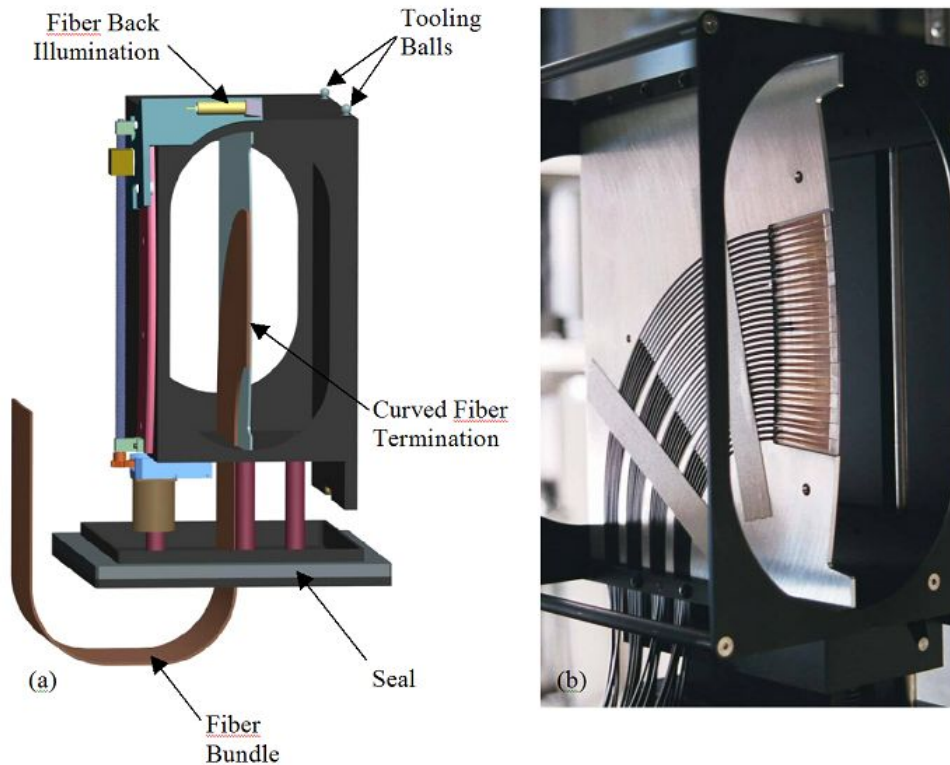


Figure 155: (a) Slithead design. The fiber bundle enters the slithead through the base, which is sealed against the surface of the optical bench. The fibers terminate along the curved edge of the central vertical plate; the radius of curvature being half the radius of the collimator. (b) Image of the SDSS slithead showing the fiber strain relief and termination.

Fibers from the telescope focal plane enter the spectrograph through the slithead, which serves as the optomechanical interface between the fibers and the optical bench; see Figure 155. As shown in the figure, the slithead is a box structure with openings in the front and rear faces so that light reflected by the collimator can pass through the system. In this scheme, the fibers are routed through the bottom of the slithead, gently bend along the surface of a thin vertical plate, and then terminate normal to an arc; the axis of each fiber being normal to the collimator. A total of 292 fibers are spaced along the vertical plate with a fiber-to-fiber spacing of $560\ \mu\text{m}$. The total height of the fiber slit is 157.5 mm. The thin vertical plate spans from the top to the bottom of the slithead and vignettes a small portion of the beam. It provides strain relief for the fibers and the curved leading edge serves as a gage for mounting the fibers on the correct arc. The fiber back-illumination system mounts to the side of the slithead and is described in detail in Section 14.2.3.9.

The slithead mounts kinematically to the side wall of the optical bench. Two tooling balls at the top of the structure engage a conical socket and a v-groove mounted to the bench. A third tooling ball, mounted to the base of the optical bench side wall, engages a hardened surface on the structure of the slithead. The slithead is held in place by a single pneumatic clamp that seats all three contact interfaces. The kinematic mount guarantees repeatable placement of the slithead in the spectrograph; a requirement for the SDSS spectrographs since slitheads were exchanged for each field observed. While not strictly necessary for WFMOS, this

kinematic mount is robust, economical, and desirable should the unit have to be removed to repair a damaged fiber.

We envision that, like the SDSS spectrographs, the fibers will be terminated in v-block modules, each module containing approximately twenty fibers.

14.2.3.4 Collimator

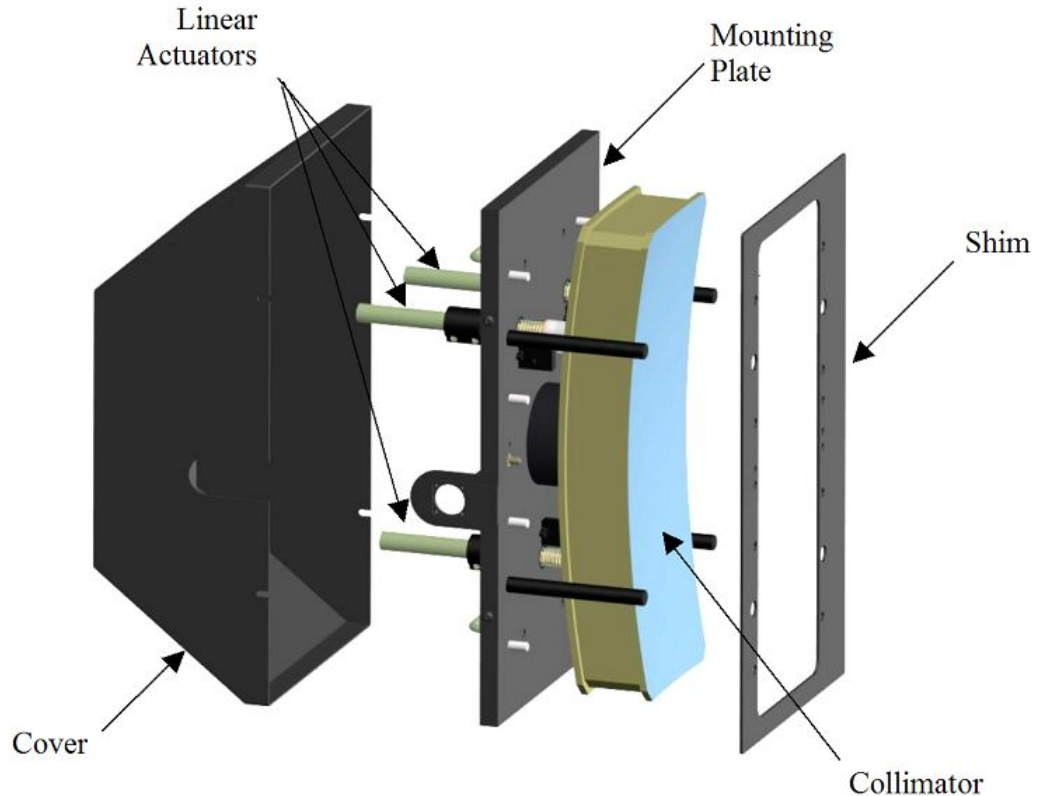


Figure 156: Collimator mount and position control. The collimator is supported in-plane by a membrane flexure and out-of-plane by three linear actuators. The three actuators provide tip, tilt, and piston control of the collimator. A shim between the mounting plate and the optical bench facilitates coarse, one-time, focus adjustments.

The collimator is the only actively controlled optic in the spectrograph. The tall rectangular collimator is controlled in tip, tilt, and piston by three linear actuators. These degrees of freedom allow for routine focus adjustment (piston), as well as spatial and spectral adjustment of the slit image on the detector (tip and tilt).

Details of the motion control system are depicted in Figure 156. The mechanical configuration is fairly simple. The mirror is supported from the back surface, at its center, by a circular membrane flexure (not visible in the figure). This flexure constrains the mirror in-plane but allows out-of-plane compliance for tip, tilt, and piston adjustment. The out-of-plane control is provided by three linear actuators that also attach to the back of the mirror. Motion of each actuator is limited (by limit switches) to ± 3 mm. The linear actuators as well as the fixed edge of the membrane flexure are attached to a common mounting plate, which is the interface to the optical bench. A shim between the mounting plate and the optical bench facilitates one-time, gross focus adjustment. Accurate and repeatable assembly of the subsystem is made possible by two dowel pins (one round and one diamond shape) that engage hardened bushings pressed into the optical bench. Safe installation is facilitated by two handles for lifting and four guide rods that

flank the collimator and ensure the collimator clears the bench opening as it is installed. A cover protects the actuators and helps cut down on stray light.

The linear actuators used for the SDSS spectrographs were DC-Mike actuators from Physik Instrumente. These devices consist of a micro DC servomotor, gearhead, lead screw, and encoder packaged in a round slender form-factor. They provide submicron resolution ($\sim 0.3 \mu\text{m}$), which is more than sufficient for this application; the required resolution $\sim 1 \mu\text{m}$.

14.2.3.5 Hartmann Doors

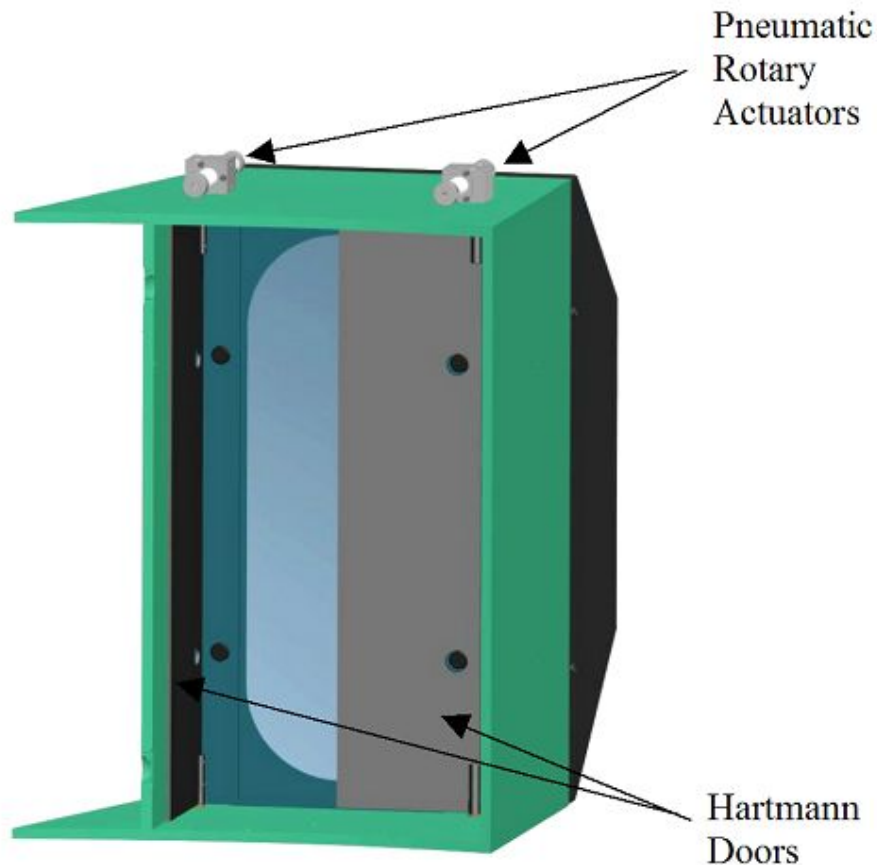


Figure 157: Cutaway view showing the Hartmann doors. The bi-fold doors reside just in front of the collimator stop and are controlled by pneumatic rotary actuators. The right hand door is shown closed in this figure.

Figure 157. The doors are used to perform a Hartmann test, which enables quick focus determination. Once complete, the out-of-focus condition is quantified in software and then corrected by a piston adjustment of the collimator. The two channels of the spectrograph are made parfocal by a one-time focus adjustment at the cameras; therefore focus in both channels is corrected by the piston adjustment.

The doors are driven by simple, 90 degree, pneumatic rotary actuators. Actuation of these devices is controlled by the embedded controller in the spectrograph electronics box.

14.2.3.6 Shutter

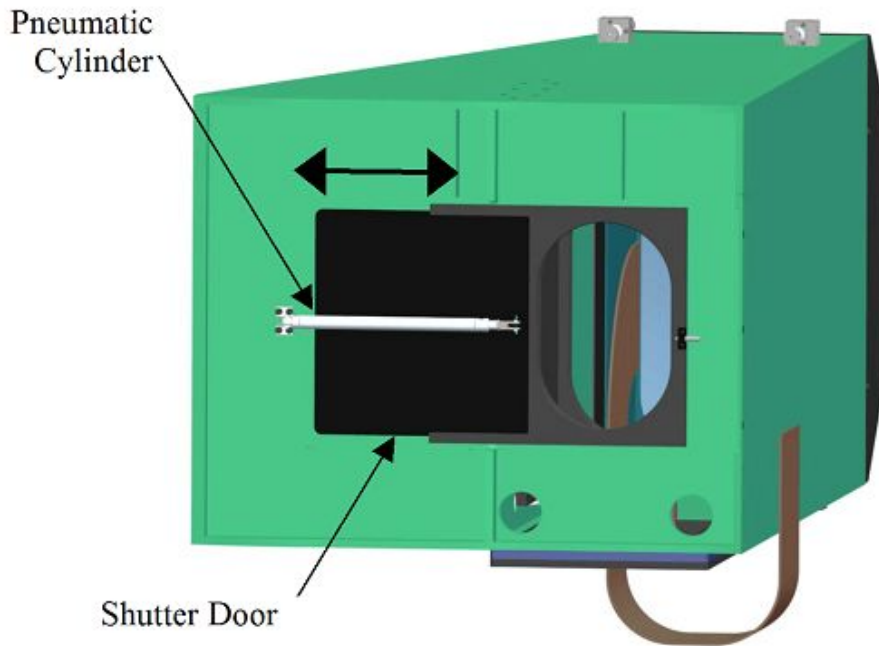


Figure 158: Cutaway view showing the shutter. The shutter is a simple sliding door driven by a pneumatic cylinder.

A single shutter is used to control the exposure in both channels. It is located just upstream of the dichroic on a dividing wall in the optical bench; see Figure 158. At this location the beam is blocked to both channels of the spectrograph when the shutter is closed.

The shutter is a very simple, reliable, sliding-door mechanism; identical to that used in the SDSS spectrographs. The pneumatically driven door slides in the slots of a picture-frame guide, which has a cut-out matched to the beam profile. Aside from guiding the door, the slots also make a light tight seal when the door is closed. Actuation is controlled by the embedded controller in the spectrograph electronics box.

14.2.3.7 Central Optics

Like the SDSS spectrographs, the dichroic and the two gratings are mounted inside the optical bench in a single optomechanical assembly referred to as the “central optics”; see Figure 159. This assembly is kinematically located by machined reference surfaces, which eliminates the need for adjustment. The “L”-shaped structure is 429 mm long, 419 mm deep, and 286 mm tall. The mass is 58 kg. It is approximately 15% larger and 40% more massive than the SDSS assembly due to the taller slit (which necessitates a taller dichroic and gratings) and the use of VPH gratings.

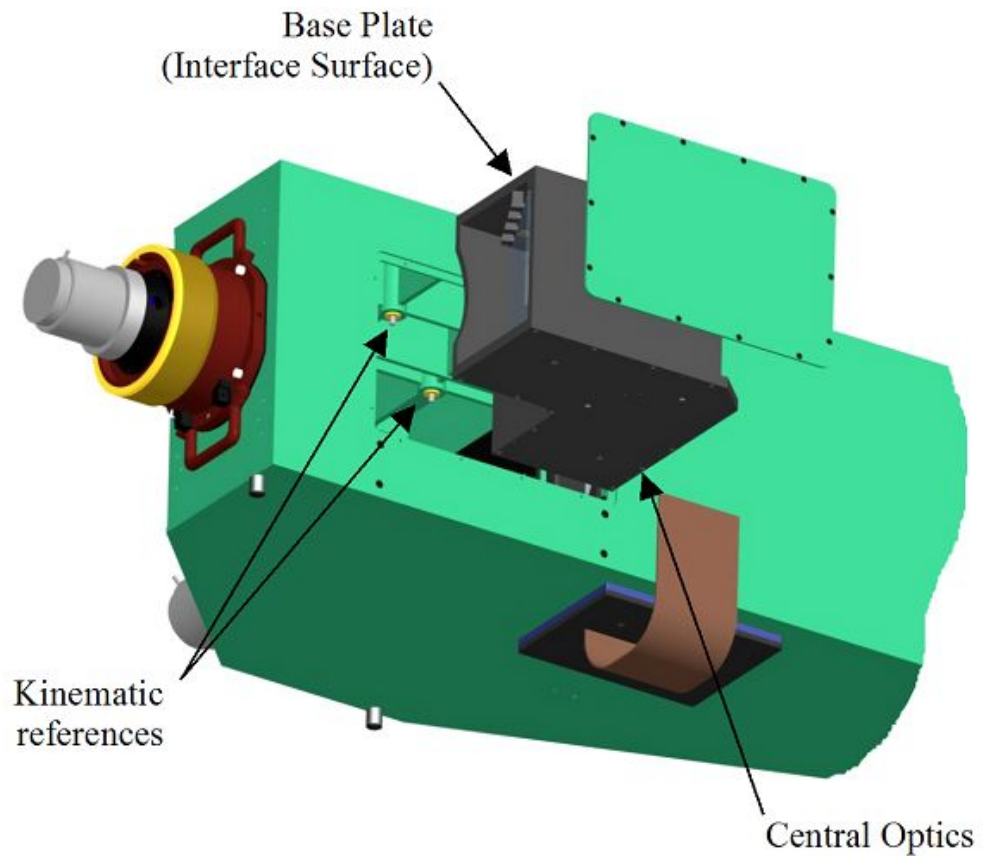


Figure 159: Central optics integration. The assembly inserted through an opening in the side of the bench and is mounted without adjustment. Kinematic reference surfaces internal to the bench interface to the base plate, precisely locating the assembly.

Details of the central optics assembly are shown in Figure 160. The three elements are each located, without any adjustment, by six machined reference surfaces. Spring plunger assemblies located on the top and base plates seat the elements against these surfaces and allow for differential contraction between the glass optics and the aluminum structure. To improve placement accuracy, the mounting scheme used here integrates all but one of the eighteen reference surfaces on the same side of the base plate, the opposite side being the interface to the optical bench. The advantage to such an approach is that these surfaces can be machined in the same setup, which is inherently accurate. The remaining reference surface is located on the top plate and it controls the tip of the dichroic. Accurate placement of this last surface hinges on tolerance stack-up within the structure, and was not an issue for the SDSS assembly.

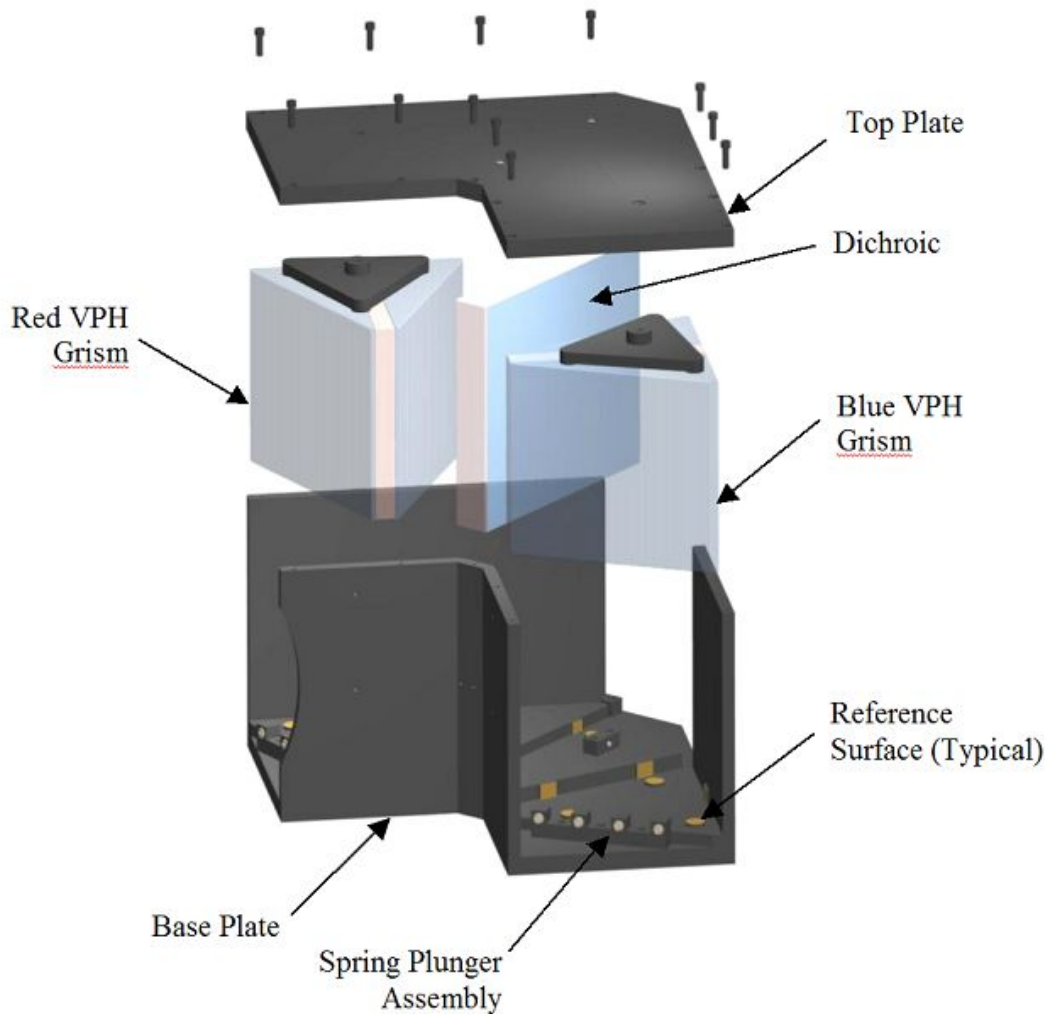


Figure 160: Optomechanical details of the central optics assembly. The dichroic and two gratings are each kinematically located by six reference surfaces. Spring plungers are used to constrain the elements and accommodate differential contraction between the glass and the aluminum structure.

14.2.3.8 Camera Optomechanics

The baseline for the camera optomechanics is the SDSS spectrograph camera design; see Figure 161. Like its predecessors (the Keck Low-Resolution Imaging Spectrometer (LRIS), and the Norris spectrograph at Palomar) the lenses and lens-groups are mounted in athermal cells. The cells are bolted together in series and mounted in a common barrel. Reference diameters, machined in the same step as the lens bores, establish lens concentricity from cell-to-cell. This technique has been successful in the past for the lens sizes, materials, and configuration described above (see Section 14.2.1.6) making it a logical approach for WMOS.

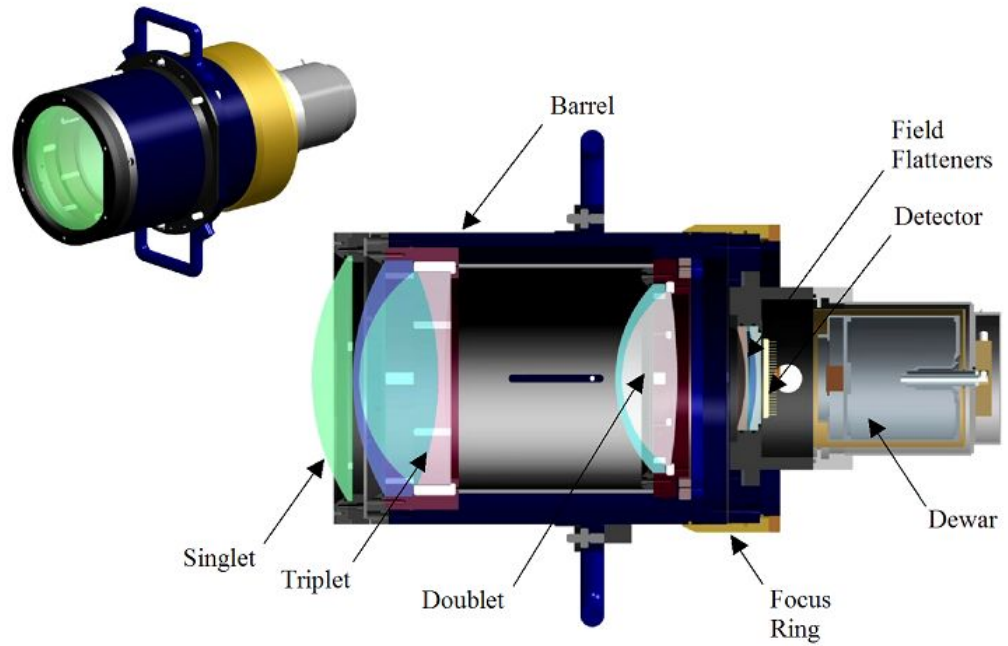


Figure 161: Optomechanical design of the SDSS cameras (blue camera shown here). Lens elements are mounted in cells which are mounted in a common barrel. The focus ring translates the dewar assembly, which contains the field flatteners. This focus adjustment is used strictly to make the two channels parfocal.

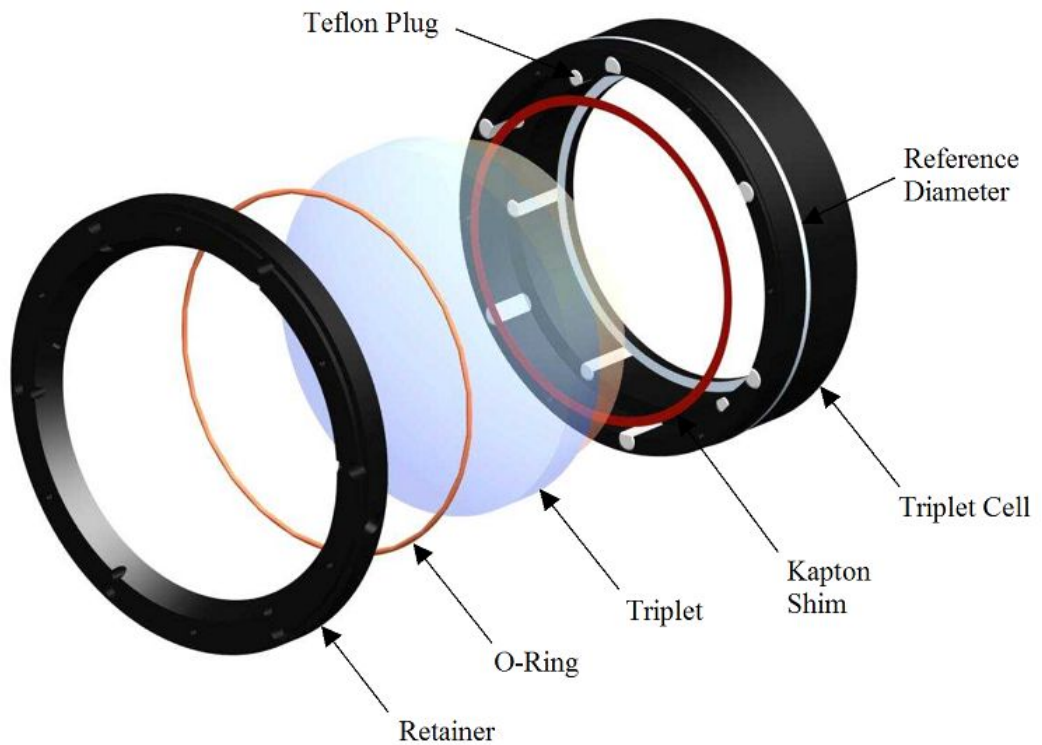


Figure 162: SDSS triplet cell. Glass-filled Teflon plugs are bored to fit the as-built lens diameters. Reference surfaces machined in the same setup guarantee accurate placement of the elements within the barrel. An o-ring between the retainer and first surface of the triplet retains the lenses and accommodates differential expansion between the glass lenses and metal cell.

The design and construction of the athermal cell design is best described as follows. A metal ring with an appropriate coefficient of thermal expansion is bored oversize to the as built lens diameter. Six glass-filled Teflon plugs are

lightly pressed into a hole pattern circumscribing the lens bore. These plugs are then bored on a lathe to a diameter that just clears the as-built lens diameter. In the same machining step, the lens axial locating faces and cell reference diameters are machined, thus achieving lens concentricity (within the limits of radial clearance) and perpendicularity to the optical axis. The plug diameter is calculated such that the net change in the diameter of the finished bore is less than the diametrical clearance to the lens over the temperature range of interest, given the coefficients of expansion for the metal ring, the Teflon plug, and the glass lens. Where lens groups are packaged in a single cell, multiple sets of plugs are used. For the SDSS cameras, aluminum was used for the singlet and doublet cells, and steel was used for the triplet cell. A Kapton shim is used between the lens locating face and the cell. An o-ring between the retaining ring and first lens surface provides force to seat the lens and compliance to accommodate differential expansion. A rendered image of the triplet cell depicting these details is shown in Figure 162.

In the SDSS camera, the singlet cell attaches to the front of the triplet cell, which in turn attaches to the front of the outer camera barrel. The doublet cell is metered with respect to the triplet by a steel inner barrel. The length of this barrel and the thickness of a shim between the singlet and triplet cells are optimized for the as-built lens dimensions. Contact and compliance between the doublet cell and inner barrel is achieved using an array of stiff springs that push against the back face of the doublet cell.

The field flatteners are mounted in the front dewar flange just in front of the detector. The entire dewar is manually translated for focus adjustment using the focus ring on the OD of the camera barrel. This adjustment is used strictly to make the two channels of the spectrograph parfocal. Routine focus compensation is done using the automated piston adjustment of the collimator.

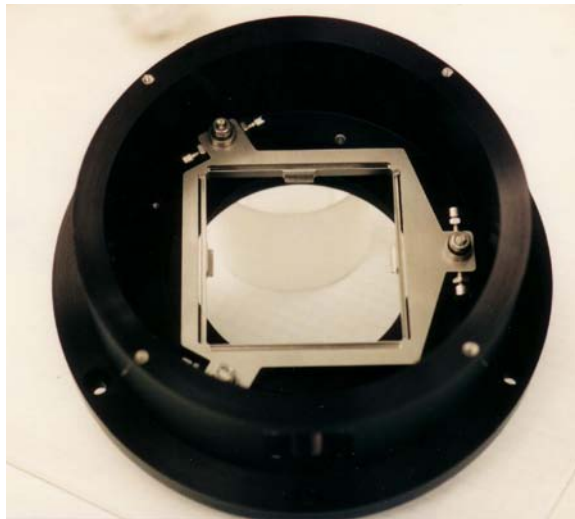


Figure 163: SDSS spectrograph detector mount. The jacking screws provide six degrees of freedom. Integral flexures mitigate stress in the package.

For WFMOs the detector will most likely be cooled by a closed cycle refrigeration system as opposed to LN₂, which was used for SDSS. Modifying the back end of the camera to accept this change should be straightforward. The detector mount however should be nearly identical, in concept, to the SDSS design (Figure 163). We envision that the 4k² array package would be nearly identical to the SITe detectors used for Sloan; hence, the invar mount and the three

point adjustment scheme would suffice for WMOS. The mount will have to be scaled, of course, to accommodate the 25% increase detector size.

14.2.3.9 Fiber Back Illumination

Like the SDSS spectrographs, a fiber back-illumination system is required to map the location of fibers in the focal plane to their respective positions on the slit. WMOS has the same requirement but the implementation is somewhat different. Here the fiber back-illumination system must be an integral part of the spectrograph since the slithead would not be removed from the spectrograph between observations. For Sloan, the plug plate and its companion slitheads are integrated into a single assembly, the fiber cartridge, which is configured off-line prior to observing. This off-line configuration made it possible to have a single back-illumination system that would temporarily mount to the slithead to map the fibers and then be removed prior to wheeling the cartridge to the telescope for installation and observing.

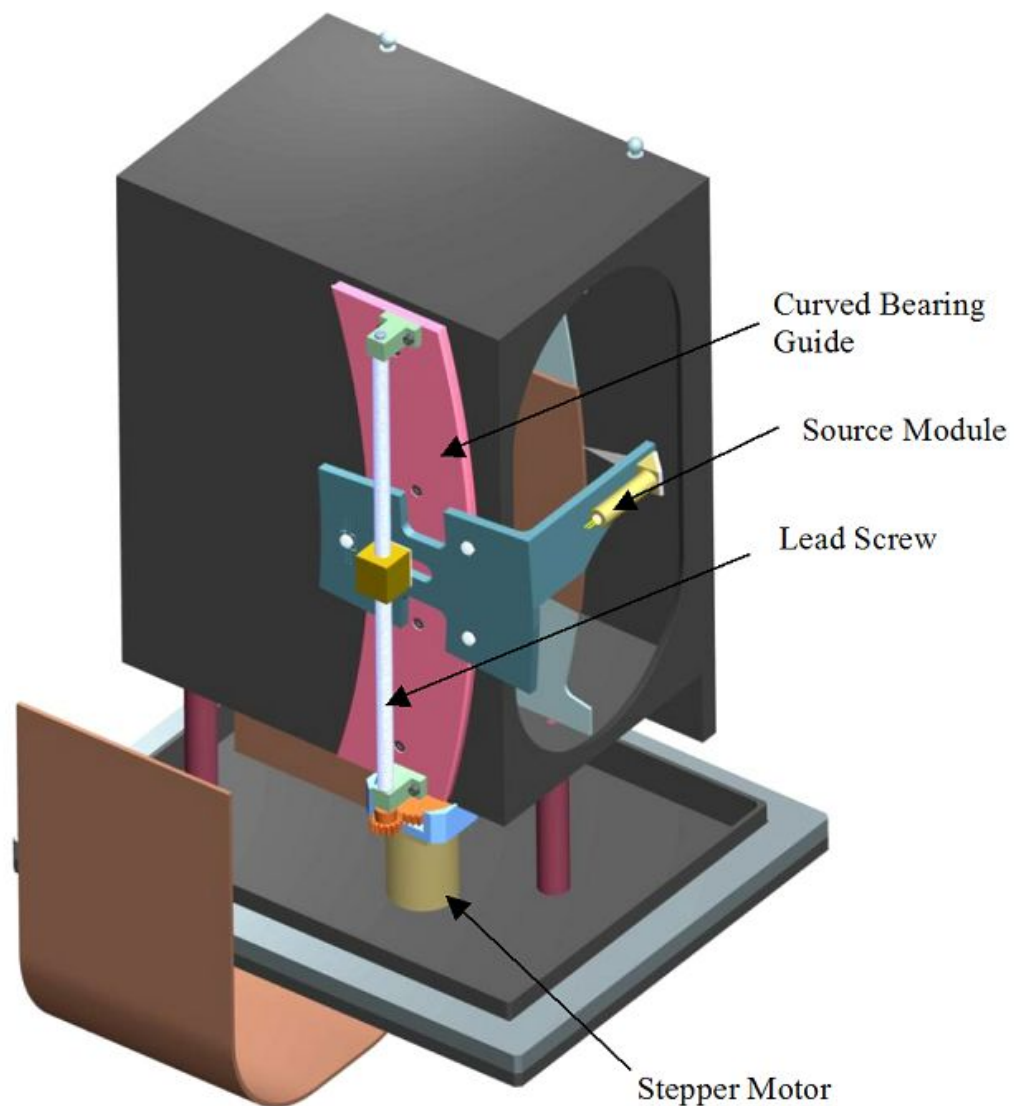


Figure 164: Fiber back illumination system. Fibers are illuminated sequentially by the focussed image of an LED as the head traverses along the curved bearing guide. Motive force is provided by the stepper motor driven lead screw.

The fiber back-illumination system envisioned for WFMOS is shown in Figure 164. Fibers are illuminated sequentially in scanning mode by a source focused on the front of the slit. As the head scans along the slit the fibers are illuminated one by one. A camera focused on the focal plane could image the fibers and determine centroids. This is similar to the method used for the SDSS spectrographs.

The optomechanics of the back-illumination system are fairly simple. The source module consists of an LED, a fold mirror, and a lens to reimage the LED source on the fiber. The module is mounted to the carriage of a curved translation stage that is driven by a stepper motor and lead screw. When parked, the head resides at the top of the slithead clear of the beam. The system shown in Figure 164 is designed to scan the 292 fiber slit in 15 seconds (an additional 15 seconds is required to return the head to the park position), which is negligible compared to the overall observation overhead. As specified, the system could scan the head much faster, or slower, by simply adjusting the motor speed.

14.2.4 Electrical System

Each spectrograph will have its own supporting electrical control system, housed in an enclosure and mounted externally to a side wall. The SDSS spectrograph electronics required an enclosure that provided heat removal and thermal insulation. The WFMOS spectrographs will be housed off the telescope in a more benign environment; therefore thermal control and thermal insulation will not be an issue. With these requirements lifted, an “off-the-shelf electronics enclosure, with minimal modification, can be employed. The electrical system will receive commands and provide telemetry via an Ethernet port using TCP/IP over a fiber interface. Refer to the system diagram in Figure 165. Control and housekeeping functions provided for the various spectrograph mechanisms are described in the following sections.

14.2.4.1 Collimator Tip/Tilt and Piston

The collimator positioning system consists of three servo motor controllers daisy-chained via an RS-485 communication interface. The embedded controller receives high-level mirror motion commands (R_x , R_y , and Z) from the Instrument Control Computer (ICC). These high-level commands are then converted to command structures understood by the motor controllers. Finally, motion commands are output from the embedded controller’s RS-485 output port. Upon motion completion, position information is harvested from the motor controllers, converted to engineering units, and telemetered back to the ICC on demand.

14.2.4.2 Fiber Back-Illumination

Motion control is provided for the fiber back-illumination system. This consists of a stepper motor indexer control, encoder feedback, and limit switch monitoring. The embedded controller communicates with the stepper motor indexer via an RS-232 communications port, similar to the collimator mirror positioning system.

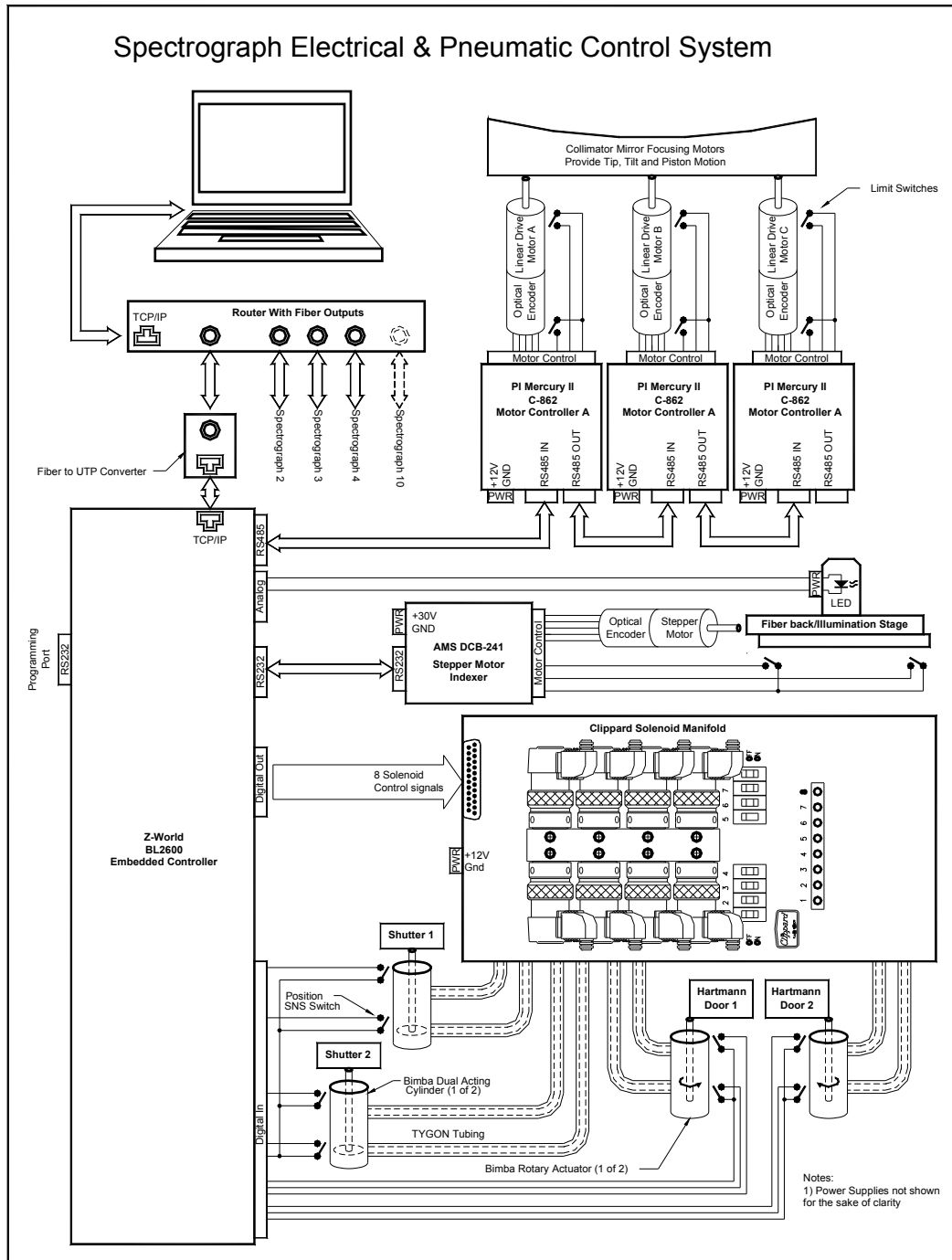


Figure 165: Electrical control system

14.2.4.3 Hartmann Doors

Hartmann door *Open* and *Close* commands are received by the embedded controller which then sets the appropriate output signals to activate pneumatic solenoid valves. The valves control air flow used activate pneumatic rotary actuators. Open and Close position sensing switches telemeter status back to the controller, available upon request to the ICC.

Table 28 SDSS spectrograph control commands.

Command	Parameter	Description
?	(none)	Returns this table of commands
a	n	Alter the exposure time to n seconds. Fails if no exposure
c	s,l,r,b	Close shutter or left/right/both Hartmann screens; note: closing one Hartmann screen opens the other
e	n	Expose of n seconds. Fails if currently exposing.
l	n	Left focus (open left Hartmann door and expose) for n seconds
m	a,b,c	Move motor a, b or c by n microns
o	s,l,r,b	Open shutter or left/right/both Hartmann doors. Note, opening one Hartmann door closes the other
P	(none)	Pause the current exposure. Closes the shutter but leaves the Hartmann doors alone. Fails if no current exposure
p	n	Piston the collimator mirror by n microns
R	(none)	Resume exposure paused with P. Fails if no paused exposure
r	n	Right focus (open right Hartmann door and expose) for n seconds
S	(none)	Stop an exposure, if present, closing the shutter and Hartmann doors.
s	(none)	Status
Z	(none)	Set Collimator mirror positions to zero

Table 29 SDSS spectrograph telemetry.

Keyword	Description of Value
SpectroID	0 for SP1, 1 for SP2
Air	On or Off
Shutter_open_sensor	On or Off
Shutter_closed_sensor	On or Off
Left_open_sensor	On or Off
Left_closed_sensor	On or Off
Right_open_sensor	On or Off
Right_closed_sensor	On or Off
Coll_motor_A	Position of collimator motor A
Coll_motor_B	Position of collimator motor B
Coll_motor_C	Position of collimator motor C
Requested_exp.time	Requested exposure time for current exposure, in sec; 0 if no exposure
Exp_time_left	Time remaining on the exposure, in sec; 0 if no exposure
Last_exp.time	Time of the last exposure, in sec
Exp_state	None, Paused or Exposing
Shutter_open_transit	Time taken by the shutter to open, in sec, for last open motion
Shutter_close_transit	Time taken by the shutter to close, in sec, for last close motion
Coll_motor_A_status	Status of collimation motor A. Motor status is 0xFF if unknown.
Coll_motor_B_status	Status of collimation motor B
Coll_motor_C_status	Status of collimation motor C

14.2.4.4 Shutter Doors

The shutter door control is very similar to that for the Hartmann doors, except that a linear cylinder actuator is used to position the shutter.

14.2.5 Software Design

Embedded control software will be stored in flash memory on a Z-World BL2600 controller. Each spectrograph will communicate with the Instrument Control Computer (ICC) via an Ethernet port using TCP/IP over fiber. Telnet interfaces will be established between the ICC and each spectrograph controller.

Spectrograph control software will be developed using Z-World's Dynamic C development system. Updates to the embedded code can be downloaded to the BL2600 via an RS-232 serial port. The embedded software will perform four main functions, described below.

14.2.5.1 Command Interpretation

The spectrograph software's main loop will continuously poll a receive buffer in expectation of ICC commands. Commands will be echoed back as receipt acknowledgement. Invalid commands will have an error code returned to the ICC. If a command is in progress, a busy character will be returned. Any errors that occur during the execution of a command will return an error code. Table 28 lists examples of commands currently used to control the SDSS spectrographs.

14.2.5.2 Telemetry Status

Up-to-date instrument status information will be stored in the local RAM of the embedded controller. This status information will be available to the ICC upon status requests. Telemetry information will be in engineering units such as microns, degrees, etc., as opposed to motor steps, counts, etc. Table 29 provides an example of the telemetry currently available from the SDSS spectrographs.

14.2.5.3 Instrument Control

The embedded controller will assume responsibility for issuing commands to various mechanisms within the spectrograph. It will monitor progress and verify proper positioning via encoder feedback and monitoring of limit and sense switches.

14.2.5.4 Health and Safety

The embedded controller will monitor internal systems for failures. It will perform prerequisite checks before issuing potentially harmful commands, such as the ICC attempting to command a motor beyond a limit position. The embedded software will provide error reporting back to the ICC.

14.3 Subaru vs Gemini

There are no direct technical or cost impacts to the SDSS-based low dispersion spectrographs associated with a Gemini versus Subaru implementation. As long as the spectrographs are fed by ~200 μm diameter fibers at $f/4$, the design will be the same. The number of spectrographs required drives the cost and is mostly dependent on the required number of low dispersion fibers, and whether Nod & Shuffle is implemented – issues decoupled to a large degree from the choice between Gemini and Subaru.

14.4 Cost Trades

14.4.1 Component Costs

Recent quotes from prospective vendors provide the basis for our estimates of the optical and mechanical component costs. Quotes were obtained for all major components, including the collimator mirror and hardware, dichroic, VPH grisms,

camera optics and optomechanics, optical bench, central optics hardware, and dewar hardware. Most other estimates are based directly on SDSS costs in today's dollars; a few are based on our best engineering judgement. Electronics components, excluding detectors and controllers (costed in a separate section), comprise a very small fraction of the overall cost and were estimated based on experience. All component costs are based on a quantity of ten spectrograph units.

14.4.1.1 Optical Components

The total cost for 10 spectrographs is broken down as follows: 42% for the cameras, 31% for the VPH grisms, 17% for the collimators, and 10% for the dichroics.

The cameras are very similar to the SDSS cameras, and we believe there are no major technical or schedule risks associated with them. There are two fairly large CaF₂ optics in each camera, but the cost and availability of CaF₂ are much improved since the SDSS days, due largely to the volume and size of UV lithography optics being manufactured today. Corning, for one, grows CaF₂ in sizes up to ~350 mm diameter. We obtained quotes from the vendor who did the SDSS optics and another vendor geared more toward small volume production work. Neither expressed any concern with the CaF₂ elements. The quote from the SDSS vendor was significantly lower per camera this time around, primarily due to the lower cost of the CaF₂ elements. Therefore we think the risk presented by the camera optics is small. There is always the risk of dropping a lens, especially when dealing with such quantities, but the vendor would be required to buy extra material up front in order to retire at least the risk associated with availability and lead time. Coating is always a concern, but the SDSS elements were successfully coated with high-performance AR coatings, suffering the loss of a single S-FPL51Y element due to a faulty temperature profile.

The VPH grisms are the only really different aspect of the WFMOS optical design as compared to SDSS. There are two vendors in the U.S. that we know of who can produce these gratings, Kaiser Optical Systems and Wasatch Photonics. Both can and have produced gratings over 200 mm in size and there would be no technology development required to produce the WFMOS gratings. While not without risk, we believe the VPH grating approach is no more risky than the ruling of two new high quality masters that would be required for traditional surface-relief grisms.

The collimator and dichroic are essentially identical to those in the SDSS spectrographs, and present no major risk above that normally associated with the production of precision optics. The fiber back-illumination system is new, but the optics associated with this system are so minimal that we are costing this hardware entirely under the mechanical components.

14.4.1.2 Mechanical Components

The optical bench is the most costly component on a per unit basis, while the cameras represent the largest overall component cost due to their greater number. The changes to the mechanical components from the SDSS design are very minor, including increasing the overall height of the optical bench as a result of the longer slit (which makes the collimator mirror taller), and reworking the central optics assembly to mount the VPH grisms instead of the SDSS-style ruled grisms. The

only new hardware is the fiber back-illumination system, which is not a technically challenging mechanism. From a mechanical and optomechanical standpoint, the risk involved in building this proven spectrograph design is very low.

14.4.2 Cost/Performance Options

The single greatest cost savings for the low dispersion spectrographs would be the elimination of the Nod & Shuffle requirement. This would halve the number of spectrographs needed from ten to five. If Nod & Shuffle is eliminated due to the use of the L3 Vision detector technology from e2v (allowing rapid readout with very low read noise), the detector savings will be less due to the higher cost of the L3 CCDs. From discussions we have had with e2v, it is not clear that the L3 technology can be implemented in the buttable 2k x 4k package. Scaling L3 to the 4k² format, while not a technological hurdle, would involve considerable non-recurring engineering costs of ~\$1M at the present time.

VPH gratings cost more than the ruled gratings used for SDSS. This is due to the additional three components in the assembly: grating substrate, grating cover plate, and a second prism. The cost of fabricating the VPH grating itself is very comparable to that of replicating a ruled master. We estimate the use of VPH gratings will add a cost premium of ~5% over the use of ruled gratings. This 5% cost premium seems well worth the price for the greatly increased efficiency, as discussed in Section 14.2.2.3.

The increased number of resolution elements required for WFMOS over SDSS (similar resolution but extended bandpass) requires more expensive cameras in order to achieve similar performance across two channels. The WFMOS camera design presented in Section 14.2.1.6 costs more than the strict SDSS design, for 20 cameras. The added cost is due to material and an additional aspheric surface per camera. The final performance with two aspheric surfaces is somewhat better than the SDSS design, but with only a single asphere the performance is somewhat worse. We believe the second asphere is warranted given the automated, computer-controlled polishing techniques widely available today for producing these types of surfaces.

Increasing the resolution in the red channel to $\sim 3 \text{ \AA}$ ($R = 3300$ at $\lambda = 1 \text{ \mu}$), as discussed in Section 14.2.2.2, involves increasing the speed of both cameras, from f/1.5 to f/1.4 for the blue channel and to f/1.2 for the red channel.

Chapter 15 High Dispersion Spectrograph

15.1 Summary of Strawman specification

The Galactic Science application for WFMOS drives the requirements for the high dispersion spectrograph. The requirements are outlined in Table 30.

Table 30: Science requirements for High Dispersion Spectrograph

Requirement	Value	Comment
Spectral Resolving Power	$\lambda/\Delta\lambda = 40000$	Optimal resolving power for abundance work
Spectral Window	390 – 1000 nm	Emphasis on 390-600 nm window
Pixel Sampling	3 pixels FWHM spectral TBD pixels FWHM spatial	Min of 2.5, max of 3.5
Simultaneous Coverage	>100 Å	Limited by detector size and pixel sampling. Free spectral range must be greater than this.
Minimum Required Spectral Regions	$\lambda_c = 400$ nm 850 nm 600 nm	Top priority [metal lines] Ca II infrared-triplet
Number of Simultaneous Targets	~1500	Likely requires multiple spectrographs
Shutter	Required, ~1 second exposure control	
Nod&Shuffle Requirements	Not required	
Image Uniformity on Detector	TBD	
Acquisition Requirements	TBD	
Guiding Requirements	TBD	
Calibration Requirements	TBD	Flat Field
	TBD	Wavelength
Fiber Back Illumination	TBD	
Sensitivity Limits	TBD (V=19, 1 hour, SN=100)?	

15.2 Spectrograph Strawman design

15.2.1 Disperser Options

The combination of high resolving power ($R=40000$) and a ~1 arc-second entrance aperture for an 8-meter telescope drives the need for a high dispersion grating and a large beam. The options for the dispersing element are limited and become a significant driver in the design and potential cost of this instrument.

15.2.1.1 Echelle Gratings

The classical disperser for consideration in the high dispersion spectrograph is the ruled Echelle grating. An advantage of an Echelle grating is that a single disperser can serve the full spectral window with the use of order sorting filters. The

disadvantage is that if the line density of the Echelle is too low, then the free spectral range (FSR) is low and therefore the bandwidth of the required sorting filter is also low. This makes it potentially difficult to achieve good efficiency and low cost for the order sorting filter.

Figure 166 shows the relationships of ruling density, blaze angle, and beam diameter that give the performance required for the WF MOS instrument. The blaze angle will define the dispersing power of the grating, the ruling density defines the size of a spectral order or the FSR, and the beam diameter will set the resolution for a given blaze angle and fiber input aperture.

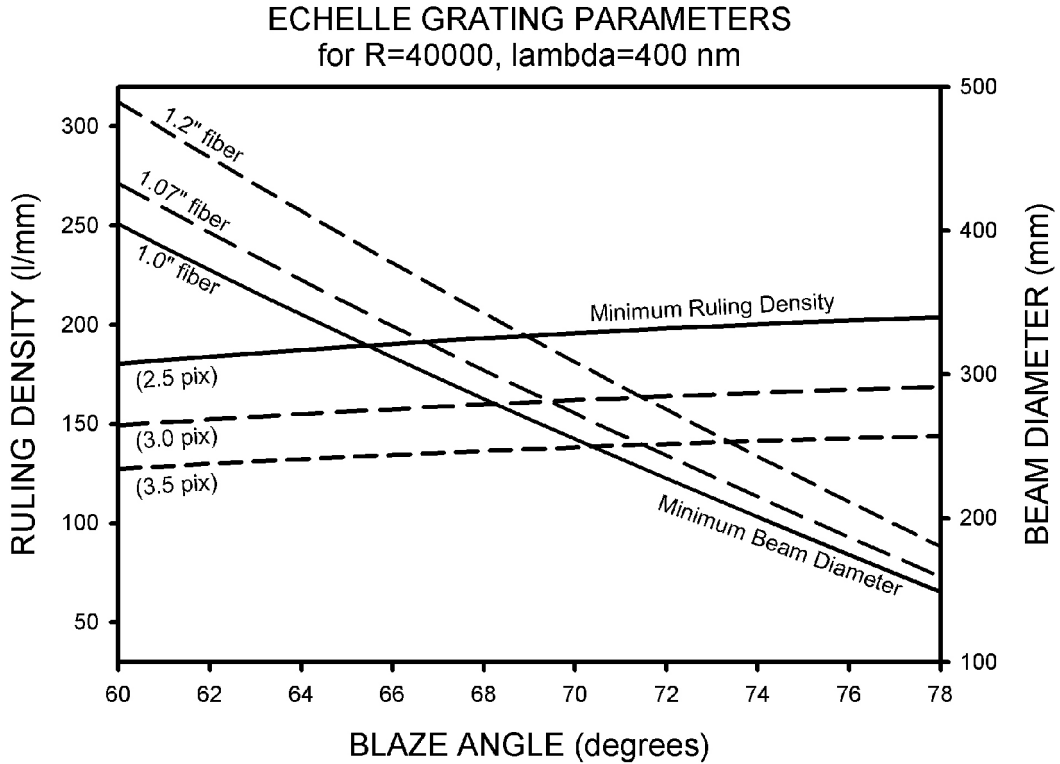


Figure 166: Ruling density vs blaze angle required to get adequate free spectral range per order on the 4k pixel detector and Beam diameter vs blaze angle required to get adequate resolving power with indicated fiber aperture on an 8-meter telescope. Acceptable values lie above the lines.

The only known source for this type of Echelle gratings is the Richardson Grating Lab (RGL) now part of Newport Corporation. They have been the sole source for large format gratings in astronomy for decades and have supplied mosaicked Echelle gratings for the VLT, Gemini, Subaru, Keck, HET, and many other observatories for use in their high resolution spectrographs. The issue then remains as to whether or not RGL can provide an Echelle that meets the needs of the WF MOS instrument.

RGL is able to create linear mosaics (1 x 2) on monolithic substrates that perform effectively as if they were a single grating. The current upper size limit on the ruling area appears to be about 310 by 820 mm.

RGL have the following master gratings available that are close to what is required for WF MOS. It is apparent that none of the currently available gratings would meet the needs for WF MOS. Gratings 53-113E and 53-121E are the closest. The most desirable grating would be a 70 degree blaze grating with a

ruling density of 160 l/mm. This would require a custom ruled master, which adds a cost of about \$60k USD (quote from RGL). The RGL quote for a 1 by 2 mosaic is \$280k USD.

Grating Number	Ruling (lines/mm)	Blaze Angle (degrees)	Ruled Area (mm)	Comment
53-417E	31.6	76	204 x 408	FSR too low (26 Å at 400 nm)
53-425E	41.59	76	204 x 410	FSR too low (34 Å at 400 nm)
53-113E	94.13	79	206 x 413	FSR marginally low (76 Å at 400 nm)
53-453E	31.6	71	308 x 408	FSR too low (27 Å at 400 nm)
53-127E	87	63	308 x 413	FSR low (78 Å at 400 nm)
53-121E	110	64	310 x 413	FSR marginal (98 Å at 400 nm) Blaze angle marginally low

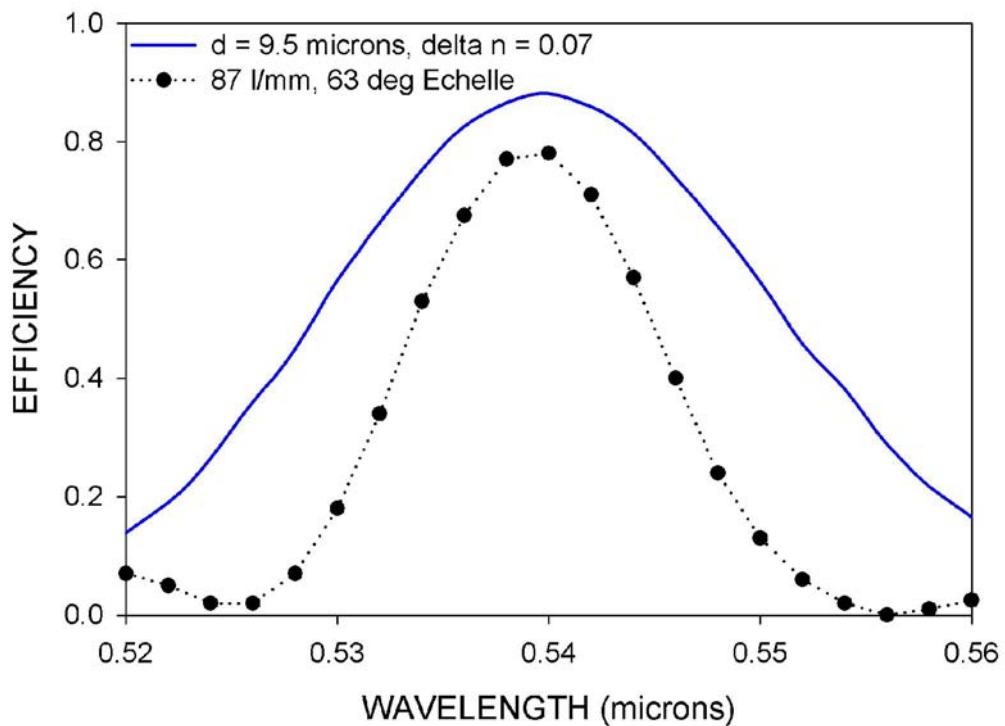


Figure 167: Comparison of theoretical 63 degree VPH grating to Classical 63 degree Echelle.

15.2.1.2 Volume-Phase Holographic Gratings

A possible alternative disperser to an Echelle is the use of volume-phase holographic (VPH) gratings. These gratings would work in first order. Their advantage is the potentially higher diffraction efficiency (80% compared to typical 60% efficiency for Echelle gratings, see Figure 167). A major disadvantage of the

VPH approach would be the need for numerous independent gratings in order to give coverage over the full spectral window.

Further details on the potential use of VPH gratings for the high resolution application can be found in the discussion of the do-all spectrograph, see section 16.4.2 in Chapter 16.

15.2.2 System Overview

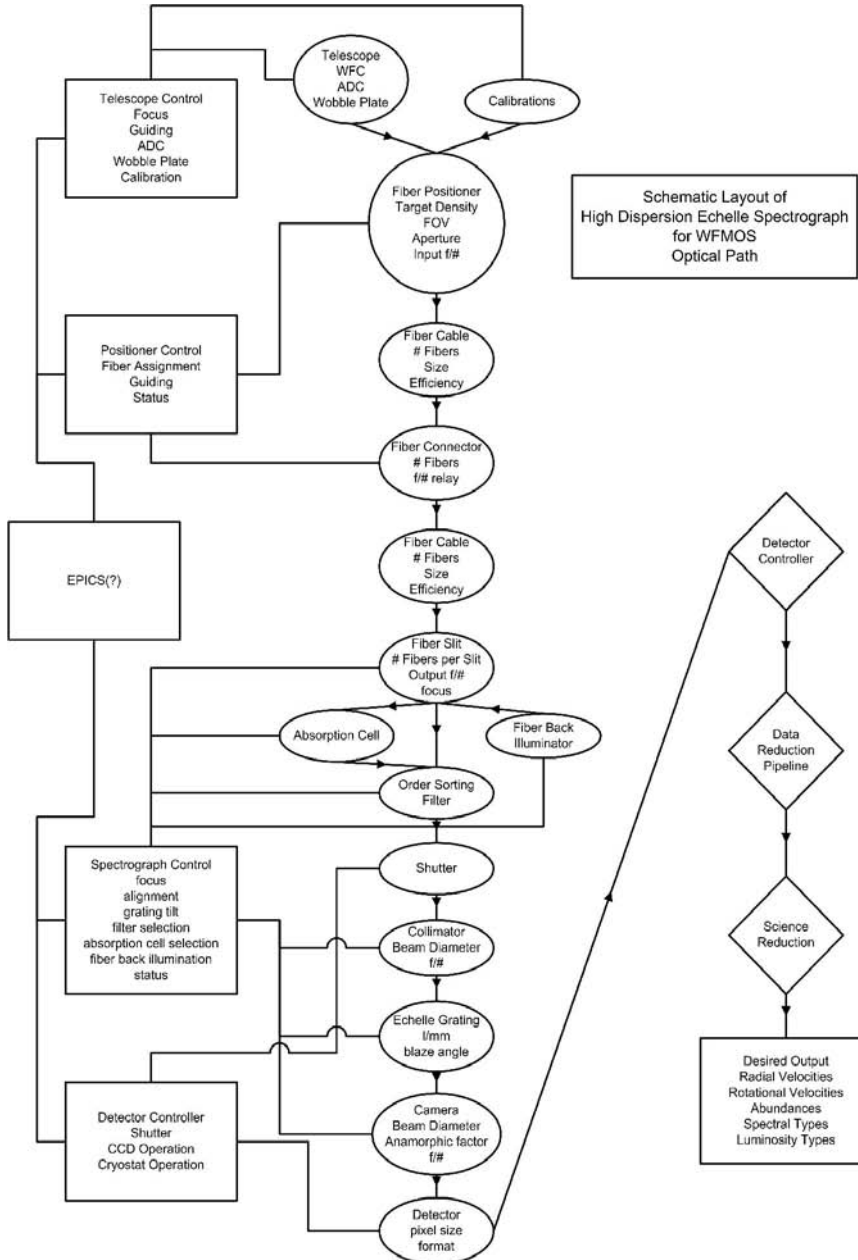


Figure 168: System diagram for the High Dispersion Echelle Spectrograph.

The system chart in Figure 168 shows the schematic of the High Dispersion Spectrograph System and its related components. This is applicable regardless of the design approach.

15.2.3 *Optical Design*

The optical design explored is based upon the use of a classical Echelle grating implemented in a white pupil optical layout. A VPH grating based design is discussed as part of the do-all spectrograph and is presented elsewhere in this document.

A white pupil approach is taken to allow the Echelle grating to work very close to Littrow, where the peak efficiency of the grating is realized, and in order to keep the camera optics at a reasonable size especially given the already large beam diameter required by the spectrograph.

15.2.3.1 *Beam Diameter*

The beam diameter, as discussed above, is influenced by the entrance aperture diameter, the telescope aperture, and the dispersion of the grating. The telescope aperture and entrance aperture are fixed parameters. The grating options are limited and imply that the spectrograph will require a beam diameter of the order of 300 mm.

Given that the beam diameter will be of this size, the preference is to have reflective optics rather than transmissive lenses wherever possible.

15.2.3.2 *Detector Influence*

The detector format will determine the amount of spectrum that can be covered. A resolving power of 40000 at 400 nm means that 0.1 Å is imaged onto a resolution element. One typically requires sampling that is greater than or equal to the Nyquist limit of 2.5 pixels. Coverage by a 4k detector format gives a maximum of 1600 resolution elements. For 3 pixel sampling, the coverage drops to 1360 elements (136 Å at 400 nm).

A 4k pixel spectral format for the detector is sufficient to give the minimum required simultaneous spectral coverage.

It will be assumed that the pixel size is 15 by 15 microns.

Nod&Shuffle observing is not considered a requirement for the high resolution case, so the spectra can be packed a factor of two closer than on the low dispersion spectrographs. It is assumed that 8 to 10 pixels are required for the centre-to-centre spacing of each fiber spectrum. Hence, a 2048 pixel format can image about 200 to 250 spectra.

15.2.3.3 *Demagnification (Camera Focal Ratio)*

The output of the fibers will be about f/4 from 200 micron diameter fibers (Note that the f/2 input beam into 100 micron fibers is converted into f/4 at the connector). The focal length of the collimator will therefore be 300 mm times 4, or 1.2 meters.

Assuming that the detector has 15 micron pixels with 3 pixel sampling, the 200 micron fiber needs to be reimaged onto a 45 micron diameter circle at the detector. This implies a demagnification ratio of 4.4 resulting in a camera focal length of 1.2 meters divided by 4.4, or 272 mm. With a beam diameter of 300 mm, the

camera focal ratio becomes $f/0.9$, which can prove to be quite challenging. The implication is that a Schmidt style of camera is likely required.

15.2.3.4 Filters

The desired Echelle grating (150 l/mm with 70 degree blaze) gives 400 nm in spectral order $m=31$. The detector sensitivity window extremes will be in order 32 (390 nm) and 12 (1.0 micron). A minimum total of ~ 21 filters would be required to allow observations to take place anywhere within the spectral window. The width of the filters needs to be matched to the FSR of the order. At order 32, the filter width would be 120 Å. For order 12, the width would be 833 Å.

It is desirable to have a top hat efficiency profile for the filters since the blaze profile of the grating will be the limiting factor in the efficiency at the limits of the FSR.

The coating technology for such filters is fairly state of the art. However, the size of the filters (300 to 400 mm diameter) is a potential risk for cost and availability. The filters should ideally be located in the collimated beam at, or very near, a pupil image. The beam collimation is desired to minimize the effects of high angle rays of light. The pupil location is to minimize the size of the filter.

The best location for the filters would be either just in front of the Echelle grating, or at the white pupil formed by the collimator. A filter exchanger would be required, but could be based upon the existing design of the GMOS slit mask exchanger.

The cost of a filter of this size is probably around \$8-10k USD.

15.2.3.5 Shutter

A shutter can be implemented as a rotating aperture wheel located behind the filters near the white pupil.

15.2.3.6 Collimator

The collimator has the task of collimating the $f/4$ output beam of the fibers. The concept explored here is a reflective mirror, used in triple pass. The first pass collimates the light for proper illumination of the Echelle grating. The grating sends the light back through the collimator where an image is formed near the fiber slit. A mirror is located at that image to send the light back through the collimator so that it is collimated for the camera and so that a white pupil is formed near the mouth of the camera.

The mirror envisioned to do this is about 2 metres in diameter of which only portions are illuminated on each pass. The parent mirror is $f/0.6$. The preference is to make the mirror spherical and then utilize transmissive optics for correcting the spherical aberration.

15.2.3.7 Camera Options

Given the $f/0.9$ speed of the camera, the most cost-effective approach is to use a Schmidt style of camera. Such a camera would not be too different from that being developed for the AAOmega spectrographs at the AAO. The do-all spectrograph

concept, described elsewhere, describes similar cameras. It would be assumed that the camera used here would be nearly identical to that described in *Chapter 16, Do-All Spectrograph*.

15.2.3.8 Number of Spectrographs Required

Given the expense of the gratings and the order separation filters, it is highly desirable to minimize the total number of spectrographs required to record the 1500 spectra. This needs to be balanced against the likely fact that the camera will be a Schmidt style system in which the detector produces a central obstruction and causes the loss of light. It is desirable to keep the detector package as small as possible. It is unlikely, therefore, that only 1 spectrograph could be designed since the detector package would become rather large in comparison to the 300 mm beam. A 12k by 4k pixel format would be required to image the 1500 spectra.

The collimator illumination pattern of the strawman concept suggests that two spectrographs can share the same collimator mirror with one spectrograph rotated 90 degrees with respect to the other. Dividing the 1500 spectra into two spectrographs reduces the detector package to 6k by 4k, which becomes a manageable size that wouldn't obstruct a significant amount of light (~10%) of the 300 mm beam.

15.2.3.9 Strawman Optical Design

The strawman optical layout is shown in Figure 169. The design was only explored to see if the collimator appeared to be feasible. The camera is only in notionally as a paraxial lens. A proper conceptual design study would flesh this design out further.

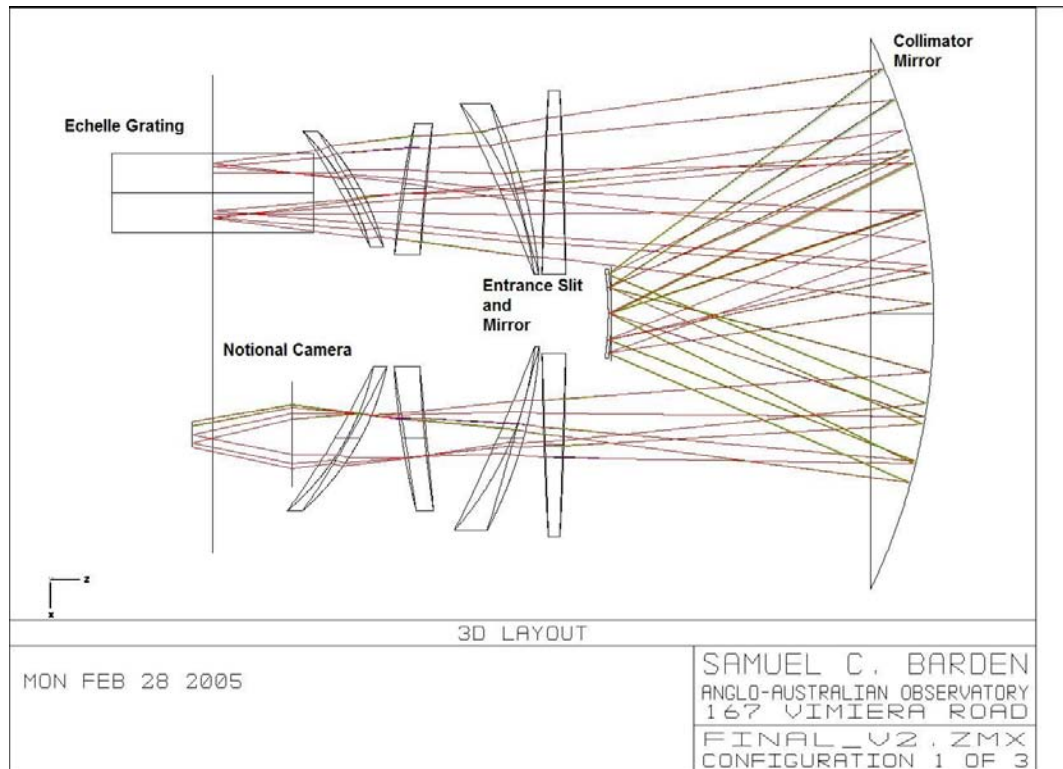


Figure 169: Schematic optical layout of the High Dispersion Spectrograph strawman concept. The camera is just a paraxial lens.

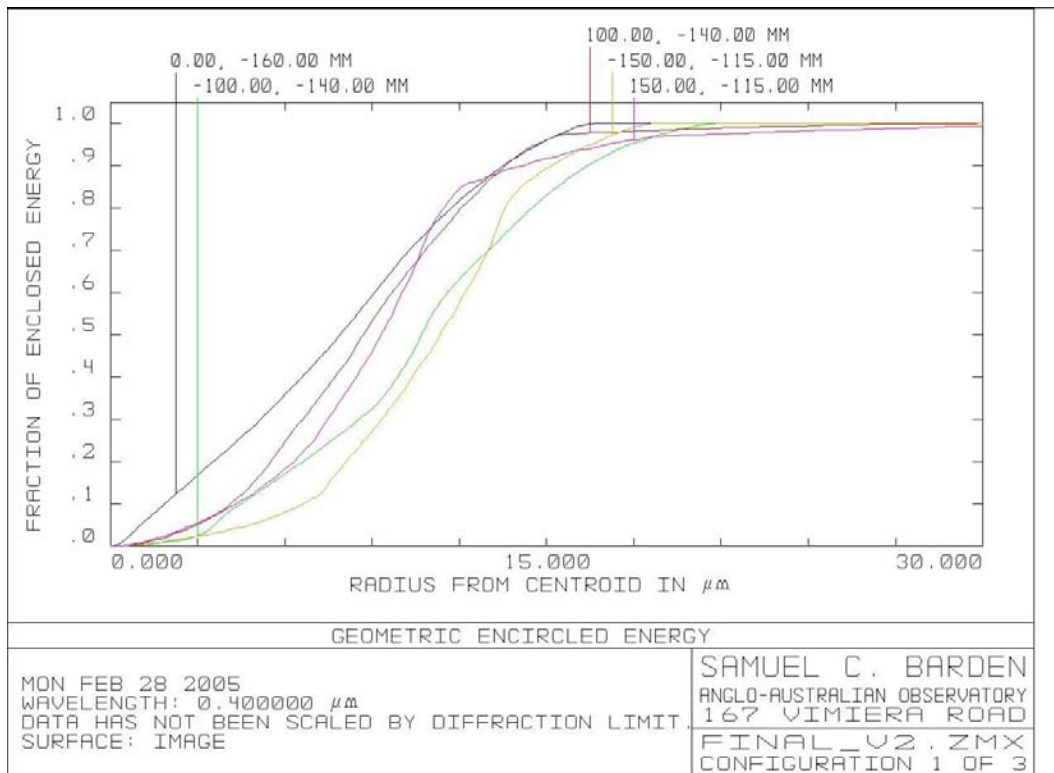


Figure 170: Encircled energy plot for 400 nm as a function of field angle for the High Dispersion Spectrograph.

Figure 170 shows the encircled energy of this collimator design (with a paraxial lens as the camera). The images fit within 2 pixels on the detector.

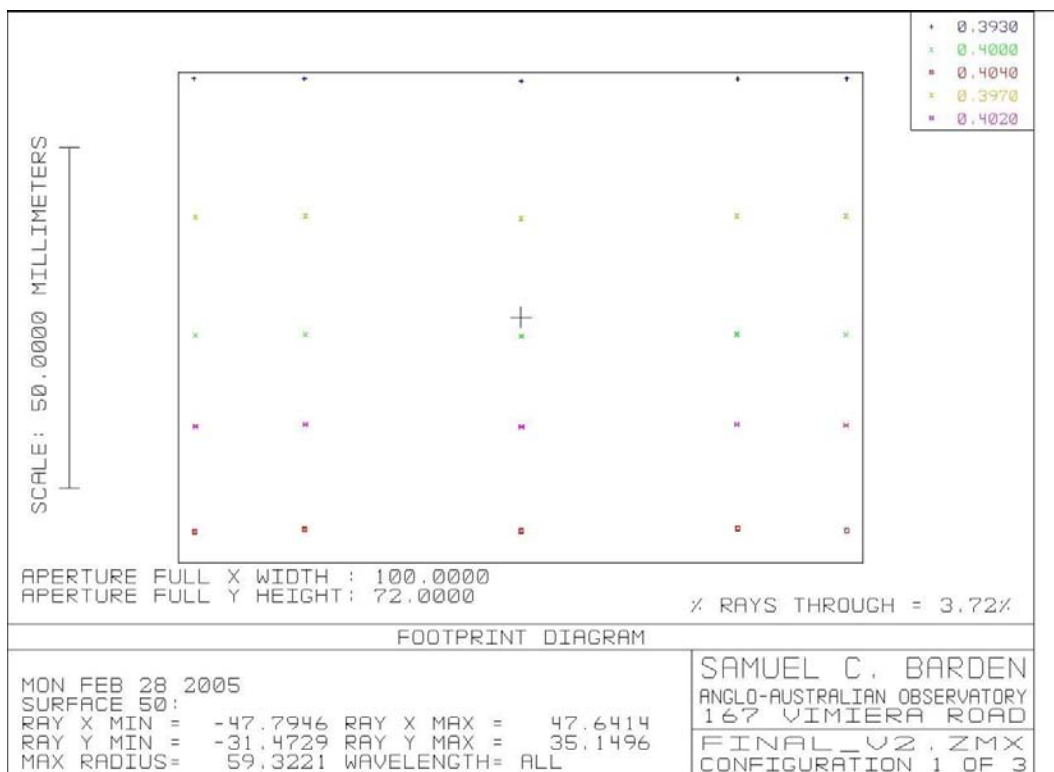


Figure 171: Detector footprint showing the wavelengths 393, 397, 400, 402, and 404 nm at 5 different slit positions on a 4k by 6k detector. The "% rays through" should be ignored as that number is invalid and is an artefact of the optical model.

The detector footprint is shown in Figure 171. In order to get the wavelengths to line up, the input slit must be curved. The input slit must also be offset from on-axis in order to not block any of the light as it passes back through the collimator. The layout of the fibers with respect to the focal plane mirror is shown in Figure 172.

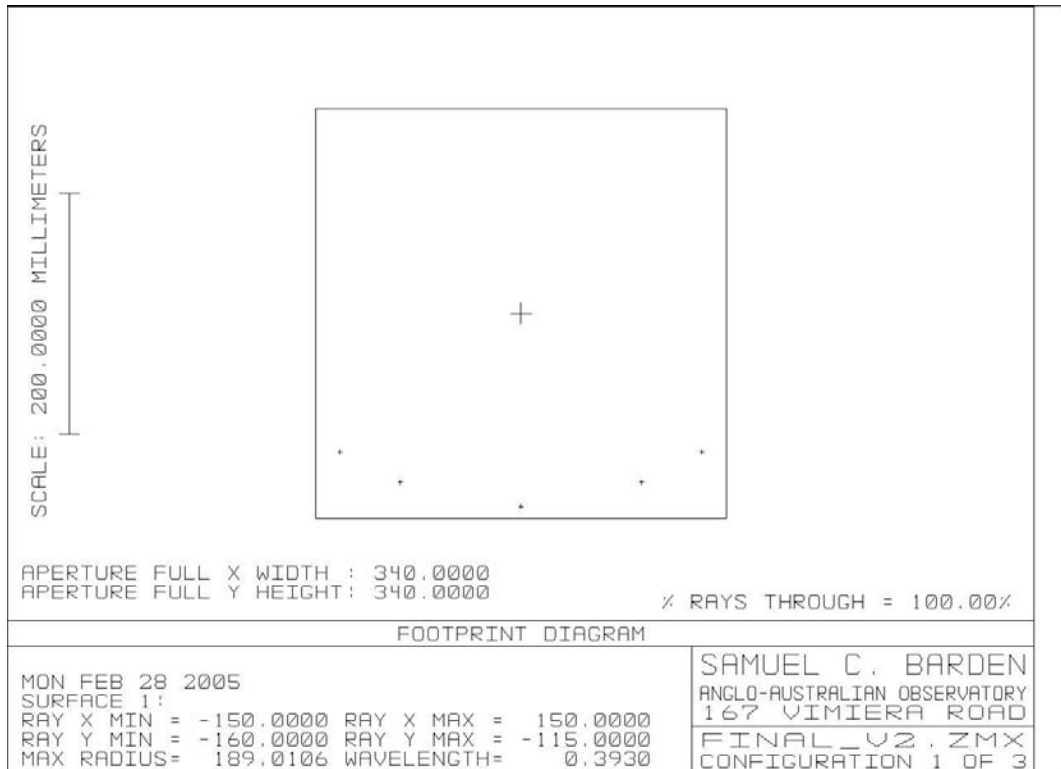


Figure 172: The footprint of the entrance slit showing that the fiber slit must be curved in order to get straight wavelengths on the detector. The slit is also offset to allow the spectra to reflect off the mirror after their second pass through the collimator.

15.2.4 Mechanical Design

Mechanically, the High Dispersion Spectrograph is a relatively simple mechanism. The collimator mirror system is able to accommodate two spectrographs. Figure 173 and Figure 174 show solid models of what this instrument might look like. The vertical orientation was selected to give minimal footprint in the spectrograph lab floor and should allow simplification of the 2-meter collimator mirror support mechanism.

The only moving components required are the following:

- Detector focus
- Echelle grating tilt (only a few degrees required)
- Shutter wheel
- Filter exchange mechanism (which could be based upon the GMOS aperture plate mechanism)

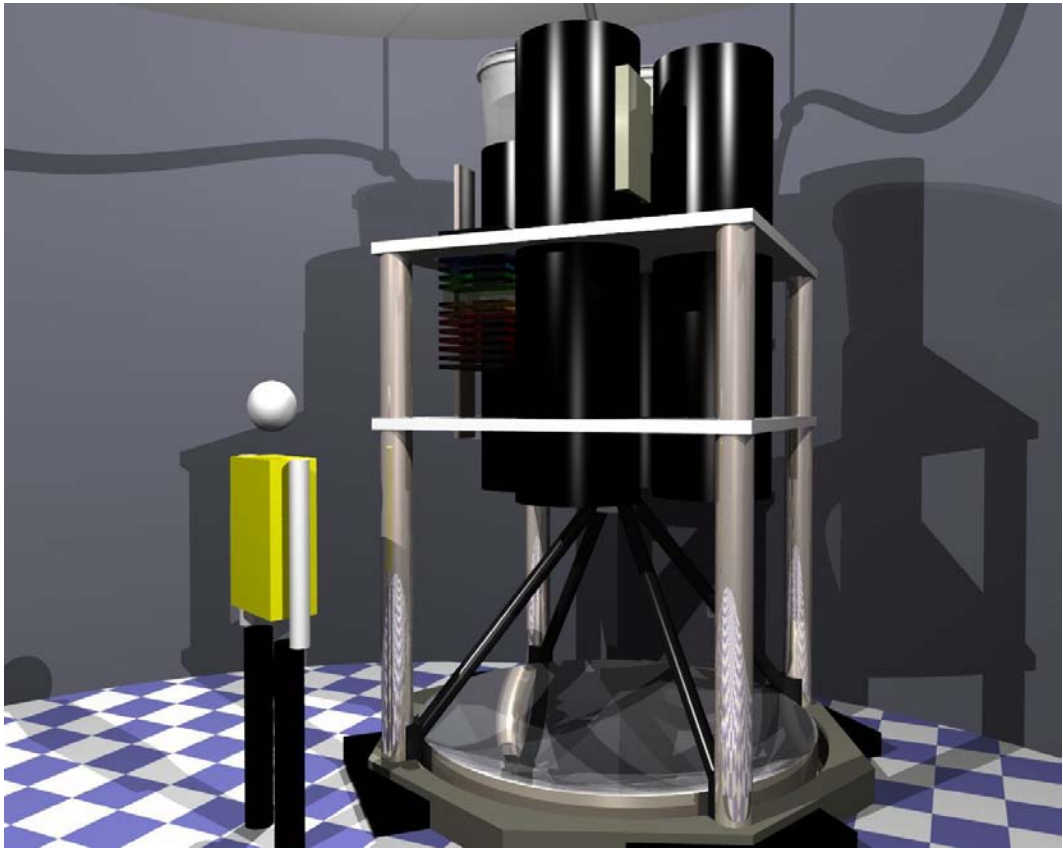


Figure 173: Solid model of the High Dispersion Spectrograph. The collimator mirror is at the bottom, the gratings and camera are mounted on the top.

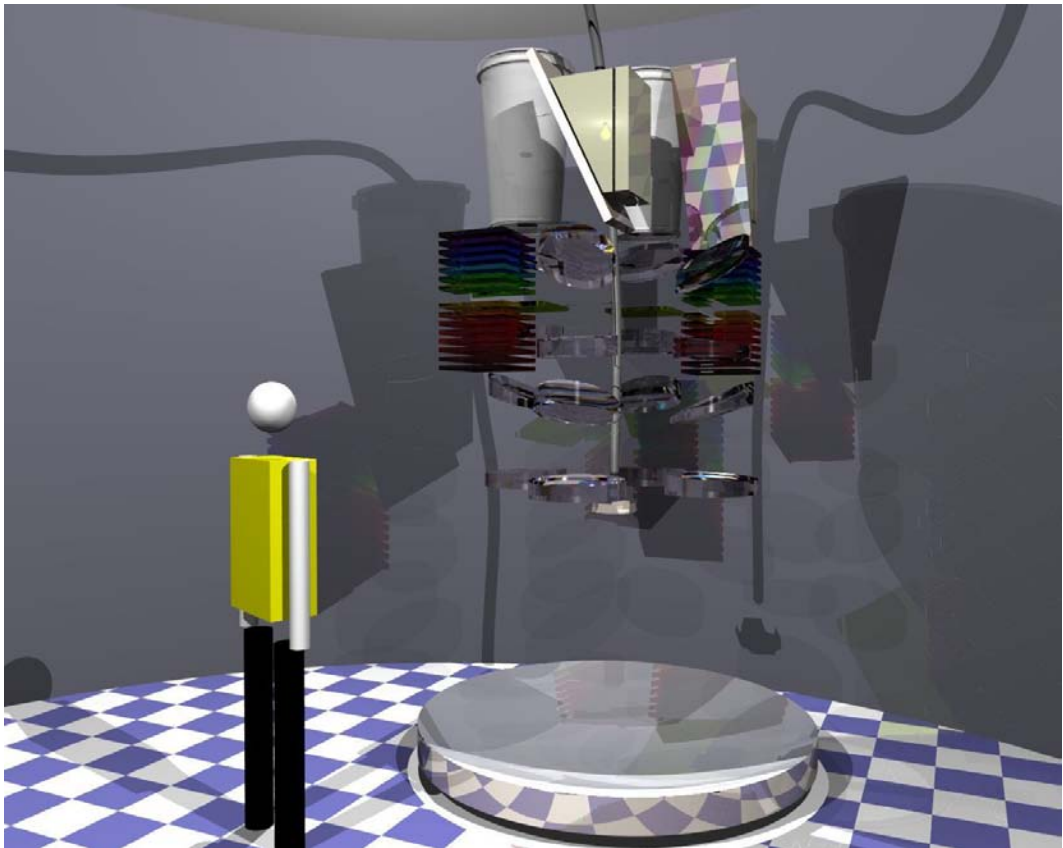


Figure 174: The optical components of the High Dispersion Spectrograph.

It is envisioned that the collimator focus and slit alignment would be done with shimming during the initial setup and that the use of thermal compensating support structures (e.g. Invar struts) will eliminate the need for active control of this focus.

15.2.5 Electronics Design

15.2.5.1 Scope

From an electronics perspective, the High Dispersion Spectrograph consists of two identical spectrographs sharing a common controller. Each spectrograph consists of a number of servo mechanisms, actuators and sensors. The functions that these mechanisms perform are largely irrelevant to the electronics design, except where there may be complex mechanisms requiring interlocking or other special requirements.

Each spectrograph has the following mechanisms, actuators and sensors:

- Back Illumination – LED sources with manually adjustable brightness, switched under computer control (or possibly direct hardware control from an external source – the fiber positioner).
- Shutter – a mechanism operated by an on/off actuator, directly controlled from an external source, usually a detector controller.
- Grating Identification – a number of encoded sensor input bits to uniquely identify each grating that may be used in the spectrograph.
- Grating Tilt – one servo axis to adjust the tilt of the grating.
- Filter Selector – one servo axis and one open loop motor, to select one of a number of filters.
- Detector Focus – three servo axes to focus the detector in the camera.

15.2.5.2 Approach

The design approach for the High Dispersion Spectrograph electronics will follow that used successfully for other AAO instruments, including 2dF, IRIS2, OzPoz and AAOmega. In this design approach, it is assumed that a servo axis includes a servo motor, incremental encoder, home and limit switches, and that an open loop motor axis includes one or more position switches.

The spectrograph electronics are split into two sections, as shown in Figure 175. These are the instrument electronics and the control electronics. The instrument electronics refers to all those electronic components and assemblies that are needed in each physical area in the body of the instrument. These may include small printed circuit boards (area interface boards) to consolidate various signals associated with mechanisms in particular areas (camera area, filter selection area, slit area etc.) and all wiring on the instrument.

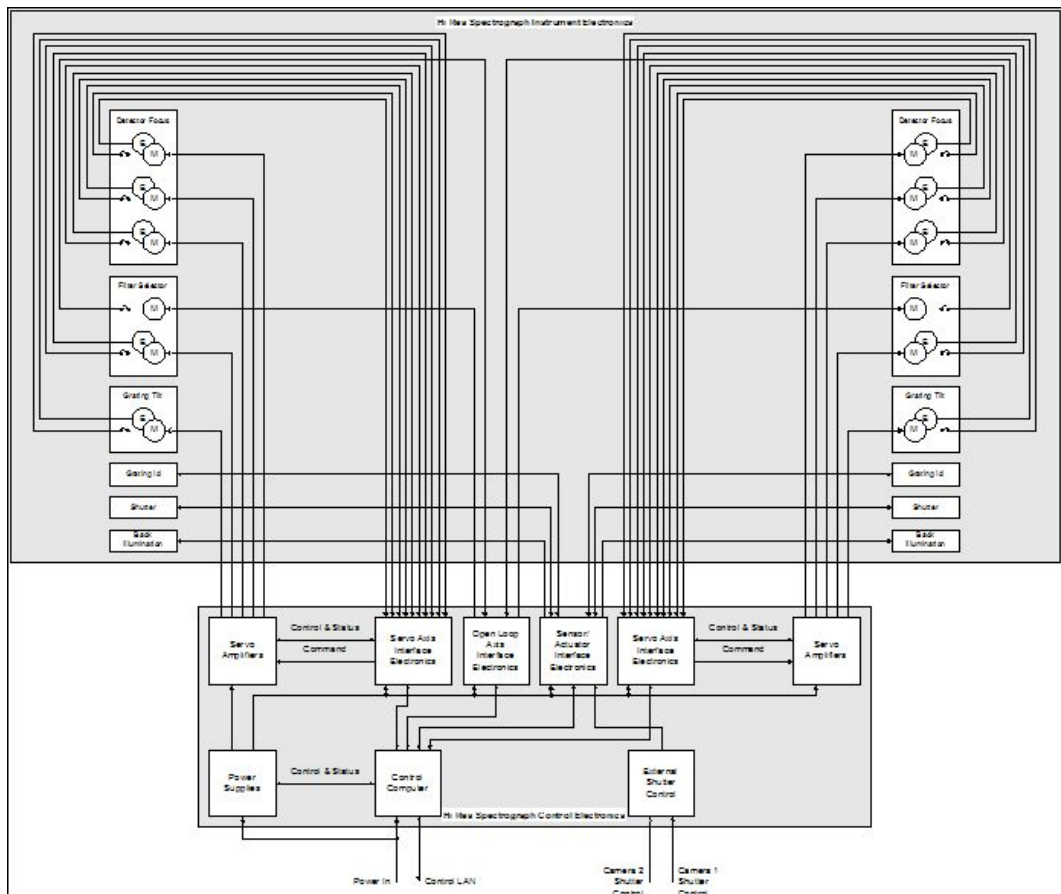


Figure 175: High Dispersion Spectrograph Instrument Control Electronics

The control electronics consists of all those components needed to provide remote control of the instrument mechanisms. The control electronics are usually located in a single enclosure or rack, and may be some distance from the instrument. The control electronics includes a control computer system containing various interfaces as required – e.g. multiple axis servo motion controllers, digital input output interfaces etc. The control computer runs the components controller software. The control electronics also includes the necessary components to interface the control computer to the instrument electronics, including servo axis interfaces, servo amplifiers and conditioning electronics for various on/off actuators and sensors.

The control computer system will be of a type that provides a cost effective solution for the task at hand. There are no hard real-time constraints required for spectrograph control, so it should be possible to use a non-real-time system such as Linux, running on an x86 processor. In addition, the control computer must have an open bus structure to support the addition of interface boards. An x86 (IA32) architecture single board computer in VMEbus (VME64/VME64X), CompactPCI (PICMG 2.0) or PCI-ISA (PICMG 1.0) format would be suitable for the task and would provide all the necessary features identified in [Guidelines for designing Aspen Instrument Software]. Ideally, this would be the same type of system as used in all instrument control computers in the WFMOS instrument.

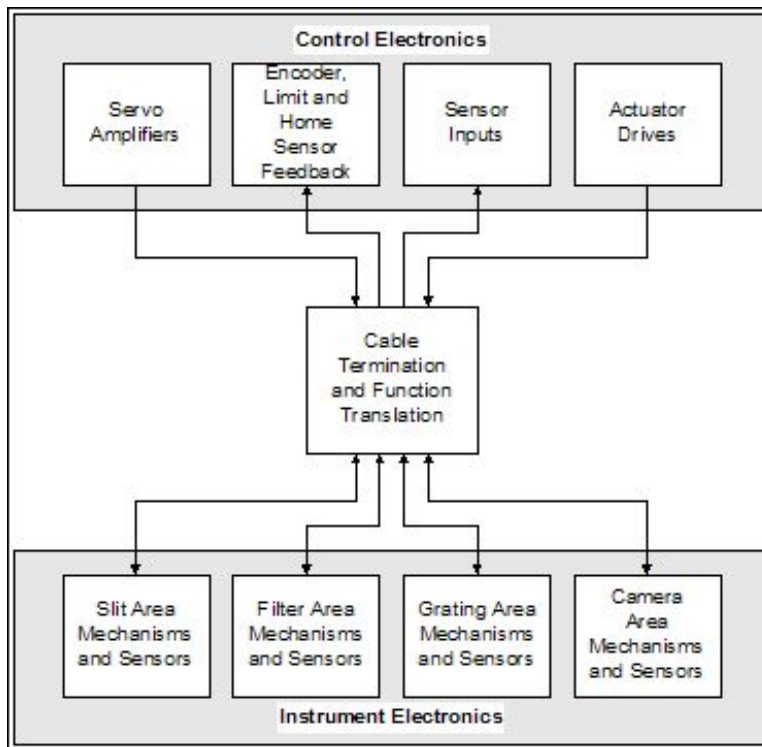


Figure 176: Spectrograph Electronics Design Approach

The instrument electronics and control electronics are interconnected with appropriate cabling, connectorised at least at the control electronics end. An intermediate cable termination box may be required to translate from electronics control functionality to spectrograph area functionality. This is illustrated in Figure 176. The cable termination box is usually located close to the instrument and is implemented as one or more small industrial enclosures containing DIN rail mounted terminal blocks.

The control electronics has an external interface to the shutter control signals from the detector controllers, to allow them to control their respective shutters.

It is unclear at this stage if there needs to be direct hardware control of the back illumination light sources. This can be done fully under software control, but with added complication to the structure of the system. The alternative is for each spectrograph to have a hardware input that is controlled by the fiber positioner electronics. This requires the fiber positioner to have one back illumination control output per spectrograph. This issue would be more fully explored during the concept design phase.

15.2.5.3 Interfaces

Assuming that back illumination control is performed at the software level, the electrical interfaces to the High Dispersion Spectrograph electronics are as follows:

- Control LAN connection
- Mains power connection
- Shutter control connection

At this stage of the design, there appears to be no requirement to connect the High Dispersion Spectrograph to the Gemini Interlock System. This aspect of the design would be explored further in the concept design.

15.2.5.4 Issues

15.2.5.4.1 Back Illumination Control

As previously noted, it is assumed for this study that back illumination control will be done at the software level via commands on the Control LAN. Software on the High Dispersion Spectrograph control computer will receive commands from the instrument sequencer or fiber positioner control system to turn on or turn off the back illumination. However, this is a departure from previous fiber positioner systems where there has been a direct (non network) link between the fiber positioner controller and the spectrograph controller to control back illumination. The concept design study will identify if it is necessary to control back illumination at the hardware level. A hardware level control would be implemented using a simple fiber optic connection.

15.2.5.4.2 Instrument Interlocks

It is unknown at this time if there are any significant interlocking requirements associated with the spectrograph that prevent either harm to humans or damage to the instrument as a result of unplanned, unintended operation of mechanisms. The concept design will identify any such requirements.

15.2.5.4.3 Servo Mechanisms

The design and cost estimates assume that standard, relatively low power brushed DC motors will be used in the spectrograph servo mechanisms, and that incremental encoders will be used for positional feedback. Any mechanisms requiring high power or brushless motors will need to be identified during the concept design.

15.2.5.4.4 Prototyping

Prototyping of circuits or systems regarded as “high risk” because they involve the use of new technology or techniques or they have a high level of complexity, is usually carried out in the concept or preliminary design phases in order to provide “proof of concept”. At this time, there do not appear to be any parts of the High Dispersion Spectrographs electronics control that require prototyping in any design phase.

15.2.5.4.5 Electronics Cooling

If the instrument control electronics are located in the same room as the spectrograph, which is of an open design, it is likely that it will be necessary to provide active cooling of the control electronics enclosure to minimise the heating effects of the electronics equipment on the spectrograph environment. This will be achieved using a cooling system that extracts the heat generated in the electronics enclosure and transfers it to the Telescope coolant system. The cooling system maintains a small temperature differential between the outside surface of the electronics enclosure and the ambient air. It is expected that a thermal analysis will be carried out during concept design to determine the cooling requirements.

15.2.5.4.6 Power

The power requirements of the High Dispersion Spectrograph electronics are not expected to be large (i.e. < 750W). However, a more thorough estimate of power consumption will be carried out during the concept design.

15.2.5.4.7 Observatory Electronics Design Requirements

As far as possible, the design of the High Dispersion Spectrograph electronics will comply with any requirements defined in the relevant electronics design specifications and standards relating to Observatory instrumentation. The concept design will identify the relevant specifications and standards.

15.2.5.4.8 Environmental Requirements

The selection and design of electronics components for the High Dispersion Spectrographs electronics will take into consideration the environmental requirements and operating conditions of the Observatory. The concept design will identify the relevant environmental requirements.

15.2.5.4.9 Electro-Magnetic Compatibility (EMC)

The design of the High Dispersion Spectrographs electronics will be undertaken to meet all the relevant requirements for Electro-Magnetic Compatibility for Observatory instrumentation. Achievement of EMC requires an understanding of interference coupling mechanisms, consideration of EMC in equipment layout, grounding and circuit design, application of appropriate filtering and shielding of interfaces and the testing and evaluation for EMC continuously through the project. Observatory EMC requirements will be identified during the concept design.

15.2.6 Software Design

The software requirements to operate this instrument are relatively simple and there isn't any foreseen technical risk or significant cost drivers associated with this item.

15.3 Subaru vs Gemini

The High Dispersion Spectrograph design will not be impacted on the choice of either Subaru or Gemini. However, the Gemini pier lab may need to have a hole placed in the ceiling to allow the spectrograph to fit.

15.4 Cost drivers

The primary cost drivers on the High Dispersion Spectrograph are the gratings, order separation filters, and the optics.

Chapter 16 “Do-All” Spectrograph

16.1 Summary of Strawman specification

The aim of the “Do-All” spectrograph design is to allow both high and low resolution spectroscopy with the same spectrograph. This reduces space requirements and spectrograph costs; it also potentially allows individual fibers to be used in either mode, giving further cost savings in the positioner. However, it does mean that low and high dispersion work cannot be undertaken simultaneously.

The input to the spectrograph is assumed to consist of either 1500 fibers in high resolution mode, or 3000 fibers in low resolution mode. We assume nominal 180 μ m fibers feeding the spectrograph at $f/4$.

At high resolution, the resolution specification is driven by the requirement to measure accurate stellar abundances. Freeman and Bland-Hawthorn (A&A. Ann. Rev. 2004) (Figure 177) have shown that the required resolution is strongly wavelength dependent. We have taken the science requirement to be that we can resolve at least 80% of the lines at all wavelengths 390-1000nm in a solar-type spectrum. The greatest possible spectral coverage is also desirable, to maximise the number of detected lines; we have assumed a nominal requirement of 1000 resolution elements covered on the detector.

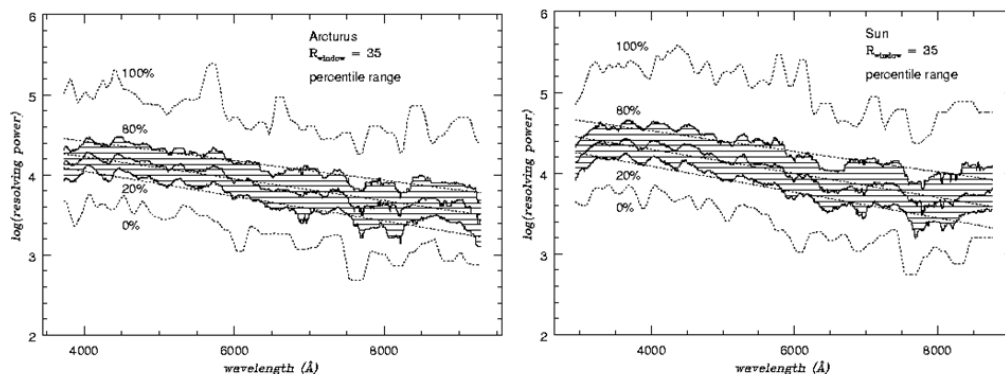


Figure 177: Fraction of lines resolved in stellar spectra as a function of resolving power and wavelength. From Hawthorn and Freeman (2004).

At low resolution, we assume a minimum resolution requirement of $R \sim 1000$, with simultaneous coverage 390-1000nm. Nod&Shuffle must be accommodated for all fibers.

16.2 Spectrograph strawman design

The design is taken directly from the AAOmega spectrograph currently in manufacture for the AAT, and due for delivery 2005Q3. The AAOmega design was also driven by the requirement to image as many spectra, as well and as efficiently as possible, at both high and low resolution, within a restricted budget and with minimum risk. The design uses all-Schmidt optics, with a dichroic beam-splitter within the collimator, and two $f/1.3$ cameras. The cameras are as fast as

readily feasible, to minimise oversampling of the spectra. The general layout is shown in Figure 178.

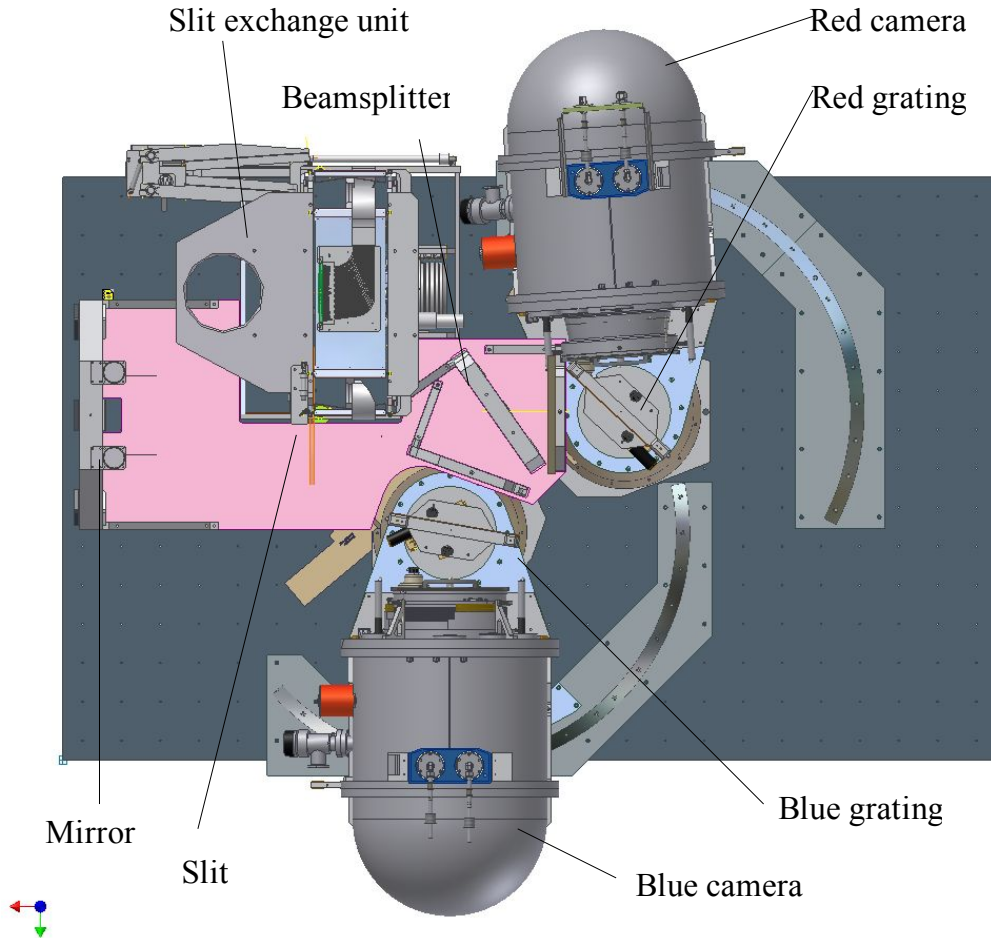


Figure 178: General layout for the AAOmega spectrograph, with the red arm in high dispersion mode and the blue arm in low dispersion mode.

16.2.1 **General considerations**

Because of the higher resolution requirements of WFMOS as opposed to AAOmega, it is necessary to increase the beam size (which is 190mm in AAOmega). However, this also means larger detector areas are possible in each spectrograph, and hence fewer spectrographs needed than if AAOmega were simply cloned. The reduction in the number of mechanisms outweighs the increased cost of optics, and so increasing the beam size also reduces the cost per unit detector area.

The VPH gratings used in AAOmega are cheap, efficient, can be made to order in terms of blaze, dispersion and bandwidth, and can be made in large sizes. They thus represent a very attractive solution for the dispersive element. At high dispersion, they are limited to grating angles less than 47° , so they have only half the dispersive power of a 63° echelle, and we cannot reach $R \sim 40,000$ with a single grating and realistic beam size. What we can do, is take advantage of their excellent performance as beam-splitters (Figure 179), to replace the dichroic in the AAOmega design with a second grating.

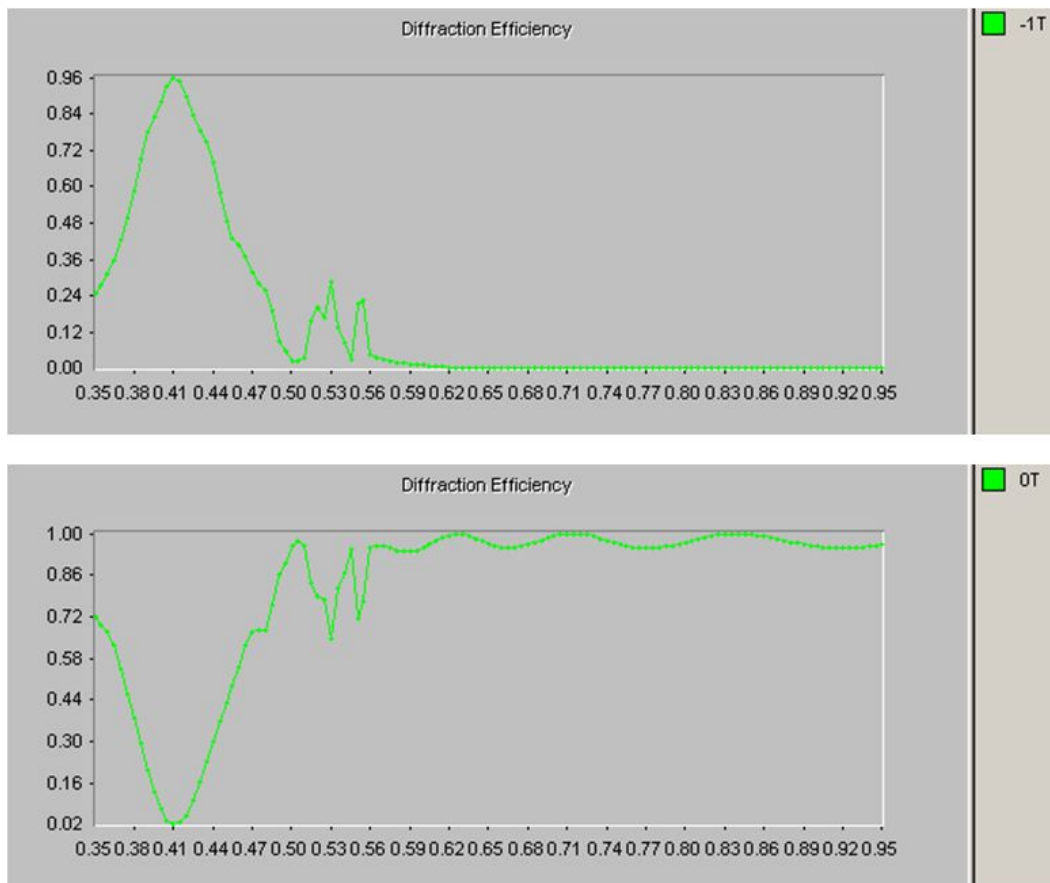


Figure 179: Theoretical efficiency of a high dispersion (47° grating angle) 'Dickson' VPH grating, blazed for 410nm, in first and zeroth orders. The grating simultaneously acts as beam splitter and blue disperser. Red arm use would be at 860nm.

We then get comparable (actually 9% better) resolution to a 63° echelle of the same beam size in the blue arm, and half this in the red arm. For our nominal 180 μ m f/4 input fibers, and a beam size of D millimetres, the maximum resolution (calculated as λ /FWHM, and including aberrations) is 116D and 58D for blue and red arms respectively. In practice we will do rather better than this, because the FWHM underestimates the resolving power of the extremely boxy PSF, as discussed below.

The resolution can be increased by reducing the fiber diameter (we are oversampled at the detector for any realistic fiber size), at the cost of increased aperture losses at the fiber input.

At low dispersion, the number of spectral pixels required is ~2000 per camera, to cover 390-910nm at a resolution $R \sim 1400$. The camera optics can accommodate 4000 or 6000 spectral pixels, so we can fit multiple banks of low dispersion spectra onto the detectors. This concept does not work well for VPH gratings, because the different slits then have different grating angles and hence blaze characteristics. However, for the large beam-sizes required for high dispersion work, the grating angles ($\sim 5^\circ$) are too small for efficient VPH gratings in any case. So at low dispersion, we assume traditional ruled transmission gratings.

16.2.2 **Beam size options**

The optimal beamsizes is determined by many considerations. The resolution requirement gives a minimum diameter of ~300mm. Optically, we find that we

can get acceptable imaging quality ($<10\mu\text{m}$ rms radius) for a system with 3 detectors (4K x 6K) per camera with 325mm beam size. The next convenient detector package shape is 6 detectors per camera (6K x 8K); to get reasonable image quality in this case demands a beam size of 475mm. In general, larger beamsizes give lower obscuration losses from the detector, and better aberrations; but the required quality of the optics increases, absorption losses within the components increase, and there is increased engineering difficulty with the dewar design. We find that the overall costs of the spectrographs, at fixed overall detector area, is rather insensitive to beamsize.

The only clear constraint we have encountered is that ruled diffraction gratings are only available from GratingLabs in sizes up to 320mm x 420mm. The beam profile is tapered, and the efficiency loss from having the grating marginally narrower than the beam is negligible.

For the purposes of this feasibility study, we have simply assumed a beamsize of 325mm. The formal maximum resolution is then $R=37,700$.

16.2.3 **Detector acreage**

We assume $180\mu\text{m}$ fibers feeding the spectrograph at $f/4$. This projects to $58.5\mu\text{m}$ on the detectors, almost identical to AAOmega. The image FWHM, including spectrograph aberrations (for overall rms radius $7.5\text{-}12.5\mu\text{m}$), is 3.2 pixels, and the full width at the 1% level is 7 pixels (Figure 180). In AAOmega, we have 10 spatial pixels per spectrum. However, these are very generously separated, as there was no incentive to pack them closer.

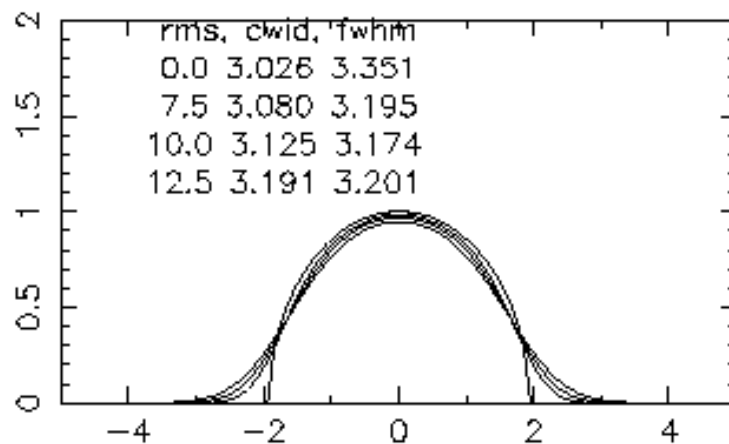


Figure 180: Expected Point Spread Function for Do-all spectrograph, for varying levels of aberration bracketing the expected performance. The x-axis units are detector pixels. Note that (a) the aberrations actually reduce the formal FWHM (because the unaberrated profile is convex); and (b) aberrated profile is still much boxier than a Gaussian.

For the high resolution WFMOS work, adjacent sources may vary by an order of magnitude or more in brightness, and the cross-talk must not compromise the target signal-to-noise of 50/pixel; therefore the maximum cross-talk (or at least, the maximum error in how well cross-talk can be removed) is $\sim 0.1\%$. For the high resolution slit, we propose 8 spatial pixels per spectrum, so the spectra are completely resolved.

At low resolution, the design specification calls for the ability to shuffle all spectra. However, all spectra are sky-limited (and hence comparably bright), and the required spectral precision is much less than at high resolution. So limited cross-talk can be tolerated as long as it can be modelled. Figure 181 shows the expected spatial profile through two adjacent spectra, separated by 6 pixels, for a variety of pixellations and aberrations. The cross-talk is negligible in all cases.

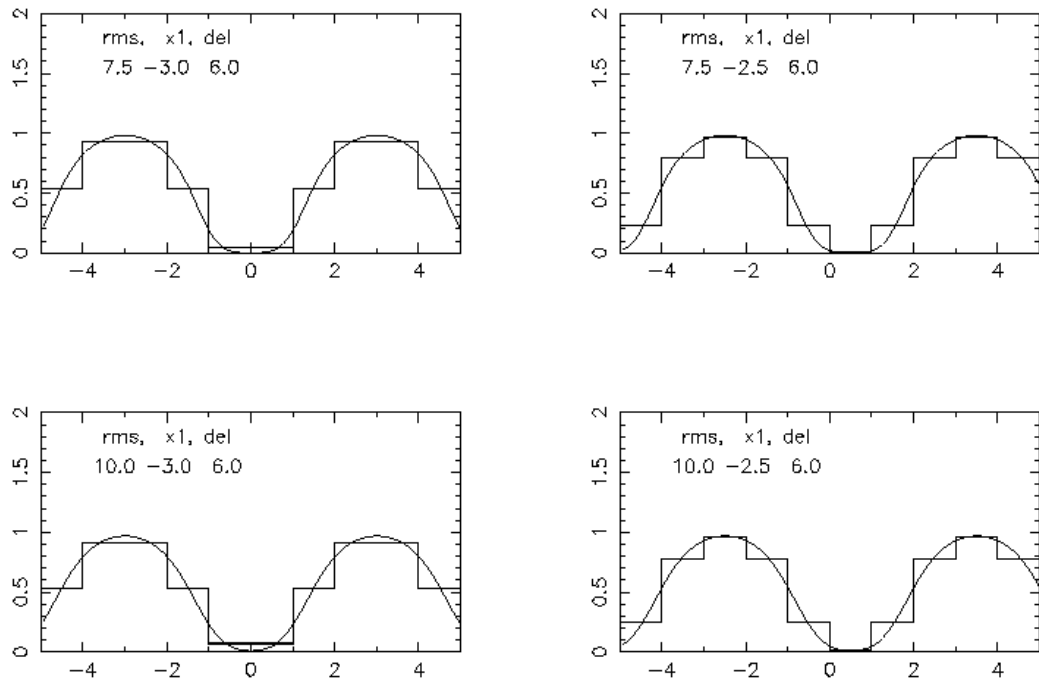


Figure 181: Expected spatial profiles for adjacent spectra separated by 6 pixels, centred on and between pixels, and for different optical aberration performance.

Spectrally, we will need $\delta\lambda/\lambda \sim 0.45$ in each arm, to cover 390-1000nm in a single observation. If we have 2000 spectral pixels in each spectrum in each arm, at a FWHM of 3.2 pixels, we then have a spectral resolution of $R=1350$.

Overall, we can then fit all low dispersion spectra, both red and blue, and including Nod&Shuffle, onto 18 x 4K (spatial) x 2K (spectral) detectors. If these are arranged to be 4K (spatial) x 6K (spectral) per camera with three banks of spectra, then we can also accommodate all high-resolution spectra, with 6000 pixels in each arm.

16.2.4 Numbers and sizes of spectrographs

At 325mm beam size, we can accommodate 3 x 4K x 2K detectors in each camera and still maintain excellent (rms radius $< 10\mu\text{m}$) imaging. The camera optics work equally well whether the long direction is spatial or spectral. We assume that the long direction is spectral, as this maximises the number of spectral pixels at high resolution.

At high dispersion, we need $8 \times 1500 = 12,000$ spatial pixels in total; at low dispersion we have 6 pixel separations twice as many spectra as fibers (to accommodate N&S) in each arm, so we must have $6 \times 2 \times 3000 = 36,000$ spatial pixels in total, for each of the red and blue arms.

Each spectrograph has 6 detectors in total (3 in each arm). We then require a total of 3 spectrographs to accommodate either 1500 high resolution fibers with a single slit per spectrograph of 500 fibers, or 3000 low resolution fibers with three slit units per spectrograph of 333 fibers each;.

To accommodate 6000 fibers (4000 low dispersion / 2000 high dispersion) would require 4 spectrographs.

16.3 Optical Design

16.3.1 Overview

The optical design is very closely derived from AAOmega, but with the use of a second grating as an alternative beamsplitter. In AAOmega, the collimator corrector is below the beamsplitter, but this must be reversed for the Do-All design because the beamsplitter is also a disperser. The cameras are essentially identical (apart from beam size) to AAOmega. The components of the design are, in order of the light train:

- 1 (high resolution) or 3 (low resolution) circularly curved slits, each made up of multiple smaller (~10 fiber) slitlets. These are mounted on a fixed kinematic mount and can be interchanged.
- For each slit, a field lens in optical contact with the fibers. This protects the slitlets, increases the efficiency and allows a pupil-centric design.
- A simple pneumatically-operated flag-type shutter.
- A pair of Hartmann shutters.
- A spherical collimator mirror.
- A fold mirror, required to keep the blue camera out of the collimator beam at high dispersion.
- The collimator Schmidt corrector lens doublet.
- A Dickson grating for high dispersion use, or dichroic mirror for low dispersion use, to separate the beams.
- In each arm, there is then a further grating. At low dispersion there is also a mirror to steer the beam into the camera.
- There is the camera Schmidt corrector doublet, also acting as dewar window
- There is a spherical camera mirror
- There is a field flattening lens
- There is the flat focal plane.

The overall dimensions of the optics are 2.5m long x 1.5m wide x 1m high.

16.3.2 Optical layout and performance – high dispersion

The layout at high dispersion is shown in Figure 182. The principal novelty of the high dispersion layout is the use of a VPH grating as a combined beamsplitter and pre-disperser. A fold mirror is necessary to avoid camera/collimator overlap, and the collimator corrector must also be trimmed to avoid conflict with the camera.

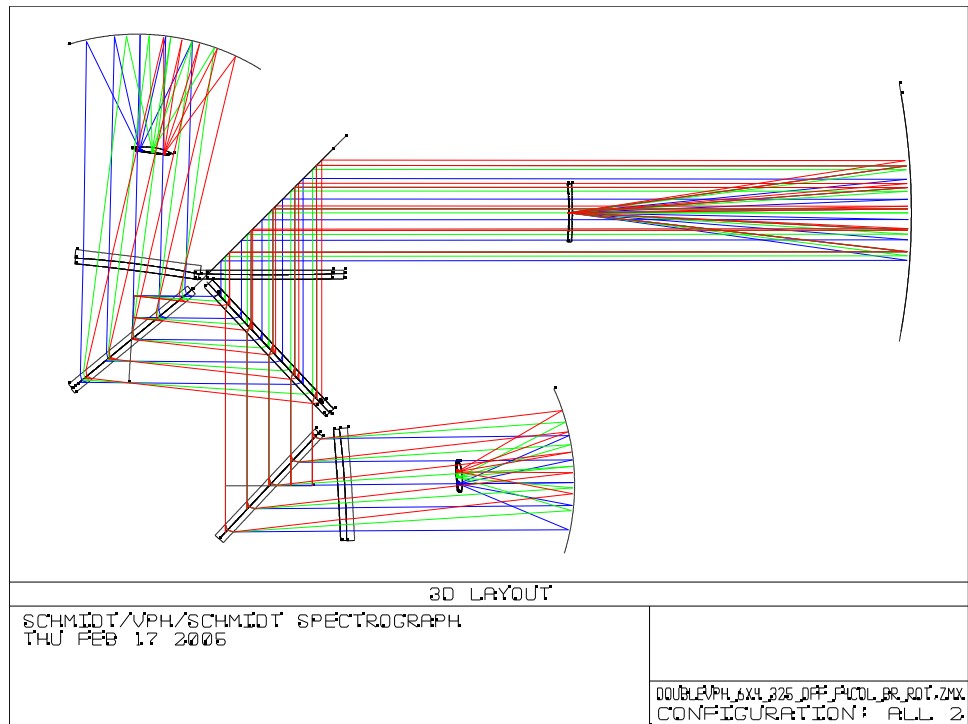


Figure 182: Do-all layout at high dispersion.

Spot diagrams are shown in Figure 183. The optical quality is satisfactory, with all rms spot sizes less than 10 μ m.

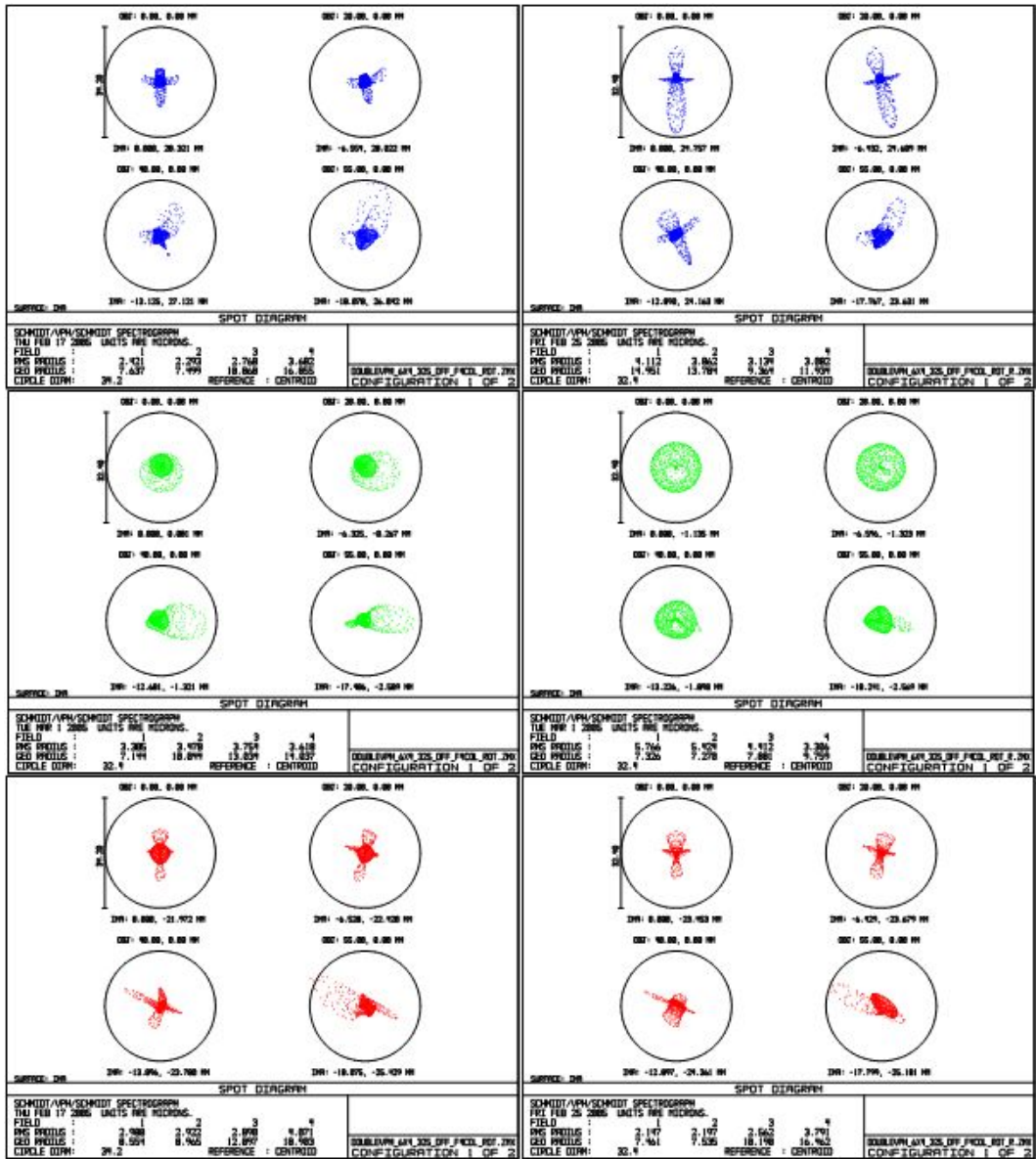


Figure 183: Do-all high dispersion spot diagrams in the blue (410nm) and red (860nm) arms. The circle represents the projected fiber size on the detector. All calculations were scaled to AAOmega dimensions, so quoted spot sizes and positions in microns must be scaled up by a factor 1.7

16.3.3 Optical layout and performance - low dispersion

Figure 184 shows the layout at low dispersion. In this mode there are three slit units; the beam-splitting VPH is replaced by a traditional dichroic; the dispersers are traditional ruled transmission gratings, and there are fold mirrors to guide the beam into the cameras, which are fixed at the same positions as at high dispersion.

The dichroic acts at 605nm, with the blue camera covering 390-640nm, and the red camera 580nm-910nm at identical grating and camera angles and hence identical resolutions.

The optical quality is acceptable everywhere, with rms spot size < 10 μ m, but can be surely improved with further work. The main challenge is that the multiple spectra on the detector have blue and red images adjacent, so the field lens must be extremely achromatic.

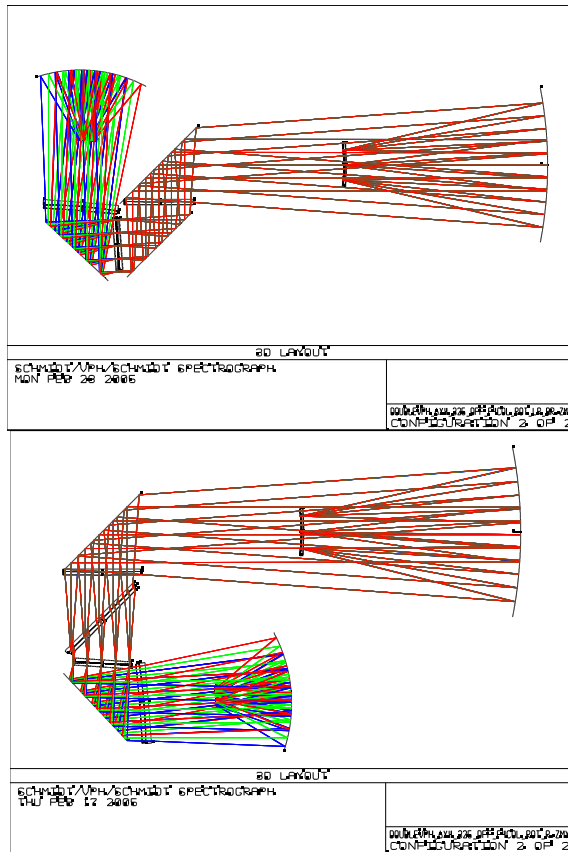


Figure 184. Do-all layout at low dispersion, shown for blue and red arms separately.

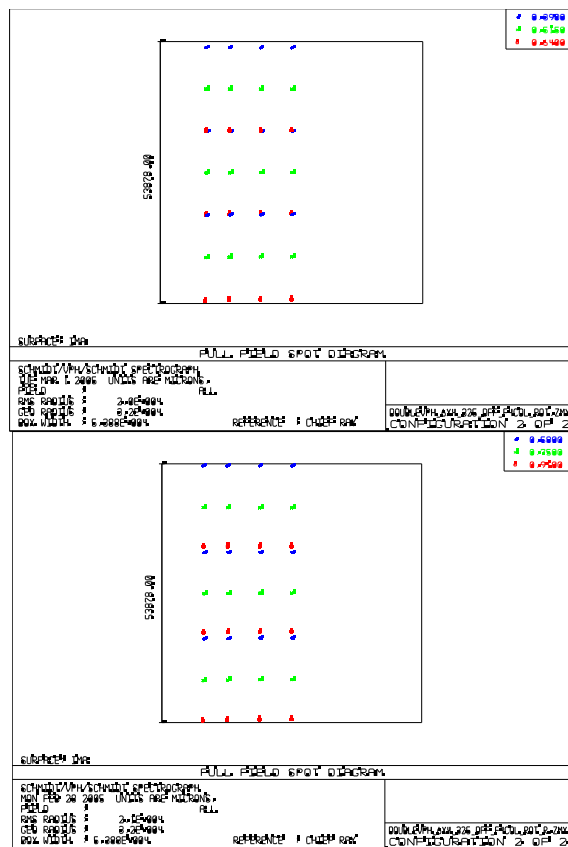


Figure 185. Full field spot diagrams for blue and red arms at low dispersion.

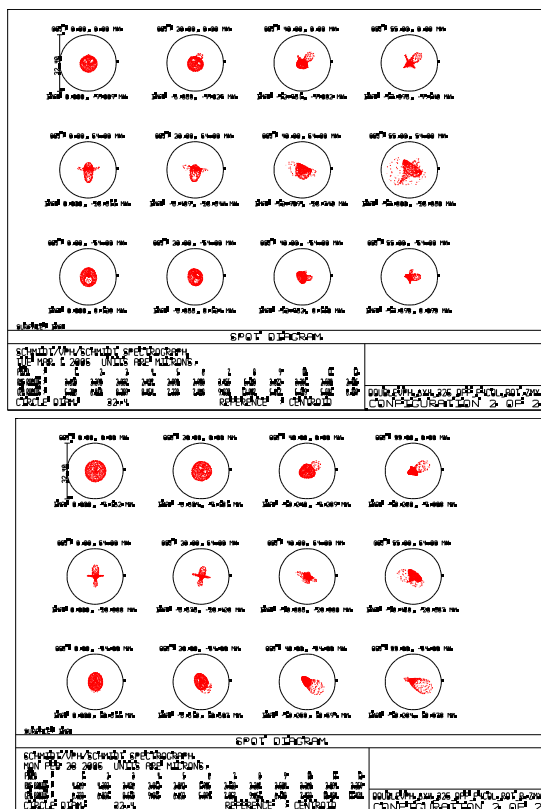


Figure 186. Do-all spot diagrams for low resolution, for 390,515 and 640nm in the blue arm, and 580, 750 and 910nm in the red.

16.4 Optical components

16.4.1 Lenses

The field lenses are BK7. The Schmidt correctors are all N-FK5/LF5 doublets as for AAOmega; these glasses are very well matched in thermal properties, so cementing is not a concern. The field flatteners are of LAK33, which is extremely achromatic and with a high refractive index giving the smallest possible lens and hence the smallest possible obstruction losses.

16.4.2 Gratings

16.4.2.1 VPH gratings as dispersers

VPH (Volume Phase Holographic) gratings offer powerful advantages over traditional ruled gratings in terms of efficiency, cost, flexibility (they can be ordered for any line density and blaze), pupil relief, scattered light performance, size, and vendor choice (two instead of one). Peak efficiencies of 90% are possible at medium dispersion (grating angles 15-35°). They do have some particular characteristics which need to be fully taken into account in the design:

- (a) Varying the grating angle changes the blaze characteristics of the grating (e.g. Figure 187).
- (b) Unlike reflection gratings, the camera angle varies with the dispersion. Full flexibility requires an articulating camera as per AAOmega; if the number of setups is restricted this can be avoided by mirrors or prisms.

- (c) Grating angles for reasonable efficient use are restricted to 8-47°.
- (d) Bandwidth is always less (in FWHM terms) than ruled gratings; however the overall higher peak efficiency means they are typically more efficient everywhere.

16.4.2.2 High dispersion grating set

For high dispersion use, we propose to use 'Dickson' gratings, where the first and second Bragg efficiency peaks of the S and P polarisations coincide to give a very efficient (though narrow bandwidth) grating. Such a grating (for use at 860nm) has been in use with 6dF for 2 years, and a larger version forms one of the core set for AAOmega. The efficiency of the AAOmega Dickson 860nm grating (uncoated) is shown in Figure 187. Unlike echelles, a separate grating is required for each wavelength region of interest. For this study we assume gratings designed for use around 410nm (where the line density peaks), at 580nm, and at 860nm for the calcium triplet.

Because the beamsplitting grating is so far from the pupil, it is very large (525mm diameter). However, there appear to be no significant constraints on VPH grating size, only that sufficiently large collimating mirrors are needed. Large VPH gratings can also be made by mosaicing, and this is routinely done.

One minor advantage of VPH gratings for this project is that the cost is almost entirely in the setup. Multiple copies of a given design come almost for the cost of the substrate, with significant savings for multiple spectrographs or multiple gratings per spectrograph.

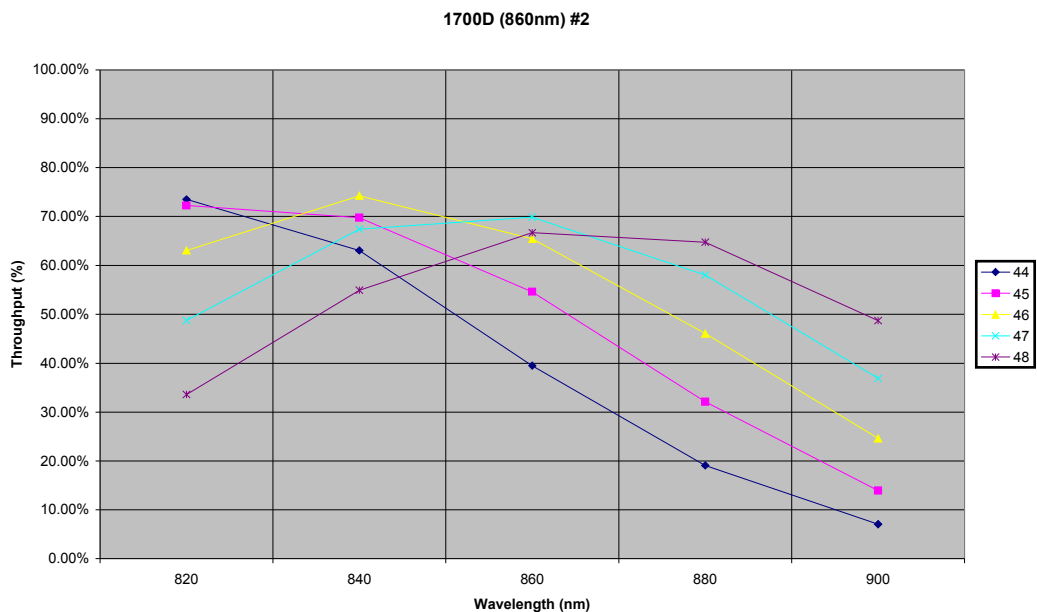


Figure 187. Efficiency for an uncoated high dispersion 'Dickson' VPH grating. Anti-reflection coating will improve all throughputs by a factor 1.08, giving a peak efficiency over 80%. The different curves are for different grating angles; the actual angle of use will be ~46.5°.

16.4.2.3 Low dispersion gratings

AAOmega uses VPH gratings throughout. This includes the low dispersion gratings, which give $R \sim 1300$ and cover 370-860nm, very close to the WFMOS requirements. The scaling up from the AAOmega design to WFMOS has two implications at low dispersion:

1. the larger and hence longer camera implies lower grating angles ($\sim 4^\circ$) for the same dispersion; unfortunately VPH gratings are not well-suited to such low dispersions because of losses to zeroth order, or absorption losses if the dichromated gelatin is thickened to reduce them;
2. the larger detector area per camera means that we would like to fit more than one bank of spectra onto the detector area; this means multiple parallel slits, which means that the grating angle is not constant for all fibers, and this has a catastrophic effect on the efficiency of VPH gratings.

At this stage, we believe that for these reasons, VPH gratings are not suitable for the low dispersion mode. However, at these low dispersions, traditional transmission gratings are almost as efficient in any case, so we propose to use traditional transmission gratings. Scattered light performance is not as good for these gratings, but at low dispersion all targets will be sky-limited and hence of comparable brightness; this means that there is a much greater tolerance to scattered light than at high dispersion, where precision equivalent widths of sources varying dramatically in brightness are required.

16.4.3 Beamsplitter

16.4.3.1 Low dispersion

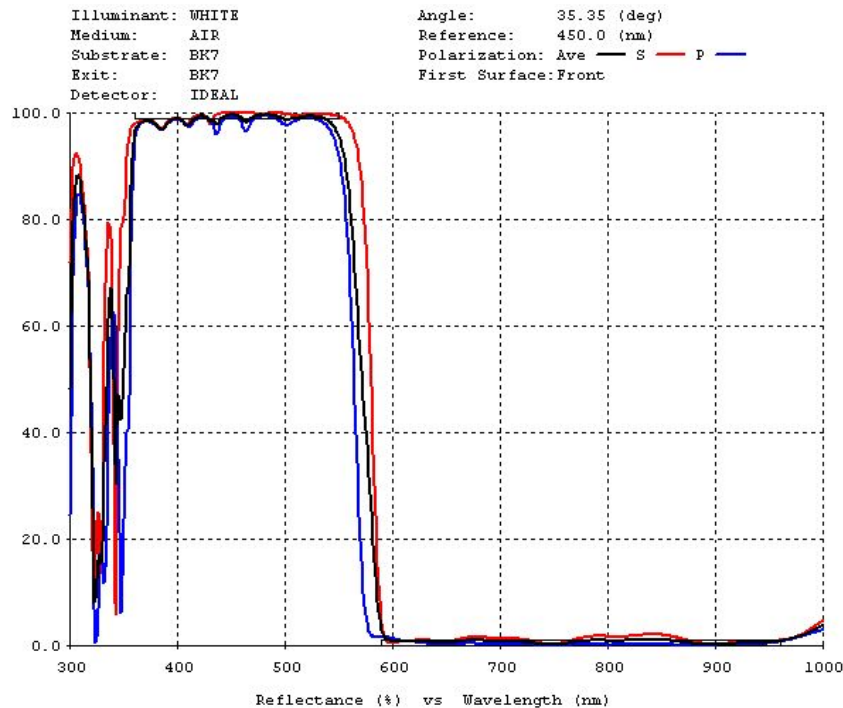


Figure 188. Transmission for the AAOmega dichroic; proposed design for WFMOS is almost identical, with all wavelengths increased by 5%.

At low dispersion, the beamsplitter is a traditional dichroic. The design used for AAOmega is shown in Figure 188; the proposed design for WFMOS is almost identical.

16.4.3.2 High dispersion

At high dispersion, the beamsplitter is the first Dickson VPH grating. The throughput in zeroth and first order mode for the 410nm grating is given in Figure 179. Although the beam-splitting performance is excellent, the crossover is nothing like as steep as a traditional dichroic, limiting how close in wavelength blue and red arms can be set up. However, since the red arm will invariably be used far into the red at 860nm, there appears to be no problem here. In particular, the blue arm can be simultaneously used at 580nm.

16.4.4 Coatings

16.4.4.1 Transmissive surfaces

One of the attractions of the dual-beamed design is the simplicity of the coatings required, since each arm covers less than an octave in wavelength. Coatings would be simple 3-layer broad-band coatings on all transmissive surfaces below the beamsplitter, giving losses <1% at each surface. There are 5 air/glass surfaces above the dichroic (field lens, 2 x corrector, 2 x first VPH); these require BBAR coatings with ~1% losses per surface.

16.4.4.2 Reflective surfaces

All reflective surfaces would be protected or enhanced silver coated, to give losses ~1% per surface in the red, rising to 3% at 400nm.

16.4.5 Detectors

For the purposes of this study, we have assumed E2V 42-80 2K x 4K detectors with 15 μ m pixels, back-illuminated and deep-depletion in the blue and red arms respectively. These detectors are buttable, have well-understood characteristics, and excellent QE, read-noise, charge-transfer efficiency and flatness. Other detectors may be equally appropriate.

16.4.6 Efficiency

Preliminary estimates of the overall throughput in each arm, at low dispersion, are given in Figure 189. They include aperture losses at the fiber input assuming 0.65" combined image size and seeing FWHM. The throughput peaks at 13% and 16% for blue and red arms respectively.

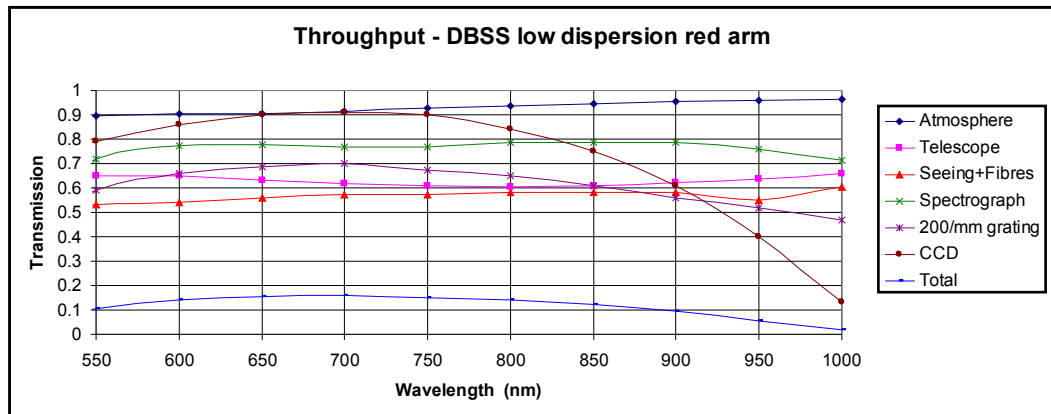
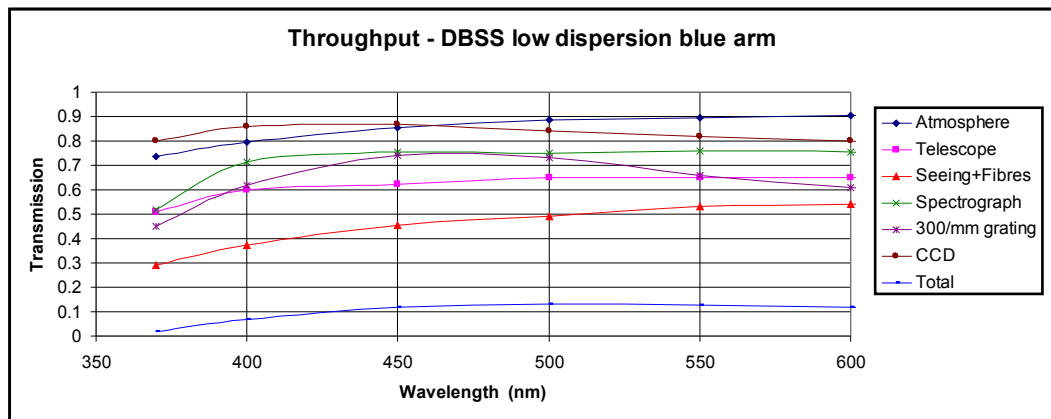


Figure 189. Estimated throughput at low dispersion for the each arm.

In high dispersion mode, the efficiency peaks at 9% at 410nm, 12% at 580nm, and 16% at 860nm.

16.4.7 Resolution

16.4.7.1 High resolution

The formal resolution R measured as wavelength/(PSF FWHM) is 37,700 in the blue arm (up to 600nm), and 18,850 in the red arm. This just fails to meet the original design goal of resolving 80% of the lines at all wavelengths in a solar-type spectrum.

However, the actual resolving power on real astrophysical targets will be better than this, because the PSF is much boxier than, for example, a Gaussian, and hence has a large FWHM compared with other measures of width, such as the rms width or the Characteristic Width (area/height). The Characteristic Width is most relevant for determining true resolving power. For a Gaussian, this Characteristic Width is 6.4% larger than the FWHM; however, for the WFMOS PSF, it is 2.5% smaller. So there is a further expected gain of 9% in resolving power over the quoted numbers for real astrophysical problems, when compared with a spectrograph with Gaussian PSF and the same nominal resolution. Subject to confirmation from more detailed spectral modelling, this design is therefore expected to meet the resolution requirements for WFMOS.

16.4.7.2 *Low resolution*

At low resolution, the resolution is $R \sim 1350$. This is sufficient to measure abundances and velocity dispersions down to 100km/s.

16.4.8 *Mechanical and thermal stability*

Because the gravity vector is fixed with respect to the spectrograph, there is no flexure. The spectrograph must be insulated from vibration; normal commercial pneumatic vibrational insulation support legs provide adequate stability. The spectrograph must also have temperature drifts no worse than 0.1°C over typical exposure times, to keep thermal shifts in the detected images less than 1/20 pixel. This means the spectrograph must be housed in an insulated chamber, and also that switching from low to high dispersion during the night is not possible without degrading the performance.

16.4.9 *Mechanisms*

Mechanically, the design is simpler than AAOmega because there is no automated slit exchange; no back-illumination within the spectrograph, and no grating or camera articulation. The mechanisms required per spectrograph are the shutter, the Hartmann shutters, and camera focus (3 motormikes) for each camera. All mechanisms are controllable from the control room.

The gratings weigh up to 34kg in glass alone. Therefore a hoist or slide is needed to allow grating changes.

16.4.10 *Cooling*

AAOmega uses LN₂ cooling, because of the articulating cameras. For WFMOS, with its cameras in fixed positions, liquid helium cooling would be used through the use of closed-cycle coolers.

Chapter 17 Near-Infrared Spectrograph option

17.1 Introduction

The baseline infrared spectrograph for Subaru WFMOS adopts the design currently used within Subaru's FMOS instrument. This is a dual mode OH-Suppression spectrograph which delivers the full range of 0.9-1.8 μ m onto a 2048 \times 2048 HAWAII-2 array within a single exposure at R \sim 600, or within four separate exposures at R \sim 3000. The Spectrograph includes an intermediate focal plane where an image of the full spectrum is formed at R \sim 3000, and where the \sim 200 brightest OH lines are removed by means of lines etched in the mirror coating. This proposal is based on the assumption that the existing pair of FMOS spectrographs can be incorporated into WFMOS with minimal effort, *provided* that the FMOS design is adopted. This assumption is itself based on the assumption that the FMOS design satisfies the WFMOS science requirements.

17.2 Summary of Strawman specification

The original KAOS proposal contains no mention of infra-red spectrographs, and hence no outline specification. For the feasibility study we have therefore adopted the FMOS specifications, since FMOS is both well-defined, and represents the forerunner of WFMOS. The scientific goals of the FMOS project were aimed at studying large-scale structure and galaxy evolution within the available field of view of the existing Subaru prime focus assembly, and so the spectrographs are well matched to the science goals of WFMOS.

Requirement	Value	Comment
Spectral Resolving Power	$\lambda/\Delta\lambda = 600$ or 3000	Resolving powers required for full wavelength coverage and OH suppression
Spectral Window	900 – 1800 nm	J-H band gap is obscured by the slit assembly
Simultaneous Spectral Coverage	900 – 1800 nm, or 900-1150, 1150-1400, 1400-1650, 1550-1800	Four exposures required for full wavelength coverage at R=3000
Detector	HAWAII-2	MBE devices preferred, VIRGO detectors may be an option for WFMOS
Imaging Performance at mask	99%EED within 360 μ m	Required for OH Suppression
Imaging Performance at detector	90% EED within 3x3 pixels	This may be reduced
Number of Simultaneous Targets	1500	Will require multiple spectrographs
Sensitivity Limits	1E-16 erg/cm ² /s @ 1700nm gives S/N=18 in 10 minutes exposure	As always, in the NIR the sensitivity is a strong function of line position.

- Input focal ratio to collimator: f/4.7
- Output focal ratio to camera: f/1.5
- Beam size (pupil stop on primary grating): 210mm
- Primary grating line density: 500l/mm

- Secondary grating line density: 370l/mm
- Operating temperature (spectrograph): 200K
- Operating temperature (camera): 75-150K
- Number of fibers/spectrograph: 2-300
- Number of spectrographs: 5-8
- Operational wavelength range: 900nm – 1800nm
- Total System Throughput (Sky-Detector): 23% (high resolution)
- Total System Throughput (Sky-Detector): 18% (low resolution)

In Figure 190 we show the performance model of the as-designed FMOS spectrographs, as this gives a better indication of the actual system behaviour than the nominal throughput values given above.

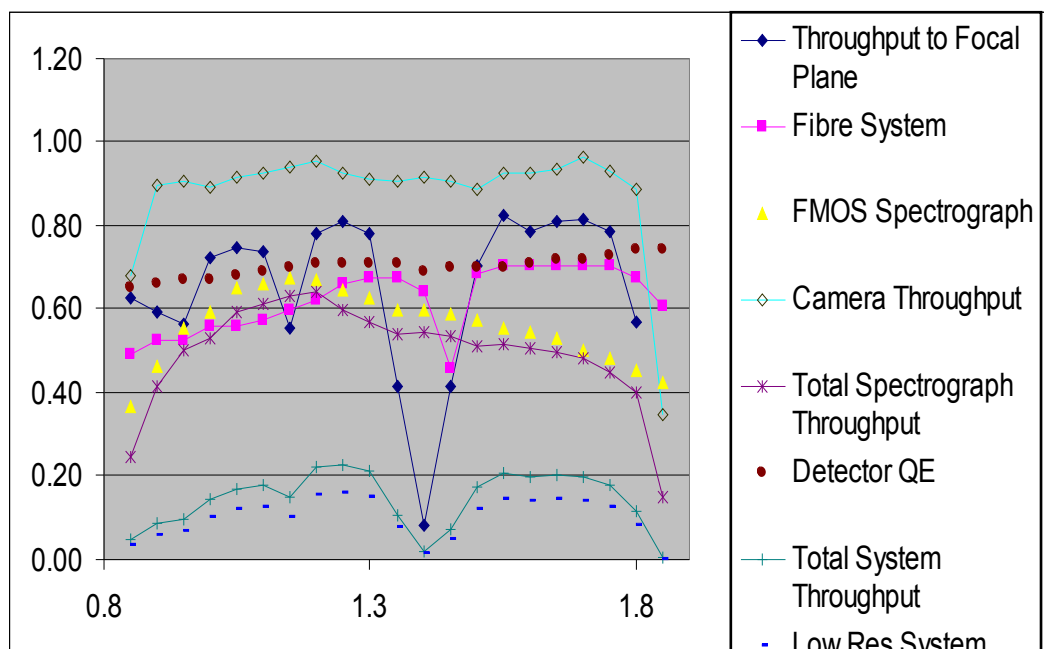


Figure 190. Performance model for the FMOS Spectrograph.

17.3 Spectrograph Strawman design

17.3.1 Thermal Design

For a NIR spectrograph operating in the OH-suppressed regime the instrument is limited by the thermal emission from the spectrograph enclosure itself which enters the camera. The out-of band component of this thermal emission can be blocked by a suitable cold filter within the camera, but the in-band contribution will still limit the performance unless the spectrograph enclosure is cooled.

The following table illustrates the requirements on the spectrograph enclosure temperature and the filter blocking efficiency that are required to ensure that the

instrument background is reduced to below the level of the expected detector dark current.

		λ : 0.5 to 0.9 μm	λ : 0.9 to 1.8 μm		λ : 1.8 to 2.5 μm	
		<i>black cam.</i>	<i>black cam.</i>	<i>reflective cam.</i>	<i>black cam.</i>	<i>reflective cam.</i>
Front elements (spectro. at T, L1+L2 at 175K) without filter	T=220K	-	5.1E-2	1.3E-1	515.6	1281.0
	T=210K	-	8.6E-3	2.1E-2	141.3	350.1
	T=200K	4.1E-20	1.2E-3	3.0E-3	34.4	84.6
	T=190K	-	1.4E-4	3.5E-4	7.6	17.7
Front elements (spectro. at T=200K baseline, L1+L2 at 175K and filter with baseline transmission spec.)		~1% spec. -> ~0 i.e. negligible	~98% transmission spec.: 1.2E-3 3.0E-3		~0.1% spec: 3.4E-2	~0.1% spec: 8.5E-2
Filter at T	T=170K	-	1.9E-8	2.6E-8	3.9E-1	5.2E-1
	T=150K	1.9E-31	3.2E-11	4.5E-11	3.9E-3	4.9E-3
	T=120K	-	4.2E-17	5.5E-17	2.0E-7	2.6E-7
Back elements at 100K (L3 to L6 + surrounding structure), detector at 70K		-	1.36E-20	1.9E-21	2.7E-11	3.8E-12
Worst-case final value: Low rejection, $T_{\text{filter}}=170\text{K}$		negligible	~0.001	~0.003	~0.423	~0.600
Best-case final value: High rejection, $T_{\text{filter}}\leq 150\text{K}$		negligible	~0.001	~0.003	< 0.01	~0.010
Intermediate case final value: Low rejection, $T_{\text{filter}}=150\text{K}$		negligible	~0.001	~0.003	~0.038	~0.090
Remarks		Filter rejection spec can be relaxed in visible	Science band background dominated by 200K environment radiation from spectrograph via camera window, no influence of filter T		This band gives the largest overall contribution; If $T_{\text{filter}} \leq 150\text{K}$, rejection spec. dictates, otherwise filter emission dominates.	

The spectrograph enclosure is cooled to 200K by circulating dry air which has been chilled to this temperature. The UK-FMOS spectrograph enclosure is currently being assembled and tested in Oxford.

17.3.2 Optical Design

17.3.2.1 General Description

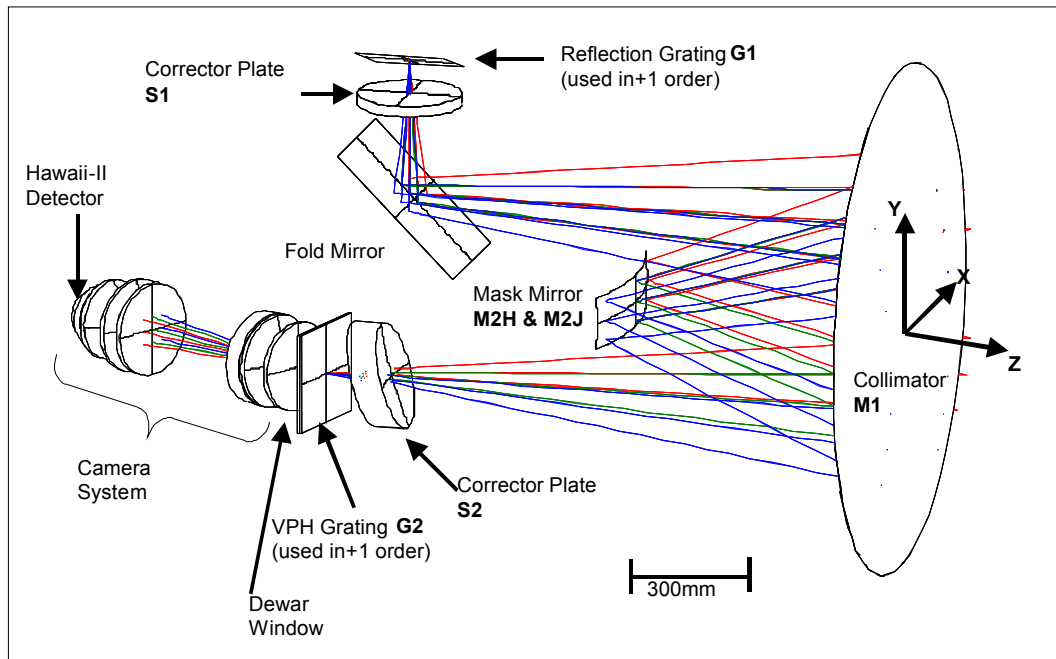


Figure 191. FMOS Optical Layout (Chief rays 1800, 1373, 900nm).

The spectrograph design (Figure 191) is based around a large (1.4m) Schmidt system with the primary collimator mirror (M1) used in triple-pass. The fiber array that forms the entrance slit is located in the centre of the secondary mirror (M2). A primary spectrum is formed on M2 by means of a reflection grating (G1) which is located beyond the first corrector plate (S1) of the Schmidt system. M2 is formed using a pair of convex spherical mirrors (M2J and M2H). M2 is used to remove the OH emission lines by the use of selective masking at this intermediate image surface. After further correction (S2) the output from the spectrograph is collected & imaged by the camera system.

The low-resolution mode is obtained by the use of a second grating (G2), placed between the second corrector and the camera allowing the spectra to be completely imaged on to the detector. The high-resolution mode is obtained by removal of G2 and rotating the camera about a point close to the position of G2.

The camera is wholly contained within a vacuum dewar to allow the detector cooling system to operate. The lens system is split into two groups with the filter located just before the second group. The detector is located just behind the second group in the $\sim f/1.5$ beam.

The spectrograph components will be accommodated within an enclosure that is maintained at 200K. To facilitate the layout within this enclosure, there will be a fold mirror inserted between M1 & G1.

This spectrograph/camera system has no chromatic correction (longitudinal or lateral), as only spectra are being imaged, which by definition does not require any 2 wavelengths to be imaged to the same point on the detector. The system is not required to be distortion free. The longitudinal chromatic aberration is corrected by tilting the detector, while lateral colour and distortion can be considered similar

aberrations that produce ‘bent’ spectra which is not considered a problem in the data recovery.

The optical system design & optimisation is highly dependant on the weighting of the wavelengths & fields. In this case no weight was given to the central wavelength & higher weight to the regions 900-1200 & 1500-1800nm.

17.3.2.2 Optical Performance

The optical performance of an OH-suppression system needs to be monitored both at the detector, and at the intermediate image surface on the mask mirror. The assumptions that have been made in the FMOS design are that the images of the 280µm fiber cores should not be allowed to blur by more than 10% at the extreme ends of the fiber slit, which implies that the spot sizes at the mask surface should be less than 120µm. Spot diagrams at the mask surface are presented in Figure 192 where lateral colour has been ignored.

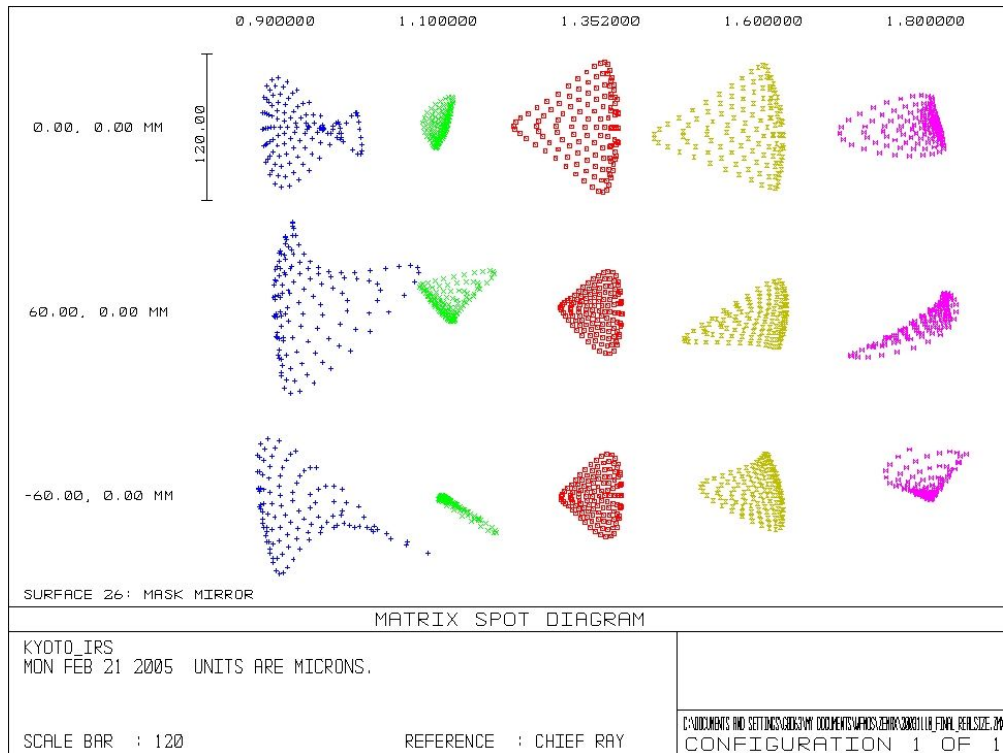


Figure 192 Spot diagrams on the mask surface for the FMOS spectrograph design.

The image quality at the detector for the FMOS design is shown in Figure 193. The design goal here was to limit the blurring effect of the optics on the image of the fiber core to less than 3 detector pixels (54µm in the case of the HAWAII-2 detectors). The encircled energy distribution for the worst case (900nm wavelength) is shown in Figure 194.

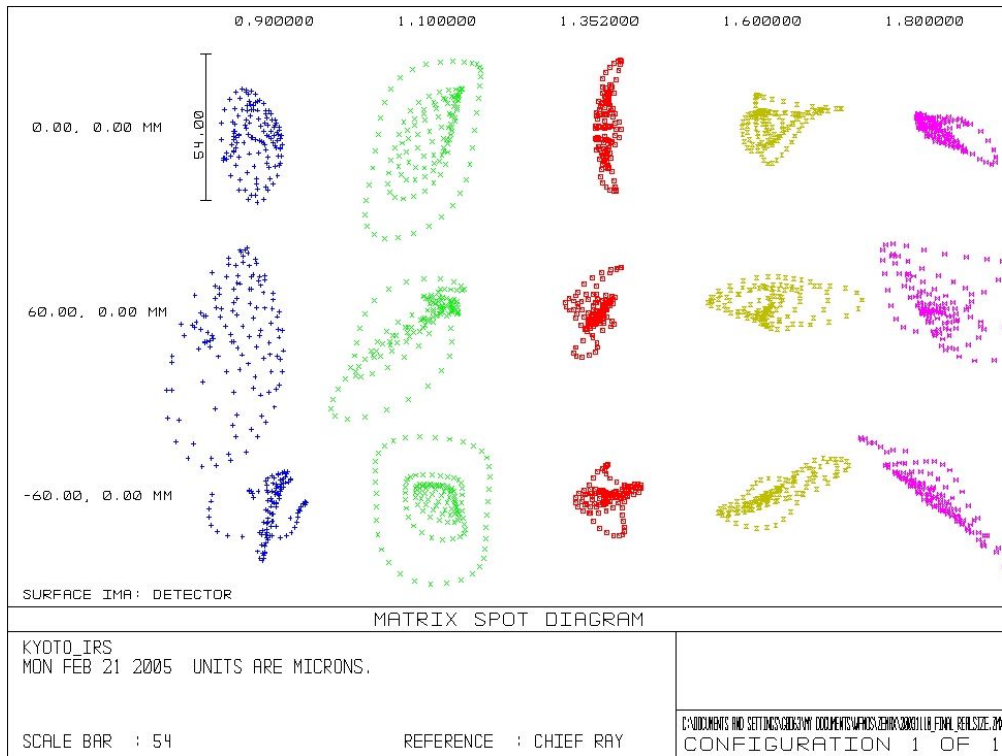


Figure 193 Spot diagrams at the detector surface for the FMOS spectrograph

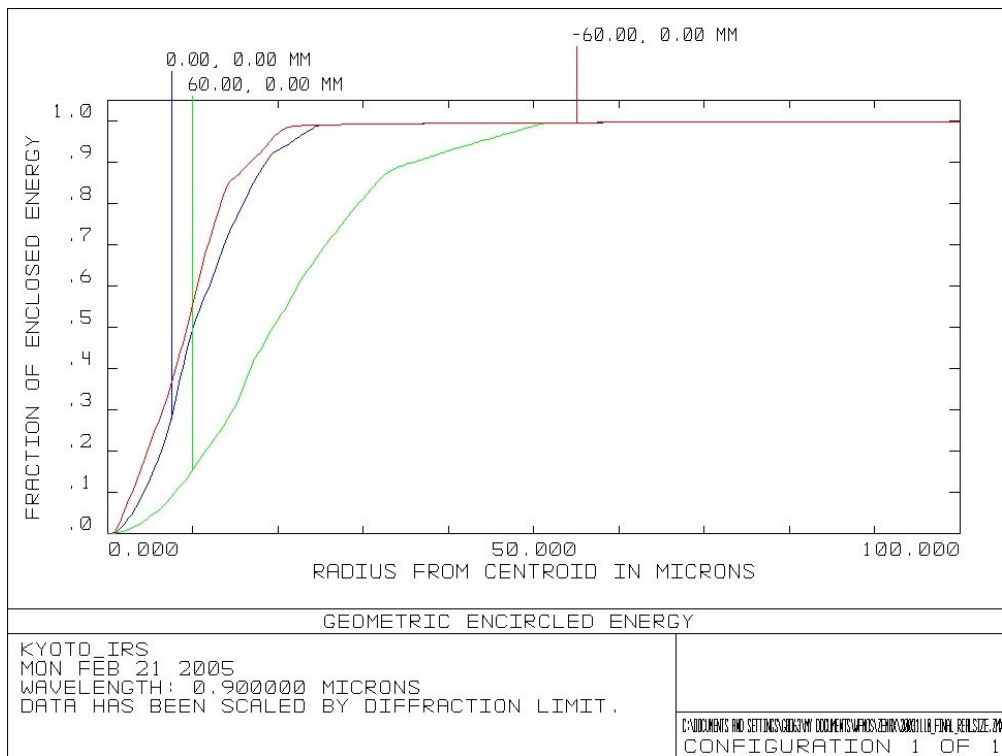


Figure 194 Encircled energy distribution for the worst case wavelength of Figure 193

17.3.3 Calibration Issues

17.3.3.1 Dithering

Unlike a classical long-slit spectrograph, we are unable to nod the telescope along the slit to sample the spatial information along different detector pixels. The

spectrograph design allows for a compromise to be reached whereby a tilt-offset of the grating is used to move all the spectra by a small amount in the spatial direction on the detector.

17.3.3.2 Fiber-Fiber Throughput Calibration

With the 2dF instrument, the best fiber-fiber throughput calibration was achieved using the relative intensities of bright sky lines within the spectra. For FMOS, this approach can be used, but is somewhat complicated by the fact that the brightest sky lines have been removed in the optical design of the system. We have therefore included provision for a controlled tilt of the slit unit in the spectral direction about its (spherical) centre of curvature. This will have the effect of moving the bright lines off the masked regions of the spectra, allowing a very short exposure of sky to be made as a throughput calibration image.

17.3.3.3 Wavelength Calibration

As the spectrographs are gravity- and temperature-stable by design, we do not anticipate any significant variations in wavelength calibration. The design of the suppression mask provides a good estimate of the wavelength calibration without any additional requirements, but if specific lamps are required for any reason then there is provision within the Subaru telescope to illuminate the prime-focus corrector from lamps located around the periphery of the telescope tertiary mirror.

17.3.3.4 Sky Subtraction

There is no analogue of the nod-and-shuffle technique that can be implemented on current IR detectors, but the individual readout times are relatively fast. On-sky test that we have performed with CIRPASS in multi-fiber mode on the AAT and WHT (Doherty et al. 2004, MNRAS 354, 7) suggest that 5 minute exposures provide adequate sampling of the JH sky for beam-switching.

17.3.4 Spectrograph Mechanical Design

17.3.4.1 Base Frame

The instrument base frame is constructed in two sections of welded steel extrusion which are bolted together in location. This allows the large base frame to be shipped and moved through the Subaru dome environment with no further disassembly.

The base frame rests on four anti-vibration feet chosen to match the vibration characteristics of the instrument structure as a whole. To facilitate movement of the whole spectrograph four jacking wheel units are also provided to raise the instrument off its anti-vibration feet and allow movement of the instrument.

The base frame supports the camera unit and the thermally insulated enclosure directly, and the spectrograph optical bench via four long thermal path legs.

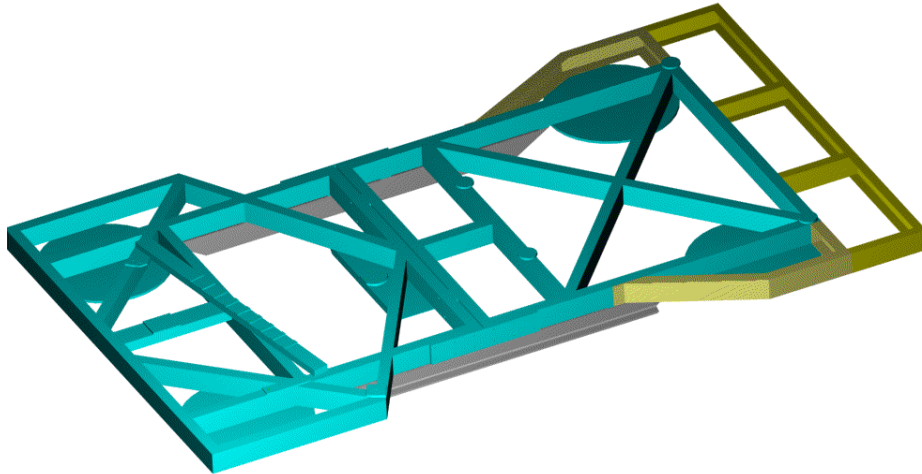


Figure 195. Showing construction of the welded baseframe structure. The anti-vibration pads are located under the circular mounting points in the corners of the baseframe. The additional bolted on section (yellow) is purely to support the insulation and is not structural to the optics support.

17.3.4.2 Support legs

The four optical bench support legs serve a number of purposes. Firstly they provide the mechanical support for the optical bench and the entire spectrograph optics. Secondly they must allow for the contraction of the optical bench as it cools to 200K relative to the base frame which remains at approximately 293K (in the lab) or 273K (at the telescope). Thirdly they must provide high thermal resistance to prevent the heat input via the legs being too large.



Figure 196. Long thermal path support leg. The lower flange is mounted to the base frame, the upper flange is connected to the optical bench. The leg is extremely stiff axially but the upper flange can move by several mm in a transverse direction to allow for thermal contraction of the optical bench.

These three aims are met by manufacturing the legs from stainless steel tubing in a nested structure with alternate ends of the tube being joined by welding. The

effective length of the stainless steel tube is then almost 0.9 metres and while it is extremely rigid axially, it can flex in a direction perpendicular to the tube axis.

17.3.4.3 *Optical bench*

The optical bench is constructed as a single welded frame structure from steel section. Attachment points are welded in place for the four legs used to support it from the baseframe, the collimator mirror mounting frame, the mask and slit unit assembly and other optical assemblies. The optical bench relies on the collimator mirror mounting frame to provide some overall stiffness. This mounting frame is dowelled and bolted to the optical bench.

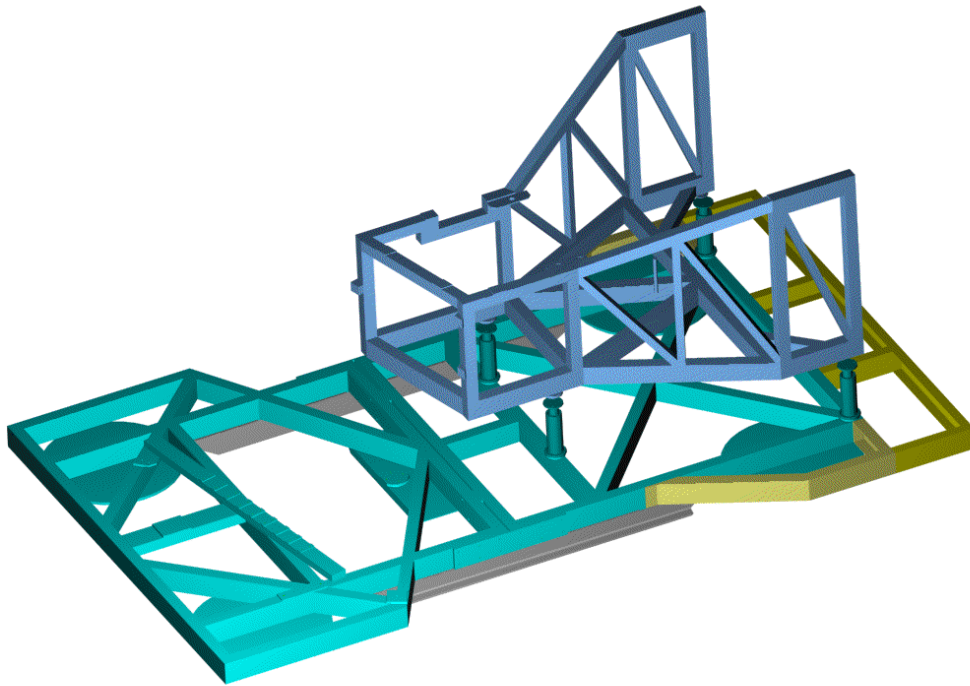


Figure 197. Figure showing the optical bench structure in place resting on the support legs and base frame. The support frame for the collimator mirror is not shown.

17.3.4.4 *Collimator mounting*

The collimator mirror is a honeycomb lightweight glass mirror approximately 1.4m in diameter manufactured by Hextek. On the recommendation of Hextek this mirror is supported in a stainless steel band with machinable lead blocks attached to the two edges. These lead blocks locate on the edges of the front and rear faceplates of the honeycomb mirror. The lead has sufficient compliance to deform to the shape of the glass at the edge contact to avoid high point loading of the mirror. It is worth noting that the walls of the honeycomb glass structure have no structural strength perpendicular to the tube axis and any pressure on the walls of the tubes must be avoided.

FEA analysis of this mounting technique with the mirror vertical has been performed and the results are shown below.

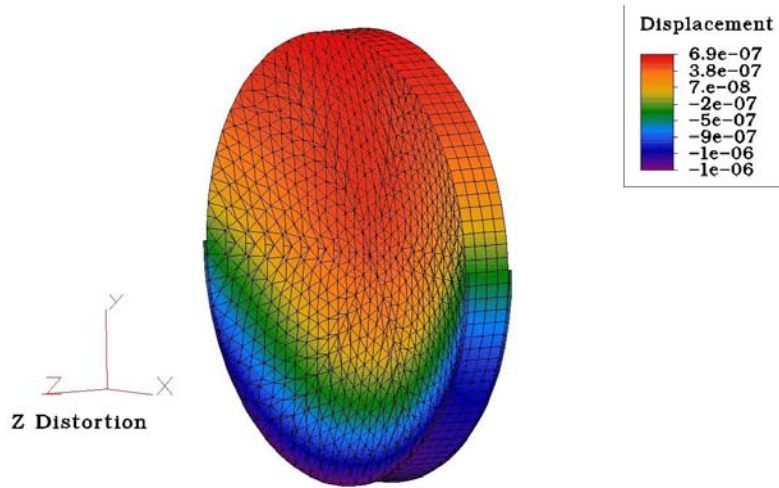


Figure 198. Results of finite element analysis of mirror support (units are metres)

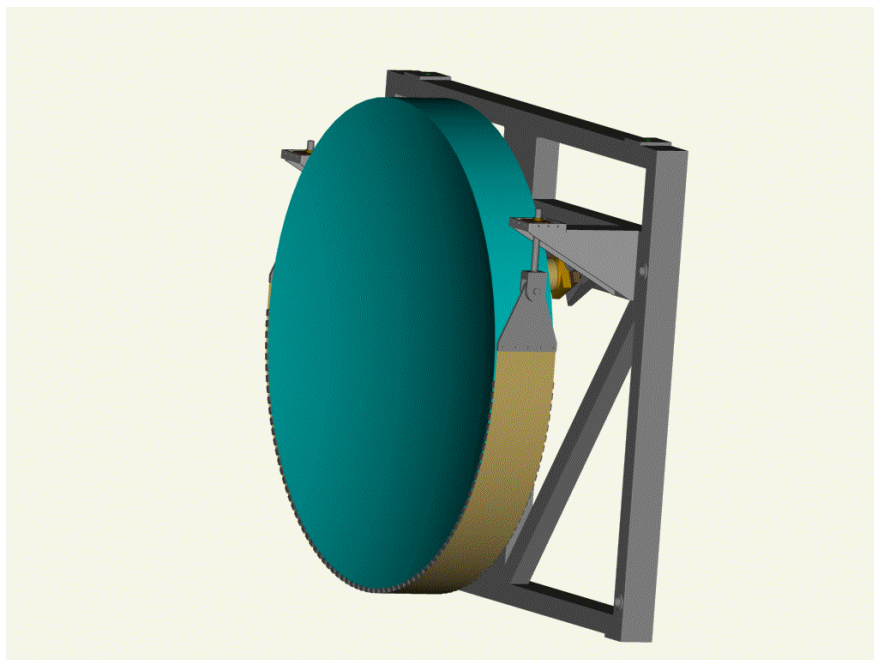


Figure 199. Mounting arrangement for collimator mirror.

The stainless steel band is suspended from two points on a mounting frame. These two mounting points have a small adjustment range to allow control over the height and position of the mirror axis. Axial location of the mirror is achieved using three of the six mounting bosses located on the rear of the mirror. At each of the rear mounting points a linear slide is attached to the mounting frame using a rotary bearing allowing it to self align (see Figure 199 and Figure 200). On the linear slide a mirror locating pin is fitted using a self aligning bearing. The overall effect is that the mirror locating pin is free to self align in the XY plane of the mirror but provides control over the Z (axial) position of the mirror.

This self alignment of the three mounting pins is important for two reasons, firstly since the honeycomb mirror has been slumped during manufacture we do not have control over the exact location of the mirror mounting points or their alignment axis. Secondly during the cooldown process the linear bearings are free to move

and the mirror and support structure can exhibit differential contraction without stressing the mirror.

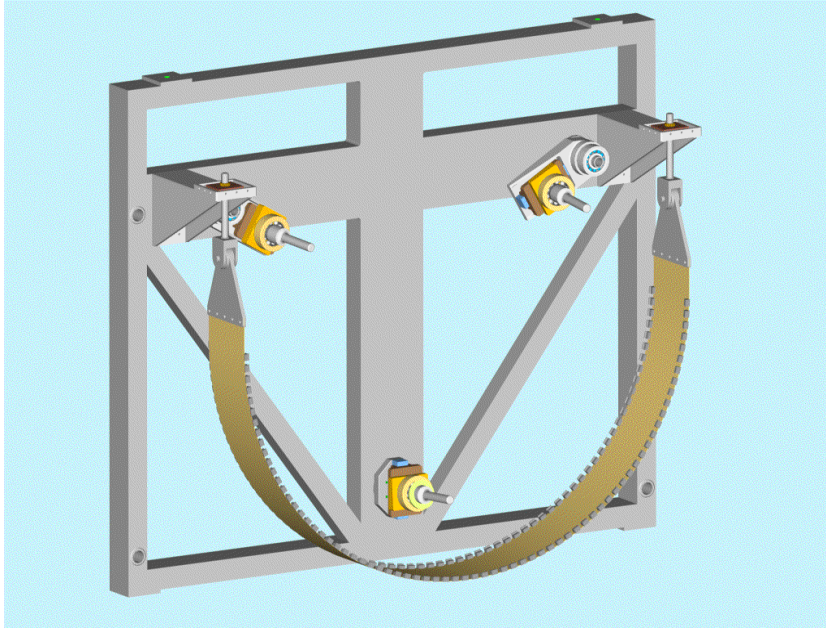


Figure 200. Main mirror support frame showing support band and axial location mountings.

17.3.4.5 Slit and mask mirror unit

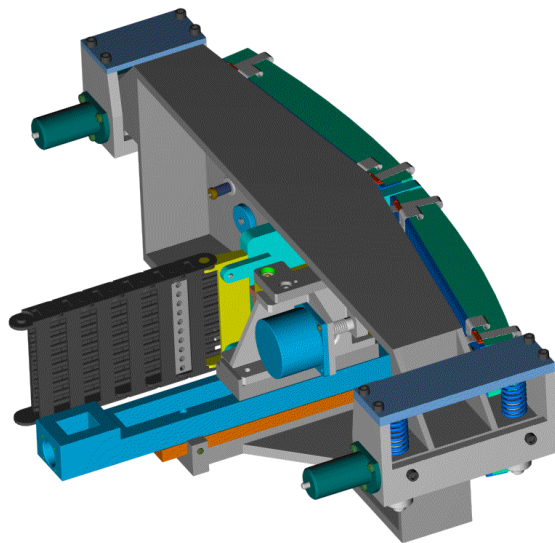


Figure 201. Cross beam with slit mechanism, slit unit and mask mirrors.

The slit unit and the two mask mirrors are mounted on a cross beam which in turn is mounted on the optical bench. The position and alignment of the cross beam can be adjusted for overall alignment of the slit unit. The masks are separately aligned relative to the slit using their individual alignment adjustments. The two mask mirrors are retained in a carrying plate using sprung clips. Each of the carrying plates is mounted on the cross beam using 3 kinematic mounts which have axial and lateral alignment adjustment.

The slit unit is mounted on a focus mechanism with long travel to allow it to be installed safely by hand in a retracted position then driving into operating position in the very narrow gap between the two mask mirrors. The slit unit is also provided with a second mechanism to allow the leading edge of the slit to be moved slightly in the spectral direction using a cam. When the cam is retracted the slit sits against an alignment hardstop.

17.3.4.6 *Fold mirror, corrector and grating*

The fold mirror, Schmidt corrector (S1) and reflection grating (G1) are all mounted within a welded framework tower which itself is supported on the optical bench. The fold mirror simply rests on a support shelf with retaining clips. The shelf has the minimal alignment requirements built into its support brackets.

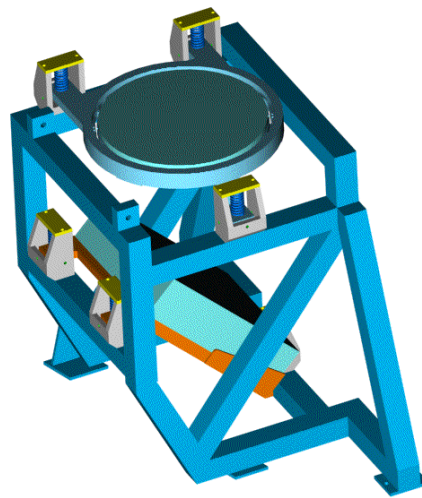


Figure 202. Figure showing the welded steel framework supporting the fold mirror and Schmidt corrector (S1). The grating (G1) support is mounted at the top of the framework but is not showing in this view. Each of the optical elements has manual alignment mechanisms.

The Schmidt corrector rests on a horizontal annular shelf and is centred using a temperature compliant mount as used in the FMOS camera. Since the temperature range for this optical element is far less severe than for the camera, we have not repeated the modelling already performed for the camera. Retaining clips are provided to prevent the optics being lifted out accidentally.

The grating (G1) consists of a mosaic of four identical elements aligned and held in a support frame designed and fabricated at Kyoto University. This complete grating unit is supported on kinematic mounts on the top of the welded tower. One of the kinematic seats is contained within a mechanism to nod the grating along the grooves in a similar manner to the slit unit. This allows the spectra to be shifted a small distance (few pixels) along the slit direction.

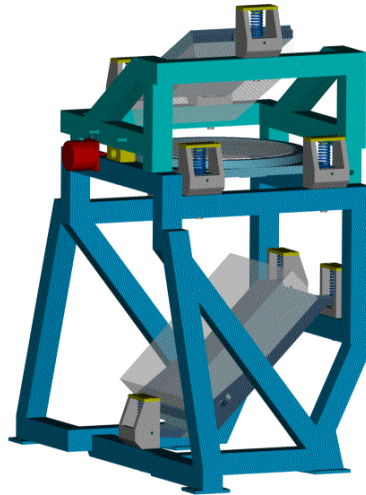


Figure 203. Grating support mounted on top of the fold mirror and Schmidt corrector.

If the design of the grating support (G1) changes then the only impact on the overall mechanical design is in the detail of the grating support frame. The tower and grating tilt mechanism remain unchanged.

17.3.4.7 Corrector (S2) mounting

The second Schmidt corrector consists of a thick pair of lenses in optical contact (silicone oil). The mounting and alignment of this optical element will be designed and fabricated by the Kyoto University team. As can be seen in figure 10, the S2 doublet lens is located near the end of the box section of the optical bench. The plan is to mount the lens in a cell and mount this from the rear of the end face of the optical bench. The VPH grating assembly is mounted from the opposite side of the end face of the optical bench .

17.3.4.8 VPH mounting

The VPH grating must be held near the optical pupil at an angle bisecting the camera and collimator axes. The VPH grating is only required for the low resolution case with the camera at a single position, the VPH grating must be removed out of the optical beam for the high resolution case with variable camera angle.

The VPH grating is mounted on a sliding carriage together with two circular apertures each defining an aperture stop. One of the aperture stops is mounted in close proximity ($< 1\text{mm}$) to the camera side of the VPH grating, the second is mounted on the carriage in the position defined by the optical beam when the VPH grating is removed from the beam. The VPH grating itself is mounted in a cell with manual rotation alignment to correctly align the dispersion direction of the grating.

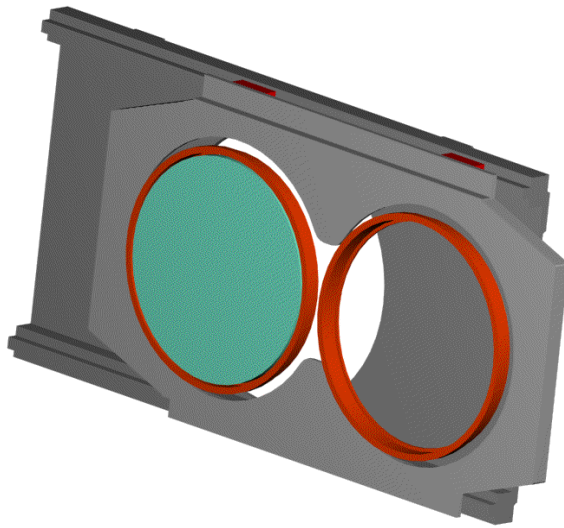


Figure 204. VPH deployment mechanism.

The VPH grating mechanism uses a stepper motor driven linear actuator and linear bearings to switch between VPH and non-VPH modes.

17.3.4.9 *Dark slide arrangement*

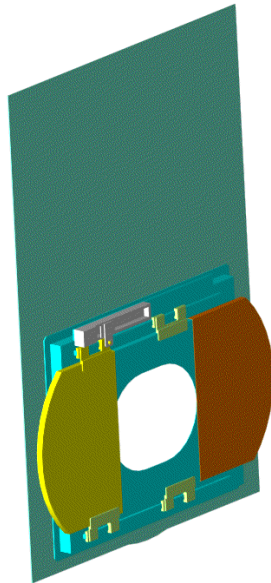


Figure 205. Darkslide arrangement with both halves of the darkslide retracted.

The dark slide is mounted on the inside skin of the thermal enclosure and has no contact with any of the optics or optical bench as there is no alignment requirement but the spectrograph to camera interface is required to be light tight. The dark slide consists of two sliding shutters which are sealed against light around the edges and overlap when joined at the centre to prevent light leaks. Either of the two shutters may be deployed individually to act as a simple

Hartmann shutter. The shutters slide on THK bearings with stepper motor driven linear actuator units.

17.3.4.10 Camera articulation

The camera is required to move through an angle of about 30° with the centre of rotation located below the centre of the VPH grating. The camera is mounted using its four feet onto a platform. This platform is attached to a pivot point below the VPH grating to define the rotation axis. The weight of the camera is supported by two cam followers running on a ground metal surface. The camera angle is set using a stepper motor driving a tangent arm and the camera position is recorded using a combination of a coarse absolute encoder (4 bit or approx 2 degrees per step) and fine resolution incremental encoder (0.01mm or 0.0006°). This mechanism and structure is outside of the thermal enclosure and operates at ambient temperature.

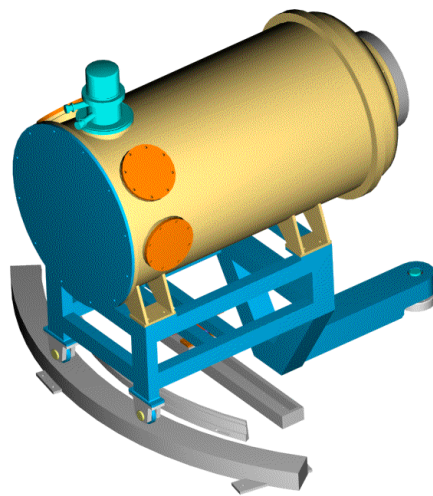


Figure 206. Figure showing cryogenic camera unit on top of the camera rotation mount.

17.3.4.11 Thermal Enclosure

The entire spectrograph is cooled to approx 200K in a dry air atmosphere to reduce instrumental thermal background. The purpose of the thermal enclosure is twofold, firstly to provide thermal insulation, and secondly to provide a gas tight sealed enclosure to prevent water vapour entering and condensing and also the loss of chilled air which must be replaced.

The basic enclosure consists of 300mm of closed cell foam insulation with an aluminium inner skin. Each of the sides of the enclosure is sealed against an inner supporting framework.

The base of the enclosure rests on the spectrograph baseframe with the inner framework attached on top. The support legs for the optical bench protrude through the base slab of insulation with a clearance hole in the insulation and a flexible gas tight seal around the inner skin of the base slab.

The side walls of the enclosure are sealed against the inner frame and base slab with the top slab likewise sealed against the inner frame and side insulation. Access ports are provided by small panels of insulation with a gasket seal against the inner framework.

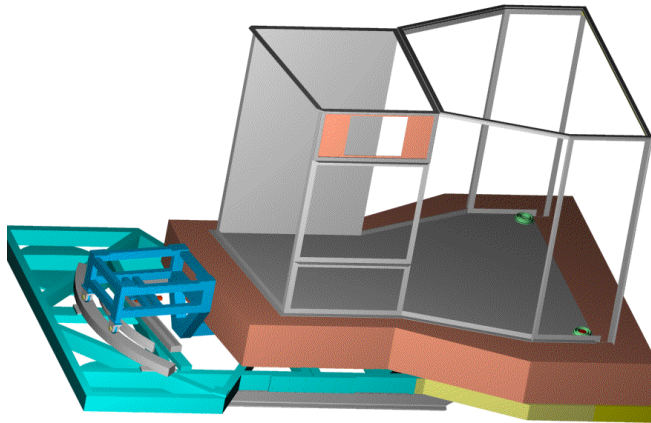


Figure 207. Inner framework sitting on base slab and base frame with camera support frame in position showing its relationship to the thermal enclosure.

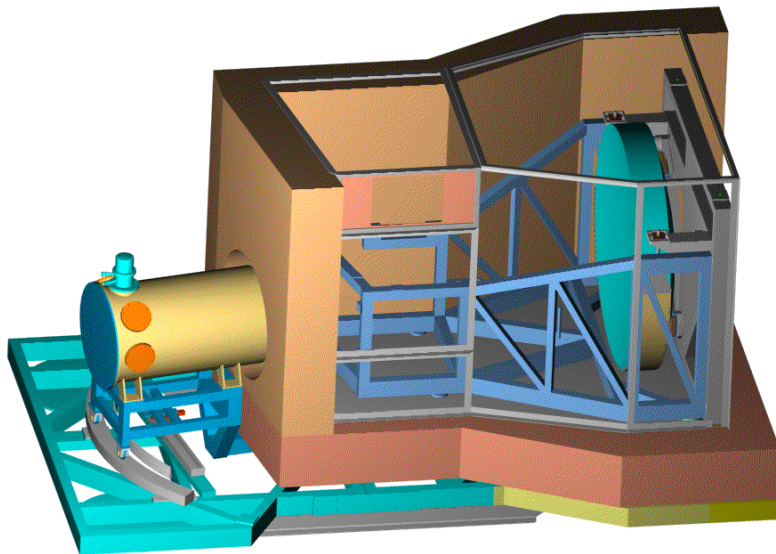


Figure 208. Cutaway representation of the thermal enclosure with camera inserted into the enclosure.

The remaining access holes in the thermal enclosure are for the camera, the fiber feedthrough, and electrical connections.

The fiber feedthrough is detailed in the Fiber to spectrograph ICD. The fibers are grouped in furcation tubing which runs through the thermal enclosure wall in an insulating tube (G10 material) and then within a gas tight conduit to a spare length box located on the outside of the spectrograph. The gaps between the furcation

tubing and the insulating tube through the wall are filled with expanding foam after assembly. Gas loss through the furcation tubing (equivalent to 50mm² hole in the enclosure wall) is eliminated by pressurizing the spare length box to the same level as the inside of the spectrograph enclosure with dry warm air.

Electrical connections from and to the interior of the thermal enclosure are made through a terminal strip panel embedded within the insulation wall. This allows the internal and external parts of the cabling loom to be split for assembly purposes.

The sealing of the moving camera body to the insulated enclosure is a complex issue. We have designed a flexible rubber tyre with attaches to the inner skin of the thermal enclosure and a flange mounted 200mm back from the camera window. Mounting flanges are bonded into the rubber tyre at the moulding stage. This rubber tyre is gas tight and by using low temperature, opaque and low thermal conductivity rubber will remain flexible at 200K. Tests of suitable material have been carried in our 200K environmental testing chamber and remain suitably elastic at this temperature.

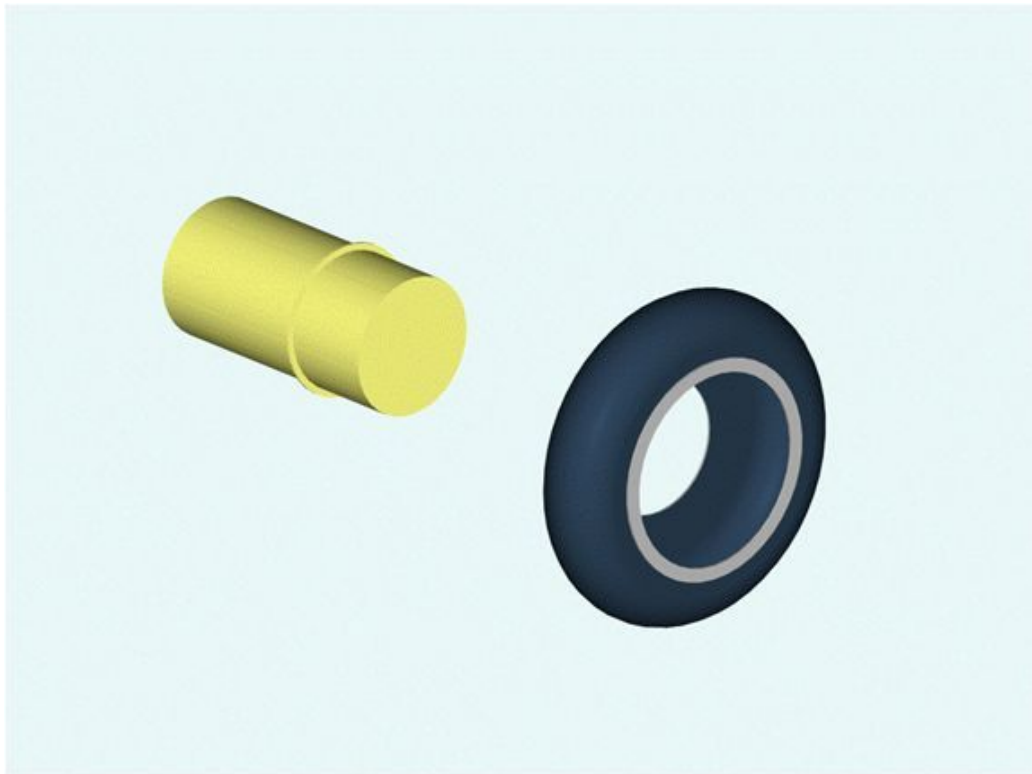


Figure 209. Diagrammatic representation of the flexible rubber 'tyre' with bonded metal attachment flanges,

17.3.4.12 Structural Analysis

A full FEA analysis of the spectrograph structure has been carried out using the ALCOR FEA package. The vibration analysis shows several modes for vibration between 15.8 and 50 Hz. This is well above the main vibration modes that have been measured at the proposed location of the FMOS spectrographs within the telescope enclosure (4 and 13 Hz).

17.3.5 Camera Mechanical Design

Thermally and mechanically there are key design requirements:

- Some of the lenses will experience temperatures down to 85K and during cool down the mount (stainless steel) must not impart significant stresses on the fused silica.
- While under thermal steady state conditions, the camera can have a 120K axial gradient which must not distort the alignment of the optical system
- The camera is a fast f1.4 system that requires accurate positioning of the detector.
- The detector is required to move to different positions as the observations switch from hi-res to the different low-res modes.
- Accommodation of the thermal control systems – cold head, cold straps, thermal shield, LN2 cool down system and GN2 warm up.

Lens Mount design

The design consists of a stainless steel lens mount, which is cut away to produce flexures, which are adhered to the outer edge of the lens. During cool down the flexures allow the outer mount to contract down around the lens. Detailed FEA shows that stresses within the flexures are well within material limits. The mounting technique is due to be trialled within the next few months.

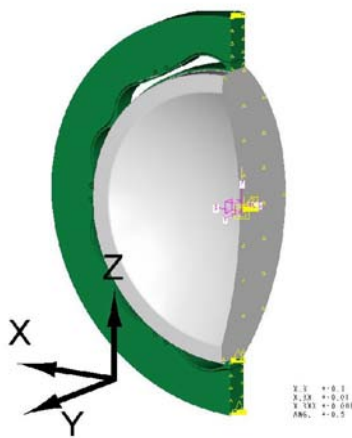


Figure 210. Typical lens mount design.

Detailed cryostat & lens barrel design

Figure 10 below shows the completed general assembly for the camera and the cryostat. To interface to the spectrograph correctly, the optical axis of the camera is required to be accurately aligned with respect to the cryostat's mounting feet. The flexible bellows to attach the cryostat to the spectrograph is attached at the front flange

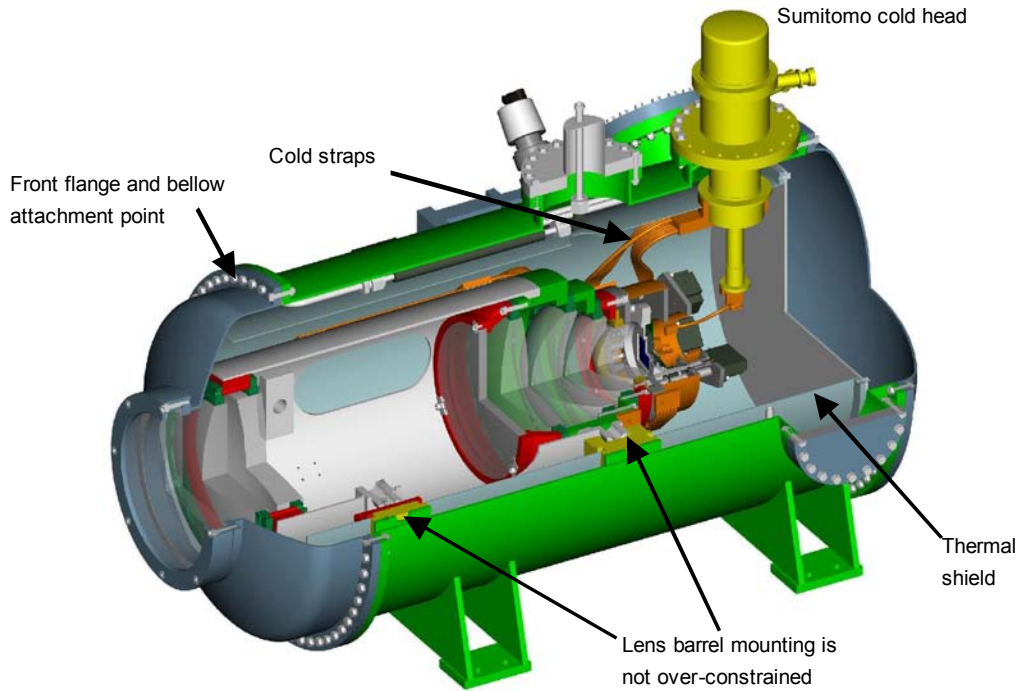


Figure 211. Detailed camera and dewar design.

FPA focus mechanism

The critical alignment of the detector the FPA requires a tip, tilt and focus mechanism. The stepper motors used are Berger-Lahr types that have been modified to operate in vacuum and down to LN2 temperatures. The focus mechanism design shown in Figure 212 and Figure 213 is capable of positioning the detector within $\pm 10\mu\text{m}$ of its desired position over a large range of travel.

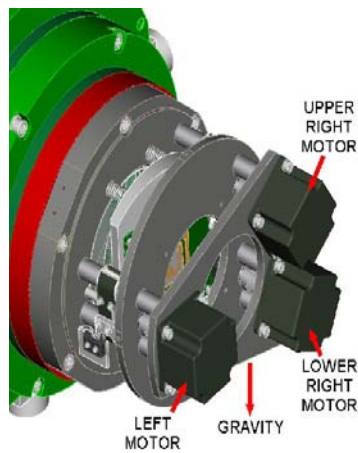


Figure 212. FPA attached to the camera.

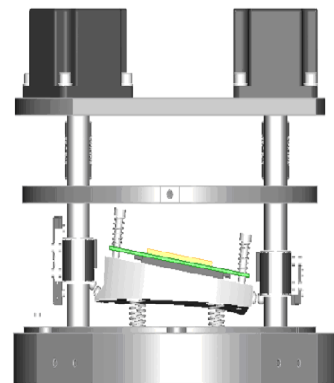


Figure 213. FPA side view.

17.3.6 Control System Design

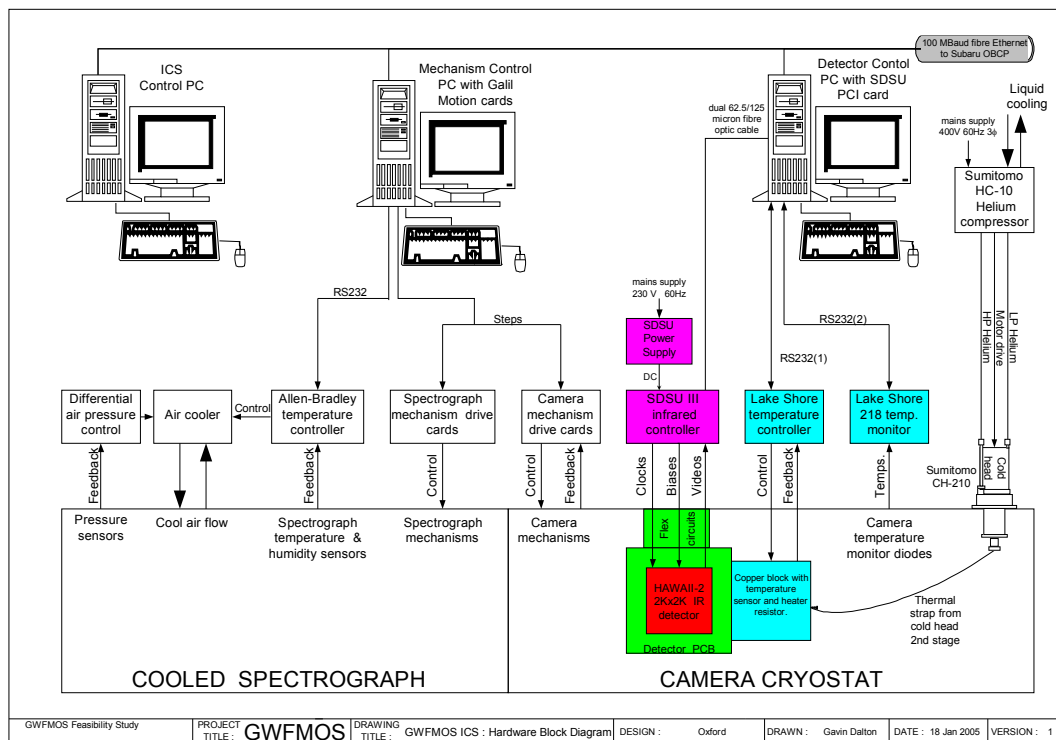


Figure 214 Block diagram for a single spectrograph

17.3.6.1 Mechanism Design & Control

The mechanisms covered by this control system include:

1. Slit focus
2. Slit nodding (for calibration)
3. Grating nod (for dithering)
4. Darkslide (2 motors)
5. VPH slide
6. Camera rotation
7. Camera tip/tilt and focus (3 motors)

This list of mechanisms requires a total of 10 stepper motors, most with end of travel limits and index marks. With the exception of the camera rotation mechanism, all motors are Berger-Lahr VRDM 564 5-phase stepper motors that have been adapted for cold/cryogenic conditions by the installation of PTFE bearings and cages. The camera rotation mechanism uses a larger 2-phase stepper motor.

All motor control instructions for the spectrograph originate within the Local Control System (LCS) PC. This PC will have two Galil 5 axis PCI motion controllers (type DMC 1850) giving a total of 10 independent channels. Each channel can accommodate servo or stepping motors, will accept encoder inputs and has opto-isolated limit and index mark inputs. Each card also has 16 uncommitted opto-isolated inputs and outputs. The PC will not be operating in

real-time and the motion control cards will provide all real-time responses. The outputs from the motion controllers go to Berger-Lahr 5 phase motor drive units, which provide the appropriate power amplification to drive the 5 phase stepper motors. The motors all have 500 full steps per revolution, half stepping is not being used so that the motors can have all power removed without losing position. All motors have a power-down function to minimise heat load inside the system during operation.

The slit- and grating-nod functions are actuated by cams driven by stepper motors against return springs. In the slit case, the cam may be driven continuously without limits to sample different detector pixels. In the grating case, the home position is defined by an index switch.

The slit focus and VPH grating and dark slides rely on linear lead screws driven by the stepper motors with end-stop sensors.

The camera rotation is a stepping motor mechanism operating at room temperature, with a "Magnasyn" high resolution (0.01mm) incremental encoder and homing reference plus a 4 bit (grey code) absolute encoder. This latter encoder subdivides the 40° rotation into 16 sectors thus minimising the time to find the homing reference on the incremental encoder. It was decided to use encoding on this one mechanism as it is rather large and heavy (approximately 500Kg) and may take a while to locate if it has to be indexed using an end of travel limit switch.

17.3.6.2 Camera Temperature Control

The camera temperature is monitored by a Lakeshore 218 temperature monitor. After an initial pre-cool with LN₂, the camera temperature profile is maintained by a two-stage (100W/6W) Sumitomo cold head (Subaru preference). The second stage of the cold head is connected directly to a copper block mounted onto the detector cooling pins. The first stage is linked by thermal straps to the camera cold shield and lens pack assembly. Temperature control is achieved using a Lakeshore 332 controller. It has been shown possible to control the detector cooling rate to less than 1K/minute using this system.

17.3.6.3 Detector Control

The detector is controlled using a generation III SDSU PCI controller as illustrated in Figure 215. The HAWAII-II detector is mounted in a 21 pin Yamaichi ZIF socket onto a custom designed 8 layer PCB which was based on the ATC-designed PCB used in WFCam. This board has now been populated and tested satisfactorily.

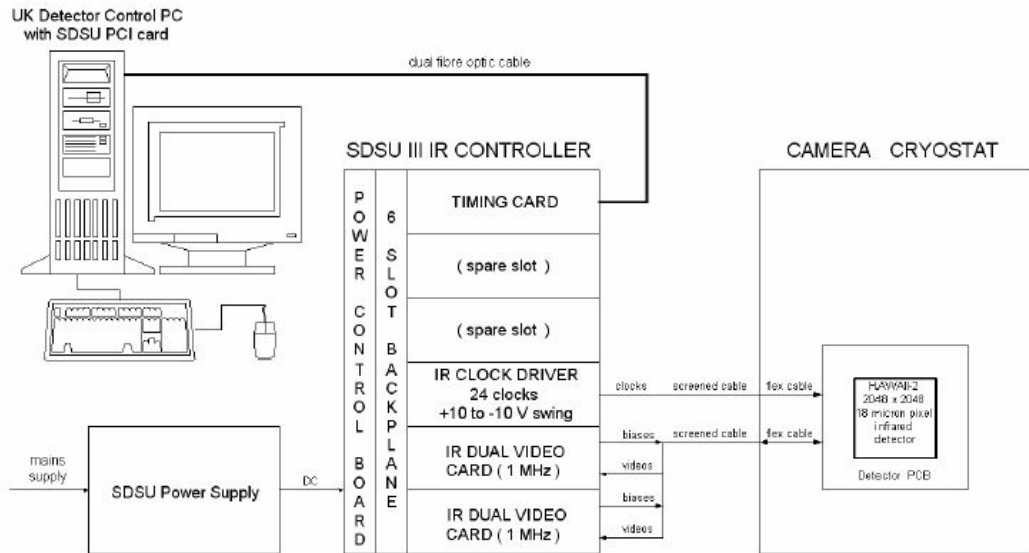


Figure 215 Detector controller block diagram

17.3.6.4 Spectrograph Environmental Control

The spectrograph enclosure is maintained at its 200K operating temperature by a heat exchanger unit which is attached directly to the wall of the enclosure behind the collimator mirror. A schematic of this heat-exchanger unit is shown in Figure 216. The heat exchanger unit contains a number of large aperture butterfly valves, these are used to isolate the heat exchanger from the enclosure so that it can be automatically defrosted without warming up the main chamber and a bypass valve.

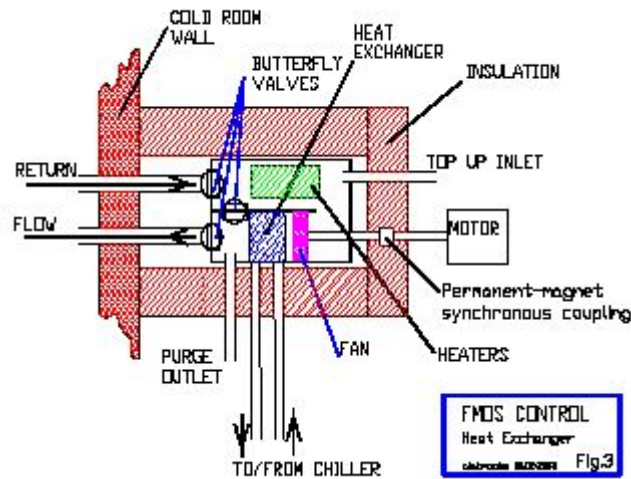


Figure 216 Schematic of the spectrograph enclosure heat exchanger.

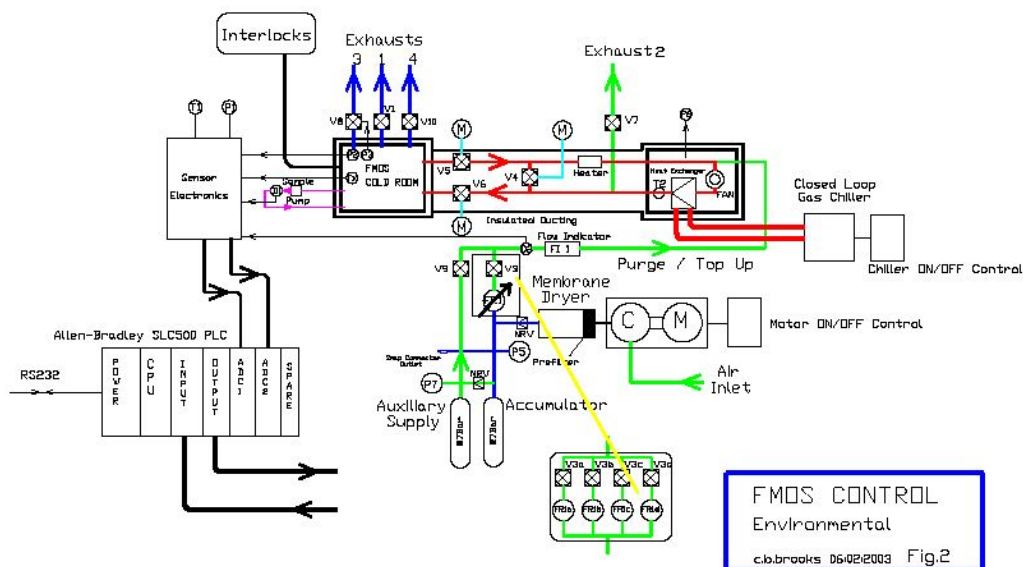


Figure 217 Block diagram of the spectrograph cooling system

Figure 217 shows a block diagram of the cooling system. The coloured lines with arrows show the various directions of air flow through the system. The cooling gas was chosen to be ordinary air for reasons of safety, but this then requires that the air be dried to a suitably low dewpoint to prevent build-up of ice within the enclosure. The system therefore consists of a small compressor feeding a membrane dryer which removes almost all the water vapour (lab tests have shown that a dewpoint of 210K within the enclosure is easily achievable within a few hours of operation). The spectrograph is flushed with dry air until the dewpoint is low enough (230K) that cooling can begin. The cooling is provided by a Polycold gas chiller unit. The enclosure is maintained at a slight (25mm water) overpressure and will track both variations in atmospheric pressure and the internal pressure of the enclosure during warm-up and cool-down cycles.

The environmental system is controlled by a standalone Allen-Bradley SLC500 PLC which can be monitored by the ICS computer via an RS232 link. Thermal load calculations suggest that the total static heat load on the enclosure (dominated by insulation losses) is around 160W which is comfortable, given the 200W capacity of the chiller unit at 200K.

17.4 Software

The instrument control software already outlined for FMOS should extend quite naturally to further spectrographs. The software interface is between the spectrograph's own instrument control computer and a top level instrument OBCP computer. The effort required for additional software development for the IR spectrographs is expected to be small.

17.5 WF MOS-IR Design Modifications & Trade-Offs

In this section we discuss the changes that are required to modify the mature FMOS design described above to produce something more appropriate to the requirements of WF MOS. In particular, we have investigated modifications to the

optical design that allow the useful slit length to be increased for a single spectrograph. The requirement for the IR version of the WMOS concept would be to accommodate 1500 fibers within the IR spectrographs. This would require 7 or 8 cloned FMOS systems (giving 1400 or 1600 fibers in total). The goal for this approach was to reduce the number of spectrographs to 5, each accommodating 300 fibers. In later subsections we will discuss a number of so-called destructive technological developments which are beyond the scope of this study, but which could open up opportunities for substantial cost savings in the implementation of the IR side of WMOS.

17.5.1 Parameters of the modified FMOS design

The FMOS design accommodates $200 \times 280 \mu\text{m}$ core fibers within a 120mm slit, and projects the spectral image of this onto a detector that has 2048 spatial pixels at $18 \mu\text{m}$ pitch. The optical blur of the fibers at the detector is 3×3 pixels. This allows 10.5 pixels for each spectral image, whereas to move to 300 fibers for each system would only allow 6.5 pixels for each image. Changing the camera f /ratio to $f/1.33$ implies that there would still be 1 clear pixel between adjacent spectra. This is tight, but is taken as the baseline for the design. At the other end of the optical system, the slit can be grown to 150mm to accommodate 300 fibers on a closer pitch without introducing substantial vignetting of the beam. This design can be developed further if it is decided to pursue the IR option beyond the level of this feasibility study, but the important aspects of the revised design are that the collimator mirror remains within the useful aperture of the existing mirrors, such that the existing spectrographs can be reused, and the camera elements remain all-silica. Spot diagrams for this system for the mask and the detector surface are shown in Figure 218 and Figure 219.

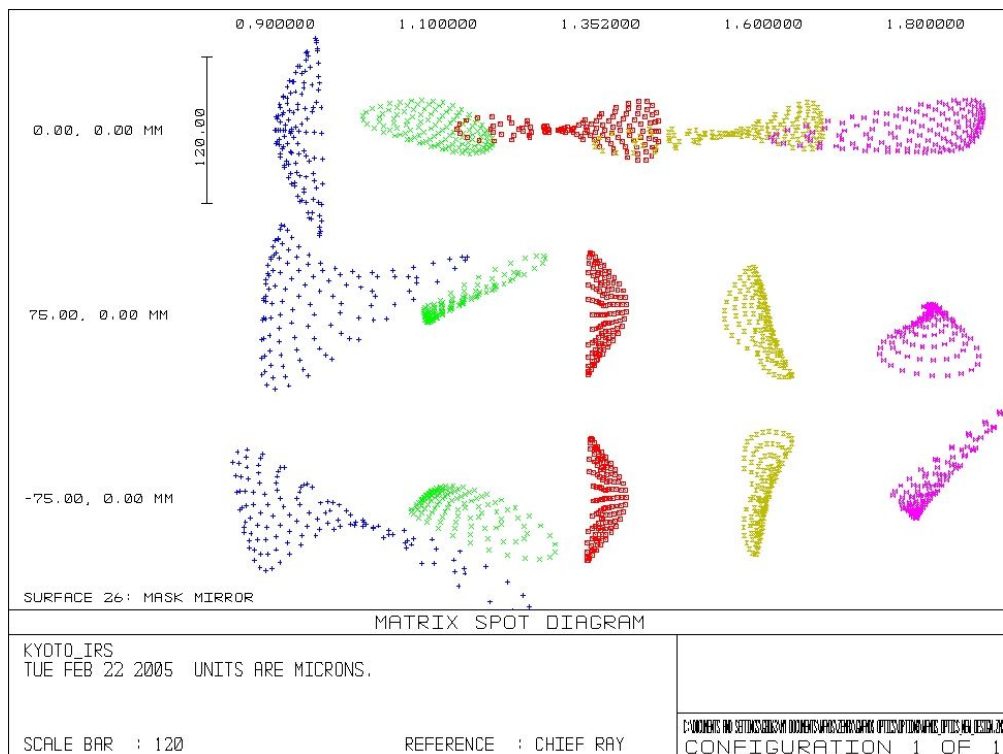


Figure 218 Spot diagrams at the mask mirror surface for the modified spectrograph.

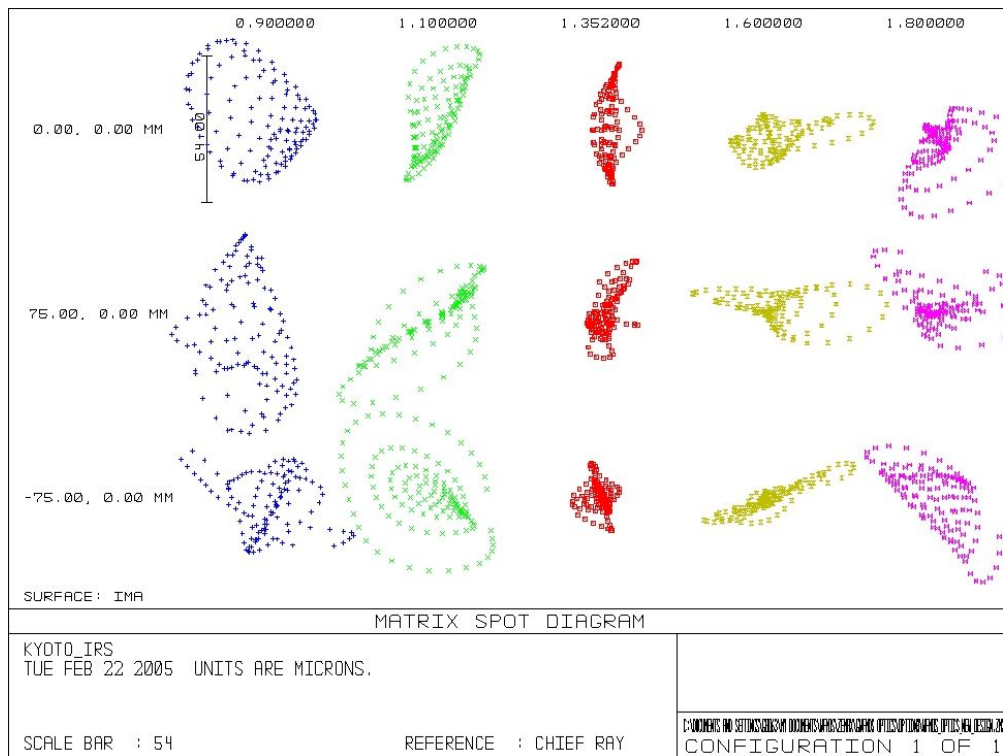


Figure 219 Spot diagrams at the detector surface for the modified spectrograph

This design would meet the operational requirements for the spectrograph. One possible further change that can be considered would be to move from Rockwell detectors with 18 μ m pixels to Raytheon VIRGO detectors which have 20 μ m pixels, as this allows more slack in the camera design. However, since the final choice of detectors will inevitably depend on developments within the next couple of years anyway, this should not be considered a major cost driver at this point. The net impact of this design change on the costings will be to reduce the required number of systems from 8 to 5, thus implying 3 complete new systems and modifications to the camera and mask mirror systems for the existing two spectrographs (the two gratings are both very close to pupils within the system, and so do not change significantly).

17.5.2 Next-Generation IR Detectors

CCLRC Rutherford Appleton Laboratory and the UKATC are currently investigating novel developments in IR detector technology (see e.g. Hall et al. 2004, SPIE 5406, 317). Within this programme there are interesting developments that could see a substantial (factor of a few) reduction in the cost of new generation IR detectors without impinging on the performance. This is clearly of interest to an instrument requiring 5 detectors at \$400,000 each!

17.5.3 Bragg-grating Fibers

New developments in the fabrication of single-mode fiber Bragg gratings (Bland-Hawthorn et al., 2004, Opt Express 12, 5902) suggest a route to providing OH-suppression at a much higher intermediate resolution than can be achieved with the current design. This could lead to a substantial simplification (and hence reduction in cost) of the IR spectrograph design, with the added benefit of the removal of 4 reflective losses, 4 transmissive losses, and one grating loss (a total

of roughly 30% loss) from the system throughput. This would clearly need to be investigated in some detail, but presents an exciting possibility that we would recommend pursuing through the design phase of WFMOS.

17.6 Cost forecast

All costs are based on the as-purchased elements of the FMOS systems, and so should be considered as robust estimates, subject only to the adopted level of inflation. Costs are summarised in *Chapter 27, Cost Structure and Cost Estimates*.

17.7 Risks

Given that the current FMOS design is already well-matured and into the final integration phase, we do not expect there to be any substantial risks associated with the design concept. There do, however, remain two outstanding risks associated with the modified design that must be mitigated by further study in the next phase, namely that the increased slit length could either force the collimator beyond the current fabrication limits for the specific lightweight design, or that the same increase could force the camera design away from simple fused-silica elements into the regime of large crystal elements (CaF₂ etc). Recent discussions with Schott at the 2004 SPIE conference suggest that there is now no major issue associated with the fabrication of CaF₂/BaF₂ blanks up to 400mm diameter, but there are still substantial schedule risks associated with the polishing of such large items of these materials.

Chapter 18 Detector Systems

18.1 Introduction

The WFMOS instrument concept considers between eight and twelve spectrographs, in a combination of optical and infrared (IR) channels.

The spectrographs will be located away from the telescope and each will be fed by a certain number of optical fibers ⁽¹⁾.

Every spectrograph will have its own detector controller system, with its own computer node connected to a higher-level supervisor, which will provide the interface to the main instrument computer.

In this document we will refer to these units using MONSOON terminology: the controller is called the DHE (Detector Head Electronics), the computer node is called the PAN (Pixel Acquisition Node) and the higher-level computer unit is called Supervisory Node (Figure 220).

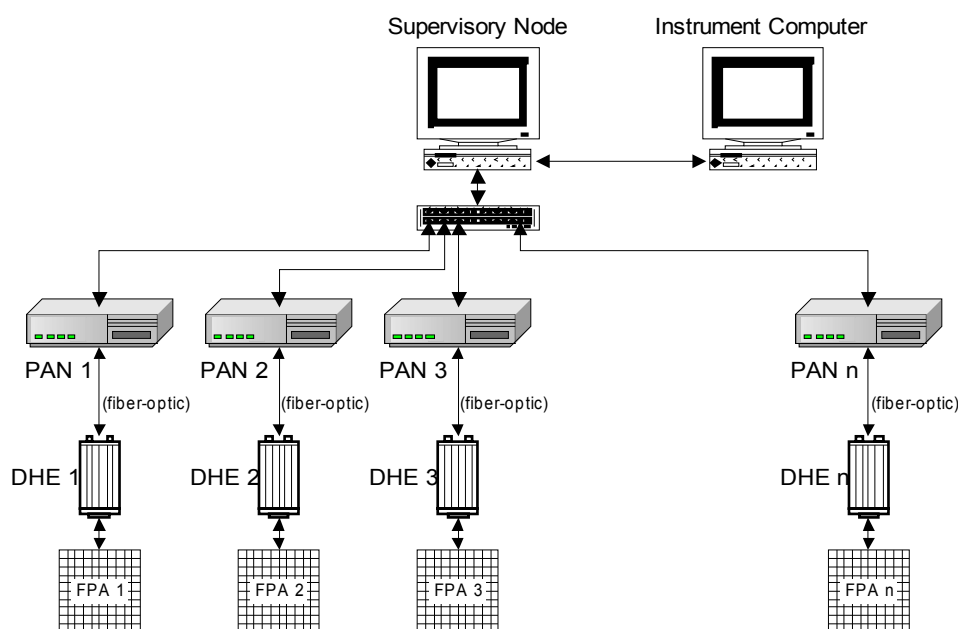


Figure 220. System Overview.

18.2 Detectors

The focal plane array (FPA) options under consideration for the spectrographs are:

- For the Optical case: FPA with format of either 4Kx4K or 4Kx6K.
- For the IR case: IR detector of 2Kx2K format.

For the CCD options, both formats can be assembled with a mosaic of 2Kx4K CCDs, two for the first case and three for the second one. The 2Kx4K format has become a standard in the astronomical detectors community for several reasons,

and therefore it makes sense to use it as the building block for the required focal plane, instead of aiming for a monolithic detector.

For the purpose of this study, the mosaic approach is assumed.

Several mosaics of detectors with this format from manufacturers like EEV and MIT/LL are currently in operation in many astronomical institutions.

When building mosaics, special attention must be given to the gap between the chips. The specifications must define the limits for the size of the gap, the parallelism and the co-planarity of the chips. It is also important to define the orientation with respect to the spectra.

The format for the IR detector (2Kx2K) is already available in monolithic arrays. The two typical manufacturers of detectors for astronomical use are Raytheon (Orion or Phoenix) and Rockwell Scientific (Hawaii-II).

Figure 221 shows examples of the format options for the optical and IR FPAs. The IR example shown is for a Hawaii-II detector.

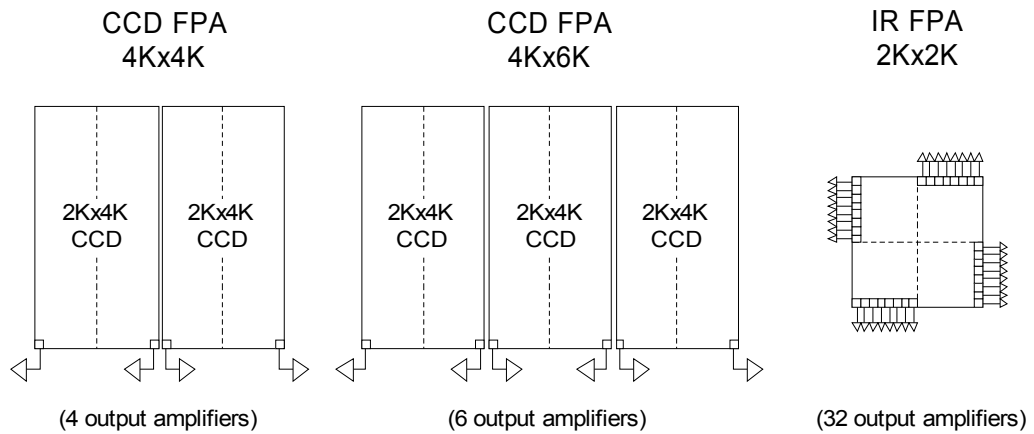


Figure 221. FPA format options for the optical and IR cases. Examples of output amplifier locations are indicated.

It must be noted that no pixel size has been yet specified. As a reference, typical values are 15 μ m for CCDs and 18 μ m for IR detectors.

This specification will depend on the overall optical design of the instrument. The scale assumed in preliminary studies is 0.3 arc-seconds per pixel⁽¹⁾.

From the operational point of view, several specification parameters determine the detector selection, like quantum efficiency (QE), readout noise (RON), dark current, well capacity and, for CCDs, charge transfer efficiency (CTE). The science objectives will have to define these requirements.

18.3 **Cryostats**

The cryostat design is primarily defined by the expected operating temperature of the detector. Options of cooling using liquid nitrogen (LN2) and cryocoolers are discussed below.

LN2, with its temperature of 74 K at ambient pressure, has been traditionally used as the cooling element for CCDs (operating range typically between 165 and 180 K) and those IR detectors with operating temperature above 75 K (like Rockwell's HgCdTe Hawaii-II at 77 K).

This option requires permanent maintenance during operation for refilling. Daily in the case of a single LN2-filled reservoir, and weekly for "continuous flow" (CF) cryostats, where an external tank is permanently connected to the cryostat.

Closed-cycle coolers, or "cryocoolers", have become the first choice for cooling, due to their lower maintenance requirements (usually every 6-12 months), and therefore a lower operational cost during its lifetime. They are especially suitable for stationary systems, which is the case of this instrument.

A cryocooler consists basically of a cold head (the cooling element that is placed inside the cryostat and is thermally coupled to the detector), a compressor and gas lines to connect both. The type of gas used determines the temperature range and the cooling power.

For operating temperatures above 75K, the commercial system "CryoTiger" (from Polycold, Inc.) is widely used, with systems in operation in several observatories giving very good results, and will be considered here as the reference for the cost estimates. It is offered with a selection of gas types and cold heads for different applications.

Its main advantage is that the cold head has no moving parts (unlike the Helium based cryocoolers), and therefore induced vibrations are not an issue.

When the operating temperature range is lower than 75 K (like Raytheon's Aladdin at ~30 K), a Helium closed-cycle cryocooling system is mandatory. It will normally be coupled to the cooling system of the whole spectrograph (optics and active radiation shields). Moreover, in the case of big thermal loads, a LN2 pre-cooling system is considered in addition, although probably it will not be the case here.

18.4 **Detector Controllers**

Here "controller" refers to the front-end electronics box (DHE), connected to the detector, which receives commands from and sends data to a computer (PAN) through a high-speed fiber-optic link (1 or 2.4 Gbps in the MONSOON case).

The spectrographs are completely independent from the point of view of the controller-detector unit. That is, they are physically isolated, and therefore the considerations for the detector controllers can be reviewed also independently.

At the time there is no specific requirement to provide synchronization between controllers. Hardware synchronization is mandatory when independent controllers operate a common focal plane (to avoid interference), which is not the case here.

In case that a synchronization requirement is defined for scientific and/or operational reasons, current systems already provide that option. To keep the systems effectively isolated, this link should be built with opto-couplers.

The selection and configuration of the controller is defined by the requirements of the detector and the environment.

Key parameters from the detector side are pixel rate, readout noise and current requirements for the controlling signals (locks and biases).

In the case of the readout noise (which is a function of the pixel rate), the ideal is for it to be “detector-limited”. That is, the controller contribution should not be comparatively significant.

For the environmental perspective, it is heat dissipation, size and weight. Due to the stationary nature of the spectrographs, it is expected that heat dissipation will be the major issue. Typical values are in the order of 40 to 60 Watts.

For the purpose of comparison, two systems are reviewed: NOAO's MONSOON and SDSU's "Leach" Controller, with their current capabilities.

SDSU's is a mature controller, in operation in many places. MONSOON is NOAO's new generation controller, designed with the new NOAO instrumentation in mind (flexibility and modularity).

18.4.1 Optical detectors

A standard 2Kx4K CCD like the EEV42 has two output amplifiers (video), requiring about 13 clock signals and 9 bias voltages.

As specified above, two options are being considered for the optical channels: 4Kx4K requiring two standard CCDs and 4Kx6K requiring three.

For the case of a mosaic, it is possible to share some clock and bias lines among chips after a careful analysis, making the total number of clock and bias lines less than simply the sum of all lines for all CCDs.

The number of acquisition (video) channels is 4 for the 4Kx4K mosaic and 6 for the 4Kx6K.

A basic MONSOON CCD configuration is enough to control either mosaic configuration:

- One Master Control Board.
- One 8-channel CCD Acquisition Board (with 32 bias voltages).
- One Clock Board (32 clocks).

A SDSU Controller, with its 2-channel Acquisition Board (which also provides 6 Bias voltages), will require two or three Video boards depending on the mosaic type, in addition to:

- One 24-channel Clock Board.
- One Timing Board.

Power supplies requirements will be typically +5V digital, +/-15V and +36V analog.

18.4.2 IR detectors

Taking the Hawaii-II FPA as reference for a 2Kx2K IR detector, the requirement is for up to 32 output amplifiers with 13 clock signals and 5 bias voltages.

A basic MONSOON IR covers easily this detector with the following configuration:

- One Master Control Board.
- One 36-channel IR Acquisition Board.
- One Clock&Bias Board (32 Clock signals and 36 Bias voltages).

The SDSU Controller offers an IR Acquisition Board with 8 video channels, and therefore four of these boards would be necessary, in addition to the Clock and Timing boards.

Power supplies requirements will be typically +5V digital and +/-15V analog.

18.5 *Detector Temperature Control and Vacuum Monitoring*

Temperature sensors are located inside the cryostat, attached to the detector mount. The information from them is used to control heaters also attached to the mount.

It is also useful to have sensors mounted on other areas of the cryostat, like for instance on the fill neck of a LN2 cryostat to provide an early warning of LN2 depletion.

MONSOON and the SDSU Controller provide ways of reading the sensors and controlling the heaters. The connection to these elements is normally done through the same connectors used for the controller-detector interface.

MONSOON has this capability implemented on its Master Control Board, and the SDSU Controller uses a special board for this purpose, called "Utility Board".

The specification of precision for the temperature control will have to be checked against the capabilities of the controllers, but it is expected that it will be good enough in the case of the CCDs, but not necessarily for the case of the IR detectors, where usually the precision required is much higher. In this case, a specialized module should be considered, independent of the controller.

Remote monitoring for the vacuum level of the cryostat is also a desirable feature, although the vacuum sensor is located away from the controller-detector connectors, and therefore must be cabled independently to the controller. As in the case of the temperature control, this feature could also be offered on a separate module.

The advantage of an independent module for temperature control and vacuum monitoring is that it is possible to keep these functions active even when the controller is off, for instance during instrument maintenance activities.

18.6 Software and Detector Controller Configuration

For both controllers reviewed above, the software to operate every independent unit exists and is operational.

All the information needed to control the FPA attached to every unit, the "configuration", will be stored in its corresponding computer node. This will allow for every spectrograph to be operated independently if needed.

The major effort will be clearly in the higher level (Supervisory node in MONSOON terms), responsible for the coordination of the cluster. The MONSOON project is currently developing the software for this layer. The first implementation of this layer will be on the MONSOON controller for NOAO's NEWFIRM instrument (NOAO Extremely Wide Field IR Imager), scheduled for delivery around the end of 2005.

18.7 Data flow

As every spectrograph will produce its own image, it will be up to the DHS (Data Handling System) to decide what to do with it.

The idea is to get the data out of the computer node as fast as possible, leaving all post-processing to take place somewhere else in order to do not interfere with the acquisition of images.

The most efficient transport of data will be determined by the specifications on pixel rate (for the throughput required) and FPA format (for the size of every image).

Possible options for the data flow to the DHS are (see Figure 222):

- (a) The Supervisory Node collects all images and takes care of relaying them to the DHS.
- (b) Every individual acquisition node sends its own image directly to a DHS receiver through dedicated links.

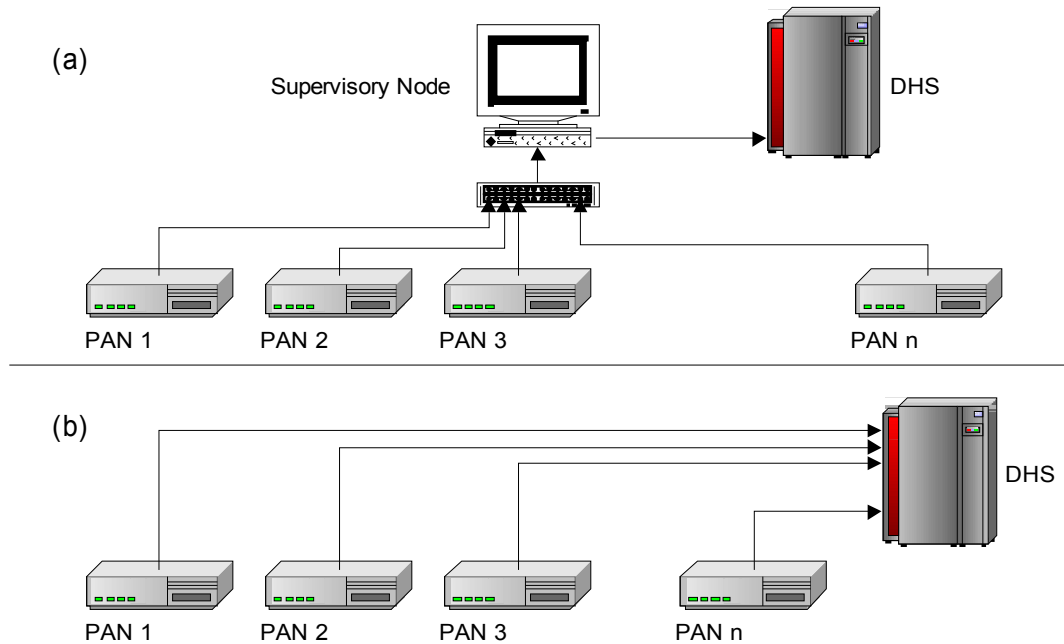


Figure 222. Pixel Data flow to the DHS. (a) Through the Supervisory Node. (b) Via dedicated links.

18.8 Cost estimates

As the exact number of optical and IR spectrographs is not yet defined, we present here the cost estimates for individual systems based on either MONSOON or SDSU Controller.

There are no significant differences in cost by using either controller system, and in all cases the cost of the focal plane represents the major part of the total.

It is assumed that the cooling systems are closed-cycle cryocoolers. Specifically for these cost estimates, CryoTiger from IGC-Polycold is considered for the CCD case, and Cryodyne from HELIX Technology for the IR case.

The cost of the design of the cryostats is not considered here, as it is a one-time cost. It should be noted that in the case of Helium-based cryocooler systems, the design of the cryostat must take in account the effect of vibrations caused by the moving parts in the cold head, which adds complexity to the design.

The costs shown below are representative of single or small quantity purchases.

It can be expected that these figures could be lower as more units are ordered, due to economies of scale and eventual discounts from detector vendors for larger orders.

18.8.1 **Optical detector systems**

4Kx4K CCD focal plane (4 video channels)	
1. Detectors (two 2Kx4K, ref: EEV42 at \$75K each)	\$150K
2. Cryostat	\$20K
3. MONSOON system (with one 8-ch CCD Acq board)	\$28K
(3. SDSU Controller (with two 2-ch CCD Video boards))	(\$25K)
4. Computer (high-performance PC)	\$4K
5. Temp/Vacuum module (optional)	\$5K
6. Cryocooler (CryoTiger, see note below)	\$11K
TOTAL (with MONSOON)	\$218K
TOTAL (with SDSU)	\$215K

4Kx6K CCD focal plane (6 video channels)	
1. Detectors (three 2Kx4K, ref: EEV42 at \$75K each)	\$225K
2. Cryostat	\$25K
3. MONSOON system (with one 8-ch CCD Acq board)	\$28K
(3. SDSU Controller (with three 2-ch CCD Video boards))	(\$30K)
4. Computer (high-performance PC)	\$4K
5. Temp/Vacuum module (optional)	\$5K
6. Cryocooler (CryoTiger, see note below)	\$11K
TOTAL (with MONSOON)	\$298K
TOTAL (with SDSU)	\$300K

18.8.2 **IR detector system**

2Kx2K IR Detector focal plane (32 video channels)	
1. Detector (ref: HgCdTe 2Kx2K Hawaii-II)	\$400K
2. Cryostat	\$20K
3. MONSOON system (with one 36-ch IR Acq board)	\$30K
(3. SDSU Controller (with four 8-ch IR Video boards))	(\$36K)
4. Computer (high-performance PC)	\$4K
5. Temp/Vacuum module	\$5K
6. Helium Cryocooler (see note below)	\$13K
TOTAL (with MONSOON)	\$472K
TOTAL (with SDSU)	\$478K

Notes:

- The cost of a CryoTiger system considers the following estimates:
Cold Head: \$6,000.
Compressor: \$4,000.
Gas lines (10 ft) and accessories: \$1,000.
- The cost of a basic He-based cryocooler system considers the following estimates (ref.: CTI Cryodyne Refrigeration Systems from HELIX Technology):

Cold Head: \$7,000 (Model 350)

Compressor: \$5,000 (Model 8200).

He lines (10 ft) and accessories: \$1,000.

18.9 Promising new technologies in detectors

Spectrograph design and costs are strongly driven by the need to shuffle the low dispersion spectra, effectively doubling the number of spectrographs. The development of the E2V L3Vision detector (http://e2vtechnologies.com/introduction/prod_l3vision_nojs.htm) strongly suggests that large format detectors, with sub-electron read-noises and MHz readout rates, will be available on the timescale of the WFMOS project. Such detectors would make charge shuffling unnecessary, and hence halve the low dispersion spectrograph requirements. We are in discussion with E2V about the development of such detectors.

18.10 Conclusions

The proposed focal plane array systems for the WFMOS instrument spectrographs can be built using existing proven technology.

Both the optical and the IR options are based on systems already in operation, and therefore the implementation of every unit independently should be known territory.

The biggest design challenge will be the implementation of the higher-level software and the data flow system.

Detector temperature specifications and maintenance issues define the design concept for the cryostats. For temperatures above 75 K, cryocoolers like the commercial CryoTiger is the recommended solution. For temperatures below that, He-based cryocoolers are mandatory.

Most of the cost of the systems will be in the detectors item, with the IR detectors being by far the most expensive.

18.11 References

1. **KAOS Purple Book**. Arjun Dey and Brian Boyle, eds.
2. **KAOS: kilo-aperture optical spectrograph**. Sam Barden et al. SPIE 2004.
3. **Gemini Wide Field: Strategic and Technical Issues**. Presentation by the Gemini Wide-Field Working Group.
4. **MONSOON Project Documentation**. <http://www.noao.edu/ets/monsoon>
5. **IGC-Polycold website**. <http://www.igc.com/polycold/>
6. **HELIX Technology website**. <http://www.helixtechnology.com/>

Chapter 19 Acquisition and Guiding

19.1 Summary of Strawman specification

The WFMOS instrument will require its own facility for target field acquisition and guiding. The following table lists the preliminary requirements for such a facility.

Requirement	Value	Comment
Number of acquisition probes	Minimum of 2 to define translation and rotation	Acquisition can be done with relatively bright stars, but need a minimum of two.
Number of guide probes	Minimum of 3 to define translation and rotation	A minimum of two could do the job, but three are highly desired to help average out astrometric errors
Magnitude limit for acquisition	TBD but probably $V=17$	To be set by sensitivity of detector, field of view for each probe, number of available probes, and stellar density.
Magnitude limit for guiding	TBD but probably $V=17$	To be set by number of guide probes, field coverage of guide probes, sensitivity of guide probes, and stellar density.
Positional Accuracy for acquisition	1 arc-second	Level to which the acquisition system must be able to determine telescope alignment. This will allow the guide probes to pick up their stars.
Guiding accuracy	TBD but probably about 0.1 arc-second	Level to which the guiding system must be able to hold the telescope in alignment with the field.

It is envisioned that the acquisition and guiding are actually done by separate facilities. The acquisition is carried out by imagers that acquire easily identifiable stars and then sends commands to the telescope to centre the target field accordingly. Once the acquisition system has centred the telescope to about 1 arc-second, the guiding system takes over. Specialty fibre probes are used for final centring onto the target field and for providing the signals to keep the telescope on the target field.

19.2 Acquisition design concept

19.2.1 Strawman Design

Target acquisition can be achieved with a set number of fixed optical imagers located around the periphery of the telescope field of view. A cost effective solution is to utilize off-the-shelf CCD cameras.

The stellar density at the galactic poles will set the limiting criteria for the number of acquisition probes required. This number is a combination of the total field of view of the combined probes and their sensitivity. The following table from Allen's Astrophysical Quantities gives a guideline to the stellar density as a function of magnitude. The final column gives an estimate of the photons detectable at the WFMOS focus with a typical CCD/CMOS detector running at about 10 Hz.

V magnitude	Number stars per square degree at galactic poles	Number stars per square arc-minute at galactic poles	Minimum Field (sq arc-min) required to see 1 star	Approximate Counts (S/N) detected in 0.1 second exposure
15	180	0.05	20	6400 (50)
16	350	0.10	10	2500 (25)
17	600	0.17	6	1000 (10)
18	1000	0.28	4	400 (4)

The KAOS Purple Book concept proposed to allocate up to four regions at the quadrants of the field. Each region is about 1.5 by 15 arc-minutes or equivalent to an areal coverage of 22 square arc-minutes. Hence each region should contain on average 1 star brighter than 15th magnitude, 1 to 2 stars brighter than 16th, 3 to 4 stars brighter than 17th, and 5 to 6 stars brighter than 17th. Hence, of order 22 stars should be imaged inside the total region available for acquisition assuming that the system can image stars as faint as V=17.

Alternatively, a single 1kx1k imager with 0.3 arc-second pixels will cover an area of sky equal to 25 square arc-minutes, which should be sufficient for the detection of target acquisition stars. This format is easily achievable with off-the-shelf CCD/CMOS camera systems such as a PixeLINK camera.

The difficulty with this approach lies in the potential difficulty in matching a 6.7 micron pixel size to the WFMOS plate scale. The f/2.16 focal ratio for the Subaru option produces a plate scale of 86 microns per arc-second or nearly 13 pixels on a camera such as the PixeLINK. An imaging system with a speed of f/0.5 is required to get optimal matching! A preliminary optical design exploration however, suggests that the problem is tractable and should only require a few custom, or possibly, off-the-shelf lenses.

As discussed in *Chapter 20, WFMOS Wavefront Sensors Subsystem Design* the wave-front sensors may also be suitable for acquisition.

19.3 Guiding system concept overview

The guiding system will be based upon the design incorporated for the FMOS-Echidna instrument and is discussed in detail *Chapter 11, Positioner*. The guide system comprises some number (14-20) of guide spines occupying some of the available spine positions in the WFMOS field. Each guide spine contains a 7-fibre bundle of 50 μ m diameter core fibres (compared to the 100 μ m core science fibres). Given each guide spine is virtually identical to a science spine (except for the nature of the fibres contained within) the relative deflection is similar enough to use the guide spines for guidance. With guide stars (R~16-18) located on a subset of the available guide spines, movement of the images on the guide fibre bundles (GFBs) can be used to track the telescope during observation, implicitly correcting for spine deflection.

19.3.1 Software

The WFMOS Guiding software will be a development of existing software developed for the FMOS project. That software was itself a development of software used with the VLT/FLAMES instrument, itself a derivative of software written for the AAT 2dF instrument. As a result, most issues are well understood.

The aim of the algorithm is to (after accounting for refraction and dispersion effects, see below) to adjust the telescope and rotator positions to ensure the Guide bundle images are centred as well as possible.

Figure 223 is a simple flowchart style representation of the algorithm. The text, which follows, is a more details explanation of the algorithm.

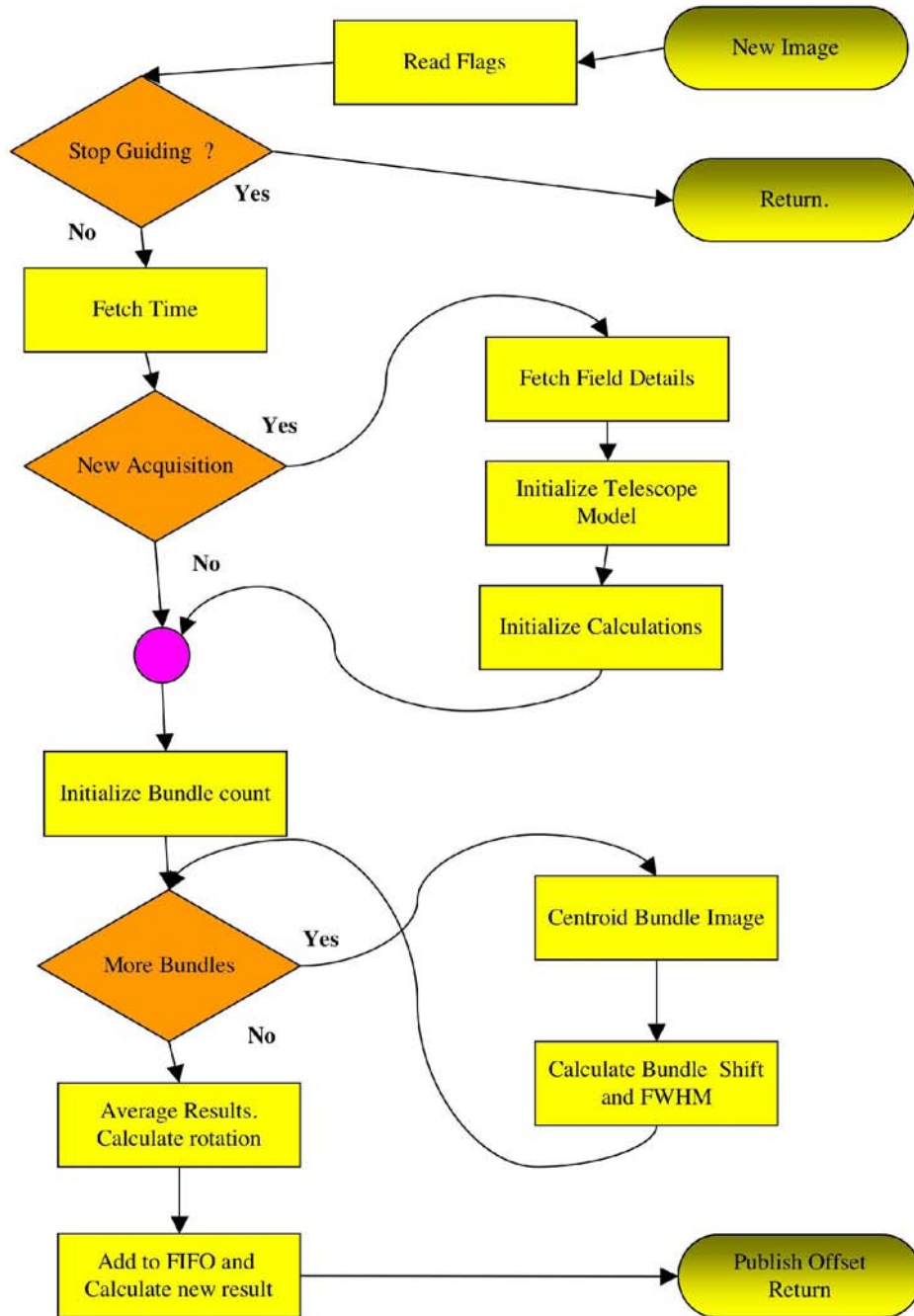


Figure 223. Guide Image processing flowchart

19.3.1.1 *Guider Image Offset Calculation Process.*

The error in each Guide Bundle position is determined by doing a centroid for each Guide Bundle that has been assigned to a guide star. Only if a valid centroid is found will that guide bundle be used in the rest of the calculations.

This result is rotated the twist of the fibre bundle. It is then scaled to account for the number of microns per pixel. Next refraction and dispersion effects (see below) are accounted for. The result is the movement of the Guide Bundle object image in microns on the field plate.

This result is then converted to an offset in Right Ascension and Declination using a matrix determined in the initialisation sequence.

The average of each of these is the telescope position error.

19.3.1.2 *Accounting for Refraction/Dispersion Effects*

The impact of the change in object positions on the focal plane due to Refraction and Dispersion effects between the Guider wavelength and the spectrograph wavelengths is considered to be significant in some cases. The change due to these effects for objects at the one wavelength is not significant (if it was, the instrument could not work).

Consider an object that has a position on the focal surface of $P_{gw_{tc}}$ at “gw” (guider wavelength) Angstroms at the central observation time. Assume its position at the spectrograph observing wavelength at the same time is given by $P_{ow_{tc}}$ at “ow” (Observing Wavelength) Angstroms. If this object is a Guide object, the Guide Spine will be positioned on the plate such that at the central observation time T_c , the Guide spine central fibre aligns with $P_{gw_{tc}}$. The difference between these two positions is given by $\Delta_{tc} = P_{gw_{tc}} - P_{ow_{tc}}$.

For any given time T_n , let the positions of these objects on the focal surface be $P_{gw_{tn}}$ and $P_{ow_{tn}}$. The difference is given by $\Delta_{tn} = P_{gw_{tn}} - P_{ow_{tn}}$. Thus at both wavelengths the object may have moved. Whilst the Guide bundles will only detect light at “gw” Angstroms, it is the light at “ow” Angstroms that we want to keep at the same relative position to the Guide Bundle centre. Thus to keep this arrangement, we must allow the object at “gw” Angstroms to be off centre by $\Delta_c - \Delta_{tn}$.

To implement this the guider software will, for each Guide bundle, run the telescope optical model for the configuration time at both wavelengths. This is done during the field acquisition with the result saved.

Then when processing each image, the telescope optical model software is again run for each Guide Bundle and each wavelength, this time for the time the image was taken. $\Delta_c - \Delta_{tn}$ and will be subtracted from the Guide bundle centroid, allowing the Guide bundle centroid to be off centre by the required amount to keep the spectrograph wavelength aligned correctly.

19.3.1.3 *Validation of the individual centroid result*

The “Full Width Half Maximum” (FWHM) of a centroid result can be used to determine if the result is reasonable. Minimum and maximum values for FWHM

will be specified. Additionally, a sensible result check is done to ensure the resulting offset is not too high.

19.3.1.4 Calculating Rotation

A formula was developed during the AAO 2dF project that determines the rotation error, given the offsets in RA/Dec for each FACB. This formula was developed using a least squares minimisation of the errors. (It also gives rise to the expected averaging formula for determination of the telescope offset). The formula applied is

$$\Delta_{ROT} = \sum_n^{i=1} \frac{RA_i * (\Delta RA_i - \Delta RA_{avg}) - DEC_i * (\Delta DEC_i - \Delta DEC_{avg})}{RA_i^2 * DEC_i^2}$$

Where

Δ_{ROT}	=	Rotation Error
N	=	Number of bundles for which we have valid centroids.
RA_i	=	RA position of bundle i's object.
DEC_i	=	Declination position of bundle i's object.
ΔRA_i	=	Error in RA position of bundle i.
ΔDEC_i	=	Error in Dec position of bundle i.
ΔRA_{avg}	=	Average error in RA position of all bundles.
ΔDEC_{avg}	=	Average error in Dec position of all bundles.

Note that if we have only one valid guide bundle centroid, the rotation is zero. Also, if all bundles experience the same offset, the result is also zero. This is expected.

The resulting rotation is validated against range errors.

19.3.1.5 Use of a FIFO to validate results

When the results are determined for a given image, they are added to a “First In First Out” (FIFO) buffer. After addition of a new value, the FIFO is analysed to throw out outliers before determination of a new offset from the average of the remaining values.

Chapter 20 WFMOS Wavefront Sensors Subsystem Design Concept

20.1 Introduction

This section contains the subsystem design concept for the WFMOS active optics (aO) wavefront sensing subsystem. The telescope model for this design concept is Gemini. In the case of the baselined WFMOS configuration with a Subaru implementation, either existing prime focus facilities could be used, or a less stringently specified version of the Gemini design concept could be applied.

Two alternative design concepts are in fact explored: one based on wide field-of-view curvature sensors with no moving parts, the other on Shack-Hartmann sensors with patrolling pickoff probes. Both systems have considerable design heritage: the first as the WFS design for the Vista survey telescope, the second in the existing peripheral wavefront sensors for Gemini. Both concepts readily meet plausible design requirements and constraints, and the design decision must trade the elimination of moving parts at prime focus against maximum compatibility with existing Gemini systems. This decision is likely to be strongly influenced by operational experience with the existing WFS, and therefore requires review input from Gemini.

Both design concepts deliver autoguiding functionality. This may be redundant as it can be accomplished using guide fibers, but as it comes for “free” (in the design effort sense), it is retained for now to preserve system-wide design flexibility. The primary financial savings from deleting this capability are visible in the cost breakdown. Space/weight savings from deleting this capability are negligible.

The majority of this report is concerned with the concept which is new to Gemini: the wide-field curvature sensors without moving parts. The patrolling Shack-Hartmann concept re-uses the current Gemini PWFS design and so the report is only concerned with the feasibility of the minimum necessary changes for prime focus operation with WFMOS. Of course, any final design would be likely to incorporate other changes based on operational experience with the existing design, but this is not really an issue for a feasibility study, provided the existing design works.

20.2 Wide-Field Curvature Sensors (LOCS)

20.2.1 Terminology

20.2.1.1 LOCS

Throughout this document the reader will find reference to Low Order Curvature Sensors (LOCS)

20.2.1.2 SDSU

Within this document reference is made to SDSUs. The SDSU comprises: a control electronics box; CCD head connection cables; fiber optic cables; and a PMC (PCI Mezzanine) interface card. The controllers commonly known as SDSU

(San Diego State University) controllers throughout the astronomical community are currently in their third generation (SDSU III). The term “SDSU” is used therefore to refer to the control electronics box alone, four of which will be required to control the WFS CCDs.

Each SDSU-3 controller requires 50W with a further shared 40W for a 24V power supply. Cooling is not required for operation but may be readily accommodated. The mass is 10.5kg each and the external dimensions are 350mm x 150mm x 200mm approximately.

20.2.2 LOCS System Overview

The key components of the Curvature-based Wavefront Sensor subsystem are:

- Two identical combined Low Order Curvature Sensor (LOCS) / Autoguider (AG) Units, subsequently referred to as LOCS/AG Units, positioned on the WFS Plate, above the ADC/corrector, on opposite sides of the field of view, each containing:
 - A pickoff mirror, to divert light into the unit
 - A filter to limit the wavelengths used by the unit to 720-920nm (I-band) and also attenuate any science band wavelengths reflected back out into the IR Camera
 - A cube beamsplitter to divide light between the pair of curvature sensor CCDs and reflect light to the autoguider CCD
 - Two 2Kx2K curvature sensor CCDs
 - One 2Kx1K frame-transfer autoguider CCD
 - A PCB containing CCD buffer and protection circuitry
 - A Mechanical assembly
 - CCD heating resistors
 - Temperature sensing diodes
 - Cryogenic enclosure and windows for the LCS and AG detectors
 - Two flexible circuit wiring harnesses to connect the LOCS/AG units to hermetic connectors on a cryostat port

External to the cryostats are:

- Four SDSU Controllers
- 24V Power Supply
- Fiber optic cables

The use of two AG/LOCS units provides the ability to distinguish all M1 wavefront aberrations with Zernike polynomials less than radial degree 3 in real-time, as well as corrector centration errors. The strawman space envelope provides space for both units. If this full capability is not required, then one unit may be deleted.

I-band operation was used in the original design, and for the purposes of establishing feasibility this is retained. This could be changed in any final design, possibly removing the need for deep-depletion CCDs, and improving AG sensitivity. Excel spreadsheets are provided with this report and these can be used to recompute sensitivity in case of design changes to operational wavelength, optical input configuration, or throughput. Consideration would also need to be given to atmospheric dispersion if a shorter wavelength band were adopted.

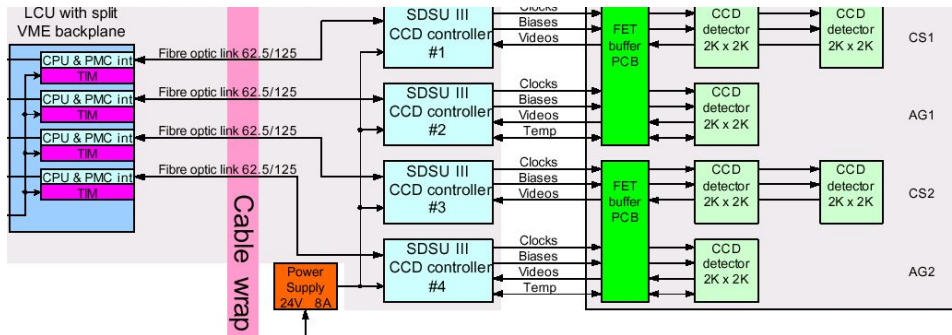


Figure 224. LOCS WFS Electrical Block Diagram

20.2.3 LOCS/AG Unit Design

This section describes the design of the LOCS/AG unit including optical, mechanical, electronic and thermal aspects of the design. The software associated with these systems is described in a later section.

20.2.3.1 LOCS/AG Requirements

The requirements for the LOCS/AG units, including individual requirements for the LOCS and AG, are adopted as follows:

- 99% sky coverage for AG and LOCS operation
- LOCS: real-time Zernikes every 30 seconds up to Z9 (Noll ordering) with 30nm RMS accuracy
- AG: 10Hz-200Hz guiding to 50mas

The main constraints on the optical and mechanical design of the LOCS/AG units come from:

- No moving parts
- Mass/space budget
- Gemini-compatible controllers and aO processing software

20.2.3.2 CCD Selection

The required footprint of the LOCS and AG are both equivalent to 2Kx2K 13.5µm pixels. The combined AG footprint is provided by two 2Kx1K frame transfer CCDs, one mounted alongside the LOCS in each of the two identical LOCS/AG units.

The CCDs themselves are custom-packaged (Invar) deep-depletion frame-transfer-wired variants of E2V's CCD4240 (BI, NIMO). To maximise cost effectiveness and minimise the need for spares, a single detector type is used but with two different mask options. The autoguider CCD in each unit will be equipped with a mask that covers half the chip allowing it to be used in frame transfer mode. The curvature sensor CCDs will have masks that cover the 40 columns nearest the readout register providing a storage area for the defocused star image during readout.

20.2.3.3 Validation of AG FOV

The adopted requirement for the autoguider field specifies that the field must be big enough for there to be a 99% probability of a suitably bright guide star being visible for any desired exposure on sky at full moon (within 10 degrees). The required autoguider field was calculated backwards through a guide star R-band magnitude of 15.6 from a desired signal to noise ratio of 20. In the accompanying spreadsheet this calculation is re-validated but, rather than working backwards from a desired signal to noise ratio, the delivered signal to noise ratio is calculated using the chosen 2Kx2K combined AG footprint with an I-band star magnitude of 15.2. This 99% guide star brightness is calculated from the Gemini (D. Simons) model of R-band star availabilities at the galactic pole for the equivalent autoguider field radius and is adjusted for I-band.

The signal to noise ratio is calculated as:

$$\frac{\sum f_{obj} t}{\sqrt{(\sum (f_{obj} + f_{bg} + f_{dark}) t + Num_{pix} \sigma_{rd}^2)}$$

where:

Numpix is the number of pixels the object image is spread over

fobj is the flux rate for the object (e-/sec)

fbg is the flux rate for the sky background (e-/pixel/sec * Numpix)

fdark is the dark current rate (e-/pixel/sec * Numpix)

t is the exposure time

σ_{rd} is the detector read noise (e-)

20.2.3.4 Validation of LOCS FOV

The low order curvature sensor signal to noise ratio is calculated in the same way as that for the autoguider but using an exposure of 30s and spreading the signal

over a larger number of pixels due to the 1mm defocus distance. The accompanying spreadsheet contains the result of this calculation showing that the sensor signal to noise ratio will be >120 . In simulation an SNR of 7 is required to meet the specified wavefront sensing accuracy.

20.2.3.5 *Operation after sunset*

The autoguider should be operable 30 minutes after sunset using a suitably bright guide star. In order to calculate if this is achievable, the same spreadsheet was used and adjusted as follows:

- A minimum exposure time of 10ms was selected
- The guide star magnitude was adjusted to provide a signal of 60,000e- in this same exposure time
- The sky brightness was then adjusted until the resulting signal to noise ratio was close to 7 (the minimum for reliable operation of the guider)

The calculation concludes that a guide star magnitude of $I = 9.2$ provides a signal to noise ratio of 7.8 with a sky brightness of 3 mag/arcsec². This calculation is somewhat nonsensical since 3 mag/arcsec² is roughly equivalent to daylight and the camera itself would saturate almost immediately.

Using a more realistic sky brightness of 13 mag/arcsec² and an exposure of 50ms, it would be possible to guide on a magnitude 14 star with a signal to noise ratio of 19.3.

20.2.3.6 *Sensor location*

The static curvature sensor has been shown by detailed modelling of work in the presence of large static aberrations (in excess of 100nm RMS on individual zernike terms). This was specifically modelled to deal with operation in the peripheral field of an optical corrector system, i.e. outside the field of stigmatic imaging. (The SH sensor can also deal with static aberrations at a broadly similar level.)

20.2.3.7 *LOCS/AG Optical Design*

The optical design of the LOCS/AG units for Vista was undertaken by Richard Bingham. The chosen LOCS design is based upon the use of a cube beamsplitter to divide light between the two CCDs. A cross-section of the design is shown in Figure 225.

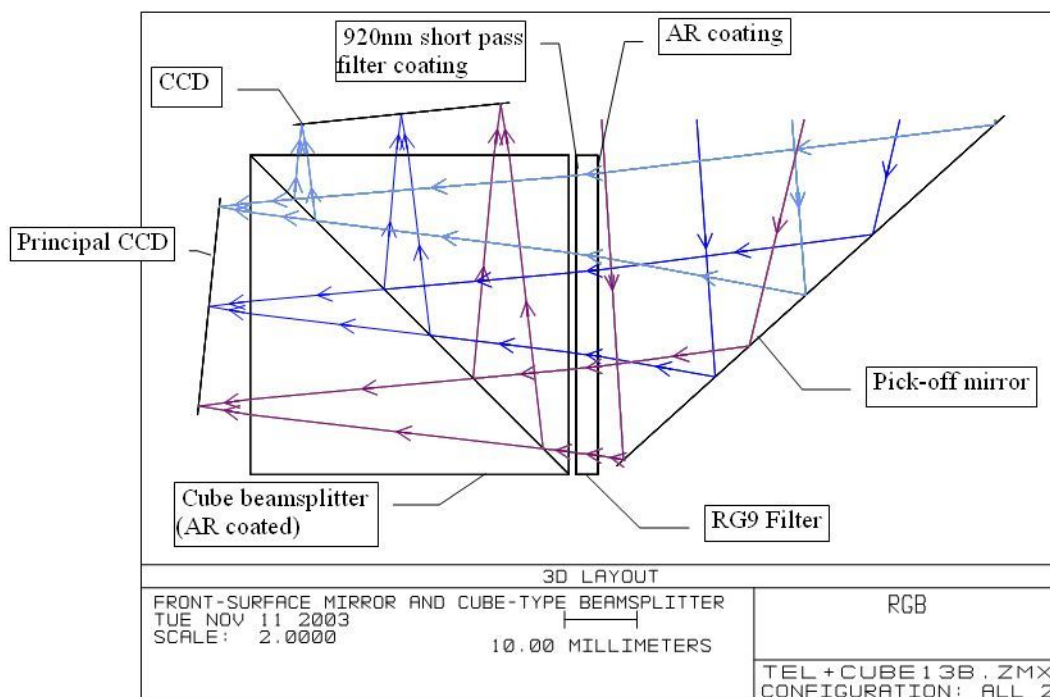


Figure 225. Cross-section of the LOCS/AG optical path.

During the detailed design phase, it became clear that it would not be possible to use a single plate beamsplitter. Such a plate beamsplitter would have introduced significant aberrations in the transmissive path to the principal CCD due to the optical path difference across the converging beam as it passes through the tilted plate. Correct operation of the LOCS would have been prevented by the different aberrations ‘seen’ by each CCD. The cube design overcomes this problem. The cube beamsplitter design has been tested successfully in a cryogenic qualification test.

20.2.3.8 LOCS/AG Filter Selection

The chosen pass-band was originally selected as 720nm to 920nm, pseudo-I band. For the purposes of establishing feasibility this choice has been retained.

The chosen CCDs will utilise deep-depletion (high-resistivity) silicon to maximise QE at these long wavelengths and to minimise the fringing normally experienced by thinned CCDs at these same wavelengths.

The filter will be implemented using 3mm-thick Schott RG9 filter glass which absorbs light below 700nm and above 1100nm. A 920nm short pass coating will be applied to the rear of the RG9 and a broad band AR coating to the front. The throughput to the CCDs will therefore be as shown in Figure 226.

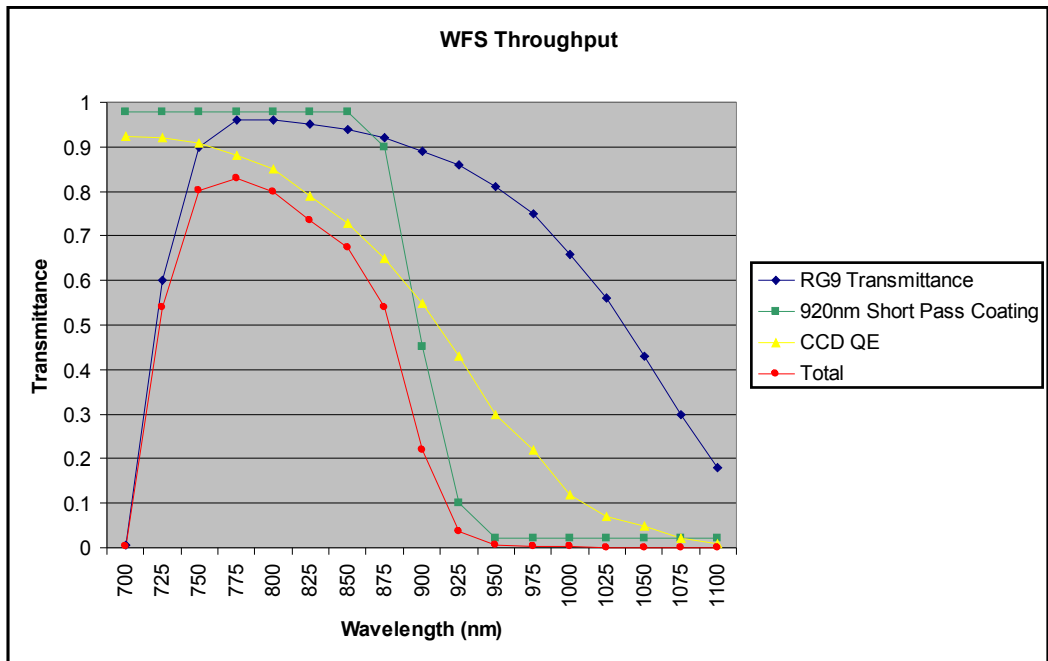


Figure 226. WFS Throughput.

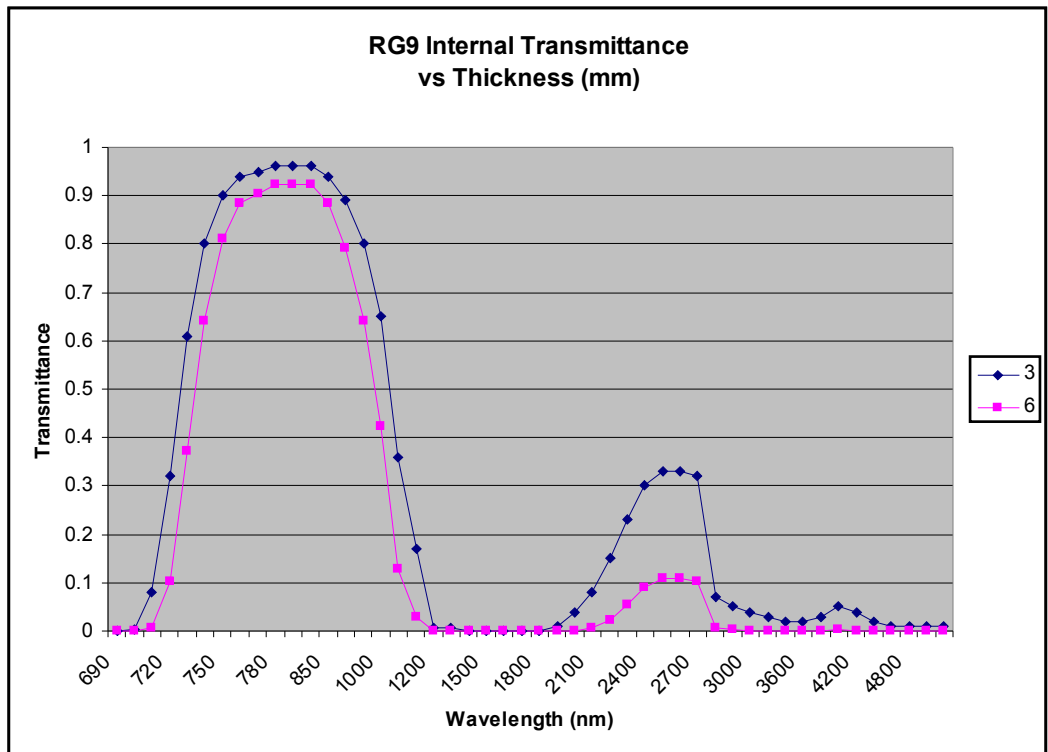


Figure 227. RG9 Transmittance.

RG9 has an unfortunate second pass-band centred on 2500nm as shown in Figure 227. A stray light analysis has been performed to demonstrate that the science wavelength light reflected off the 920nm filter coating and which exits the RG9 after a second pass (6mm) does not cause unwanted ghosting on the science array. The analysis is presented in Appendix 9 and concludes that a magnitude 1 star image reflected back from the filter will cause ghosting equivalent to 1% of the sky background in Y and Zsloan. The ghosting is therefore considered acceptable

and the RG9-based design valid. If the RG9 were to be replaced by standard glass then the same level of ghosting would occur from a magnitude 5 star.

20.2.3.9 Alignment Sensitivity

The optical design of the LOCS/AG unit utilises the angle of the pick-off mirror to desensitise the system to misalignment in Y relative to the optical axis. Lines extended from the surfaces of the mirror and principal CCD would meet on the focal plane. In this way, any misalignment in Y (or X) only results in a shift of the part of the FOV seen by the CCDs and not a change in focus.

An analysis of the (mis-) alignment sensitivity has taken place and a movement of the unit by up to 5mm in either X or Y will introduce a maximum P-V change in the image aberrations of less than 0.3 waves. This LOCS software can easily cope with much large level of static aberration.

20.2.3.10 Mechanical Design

The mechanical design of the LOCS/AG units is governed by the physical location of the optics and detector surfaces from the optical design plus the mechanical and mounting constraints. The internal construction of the LOCS/AG units is as shown in the following figures. The mechanical components of the LOCS/AG units will be made from the same material as the mounting plate. The surrounding cryostat is excluded. The external dimensions of a LOCS/AG unit without cryostat are 190mm x 170mm x 100mm.

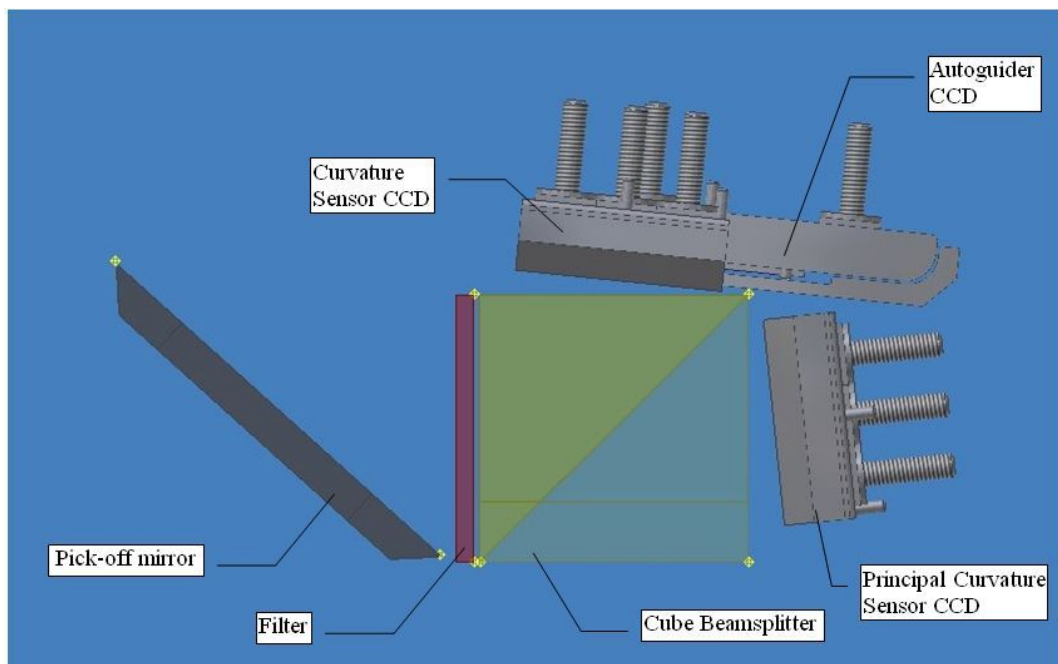


Figure 228. LOCS/AG Optics and Detectors, Side View.

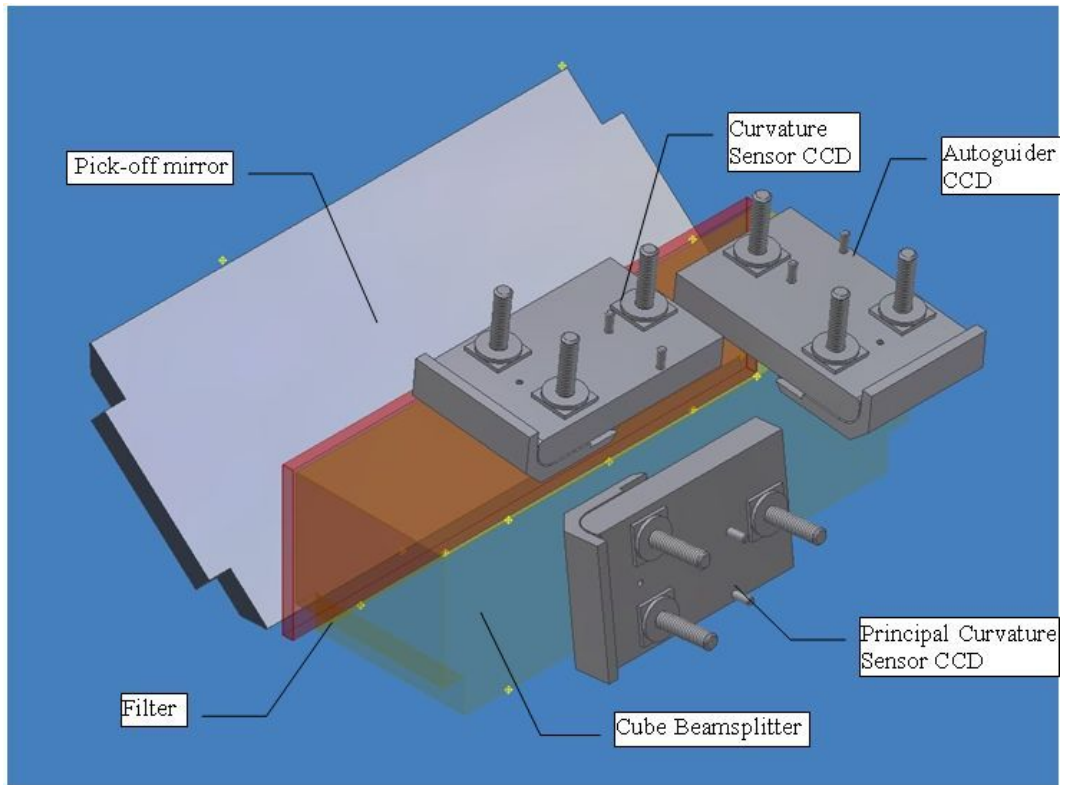


Figure 229. LOCS/AG Optics and Detectors.

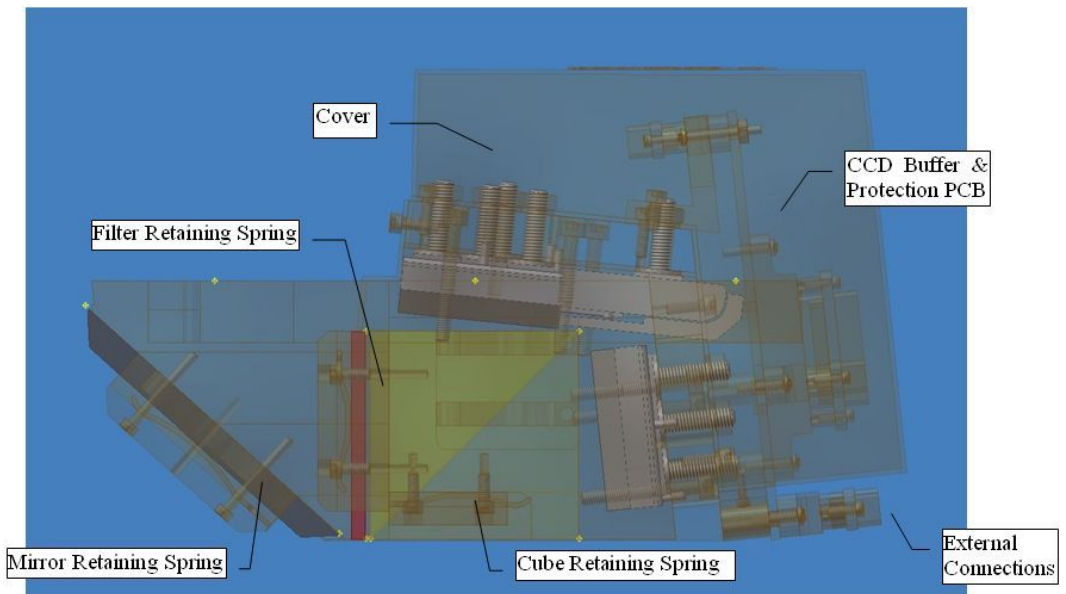


Figure 230. LOCS/AG Unit Transparent Side View.

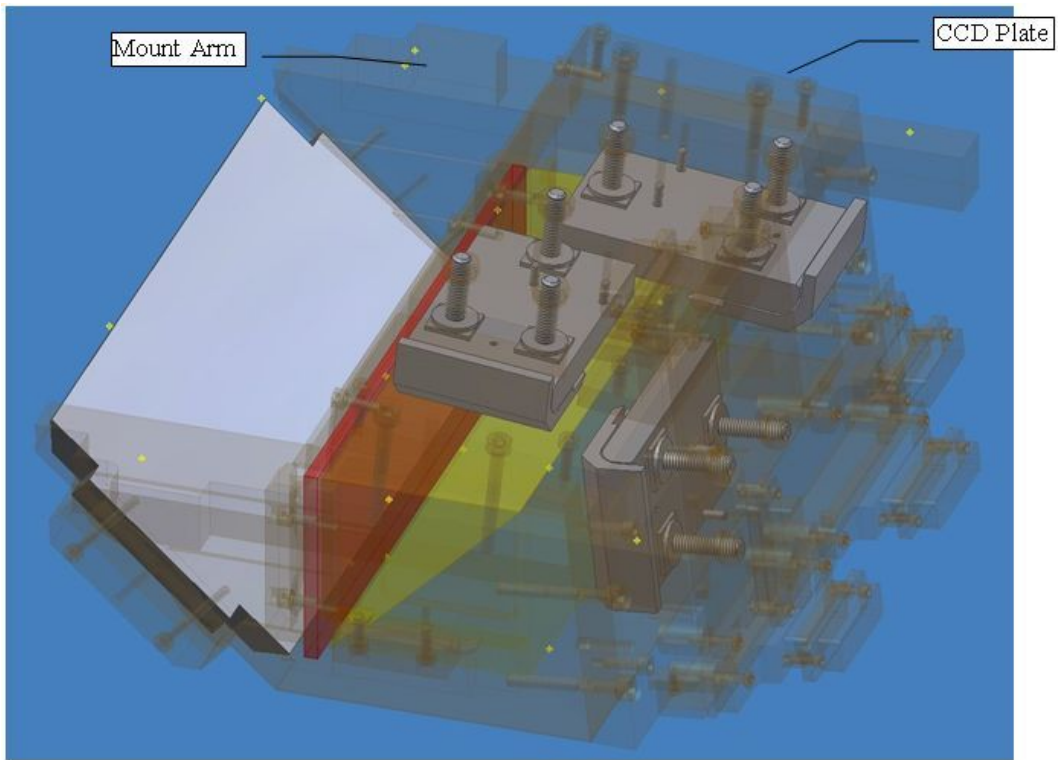


Figure 231. LOCS/AG Unit Transparent View (Cover Removed).

20.2.3.11 LOCS Thermal Design

The thermal design of the LOCS/AG units is summarised in Figure 232.

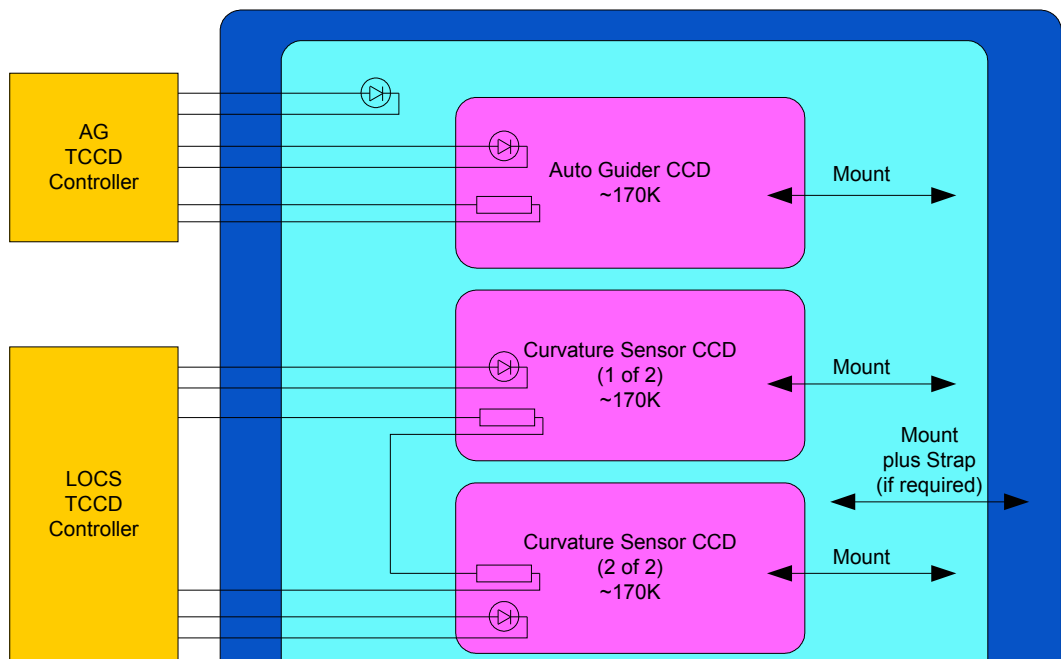


Figure 232. LOCS/AG Unit Thermal Design.

The LOCS/AG CCDs are to be maintained at a constant temperature of approximately 170K. The temperature needs to be above 150K for correct operation and below 210K to reduce the dark current to acceptable levels. The CCDs will be slightly over-cooled by thermal conduction into the CCD plates, through the remainder of the LOCS/AG unit assembly and into the surrounding

WFS plate. Provision will be made to include additional cooling straps between the LOCS/AG units and the WFS plate should the thermal path through the intermediate mounting surfaces not be sufficient. CCD temperatures will be servo-controlled by the SDSU controllers via heating resistors and temperature sensing diodes. Each Controller has two temperature-sensing channels and one heating channel. For the LOCS, each CCD will have its temperature monitored by a single diode and heating power shared between each pair. For the AG, the temperature of the CCD will be monitored by one diode, the other being used to monitor the temperature of the surrounding metalwork.

The power dissipated by each LOCS CCD will be of the order 250mW while the AG CCD will dissipate of the order 760mW due to its almost constant clocking.

20.2.3.12 LOCS/AG Unit Mass

The predicted mass of each complete LOCS/AG unit has been confirmed as 2.25kg

20.2.3.13 LOCS Predicted Accuracy

Simulation predicts that the LOCS will achieve the required accuracy of 30nm RMS per term from Z4 to Z10 (defocus, astigmatism, coma and trefoil) in the presence of aberrations up to $\pm 120\text{nm}$ from their nominal value in 0.75" seeing.

20.2.3.14 LOCS Processor Requirements

In order to achieve 15-second LOCS coefficient processing time requirement, tests indicate that a 1GHz-class processor is likely to be required. Coefficient processing will be performed on a VME processor card. The Motorola MVME5500 offers a 1GHz (Power-PC) processor.

20.2.3.15 LOCS Software

The software which has been used for the accuracy testing simulations and for the processor requirement tests uses a simple minimisation technique (the Nelder and Meade algorithm) which calls a merit function with the trial Zernike coefficients as parameters. The merit function then uses raytrace code together with a seeing blurring function to predict extra focal images which are compared with the ones actually measured. The blurring function can be adjusted using measured seeing but results are insensitive to ± 0.25 arcsec. The advantage of this algorithm is that it is robust across a wide range of trial aberrations and is insensitive to working in the presence of large static aberrations if that is required. It is however very CPU intensive for what it does and work is underway on evaluating more direct methods. This is not required for the establishment of feasibility however.

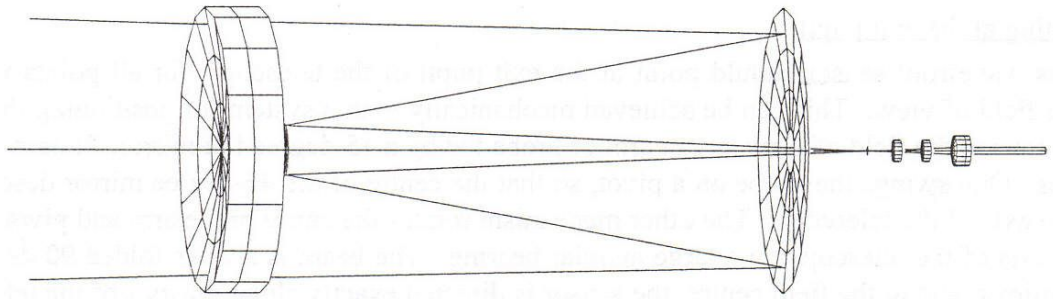


Figure 233. Original PWFS f/16 input beam shortener design. On the left is a 127mm diameter cemented-doublet corrector. On the right are the field stop, filters and Shack-Hartmann collimator. (Richard Bingham, Gemini WFS CDR, 1996)

The LOCS/AG design concept described above provides a method of operating without moving parts in a fast beam at the periphery of the prime focus field. An alternative to this approach is simply to reproduce the current Cassegrain patrolling Shack-Hartmann PWFS at prime focus. For the purposes of establishing feasibility, it is then necessary to examine the minimum design changes that would be required to accomplish this. In fact these turn out to be fairly limited:

- Operating upside down
 - Simply flip the 45 degree folding flat at the entrance.
- Operating in a faster beam, physically closer to focus.
 - The original catadioptric design could be adjusted with some changes to the arm external mechanical space envelope.
- Operating with a changed plate scale
 - Relaxation of the physical patrol field to attain the same sky coverage
- Operating in the available space envelope at Prime
 - Space is available for 2 units: an AG unit and low-order WFS unit.

All other design features would remain the same: detectors, electronics/controllers, real-time processor, software, and interfaces.

20.4 Design trades

Two design concepts have been offered. The first is purpose-built for prime focus operation at the field periphery, and as a new system, has been dealt with in some detail. The other is a minimally changed version of existing Cassegrain facilities. There are no significant differences in feasibility, cost, space, weight or thermal load. The choice is therefore one of system compatibility against the elimination of moving parts, and can only be made in the light of operational experience with the existing design.

20.5 Potential descopes

Gemini's current operational practice is not in fact to use the aO WFS systems during observation but rather to use them for initial calibration, at most nightly. In this case the choice of guide star is much more freely determined, and is probably only constrained by a fairly broad range of acceptable brightness, and the zenith distance for the calibration being conducted. If this were accepted as the actual requirement (i.e., that the requirement for operation during observation were removed) then the sky coverage and consequent WFS field of view and sensitivity requirements would be greatly relaxed.

The relaxation of the aO sky coverage requirements would not by itself engender large-scale cost or space savings so long as the fast guiding and controller compatibility requirements remained. However if all three constraints were removed then very significant savings of cost, space, weight could be made. Such a broad relaxation would mean that guide spines were being used, and were fully-specified for all wind-shake conditions, and it would also mean that a low cost non-SDSU CCD controller were acceptable. We note that the recent Altair (Cass AO) Laser Guide Star upgrades have adopted a low-bandwidth natural guide star focus sensor based not on Gemini's usual SDSU approach, but on a very low cost "amateur" integrated CCD/controller combination. If this de facto derogation were extended to WFMOS, guide spines were adopted, and continuous operation during observation never required, then large-scale cost/space/weight savings become feasible.

Under this combination of circumstances the entire WFS CCD/controller system could be eliminated and replaced by a detector unit costing around US\$10K, including mechanical mounting. The Shack-Hartmann or Curvature options are both feasible and would trade compatibility with existing operation (SH) against very easy acquisition into what would still be quite a large FOV (CS). Assuming the opto-mechanical options remain unaltered from the design concept in both cases, then the remaining differential cost compared to the current WFS costing would be increased software effort to deal with a new data interface for the low-cost controller. Given a reasonable choice of controller this could probably be around 3 mm in total.

LOCS option descopes:

Capability Removed	Main Items Removed	Saving
AG	2 Controllers	\$65K
	3 CCDs (inc spare)	\$133K
AG/SDSU/Continuous	4 controllers	\$130K
	6 CCDs	\$265K
	Mfr	\$40K

20.6 Sensitivity Spreadsheets

20.6.1 AG

Wavelength	
Sensor Wavelength Coverage	50% Cut-On 730nm 50% Cut-Off 910nm pseudo-I
Telescope Properties	
Telescope Diameter (m)	8.1
Telescope Central Obscuration Diameter (m)	1.635
Effective Collecting Area (m ²)	49.43
f/#	2.40
Focal Length (mm)	19440.00
Plate Scale (arcsec/mm)	10.61
Throughput	
Primary Reflectance	0.97
Secondary Reflectance	0.97
Camera Window,L1,L2,L3 Throughput	0.85
Pick-Off Mirror Reflectance	0.97
RG9 Filter Transmittance	0.92
Short Pass Filter Transmittance	0.85
Autoguider Beamsplitter Transmittance	0.9
CCD QE in I-Band	0.85
Autoguider Total Throughput	0.46
Detector & Sky Properties	
I-Band $\Delta\lambda/\lambda$	0.19
1 μ Jy (photons/second)	141.82
0th Magnitude in I-Band (μ Jy)	2.55E+09
CCD Pixel Size (mm)	1.35E-02
Pixel Area (m ²)	1.8225E-10

Pixel Width (arcsec)	0.14324
Pixel Area (arcsec ²)	0.02052
Combined Autoguider Area on Sky 2040x2040 Pixels (arcmin ²)	23.72
Autoguider Equivalent Radius on Sky (arcsec)	164.86
FWHM including seeing (arcsec)	1
Autoguider Star Image Area (pixels)	153.12
Worst case sky brightness I-Band, full moon 10° away (mag/arcsec ²) R 17.2 - R-I 0.5	16.7
Background Flux (μ Jy/arcsec ²)	532.77
Background Flux (photons/sec/arcsec ²)	75555.33
Background Flux At Autoguider (e-/sec/arcsec ²)	35064.48
Background flux at autoguider (e-/sec/pixel)	719.44
CCD Read Noise at 1MHz (e-)	8
CCD Dark Signal at 190K (e-/pixel/second)	1
Autoguider Properties	
Autoguider Exposure Time (seconds)	0.09
I-Band Guide Star Magnitude 99% Probability at Equivalent Radius near Pole R 15.6 - R-I 0.5	15.2
Guide Star Flux (μ Jy)	2121.00
Guide Star Flux (photons/sec)	300791.18
Guide Star Signal including Throughput (e-/sec)	139594.21
Autoguider Signal/Noise Ratio	69.91

20.6.2 LOCS

Wavelength	
Sensor Wavelength Coverage	50% Cut-On 730nm 50% Cut-Off 910nm pseudo-I
Telescope Properties	
Telescope Diameter (m)	8.1
Telescope Central Obscuration Diameter (m)	1.4
Effective Collecting Area (m ²)	49.99
f/# (change to corrector f/# ?)	2.40
Focal Length (mm)	19440.00
Plate Scale (arcsec/mm)	10.61
Throughput	
Primary Reflectance	0.97
Corrector Throughput	0.97
WFS Camera Window Throughput	0.85
Pick-Off Mirror Reflectance	0.97
RG9 Filter Transmittance	0.92
Short Pass Filter Transmittance	0.85
Curvature Sensor Beamsplitter Transmittance	0.45
CCD QE in I-Band	0.85
Curvature Sensor Total Throughput	0.23
Detector & Sky Properties	
I-Band $\Delta\lambda/\lambda$	0.19
1 μ Jy (photons/second)	143.42
0th Magnitude in I-Band (μ Jy)	2.55E+09
CCD Pixel Size (mm)	1.35E-02
Pixel Area (m ²)	1.8225E-10
Pixel Width (arcsec)	0.14324

Pixel Area (arcsec ²)	0.02052
Curvature Sensor Area on Sky 2008x1968 Pixels (arcmin ²)	22.52
Curvature Sensor Equivalent Radius on Sky (arcsec)	160.65
FWHM including seeing (arcsec)	1
Worst case sky brightness I-Band, full moon 10° away (mag/arcsec ²) R 17.2 - R-I 0.5	16.7
Background Flux (μ Jy/arcsec ²)	532.77
Background Flux (photons/sec/arcsec ²)	76411.55
Background Flux At Curvature Sensor (e-/sec/arcsec ²)	17730.92
Background Flux At Curvature Sensor (e-/sec/pixel)	363.80
CCD Read Noise at 1MHz (e-)	8
CCD Dark Signal at 190K (e-/pixel/second)	1
LOCS Properties	
Curvature Sensor Defocus (mm)	1
Curvature Sensor Image Diameter Including Seeing (pixels)	44.83
Curvature Sensor Image Area (pixels)	1578.21
Curvature Sensor Exposure Time (seconds)	30
I-Band Guide Star Magnitude 99% Probability at Equivalent Radius near Pole R 15.7 - R-I 0.5	16
Curvature Sensor Star Flux (μ Jy)	1015.17
Curvature Sensor Star Flux (photons/sec)	145599.21

Curvature Sensor Signal including Throughput (e-/sec)	33785.58
LOCS Signal/Noise Ratio	236.38

Chapter 21 Calibration

21.1 Calibration requirements

The WFMOS instrument requires calibration information for all data taken. This is in order to:

- Determine the bias level on the data (discussed in Section 21.1.1)
- Correct for pixel-to-pixel detector sensitivity variations (Section 21.1.2)
- Identify the loci and profiles of the spectra on the 2D frames (Section 21.1.3)
- Subtract scattered light (Section 21.1.4)
- Correct for fibre-to-fibre spectral variations (Section 21.1.5)
- Correct for fibre-to-fibre throughput variations (Section 21.1.6)
- Wavelength calibrate the data (Section 21.1.7)
- Flux calibrate the data (Section 21.1.8)

This calibration information allows raw 2D frames to be turned into flux and wavelength calibrated 1D spectra. The calibration must not limit the spectral or photometric precision of the instrument, so the calibration frames must allow calibration to a better accuracy than either (a) the statistical error from the highest S/N observations envisaged for the instrument, or (b) unavoidable systematic error arising from observational or instrumental variations during a set of exposures. The time taken to take calibration frames should be small compared with the typical sets of science exposures.

21.1.1 Determination of bias level

This can be via bias frames or bias (overscan) strips. The bias level for each pixel must be determined to much better accuracy than the read noise.

21.1.2 Pixel-to-pixel variation

The pixels on the CCDs have differing sensitivity due to area and QE variations; in principle these variations may be wavelength dependent. Calibration of pixel-to-pixel variations must be at an accuracy $<1\%$ to avoid compromising high S/N data.

21.1.3 Spectrum mapping

There is a need to map the loci and profiles of the spectra on the detectors, to allow efficient extraction of 1D spectra. In practise, the requirements for this are always easily met by the throughput variation calibration requirements. However,

there is an improvement in the quality of the extractions if pixel-to-pixel flat fielding is performed before the extractions.

21.1.4 *Scattered light subtraction*

In all multi-fibre spectrographs, there is a need to accurately subtract off the scattered light, in order to get the correct continuum level for each spectrum, and hence measure meaningful equivalent widths. This may be done either spatial row by row (as with 2dF), or using the full 2D frame (as intended for AAOmega). In either case, unilluminated space is needed on the detector to determine any free parameters used in fitting the scattered light. These are provided for free if there are gaps (4 is sufficient) within the bank of fibres. Such gaps are invaluable in any case for automatically identifying each spectrum with its fibre number by simple pattern recognition, as used with complete success for 6dF. Therefore, no additional calibration information is required for scattered light subtraction.

21.1.5 *Fibre-to-fibre spectral variation*

Each fibre has its own wavelength dependent transmission function. For WFMOS, these will be small (few %) because there are no glued joints. However, calibration of fibre-to-fibre variations must be at a level <1% to bring all spectra onto the same spectrophotometric system, and to allow sky subtraction via dedicated sky fibres. This requires an exposure of the same continuum source through all fibres, ideally with the same spectrograph pupil-illumination as the science data.

21.1.6 *Fibre-to-fibre throughput variation*

As well as spectral variations, there will be absolute throughput variations between fibres, and these must be accurately determined if sky subtraction is to be performed or if relative spectrophotometry between different fibres is to be performed. This requires illumination of all fibres by a source of uniform brightness. Traditionally this has involved twilight flats, but this is an uncertain procedure easily spoiled by weather or background stars, not very accurate for the huge WFMOS field of view, and not available for fields other than the first and last of each night.

An alternative method extensively used in 2dF and 6dF, is to use bright sky lines, on the assumption that the sky brightness in these lines is uniform. This method requires no special calibration data, and by definition leads to good sky subtraction of at least these strong lines. The disadvantages are that (a) variations in the sky brightness may lead to poor spectrophotometry and poor moonlight subtraction; and (b) at high resolution, or in the blue, no sky lines may be available; and (c) the method works poorly for very bright targets.

The ideal method will allow artificial uniform illumination of all fibres at any time, to a precision of 1% or better. As well as being uniformly illuminated, they should be illuminated as closely as possible in the same way as sky light, because the throughput of each fibre and the spectrograph is itself slightly dependent on the f-ratio of each incoming beam.

21.1.7 Spectral calibration requirements

Spectral calibration requires arc lines of known wavelength with sufficient spectral density and sufficient intensity throughout the spectral range of the instrument, in all setups. This is taken to mean that there shall be at least 10 useable lines in all setups, and that the largest gap between useable lines not exceed 20% of the length of the spectrum. The required intensity is such that the statistical noise be smaller than the best required spectral accuracy of $\sim 1/20$ pixel; this leads to a requirement of at least 10^4 counts per arc line per fibre. The maximum integration time per arc lamp exposure is taken to be 30s, since this is less than the read-time for normal read-out mode. Any differences in the way the spectrograph pupil is illuminated by the arc lamps as compared with the science data, leads to error in the wavelength calibration due to aberrations within the spectrograph; the requirement is that this error be smaller than $1/20$ pixel.

21.1.8 Spectrophotometric calibration requirements

The overall averaged instrumental spectral response varies with setup, weather, seeing and target elevation. Lookup tables can provide approximate relative spectrophotometric calibration for any setup, but full spectrophotometric calibration requires observation of a standard star through a science fibre with the same instrumental setup as the science data; and as closely as possible matched observationally in terms of conditions, elevation etc; this must be reduced exactly as the science data and divided by the true spectrum of the star to get the instrument function for that setup. This instrument function can then be applied to all spectra. No special calibration facilities are required to take spectrophotometric standards.

21.2 Calibration system design and performance

It is proposed that the calibration facilities provided for WFMOS shall consist of a variety of arc lamps and quartz-halogen lamps, all mounted on the top end of the telescope, within the primary beam of the telescope, and all pointing downwards towards the primary mirror. The philosophy is that this allows (a) focussing of the very faint arc-lamps onto the fibres at the focal plane; (b) that very uniform illumination of the fibres by the flat-field lamps is easily achieved, and (c) it is straightforward to match the average input f-ratio of the telescope.

There may optionally – depending on final spectrograph design – be long-slit calibration unit within each spectrograph.

21.2.1 Arc lamps and mounting

We propose to use standard hollow cathode arc lamps (Figure 234) for wavelength calibration. These lamps are compact, with well-understood properties and good availability.

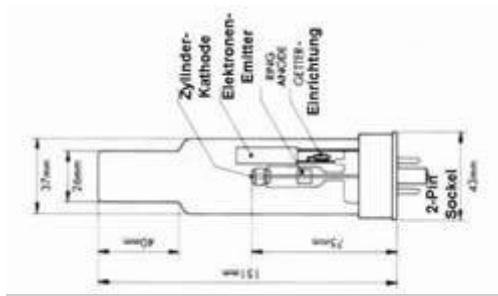


Figure 234. Typical hollow cathode arc lamp.

Traditionally, these lamps are used to illuminate a diffuser screen either in front of the entire telescope (a white spot) or deployable below the prime focus corrector lenses (as for 2dF). However, the first of these means closing and slewing the dome, and slewing the telescope; the second means that the fibres are fed at an f-ratio completely different to the science data. Both of these arrangements lead to very faint illumination of the fibres, and exposure times and signal-to-noise of the arcs becomes a real issue. We therefore propose a novel method of illuminating the fibres for WFMOS.

The light from the hollow cathode arc lamps is emitted from a circular area 4mm in diameter, in a roughly f/4 beam out of the end of the lamp. It is easy to crudely collimate this beam with a simple lens in contact with the end of the lamp, of focal length 90mm and diameter 37mm, to produce an approximately f/20 beam.

We propose that such lamps be mounted parallel with the telescope axis, within the primary beam of the telescope and directed down at the primary mirror. The primary then reflects the light onto the focal plane, with the returned image comfortably overfilling even a 2° field (Figure 235).

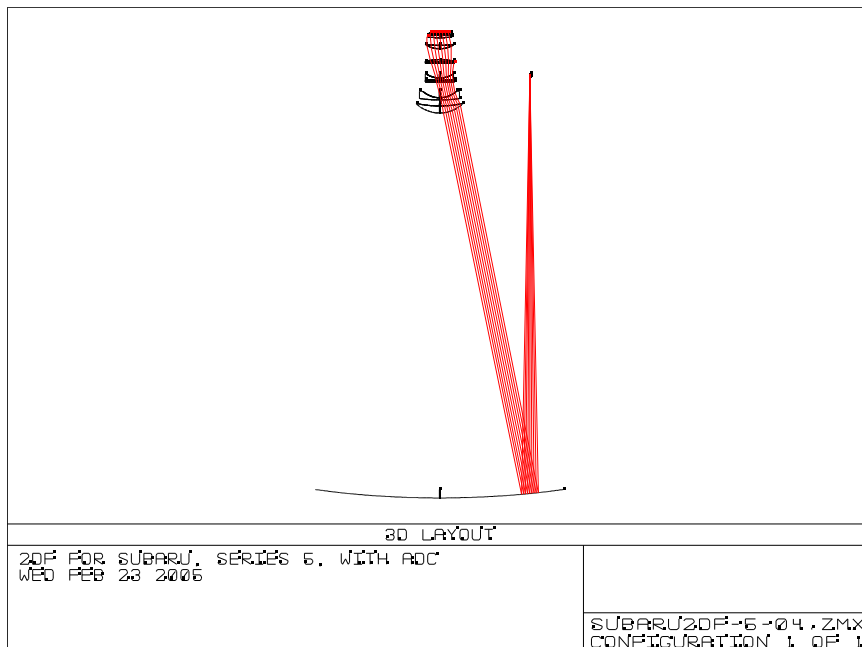


Figure 235. Proposed arc and quartz-lamp field illumination for WFMOS.

This arrangement has been successfully been tested on the AAT with 2dF, and will be implemented for AAOmega. In the test, the arc-light intensity (per lamp) was 30 times greater than the previous arrangement, allowing integration times to

For red arm low dispersion observations, a CuAr arc is adequate (Figure 237) but more lines would be better; these can easily be added via a NeAr lamp (Figure 238)

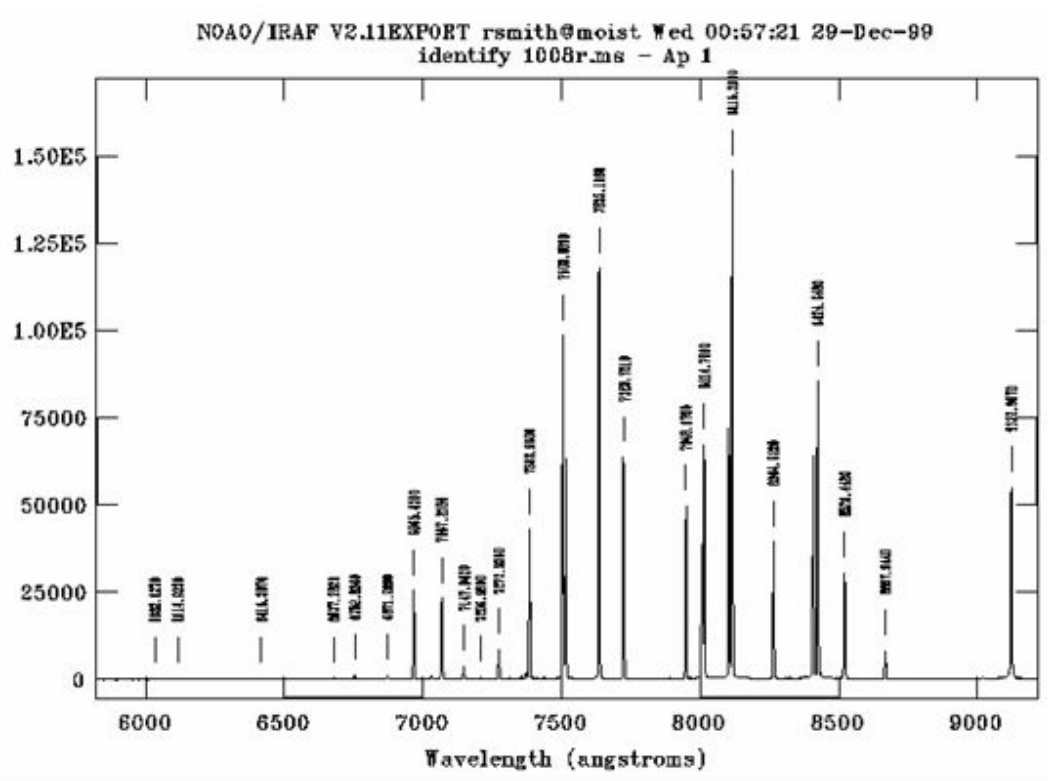


Figure 237. CuAr red spectrum.

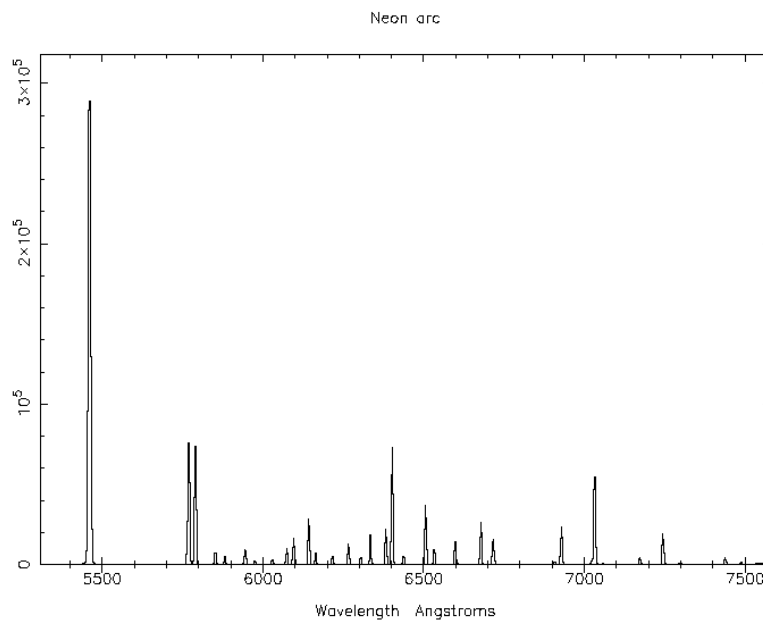


Figure 238. Neon arc spectrum.

For high resolution work, a ThAr lamp provides excellent calibration over the entire spectral range. Figure 239 and Figure 240 show ThAr frames in the blue (3522-4653 Å) and the red (4824-9386 Å) with the UCLES high dispersion spectrograph on the AAT. Each order represents $\delta\lambda/\lambda \sim 0.016$, versus $\delta\lambda/\lambda \sim 0.028$

for WFMOS HIRES spectrograph. So this single lamp apparently provides a sufficient density of lines everywhere.

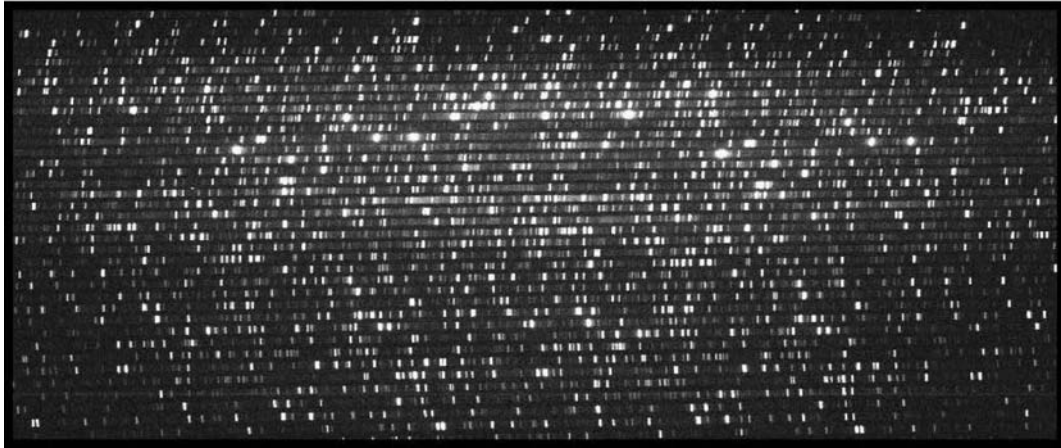


Figure 239. ThAr blue arc spectrum.

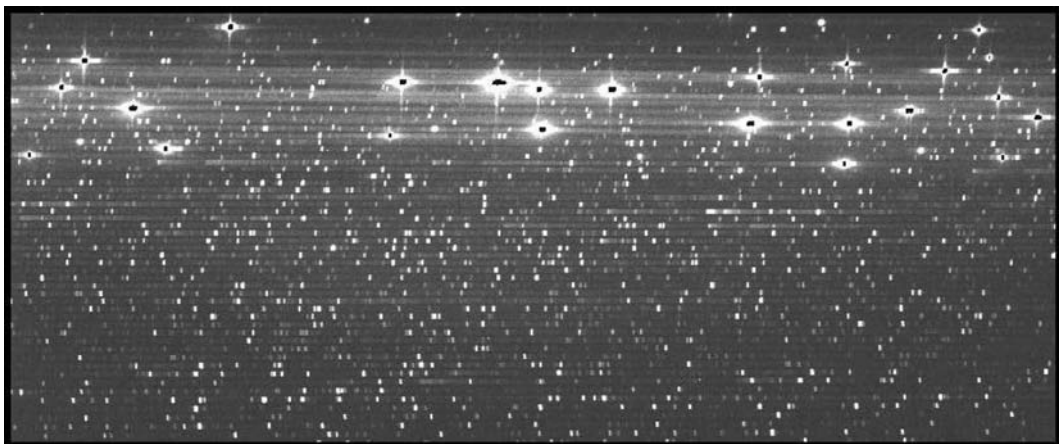


Figure 240. ThAr red arc spectrum.

Additional lamps (FeAr, CuHe) may also be implemented as needed. The electronics allow for any two lamps to be used simultaneously.

21.2.3 ***Quartz-halogen lamps and mounting***

The same mounting arrangement has equally powerful advantages for the quartz-halogen lamps. It is proposed that 20-50W lamps be used as for AAT/2dF. These lamps produce an $\sim f/1$ beam. Because the part of the beam reaching the fibres amounts to only the central $\sim f/30$, it is extremely angularly uniform. This uniformity can be further increased by putting a diffuser of frosted glass in front of the lamps. Light outside the required $f/30$ beam would have to be masked out at the lamp; the heat generated by this masking may limit the wattage of the lamps. However, 6dF masks out most of the light from 50W bulbs without problems. Obviously the lowest power possible is also desirable from a seeing quality point of view.

An issue with these lamps at low dispersion is obtaining enough counts at all wavelengths without saturating anywhere. Colour balance filters can be used to rectify the spectrum, and for WFMOS we propose to use 1mm UG3 + 2mm BG14 Schott filters. The counts from lamp + filters + detector is shown in Figure 241.

The fibres and spectrograph optics will further suppress the blue end, leading to an excellent overall uniformity of counts to within a factor of a few over the entire low dispersion wavelength range.

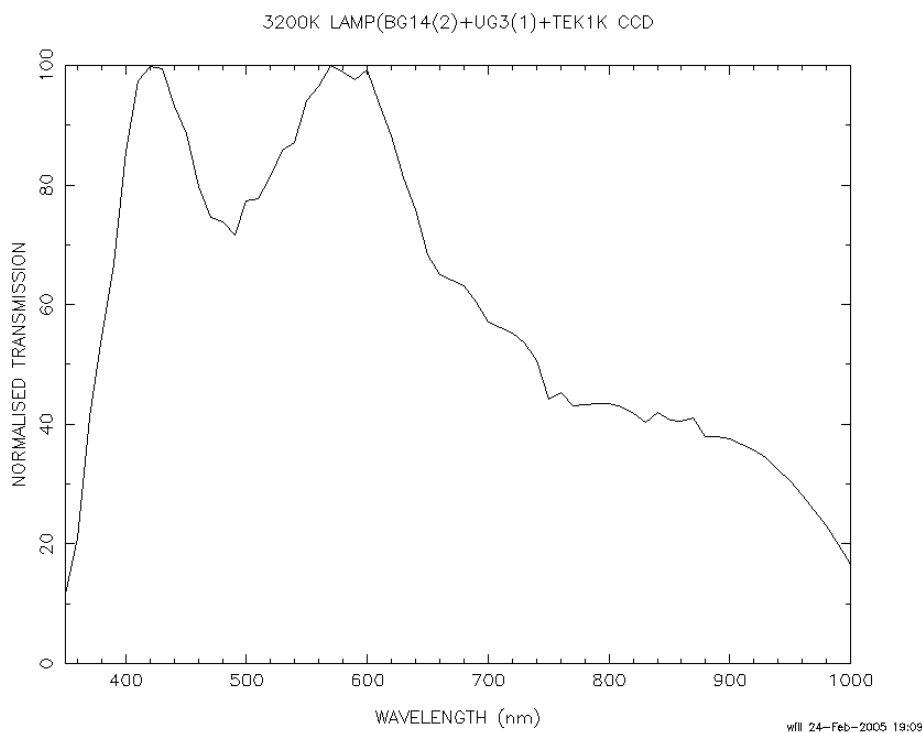


Figure 241. Expected counts from quartz-halogen lamp, filters and detector.

A variable voltage supply is provided with each lamp, since this allows considerable control over the spectral shape and intensity, especially below 4000Å.

21.2.4 Bias determination

Depending on the stability of the CCD controllers, bias frames may not be required at all. The bias can be determined from overscan strips. If bias frames are deemed necessary, they require no special equipment or procedures. However, they are extremely time-consuming, as many frames are required to beat the read-noise; this means they will often be taken many hours from the data they are applied to. The stable temperature of the controllers means that the bias levels should also be very stable.

21.2.5 Pixel-to-pixel flat-fielding

Pixel-to-pixel variation is not a major source of error for WFMOS. The typical rms variation of modern CCD pixel sensitivity is ~1-2%, while the flat-fielding requirement is only 1% even for high S/N data. 2dF and 6dF do no pixel-to-pixel flat-fielding prior to data extraction, even for high signal-to-noise RAVE data; the pixel-to-pixel variations in the spectrum after extraction are removed as part of the spectral throughput calibration. However, proper 2-D pixel-to-pixel flat-fielding in principle allows slightly better extractions.

Calibration frames taken with a long-slit continuum source allow simple determination of the pixel-to-pixel sensitivity variations at the actual wavelength

of use. Some spectrograph designs allow interchangeable slit units, and hence straightforward use of a calibration long-slit during setup.

However, where this is not straightforward, adequate determination of the pixel-to-pixel variations is in any case possible using simple median filtering and quotient taking of normal fibre flat-field frames. Figure 242 shows a flat field constructed from a series of 12 low resolution 2dF fibre flat-field frames. No increase in noise in the gaps between spectra (which run horizontally with blue on the left) is apparent.

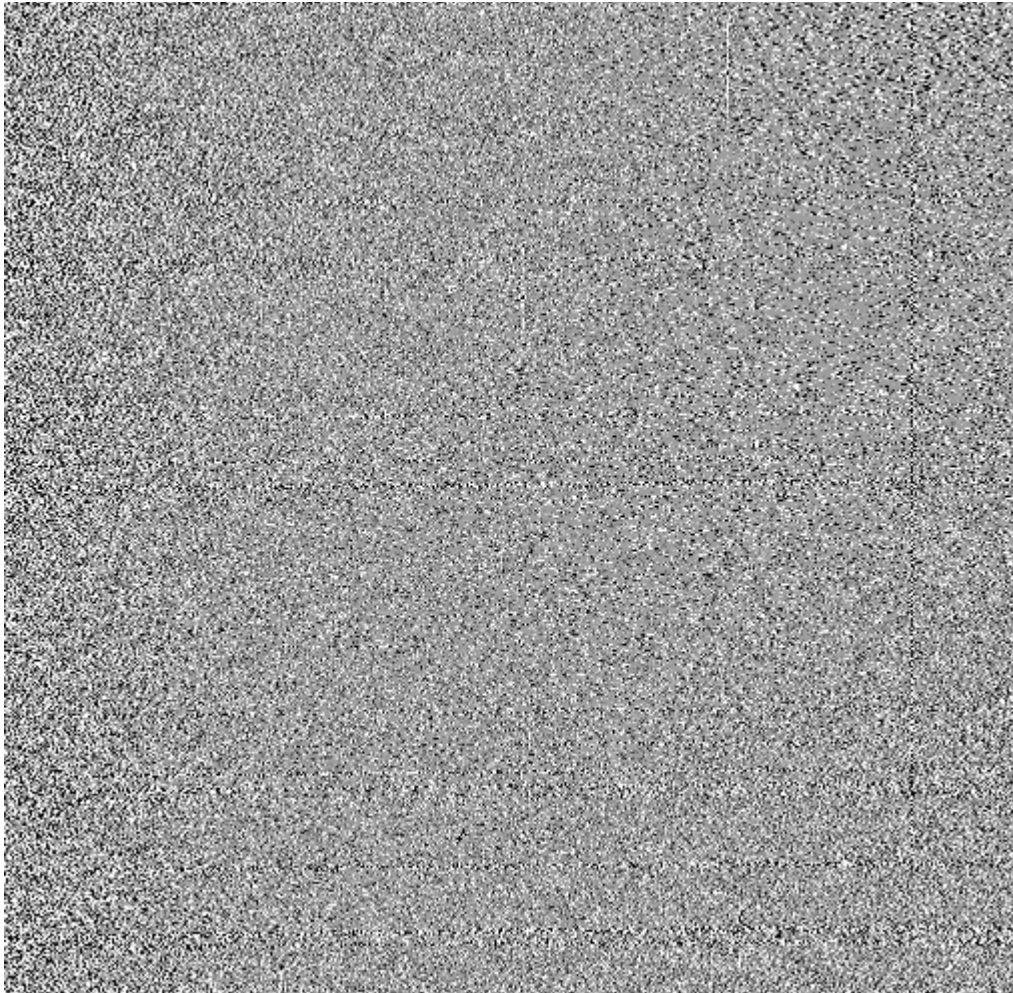


Figure 242. Pixel-to-pixel flat field frame made from a set of 12 low dispersion 2dF fibre-flat field frames.

Since the pixel-to-pixel variations will remain constant for each setup, a series of fibre flat-field frames can always be taken following each instrument change, and a large number of frames can always be taken. Since even the best spectrograph designs will have 5-10% scattered light, a series of ~10 fibre flat-field frames will always give enough counts to reach better than 1% flat-field accuracy even between the spectra. Formally, if the flat-field has high enough precision to beat the shot noise in the actual data within the spectra, it will always have enough precision to beat the shot noise between the spectra.

Therefore a system of calibration slits is not included in this feasibility study.

21.3 *Data reduction calibration steps*

For a given science data set, the calibration information then consists of the following:

- Bias level (scalar or 2D image) determined from overscan strip or multiple bias frames
- Pixel-to-pixel sensitivity map, derived either from a long-slit calibration unit or from multiple fibre flats
- Scattered light fitting, from the data frames themselves
- Spectrum locus and profile information taken from a fibre flat-field
- Wavelength calibration information derived from an arc spectrum
- Spectral throughput variation taken from the (wavelength calibrated) fibre flat-field
- Total throughput variations taken from fibre flat-field, twilight or offset skies, or night sky line strengths
- Instrument function derived from observation of a spectrophotometric standard

The reduction steps are to apply these in sequence to each data frame as follows:

- Subtract bias level or image
- Divide by pixel-to-pixel flat-field
- Fit free parameters in scattered light model, and subtract resulting model
- (Do shuffle subtraction if in Nod&Shuffle mode)
- Extract spectra using loci and profiles from fibre flat-field
- Solve dispersion relation using arc spectrum, apply this solution to science data
- Divide out spectral throughput variations - i.e. the observed flat-field spectrum for each fibre divided by the average for all fibres
- Divide by the throughput measured by whichever method
- (Subtract sky from average of dedicated sky fibres if not in Nod&Shuffle mode)
- Turn counts into fluxes using the instrument function.

21.4 Electronics

21.4.1 Scope

The Calibration Lamp Controller provides a means of remotely controlling the system calibration lamps. Two types of lamps are required:

- Hollow Cathode (HC) lamps
- Quartz Tungsten Halogen (QTH) lamps

21.4.2 Description

It is expected that there will be four groups of Hollow Cathode lamps, with two lamps in each group. Each group will have the same lamp type. The groups may include the following types:

- Copper Argon (CuAr)
- Thorium Argon (ThAr)
- Iron Argon (FeAr)
- Spare

Hollow Cathode lamps require a high voltage low current DC supply. The supply provides a voltage typically 100V in excess of the nominal operating voltage startup to strike the lamp, and then falls to nominal voltage after the lamp has fired. The supply provides typically 10-20mA (adjustable) of current. Each Hollow Cathode lamp will require its own power supply, although it may be possible to share the power supplies between the lamps in each group using a suitable switching arrangement.

Four sets of Quartz Tungsten Halogen lamps are envisaged, with two lamps in three sets and a single lamp in the fourth set. The lamps in each set would be the same and each set would operate at a different wattage (in the range 20-50 Watts). The single lamp set would be used for spectrograph slit illumination.

Quartz Tungsten Halogen lamps require a low voltage stabilised DC supply. Ideally, this should be a constant current supply. It may be possible to operate multiple lamps off a single supply, depending on the lamp specifications and the supply capacity. However, it is likely that multiple supplies will be required. It should be possible to share the power supplies between the lamps in each group using a suitable switching arrangement. Typical precision DC current sources specifically designed to accurately operate tungsten filament lamp standards and calibration sources have a power output range of 10 to 1000 Watts. Such power supplies include the following features:

- Output current accuracy of $\pm 0.01\%$ or better.
- Controlled ramp up/ramp down of the lamp current to prolong lamp life.
- Ability to set lamp current, voltage or power.

One lamp from each group will be mounted on opposing top end spiders, illuminating the telescope primary mirror. On the Subaru telescope, the lamps will be mounted on the upper spider and require a mechanism to drive them clear of the lower spider. On the Gemini telescope, the lamps can be mounted on the underside of the spiders. The mechanism to drive the lamps can be a simple open loop system.

A block diagram of the calibration lamp system is shown in Figure 243.

The calibration lamp controller can be some sort of suitable microcontroller with an Ethernet interface and digital input/output capability. The microcontroller, together with its power supply, drive and control electronics for the calibration unit motors and the lamp selector electronics, can be mounted in a 3U 482.6mm electronics chassis and located on the top end. The lamp power supplies, depending on their number and size, could either be mounted on the top end or else where on the telescope structure. Ideally, cable lengths should be kept to a minimum.

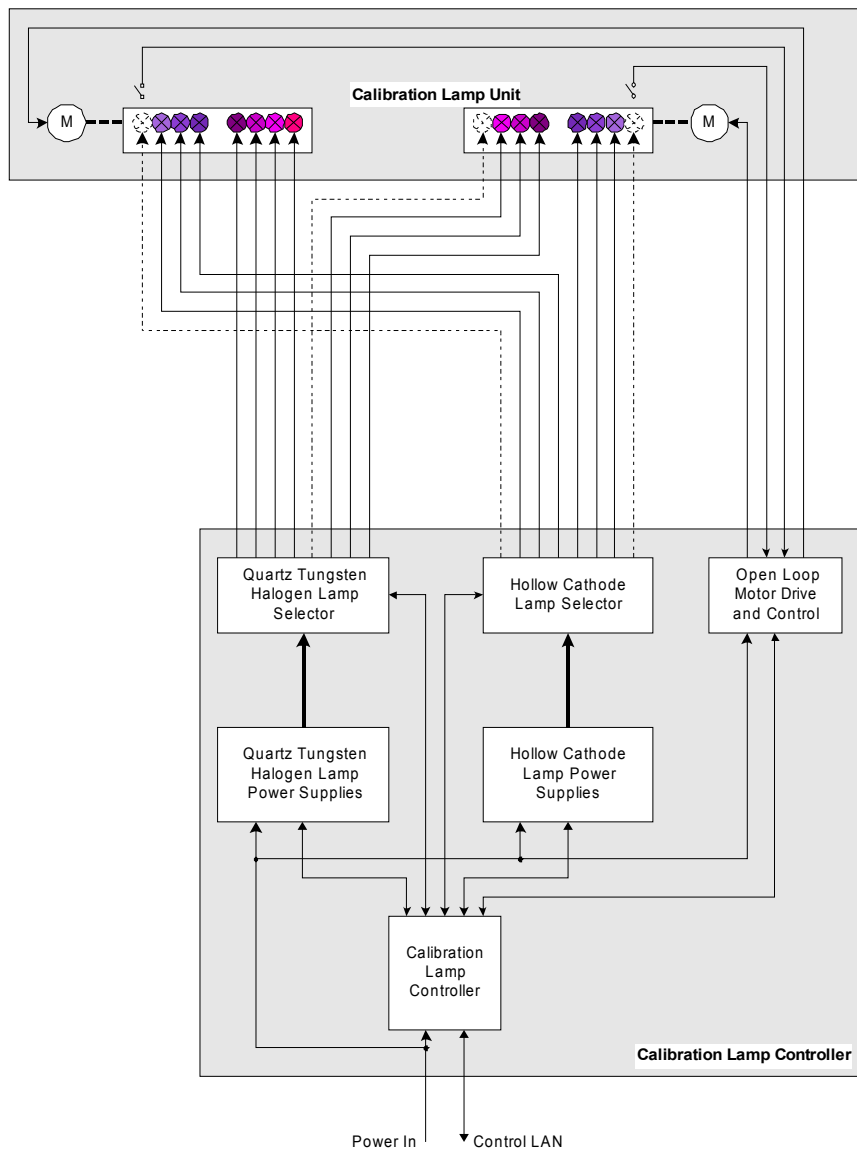


Figure 243: Calibration Lamp Control System

21.4.3 Interfaces

- Control LAN connection
- Mains power connection

21.4.4 Issues

21.4.4.1 Power Supply Number, Size and Weight

It is hoped that no more than two supplies for each type of lamp are needed, to keep the size and weight of the calibration electronics to a minimum. This should be achievable with the Quartz Tungsten Halogen lamp supplies, if they have programmable current settings. However, in the case of the Hollow Cathode lamps, different lamp types usually have different operating voltages and currents and so may require different power supplies if the supplies do not have programmable voltage and current settings. Alternatively, the lamp selection scheme may be able to provide external voltage and current selection. Further investigation of this issue will be required during the concept design.

21.4.4.2 Prototyping

Prototyping of circuits or systems regarded as “high risk” because they involve the use of new technology or techniques or they have a high level of complexity, is usually carried out in the concept or preliminary design phases in order to provide “proof of concept”. At this time, there do not appear to be any parts of the calibration lamp control electronics control that require prototyping in any design phase.

21.4.4.3 Electronics Cooling

The calibration lamp control electronics are likely to be located on the Telescope Top End, it is likely that it will be necessary to provide active cooling of the control electronics enclosure to minimise the heating effects of the electronics equipment on the Telescope environment. This will be achieved using a cooling system that extracts the heat generated in the electronics enclosure and transfers it to the Telescope coolant system. The cooling system maintains a small temperature differential between the outside surface of the electronics enclosure and the ambient air. It is expected that a thermal analysis will be carried out during concept design to determine the cooling requirements.

21.4.4.4 Power

The power requirements of the calibration lamp control electronics are not expected to be large (i.e. < 500W). However, a more thorough estimate of power consumption will be carried out during the concept design.

21.4.4.5 Observatory Electronics Design Requirements

As far as possible, the design of the calibration lamp control electronics will comply with any requirements defined in the relevant electronics design specifications and standards relating to Observatory instrumentation. The concept design will identify the relevant specifications and standards.

21.4.4.6 *Environmental Requirements*

The selection and design of electronics components for the calibration lamp control electronics will take into consideration the environmental requirements and operating conditions of the Observatory. The concept design will identify the relevant environmental requirements.

21.4.4.7 *Electro-Magnetic Compatibility (EMC)*

The design of the calibration lamp control electronics will be undertaken to meet all the relevant requirements for Electro-Magnetic Compatibility for Observatory instrumentation. Achievement of EMC requires an understanding of interference coupling mechanisms, consideration of EMC in equipment layout, grounding and circuit design, application of appropriate filtering and shielding of interfaces and the testing and evaluation for EMC continuously through the project. Observatory EMC requirements will be identified during the concept design.

Chapter 22 Telescope Infrastructure Upgrade

22.1 Telescope Infrastructure Upgrade – Subaru

The baseline WFMOS configuration considered in this feasibility study involves implementation on the Subaru telescope. This section includes an exploration of issues related to handling equipment, storage requirements, spectrograph location, etc. in the Subaru environment.

22.1.1 Summary of Strawman specification

The telescope infrastructure needs to be upgraded to accommodate the WFMOS system.

The upgraded observatory systems must allow removal/refitting, relocation and storage of the WFMOS top-end components, without compromising the fit and handling of other instrument components. An attractive possibility would be to allow storage of the fiber positioner within the same room as the spectrographs, to facilitate test and maintenance.

Accommodation must be provided for the spectrograph suite, along with power and any other required services to operate the spectrographs.

Discussions with Subaru suggest that telescope counterweight issues are likely to be tractable with existing Subaru infrastructure, depending on the final total weight of the WFMOS top-end components.

Other components that may be regarded as part of the support infrastructure for WFMOS are discussed and costed as part of the relevant subsystems – routing of the fiber cable, services for top-end components, modification of the central top-end hub to mount the WFMOS components, structures and support for calibration systems, system control software interfacing to the Subaru telescope control system, etc.

22.1.2 Design concept

Instrument and telescope components mounted at the top end of Subaru are presently accommodated by a semi-automated exchange system involving an overhead crane and “cherry picker” system. Components clamp precisely to a hub mounted centrally to the telescope top end.

The WFMOS top-end components are larger than any existing Subaru top-end components, and may well exceed handling limits of the existing equipment.

A site visit to the Subaru telescope in mid-2004 identified a plausible space, presently unused, to accommodate the WFMOS spectrographs. This space is the floor in between the Nasmyth platform and the top-end component storage room, on the “optical side” of the telescope dome (Figure 244). The FMOS spectrographs currently under construction are to be installed in the equivalent space on the “infrared side” of the telescope.

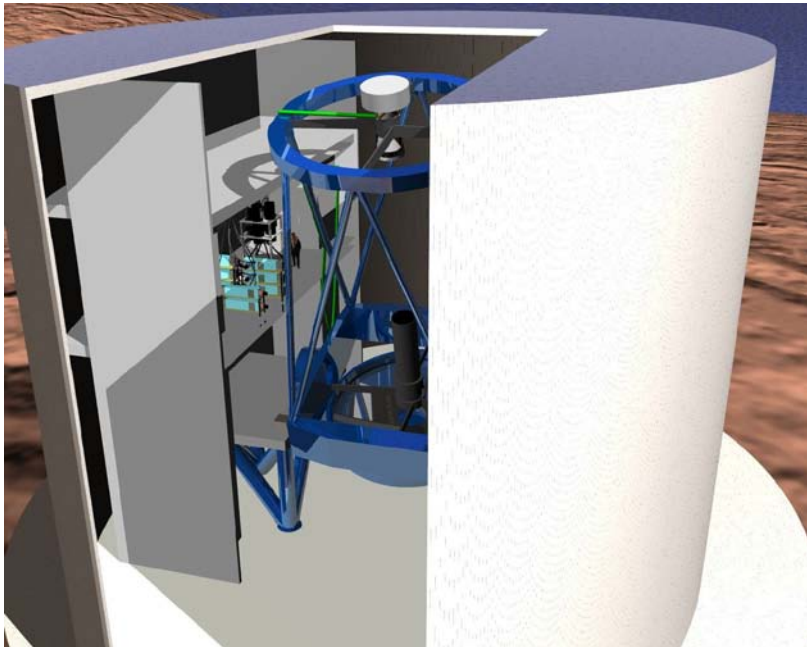


Figure 244. This figure shows the proposed location of the spectrograph suite within the Subaru dome.

An analysis of the available space in this area indicates that there is more than adequate room to accommodate the baseline spectrograph options (Figure 245), including required cryocoolers and support equipment. The room is not presently in a suitable form, and work similar to that undertaken for FMOS will be required to upgrade it.

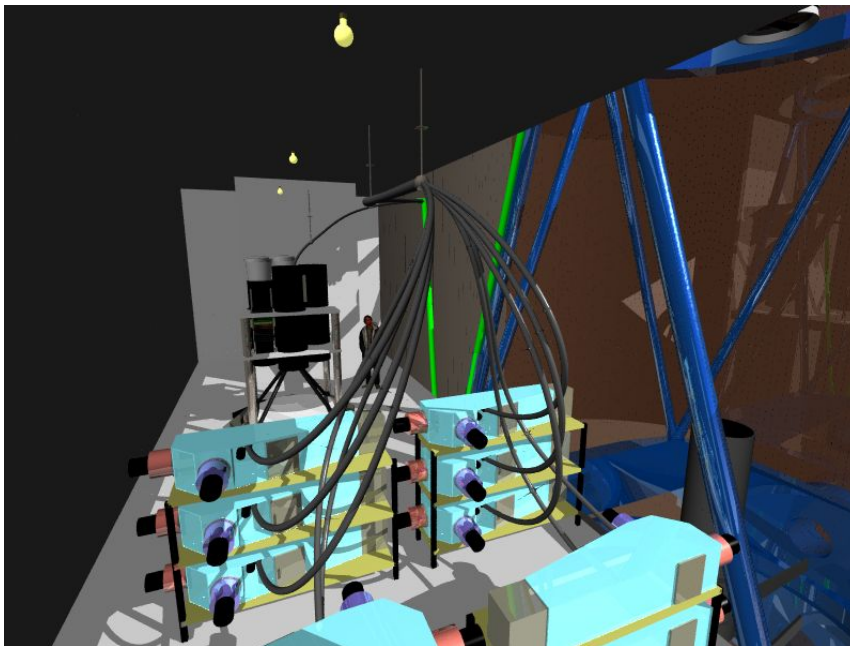


Figure 245. Baseline spectrograph suite contained in proposed new room. The "Great Wall" has been omitted from this figure to show the location with respect to the telescope.

Clearly, some lifting/handling equipment will also be required to deal with the WFMOS subsystems for storage, maintenance and transport.

It is regarded as plausible that accommodation for the fiber positioner component maybe possible in the same room as the spectrographs. This could have significant

advantages, allowing the fiber cable to remain connected from the spectrographs to the positioner – in this case, the cable would be ‘unclipped’ from the telescope structure when the positioner is removed, and be stowed hanging against the enclosure wall. Testing and maintenance of the WFMOS system would be greatly facilitated by such an arrangement, and scope may exist for simplifying the fiber cable connector if routine disconnection is no longer required. Implementing such an option would involve installing a door in the Great Wall, to allow the positioner to be passed through. The wide field corrector would most likely still be stored in the existing top end exchange room, although weight limitations of the existing “cherry picker” need investigation and may impact handling and storage of this component.

If the cable is routinely disconnected, it is anticipated that some additional systems will be required to allow off-telescope testing of WFMOS components – for example a unit to back illuminate the fibers for testing of the fiber positioner.

22.1.3 **Cost Forecast**

Substantial uncertainties in the existing capabilities and limitations of the Subaru telescope systems preclude the possibility of accurate cost forecast for the infrastructure upgrade. Much of this can only be accomplished with significant input from Subaru. Accordingly, estimates are offered for a plausible breakdown of work package components as follows, although with a somewhat greater degree of uncertainty than for other components considered in this feasibility study.

Design	USD 50,000
Spectrograph room preparation	USD 650,000
Power/services	USD 30,000
Modifications to “Great Wall”	USD 100,000
Lifting equipment (off telescope)	USD 50,000
Counterweight	USD 20,000
Cherry picker modifications	USD 50,000
Other infrastructure	USD 50,000
Labour	USD 150,000
Logistics/management	USD 50,000
Total infrastructure upgrade cost	USD 1,200,000

22.2 **Telescope Infrastructure Upgrade – Gemini**

Although the baseline WFMOS configuration for this feasibility study involves implementation on the Subaru telescope, the possibility remains open for a Gemini implementation. Accordingly, as part of the costing of a Gemini fit as an option, this section includes an exploration of issues related to handling equipment, storage requirements, spectrograph location, etc., as relevant to the Gemini telescope.

22.2.1 Summary of Strawman specification

The telescope infrastructure needs to be upgraded to accommodate the WFMOS system.

Although the Gemini telescope was designed for easy top-end exchange, this operation has never been done. Accordingly, the upgraded observatory systems must allow removal/refitting, relocation and storage of the both the existing and the new WFMOS top ends.

When the WFMOS top end is not on the telescope, it must be possible to remove, refit and handle the major WFMOS top-end components (corrector and fiber positioner).

Accommodation must be provided for the spectrograph suite, along with power and any other required services to operate the spectrographs.

Telescope counterweight issues are dominated by the selection of a steel vs. composite structure for the WFMOS top end, and counterweight requirements are discussed in *Chapter 10, Top End Structure*.

Other components that may be regarded as part of the support infrastructure for WFMOS are discussed and costed as part of the relevant subsystems – routing of the fiber cable, services for top-end components, structures and support for calibration systems, system control software interfacing to the Gemini telescope control system, etc.

22.2.2 Design concept

As laid out in the Purple Book, the strawman layout houses the spectrographs in the Pier Lab. Estimates of the size and number of spectrographs confirm that the Pier Lab offers sufficient space for this. Little modification is required to serve this purpose, however the vinyl floor tiles presently fitted are likely to be somewhat phosphorescent and so new floor covering and paint is likely to be required. We expect the spectrographs' cryocoolers to be best located against the outside wall of the Pier Lab, with helium lines run through the wall, in a similar manner to those presently in that location for GMOS. In the order of 6 to 8 "Cryotigers" are likely to serve the needs of all the WFMOS spectrographs, and a site inspection confirmed the availability of sufficient space to accommodate these.

Since the observatory would now be operating two top end units, some accommodation would need to be made to protect the off-telescope unit. The expectation is that this would be accommodated at the same level as the coating chamber, but on the other side of the pier. We understand that this was the planned location for top end unit storage from the outset of Gemini design. Some structures will need to be constructed to provide better environmental protection to the top end unit in storage.

Clearly, some lifting/handling equipment will also be required to deal with the WFMOS subsystems mounted to the top end structure. It is also anticipated that some additional systems will be required to allow off-telescope testing of WFMOS components – for example a unit to backilluminate the fibers for testing of the fiber positioner.

Top end exchange was designed into the Gemini telescope from the outset, and a top end handling carriage already exists, capable of loading and transporting the present top end. A new top end handling carriage is proposed, dedicated to the WFMOS top end, and based on the existing design. It cannot be assumed that a new WFMOS top end will be compatible with the existing carriage design.

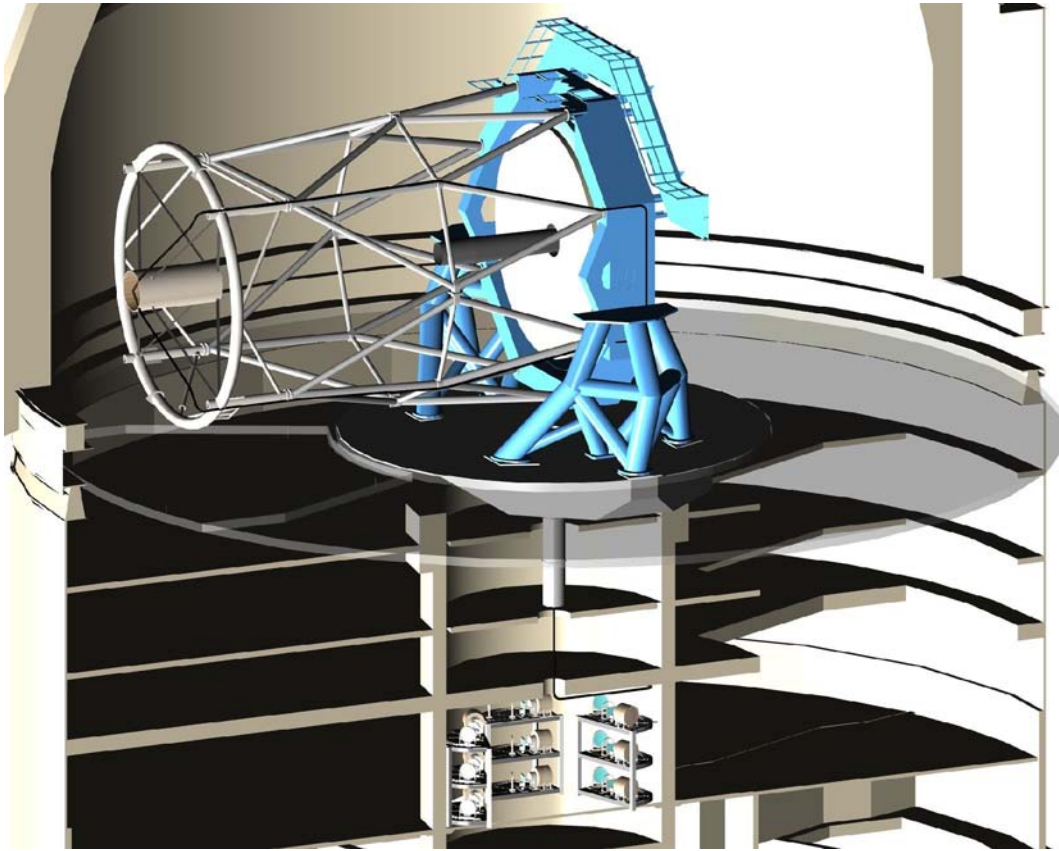


Figure 246. Gemini telescope with WFMOS instrument installed.

Because it will be necessary to install and remove the top end structure to switch between WFMOS and the Cassegrain instruments, the size and carrying capacity of the dome and its affected subsystems becomes another area of concern. Figure 246 shows the Gemini telescope with the WFMOS instrument installed, illustrating the space in which the top end changes must take place.

Prior estimates of the clearance between the WFMOS prime focus unit and the dome should be verified to confirm that there are no interferences with the dome or any in-dome facilities during normal operation. The clearance available for removing the top end in the horizon pointing, as shown in Figure 246, should be verified to confirm that there is adequate space to work around the top end during the installation and removal processes. The clearance of the WFMOS top end and any necessary handling fixtures through the dome floor trapdoor should also be verified, as should the load-bearing capacity of the dome floor and trapdoor (when closed). The lifting capacity and lifting range of the dome crane should also be confirmed, to verify that it is capable of lifting and lowering the WFMOS top end and its handling fixture to and from the below-dome storage area. Finally, the available space in the below-dome storage area should be evaluated to ensure that both the WFMOS and f/16 top ends can be handled and moved in that space during the change procedures.

The Gemini facility was originally designed to permit changes between the existing f/16 top end and a never-built f/6 wide-field model, so it is not expected that any of these issues will present serious problems, but that should be confirmed. Also, detailed review of the interfaces among the instrument, the telescope, and the rest of the observatory systems should be undertaken jointly with the Gemini staff to ensure that all relevant issues have been addressed.

22.2.3 **Cost Trades**

The greatest single cost trade associated with the telescope infrastructure upgrade for a Gemini implementation of WF MOS is likely to be associated with the choice of a composite versus steel top end – the more expensive composite structure needs to be balanced against the counterweight and telescope load issues associated with a heavier steel top end unit. Chapter 10 expands on this area, with a discussion of issues specific to the top end structure.

Another cost trade that should be made in the WF MOS concept design phase is to assess the cost-effectiveness of using two top end carriages rather than just one carriage and two static storage positions.

22.2.4 **Cost Forecast**

Substantial uncertainties in the existing capabilities and limitations of the Gemini telescope systems preclude the possibility of accurate cost forecast for the infrastructure upgrade. Most notably, we do not presume to estimate in detail the cost of implementing an 18,600kg counterweight, its handling equipment, or of any related upgrades to telescope structure, bearings or axis drive motors. Accordingly, estimates are offered for a plausible breakdown of work package components as follows, based on the expectation of a composite top end without significant telescope counterbalance requirements.

Design	USD 50,000
Spectrograph room preparation	USD 40,000
Power/services	USD 30,000
Lifting equipment/cradles	USD 100,000
Counterweight analysis	USD 10,000
Other infrastructure	USD 95,000
Labour	USD 150,000
Logistics/management	USD 25,000
Total infrastructure upgrade cost	USD 500,000

Chapter 23 Data Analysis and Handling

23.1 Overview

We present here a discussion of the data analysis and handling software required for the WFMOS instrument. This section only focuses on tasks associated with extracting, and storing, science-quality data and information. Software for the preparation of observations and controlling the instrument are presented elsewhere in this study. Throughout this document, we refer to two associated data analysis software packages (known as Package A & B), which kept separate because of their differences in functionality and cost. We will define these packages below.

23.2 Software Requirements

The data analysis and handling requirements are driven by the science goals of the instrument. These will be refined over the course of the project, but we list below a set of fundamental goals for the WFMOS analysis:

- Compatible with present and future Gemini infrastructure;
- Provide “real-time” reductions of all data (i.e. initial results within 15 minutes of “wall-clock” time). This will facilitate immediate diagnostics of the science quality of the data;
- Attempt to re-use existing software where possible to reduce costs;
- Store and disseminate data in compliance with Virtual Observatory, and other, international standards.

23.3 Software Packages

The WFMOS data analysis can be naturally divided into two separate packages based on the types of tasks involved in both packages. The first package (which we call Package A) will be centered around the reduction of the 2-D data frames from the spectrographs to 1-D “science-ready” spectra of individual objects. The second package (which we call B) will focus on the software required to extract scientific results from the 1-D WFMOS spectra as well as provide the WFMOS team with robust source lists of objects. The observation preparation software and tools will be covered elsewhere in this report as well as within the Gemini Observing Tools. We briefly outline packages A & B below.

Package A:

- Real-time data processing for quality assessment,
- Science-ready data reductions and spectral extraction
- Gemini Science Archive (GSA) operations
- Data simulator for pre-commissioning tests

- Virtual Observatory database and tools

Package B:

- Target selection software
- Enhanced science analysis software e.g. to extract publishable results

23.4 Software Systems

23.4.1 Data Retrieval and Analysis Environment

The Aspen instruments are required to output their raw data as standard FITS files and store them on the Gemini Data Storage Network (GDSN). The exact details of the GDSN are still unclear, but we will assume here that WFMOS will interact with this system and it will be the mechanism for delivering the data to the analysis software. The raw data on the GDSN will be analysed using the Gemini Online Data Pipeline (OLDP), which has been developed by Gemini to provide a very flexible framework within which to perform a variety of data reduction tasks (see Walker, Gillies & Brighton 2004, SPIE publication). The key concept of the OLDP is to provide a visual programming environment for data analysis modules, thus allowing users to interactively construct pipelines and detach the user from the overhead of scheduling these pipelines on a cluster of computers available for the on-line processing.

The OLDP is built upon Jini, a Java-based technology for the construction of advanced distributed application. Within Jini, is the concept of a JavaSpace, which is a service registry or “lookup table” for independent tasks - for instance, the analysis of different spectroscopic frames - are written into the “space”. Each participating computer in the compute server then searches this space for an unassigned task, removes it, completes the necessary computational work, dropping the results back into the space, and then continues. The JavaSpace technology is simple with well-documented APIs and is designed to have error handling and a high level of abstraction, allowing for simple design and understanding. The main issues therefore, with using OLDP for WFMOS data reduction are scalability, book-keeping and speed, which we address below.

In terms of scalability, each WFMOS observation will produce of the order of a hundred tasks for the OLDP (see Figure 247) and therefore, we would wish to spread these tasks over the available compute server to optimize the reductions. In consultation with the Gemini staff, we believe the OLDP naturally scales to such data volumes and JavaSpaces should work fine with hundreds of separate tasks in the space. Even by today’s standards, parallelizing such a computation (i.e., with hundreds of individual components) is not a major problem on Beowulf clusters of computers and, by the end of the decade, this technology will be much more mature. Furthermore, JavaSpaces naturally support load-balancing as each computer in the server will take as much work as it can handle, so slower processors will pick up less tasks. Also, the scheme outlined in Figure 247 is naturally robust against data acquisition errors (i.e., a faulty spectrograph or missing data frame) as each CCD is treated as a separate entity in the space with no requirements for other frames to be available.

During the design phases, we will clearly need to work with the Gemini staff to understand the scaling of OLDP to the WMOS regime as well as study the optimal granularity of the individual tasks. Furthermore, we may require the purchasing of new computer hardware to provide WMOS with several hundred available CPUs, thus minimizing the computational time and ensuring results can be delivered in real-time (15 minutes). By the end of the decade, such computational hardware should be inexpensive and straightforward to purchase and install. We would work closely with the Gemini staff to ensure any new hardware was compatible with their existing infrastructure and there are available resources to install and maintain this new hardware. In addition, we will investigate the use of the emerging computational grid for both on- and off-line data analysis; for example, “GigaSpaces” now extends the JavaSpaces methodology to sets of distributed clusters of computers. Such a grid solution would allow WMOS to demand extra resources off-site in times of heavy load, thus minimizing the size of compute cluster solely dedicated to WMOS. Also, non-time-critical analyses could be done over the computational grid, again reducing the need for major new resources at Gemini.

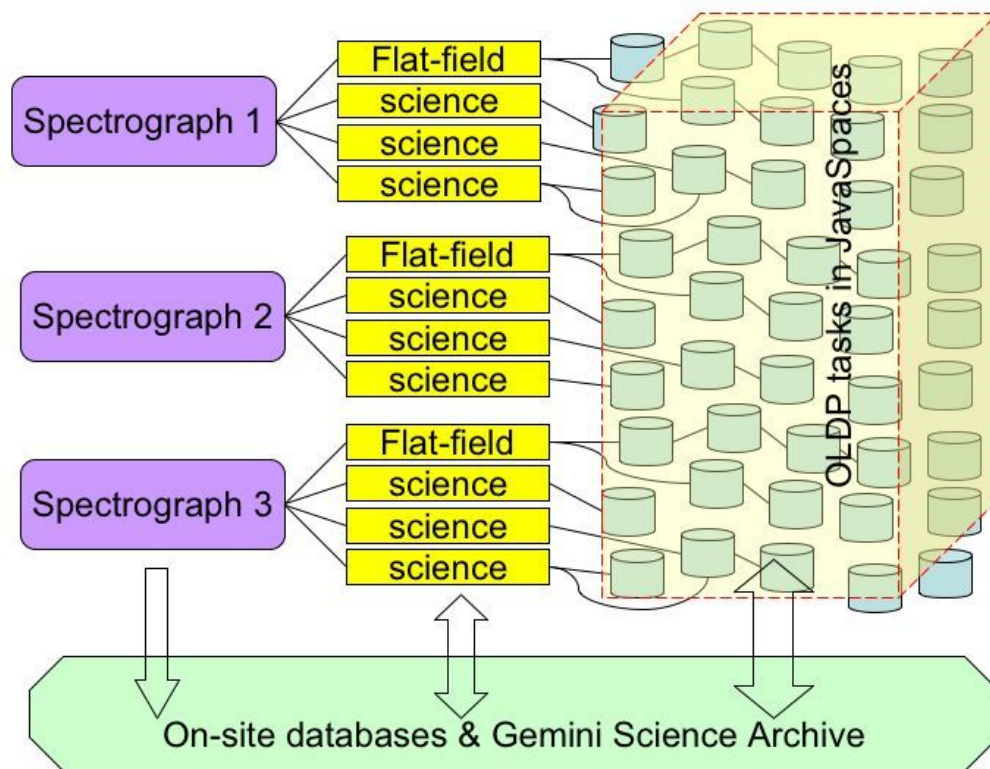


Figure 247. Schematic view of the data and task flow from the WMOS spectrographs into hundreds of individual tasks within the OLDP and then storage data and metadata in the on-site databases and GSA. Each spectrograph will have 2 CCDs which in turn will produce multiple frames per observation. Each frame can be sub-divided into a series of tasks, which can be represented in the “space” as a separate entity.

For book-keeping and logging, OLDP presently allows for the monitoring of all individual tasks and provides access to all log-files, I/O information and error messages generated by each task. The user can drill down to whatever level is necessary and this metadata can be displayed interactively if required. Therefore, we believe OLDP has the infrastructure in place for the extensive book-keeping required to create and monitor hundreds of task running simultaneously. The key issues will be two-fold. First, this metadata (about the success or failure of each

task) must be captured and stored with the reduced data. This requires the OLDP to interact directly with the Gemini Science Archive (GSA) and routinely ingest the metadata, and the reduced data, from the OLDP (see Figure 247). Such an arrangement between the OLDP and GSA is already planned over the next few years and we will work closely with the Gemini staff and CADC (hosting the GSA) to define the metadata required to be stored alongside the data. Secondly, we will require more advanced visual monitoring tools (to handle hundreds of simultaneous tasks) than are presently available within OLDP. We will also need to develop automated routines for highlighting potential problems in the analysis and data; we cannot expect an operator to monitor all these tasks simultaneously, but will need alarms to trigger in the OLDP if there is any suspicious behavior, e.g., reductions take longer than expected, number of fibers traced in frame is less than expected, etc. Again, the flexibility of the OLDP infrastructure should allow us to create such automated testing routines.

The final issue for the OLDP is computational speed, as JavaSpaces is based on the Java language, which is slow compared to more native computational languages like C/C++. Initial studies of OLDP (see Walker, Gillies, Brighton 2004) suggest the overhead of the OLDP workflow system is small and adds little to the overall time of computations compared to running them outside OLDP. However, we will write the computationally intensive tasks in C, Fortran and/or IDL, and call them from the JavaSpaces. Even today, the SDSS spectroscopic pipeline is able to keep-up with the analysis of the SDSS 2-dimensional raw CCD data from the SDSS using a dual-processor workstation at the mountain.

In summary, the OLDP should provide the necessary environment within which to perform online WFMOS data reductions. Future planned improvements to the OLDP, including the facility to automatically search for other sources of data like the “best” available calibrations, should greatly increase its functionality as well. We will work with the Gemini staff over the design phase to fully understand the optimal approach to splitting the WFMOS data analysis pipelines into independent tasks: this is key to the success of OLDP and load-balancing the reductions.

23.4.2 Data Analysis Components

Within the OLDP, we must provide individual tasks or components that can be connected together to develop a data reduction pipeline for the WFMOS data. This will be straightforward as the OLDP provides a generic framework within which tasks can be defined and executed. This is achieved through a task registry and descriptor (see Walker, Gillies and Brighton 2004).

The individual data analysis components we plan to use for WFMOS are now well understood and tested, and we do not envisage any major uncertainties in these components. These data analysis components traditionally include:

- Correct 2-D data for bias,
- Correct 2-D data for flat-field (including fringing if necessary),
- Trace fiber positions in 2-D flat-field,
- Optimally extract spectra from 2-D data,

- Measure and subtract scattered light,
- Calibrate wavelength (using observations of arc lamps and/or sky lines),
- Re-bin spectra to common wavelength,
- Create, calibrate and subtract sky spectrum (see below),
- Co-add science spectra (reject cosmic rays)
- Flux calibrate (calibration stars and/or using sky lines etc.)
- Compute error matrix for the spectrum
- Provide mask array for each spectrum
- Update metadata associated with each spectrum
- Ingest data into the on-site GSA

Within our collaboration, we have access to existing code for a majority of these spectroscopic analysis tasks, e.g., through our involvement in the SDSS, 2dFGRS and the GDDS collaborations. We will endeavor to re-cycle these available algorithms within WFMOS as these tools are already well tested and documented; for example, there are efficient algorithms within the SDSS for the automated detection and tracing of 300 fibres on a single CCD frame (robust against lost fibers etc.). This re-use of such legacy code will help control development costs. The key concern here is the diversity of languages used by these existing pipelines including IDL, C, Fortran and certain Starlink software packages. We will need to revisit these codes to ensure they have consistent I/O standards to work together within the OLDP, which will probably require re-writing parts of the software.

Sky subtraction of the WFMOS spectra will be critical, especially in the red end of the spectra where the OH skylines are dense. Therefore, we plan to explore the use of the Nod & Shuffle (N&S) methods (including mini-shuffling as presently planned for AAOmega at the AAT) to obtain more accurate sky subtraction. In this mode of observation, the data analysis tasks will be quite different as bias subtraction, flat-fielding and sky subtraction can in theory all be done on-chip removing the need for any post-processing. The flexibility of OLDP will allow us to add or change data analysis components to accommodate such changes and we will need to explore these options during the testing and commissioning phases. We will also need to explore in more detail accurate sky subtraction methods for more traditional observations. We will provide a set of pipelines within OLDP to correspond to the different observing modes; both classic and N&S observing modes. IRAF software is already available for N&S observations on GMOS and Glazebrook et al. have already performed N&S observations using the AAT 2dF fiber-fed spectrograph. The AAOmega 2dfdr software package will also include N&S tasks which we can utilize.

Once these tasks are connected within the OLDP, we will have a pipeline capable of removing the instrumental response from each spectrum, thus providing the scientist with a “science-ready” spectrum. The OLDP will analyse each CCD frame independently (placing it into the “task space” as a set of tasks) thus

removing the need for the OLDP to wait for a full set of science and calibrations frames to be taken and written to the GDSN. Each spectrograph will also be treated separately. Calibrations frames will be reduced (using the header information to identify them) and placed into an on-site database (Figure 247), which will include the latest (and historical) arc, bias and flat-field calibrations for each CCD. It will also include the latest (or “best”) fiber-mapping solutions for each CCD, fiber throughput measurements and flux calibration solutions. This database therefore provides the OLDP with the appropriate calibration data (both in time and for each CCD) for the reduction of science frames. We envisage that many of these pipelines (one per CCD frame) will be running concurrently within the OLDP thus exploiting the parallelization of the OLDP discussed above. As mentioned in the previous section, we will require automated monitoring and logging of these separate pipelines, as well as support multiple, simultaneous interactions with the on-site GSA (see Figure 247).

At the present time, we have decided against IRAF even though it is integrated into the OLDP already. We realize this is against the advice of Gemini for the data reduction of the Aspen instruments. Our decision is based primarily on our desire to re-use the enormous amount of legacy code available to us. Also, during the development of the SDSS spectroscopic pipeline, we found the IRAF routines to be beyond the capabilities needed for the SDSS 2-D reductions and were forced to develop our own algorithms; this was primarily due to the uniqueness of the underlying IRAF language and difficulties in scripting IRAF tasks together. These problems may now be resolved, but we feel we can scale-up the existing SDSS & 2dFGRS codes easier than re-discovering the IRAF commands; for example, WFMOS will use similar low resolution spectrographs as the SDSS and therefore, we expect the SDSS software to be most appropriate for these spectrographs (in terms of matching their resolution etc.). In the design phase, we will provide a more quantitative analysis of the pros and cons of using the SDSS & 2dFGRS code compared to IRAF.

23.4.3 Post-Processing Tasks

One of the major additions to the OLDP and existing analysis software will be the design and construction of tools for the visualization of both the raw and reduced data (both 2-D and 1-D spectra), as well as visualization tools for the host of metadata produced during a signal WFMOS observation. For example, we can not expect the operator to study each frame individually but must design a tool that allows the operator to see all data in an abstract form, and provide simple mechanisms for drilling down to individual frames if need be. For example, one could present a “photo album” of all images taken in the last hour (i.e. small postage stamp images arranged in time logical sequence) and provide the facility to interrogate any image at the click of a button. We can also provide some level of background error checking that can highlight frames in the clickable “photo album” that appear to be abnormal (e.g. higher than expected bias, unexpected wavelength solution etc.). Similarly, we can provide a clickable “photo album” of extracted spectra with associated metadata like redshifts (see below), error matrix, etc., for the operator. Finally, we will require a visualization tool to provide summary statistics of all aspects of the WFMOS observation and reduction, again providing the operator with a rapid interactive overview of the real-time performance of the instrument. For example, plots showing the distributions of signal-to-noise per frame and spectrum, fibre throughput measurements, redshift histograms etc. At present OLDP provides simple “quick look” visualization tools

but the OLDP infrastructure should again provide the necessary flexibility to construct more sophisticated tools. Such visualizations can be displayed on large flat-screen monitors in the control room, and will be essential for the commissioning and testing stages of WFMOS.

As mentioned above, it will be essential to automatically monitor the performance of the OLDP and any WFMOS observations, e.g., study the obtained signal-to-noise in each spectrum compared to expectations and requirements. We believe however that one can also provide real-time redshift measurements for each spectrum for little extra computational overhead (see section below on Package B). This would allow the operator to monitor the progress of an observation as a function of a scientifically interesting quantity (redshifts) as well as allow for the option of re-allocating of fibers during an observation, thus maximizing the number of redshifts obtained per unit time, which is optimal observing strategy for the Dark Energy science case. Software already exists within IRAF, and the SDSS & 2dFGRS pipelines, to gain redshifts via cross-correlation against known templates and detected emission lines for the WFMOS spectra. Such redshift measurements can be highly parallelized in the OLDP (one spectrum per CPU) and can be trivially automated e.g. the existing 2dFGRS redshift code can be run in interactive or batch mode providing redshifts for 200 spectra in less than a minute on a standard workstation. We believe the addition quality assurance measures that are provided by such an analysis outweigh the addition computational and development time within OLDP.

A key requirement for the Aspen instruments is the publication of science-quality data to minimize the time between data collection and publication of results. To achieve this, WFMOS must provide its reduced data to the WFMOS community quickly and in a standard, well-understood, flexible format. To this end, we expect WFMOS data to be made available through the GSA in format compatible with the emerging Virtual Observatory (VO) paradigm. This is relevant on two levels: First, the data will need to be exported to scientists in VO-compliant data formats like VOTables (an XML template developed by the US VO collaboration) which can be read by a host of emerging VO tools and infrastructure. VOTables has the advantage of allowing a rich array of metadata to be associated with the raw and reduced data. Unfortunately, VOTables is not designed for spectral data, but work is underway to solve this deficiency. Secondly, WFMOS and GSA should provide a VO-compliant database that can be part of the growing Open SkyQuery network of distributed astronomical databases i.e., WFMOS data could become a SkyNode in this network allowing for complicated cross-matching of WFMOS data with a host of other data sources. Also, webservices designed to operate on this network could then be used to provide advanced analyses of the WFMOS spectra and redshifts, e.g., correlation function webservices, as well as the VOSTats webservices to provide a suite of statistical analyses. In summary, the VO is evolving rapidly and will continue to progress significantly over the next decade. Gemini and the GSA staff are already aware of these technologies and plan to exploit them in future data releases. We will work closely with the Gemini and GSA staff in this regard as members of our team are also involved in the AstroGrid and US VO initiatives, as well as the GSA.

23.5 **Package B Software**

As discussed in Section 23.3, we envisage two software packages (A & B). We have outlined the functionality of Package A in Section 23.4 as this will be the main effort in the development of the WFMOS pipeline. In this section, we briefly outline Package B which would provide important software and tools for the extraction of science from the WFMOS data; rather than producing “science-ready” data as discussed on Package A. We believe this is vital for achieving one of the goals of the Aspen instruments to minimize the time between taking the data and producing scientific publications.

Package B will include tools for the construction and storage of target lists and catalogs. In particular, these tools will allow the scientist to select targets from a database (either locally or distributed via the VO) and perform quality assurance tests and cuts on the data. The tool will also perform optimal field tilting (as performed now with the SDSS and 2dF surveys) to maximize the coverage of targets by the minimum of fields and thus fibers. For galaxies, this can become complex because of the angular clustering of galaxies thus leading to many possible local sub-optimal solutions for the tilting of fields. As part of these target preparation tools we will provide the scientists with software to perform Monte Carlo simulations of different fiber placements options and score these different scheme automatically. We will also provide tools for constructing sets of target list FITS files for automatically configuring the WFMOS fibers (the software for configuring the fibers will be written elsewhere and take standard input FITS files) as well as storing these input files in the GSA for later analysis alongside the spectral data.

Package B will also contain a set of more advanced data analysis tools, which can be applied to the “science-ready” WFMOS spectra. These include:

- Emission line detections and identification (for redshift estimation)
- Emission line measurements including equivalent widths, profile-fitting and joint stellar absorption estimation (via joint fitting of emission and absorption features)
- Redshift determination (plus error and confidence) via cross-correlation with known templates (see above)
- Spectral classification (stellar type, galaxy type, quasars etc.)
- Real-time detection of anomalous spectra, e.g., supernovae
- PCA analysis or similar spectral data compression methods (MOPED etc)
- Measure known indices and abundance measurements e.g. Lick indices
- Spectral modeling fitting
- Power spectrum analyses and clustering algorithms for the WFMOS survey

These analyses will be desired by a majority of WFMOS users and we advocate providing the WFMOS community with a database of such spectral parameters in

parallel to the “science-ready” spectra from Package A. This is the SDSS model where most users are happy to use the SDSS-derived quantities (like redshift, classification etc) rather than derive them themselves. By the end of the decade, software to perform these advanced tasks will be readily available and could be integrated into the OLDP without much extra work.

23.6 Testing and Commissioning Milestones

During the design and fabrication phases of WFMOS, we will embark on a series of tests for the data analysis software. To initial such early tests, we will begin by constructing a data simulator (see Package A outlined in Section 23.3), which will be designed to create realistic mock WFMOS raw data e.g., 2D CCD frames with high redshift galaxies etc. These mock data can then be used as simulated inputs to OLDP and be used to test any WFMOS pipeline we construct. These mock data will be critical for the final design of the data analysis pipelines as well as the suitability of the OLDP environment for handling multiple pipelines with hundreds of individual tasks. In this way, we will be able to focus our time during the fabrication stage on deploying the WFMOS pipelines at Gemini and testing them on-site, and providing documentation and well-studied tested examples and test code, as required of the Aspen instruments. We will also focus on the optimization of the OLDP for the volume of WFMOS, which may include installation of new hardware and/or data transfer between telescopes and Hilo (see below). Finally, during the fabrication stage we will work with the GSA staff to define the structure of the WFMOS database and work towards building this database and ingesting mock data.

During the commissioning phase, we will work closely with the Gemini staff and other WFMOS team members to test all aspects of the data analysis pipeline (target preparation, reductions, GSA interactions etc.) with real data. As discussed below, we expect something unusual with the real data, compared to the mock data, which will force us to revisit our pipeline design. However, we believe the flexibility of the OLDP, and the extensive pre-commissioning testing with mock data, will keep such surprises to a minimum.

At the end of commissioning, we will deliver a suite of working pipelines within OLDP that will support the main observing modes of WFMOS and will control the flow of data from target selection, through to redshift determinations and other advanced analyses. We will publish the data via GSA in a VO-compliant distributed database.

23.7 Cost Mitigation

The last decade has seen an explosion in the number and size of software projects undertaken in physics, astronomy and astrophysics, e.g., SDSS, VO, AstroGrid, GriPhyN, iVDGL, CADC, NOAO Data Products group etc. This trend will continue, driven by ubiquitous computing, massive datasets and high-speed networks. Therefore, the WFMOS analysis pipelines and archiving will not be developed in vacuum, but will learn from these past and present software endeavors.

During the WFMOS software development, we will employ established software development practices and standards for managing large software projects, both in industry and academia. These practices include:

- Version control of software within development archives like CVS which allow branching of codes, thus allowing beta-versions of pipelines to be created and frozen;
- Regression testing of the pipeline using mock (or real data) i.e., when the software is changed substantially it is tested against a set of standard data to ensure consistent and reproducible results;
- Bug reporting and archiving, which allows developers and users to report errors in the code and test against them;
- Prototyping of the pipelines using interactive languages (like IDL, Matlab) by expert scientists, but then re-design the code for speed and robustness;
- Strict documentation of all code.

We will also follow the model of AstroGrid that employs scientists to rapidly prototype and test algorithms and codes, which are then optimized and deployed by professional software developers. Careful management of software, with well-controlled deadlines, dedicated people and clear objectives, is critical to controlling the cost of software development. Finally, we again stress our desire to re-use existing data analysis software within OLDP and believe our team (which includes members from SDSS, 2dFGRS, GSA and NOAO, as well as industry) have the experience to manage such a software development programme.

23.8 Potential Risks

- **OLDP:** The Online Data Pipeline should be sufficient for running the data analysis of WFMOS. However, there is uncertainty about the scalability of the infrastructure to the WFMOS regime i.e., potentially hundreds of tasks running simultaneously. We will need to work with the Gemini people to understand this up-grade and the on-site computer hardware requirements. Overall, we believe this is a low risk but highlight it here for completeness.
- **Subaru:** We will rely heavily on the OLDP, GDSN and GSA infrastructure. These facilities, which are improving all the time, will allow for great cost and efficiency savings. However, it remains unclear if this infrastructure will be available at the Subaru telescope, either requiring us to either build such a facility there, or move the data from Subaru to Gemini. This may require dedicated fiber-optic links between the telescopes and/or Hilo (some of which may already be in place). This is a medium risk, but straightforward to solve if required.
- **Legacy Code:** We plan to extensively re-use legacy code from 2dFGRS and SDSS. This code is written in a variety of languages and connecting them together, within the OLDP, maybe more effort than expected. This will be a large unforeseen expense but we should be able to test against this in the design and fabrication stages. We believe this is a medium risk.

- **Commissioning & Testing:** There are likely unforeseen features and errors in the final WFMOS instrumentation and data, e.g., worse fringing than expected, scattered light etc. These will require some level of re-design and re-writing of the data analysis codes and pipelines during commissioning. The risk is low.
- **Sky Subtraction:** The accurate subtraction of skylines in the red edge of the WFMOS spectra will be critical, as we will be looking for emission lines amongst the strong OH lines. We will explore the use of nod & shuffle to achieve this goal as well as more advanced traditional sky subtraction methods. We will need to explore these in detail during the testing and commissioning phase. Overall, this is a low risk.

Chapter 24 Operations

24.1 Site selection North versus South

24.1.1 Scientific considerations

24.1.1.1 Dark Energy

The dark energy science case is agnostic as to hemisphere. It is expected that good imaging data sets (in optical, NIR, and UV) will exist in both hemispheres and along the celestial equator.

Similarly, the dark energy science case does not depend on the question of Gemini-N versus Subaru, save in the availability of telescope time and speed of deployment.

24.1.1.2 Galactic Archeology

Different parts of the Galaxy are observed more efficiently from different hemispheres: the outer Galactic disk, particularly in the anti-center, is better studied from the North, while the Galactic central regions are better studied from the South.

The science for M31 and M33 discussed here is, of course, only feasible if WFMOS has northern hemisphere access. If WFMOS is limited to the southern hemisphere, the case for using it to explore the fossil record in large galaxies is substantially diminished. The next nearby galaxy group in the south is the Sculptor Group, which contains 5 moderately-sized disk galaxies. Located at 2.5–3.5 Mpc, the most luminous red giant branch stars in these systems have magnitudes of $I \sim 23$ – 24 , putting them essentially out of range for detailed spectroscopy with 8-m class telescopes.

The satellite galaxies of the Milky Way are distributed such that the gas rich Magellanic Clouds are Southern objects, while the gas-poor dwarfs are approximately equally divided. Many of these systems will be targets of other 6–8m class facilities, particularly in the South e.g. VLT/FLAMES; Magellan/MIKE.

On balance, the Northern Hemisphere is preferable for the galactic archaeology aspect of the science case.

24.1.1.3 Input catalogues

Target selection for all science cases will require multicolour imaging data. The basic requirements on coverage and depth for both lead science projects are compiled in Table 31. Considering the existing and ongoing surveys (Table 32) plus planned surveys and new survey telescopes (Table 33 and Table 34), a wealth of resources to create appropriate input catalogues has been recognised.

Table 31 Identified requirements

Requirements	Galaxy Genesis & Stellar Archeology		Dark Energy		
	low resolution	high resolution	z<1	1<z<2	z>2.5
area	400	1500	1000	1000	200
U (u')			20.5	23	25.5
V (g')	22.5	18			
R (r')				24	

Table 32 Existing and on-going surveys

NAME	area [sqdeg]	depth (filters)	Sky Region
SSS	hemisphere	23.0, 22.0 (Bj, R)	south+equatorial
DSSII	hemisphere	22.5, 22.0 (Bj, R)	north+equatorial
SDSS		22.0, 22.2, 22.2, 21.3, 20.5 (u', g', r', i', z')	north+equatorial
SDSS (SGC)	225	24.4, 25.3, 25.1, 24.4, 22.9 (u', g', r', i', z')	equatorial
CFHTLS(VW)	1200	25.0, 25.5, 24.4 (r', g', i')	north+equatorial
DENIS	hemisphere	18.5, 16.5, 14.0 (i, J, Ks)	south+equatorial
2MASS	all sky	15.8, 15.1, 14.4 (J, H, Ks)	all sky
GALEX (AIS)	>35000	20.5 (U_AB)	gal. caps first
GALEX(MIS)	1000	23.0 (U_AB)	SDSS+2dF overlap
GALEX (DIS)	80	25.0 (U_AB)	12 separate fields

Table 33 Planned surveys

NAME	area [sqdeg]	depth (filters)	Region	Geometry
UKIDSS(LAS)	4000	20.5, 20.0, 18.8, 18.4 (Y, J, H, K)	north+equatorial	Sloan strips
UKIDSS(GPS)	1800	20.0, 19.1, 19.0 (J, H, K)	galactic plane	b < 5 deg strip
UKIDSS(GCS)	1400	19.7, 18.8, 18.7 (J, H, K)	north+equatorial	galactic clusters
DES	5000	24.6, 24.1, 24.0, 23.6 (g', r', i', z')	south+equatorial?	??

Table 34 New survey facilities

NAME	hemisphere	Spectral Region	Expected Availability
VST	south	optical	2005
VISTA	south	NIR	2006
NEWFIRM	north	NIR	2006
WISE	all sky	MIR	??
PanStars	north	optical	??
LSST	not decided	optical	2012

Conclusion: Both hemispheres provide sufficient resources in terms of existing data and telescope facilities to obtain any missing data items. The equatorial region with its strong existing and planned coverage can be reached from both hemispheres.

24.1.2 **Resulting instrument complement**

We consider the resulting instrument suites available to the Gemini community for three cases: WFMOS is mounted on (a) Gemini-N (b) Gemini-S (c) Subaru

Assumptions:

- All next-generation instruments should have a significant amount of time available, i.e. at least 6 months per year.
- MCAO is operational on Gemini-S and remains there (since the effort to move it would be considerable)
- On the timescale that WFMOS would be operational, Ex-AO and HRNIRS are also operational.
- The currently existing (or soon-to-exist) Gemini instruments mature as follows:
 - NIRI - retires
 - GMOS-N - stays (need some optical imaging capability)
 - ALTAIR+LGS - retires if Ex-AO on GN (AO capability replaced by ExAO)
 - NIFS - retires if ExAO on GN (NIR IFU capability replaced by ExAO-IFU?)
 - MICHELLE - retires (Mid-IR capability maintained with T-ReCS move T-ReCS North to take advantage of MK)
 - GNIRS - retires (capabilities replaced by HRNIRS, F2, ExAO-IFU)
 - GMOS-S - retires (capabilities covered by GMOS-N and WFMOS)
 - T-ReCS - stays (need Mid-IR capability)
 - Flamingos-2 - stays (near-IR MOS capability likely to be very popular)
 - bHROS - retires
 - NICI - retires (capability replaced by Ex-AO)
 - GSAOI - stays (need IR imaging capability)
- Ex-AO could operate in either hemisphere but South may be preferred because of access to the galactic plane.
- HRNIRS (in MOS mode) operates with MCAO.

Below we present possible instrument suites resulting for the Gemini community. These are suggestions - in practice the demand from the community and the observatory's support model (i.e. the number of instruments that can be supported by Gemini staff) should influence which of the 1st-generation instruments remain in operation.

Table 35 Instrument complement resulting with WFMOS in operation on Gemini-N, Gemini-S or Subaru.

SUBARU	Gemini-N	Gemini-S
<i>Gemini-N option</i>		
	WFMOS	[MCAO]
	Top end change 1 or 2 times/yr	- Flam2 -GSAOI
	GMOS-N T-ReCS [ALTAIR+LGS] NIFS or GNIRS	HRNIRS Ex-AO
<i>Gemini-S Option</i>		
	Ex-AO GMOS-N T-ReCS GNIRS?	WFMOS
		Top end change 1 or 2 times/yr
		[MCAO] -Flam 2 -GSAOI HRNIRS
<i>Subaru Option</i>		
WFMOS	GMOS-N T-ReCS [ALTAIR+LGS] NIFS or GNIRS	[MCAO] - Flam2 -GSAOI HRNIRS Ex-AO

24.2 Support requirements for instrument operation

24.2.1 Instrument change

24.2.1.1 Top end change

The following table outlines the steps and gives estimates of the time involved with a Top-end change.

Table 36. Two operational scenarios for top end change: (I) Staffing level at the observatory allowing only a single shift working some overtime over three days with two nights of telescope shutdown; (II) Increasing staffing level allowing three shifts working over two days and one night with one night of telescope shutdown. Similar would apply to Subaru.

WF MOS Top End Change Steps	Time [hours]	GEMINI I	GEMINI II
Removal of prime focus instrumentation or telescope top end	2	DAY 1	DAY 1
Storage of f/16 top end (* Gemini only)	2	8:00 – 18:00	8:00 – 16:00
Transport of WF MOS top end to dome floor (*Gemini only)	1	incl. 1hr break	incl. 1hr break
Installation of WF MOS top end onto Gemini/Subaru	2		
Installation of WFC front end onto bottom of mounting ring	2		EVENING 1
Installation of WFC back end onto top of mounting ring	2	DAY 2	16:00 – 24:00
Installation of WF MOS instrument package	2	8:00 – 18:00	incl. 1hr break
Service connections	1	incl. 1hr break	
Fiber cable connections	1		NIGHT 1
Counterbalance installation	2		00:00 – 08:00
Storage of handling equipment	1		incl. 1hr break
Configuration of spectrographs	3	DAY 3	
Test of instrument subsystems	4	8:00 – 17:00	DAY 2
Software preparation	1	incl. 1hr break	8:00 – 13:00

The expected time requirement for top end change is 26 and 23 hours on Gemini and Subaru Telescopes respectively. The number of staff required for top end change is a strong function of the availability of assisting technology and training level and could not be assessed at this stage of the project.

24.2.1.2 Spectrograph configurations

The spectrographs will need to be configured and cooled down upon installation of the instrument. It is anticipated that this effort could take 2 days for 1 person given the large number of spectrographs. Gemini should give goals for automation and ease of the spectrograph configuration and initial setup testing in order to minimize the manpower effort required.

It is not yet known if the cryostats should remain cool at all times, including when the WF MOS instrument is not mounted on the telescope or what the cool down times might be. This will depend on the frequency of WF MOS installation. In other words, if WF MOS is used many times throughout the year, it may be better to keep the cryostats cooled down all the time whereas if WF MOS is only

installed for one or two blocks during the year, it may be possible to allow the cryostats to warm up.

Grating changes should be minimal to non-existent depending on the spectrograph design. A VPH high dispersion spectrograph might require frequent grating changes. All other aspects of the spectrographs should be automated.

The manual focus and alignment of a dozen spectrographs can prove to be a very time consuming process. Focus and alignment should be as automated as possible with software that is able to execute a focus run without significant human interaction. The only human input should be to initiate the process and to verify that the correct solution was achieved.

The baseline Subaru option with SDSS and High Dispersion Spectrographs will not require fiber slit changes. They will be effectively mounted permanently to the spectrograph. However, there are potential descope options that might be considered in a conceptual design phase in which high resolution fibers might be interchanged with low resolution fibers. If such descopes are considered for saving expenses in the production of the instrument, it must be noted that the support expenses will increase due to the added effort required to switch the fiber slits.

Likewise, the detectors should remain aligned and fixed to a given spectrograph. The only issue is whether or not to keep them cooled when WFMOS is not in use.

24.2.1.3 *Fiber cable*

The fiber cable will have a connector located near the fiber positioner. This connection will need to be disconnected and reconnected whenever the WFMOS instrument comes off or goes on to the telescope for the Gemini option. The same would be true for the Subaru implementation if the fiber cable is not allowed to drape off the telescope as described in *Chapter 12, Fiber Cable*. However, if the cable is allowed to drape off of Subaru, and proper infrastructure modifications are made for the storage of the fiber positioner, it may be possible to leave the fiber cable connector connected. This would greatly simplify the installation and removal process and would minimize the potential for damage to the connector during installation and removal. It would also allow the full instrument to be operated for maintenance and test modes while off of the telescope.

24.2.2 **Maintenance**

The Subaru baseline with a draped fiber cable allows the instrument to be fully operational for maintenance and testing while off the telescope with minimal accessory equipment. Such off the telescope effort will likely be required on a routine basis in order to maintain proper, healthy operation. It is likely that a full set of tests be performed a few days prior to installation of WFMOS onto the telescope, especially if WFMOS is only used in long blocks separated by lengthy periods of time.

Other times for maintenance would be when failures occur either on or off the telescope.

A proper set of spare components will be required and it is highly desirable to share common components throughout the WFMOS system in order to minimize the number of spare components required to be on the shelf.

At least one observatory staff member will need to be fully trained in the operation, maintenance, and repair of the WFMOS equipment.

24.2.3 Software

24.2.3.1 Data reduction packages

Software for observation preparation, data reduction and archive facilities will be delivered with instrument within the scope described in *Chapter 23, Data Analysis and Handling*. It is intended to use well proven solutions minimising maintenance requirements. A staffing level of 0.25 FTE is expected to ensure implementation of upgrades and inner observatory distribution.

24.2.3.2 Reduction pipeline

Data handling and reduction will be taken over by pipelines with minimal level of human interference. However, some visual data assessment for the purpose of quality control must be implemented. A staffing level of 2 FTE for quality control and 1 FTE for supervision of data flow and distribution will be required.

24.3 Observing scenarios/strategies

Observing scenarios for the Galactic Archaeology survey are described in Section 4.4. Observing scenarios for the Dark Energy survey are given in Section 3.5.

24.4 Scheduling of observations

Scheduling particular WFMOS observations will be based on lunar phase, sky placement, and atmospheric conditions during a WFMOS observing block. Because the fields from the WFMOS Dark Energy case are close to contiguous, in order to achieve high observing efficiency, a given night should likely observe fields that cover a larger range in sky position. Thus, fields from any of the Dark Energy survey, the Galactic Archaeology program, and future programs that are of a smaller P.I. (principal investigator) scale could be optimally selected for observing on any given night. We do not view it as efficient to restrict a given night to a specific program.

Because the time to install or remove WFMOS on Gemini is considerable (approximately 3 days), it is expected that the WFMOS blocks on the telescope will be long. With our current level of understanding, we do not envision WFMOS blocks much shorter than 3 months. Based on the Galactic Archaeology program alone, Section 4.4.5 suggests a block length in the North of 110 days.

24.5 Time allocation selection

The depth and diversity of talent in the Gemini Partnership is a significant enabler toward carrying out the WFMOS Dark Energy and Galactic Archaeology programs. Also, because considerable telescope time is required for the surveys, it

is important to access time from all/most of the national Gemini allocations. Finally, because WFMOS will be funded by the entire partnership, it seems important for representatives from all the partners to participate in the major scientific endeavours.

Gemini time is allocated by the National Gemini time allocation committees (NTACs). One can submit a proposal to multiple NTACs, and such joint proposals are merged into one program at the ITAC (international TAC, which is made up of delegates from each NTAC). Under the current system, a WFMOS survey team would recruit members from each partner and submit the same proposal to each partner TAC. For the countries/partners that give time to this program, the sum of their allocated hours would be given to the WFMOS survey team. This system has two disadvantages for large programs, and perhaps one advantage. The perceived advantage is that the WFMOS science is judged directly relative to other submitted proposals, and the survey team is strongly motivated to produce science competitive with the best other proposals. The current system has made allocations to several joint proposals of fairly large scale, such as the Gemini Deep Deep Survey. However, the scale is small relative to the two surveys proposed for WFMOS.

One disadvantage of the current system relates to multiple teams proposing to undertake a WFMOS survey. It is possible that some NTACs could choose one team, while other NTAC(s) could choose another. This would result in competing teams undertaking the same survey with Gemini, which is not in anyone's best interest. This could be solved by having a partnership-wide competition, organized by Gemini, as to which team would best carry out a given WFMOS survey. This would be announced by a Call for Proposals, and only the team selected by Gemini would be allowed to undertake the WFMOS survey. The NTACs would still determine how much time any partner allocates to the survey.

Another disadvantage of the current system is that the WFMOS survey proposal faces multiple jeopardy over the NTACs. In a more centralized allocation, WFMOS survey time could be taken off the top from the time allocated by the NTACs. This would likely require action by the Gemini Board and Gemini Science Committee to determine the appropriate balance between WFMOS survey time and other time. All the partners would then contribute time to the survey in proportion to their Gemini share. The WFMOS survey would then be allocated a certain number of hours/nights over a certain number of years. Teams would compete to be selected for a particular WFMOS survey. This competition could be done by a special panel that would make a recommendation to the Gemini Director. Criteria might include science experience, planned approach, likelihood of timely analysis, partner representation, and resources brought to work on the survey. This model has the advantage that it assures Gemini time will be allocated over the lifetime of the survey. One potential disadvantage is community protests that too much time is allocated to a survey without a direct competition between P.I.-class science and survey science.

A model similar to that just described was discussed for key projects at the Gemini Operations Working Group meeting in February 2005. Gemini Observatory is discussing such a model with its committee and advisory structure. Gemini is considering implementing a revised time allocation model for a key project that would be done with the Near Infrared Coronagraphic Imager (NICI). Gemini-supported key projects would be the only exception to the current system.

NICI is anticipated to see first light on Gemini South in 2005. Experimenting with allocations for key projects with NICI would be of significant help in having a working process in place for WFMOS.

24.6 *Interleaving WFMOS science campaigns*

The WFMOS Dark Energy case requires a fairly contiguous area of sky (1000-2000 square degrees; survey regions must be at least 15 degrees across). The WFMOS Galactic Archaeology case requests 10-degree-wide stripes in the directions of $l = 0, 90, 180, \text{ and } 270$ with $|b| > 45$. Thus, there is little field overlap between the two major surveys. Thus, for the purpose of estimating the time to complete the surveys, it is practical to think of the two key surveys as independent. Carrying out the surveys independently also simplifies the issue choosing a compromise exposure time per field and a compromise spectrograph configuration common to the two surveys.

However, it should be possible and profitable to interleave future science projects in the two surveys. As described in Section 3.8, one can imagine allowing other investigators to propose for parallel targets in the fields of the WFMOS Dark Energy and Galactic Archaeology survey fields. Such parallel investigators would be required to accept the exposure times and spectrograph configurations of the major surveys. Also, their targets would presumably only be observed if a suitable WFMOS Dark Energy or Galactic Archaeology target is unavailable for a given fiber (plus sufficient sky fibers had been allocated). A parallel capability would be highly advantageous for surveys for rare objects. This capability is not without cost, however. No mechanism currently exists to allocate parallel time in this manner, and the number of fibers/spectra available is not known until the primary program specifies its fiber configuration. Also, special software and operational effort would be required to add these parallel targets, carry out the bookkeeping as to which program is charged, and route the proper data to the proper team. In such a model, individual spectra are the data product, as opposed to the two-dimensional images of MOS spectra.

24.7 *Distribution of data products for maximum science impact*

The distribution of data products including the issue of proprietary rights should be looked at by Gemini Strategy and operations Committees. The committee may want to consider for example (a) ensuring a good balance across the partnership for those involved in the primary science projects (b) securing some benefits for science and instrument teams.

SECTION V: WFMOS PROJECT ORGANISATION AND MANAGEMENT

Chapter 25 Organisation and Management

25.1 Introduction

This section outlines the organisation and management arrangements that will be required for the project to design, build, test, integrate, deliver and accept but not commission (the design/build project) a WFMOS instrument to Hilo in accordance with the requirements stated in AURA Contract No. 0084699-GEM00385 and judged as necessary by the AAO consequent on the outcome of this Feasibility Study Report.

Organisation structures generally develop as a result of perceived and planned actions and also as a reaction to problems experienced in achieving an organisation's goals. The experience of the WFMOS Feasibility Study combined with the past experience of the AAO with astronomy instrumentation projects has been drawn from to develop a model for the design/build phase of WFMOS.

It is likely that the range of expertise and resources required to build such an instrument and have it delivered and ready for commissioning some 5 to 6 years after contract approval will require a consortium of expert organisations to achieve and good management.

Different culture, methods and project effort spread over a number of organisations will place significant focus on organisation and management arrangements, on risk management and on quality aspects achieved through progressive test/acceptance regimes and through configuration control.

WFMOS is by any astronomy instrumentation standards, a very large and high cost instrument and has significant cost / delivery risks. These are discussed below and a model for managing such issues is proposed.

25.2 Organisation

The focus and effort required to deliver the design/build project outputs has to be clear and subject to regular review by the design/build organisation in conjunction with Gemini. The lead organisation would be the Prime Contractor; all support organisations would be sub contractors to the lead organisation.

Expertise and availability of the key resources needs to be taken into account when setting objectives within the build plan. The performance of various organisations that have participated in the Feasibility Study and the preparedness to commit to firm planning objectives should be a major factor in the selection of the build team.

The organisation that is established will have to reflect the fact that work is likely to be distributed across a number of sub contractors that are spread across the world. Configuration management, change control, quality assurance, integration and acceptance testing will be critical issues and arrangements will need to be put in place to achieve the required level of control and to minimise risk.

The key risks will be cost escalation through prolongation as a result of poor interfacing, protracted integration activities and the identification of technical and performance issues late in the schedule of work.

Although organisational arrangements need to reflect cultures and styles, track record and commitment of resources to meet the agreed distribution of work must be the essential factor in determining the participants and the organisation structure has to be able to exert control. Agreement in advance to the allocation of resources to the plan and the acceptance of direction from the Prime Contractor's representative is needed.

It will be essential to achieve a sound plan at the start that recognises the relationships between the various activities and the coordination and management arrangements that are necessary to provide the deliverables at the milestone dates indicated in the build schedule.

25.2.1 Proposed Organisation Structure

The need for tight management and coordination will require the establishment of a Project Office.

The Prime Contractor would operate the project office with members of the Gemini organisation being part of the function from time to time. The project office would be a full time activity and would focus on project management with emphasis on planning and control.

Although quality would be part of the project management function along with acceptance procedures, interface control, configuration management and technical liaison responsibilities, if indeed there is likely to be a significant level of work distribution across a number of other organisations acting as sub contractors, the level of interface control, resolution of technical issues and integration would be high at times and should not degrade quality and acceptance procedures. A sound plan and active risk management practices will be required.

It will be important to introduce a strong QA focus on a progressive basis with focus on integration issues and acceptance during production as early as possible in the cycle and being conducted at the manufacturing organisations premises.

Integration and testing prior to commissioning will be a major issue in such an instrument and focus must be placed on management of the risk associated with these activities, as failure to do so will incur delay and cost penalties if significant problems are detected later in Hilo or during commissioning.

A separate Quality and Acceptance Cell should be considered. This should be staffed by Gemini and the Prime Contractor to focus on early checking, testing and acceptance prior to shipping components and sub assemblies to Hilo. The prime contractor project office would coordinate the operation of this cell but the QA cell would report directly to the Prime contractor's management and the Gemini Project Office.

A typical organisation structure is shown in Figure 248.

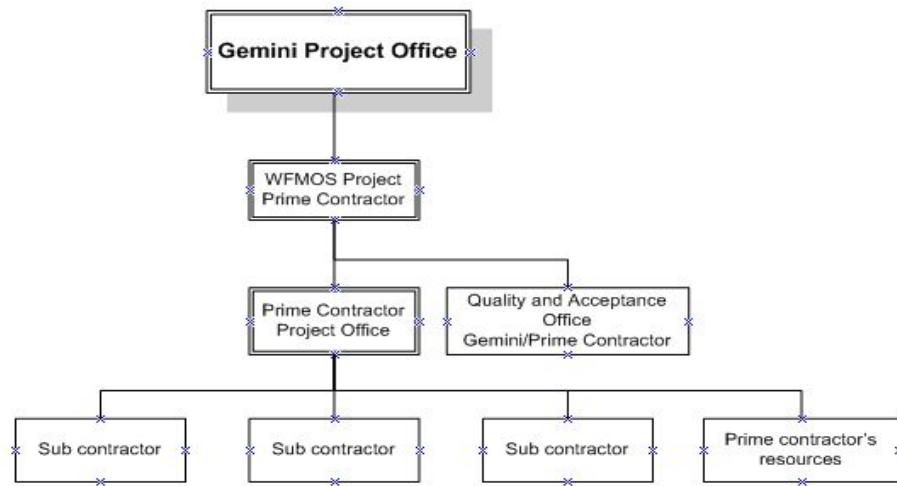


Figure 248 Typical organisational structure

Without getting into deep philosophical discussion regarding pure project organisations vs. matrix organisations, it is clear that the WFMOS project will face a large-scale, one off type activity with geographical disbursement of work, drawing resources from different independent organisations with different local work practices and reporting/responsibility arrangements. These issues must be addressed by Prime to sub contractor relationships using strong “integrator” activities applied through a strong matrix type project management arrangement with all participating organisations bound by an appropriate contract and MOU.

Project Management is about planning and control; a strong matrix style has to be able to apply sufficient control to maintain both schedule and cost objectives whilst allowing expert team members sufficient freedom to react appropriately to the emerging technical and logistic issues.

25.3 Management

The design/build project activities for WFMOS will require strong management arrangement as shown below.

25.3.1 Key Management Issues

The key issues that have to be managed are:

- Control of work - across a number of sub contractors
- Maintaining a relevant plan including a sound schedule for all work
- Schedule Management – this means achieving good feedback into the planning cell to maintain a relevant plan that points to issues of slippage in the program.
- Cost Management and Control – watching cost trends, anticipating cost escalation and taking appropriate mitigation action

- Project Risk Management – conducting a thorough risk assessment at the planning stage, maintaining a sound risk register and risk watch list and initiating appropriate mitigation actions.
- Configuration Management – operating and maintaining good control over documentation and change management.
- Progressive testing and QA – to ensure that all variations from specified performance are identified as early as possible, are rectified in process and are not allowed to accumulate to the formal testing and acceptance phase of the project.
- The disbursement of work to various subcontractors will emphasize the need for a formal and active QA program operated at the point of acceptance and as early in the process as possible.
- Reviews will be an important part of the QA process and the nature of the instrument and the likely consortium arrangements for design/build etc will require that reviews are held for major component parts of the instrument such as the fiber positioner or the spectrographs. An additional consideration will be the location of manufacture and the critical path/time and integration considerations. The fastest way through the schedule should have a major influence on the grouping of components for reviews.
- Commissioning issues – needs to be planned on the basis that time periods are allocated in advance based on an agreed and formal program of commissioning activities. Commissioning may be able to be progressive enabling particular features of the WFMOS instrument to become operational on a progressive basis.
- The time planned for the telescope area should be minimised to avoid staff stress and low efficiency. The maximum amount of testing that can be done prior to going on to the telescope will reduce expensive and disruptive on – telescope activities. The scope of this Feasibility Study has not covered commissioning detail.

25.4 Management Arrangements

25.4.1 Contracting Arrangements

A single Prime Contractor would manage the design/build/commission project. This Prime Contractor may need to be supported by other institutions operating as sub contractors all of which would bring specific scientific and technical experience relevant to the requirements of the scope of work expressed in the contract.

The nature of the contract will be an important issue to be decided. Firm fixed price contracts place a high risk on the Prime Contractor and in order to hedge against this risk a contractor will need to inflate price. Some risk sharing basis for the build contract must be investigated or at least cost risk minimised to avoid contract cost escalation.

Significant costs will be involved and progress payments including advanced payments on project start up and on receipt of equipment and component parts needs to be agreed.

25.4.2 Management Arrangements and Focus

The key focus of the management arrangements would be on the following aspects:

- Maintaining progress to meet scheduled dates for the deliverables
- Monitoring the quality of the deliverables of the project
- Managing the logistics created by geographical separation of the production centres, and
- Controlling cost

The management arrangements must be strong in terms of the level of control that can be applied – this is a feature of the contract and the track record of the participants.

A sound Project Management approach based on an agreed project cycle will be needed. Regular “in-process” QA will reduce the risk of cost escalation and prolongation. Also it will be necessary to implement significant pre-commissioning testing and acceptance regimes to avoid long and disruptive periods of commissioning at altitude.

Logistics management will be a feature of a dispersed production arrangement – as major parts will come together for integration in Hilo. This places importance on “in-process” QA and may offer an opportunity for progressive commissioning as various parts of the overall WFMOS system functionality become available.

Project Management will cover the Initiating, Planning, Executing, Controlling and Closing the project. A project team will be required to ensure progress, quality and cost control. It is recommended that a Project Office be established for the WFMOS design/build project.

A strong matrix management form of organisation structure has to be agreed with all participating consortium members in advance and track record and commitment to the objectives is an essential feature of the selection of such participants. The structure will bring together the essential mix of experience and commitment necessary to manage the project and contain costs.

Matters that will require management effort are:

- Establishing clear project goals
- Preparation and maintenance of an agreed and fully resourced schedule of activities with all resources committed to the goals and milestones set
- Coordination and integration of effort between the various centres of expertise (team members)

- Establishing the progress of work and reporting to the Prime contractor's project office and to Gemini
- Maintaining arrangements within the team for information exchange, reporting of progress and for the direction of corrective actions as required to meet previously agreed and scheduled objectives
- Timely exchange of knowledge and experience relevant to the goals set
- Maintaining coherent and timely action by all subcontractors (the other Institutions) within the overall project responsibility of the Prime Contractor.
- Monitoring of budget and costs

25.4.3 Management arrangements for control of work

The management arrangements for control of all work are indicated at a high level in paragraph 25.2.1, on page 448.

The tasks required to deliver the design/build scope of work are shown in the schedule and in the Work Breakdown Structure (WBS), detail of both are in Chapter 26.

Wherever possible, work packages that are self-contained and allow for design, build, test and acceptance to pre-determined test/acceptance criteria should be managed and controlled for quality within that one organisation with audit from the Prime contractor's project organisation.

25.4.3.1 Quality Management

This will cover documentation, version control and the deliverables. A procedures and documentation format for the design/build project would be prepared by the Prime contractor's project office and issued as a template outline for guidance of all team members.

25.4.3.2 Schedule Management

The Prime contractor's project manager would manage the scope of work and the schedule issues. The schedule for the design/build will show the key deliverables and will be populated with sufficient milestones to provide for monitoring and control of the scope and timeline aspects of the deliverables.

Regular and periodic reporting to the Prime contractor's Project Office by the sub contractors will be essential to enable the project plan to be maintained and allow for corrective action in the event that variances occur that threaten the objectives.

25.4.3.3 Cost Management

This is discussed in more detail in Chapter 27, which addresses cost structure and cost estimates.

The schedule issued for the scope of work would be the authority to incur expense on the project and all variances to the issued plan would need to be reported with

recommended actions to compensate or correct the variances. Control of this process would need to be distributed at the work interface level but overall management control would be required at the Prime contractor's project office.

The Feasibility Study report provided cost estimates for the baseline case and for various options. These cost estimates are considered to be reasonably reliable having been based on existing or low risk technology. All costs have been estimated using experience and after breaking system component costs down to provide for better analysis and accuracy.

Cost estimates are expected to reduce with further work during the concept design phase as the prime contractor will then be able to focus on the use of common design features across all areas of the design effort and this in turn would enable a degree of commonality in component and equipment selection enabling lower procurement and running costs. The use of common components may require issue of standards from a project technical office.

The prime contractor's project office would be expected to maintain a program of cost reduction initiatives such as the following:

- during concept design; look at the use of 'other' instrument designs to reduce design effort
- look at commonality of spectrograph software
- software could benefit of common approach and by getting standards set and compatible to reduce interface issues and management effort
- software effort could be co-located and design effort shared
- seek to share designs and ensure cohesive approach

25.4.4 Grouping of work scope components

Grouping of work components will be essential to facilitate ease of management and to reduce overhead costs. There are sound arguments for identifying work grouping such that closely assembled and tightly integrated arrangements with complicated and interrelated interfaces are kept together.

The following table indicates a possible separation of work:

Group 1

Fiber positioner

Top end – design and integration issues

Corrector

Structure

Optics design

Optics procurement and acceptance

Fiber cable

Fiber connector

Guiding (in fiber positioner)

Acquisition System

Wave Front Sensing System

System Architecture

Group 2

High Resolution Spectrographs

Group 3

Low Resolution Spectrographs

Group 4

Infrastructure

Group 5

Calibration System

Group 6

System Software

Group 7

Data Pipeline and Archiving

25.4.5 *Management aspects of logistics issues*

There could well be benefits and cost reductions that derive from good planning and foresight such as:

- Use of a common carrier for the movement of personnel and equipment; it is possible that Gemini could organise this.
- Where the cost of movement of large items is high, cost containment should be investigated by seeking opportunity to manufacture such items close to the final destination (Hilo).
- Optics may need to go to the prime contractor or that part of the organisation manufacturing the corrector prior to going to Hilo.
- Another example of potentially high cost logistics is the Top End. The top end can go direct to Hilo post manufacture or possibly manufactured in Hilo.

- There is a sequence that may offer easier and cheaper acceptance and make for better handling of component parts in Hilo, this order would likely be as follows:
 - Infrastructure
 - Top end structure – can wait to be fitted
 - Corrector
 - Low Resolution Spectrographs
 - High Resolution Spectrographs
 - Fiber Cable
 - Positioner and related top end system components

25.5 Project Documentation

During the conduct of a design / build contract for the WFMOS instrument, documentation systems will be necessary to control work scope, quality aspects and to drive the effort of the design, build, test, integrate and deliver phases.

25.5.1 Configuration Management

The WFMOS instrument will be a high-technology product and it is very likely that a number of institutions from various parts of the world will contribute to the design, build, test and later the commissioning of such an instrument.

In order to avoid any adverse effect on project cost, schedule or technical objectives, a formal process of systematic change control and coordination must be integrated into the overall project management and control arrangements.

Proper configuration management will be essential to ensure that the end product is built, assembled, tested and set to work in accordance with the projects stated and confirmed objectives.

The aim of such a system would be as follows:

- To ensure that the original or formally amended work scope and work release orders with accompanying schedules, budgets and statements of work are clearly agreed to by the persons responsible for execution.
- To monitor the work to ensure that it is meeting and not exceeding specifications.
- To screen tasks for potential cost or schedule overruns that may signify increased work scope and to initiate quick action to correct any problems identified.
- To require that any engineering and work changes are documented as to their effect on work orders, budgets, schedules and contracted prices and are reviewed and authorised by sign off.

The components of this plan include:

- The handling of the contractual changes
- The handling of the interfaces internal and external to the instrument
- The handling of technical changes

A series of design reviews would be necessary to maintain a level of audit control on the design but configuration management will be necessary to ensure that the agreed “paper” output of the design effort is properly maintained and is later followed to deliver the functioning “as designed” end product.

The output of the joint engineering effort will be paper drawings, code, specifications and process instructions to define the construction and function of the instrument. This is particularly important when the production boundaries spread across a number of organisations on different continents with different culture and standards.

A proper configuration management system will be required to ensure that all drawing and documentation is well managed to see that it is correct; changes are approved and properly implemented with agreed numbering systems and change procedures.

Software will require special arrangements to ensure control of configurations, versions, releases, changes and defects.

Gemini have allocated a block of drawing numbers, there will be a requirement for written drawing and document control from numbering through to change, release arrangements to tie up all details.

The successful project organisation will need to set up and manage the requirements of the contract and apply quality and configuration management that focuses on the above objectives

25.5.2 Configuration Item Data

As discussed at 25.5.1 above, proper configuration management will be essential to ensure that the end product is built, assembled, tested and set to work in accordance with the projects stated and confirmed objectives.

A full listing of all configuration item data will need to be maintained. Such a list would include:

Applicable Documents

No AD	Document Title	Reference

Reference Documents

No RD	Document Title	Reference

Top Level Requirements Documents

A typical range of documents would be maintained as shown below.

DOCUMENT TITLE	REFERENCE	ISSUE	DATE
Fiber Positioner, Statement of Work			
Software Management Plan			
Software Configuration Control Plan			
Management Plan			
Project Plan and Schedule			
Configuration Control Plan			
Product Assurance Plan			
Safety Compliance Plan			
Design and Development Plan			
Configuration Item data List			
Instrument Commissioning, Calibration and Science Verification Plan			

Requirement Specification/Design Specification on item level

A typical range of documents would be maintained as shown below.

DOCUMENT TITLE	REFERENCE	ISSUE`	DATE
Directive for Preparation of Technical specification			
Requirements for Safety Analysis			
Optics: Design of Telescope Optics			
Observatory Requirements for Instruments			
Environmental Specification			
Service Connection Point, Technical Specification			
Electronic Design Specification			
Electromagnetic Compatibility and Power Quality Specification			
Electromagnetic Compatibility and Power Quality Specification			
General Safety Requirements for Scientific Instruments			
Instrumentation Software Specification			

Software Configuration Control Plan

While this document largely describes what will happen from delivery of the software, certain aspects must be implemented from early in the project in order to provide the necessary support. It is also necessary that we correctly document software changes throughout the development stage.

The basis of our source code management system must be described.

System Release Management should be consistent across the Gemini Observatory.

DOCUMENT TITLE	REFERENCE	ISSUE	DATE
Instructions for Provisional Acceptance of Products			
Lower Level Specification			

Identification of Deviation (Change Notice - Request for waiver)

Technical Changes must be managed as described in a contract Statement of Work.

Changes would be listed as follows:

DOCUMENT TITLE	REFERENCE	ISSUE	DATE
Change detail			
Change detail			

Both contractor and Gemini initiated changes must be listed.

25.5.3 Definition of Hardware / Software

During a major design / build contract, a wide range of documentation will need to be maintained including the following:

25.5.3.1 List of Manufacturing Drawings

Drawing Number	Title	Revision

25.5.3.2 Analysis Documentation

A list of deliverable documents to be provided under the contract:

DOCUMENT TITLE	REFERENCE	ISSUE	DATE

25.5.3.3 Design Documentation

A list of design documents to be provided under the contract:

DOCUMENT TITLE	REFERENCE	ISSUE	DATE

25.5.3.4 *ICDs and Data List*

A list of ICD and Data Lists to be provided under the contract:

DOCUMENT TITLE	REFERENCE	ISSUE	DATE

25.5.3.5 *I/F Control Drawings*

A list of interface documents to be provided under the contract:

DOCUMENT TITLE	REFERENCE	ISSUE	DATE

25.5.3.6 *Drawings*

Drawing Set

This list would provide details of how drawings would be prepared including the likely coverage of the drawing set and the drawing format to be used.

Drawing Numbering System

The drawing numbering system to be used would be as required by Gemini – a block of numbers has been allocated during the Feasibility Study.

Chapter 28 Risk Management & Cost Mitigation

28.1 Introduction

Risk management will be an essential management component of the WFMOS design/build as this project will most likely be required to manage technical, cost and logistics risks across a number of organisations in different parts of the world.

The major focus of management during the proposed WFMOS design/build project will be the management of cost. Technical risks are seen as low as much of the technology proposed exists already or is based on existing and well understood technology.

There are a number of factors that will affect the ability of the project team to complete the project within budget and these include:

- Resource planning (who will do what, when and also the equipment and materials required to do the project)
- Cost estimating (developing the cost for the resources required to do the project)
- Cost budgeting (allocation of project cost estimates to the various tasks and work centres)
- Cost control (management of project budget changes)

The WFMOS project will also be sensitive to logistics and failure to manage logistics will result in prolongation (with consequential cost impacts).

Cost escalation is a factor of poor initial planning, poor estimating and lack of proper control during the development phase.

The following details recommend an approach for identification and management of risk.

28.2 Risk Management

28.2.1 Approach to Risk Management

A formal risk management process is required and must be applied across all phases of the design, build, integrate, test and deliver work program.

To be successful in the management of such a large and high cost project with the likely involvement of a number of organisations working in a contractor/sub contractor relationship and very likely in different continents, a good culture of risk management will be essential under the umbrella of project management.

The following definitions need to be understood:

Risk - an uncertain event or condition that, if it occurs, has a positive or negative effect on the project's objectives (clearly our major concern is with negative effects).

Risk assessment - the overall process of risk analysis and risk evaluation.

Risk management - the culture, process and structures that are directed towards the effective management of potential opportunities and adverse effects, see Risk Management overview figure below.

Risk Management overview

The purpose of the risk management will be to minimise the risk of not achieving the project objectives and to identify and take advantage of opportunities that may emerge.

The process is continuous throughout the project and relies on establishing the context and then identification, analysis, evaluation and treatment. There is a need for effective on going communication and for monitoring and review. Figure 252 has been extracted from the Australian Standard for Risk Management and outlines a typical process:

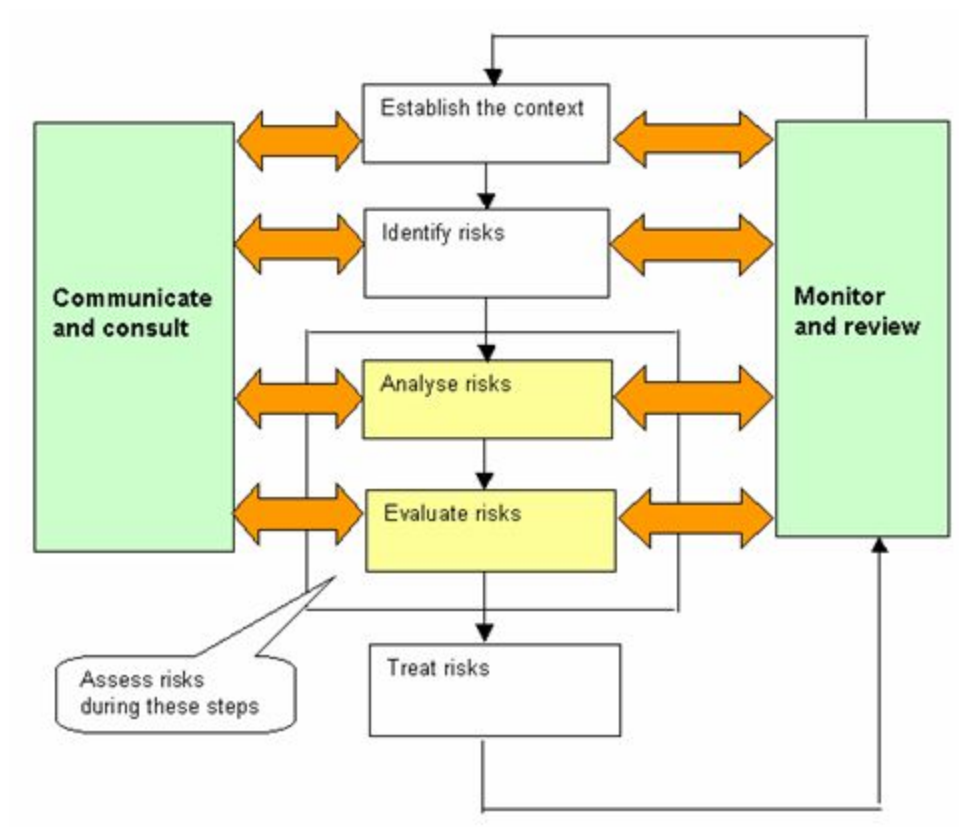


Figure 252 Risk Management Process Extract from AS/NZS 4360:1999

Process starts - when we establish the context and is an iterative process of continual improvement. It applies throughout the typical project cycle from initialisation until completion.

Monitor and review - the performance of the risk management system is assessed by the Project Manager together with Resource Centre Managers and key project staff such as the Project Engineer

Communicate and consult - is continuous between the project team and all stakeholders.

The nature of risks that are identified changes as work progresses through the project cycle. Early in the cycle concepts and technology issues are paramount whilst later in the cycle supply issues, facility problems, resource availabilities and matters impacting transport, access and commissioning come into better focus.

28.2.2 **Application of Risk Management**

As Risk Management is a continuous process during the project cycle, efforts are directed at the establishment and maintenance of risk assessment as shown below.

Risk assessment would be conducted regularly by the project manager together with the project engineer and the key technical and scientific staff involved across the entire project team.

The aim would be to establish a Risk Assessment table that lists risks together with their probability, impact on the project and to rank these such that those that have the greatest potential to bring negative impact on the objectives in terms of compliance with specification and cost and schedule goals are identified and managed. This has to be a dynamic process as things change during the cycle.

Management of risk may mean elimination of the risk but in many cases it means mitigation and this requires a course of action to be determined, responsibility to be allocated for applying and monitoring the course of action and making corrections as necessary.

28.3 **Risk Mitigation**

28.3.1 **Identification of Key Risks**

The following have been identified as being the more significant risks that can either hinder deployment of the WFMOS instrument or impact the scientific viability.

28.3.1.1 *General*

The following risks apply to the overall instrument:

Risk	Consequence
Funding is not forthcoming	Project does not proceed
Gemini / Subaru political alliance issues	Project does not proceed
Working at high altitude (health)	Environmental aspects of working at altitude need to be factored into planning and quality testing prior to final tests and commissioning at telescope. Risk to commissioning
Environmental	Risk that selected materials may degrade
	Risk that components and/or assemblies may fail to work to specification

Risk	Consequence
Lack of standards and well defined interfaces (ICDs) - e.g. earthquake tolerance	Risk that components won't fit to existing infrastructure – e.g. Failure of Top end to telescope interface would lead to major impact on the project
	Risk that components may not fit and/or will fail to perform to specification. Extensive on-site work may be required (at altitude) to get things working
	Failure to achieve technical compliance with specification

28.3.1.2 Management and Logistics

The following risks apply to the overall management and logistics:

Risk	Consequence
Inadequate or ineffective Project Control	Impacts cost, schedule and system performance
Late delivery of major system components to meet schedule	Delays schedule and integration, adds cost
Work distributed across a number of different institutions	Risk that the project coordination is poorly controlled
Standardization	Risk that different design tools used in different institutions cause confusion and errors
	Duplication of effort
Single point specialists	Risk of delay and/or loss of expertise
Security of long term partners	Continuity of work packages and delivery to schedule threatened
Exchange rate variations	Cost variations – could increase
Inadequate planning and estimating (this goes on during the project)	Risk to cost and schedule compliance
Cost escalation and prolongation due to poor estimating	Risk to cost and schedule compliance
Poor risk management process	Risk to cost and schedule and technical performance
Damage in transit	Cost for repair and/or remanufacture and delay to program
Inadequate integration, test and acceptance procedures	Emergent technical and performance issues that delay the program and add cost. May also increase work done on site.

28.3.1.3 Science

Risk	Consequence
Science gets enabled by others	Instrument usefulness gets devalued.

28.3.1.4 Electronics

The following risks apply to the overall electronics:

Risk	Consequence
Electronics packaging and space availability – top end is inadequate	Needs more space and degrades instrument performance
Instrument power dissipation	Heat problem cause degraded instrument performance, cooling adds cost and mass

Risk	Consequence
Too heavy	Telescope performance impacted and/or cost incurred for counterbalancing
Interfacing issues not managed properly	Degraded instrument performance or failure to function to specification, delay and cost impact and more work required on site.
Component environmental compliance	Degraded material and instrument performance
Electro magnetic compliance (EMC) not achieved	Degraded instrument performance, interference to existing systems
Failure to standardise components to limit variations wherever possible	Higher cost and effort for manufacture and maintenance

28.3.1.5 Detectors

The following risks apply to the detectors selected:

Risk	Consequence
Higher cost than estimated	Cost impact
Availability	Delays development or forces alternate component selection – performance could be degraded
Characterisation is not done to schedule or to specification	Cost escalation and extension of schedule – instrument does not meet specification
Availability of new higher performance detectors during committed work program	Redesign – time and cost impact, major program disruption

28.3.1.6 Software

There are some overall software type risk issues, more detail is given in the parent chapters:

Risk	Consequence
Estimates wrong	Project cost and schedule extensions
Instrument Software integration fails	Project cost and schedule extensions
Gemini (or Subaru) Integration fails	Project cost and schedule extensions
Hardware not delivered early enough to enable proper and timely software testing (reflected in the deliverable schedule).	Project cost and schedule extensions
Lack of understanding of data reduction techniques required	Impacts data quality
Algorithms don't work	Project cost and schedule extensions

28.3.1.7 Product Specific Risk Comments

28.3.1.7.1 Corrector

The following risks apply to the corrector:

Risk	Consequence
Availability of appropriate quality glass materials	Degraded performance and potential time and cost impacts
Fabrication of surfaces - design requires aspheric surfaces	Performance and delivery impacted
Design risk – can the same design be used for both WF MOS and HyperSuprime Cam?	Cost and performance impact
Breakages	Delivery and cost impact
Test issues and alignment	Performance, time and cost impact
AR coating	Performance, time and cost impact

Risk	Consequence
Mechanical flexure and the ability to maintain tolerances	Performance impact

28.3.1.7.2 Top End

The following risks apply to the top end structure:

Risk	Consequence
Mass/ stiffness	Impacts telescope performance

28.3.1.7.3 Fiber Positioner

The following risks apply to the fiber positioner:

Risk	Consequence
Packing into available space	Performance impacted
Robustness not adequate	Reduced reliability and increased cost of maintenance
Maintainability difficult	Increased support costs and extended down time

28.3.1.7.4 Fiber Cable

The following risks apply to the fiber cable:

Risk	Consequence
Fragility – breakage and strain	Degraded performance and / or instrument inoperable
Throughput poor	Degraded performance
Excess weight of fiber cable	Impact on telescope performance
Availability of selected materials (single supplier for high performance fiber)	Degraded performance, longer delivery, and higher cost

28.3.1.7.5 Fiber Connector

The following risks apply to the fiber connector:

Risk	Consequence
Throughput falls below goals	Degraded performance
Tolerances on components not met	Degraded performance
Poor image quality of microlens arrays	Degraded performance
Poor ease of use	Impacts operations and maintenance
Durability	Degraded performance and / or instrument inoperable

28.3.1.7.6 LoRes Spectrograph

The following risks apply to the low dispersion spectrographs:

Risk	Consequence
Non availability of optical materials (CaF2 in particular)	Forces redesign – delays program, cost and schedule impact
Inadequate resolving power	Degraded performance
Inadequate spectral coverage	Degraded performance
Low throughput	Degraded performance

28.3.1.7.7 HiRes Spectrograph

The following risks apply to the high dispersion spectrographs:

Risk	Consequence
Late delivery of materials for the custom Echelle gratings	Cost and schedule impact
Inadequate resolving power	Degraded performance
Inadequate spectral coverage	Degraded performance
Low throughput	Degraded performance

28.3.1.7.8 Acquisition & Guiding

The risks for acquisition and guiding are considered to be relatively minor.

28.3.1.7.9 Wave Front Sensing

The following risks apply to the wavefront sensors:

Risk	Consequence
Does not perform to specification	Degraded instrument performance

28.3.1.7.10 Calibration Systems

The following risks apply to the calibration system:

Risk	Consequence
Does not perform to specification	Degraded instrument performance

28.3.1.7.11 Wobble Plate

The following risks apply to the wobble plate:

Risk	Consequence
Does not perform to specification	Degraded instrument performance
Premature component failure	Degraded instrument performance, higher cost and increased maintenance cost

28.3.1.7.12 Subaru Infrastructure

The following risks apply to the Subaru facilities:

Risk	Consequence
Lack of definition	Extended commissioning period, impact on cost and schedule

28.3.2 Risk Management Plan

The key is to establish regular risk watch activities based on progressive assessment of the risks that exist at that time in the project cycle. As mentioned above, risk assessment is continuous and a Risk Register is maintained with action items that allocate responsibility for control and management of the identified factors in a pro-active manner.

An example of the Risk Register is shown at section 28.5. Explanations of the various components of the table are at sections 28.6 and 28.7. An example of how this may be applied to a specific component is given at section 28.8.

The Risk Register sets the basis for identification and management of risk and assigns responsibility on a priority basis.

A risk watch process should be operative throughout the entire project under project management with both contractor and subcontractor representatives involved in monitoring actioning and updating the Risk Register as risk is identified and corrective action taken.

28.3.3 Insurance

The WFMOS instrument and a number of the major components will be high cost. Risks exist during manufacture, test and specifically during movements of component parts, equipments and assemblies.

The major contractor for the design/build of WFMOS should carry combined public and product liability insurance. The risks of damage during movement of component parts, equipment and assemblies should be handled on a case-by-case basis as part of the logistics management arrangements.

For the purpose of insurance, the insurance value would be calculated as the commercial value of the items plus freight and other transport charges and then marked up by say 10% to cover the unplanned costs for associated with repair and replacement actions.

In our cost estimating for the WFMOS project, an allowance has been made for the cost of logistics and this covers staff labour for planning and management of logistics and for transport, packing and insurance.

28.4 Cost Mitigation

28.4.1 Cost risks

The major cost risks have been identified as an output of this Feasibility Study and must be confirmed at each phase of the design/build program.

Cost estimates have been made on the basis of experience and actual prices obtained from potential suppliers.

During planning, most major elements should be estimated as a “most likely” cost qualified with confidence limits. Such cost estimates would be represented as “optimistic”, “pessimistic” and “most likely” costs for the purpose of analysis.

Cost components can be subjected to an analysis within a model using the levels of uncertainty identified using a simulation technique to provide a single point estimate with a probability distribution. Each major item and/or assembly that is made up of a number of estimates represents a single point estimate with a confidence level – this confidence level is a measure of cost risk. This is the same for both labour and capital cost estimating.

Regression analysis provides details of those components within the major item or assembly that will contribute most to the total cost and to cost variations and so by management of these items we can establish a focus for cost control and achieve best effect in terms of controlling cost variations.

The use of software tools (such as Palisade @Risk) to simulate variations in the estimates and to create a single point estimate with a statistical probability

attached – will enable assessment of possible cost risk. The continued use of such a tool to update and provide the best set of data within a cost model is recommended for cost risk management. This tool can also be used integrated within the project schedule and will provide forecasts of both schedule and cost variation.

28.4.2 Cost mitigation approach

Cost mitigation can be achieved by use of the Risk Watch system and by seeking to progress through the schedule of work by the fastest route. Reviews are important but it will incur delay on some items if we force all components and sub assemblies to be reviewed at the same time. The fact that the team to build such an instrument is likely to be located in different parts of the world also adds a cost dimension to this.

Attention to scope of work and ensuring that scope creep does not occur and that progress is maintained expeditiously are the best means of keeping costs under control.

Project Management must be centralised for planning and overall control but local project management (or work package management) will need to be active in each part of the organisation that is involved with the WFMOS project.

As progress is made through the scheduled work, opportunities will emerge to use different technology or other means to achieve the scope of work agreed. These opportunities may also come up from the risk watch as risk can have a positive or negative effect on the project's objectives.

28.4.3 Logistics Risks

The movement of items from various manufacturing points around the world to a single point for integration and pre-acceptance testing is a cost driver and will introduce the risk of damage, loss and delay.

Logistics issues cover, packing, transport of materials and equipment, the movement of people to meet planned project requirements.

Delays can result if we allow the manufacture and progress of component parts and sub systems to move independently or to meet some artificial "latest date" milestone. Delays will cumulate and so early dates should be targeted and movement of components and sub systems would be achieved to meet the plan early rather than at the latest possible date.

Grouping of work packages and tight integration of those that are clearly tightly interdependent with interfaces that require tight management should be considered, the following groupings indicate a possible arrangement for the various system components:

Group	Work package
1 (top end-mounted components)	Fiber positioner
	Top end – design and integration issues
	Corrector
	Structure
	Optics design
	Optics procurement and acceptance
	Fiber cable
	Fiber connector
	Guiding (in fiber positioner)
	Acquisition System
	Wave Front Sensing System
	System Architecture
	2
3	Low Resolution Spectrographs
4	Infrastructure
5	Calibration System
6	System Software
7	Data Pipeline and Archiving

28.4.4 Technical Risks

The technical risks for the project are considered to be manageable. All major technologies planned for use and reflected in the costing and schedule output from this feasibility study are well understood and at most, the WFMOS project makes only incremental advances in this area.

Technical risks associated with each sub system are discussed within the relevant chapters; none of these are seen to be insurmountable with proper risk management procedures in place.

28.5 Example Risk Register Format

E	Element	Risk Number	Risk	Controls	L	C	Risk Priority	Actions	Status
1	Element 1	1.01							
1	Element 2	1.02							

Key

E Element number

28.6 Risk Priority Ratings

Risk priority ratings

Likelihood	Consequences				
	Negligible E	Minor D	Moderate C	Major B	Catastrophic A
A: Almost Certain	Medium	Major	Extreme	Extreme	Extreme
B: Likely	Minor	Medium	Major	Extreme	Extreme
C: Moderate	Minor	Minor	Medium	Extreme	Extreme
D: Unlikely	Minor	Minor	Medium	Major	Extreme
E: Rare	Minor	Minor	Minor	Medium	Major

28.7 Likelihood ratings

Likelihood ratings

Rating	LIKELIHOOD
A	ALMOST CERTAIN: Very high probability of occurrence could occur several times during the project or coming year.
B	LIKELY: High probability may arise once or twice during the project or in a one to two year period.
C	MODERATE: Possible, reasonable probability that it may arise during the project or in a five year period
D	UNLIKELY: Plausible, unlikely during the project, reasonable probability that it may arise in the next ten years.
E	RARE: Very low likelihood, but not impossible, unlikely during the next ten years.

28.8 Example of Risk Register – CFRC Top Ring for Gemini

E	Element	Risk Number	Risk	Controls	L	C	Risk priority	Actions	Status	Responsibility
1	Concept Design	1.01	Too high or too wide to fit in the dome	Careful checking and review on site	B	B	Extreme	Obtain up to date drawings and data from Gemini. Check the clearances in all positions of the telescope. Discard proposals which are too close for comfort.	Under review	
1	Concept Design	1.02	Design structurally not sound	Design analysis	D	A	Extreme	Obtain FEA model Of the telescope. Conduct and verify the FEA under all conditions.	Under review	
1	Concept Design	1.03	Mass and/or dimensions of the payload (instrument) different than expected	Schedule	B	B	Extreme	Allow in schedule for substantial changes and additional FEA	Under review	
1	Concept Design	1.04	Material not suitable for environmental conditions	Analysis	D	C	Medium	Supply appropriate ICD to the manufacturer. Request the statement of compliance. Consider protective coating if necessary. Review. Draw an appropriate	In progress	
1	Concept Design	1.05	Cost higher than projected	Contract	C	C	Medium	Contract with the manufacturer	Under review	
1	Concept Design	1.06	Fibre bundles routing too difficult	Design progress review	C	B	Extreme	Review proposals at early stage.	Under review	
2	Final Design	2.01	Interface with the Telescope Truss error.	Careful checking and review on site. Design features.	D	C	Medium	See 1.01. Avoid machining on assembly. Melding of the components on the telescope with use of jigs.	Under review	
2	Final Design	2.02	Manufacturability problems	Test	E	B	Major	Conduct tests on real scale components	Under review	
2	Final Design	2.03	Special equipment and tooling requirement to cope with the size of the job	Contract	C	C	Medium	Assure sufficient fund allocation for tools and equipment		
3	Manufacturing/Installation	3.01						If decision is made to carry on melding in place (on the telescope in zenith position), an appropriate scaffolding and protective barriers have to be installed.		
3	Manufacturing/Installation	3.02	Lack of preparation of the safe and functional environment on site	Planning	B	C	Major			
4	Transport costs	4.01	Departure from the idea of melding on site may cause escalation of the transport costs and increase the risk of damage	Planning	D	D	Minor	Manufacture of a complete top ring in the factory may be seen as potential saving on the preparation of working environment at the telescope. The cost and risk of damage during transport may outweigh those savings. It needs to be carefully analysed and planned.		

Chapter 29 Logistics

29.1 Introduction

Logistics means having the right things in the right place at the right time.

Logistics in the context of the WFMOS project is seen as the process of planning, implementing and controlling the efficient flow of materials, equipment and in-process components and sub assemblies from point of origin (manufacture/test/acceptance) to locations for integration and final acceptance prior to the final instrument commissioning phase.

29.2 Logistics

This section discussed the various aspects of logistics.

29.2.1 Importance of logistics for WFMOS

The way the design process and the consequent design reviews are planned and variations in the time required to design and develop major components of the WFMOS system will result in progressive delivery of component parts and equipments to Hilo. Movement of these items to the telescope platform for installation and for final integration and acceptance prior to commissioning will be progressive.

There will be logistics issues associated with many of the WFMOS project phases. It is very likely that movement of major components and sub assemblies will occur for the purposes of integration and acceptance prior to movement to the final point of acceptance (Hilo or in some cases the final telescope platform). Poor planning and management of these movements will add time and cost to the project.

29.2.2 Logistics planning

WFMOS component parts and assemblies will almost certainly be manufactured in different places and by different organizations. The needs of integration and progressive QA inspection and acceptance will drive logistics costs in terms of travel for technical staff, packing, shipping and insurance costs for components and assemblies.

The availability and location of various components could have a significant impact on the schedule and the elapsed time required for WFMOS to be manufactured, for acceptance and ultimately for availability at the selected telescope platform.

Logistics planning will be an important part of the Project Management and will need to be staffed within the Project Office. Logistics planning should maintain a high profile as it will offer opportunities for compression of the project schedule.

29.2.3 Protection and Packing requirements

Items that have to be moved will require appropriate protection and transport from point of acceptance to Hilo.

29.2.3.1 Standards for packing

Items will be packed for all movements and these movements may be inter-organisational for the purpose of interface and functionality checking as well as for movement to the point of acceptance and eventually to Hilo for final acceptance.

The standards should be as appropriate for air movements in the main and reflect IATA standards. This means being protected within a purpose built outer timber packing cases with internal protection as appropriate and for sensitive items packing cases shall be fitted with tilt, shock and possibly temperature monitors.

Packing should be undertaken by organisations that are familiar with airline freight requirements and who are professionals in that business.

29.2.3.2 Vacuum packs and moisture control agents where required

Sensitive components and subassemblies should be protected from impact and also from dust and moisture. Vacuum packing should be used for sensitive equipment.

29.2.3.3 Number of crates

We have estimated the number of crates required for the movement of equipment within the team and from point of manufacture to Hilo as being around 30 in number.

29.2.3.4 Likely inter-organisation movements for QA and integration checks

There are likely to be a number of inter-organisational equipment movements required for the purpose of proving interfaces and to facilitate quality.

29.3 Component and Equipment Handling

29.3.1 Approach

WMOS comprises a number of parts and assemblies that require special handling. The most obvious component parts will be:

- Corrector
- Top End
- Fiber cable runs
- Other

29.3.2 Special Tools

Handling of the Top End will require special tools and equipment.

29.4 Transport

29.4.1 Approach

The majority of components and sub assemblies will be moved by air freight, the benefits are outlined below. Where items are robust and the schedule allows for slower movement, they should be moved using ocean freight and this will offer cost savings. Security, protection and the overall schedule impact should be considered as protracted delivery may introduce unnecessary delay.

29.4.2 Freight arrangements

Freight arrangements shall be appropriate to meet the needs for protection and be cost effective. The standards required for packing are discussed at 29.2.3 above.

There is a choice of air and ocean freight arrangements for the typical items that will be delivered under a WFMOS build contract.

IATA (International Air Transport Association) standardizes the rules and regulations for air carriers throughout the world and provides a good basis for save and cost effective movement.

Air freighters like the Boeing 747-400F can carry loads weighing up to 110.67 metric tons and are effective for carrying quite large items in IATA Type 2H pallets or containers (10'-high main deck pallet or container, dimension is 96" x 125" x 118") or IATA Type 8 containers (lower deck container, dimension is 60.4" x 61.5" x 64").

Airfreight is often used for high value but low volume cargo. Although often perceived as expensive, there are benefits with airfreight:

- Faster delivery

Ports worldwide can be reached in 1 or 2 days or in a few hours by airfreight, thus reducing the risks of theft, pilferage and damage to the goods.

- Better security

Airfreight has tighter control over its cargo, thus it has better security that reduces the cargo exposure to theft, pilferage and damage.

- Less packaging

Usually requires less packaging because of faster delivery and better security. Less packaging can mean saving freight, packaging and labour costs but in many instances our case the packing standards will be determined by technical need and risk assessment.

- Lower insurance

Faster and has better security than the land and ocean freight, thus the insurance premium rate generally is lower.

29.4.3 Air and Ocean freight movements to Hawaii

29.4.3.1 Air movements to Hawaii

The movement of the majority of equipment to Hilo will be by airfreight. This is because the costs and time involved are reasonable and time available may not allow all items to go by sea. The time required for movements by air from Sydney to Hilo will be up to 9 days point to point.

29.4.3.2 Ocean movements to Hawaii

Ocean freight clearly takes longer and equipment may be more vulnerable to moisture and transit damage.

The time required for ocean freight movements from Sydney to Hilo is about 30 days point to point but this can be extended if the timing of movements in out of synchronization with ocean freight schedules.

29.4.4 Ground Transport - Hawaii

Receipt inspection is an expected requirement and would be carried out within days of arrival in Hilo. Movement of various items to different assembly points is likely following receipt inspection.

It may save money and make better sense for Gemini to arrange for pick up of equipment from the Hilo terminal on advice of its availability so that receipt inspection can be organised and movement to the preferred locations can be arranged. Delivery points may vary with large items that have been accepted overseas being move directly to the telescope area and instrument components being moved to assembly and preparation points.

29.4.5 Timing of Transport to Hawaii

In general it is expected that a complex instrument such as WFMOS would be accepted at the point of manufacture as far as is possible and that the timing of transport to Hilo would be phased to allow progressive receipt, delivery acceptance and movement to the point of either final assembly and test or in the case of large structural items, direct to the telescope.

A typical delivery sequence could be:

- Infrastructure items
- Top end and associated structures together with special tools and equipment
- Spectrographs – by type and/or final location

- Fiber runs
- Electronics cabinets and associated systems
- Wide field corrector, and
- Fiber positioner

29.5 Cost estimate

A ROM cost estimate has been developed for probable transport and handling to meet the forecast logistics needs. This contains costs for both air and ocean transport as necessary and the cost of packing, insurance and door-to-door movements for all deliverable items.

The costs estimate is based on information received from a reputable logistics organisation and assumes mass, size and numbers of crates necessary for the movement of all components and assemblies required for the WFMOS instrument.

29.5.1 Transport and packing costs

The costs for transport and packing are as follows:

All items moved by both air and sea as determined by priority and mass/size are estimated as USD 507,000. This is made up of the following components:

Item	Costs - USD
Transport costs	310,000
Insurance costs	135,000
Packing and protection	62,000
Total	507,000

29.5.2 Other associated costs

Insurance costs are estimated for replacement of loss due to damage in transit. The estimate assumes that design and development work will not be lost and that as the instrument will be moved in multiple containers and from various ports of embarkation, the insurance risk extends largely to the purchased and manufactured items and that these will total no more than USD 30 M.

The insurance cost is estimated at USD 135,000.

This is in 2004 dollars and is based on an estimate received from a reputable logistics organisation.

29.5.3 Typical ocean transport costs

Ocean transport is likely to be required for large items and it is a cost saving option that can be considered for items that are manufactured early and where time is available for slow-time movement of the deliverable to Hilo. This would typically cover such items as the top end, major fiber runs and any support structures.

Typical ocean transport costs for the large items likely to be moved from Sydney to Hilo would cost up to USD 70,000.

Transit times door to door from Sydney to Hilo for ocean transport are estimated as around 30 days.

29.5.4 **Typical air transport costs**

It is envisaged that the majority of components and sub assemblies will be moved by air freight as time will be important in terms of the overall schedule and to facilitate the quality and acceptance processes.

Typical air transport costs are shown below for a sample range of packing cases. The total cost of air movements has been developed from the quoted prices based on estimated numbers of cases and their likely mass and dimensions.

Airfreight	Dimensions - metres			Volume	Mass	Cost
	Length	Width	Height	Cubic metres	Kg	AUD
Sydney to Hilo	2.5	2.5	1.2	7.5	400	\$52,000
Sydney to Hilo	1	0.5	1	0.5	60	\$1,600
Sydney to Hilo	2	2	1	4	1,000	\$10,000
Sydney to Hilo	2	2	3	12	500	\$62,000

A similar range of costs has been developed for mainland USA to Hilo and UK to Hilo to provide a reasonable estimate of total movement costs.

Transit times for air transport, door to door are estimated as follows:

Sydney to Hilo	<9 days
UK to Hilo	<9 days
Mainland USA to Hilo	<5 days

29.6 **Grouping and Movement of components**

Chapter 25, Organisation and Management discusses the possible separation of work and there are clearly implications for logistics planning and for cost management (see section 25.4.5 specifically).

A possible separation of work is shown in section 25.4.4.

Logistics Issues

There could well be benefits and cost reductions that derive from good planning and foresight such as:

1. Use of a common carrier for the movement of personnel and equipment; it is possible that Gemini could organise this.
2. Where the cost of movement of large items is high, cost containment should be investigated by seeking opportunity to manufacture such items close to the final destination (Hilo).
3. Optics may need to go to the prime contractor or that part of the organisation manufacturing the corrector prior to going to Hilo.

4. Another example of potentially high cost logistics is the Top End. The top end can go direct to Hilo post manufacture or possibly manufactured in Hilo.
5. There is an order that may offer easier and cheaper acceptance and make for better handling of component parts in Hilo, this order would likely be as follows:
 - Infrastructure
 - Top end – can wait to be fitted
 - Corrector
 - LoRes Spectrographs
 - HiRes Spectrographs
 - Fiber Cable
 - Positioner and the rest

Chapter 30 Applicable Documentation

30.1 Documentation

The following documentation is relevant to the Feasibility Study. The various sections below discuss the major project documentation required to control work scope, quality aspects and to drive the effort of the design, build, test, integrate and deliver phases.

30.1.1 **AURA Contract No. 0084699-GEM00385 – Design Study for the Wide Field Fiber-Fed Optical MOS (WF MOS)**

The Feasibility Study has been carried out under the terms of an AURA contract. This contract is made up of the following documents:

- Main Document
- Statement of Work
- Science Case
- Terms and Conditions
- Proposal

During the conduct of the Feasibility Study, three (3) amendments to the contract have been entered into and agreed between AURA and the Anglo-Australian Telescope Board (AATB).

It is assumed that the effort to design, build, test, integrate and deliver the WF MOS instrument will be covered by the standard AURA contract in the form of a Main Document, Statement of Work and Terms and Conditions. The contract would be supported by the Feasibility Study Report, IOCDD and IFPRD documents delivered under the terms of AURA Contract No. 0084699-GEM00385.

The AAO has raised specific objections as part of the Proposal Document made in response to RfP N231804; and if the AAO were to be involved in a future design, build contract; these objections would still stand.

Technical and scientific details provided by the AAO as part of the Feasibility Study report, the IOCDD and /or the IFPRD are for use by Gemini for the purpose of building the WF MOS instrument and the contract should protect this by use of non disclosure agreements before disclose to any third party.

30.1.2 **Statement of Work**

Any contract issued for the design, build, test, integrate and deliver a WF MOS instrument would include or refer to a Statement of Work that will define in precise terms the scope of all work required to be undertaken.

The presentation style and language used will allow the selected contractor to design and manufacture to meet technical and performance standards in an unambiguous manner and will provide the basis for verification and acceptance by AURA.

30.1.3 The KAOS Purple Book

The Purple Book describes the main scientific drivers for KAOS and its technical feasibility.

30.1.4 Gemini WF MOS – Proposal Document in Response to RfP N231804

The proposal was prepared jointly by the AAO, CADC, Johns Hopkins University, NOAO, University of Durham, University of Oxford and the University of Portsmouth. The proposal was released and submitted to Gemini on 25th March 2004.

30.1.5 Guidelines for Designing Gemini Aspen Instrument Software – AspenSoft-03072004-6

This document provided guidance for software development for Aspen instruments and was relevant to the Feasibility Study efforts for feasible software design and development and was used to guide approach and cost estimating.

This document also appears in the interface control listing below and is referred to as the “Gillies document RD1”.

30.1.6 Interface Control Documents

All interface information required by the contractor building the WF MOS instrument must be provided in manageable form and be maintained by AURA under proper change management arrangements.

Where documents supersede the ICDs, these documents must be identified and made available at the time that price negotiations are being undertaken and also be maintained by AURA under proper change management arrangements. An example of this is the Guidelines for Designing Gemini Aspen Instrument Software by Kim Gillies; AspenSoft-03072004-6.

The following list that was relevant to the Feasibility Study was prepared on 25th August 2004

	Number	Title	Mech	Elec	Soft	Comments
1	ICD 1.1.1/1.9	Telescope Structure to Science Instruments Interface Control Document	Yes	No	No	Not related to prime focus.

2	ICD 1.1.11/1.9	Science Instrument to Telescope Control System	No	No	Yes (AKA ICD6)	Reference only (subject to Gillies document RD1)
3	ICD 1.1.13/1.9	Interlock System to Science Instruments Interface Control Document	No	Yes	No	Not related to prime focus.
4	ICD 1.4.4/1.9	SCS to Science Instrument Interface	No	No	No	Can be ignored.
5	ICD 1.5.3/1.9	Instrument Support Structure to Science Instruments Interface Control Document	Yes	No	No	References to thermal control, thermally conditioned electronics, allowed heat release from instrument.
6	ICD 1.6/1.9	A&G System to Science Instruments	No	No	Yes	Can be ignored.
7	ICD 1.6/1.10	A&G to On- Instrument Wavefront Sensors	No	Yes	Yes	Probably subject to Gillies document RD1.
8	ICD 1.9	Science Instruments Interface Control Documents Overview and Guide	Yes	Yes	Yes	Covers heat sources and references to Gemini standards and VME slots. May be superseded by Gillies document RD1.
9	ICD 1.9/1.10	Science Instruments to On Instrument WFS	No	Yes	Yes	Ignore?
10	ICD 1.9/2.7	Science and facility instruments to facility handling equipment interface control document	Yes	Possibly	No	May be of relevance to handling top end when off the telescope and to parts of the spectrographs.
11	ICD 1.9/3.1	Science Instrument to Observatory Control System	No	Partly	Yes (CICS Details from ICD14?)	Refers to ICD 13 and 14. Probably superseded by Gillies document RD1.
12	ICD 1.9/3.2	Science Instrument to Data Handling System	No	Partly	Yes (CICS Details from ICD15?)	Refers to ICD 13 and 14. Probably superseded by Gillies document RD1.

13	ICD 1.9/3.6	Science and Facility Instruments to System Services Interface Control Document	Yes	Yes	No	Possibly relevant to top end and pier lab.
14	ICD 1.9/3.7	Science Instruments to Facility Thermal Electronics Enclosures	Yes	Yes	No	Possibly relevant to the pier lab.
15	ICD 1.10	On-Instrument WFS	No	Yes	Yes	Refers to 1.1.11/1.10, 1.6/1.10 and 1.9/1.10.
16	ICD 1a	The System Command Interface	No	No	Yes	Reference only subject to Gillies document RD1.
17	ICD 1b	The Baseline Attribute/Value Interface	No	No	Yes	Reference only subject to Gillies document RD1.
18	ICD 1c	Baseline DHS Interface	No	Partly	Yes	Reference only subject to Gillies document RD1.
19	ICD 2	Systems Status and Alarm Interfaces	No	Not directly	Yes	Reference only subject to Gillies document RD1.
20	ICD3	Bulk Data Transfer	No	Partly	Yes	Reference only subject to Gillies document RD1.
21	ICD5	Wavefront Sensing Information Interface	No	No	Yes	Contains ICD7a – ICS Subsystem Interfaces. Reference only subject to Gillies document RD1.
22	ICD9	EPICS Time Bus Driver	No	Yes	Yes	Reference only subject to Gillies document RD1.
23	ICD10	EPICS Synchro Bus Driver	No	Possibly	Yes	Needed for fast, deterministic information transfer between IOCs. Reference only subject to Gillies document RD1.
24	ICD12	Interlock System	No	Yes	Yes	Reference only subject to Gillies document RD1.
25	ICD-G0013	Gemini Environmental Requirements	Yes	Yes	No	

26	ICD-G0014	Gemini Observatory Optomechanical Coordinate Systems	Yes	No	No	
27	ICD-G0015	Gemini Facility Handling Equipment and Procedures for Instrumentation	Yes	Partly	No	Only references Cass instruments. Not yet inclusive of top end or pier lab instrumentation.
28	ICD 16	The Parameter Definition Format	No	No	Yes	Reference only subject to Gillies document RD1.

Missing ICDs and other documents/standards?

	ICD 1.5.2/1.9	Cassegrain Cable Wrap to Science Instruments		Possibly		Referenced in ICD 1.9. Contains details on how connections are made to power, signals, cooling water and helium, which may be relevant to the top end, and pier lab.
	ICD 13	Standard Controller			Yes	Out dated or not relevant and can safely be ignored
	ICD 14	Core Instrument Control System			Yes	Out dated or not relevant and can safely be ignored
	ICD 15	DHS Database Interfaces			Yes	Out dated or not relevant and can safely be ignored

Additional Documents

RD1		Guidelines for Designing Gemini Aspen Instrument Software, Kim Gillies, 13/5/2004	No	Yes	Yes	We have a copy of this, but not under Copy Control
RD2	GSCG.grp.005	Gemini System Interfaces				
RD3	GSCG.grp.006	Overview of Gemini System Interfaces				
RD4	SPE-C-G0009/02	Gemini Software Programming Standards				
RD5	SPE-ASA-G0008	Gemini Electronic Design Specification				

30.1.7 Drawings

There are a number of CAD models and drawings that were released to the AAO and the team for guidance and direction whilst conducting the Feasibility Study, these are referred to below.

A CDROM with many CAD files from KAOS development was supplied by Gemini. They have been viewed for assessment of suitability of use by AAO.

KAOS assembly model created in Solid Works contained most of the information needed. On our request the file has been converted to STEP format and delivered to AAO. We have converted the file to Autodesk Inventor model and used it for all Gemini Telescope related work.

Availability of Subaru documentation was limited. We have used some models of the Top End supplied earlier for FMOS project. Other data was gathered from commonly available sources like brochures, published documents etc.

30.2 *Operational Concept Definition Document*

The OCDD is a deliverable of the Feasibility Study and must become a part of the contract documents provided for any future stages of the design / build phases of the WFMOS instrument.

30.3 *Functional and Performance Requirements Document*

The FPRD is a deliverable of the Feasibility Study and must become a part of the contract documents provided for any future stages of the design / build phases of the WFMOS instrument.

SECTION V: ACKNOWLEDGEMENT OF CONTRIBUTORS

Chapter 31 People Involved

The WFMOS feasibility study was a joint international effort of the following organizations:



Prime Contractor

Anglo Australian Observatory (AAO), Australia – brings expertise in fiber fed multi-object spectroscopy (2dF), VPH gratings, and robotic positioners, in particular its revolutionary Echidna technology under development for the FMOS instrument on Subaru.



Subcontractor

The Canadian Astronomy Data Centre (CADC) brings expertise in data archiving particularly for large-scale sky surveys and are at the leading edge of development for the Virtual Observatory. They also bring Gemini experience through their management of the Gemini data archive.



Subcontractor

Johns Hopkins University (JHU) brings expertise in spectrograph design and fabrication, VPH grating experience, optical/IR imaging cameras, spacecraft and space instrumentation, and science from the Sloan Digital Sky Survey. They have expertise in cosmology, large-scale surveys, and galactic structure.



Subcontractor

National Optical Astronomy Observatory (NOAO) brings expertise in broad areas of optical and infrared astronomical instrumentation, including wide-field prime focus correctors, detector development and characterization, and design and development of detector controllers.



Subcontractor

University of Durham (Durham) brings expertise in the development of large fiber bundle and fiber connector technology in a variety of instruments (e.g. GMOS and FMOS).



Subcontractor

University of Oxford (Oxford) brings expertise in fiber-fed spectrograph design (e.g. FMOS spectrograph) backed by substantial practical experience with the exploitation of fibre-fed spectroscopy through FOCAP, AUTOFIB, AUTOFIB-2, CIRPASS, and the 2dF galaxy and QSO redshift surveys.



Subcontractor

University of Portsmouth (Portsmouth) brings scientific and data handling leadership experience from experience with the Sloan Digital Sky Survey and related cosmological survey projects. They bring expertise in cutting edge theoretical models of Dark Energy and the early Universe.

<i>Anglo-Australian Observatory</i>	
Samuel Barden	Feasibility Study Manager, high-disp spectrograph, calibration, acquisition/guiding
Chris Evans	Project Manager, leader on management and costing
Andrew McGrath	Systems Engineer, fiber positioner, document generation
Stan Miziarski	Engineer, Subaru top end, fiber positioner
Jurek Brzeski	Engineer, Subaru top end
Peter Gillingham	Engineer, WFC corrector evaluation
John Dawson	Mechanical engineer, mechanical systems
Greg Smith	Mechanical engineer, costing of systems
Lew Waller	Electrical engineer, electronic systems
Tony Farrell	Software engineer, software systems and data pipeline
Will Saunders	Scientist, do-all spectrograph, calibration system
Roger Haynes	Scientist, fiber cable
Matthew Colless	Scientist, w(z) science case
Joss Bland-Hawthorn	Scientist, Galactic science case
Scott Croom	Scientist, w(z) science case
Scott Smedley	Software engineer, fiber positioner software
Helen Woods	Administrative assistant, management assistance
<i>Canadian Astronomy Data Centre</i>	
David Schade	Scientist, data pipeline and archive
Severin Gaudet	Scientist, data pipeline and archive
David Bohlender	Scientist, data pipeline and archive
<i>Johns Hopkins University</i>	
Rosie Wyse	Scientist, leader of Galactic science case
Karl Glazebrook	Scientist, w(z) science case
Stephen Smee	Engineer, low-res spectrograph
Robert Barkhouser	Engineer, low-res spectrograph
Ivan Baldry	Scientist, low-res spectrograph
Joe Orndorff	Engineer, low-res spectrograph

National Optical Astronomy Observatory

Arjun Dey	Feasibility Study Scientist, w(z) and Galactic science cases
David Sprayberry	Scientist, Gemini WFC, Gemini top end, detectors/controllers
Jeremy Mould	Scientist, Galactic science case
Taft Armandroff	Scientist, leader operational impact, Galactic science case
Ming Liang	Optical designer, Gemini WFC optical design
Gary Poczulp	Engineer, Gemini WFC
Larry Daggert	Engineer, Gemini WFC
Bruce Fitz-Patrick	Engineer, Gemini top end
Rick Robles	Engineer, Gemini top end
Gustavo Rahmer	Engineer, detector/controllers
Mark Hunten	Engineer, detector/controllers
Knut Olsen	Scientist, Galactic science case, operational impact
Verne Smith	Scientist, Galactic science case

University of Durham

Simon Morris	Scientist, w(z) science case
Ray Sharples	Scientist, fiber connector
Marc Dubbeldam	Engineer, wobble plate
Richard Myers	Scientist, WFS
David Robertson	Engineer, management and costing
Carlton Baugh	Scientist, w(z) science case
Raul Angulo	Scientist, w(z) science case
Richard Bower	Scientist, w(z) science case
Carlos Frenk	Scientist, w(z) science case
Graham Murray	Engineer, fiber connector
George Dodsworth	Engineer, fiber connector
Robert Content	Optical designer, fiber connector
Stephen Goodsell	Engineer, wobble plate
Paul Clark	Engineer, WFS

University of Oxford

Gavin Dalton	Scientist, IR spectrograph, w(z) science case
--------------	---

Isobel Hook	Scientist, operational impact
Ilona Soechting	Scientist, operational impact
Roger Davies	Scientist, operational impact
Ian Lewis	Scientist, IR spectrograph
Alan Holmes	Engineer, IR spectrograph
Barney Brooks	Engineer, IR spectrograph
Ian Tosh	Engineer, IR spectrograph
Hanshin Lee	Engineer, IR spectrograph
Tim Froud	Engineer, IR spectrograph
Guy Woodhouse	Engineer, IR spectrograph
Marc Ferlet	Engineer, IR spectrograph
<i>University of Portsmouth</i>	
Robert Nichol	Scientist, leader on data pipeline and archive, w(z) science case
Bruce Bassett	Scientist, w(z) science case
Martin Kunz	Scientist, w(z) science case
Chris Miller	Scientist, w(z) science case
David Wake	Scientist, w(z) science case
David Parkinson	Scientist, w(z) science case
<i>Additional contributions from non-participating organizations</i>	
Daniel Eisenstein	Scientist, leader of w(z) science case
Hee Jong Seo	Scientist, w(z) science case
Chris Blake	Scientist, w(z) science case
James Bullock	Scientist, Galactic science case
Walter Dehnen	Scientist, Galactic science case
Annette Ferguson	Scientist, Galactic science case
Ken Freeman	Scientist, Galactic science case
Kathryn Johnston	Scientist, Galactic science case
Dionne James	Document formatting
Colin Dawson	Document formatting

Chapter 1 APPENDIX: Extended Value-added Science Cases

We present here several case studies of new scientific studies that can be undertaken using the WFMOS instrument, and the data from it.

1.1 Constraints on the Primordial Power Spectrum

In addition to constraining Dark Energy, the WFMOS surveys outlined in this proposal will provide a unique constraint on the shape of the primordial power spectrum coming out of Inflation. In particular, most Inflationary models predict that the primordial power spectrum should exhibit some departures from pure scale-invariance, which can be characterized by a scale-dependent spectra index, $n(k)$. Moreover, inflationary models can also give rise to isolated sharp features in the primordial power spectrum and there is evidence for such features in the SDSS power spectrum [1]. Therefore, it is imperative that we try and constrain the primordial power spectrum, as it will provide new insights into Inflation and thus the first instant after the Big Bang.

We present here a brief examination of the likely constraints on the primordial power spectrum. Following standard practice, we consider a two-parameter dependence of $n(k)$ on wavenumber k , e.g. $n(k)=n_0 + n_1 \log(k/k_*)$, where $k_* = 0.05\text{hMpc}^{-1}$ is a reference scale, $(n_0 - 1)$ is known as the *tilt* and the second term controls the running of the spectral index. To quantify the likely WFMOS constraints on n_0 and n_1 , we employed the Fisher matrix approach with the default WFMOS survey configuration described in Seo and Eisenstein [2]. The details of the approach we follow is described in detail in [3] and [4].

We consider two different approaches to the problem. We can consider only the linear part of the power spectrum and then consider a time-dependent two-parameter model of bias with no scale-dependence (left panel of Figure 1). We also consider the fully nonlinear power spectrum allowing for a four-parameter time and scale-dependent biasing (right panel of Figure 1). The results are rather similar once we marginalize over the corresponding bias parameters in each case and the dark energy equation of state w (assumed constant). For these simulations we assumed a flat universe and fixed $\Omega_m=0.28$, two parameters that will be known to very good precision with Planck and related surveys before WFMOS.

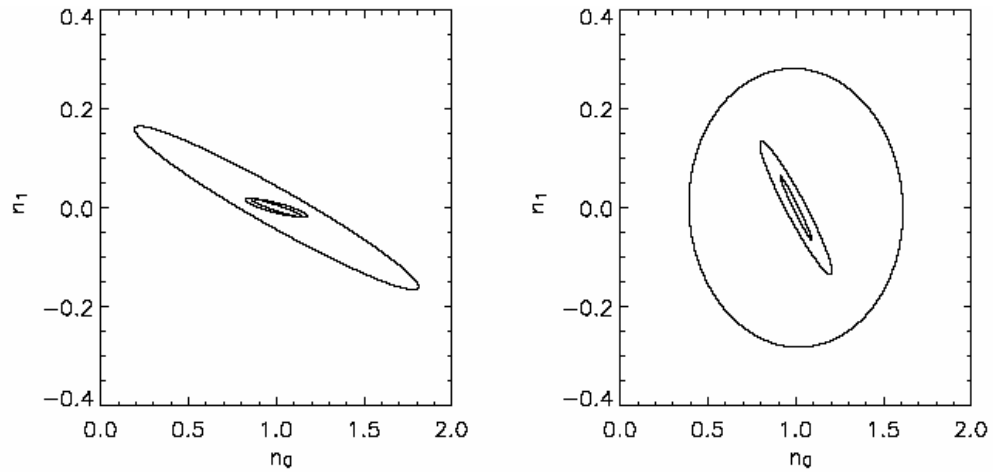


Figure 1 (preliminary – does not include the high- z survey): The expected error ellipses for LCDM from the $z < 1.5$ part of the fiducial WFMOS survey for the linear part of the power spectrum (left panel, two bias parameters) and full nonlinear spectrum (right panel, four bias parameters). The inner ellipses are the full constraints while the outer two ellipses show the constraints from the monopole and quadrupole (outer ellipse) of the redshift-space power spectrum respectively.

Figure 1 shows that a particular linear combination of n_0 and n_1 will be very tightly constrained to within an accuracy of about 2-3% (the precise linear combination depends on the slope of the degeneracy ellipse). The CMB experiment Planck will break the degeneracy and hence we can hope to constrain both n_0 and n_1 to this high accuracy, allowing significant constraints to be placed on the space of possible inflationary model parameters. If, in addition, we assume that the bias parameters will be determined through some other means (for example through weak lensing or higher-order correlation functions which could be extracted from WFMOS) then the precision will be significantly better. Hence, WFMOS will provide a significant contribution to our understanding of the early universe.

The other possibility – that of sharp features in the spectrum – is easy to address at the qualitative level. Assuming that the feature is sharp then we may extract it using standard techniques. Cross-correlation with the CMB may then allow its use as an additional standard ruler (complementary to that provided by the baryon oscillations). Distortions to the spectrum are also expected at small scales due to neutrino masses, which suppress small-scale power. A high-redshift component to WFMOS will allow this effect to be uncovered even if the sum of the neutrino masses is as small as 0.16 eV when combined with Planck, and 0.10 eV (2 sigma) when combined with the proposed CMBpol experiment [4].

1.1.1 References

1. D. Tocchini-Valentini, M. Douspis, J. Silk, astro-ph/0402583.
2. H-J. Seo and D.J. Eisenstein, *Astrophys.J.* 598 (2003) 720
3. K. Yamamoto, B. A. Bassett and K. Nishioka, astro-ph/0409207
4. B. A. Bassett, J. Lesgourgues and K. Yamamoto, in preparation (2004).
5. J. Lesgourgues, S. Pastor, L. Perotto, *Phys.Rev. D*70 (2004) 045016

1.2 Formation and Evolution of the Highest Redshift Galaxies

How do galaxies form and evolve? Primeval galaxies undergoing their very first episodes of star formation have remained elusive, either because these nascent systems are shrouded in dust or because galaxy formation is a slow hierarchical process wherein galaxies are assembled over time from small building blocks. The aging of galaxies has also remained a puzzle: so many factors contribute to the chemical, dynamical and morphological development of a galaxy, that the small observational data sets painstakingly obtained barely provide us with clues even to the most global issues (e.g., the evolution of the luminosity function) over a large range in lookback time.

Our investigation of the processes of galaxy formation and evolution is currently restricted to theoretical simulations and small observational data sets. Current simulations suggest that galaxy assembly is a hierarchical process, wherein mergers and interactions play a significant role in determining the present-day morphologies and stellar constituents of galaxies. At present, the observational data are ambiguous, and results suffer from selection effects and small number statistics. The pioneering studies during the last decade have been largely restricted to small pencil beam surveys or shallow surveys of the low-redshift galaxy population (e.g., CFRS - Lilly et al. 1996; LDSS/Autofib - Ellis et al. 1996; various Keck surveys - Cowie et al. 1996, Koo et al. 1996, Cohen et al. 1999). More recently, observations with *HST* and the Keck telescopes have demonstrated the existence of star-forming galaxies at redshifts beyond 3 (Steidel et al. 1996, 1999). These galaxies are believed to be the building blocks of the present-day galaxies, but their properties (masses, chemical composition, stellar content, ages and evolutionary histories) remain largely unknown.

In order to address the question of galaxy formation and evolution for the entire population, we would ideally want to trace the evolutionary history of galaxies (i.e., their star-forming history, chemical evolution, merging and morphological evolution) as a function of mass, redshift and environment. It is critical to understand and interpret the formation of galaxies in the context of structure formation and evolution. These astrophysical problems are inextricably linked, since the large-scale environment plays a crucial role both in the assembly of galaxies and in their evolution (through merging, exclusion, harassment, etc.).

1.2.1 Need for Large Area / Depth / Large Samples

To trace the evolutionary history of galaxies as a function of environment, we need to sample galaxies over the entire range of environments: from the lowest density regions (voids) to the rarest high-density environments (cores of rich clusters). Surveys over large volumes (~ 100 square degrees — see previous section) are needed to accomplish this.

In order to explore the early evolutionary history of galaxies ($z \sim 4-6$), deep spectroscopic surveys (to ~ 25 AB mag) are essential. These depths are needed not only to probe the highest redshifts, but also to ensure that the samples are not restricted to the rarest, most luminous objects, and instead sample more typical objects as well (i.e., as much of the luminosity function as possible).

Galaxies in the present epoch exhibit a large range in physical properties (e.g., masses, chemical abundances, star forming histories, morphologies, gas and stellar content). Since the evolutionary processes responsible for these properties are numerous and complex (e.g., star formation, mergers and interactions, infall),

an observational program to unravel the formation histories of present-day galaxies inherently requires large samples ($\sim 10^6$ galaxies). For example, in order to trace the evolutionary history of galaxies as a function of mass, redshift and environment, we would need at least 5 redshift bins ($1 < z < 6$), 4 mass bins (logarithmic intervals spanning $10^8 - 10^{12} M_{\odot}$), 5 bins in mean stellar age or star-formation rate (0.1 – 10 Gyr or $0 - 10^3 M_{\odot}/\text{yr}$), 4 bins in morphology (E/S0, S, Irr, multi-component), 4 bins in mean chemical abundance ($0.002 - 2Z_{\odot}$), and 3 bins in environmental density (field, groups, clusters). With at least 100 galaxies per bin, this implies a total sample size of at least 500,000 galaxies. This is truly a lower limit since we have required that the bins of rare objects be also well populated. Populating such rare bins is critical in order to address questions such as the formation history of the most massive galaxies, or the evolutionary history of the most metal-poor galaxies.

1.2.2 A Representative WFMOS Project

The surface densities on the sky of $R < 25$ AB mag $z \approx 3$ and $I < 25$ AB mag $z \approx 4$ galaxies are ≈ 4000 and 800 per square degree respectively. A survey of 5×10^5 galaxies over 100 square degrees requires a wide-field, highly multiplexed multi-object capability. We are only beginning to scratch the surface with current studies: a typical Keck+LRIS campaign results in \sim a dozen redshifts of $R \sim 24 - 25$ galaxies per night. The low-resolution spectra that are obtained probe only a restricted class of objects (mostly low-extinction, star-forming systems) and are generally only sufficient for measuring redshifts. Detailed investigations of the physical properties of these objects and their evolution require spectroscopic capabilities, which are neither available nor planned.

For the detailed spectroscopic studies described here, we need a minimum resolution of $\lambda/\Delta\lambda \approx 2000$ and signal-to-noise ratios per resolution element of ~ 20 . The redshift range targeted by this survey requires spectroscopy at both optical and infrared wavelengths. In 0.7" seeing with DEIMOS on Keck, this requires an exposure time of ≈ 1 night per 80-object mask; hence it will take 6250 clear nights to obtain spectra of 5×10^5 galaxies, or a minimum of 17 clear observing years with Keck and DEIMOS dedicated to this one project. In comparison, WFMOS would execute this project in only ~ 100 clear nights.

1.3 Physics of AGNs and Quasars at $z < 6.5$

The aim of this project is to understand the physics of AGN evolution from the end of the epoch of re-ionization ($z=6.5$) to the present day ($z=0$). This will be achieved by a conducting a comprehensive survey for over 30000 AGN with which to carry out detailed studies of their demographics and physical properties (space density, clustering, environments and black hole masses). This will complement the increasingly detailed dynamical studies of local AGN with similar luminosities that will be carried out over the coming decade with space-based facilities and IFU capabilities on ground-based telescopes.

1.3.1 Current Position:

Our knowledge of the statistical properties of the AGN population has been greatly enhanced by the two major QSO surveys of recent years: the 2QZ (Croom et al. 2001) and the SDSS (Richards et al. 2001). In many respects the surveys

provide complementary information; the deeper ($g < 21$) 2QZ survey probes ~ 1 mag below the break in the QSO luminosity function (L^*) at $z < 2.5$, whereas the shallower SDSS survey extends to much higher redshift, $z < 6.5$, courtesy of its superior CCD-based photometric selection techniques.

The statistical precision provided by samples of over 20000 AGN has yielded new insights into many aspects of the QSO phenomenon, the QSO luminosity function (Boyle et al. 2000) QSO clustering (Croom et al. 2001), the $z > 5$ Universe (Fan et al. 2001), limits on cosmological parameters (Hoyle et al. 2002) new populations of AGN (Brotherton et al. 1999, Hall et al. 2002) the physics of QSO emission lines (Croom et al. 2002) and QSO black hole masses (Corbett et al. 2003).

However, even surveys such as these still provide us with an incomplete view of the QSO phenomenon – missing a vital area of observational parameter essential for building up a full understanding of AGN physics and evolution. Both the SDSS and 2QZ are limited to magnitude ($g < 21$) which at best probe only 0.5 – 1 mag below L^* at low redshift ($z < 2$) and only sample the very brightest end of the AGN luminosity function at $z > 4$.

To achieve the a comparable range in luminosity coverage of the $z \sim 2$ AGN luminosity function (the peak epoch of QSO activity) compared to the existing $z = 0$ galaxy LF requires samples extending to $B < 25$. Equivalent depths ($I \sim 24$) for $z > 5$ would reach ~ 2 mags below the break at these redshifts providing, for the first time a full picture of the high redshift AGN demographics.

Unfortunately, due to the relatively low surface density of QSOs (< 0.1 QSOs/sq arcmin even at $g \sim 25$) and the small fields-of-view available to MOS devices on 8m-class telescopes required to identify AGN at faint magnitudes, the faintest AGN studies conducted to date have been limited to $B < 22$ and comprise less than 100 QSOs in total.

1.3.2 WFMOS contribution

With its uniquely wide field-of-view, WFMOS is the only instrument, either constructed or planned, capable of conducting a major new spectroscopic survey of AGN at the depths required to provide a full statistical picture of the AGN phenomenon over the full range in redshift between the end of the epoch of re-ionization and the present day. Although the shape and form of the AGN LF is unknown outside the L, z range probed by current surveys ($B < 22, I < 21$), extrapolation of the current AGN LF evolutionary models for $z < 2.5$ obtained from the 2QZ (Boyle et al. 2001) and $z > 3$ from the SDSS (Fan et al. 2002) yield the following AGN space densities at typical depths attainable with Gemini using nod-and-shuffle techniques:

Mag Limit	Redshift Range	Space Density of QSOs	Space Density of Other AGN
$B < 25$	$0 < z < 2.5$	300 deg^{-2}	300 deg^{-2}
$R < 24.5$	$2.5 < z < 4$	30 deg^{-2}	300 deg^{-2}
$I < 24$	$4 < z < 6.5$	3 deg^{-2}	50 deg^{-2}

To ensure completeness, complete color-selected samples of AGN will also contain significant contamination from galactic stars. Indeed, for the key redshift range $2.5 < z < 3.5$ (i.e. the epoch of peak QSO activity) this contamination can be as high as a factor 10 of greater. With its extremely high multiplex capability,

WF MOS is unique in being able to access simultaneously all AGN candidates (1500 per field) based on a color selection designed to yield a complete sample of the full range in redshift from $0 < z < 6.5$.

1.3.3 Proposed WF MOS experiment

To remove the effects of cosmic variance from any studies of QSO clustering, the survey will need to be conducted over an area whose minimum spatial dimension corresponds to a comoving length of $\sim 200/h$ Mpc. At $z > 0.5$ this corresponds to a maximum angular size of 10° . A survey covering 100 deg^2 would therefore produce 30000 $z < 2.5$ AGN, 3000 AGN with $2.5 < z < 4$ and 300 AGN in the range $4 < z < 6.5$. Based on these numbers the AGN power spectrum would be determined to better than 5 per cent precision at $z < 2.5$, and an estimate of the scale length of the AGN correlation length determined to better than 20% for all $\Delta z = 1$ between $z = 0$ and $z = 6.5$. At resolutions of $\Delta z = 0.25$, $\Delta m = 0.5$ mag, errors on the estimates of the QSO LF would be better than 5% for all redshifts $z < 4$. At the very highest redshifts, errors of the $z \sim 6$ LF would be typically 10%. Note that the proposed survey would probe a factor of more than 10 further down the AGN LF at all redshifts than any previous survey. Indeed 90% of the AGN identified in this probe a region of (L, z) space unexplored by any previous survey.

The survey would provide information on high redshift AGN at similar luminosities to those low redshift AGN that will be studied with increasingly detailed dynamic/kinematical observations over the coming decade. Coupled with surveys such as SDSS and 2QZ, it will provide an unprecedentedly wide baseline in luminosity and redshift over which to:

- test the luminosity-dependence of AGN clustering predicted by recent hierarchical models of QSO formation (Kauffmann & Haehnelt 2002).
- determine the redshift-dependence of AGN clustering from $0 < z < 6.5$ independent of luminosity. The redshift evolution of AGN bias at a fixed luminosity is a fundamental input parameter to models of QSO formation.
- extend our knowledge of the $z > 4$ AGN LF below L^* . This will provide discrimination between models of AGN evolution (density vs. luminosity) at these redshifts and providing an accurate (convergent) estimate of the ionizing background due to AGN in the early Universe.
- use the mean spectral properties of AGN (see Corbett et al. 2003) to derive black hole mass estimates over a wide range of luminosities and redshifts. Direct comparison of black hole mass estimates obtained from a WF MOS survey for AGN at high redshift may be directly compared to black hole mass estimates in low redshift AGN of similar luminosity obtained directly from dynamical studies, to infer the evolution of fuelling rates/black holes masses within AGN.
- coupled with the Dark Energy project, it will provide a unique opportunity to investigate the evolution of AGN environment over the redshift range $1 < z < 3$.

The proposed survey relies on the availability of deep $B < 25$, $I < 24$ digital data covering the full range of the optical/IR passbands $U \rightarrow K$ for optimal AGN selection. It is assumed that, by the time WF MOS is completed, that this data will exist (at least over 100 deg^2) accessible from both hemispheres (i.e.,

PANSTARRS/UKIDSS combination in the Northern Hemisphere, VST/VISTA in the Southern Hemisphere).

The survey can also be viewed as providing important complementary information to proposed deep surveys in other wavebands (X-ray: *Chandra*, radio: eVLA, UV: *GALEX*), many of whose source detection will be AGN.

The proposed survey will require approximately 70 pointing to cover the full 100 square degrees. Over each 1.5deg^2 WFMOS field-of-view there will be 2,000 AGN candidates; ideally matched to WFMOS's 4,000 fibers to enable a 'sky-object' paired fiber configuration, so that nod-and-shuffle can be implemented with 100% time on target, i.e., with no efficiency loss. Based on previous experience (2QZ), a minimum signal-to-noise ratio $\text{SNR} \sim 5$ per 4\AA resolution element will provide 95% complete identification rate amongst an AGN sample. For the magnitude limits specified above, this SNR is achieved in 10,000 secs exposure; assuming median seeing of 0.8 arcsec (*R* band), system efficiencies of 0.1, 0.24 and 0.31 at 440nm, 670nm and 870nm respectively. In total, this survey could be completed in 25 dark nights.

The combination of high target density yet large coverage means that this survey would be impractical on any other existing facility. It would take over 10 times as long to complete using Magellan/IMACs (field of view 6 times smaller than WFMOS, integration times longer by factor 2), 20 times as long with either VLT/FLAMES (f.o.v. 6 times smaller target density 3 x higher than offered by FLAMES) or MMT/Hectospec (f.o.v. 3 times smaller than WFMOS, integration times 2 times longer, survey target density 3 x higher than offered by Hectospec). Furthermore, at the proposed survey depths (2 per of sky), the use of nod-and-shuffle is crucial. Currently, the lack of nod-and-shuffle on these other facilities would make the proposed survey impossible, no matter how much time was devoted to it.

1.4 The Relationship Between the IGM and Galaxies at High Redshift

One of the long-standing problems in investigations of the intergalactic medium (IGM) is the nature of the relationship between the gaseous and luminous constituents of the universe. By mapping the distribution of galaxies and of the IGM over the same volume, we can examine how these two constituents affect each other during the process of the formation and evolution of galaxies. Observations of this nature can provide statistical constraints on the feedback (radiation, winds, metal enrichment) from star formation in galaxies to the surrounding IGM.

To be specific, moderate resolution ($R=1000$ to 5000) spectroscopy of 120 quasars with redshifts between 2 and 4 drawn from a contiguous 10 square degree region of the sky will provide a mapping on scales of 10 to 80 Mpc of the properties of the IGM. When combined with extensive galaxy redshift surveys in the same field we will be able to investigate the relationship between the IGM and luminous matter in the same volume of the high redshift Universe. While these observations will not resolve individual subcomponents of the Lyman-alpha forest, the variation in the column density of absorption by neutral hydrogen will be traceable from $z=1.6$ to the redshifts of the available background quasars. In addition, metal absorption lines are sensitive tracers of the gas associated with the ISM of galaxies along the sight-lines to the background quasars. Even galaxies too

faint to observe spectroscopically in the galaxy redshift survey would still be detectable by the absorption the gas in their interstellar media would cause in the quasar spectra. Quasar absorption line systems with significant absorption by metals (like the higher column density systems produced by gas directly associated with the ISM of galaxies), will produce identifiable absorption by Mg II (observable with WFMOS over the range $0.3 < z < 2.9$) and C IV (observable with WFMOS over the range 1.3 to 6.1).

Combined with similar studies at lower redshifts, we will be able to trace the evolution of the IGM, stellar populations, and their impact on each other from redshifts of $z \approx 4$ to the present epoch.

1.4.1 The IGM in 2004

The combination of the UV spectrographs on the Hubble Space Telescope and Echelle spectrographs on large ground-based telescopes have enabled us to study the properties of the IGM from redshift 6 to 0 (e.g., Kim et al. 2002; Kim et al. 1997; Weymann et al. 1998). Such data, when combined with the interpretive insight provided by modern cosmological simulations (e.g., Dave et al. 1999; Cen et al. 1998), have provided new insights into what drives the evolution of the observed properties of the IGM. Measurements of the fluctuations in the IGM have been used to map the underlying dark matter distribution (e.g., Croft, R. et al. 2002) and help constrain the most accurate determination of cosmological parameters (*WMAP*; Bennet et al. 2003, Spergel et al. 2003).

There have been extensive efforts to study the relationship between the IGM and the luminous matter (as traced by individual, groups, and clusters of galaxies). However, these are generally frustrated by the difficulty of obtaining detailed information about the distribution of the IGM and of galaxies in the same cosmological volume. Most studies have used *HST* spectroscopy of a small number of lines-of-sight toward quasars (generally less than 20) and incomplete redshift surveys of the brighter galaxies in modest fields (less than 15' in field-of-view) centered on the quasars (e.g., Chen et al. 2001; Chen et al. 1998; Le Brun, Bergeron, Boise, 1999). The small fields-of-view and low redshifts, $z < 0.8$, of the quasar absorption line data make it difficult to identify the larger scale structures with which both the IGM and individual galaxies might be associated. This has complicated the interpretation of the observational results, yielding conflicting interpretations of effectively the same observational results. A few studies have used extensive redshift surveys over larger areas, but have been limited by the available UV spectroscopic data (e.g., Morris et al. 1993; Grogin and Geller 1998).

Another approach has been to obtain spectra of multiple quasars in a single large field in order to improve the knowledge of the distribution of gas in the IGM in the surveyed volume (e.g., vanden Berk et al. 1999; Impey, Petry, and Flint 1999). While yielding interesting constraints on the correlation lengths and/or sizes of structures traced in the IGM, these studies have still provided less than 10 probes of the IGM across scales of several degrees (i.e., only ~ 10 sight-lines over a region of more than 25 square degrees).

Similar investigations at high redshift are only just beginning. Working with the world's largest telescope, researchers are now obtaining many redshifts (i.e., hundreds) of Lyman-break galaxies in the fields of high redshift quasars. This has allowed the investigation of the interaction between galaxies with strong winds

(driven by the forming stars they contain) and the surrounding IGM (Adelberger et al. 2003). Such studies are still limited to a relatively small number (<10) of isolated lines-of-sight (i.e., a single quasar in a survey region of 10s of arcminutes) and sampling a limited redshift range (centered around $z=3$, where the Lyman-break technique used to feed the galaxy redshift survey in this study was optimized).

Modern cosmological simulations can provide detailed predictions for the relative distribution of gas in the IGM including modeling the metal enrichment of the gas (e.g., Cen and Bryan 2001; Croft et al. 2002). This enables the prospect of being able to interpret the richer data set that would be provided by a program using WFMOS to obtain a redshift survey and spectra of AGN in the same high redshift volume.

1.4.2 A WFMOS Survey of the IGM

High spectral resolution ($R\sim 40,000$) spectroscopy of the majority of the background QSOs, while desirable, would be prohibitively expensive in 8-m class telescope time even with the multiplexing advantage of WFMOS. However, low-to-moderate resolution ($R=1000$ to 5000) spectroscopy, while still requiring many long exposures, would be feasible for quasars as faint $R\sim 22$. This would make possible obtaining spectra of 30 to 100 high redshift ($2<z<4$) AGN over the survey area. Such spectra, while not capable of resolving the individual sub-components of the Lyman-alpha forest, could provide maps of the variation in the opacity caused by fluctuations in the column density of neutral hydrogen along each line-of-sight. These can be compared to the distribution of galaxies in the complimentary redshift survey. To probe variations in the column densities as low as 10^{14} cm^{-2} in neutral hydrogen will require a SNR per spectral resolution element (5.23\AA for $R=1000$ mode of WFMOS) of at least 10. Interpretation of the spectra will be limited by our ability to determine or model the intrinsic AGN continuum emission, observed as modified by the IGM in our data. The SDSS is currently in the process of developing techniques identifying significant variations in individual QSO spectra when compared to a low-resolution template, based on their low-to-moderate-resolution spectra of high redshift ($z>3$) AGN (Burles 2003), but this will be the major constraint in interpreting the spectra. The spectra will provide information about the distribution of $N(H)$ over the redshift range 1.6 out to the redshifts of the background AGN.

Simultaneously, we will gather information about the distribution of metal-line absorbing gas in systems with $N(H)>10^{13.5-14.0} \text{ cm}^{-2}$ over a redshift range 0.28 to 6.1 (or the redshift of the background AGN). Over this range of column densities, the Mg II $\lambda\lambda 2796, 2803$ doublet should be observable in the optical window for intervening gas at redshifts $0.28<z<2.9$ and the CIV $\lambda\lambda 1548, 1550$ doublet will allow investigation over the redshift range 1.3 to 6.1.

The surface density of quasars with $R<22$ mag is approximately 150 per square degree (Boyle 2003), yielding about 250 QSOs per WFMOS field. Most of these quasars will not have high enough redshifts to be of use in studying the distribution of $N(H)$ (as traced by the absorption by the Lyman-alpha forest) at high redshifts ($1.6<z<6$), but there should be between 5 to 25 such objects per WFMOS field, 30 to 150 in the entire survey area.

Total exposure times with WFMOS are significant, but not prohibitive. For example, to obtain an $R=1000$ spectrum at 5000\AA with SNR of 10 per 5.2\AA

spectral resolution element for an $R=22$ mag AGN (power-law spectrum) 4.5 hours per field, or roughly 30 hours for the entire survey. Covering larger areas than 10 square degrees (to mitigate the effects of cosmic variance on the conclusions) is therefore not out of the question. To increase the spectral resolution to $R=5000$ would require an increase to a total integration time of 20 hours per WFMOS field. This would move the project into one requiring a large time commitment (100+ hours to complete the proposed survey), but might be possible as a major project for the instrument.

No existing facility can provide the data as efficiently with WFMOS. Since the typical separations between target quasars will be ~ 5 -20 arcminutes, current wide-field spectrographs like DEIMOS would be able to observe only 1 to 3 QSOs at a time, requiring ~ 80 pointings for every one of WFMOS. The proposed survey requires the large field of view of WFMOS and the light gathering capability of Gemini or larger telescopes.

1.4.3 References

- Adelberger, K. L., Steidel, C. C., Shapley, A. E., and Pettini, M. 2003, ApJ, 584, 45
- Boyle, B. 2003
- Cen, R., and Bryan, G. L. 2001, ApJ, 81, 546L
- Cen, R., Phelps, S., Miralda-Escude, J., Ostriker, J. P., 1998, ApJ, 496, 577
- Croft, R., Weinberg, D. H., Bolte, M., Burles, S., Hernquist, L., Katz, N., Kirkman, D., and Tytler, D. 2002, ApJ, 581, 20
- Croft, R., Hernquist, L., Springel, V., Westover, M., and White, M. 2002, ApJ, 580, 634
- Dave, R., Hernquist, L., Katz, N., Weinberg, D. H., 1998, ApJ, 511, 521
- Impey, C. D., Petry, C. E., Flint, K. P. 1999, ApJ, 524, 536
- Kim, T.-S., Carswell, R. F., Cristiani, S., D'Odorico, S., and Giallongo, E., 2002, MNRAS, 335, 555
- Kim, T.-S., Hu, E. M., Cowie, L. L., and Songaila, A., 1997, AJ, 114, 1
- Morris, S., Weymann, R. J., Dressler, A., McCarthy, P. J., Smith, B. A., Terrile, R. J., Giovanelli, R., and
- Irwin, M., 1993, ApJ, 419, 524
- Grogin, N. A., and Geller, M. J. 1998, ApJ, 505, 506
- vanden Berk et al. 1998, ApJS, 122, 355
- Weymann, et al. 1998, ApJ, 506, 1

1.5 The Structure of the LMC's Disk

The Galaxy Genesis project described in this Purple Book seeks to unravel the formation history of the Milky Way disk by identifying the remnants of the disrupted early generations of star clusters that populate the thick disk. Carrying out a similar project in the disk of the Large Magellanic Cloud (LMC) will in many ways be easier, and would allow us to study disk formation in a galaxy with

mass and age close to that of the primordial galaxy building blocks. Here, we propose to survey approximately 10^5 LMC red giants with WFMOS at high resolution ($R \sim 20,000$), so as to identify disrupted ancient star clusters through their unique chemical signatures. By observing near the Na D lines at $\sim 5890\text{\AA}$, our single-order echelle spectra will include lines of Ba, Ca, Fe, Ti, and Si in addition to Na; Na and Ba are particularly interesting, since they have been found to vary between globular clusters (Snedden et al. 2000). This survey will demonstrate the concept of chemical tagging (Freeman & Bland-Hawthorn 2002) at a much lower cost in telescope time than the Galactic survey. At the very least, the results of this survey will provide a massive database through which we will study mean stellar abundance trends and dispersions for a clear understanding of dwarf galaxy chemical evolution.

1.5.1 Chemical evolution in the LMC: the current state of the art

By contrasting the abundance patterns in the LMC with those in the Milky Way, we may highlight the physical processes that affect galactic chemical evolution. However, only with the availability of high-resolution spectrographs on 8-m class telescopes in the southern hemisphere has it become possible to study the chemical evolution of the LMC in detail. Smith et al. (2002) used Gemini South and the Phoenix high-resolution infrared spectrograph to measure oxygen and heavy element abundances in 12 LMC red giants. First, Smith et al. found that in the LMC, the [O/Fe] ratio begins to drop at a lower [Fe/H] than in the Milky Way. This observation is consistent with the LMC having experienced a strong early burst of star formation (Gilmore & Wyse 1991), while the Milky Way formed stars at roughly constant rate. Second, the LMC reaches lower [O/Fe] ratios at high [Fe/H] than does the Milky Way. This observation could be explained by a higher ratio of SN Ia to SN II in the LMC than in the Milky Way.

The Smith et al. results demonstrate how the comparison of abundance patterns in the LMC and Milky Way strengthens our general understanding of chemical evolution. With a much larger LMC abundance dataset, we could explore the source of the evident intrinsic scatter in the abundance patterns. Although our proposed WFMOS project will not include the measurement of O, Ti and Si (which behave in a similar fashion to O (Edvardsson et al. 1993)). The Smith et al. results thus provide strong motivation for the WFMOS proposal.

1.6 The globular clusters of the LMC: tracers of early star formation

The globular clusters (GCs) of the Milky Way halo are widely considered to represent the oldest known stellar population in the Galaxy, with the disk population being a few Gyr younger. The LMC has 13 known old GCs, which are remarkably similar to those of the Milky Way. Comparisons of the *HST* color-magnitude diagram of the LMC cluster NGC 2019 (Olsen et al. 1998) with the MW GC M5, show an extremely good match implying that NGC 2019 and M5 have the same age to within 1 Gyr and nearly identical abundances. Indeed, *all* of the LMC's old GCs studied to date have ages, abundances, and integrated luminosities which could have been drawn from the same parent population as the Milky Way GCs (Olsen et al. 1998, Johnson et al. 1999). The GC systems do, however, have one major difference: the MW GCs have halo kinematics, while the LMC GCs revolve with the HI disk (Schommer et al. 1992). Thus, the LMC

contains the *oldest* disk that we know of in the Local Group; understanding the formation of this disk is potentially extremely exciting. There is no plausible way to form a disk GC system from the accretion of fragments (e.g., Searle & Zinn 1978) without also forming a stellar halo (Abadi et al. 2002). While many have looked (cf. Olszewski et al. 1996), there is not yet any evidence for a halo in the LMC. In the absence of a halo, a compelling explanation is that galaxies such as the LMC are indeed the ‘building blocks’ out of which the halos of larger galaxies formed (e.g., Côté et al. 1998). Kinematics of a large set of metal-poor LMC stars would establish whether the LMC indeed lacks a stellar halo.

1.6.1 Selecting an old LMC population

Unlike the Milky Way, the star formation history of the LMC has been punctuated by bursts. The LMC experienced an initial burst of star formation coinciding with the epoch of globular cluster formation. This was followed by an approximately eight-Gyr-long period of lower star formation rate, and a subsequent renewed star formation burst beginning approximately four Gyr ago and continuing to the present (e.g. Geha et al. 1998, Holtzman et al. 1999, Olsen 1999).

The star formation history is such that a random sample of LMC red giants with $V \leq 20$ will contain $\sim 30\%$ stars formed at early times. Moreover, these stars are easily selected by their metallicity, since the initial burst produced rapid enrichment to $[\text{Fe}/\text{H}] \approx 1$ (Gilmore & Wyse 1991; see also Dopita et al. 1997), as seen in the cluster metallicity distribution (Pagel & Tautvaisiene 1998).

1.6.2 The Experiment

The main goal of this experiment is to identify through abundances and kinematics the population of disrupted low-mass star clusters that accompanied the formation of the LMC's existing globular clusters. How many clusters do we expect to identify, and how many objects will be available to WFMOS? If the globular clusters are the surviving remnants of an LMC cluster population with a power-law mass spectrum similar to that of young LMC clusters (Elmegreen & Efremov 1997), then we expect the initial burst to have produced roughly 2000 star clusters with masses in excess of $10^3 M_{\odot}$. In order to identify ~ 10 chemically unique stars per parent cluster, we will thus need to survey 60000 LMC stars, assuming 30% of the stars are ancient. Using the 9-million star color-magnitude diagram of the MACHO project (Alcock et al. 2000) as a guide, there are ~ 300000 LMC red giants with $V < 18$ distributed over an area in excess of 100 square degrees. To sample stars over the entire LMC disk, we will thus require ~ 45 WFMOS pointings. Within the inner ~ 3 degrees of the LMC, the object density will exceed the number of fibers available, while at a 5 degree radius the density will drop to ~ 1000 objects per pointing. The high object density in the central regions led us to suspect that crowding might be problematic. However, as demonstrated by observations taken by the SuperMACHO project (Stubbs et al. 2003) with the CTIO 4-m of the LMC Bar, crowding is not a problem at $V=18$. Analytical considerations of crowding (Olsen et al. 2003) suggest that accurate photometry at $V=18$ in the LMC is possible even in regions with surface brightness $\sigma_V=20$ mag arcsec $^{-2}$, while the LMC has central surface brightness $\sigma_B=21.5$ mag arcsec $^{-2}$ (Bothun & Thompson 1988). The 45 pointings will allow WFMOS to obtain spectra of $\sim 140,000$ red giants, or ~ 20 stars per disrupted cluster; the capabilities of WFMOS are thus an excellent match to this project.

Assuming 1 night of integration per pointing to achieve $S/N=100$ with $R=20000$ at 5800\AA , this project will require ~ 45 nights of telescope time.

1.6.3 The LMC-SMC-Milky Way interacting system

The LMC has clearly interacted with its close companion SMC and the Milky Way, the most spectacular evidence coming from the Magellanic Stream (Mathewson et al. 1974) and its leading arm (Putman et al. 1998). Understanding this interaction is important for the analyses of the kinematics of both the LMC and Milky Way projects described in this Book, since the Clouds may be responsible for the Galactic warp (Weinberg 1998). While the SMC has borne the brunt of the damage from the interaction (e.g., Caldwell & Coulson 1986), in the LMC the effects are more subtle. van der Marel & Cioni (2001) found that the LMC is intrinsically elliptical with an asymmetric stellar density profile, which they ascribe to tidal interaction with the Milky Way. The kinematics of LMC carbon stars (Kunkel et al. 1997, Graff et al. 2000, van der Marel et al. 2002) most clearly show the rotation of the LMC disk, but also show intriguing evidence for kinematic disturbances. One of these disturbances corresponds in location to the region that Olsen & Salyk (2002) found from photometric analysis contains a warp. The analysis of LMC kinematics is particularly important, since the irregularities might be revealing structure that could be responsible for the microlensing rate seen in the direction of the LMC (Graff et al. 2000). The experiment proposed here will provide accurate kinematics for 10^5 LMC stars, a sample that is two orders of magnitude larger than all other samples combined. Thus, kinematic features that are invisible in today's data will be readily apparent in the WFMOS dataset.

1.6.4 References

- Abadi, M.G., Navarro, J.F., Steinmetz, M., Eke, V.R., astro-ph/0212282
- Alcock, C., et al. 2000, AJ, 119, 2194
- Bothun, G.D., Thompson, I.B. 1988, AJ, 96, 877
- Caldwell, J.A.R., Coulson, I.M. 1986, MNRAS, 218, 223
- Côté, P., Marzke, R.O., West, M.J. 1998, ApJ, 501, 554
- Dopita, M.A., et al. 1997, ApJ, 474, 188
- Edvardsson, B., Andersen, J., Gustafsson, B., Lambert, D.L., Nissen, P.E., & Tomkin, J. 1993, A&A, 275, 101
- Elmegreen, B.G., Efremov, Y.N. 1997, ApJ, 480, 235
- Freeman, K.C., Bland-Hawthorn, J. 2002, ARAA, 40, 487
- Geha, M., et al. 1998, AJ, 115, 1045
- Gilmore, G., & Wyse, R.F.G. 1991, ApJ, 367, L55
- Holtzman, J., et al. 1999, AJ, 118, 2262
- Johnson, J.A., Bolte, M., Stetson, P.B., Hesser, J.E., Somerville, R.S. 1999, ApJ, 527, 199
- Kunkel, W.E., Demers, S., Irwin, M.J., Albert, L. 1997, ApJ, 488, L129
- Mathewson, D.S., Cleary, M.N., Murray, J.D. 1974, ApJ, 190, 291

Olsen, K.A.G., Hodge, P.W., Mateo, M., Olszewski, E.W., Schommer, R.A.,
Suntzeff, N.B., Walker, A.R. 1998, MNRAS, 300, 665

Olsen, K.A.G. 1999, AJ, 117, 2244

Olsen, K.A.G., Salyk, C. 2002, AJ, 124, 2045

Olsen, K.A.G., Blum, R.D., Rigaut, F. 2003, AJ, submitted

Olszewski, E.W., Suntzeff, N.B., Mateo, M. 1996, ARAA, 34, 511

Pagel, B.E.J., Tautvaisiene, G. 1998, MNRAS, 299, 535

Putman, M.E., et al. 1998, Nature, 394, 752

Schommer, R.A., Suntzeff N.B., Olszewski E.W., Harris H.C., 1992, AJ, 103, 447

Searle, L., Zinn, R. 1978, ApJ, 225, 357

Smith, V.V., Hinkle, K.H., Cunha, K., Plez, B., Lambert, D.L., Pilachowski, C.A.,
Barbuy, B., Melendez, J., BalaChandran, S., Bessell, M.S., Geisler, D.P., Hesser,
J.E., Winge, C. 2002, AJ, 124, 3241

Snedden, C., Pilachowski, C. A., Kraft, R. P. 2000, AJ, 120, 1351

Stubbs, C.W. et al. 2003, 2002, BAAS, 201, #7807

van der Marel, R.P., Alves, D.R., Hardy, E., Suntzeff, N.B. 2002, AJ, 124, 2639

van der Marel, R.P., Cioni, M.-R.L. 2001, AJ, 122, 1807

Weinberg, M.D. 1998, MNRAS, 299, 499